1 OF 6

N84-29978 UNCLAS

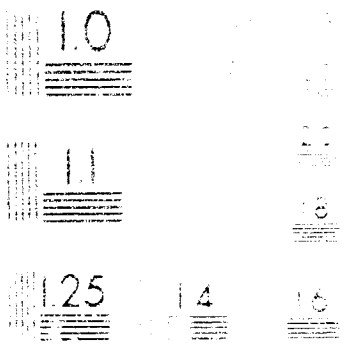

NASA Contract Report CR-172211

A Study of Stiffness, Residual Strength and Fatigue Life Relationships for Composite Laminates

J.T. Ryder
F.W. Crossman

LOCKHEED-CALIFORNIA COMPANY
A Division of Lockheed Corporation
Burbank, California 91520

Contract NAS1-16406
October, 1983

National Aeronautics and
Space Administration

Langley Research Center
Hampton, Virginia 23665

NASA Contract Report CR-172211

A Study of Stiffness, Residual Strength and Fatigue Life Relationships for Composite Laminates

J.T. Ryder
F.W. Crossman

LOCKHEED-CALIFORNIA COMPANY
A Division of Lockheed Corporation
Burbank, California 91520

Contract NAS1-16406
October, 1983

National Aeronautics and
Space Administration

Langley Research Center
Hampton, Virginia 23665

TABLE OF CONTENTS

TABLE OF CONTENTS - Continued

TABLE OF CONTENTS - Continued

LIST OF TABLES

LIST OF TABLES - Continued

LIST OF TABLES - Continued

LIST OF TABLES - Continued

LIST OF TABLES - Continued

LIST OF TABLES - Continued

LIST OF FIGURES

LIST OF FIGURES - Continued

LIST OF FIGURES - Continued

LIST OF FIGURES - Continued

FOREWORD

This report describes the nature and results of a research investigation into the relationship among strength, fatigue, residual strength, and stiffness properties of several tensile loaded graphite/epoxy composite laminates. The investigation was conducted by two companies of the Lockheed Corporation between September 30, 1980 and July 15, 1983 in fulfillment of National Aeronautics and Space Administration Contract NAS1-16406. Because of the breadth of the investigation, experimental and analytical results from other studies supported by the Lockheed Corporation are included in this report. These studies were conducted independent of this program, but their results or experimentally generated data were of significant importance to the overall understanding developed on the NASA sponsored program. While a joint analytical effort took place, experimental work was performed by the Lockheed-California Company at the Kelly Johnson Research and Development Center at Rye Canyon while computer aided, mathematical modeling was done by the Lockheed Missiles and Space Company at the Palo Alto Research Laboratory. The work was sponsored by the NASA Langley Research Center, Hampton, Virginia, under the constructive management and leadership of Dr. T. K. O'Brien. The contract effort which has led to the results in this report was financially supported by the Structures Laboratory, USARTL (AVRADCOM).

The program was performed by the Fatigue and Fracture Mechanics Laboratory of the Lockheed-California Company and by the Applied Mechanics Laboratory of the Lockheed Missiles and Space Company. Throughout the program, the Lockheed engineering project leader was Dr. J.T. Ryder who was also directly responsible for the experimental effort. Dr. F.W. Crossman of the Lockheed Missiles and Space Company was responsible for the computer aided mathematical modeling. Development of insights gained during the program and

many of the technical decisions as to program direction were very much the result of a cooperative effort among Drs Ryder, Crossman, and O'Brien. The help of Dr. O'Brien in many phases of the program is therefore gratefully acknowledged.

The authors of this report warmly acknowledge the major contributions of several individuals. Mr. P. M. Steinert faithfully performed the computer aided/mathematical modeling while spending many long hours at the computer terminal. Mr. J. R. Zumstag was instrumental in developing much of the computer software capability used in the investigation. To Mr. C. J. Looper and Mr. D. R. Diggs goes our deep appreciation for skilfully conducting the majority of the experimental work. Ms. A. Denny was also called upon to conduct some of the experimental work which she did in an excellent manner. Mr. P. L. Mohr helped greatly by collecting and collating a significant portion of the extensive amount of data into a useful format. The many technical discussions with Ms. K. N. Lauraitis were extremely helpful. In fact, without them the ideas and concepts presented would not have developed nearly as well; thus her contribution was much larger than clearly shown in this report. The authors are pleased to extend their appreciation to Ms. D. M. Riley for her sustained typing and manuscript preparation efforts throughout the many monthly reports and during the much larger final report. Finally, much appreciation is extended to Mr. E. K. Walker whose early inspiration at Lockheed in the field of composites allowed the eventual development of this manuscript.

SUMMARY

The purpose of this research investigation was to explore, in both a qualitative and quantitative fashion, the relationship among stiffness, strength, fatigue life, residual strength, and extent of damage of unnotched, graphite/epoxy laminates subjected to tension loading. The more complex cases of notches or compression loading were eliminated not because of their lack of importance, indeeed in many cases they may be more important, but because we do not yet understand the mechanics of the so called simple tension case. Clarification of the mechanics of the tension loading case was intended to accomplish several purposes. First, the valuable results and conclusions of many previous investigations could hopefully be combined in a unified way which would explain the many apparently contradictory observations and hypotheses. Second, the development of a relatively simple procedure to anticipate strength, fatigue life, and stiffnesss changes was desired. Third, the intent was to provide a solid foundation upon which to extend the work to the more complex cases of compression, notches and spectrum fatigue loading.

An outline of the investigation and an overall philosophy is given in Section 1. The experimental and analytical results are discussed and compared in Section 4 with the conclusions and implications summarized in Section 5. Section 2 is devoted to a detailed presentation of the experimental results while Section 3 is similarly devoted to a presentation of the analytical and mathematical modeling study. A basic understanding of the program can be gained by reading Sections 1.1, 1.4, 4 and 5.

The dominant damage type of analytical concern during the program was matrix cracking (both interlamina and intralamina) and 0° fiber fracture. Mathematical models were developed based upon analysis of the damage states. A

mechanistic approach to modeling was selected to represent damage development instead of the statistical approach. Because a primary objective was to investigate whether the nature of macroscopically observed phenomena can be understood based on knowledge of the lamina properties, the laminate construction, and the damage state, a statistically based modeling approach was not appropriate.

Coupons from several different layups $((0)_4$, $(0/90/\pm45)_s$, $(0/\pm45)_s$, $(0/45/0_2/-45/0)_s$, $(0_2/90_4)_s)$ were subjected to monotonic tension load to failure, constant amplitude tension-tension fatigue loading, or to monotonic tension load to failure after prior fatigue loading. Stress, strain, and stiffness were recorded throughout each experiment. Plastic cast edge replication and enhanced x-ray were used to record both inter and intra lamina matrix cracking. Observed damage states were analyzed and mathematically modeled. Estimates of stiffness, strength, strain to failure, extent of scatter, fracture appearance, and shape of the stress-life curve based on the models were compared to experimental data for each of the three types of experiments: initial strength, fatigue, and residual strength. Mathematical models were based on laminate analysis, free body type modeling, or upon a strain energy release rate approach combined with a finite element procedure.

Changes in laminate stiffness were attributed to: transverse, intralamina matrix cracking, with and without end delamination; interlamina matrix cracking, delamination; ply isolation due to combined delamination and transverse matrix cracking; 0° ply splitting; and 0° fiber fracture. During development of 0° ply failure criteria, several possible theories and means of strain concentration were considered. These were: deterministic strength theories, statistical fiber bundle theory, linear elastic fracture mechanics, transverse matrix cracks, and ply isolation. Three dimensional finite element modeling was conducted of several types of delamination. This modeling was performed to further examine the stress field in the 0° ply as influenced by delamination. The possible differences between strain

to failure in unidirectional and multidirectional laminates was also analyzed. This study led to consideration of the relationship between volume and strength of a 0° ply.

Essentially, stiffness was found to be only loosely related to fatigue life or strength. Strain was found to be the primary measurement of greatest significance. Stiffness changes were found to be primarily due to delamination, transverse matrix cracking, and local ply isolation (due to combined delamination and transverse matrix cracking). All other possible contributions were found to be small. A simple analysis based upon a free body type analysis approach was found to account for stiffness change due to combined matrix cracking and delamination (ply isolation) while matrix cracking, which was at most less than a 3 percent effect, was determined using simple master plots for each ply.

Coupon failure requires fracture of the 0° plies and this was attributed to essentially three factors: 1) small strain increases due to transverse matrix cracking; 2) local strain increases in the 0° plies due to specific combinations of delamination and transverse matrix cracking resulting in local ply isolation, and 3) strains in the 0° plies being high enough that fatigue failure would occur even for a 0° unidirectional laminate. Scatter in properties was found to be due to: 1) the intrinsic size of the microstructure relative to the geometry; 2) the variability in fiber strength; 3) the requirement of only a few adjacent statistically significant fiber fractures for general coupon failure; and 4) the magnitude of local strain concentration due to ply isolation.

Comparison of three dimensional to two dimensional modeling of stress concentration in a 0° ply due to delamination between adjacent plies showed that the more complex analysis did not provide any fundamental improvement in accuracy. Further, damage growth, both direction and rate, were found to be dependent on complex relations among G_I, G_{II}, and G_{III}. This fact combined with the necessity of constantly and drastically changing models as

damage grows rendered the use of complex three dimensional models questionable. Both two dimensional and three dimensional analyses showed that high peak stress concentration did not develop in 0° plies adjacent to either delamination or transverse matrix cracks. This result indicated that fracture toughness concepts could not be used to provide a failure criteria for the 0° plies.

By assuming that strain is the primary variable of importance, accounting for possible stiffness changes by a simple rule of mixtures, and by applying the derived 0° failure criteria, all of the observed mechanical properties for each loading condition and layup could be quantitatively and qualitatively calculated by using lamina properties. Therefore, a simple procedure is proposed to calculate strain to failure, stiffness, strength, data scatter, shape of the stress-life curve, and stiffness changes for any laminate based only on lamina properties. The lower bound of the stress-life curve, "runout" life, was determined by free body type of analysis. Strain energy release rate analysis is required for determining the lower bound for the onset of matrix damage (transverse cracking or delamination), but not for the fatigue life curve. The complex analyses performed in this study were found to be extremely useful and worthwhile for confirming and supporting the validity of employing the proposed relatively simple procedures.

SECTION 1
INTRODUCTION

1.1 PROGRAM OBJECTIVE

The purpose of this research investigation was to explore, in both a qualitative and a quantitative fashion, the relationship among stiffness, strength, fatigue life, residual strength, and extent of damage of unnotched, graphite/epoxy laminates subjected to tension loading. The unnotched geometry condition was selected to avoid the complexities attendent to modeling damage from a hole or notch. Likewise, the program was restricted to tension load and constant amplitude fatigue because of the inherent mathematical difficulties which occur with the more complex case of compression dominated or spectrum loading. In short, the simplest case possible was selected for study. However, this case was selected precisely because, despite the apparent simplicity, the relationship among such quantitatively measured properties as stiffness, damage extent, strength, and fatigue life is not well understood. Thus the more complex cases were eliminated not because of their lack of importance, indeed in many cases they may be more important, but because we do not yet understand the mechanics of the so called simple case.

Clarification of the mechanics of the tension loading case was intended to accomplish several purposes. First, the valuable results and conclusions of many previous investigations could hopefully be combined in a unified way which would explain the many apparently contradictory observations and hypotheses. Second, the development of a relatively simple procedure to anticipate strength, fatigue life, and stiffness changes was desired. Third, the intent was to provide a solid foundation upon which to extend the work to the more complex cases of compression, notches, and spectrum fatigue loading.

This was not thought to be fully possible without this basis. Finally, the intent was to aid in the establishment of a basis for succinctly relating laboratory coupon type data to structural application.

Throughout this research study, primary emphasis was not upon collecting the necessary experimental data for developing mathematical models to specifically predict residual strength or fatigue life. Instead empnasis was upon analysis of observed experimental data, upon developing mathematical models to represent the assumed pertinent features of a selected laminate and an experimentally observed damage state, and upon the qualitative and quantitative comparison of such derived properties as stiffness and strength to experimentally based data. Comparative agreement for many different cases was taken as verification that the mechanics of a particular laminate and damage state was understood. Thus the intent was development and improvement of our technical understanding of the mechanics of laminated composites. For this reason, much attention was given to the generation of detailed, accurate experimental data, to the detailed analysis of those data, and to the exploration and development of many different, though related, models and aspects of both the models themselves and variations in them. In certain restricted cases, predictive capability may of course be derived from the models, perhaps rather easily as will be shown in Section 4, but such concepts as prediction of fatigue life and cumulative damage were not of basic concern.

Success in developing a definitive understanding of the mechanics of laminated composites even for this supposedly simple case is believed to be of value for two reasons. First, confidence would be gained that the basic mechanics is understood. Second, that basic mechanics would form a solid foundation under efforts to understand more complex cases thereby avoiding many unfounded assumptions and undoubtedly much inefficient effort.

1.2 DEVELOPMENT OF A POINT OF VIEW

A specific point of view underlies this program concerning the mechanics of damage development in graphite/epoxy laminated composites and thus

influenced subsequent analysis as well as the selection of representative models and their associated mathematical procedures. This subsection discusses that point of view while the next subsection addresses mathematical modeling.

Fundamentally the nature of damage, or change in state, for both metals and composites is the same, namely: the extensional breakage of atomic bonds. The small molecular dimensions of most materials formed of metallic elements allows them to be considered homogeneous, continuous and isotropic at small dimensions (generally at any dimension greater than 1 or 2 mm). These small dimensions plus the nature of the interatomic bonds allows metallic materials to exhibit the macroscopic phenomenon termed plasticity. Thus, state change (damage) manifests principally as the processes termed slip, twinning, cleavage, and microcracking. These microscopic processes are the most important ones of concern for most macroscopic studies. In some cases, they result in macroscopic size flaws which dominate the microscopic damage.

The macroscopic expressions of damage exhibited by laminated composite materials are not normally encountered in similar studies of metals except in the case of bonded bimetallics. Although laminated composites are made up of at least two material phases of quite different properties, this is not unique since the same fact is usually true for metallic materials. The unusualness of composite materials lies in the fact that their method of formation results in a state where conditions of homogenity, continuity, and isotropy occur only at large macroscopic levels (at least on the scale of cms if not meters). In fact, for most practical applications of laminated composites, such a state is not actually ever reached in a direction perpendicular to the plies. Therefore, the dominant manifested form of damage which needs to be considered for qualitative understanding of most composites, up to the onset of 0^{o} fiber breakage, is matrix cracking (inter and intra lamina) as influenced by the anisotropic nature of the material. Thus in order to understand the mechanics of the change in state damage process,

the nature of matrix cracking and delamination must be of primary interest. This understanding needs to be combined, for certain applications, with a detailed formulation of fracture in the primary load carrying plies.

The fact that the microstructure of laminated composites always directly enters into consideration of macroscopic phenomenon is a point requiring further discussion. The large scale microstructure essentially insures, for example, that scatter in fatigue life of unnotched coupons will always be relatively large compared to that usually encountered for metals. The scatter in fatigue life of metallic coupons is also large when the microstructure and not surface finish dominates fatigue life[1]. This happens, for instance, when the coupon surfaces are carefully prepared by special polishing techniques thereby effectively reducing surface residual stresses and micronotch induced stress concentrations to such an extent that microstructural variations predominate. Normal surface preparation, even for ASTM type standard tests, is not nearly so careful, therefore, surface preparation dominates fatigue life, not microstructure. For normally recommended surface preparation procedures[2,3], resultant fatigue life scatter is relatively narrow[4]; much less than the differences induced by microstructure alone. However, average fatigue life can be much less than for the case where microstructure predominates especially in the long life region[4].

Laminated, un-notched composites coupons are, in essence, usually in the state of being "carefully polished" coupons in that microstructure predominates. Most edge defects are unimportant in that statistical variations in the large scale microstructure continue to dominate fatigue life leading to large scatter and long life. Certain types of defects can significantly reduce fatigue life if they are large relative to the microstructure. Among these defects are: alignment of prepreg tape edges in plies of the same orientation through the thickness[5], large groups of misaligned load carrying fibers within a ply[6]; and rows of dimples distorting the load carrying plies, such as happened to some of the $(0/\pm 45)_s$ coupons of this

study, see Section 2.3. The primary point is that relatively large fatigue life scatter is inherent to graphite/epoxy laminated composites because of the microstructure. This point will be discussed much further in Section 4.

The significant microstructural influence for laminated composites not only manifests in large fatigue life scatter, but also in the very nature of the stress-life curve representation. Stress-life curves for metals are similar regardless of whether the data are for notched or unnotched coupons. The actual fatigue life differs numerically, but not the general response to load, hence the curves look similar but shifted. For laminated composites, however, the stress-life curve for, as an example, tension-tension fatigue loading of notched coupons looks significantly different than that for unnotched coupons[7]. In addition, bonding a thin strip of glass/epoxy along the free edge results not only in greatly increased life, but also in reduction or even elimination of delamination[8]. Even the type of fatigue loading, for example a stress range ratio of -1.0 versus -0.3, totally changes the direction and type of damage growth and thus the resultant shape of the stress-life curve[9]. All of these changes are due to the much more significant influence, relative to metals, of geometry and loading on the resultant behavior of laminated composites which is in turn due to the large scale microstructure, see Reference 1 for an in-depth discussion. Thus the significant effect of microstructure of laminated composites on both fatigue life scatter and the nature of the relationship between stress and fatigue life must always be kept in mind.

Based upon the above discussion, a comprehensive analysis of how matrix crack formation and growth (inter and intra lamina) are influenced by load application is required. A mathematical representation of the process will result in a quantitative description, the accuracy of which is dependent upon the previous analysis, the practical difficulties of obtaining appropriate experimentally based input data, and the human labor required for achieving a desired level of accuracy. Having concluded that for laminated composites, damage in the form of crack development and extension,

whether inter or intralamina, is the dominant one of interest, qualitative analysis of what influences crack formation, location, and growth is believed to result eventually in an understanding of macroscopic phenomena.

Consider, as an example, the case of an unnotched multidirectional laminated composite subjected to steadily increasing tension load. The experimentally observed location of crack formation (intralamina matrix cracks, interlamina delamination) and their saturation numbers in transverse plies can be approximated by mathematical analysis.[10,11] An energy approach to this problem appears to be the most fruitful since an energy concept allows for volumetric effects. This was confirmed by Wang and Crossman.[11,12] Crack formation and extension is, of course, caused by the load (energy) increase. Final fracture is due to localized transfer of load into the 0^{o} plies, localized fracture of 0^{o} fibers which in turn influence the breakage of the 0^{o} plies, and further crack extension followed by coupon fracture at a region where a critical number of such fiber breakages interact.

For the case of constant amplitude tension-tension fatigue, cracks are formed on the first load cycle, if high enough, because of the increasing load, as in static tension. Each additional input of energy (cycle) extends the cracks (damage), however minutely, or increases their number. Crack extension occurs either due to a stable rate of breakage and partial reformation of atomic bonds near the peak load or to breakage and complete or partial reformation of atomic bonds during each energy (load) input cycle in such a manner that the original state is changed slightly on each cycle. Final fracture occurs for similar reasons as in the static tension case, namely: transfer of load to 0^{o} plies, fracture of 0^{o} fibers at various locations, and final coupon fracture in a region where the 0^{o} fiber breakages sufficiently interact. Similar to the static tension case, the location, type, and number of, at least, initial cracks can be approximated by an appropriate laminate analysis.[10-12]

Although final fracture state under either monotonic (static) tension loading or tension-tension fatigue loading is deterministically related to the initial state of the coupon, the final damage state prior to fracture is path dependent, i.e., dependent upon the type of prior loading. The significant point, of course, is that a developing damage state is always peculiar to or characteristic of a particular laminate. At some point of damage development, a specific state may, however, manifest in some laminates regardless of whether loading is monotonic or fatigue cycling.[10] However, other layups do not appear to reach such a state prior to coupon fracture.[12] For those laminates which do reach a specific, often termed characteristic state[10], damage development can be said to be path independent up to that point. However, for such laminates subsequent damage development is load path dependent, as it always is for all other laminates, because both delamination and extent of matrix cracking under fatigue loading prior to fracture can be significantly greater than and much different than that which occurs under monotonic tension loading.[7] Thus, the transfer of load into the 0^{o} plies will be different for the two loading types resulting in a path dependent state. This property, as the results of this program will clearly show, and prior work indicated[7,13], manifests in the significant difference between strain to failure which occurs under fatigue loading and that which occurs under residual strength loading.

Other aspects of laminated composites requiring analysis are the problems of representing fatigue-life scatter and the nature of the stress-life curve which reflects the interaction of the microstructure, geometry and loading. Representation of fatigue life scatter is undoubtedly theoretically possible, but would require collection of extremely detailed experimental data beyond the scope of any normal necessity. Thus the problem appears to be more one of understanding and bounding the scatter, not modeling. In any case, the extent of scatter is dependent on the part geometry and loading [7,9] and thus is problem specific. The question of reviewing and modeling damage state development as influenced by geometry and loading was considered to be one of future concern since the basic mechanics have to be understood first.

A descriptive analysis similar to that just given for tension loading could be done for compression loading and for tension-compression or compression-compression fatigue. Although, damage state development is significantly different, the principles remain unchanged. Therefore, a point of view as to the nature of damage initiation and growth for laminated composites was formulated as follows:

- The dominant damage type of analytical concern is matrix cracking.
- Matrix cracking can be intralamina or interlamina (delamination).
- The damage state is characteristic of the laminate, loading direction, and geometry; at any time is deterministically related to the initial state, and is, in general, path dependent (although specific cases of path independency exist up to some state).
- Microstructure always has a dominating influence on observed mechanical properties such as in fatigue life scatter and the stress-life curve.

This point of view implies several inferences, among which are:

- The laminate stacking sequence determines the inter and intra laminar normal and shear stresses which, in turn, determine: location and eventual density of intralamina cracks; and location and propagation of delaminations. These can be calculated, at least approximately, by known mathematical procedures.
- Stiffness is dependent on both layup and damage state.
- Final fracture must be ascertained by determining the manner in which load is transferred to the primary load carrying plies. For coupons of this program, this required analysis of the influence of local delamination on the fracture of 0^{o} fibers and the effect of such fiber fractures on 0^{o} ply integrity and coupon failure.
- Temperature, width, and notches affect static strength and fatigue life because they alter matrix properties and stress states.

- Fatigue life depends on the definition of failure. If defined as an amount of stiffness change, fatigue life will be much different than if defined as the number of cycles to a damage state characteristic of the laminate or as fracture into two or more pieces.

1.3 MATHEMATICAL MODELING

Analysis of the laminates, damage states and associated properties was followed by mathematical modeling of the interaction of the separated elements. This required selection of a modeling procedure. Two major approaches to represent damage development in laminated composites have been historically employed. These may be called statistical and mechanistic (where the emphasis here is upon the detailed mechanics of the damage process). In the statistical approach, such macroscopic phenomena as global stress, number of cycles, time, or tensile strength at any point in time are tabulated. Relationships among the parameters are sought by considering them as statistical variables and thus formulating statistical probability equations which describe observed rates of change. Physical mechanisms are postulated to explain hypothesized relationships between the variables and their rate of change. In contrast, the mechanistic approach considers the physical details of both a laminate and an assumed damage state, formulates mathematical descriptions and, in theory, derives the expected macroscopic relationships from the microscopic phenomena. The nature of the two analytical approaches are thus quite different. One leads from the macroscopic to the microscopic on the basis that the mechanics of damage may be too complex for direct formulation, and the other from the microscopic to the macroscopic on the basis that the broad spectrum of often unsuspected macroscopic relationships can not otherwise be fully understood.

Essentially, all statistical approaches emphasize representing rates of change in observed mechanical properties, such as residual strength. All such procedures (see those postulated by the authors of References 14 to 17) have common elements in that the same four basic assumptions are stated. First, the distribution of observed phenomena can be represented by an

exponential equation (this is usually chosen as a two parameter Weibull equation). Second, change in strength can be represented by a power law. Third, fatigue life and macro stress are related by a power law. Fourth, there is a one-to-one relationship between residual strength and fatigue life. The last assumption is equivalent to stating that the stress required to fracture a coupon into two pieces is path independent. Different mathematical exponents have been selected for the various proposed power laws depending on the interpretation of the form of variable relationship. Hahn, has put this statistical procedure on a more rigorous basis.[18] Yang and Jones[17] have shown how the various statistical approaches are related. Other approaches such as that of Halpin and Waddoups[19] have postulated damage growth concepts, but in a manner general enough and with the same four assumptions that they reduce to a statistical approach[17].

Statistical approaches for life prediction and strength degradation have the unfortunate property that they do not easily lead to an understanding of physical phenomena. They also have the requirement that data be obtained for each layup under each type of loading and environment. The accuracy of such approaches is dependent upon the correctness of the assumption that fracture strength is path independent (that a one-to-one rank order relationship exists between strength and fatigue life). Previous studies[7] have indicated that this key assumption is, at best, only superficially valid. In fact, the necessary conditions for fracture under fatigue load appear to be quite different than those for residual strength loading as the results of a prior investigation indicated[7]. Another problem with the statistical approach is that generalized formulations are difficult to devise. For instance, most layups increase in static tensile residual strength due to tension-tension fatigue loading if they contain a notch and can even increase under tension-compression loading depending on the stress ratio.[7]

Mechanistic approaches[10,11,12] are based on detailed analysis of the mechanics of both the laminate and the damage process and thus attempt to model damage development from initiation through growth and up to fracture.

Such approaches, at least idealistically, come close to starting from lamina properties and lead to stiffness, damage development, and fracture development properties. Because a primary objective of this program was to investigate whether the nature of macroscopically observed phenomena can be understood based on knowledge of the lamina properties, the laminate construction, and the damage state, a statistical approach was not selected. Instead the approach was taken to model observed damage, calculate stiffness changes, estimate effects on primary load carrying plies, and compare results to experimentally observed stiffness and strength. The hoped for result was the development of a capability to, at a minimum, anticipate for any given layup: both stiffness and strength under monotonic loading as well as the general matrix cracking and delamination state; the threshold for onset of delamination growth and/or matrix crack saturation under fatigue loading thus allowing an estimate of the bounds of the fatigue life curve; and, lastly, given a known damage state, to estimate residual strength.

1.4 OUTLINE OF PROGRAM

This research study consisted of: 1) detailed experimentation; 2) analysis (separation) of the various aspects of the laminates and the observed damage states and associated mechanical phenomena; 3) modeling of the laminates and damage states, and; 4) comparison of analytically and mathematically based conclusions with experimental results. A brief outline of each of those phases will be described.

1.4.1 Experimental Program

Twenty-five to thirty coupons of each of five different layups were subjected to experimentation. Those experiments consisted of monotonic tension load to failure, constant amplitude tension-tension fatigue loading to failure or to 10^6 cycles, and monotonic tension residual strength loading to failure of coupons previously subjected to fatigue loading. Throughout

each experiment, stress and strain were recorded and stiffness calculated (both monotonic and dynamic stiffness for fatigue experiments). During each experiment, the two NDI techniques, plastic cast edge replication and enhanced x-ray photography, were used to periodically record both inter and intra lamina matrix cracking. As previously mentioned, only tension loading of unnotched coupons was conducted in order to explore a relatively simple, yet by no means fully understood situation. All fatigue experiments were conducted under load control in order to allow strain to increase, if stiffness decreased, and to guarantee eventual coupon fracture.

There were five layups experimentally investigated in this program: $(0)_4$, $(0/90/\pm45)_s$, $(0/\pm45)_s$, $(0/45/0_2/-45/0)_s$, and $(0_2/90_4)_s$. The unidirectional layup was selected to give baseline information on the fracture of 0° plies unaffected by off axis plies. The $(0/90/\pm45)_s$ laminate tends not to delaminate during monotonic tension loading to fracture, but does during fatigue loading. Thus the data of this layup, when combined with other quasi-isotropic layups which tend to delaminate during monotonic loading or with other layup configurations, provided a data set suitable for analysis for the entire range of quasi-isotropic laminates. The $(0/\pm45)_s$ layup provided information on a laminate influenced only by $\pm45^\circ$ plies and one which would tend not to delaminate under either monotonic or fatigue loading. The $(0/45/0_2/-45/0)_s$ layup was selected because of its known tendency to delaminate under fatigue loading[7], but without associated stiffness change. Finally, the $(0_2/90_4)_s$ layup allowed analysis of the extreme effect of 90° plies only. Thus, these layups were chosen not for their practical utility, but because the data obtained from them when combined with other data allowed study of a wide range of possible states of damage (intraply matrix cracking with and without delamination), associated stiffness change (with and without macroscale delamination), or no stiffness change with delamination, and effects of off axis plies alone and in combination. Note, however, that most practical layups are combinations of these basic simple layups.

1.4.2 Data Analysis

The collected damage, stiffness, and fracture data were analyzed for the purposes of determining both the details of the damage states and the associated mechanical phenomena. This analysis entailed, as a first step, tabulating lists of matrix crack spacing; of extent, shape, and area of delamination, if any; the recording of unusual or non-regular types of matrix cracking, such as occurred in some layups; and the recording of associated monotonic, and for fatigue loading dynamic, modulus plus the final fracture data. Because of the scatter in fracture and fatigue life, precise correlation of the output of a mathematical model for some damage state with observed stiffness or fracture data was not considered pertinent. Instead, the goal was to select from the damage state that representation for modeling purposes which would most affect observed stiffness or fracture characteristics. Thus the number of matrix cracks, delamination location, extent and shape were modeled. Even the effect of small delaminations at the ends of matrix cracks were considered. However, the complexity of matrix cracks at angles to the load direction, such as in $(0/\pm45)_s$ and $(0/45/0_2/-45/0)_s$ coupons or more complex subsidiary matrix cracking in $(0_2/90_4)_s$ coupons were not considered of primary significance and thus were not modeled. The effects of these variations were believed to manifest more in statistical variations among coupons than in average strain to failure values or stiffness. If this assumption proved to be incorrect, much more extensive modeling would be required than undertaken in this study.

The experimental data obtained in this study were combined with those available in the literature[12,21] for several other layups, specifically those for :$(\pm25/90_n)_s$, $(\pm45_n/0_n/90_n)_s$, $(0/45/90/-45)_{2s}$, $(0/45/0_2/-45/0)_{2s}$, $(0)_8$, and $(0)_{16}$. Thus a set of data for a broad range of layups was available for detailed analysis. The data for the $(0)_4$, $(0)_8$, and $(0)_{16}$ layups were used to investigate fracture criteria of 0° plies unaffected by cross plies. The data for the other layups were used to attempt to delineate the mechanics of unnotched, graphite/epoxy laminated coupons subjected to

tension loading. The specific experimental observations which we wished to analyze for these laminates are detailed for each loading type in Figure 1. If the mechanics of the laminates and load induced state changes are understood, each of the observations in Figure 1 should be qualitatively and quantitattively explainable. The success of this effort, to date, is discussed in Section 4.

1.4.3 Mathematical Modeling

The analytical objective of deriving quantitative relationships between laminate stiffness, residual strength, fatigue life and damage state imposed a number of requirements. The nature of these requirements can best be understood by recalling the general state of damage growth in laminated composites as described in Section 1.2. The experimental data obtained in this program, when combined with those available from other investigations, were sufficient to demonstrate the general applicability of the selected modeling and mathematical approach. As described, the nature of the load-induced damage under fatigue loading and the manner of growth was recorded and the relationship between this damage and laminate stiffness was experimentally established. The nature of the relationship between subsequent damage growth and failure and stiffness under residual strength tensile loading after prior fatigue loading was also established.

Except for the case of a dominant flaw at the laminate scale, the mathematics to quantitatively describe fracture were as yet quite undeveloped due to the complex state of cracking. Certain procedures were available to give qualitative and even quantitative predictions of early damage states under both static and fatigue loading.[10,11] The simplest procedures appeared to be energy approaches.[11] Because of the complexities of the mechanistic approach and the limitations of the statistical approaches previously mentioned, essentially empirically based crack growth laws have often been formulated[22]. These have been based upon an assumed damage mode with assumed growth characteristics believed to be of importance in a particular

LOADING TYPE	EXPERIMENTAL OBSERVATIONS
Monotonic Tension	o Stiffness o Onset of matrix cracking and saturation o Onset of delamination o Fracture o Extent of scatter
Tension-Tension Fatigue	o Onset of matrix cracking and saturation o Onset of delamination o Stiffness changes o Strain at failure o Fracture o Extent of scatter
Monotonic Tension-Residual Strength	o Stiffness o Damage growth o Fracture o Extent of scatter

Figure 1: Experimental observations requiring explanation.

loading environment. Such approaches have only been successful if a quasi-dominant flaw can be considered as being the most important damage mechanism. For many (perhaps most) layups and loading conditions, this concept was considered much too restrictive and thus was not employed in this study.

In this investigation the experimental data were used in the following manner. After analysis and selection of assumed pertinent features, the laminate and the experimentally observed damage were modeled by the selected mathematical procedure and resultant stiffness calculated and compared to measured stiffness. The observed extent of damage near static or residual strength tensile failure and near fatigue failure was analyzed for the amount and location of load transfer into the 0° plies. The distribution of stresses and strains within the 0° plies was calculated and compared to the strength data of the unidirectional laminate. The cause of fracture within the 0° plies was critical to the analysis. Without an analytical understanding of the 0° ply fracture, only an empirical relationship among stiffness, residual strength and fatigue life would result. Thus the modeling procedure attempted to determine the distribution of stresses and strains within the 0° ply just prior to failure because a failure criterion for the 0° ply was required to determine expected tensile strength and fracture.

This problem of delineating a failure theory for the 0° plies was concerned with the fact that the average failure stress within the 0° ply of a multiply laminate is not necessarily equivalent to the strength of a 0° unidirectional laminate, but may be in the local region of fracture. One concept to handle this problem is the analysis of the statistical linkup of individual or groups of 0° fiber breakages in a region of high stress induced damage. Such a linkup would be followed by rapid growth of a critical crack which parts the specimen. The mathematical basis for such a concept has been developed and used for metals.[23] In the regions of high 0° ply stress, the concept of a single region of fiber breakage causing fracture was analyzed as a local dominant flaw because there was evidence that a 0.5

mm (0.020 in.) long broken fiber region is sufficient to cause fracture of a 0° ply.[24,25] These concepts all depend on stress volume and appeared to be more applicable than local application of Tsai-Wu[26] or Hoffman[27] maximum stress failure theories. This was supported by the suggestion of Wu[28] that stress gradient at the tip of a transverse matrix crack may need to be taken into account. This suggestion and the more general one of a local strain gradient in a 0° ply due to the presence of combined matrix cracking and delamination[13] were investigated for several layups.

Fracture in unidirectional 0° plies has also been analyzed by statistical bundle theories.[29,30] These theories do not appear to be directly applicable to fracture of 0° plies in multidirectional layups as Wang has recently concluded.[31] In such cases, the degree of uniformity of load within the 0° ply is dependent on the extent of transverse cracking and delamination damage within the laminate.

Because of the lack of a failure theory to anticipate the residual strength of the laminates, the nature of the stress field in the 0° ply was evaluated as a function of longitudinal position X, depth Y and height Z. For example, the depth of delamination was documented since this depth has been found to be a function of the number of fatigue cycles.[7,32,33] Therefore, an analysis of the laminate coupons in a given damage state was conducted: 1) X-Z analysis of a plane section at the surface free edge thereby modeling typical observed crack densities and delamination if present; 2) analysis of an X-Z plane section at the midplane modeling transverse cracks and any delaminations which cross the specimen; 3) analysis of a Y-Z plane section using effective properties for cracked 90° and 45° plies and modeling the depth of observed delaminations.

1.5 REPORT OUTLINE

Section 2 of this report discusses the experimental results while Section 3 gives the results of the analysis and the various modeling procedures. In

Section 4, experimental results are compared to the results of the models and the inferences drawn from that comparison are discussed. A summary along with conclusions is given in Section 5. Four appendices give, respectively, the material and layup background, experimental procedures, detailed experimental data, and mathematical analysis procedures.

SECTION 2
EXPERIMENTAL RESULTS

In this section only that information considered pertinent for understanding the experimental results is presented. Details concerning material properties, coupon manufacturing, experimental procedures, and tabulated test results are given in report Appendices A, B, and C.

The experimentation was conducted using un-notched 38.1 mm (1.5 in.) wide, 254 mm (10 in.) long coupons with a 152.4 mm (6 in.) test section. A 101.6 mm (4 in.) extensometer was used to obtain strain measurements in order to derive average stiffness values relatively unaffected by local stiffness changes. The 101.6 mm (4 in.) length of the extensometer was defined as the coupon gage length. Coupons were manufactured from five different laminates of T300/5208 material. The $(0)_4$ layup provided information on coupons whose properties were totally dominated by the fibers. A quasi-isotropic $(0/90/\pm45)_s$ layup was selected as being one which did not tend to delaminate under monotonic load, but would under fatigue load. The $(0/\pm45)_s$ layup was selected because the laminate would not tend to delaminate under either monotonic or fatigue load. The $(0/45/0_2/-45/0)_s$ layup was expected to respond similarly to the $(0/\pm45)_s$ layup, but was expected to tend to delaminate under fatigue load. Unlike the quasi-isotropic layup, little or no stiffness change was expected to accompany the delamination in the $(0/45/0_2/-45/0)_s$ laminate. Finally, the $(0_2/90_4)_s$ layup was selected as a limiting case where the effect of the 90° plies was highly dominant. The data for these five laminates were combined with the results of several others available in the technical literature. Of these layups, key ones were: a $(+45_n/-45_n/-0_n/90_n)_s$ layup investigated by T. K. O'Brien at NASA/Langley[21,34], a $(0/45/0_2/-45/0)_{2s}$ and a $(0/45/90/-45)_{2s}$ layup investigated at Lockheed[7,32], and a $(\pm25/90_n)_s$ layup also studied at Lockheed[12]. These laminates provided a full range of configurations covering all of the various possibilities of matrix cracking and delamination tendency.

For each of the five laminates, the experimental procedures, the number of coupons, and the type of data collected were similar. At least five coupons were loaded to failure under monotonic tension load. An additional group (at least 9 coupons) were cycled to failure under constant amplitude fatigue load (R = +0.1) at various stress levels. Coupons were loaded to a particular initial stress or strain, and subsequently cycled to failure under constant load thus allowing the strain to increase as stiffness decreased. A third group of coupons were also load cycled at constant amplitude, R = +0.1, for either a set number of cycles or until a specific change in stiffness had occurred. These coupons were subsequently loaded to failure under monotonic tension load. Except for the $(0)_4$ coupons, the NDI techniques of edge replication and enhanced x-ray were used to document the extent of matrix cracking and delamination in these coupon during either monotonic or fatigue loading.

Coupons for the $(0)_4$, $(0/90/\pm45)_s$ and $(0/\pm45)_s$ laminates were supplied by NASA. Coupons for the other two layups were manufactured by Lockheed-California Company.

2.1 RESULTS FOR $(0)_4$ COUPONS

Monotonic tension tests of the $(0)_4$ coupons were difficult to conduct due to the extreme fragileness of these four ply coupons. A summary of the monotonic tension test results is given in Table 1. The stress-strain curves were slightly concave, showing an increasing stiffness, rather typical of unidirectional layups[7,13,32,35] as shown by the difference between the secant modulus at failure compared to that at 517 MPa (75 ksi). This is due to the non-Hookeon behavior of the fibers[36,37]. Coupon fracture was characterized by splintering into many small, short linear pieces. The original data set obtained in March 1981 showed strain to failure and strength values of this material to be lower than expected. A check of the material batch information revealed no obvious reason for the lower than expected values.

TABLE 1a
SUMMARY OF MONOTONIC TENSION
TEST RESULTS FOR $(0)_4$ COUPONS

Coupon ID	Average Area mm^2	Failure Stress MPa	Failure Strain	Secant Modulus at Failure, GPa	Secant Modulus at 517 MPa CPa
EXPERIMENTS CONDUCTED MARCH 1981 WITH EXTENSOMETER					
6-6	22.7	1251	0.0094	134	128
6-62	21.1	1258	0.0090	141	134
6-65	20.7	1418	0.0096	147	139
6-68	21.3	1261	0.0090	141	134
6-67	21.0	1371	0.0094	134	128
EXPERIMENTS CONDUCTED MARCH - APRIL 1982 WITH EXTENSOMETER					
6-28	22.2	1502	0.0108	139	135
6-85[a]	20.6	1247	0.0092	136	127
6-111	21.0	1538	0.0108	146	139
6-122	20.8	1586	0.0106	149	143
EXPERIMENTS CONDUCTED MARCH - APRIL 1982 WITHOUT EXTENSOMETER					
6-102	20.8	1409	-	-	-
6-104	21.2	1224	-	-	-
Average		1374	0.0098	141	134

a = Coupon had noticeable longitudinal crack observed after insertion into the loading machine.

TABLE 1b
SUMMARY OF MONOTONIC TENSION
TEST RESULTS FOR $(0)_4$ COUPONS

Coupon ID	Average Area, $in.^2$	Failure Stress, ksi	Failure Strain	Secant Modulus at Failure, Msi	Secant Modulus At 75 ksi, Msi
EXPERIMENTS CONDUCTED MARCH 1981 WITH EXTENSOMETER					
6-6	0.0352	181.4	0.0094	19.5	18.5
6-62	0.0327	182.4	0.0090	20.4	19.5
6-65	0.0321	205.6	0.0096	21.3	20.1
6-68	0.0330	182.9	0.0090	20.5	19.5
6-67	0.0326	198.9	0.0094	19.5	18.5
EXPERIMENTS CONDUCTED MARCH - APRIL 1982 WITH EXTENSOMETER					
6-28	0.0344	217.9	0.0108	20.2	19.6
6-85[a]	0.0320	180.9	0.0092	19.7	18.4
6-111	0.0326	229.6	0.0108	21.2	20.2
6-122	0.0323	230.0	0.0106	21.6	20.7
EXPERIMENTS CONDUCTED MARCH - APRIL 1982 WITHOUT EXTENSOMETER					
6-102	0.0323	204.4	-	-	-
6-104	0.0329	177.5	-	-	-
Average		199.2	0.0098	20.4	19.4

a = Coupon had noticeable longitudinal crack observed after insertion into the loading machine.

Therefore, further experiments were conducted with much greater care and with detailed inspection of coupon damage prior to loading. The experimental results, see Table 1, indicated that perhaps the laminate strain to failure for the $(0)_4$ laminate was indeed higher than originally estimated, perhaps 0.0100 to 0.0108, and the strength approximately 1379 to 1586 MPa (200 to 230 ksi). The lower strength/strain results for most coupons were initially hypothesized to be due to unobserved damage in the coupons which occurred during coupon manufacture, end tabbing, and insertion into the loading frame. However, two subsequent experiments conducted without an extensometer, to prevent any damage from that source, did not support this conclusion, see Table 1. As discussed in Section 3, the strain to failure results may possibly be better understood based on a Weibull statistics basis.

The fatigue test data obtained for this layup are shown in Table 2. All coupons fractured across the 0° fibers near the center of the test section. Considerable 0° splitting and some shattering of the coupon usually occurred. The data show the extremely large scatter typical of a unidirectional layup (see Reference 38). Coupons were not cycled below 1103 MPa (160 ksi) because lives were exceeding 10^6 cycles nor above 1172 MPa (170 ksi) because the lives of most coupons were short. For coupon 6-72, dynamic stiffness was measured at 10, 1 000, 10 000, 100 000, and 250 000 cycles. The average dynamic stiffness of the five readings was 140.2 GPa (20.34 Msi) $\pm$ 0.6 percent. This value was essentially identical to the average secant modulus value of 140.6 GPa (20.4 Msi) $\pm$ 0.5 percent obtained on the monotonic tension tests. Periodic stiffness measurements were also obtained during other $(0)_4$ coupon fatigue tests. All of the data indicated that the stiffness did not change during fatigue loading.

The results of the residual strength experiments for this $(0)_4$ layup are shown in Table 3. Only three coupons were tested because so many had been used to obtain reasonable tension and fatigue data. Extreme care was taken

TABLE 2
SUMMARY OF CONSTANT AMPLITUDE
FATIGUE EXPERIMENTS FOR $(0)_4$ COUPONS
R = +0.1, F = 10 Hz

Stress Level, MPa	ksi	Coupon ID	Cycles to Failure, N_f
1103	160	6-4	599 285
		6-25	30 000
		6-17	10^6 NF[a]
		6-50	10^6 NF[a]
		6-115	352 460
1172	170	6-72	350 820
		6-81	1 610
		6-91	2 550
		6-112	360
		6-120	2 001

a = NF, no failure

TABLE 3a
SUMMARY OF MONOTONIC TENSION
RESIDUAL STRENGTH EXPERIMENTAL
RESULTS FOR $(0)_4$ COUPONS
R = +0.1, f = 10 Hz, Max. Stress = 1103 MPa

Coupon ID	Average Area, mm^2	Failure Strain MPa	Failure Strain	Secant Modulus At Failure GPa	Secant Modulus At 517 MPa GPa
6-11[a]	22.6	1569	0.0113	139	134
6-17[b]	22.4	1500	0.0106	142	133
6-50[b]	22.1	1517	--[c]	-	-

a = Coupon monotonically loaded to failure after 407 500 cycles.

b = Coupon monotonically loaded to failure after 10^6 cycles.

c = No extensometer used on this coupon.

TABLE 3b
SUMMARY OF MONOTONIC TENSION
RESIDUAL STRENGTH EXPERIMENTAL
RESULTS FOR $(0)_4$ COUPONS
R = +0.1, f = 10 Hz, Max. Stress = 160 ksi

Coupon ID	Average Area, $in.^2$	Failure Stress, ksi	Failure Strain	Secant Modulus At Failure Msi	Secant Modulus At 75 ksi, Msi
6-11[a]	0.0351	227.5	0.0113	20.1	19.5
6-17[b]	0.0347	217.6	0.0106	20.6	19.3
6-50[b]	0.0342	220.1	--[c]	--	--

a = Coupon monotonically loaded to failure after 407 500 cycles

b = Coupon monotonically loaded to failure after 10^6 cycles

c = No extensometer used on this coupon

to prevent damage to these coupons prior to loading. A comparison of the limited results of Tables 1 and 3 show that there was no effect of fatigue cycling on subsequent tensile strength, strain to failure or stiffness. This result is consistent with the observation that no delamination occurred during fatigue loading and with the hypothesis that damage in the matrix does not affect unidirectional strength.

2.2 RESULTS FOR $(0/90/\pm45)_s$ COUPONS

A summary of the monotonic tension tests to failure is given in Table 4. Coupon 11-5 was tested because the failure data on coupon 11-2 were inadvertently not recorded. The observed stresses and strains to failure and the stiffness were typical of other quasi-isotropic laminates[6,7,8,-21,32,34]. Loading in these coupons was periodically interrupted in order to obtain NDI data after which the coupons were reloaded to a higher strain level. The stress-strain curves at each load level were quite straight lines to failure, thus the stiffness data are not secant values. Table 5 lists the stiffness values obtained for each strain level. For four of the five coupons, stiffness decreased slightly, an average of 1.4 percent, but not in a consistent trendlike manner. This result is consistent with the observation, made by using both edge replications and enhanced x-ray photographs, that no large delamination occurred in these coupons prior to failure. Delamination was confined to short distances extending from the ends of the transverse matrix cracks and these were not visible by enhanced x-ray. The mathematical modeling in this layup, see Section 3, indicated that there should be only a few percent change in modulus due to matrix cracks alone.

The matrix crack spacing data obtained from the edge replications are shown in Figure 2. The data are shown as smooth "eye based" average curves of the data points which are individually tabulated in Appendix C, Table C1. No matrix cracks were observed in the -45° plies. The number of cracks reached an apparent plateau in the 90° plies at a minimum crack spacing consistent

TABLE 4

FAILURE STRESSES AND STRAINS FOR MONOTONIC TENSION EXPERIMENTS OF $(0/90/\pm45)_S$ COUPONS

Coupon I.D.	Average Area mm^2	Average Area $in.^2$	Stress At Fracture, MPa	Stress At Fracture, ksi	Strain At Fracture, mm/mm in 101.6 mm	Stiffness To Failure GPa	Stiffness To Failure Msi
11-2	41.4	0.0642	---[a]	---[a]	------[a]	----[a]	---[a]
11-5	41.6	0.0645	568	82.4	0.01065	53.3	7.74
11-6	41.7	0.0647	534	77.4	0.01050	50.8	7.37
11-15	42.6	0.0660	538	78.0	0.01009	53.4	7.74
11-22	41.7	0.0647	563	81.6	0.01023	35.0	7.98
11-24	41.2	0.0639	538	78.0	0.01023	52.6	7.62
		Average	548	79.5	0.01034	53.0	7.69

a = Failure data inadvertently not recorded, see Table 5 for detailed stiffness data.

TABLE 5
STIFFNESS DATA OBTAINED DURING MONOTONIC TENSION EXPERIMENTS OF $(0/90/\pm45)_s$ COUPONS

COUPON ID	STRAIN LEVEL mm/mm in 101.6 mm	STIFFNESS GPa	Msi	
Laminate $(0/90/\pm45)_s$				
11-22	0.00394	52.5	7.61	
	0.00648	53.2	7.71	
	0.00979	53.5	7.76	
	0.01023	55.4	8.03	Failed on Loading
11-24	0.00641	53.3	7.73	
	0.00782	53.0	7.69	
	0.00909	53.1	7.70	
	0.00928	53.2	7.72	
	0.00953	52.9	7.67	
	0.00983	53.1	7.70	
	0.01023	52.5	7.61	Failed on loading
11-2	0.00737	53.5	7.76	
	0.00925	52.3	7.58	
	0.00958	52.4	7.60	
	0.00983	53.3	7.73	
	0.01003	53.2	7.72	
	0.01025	53.1	7.70	
	Data on Failure Not Obtained			
11-6	0.00912	53.3	7.73	
	0.00937	53.5	7.76	
	0.00984	52.5	7.62	
	0.01005	52.6	7.63	Failed on loading
11-15	0.00881	54.9	7.96	
	0.00968	53.6	7.77	
	0.01009	53.4	7.74	Failure During NDI

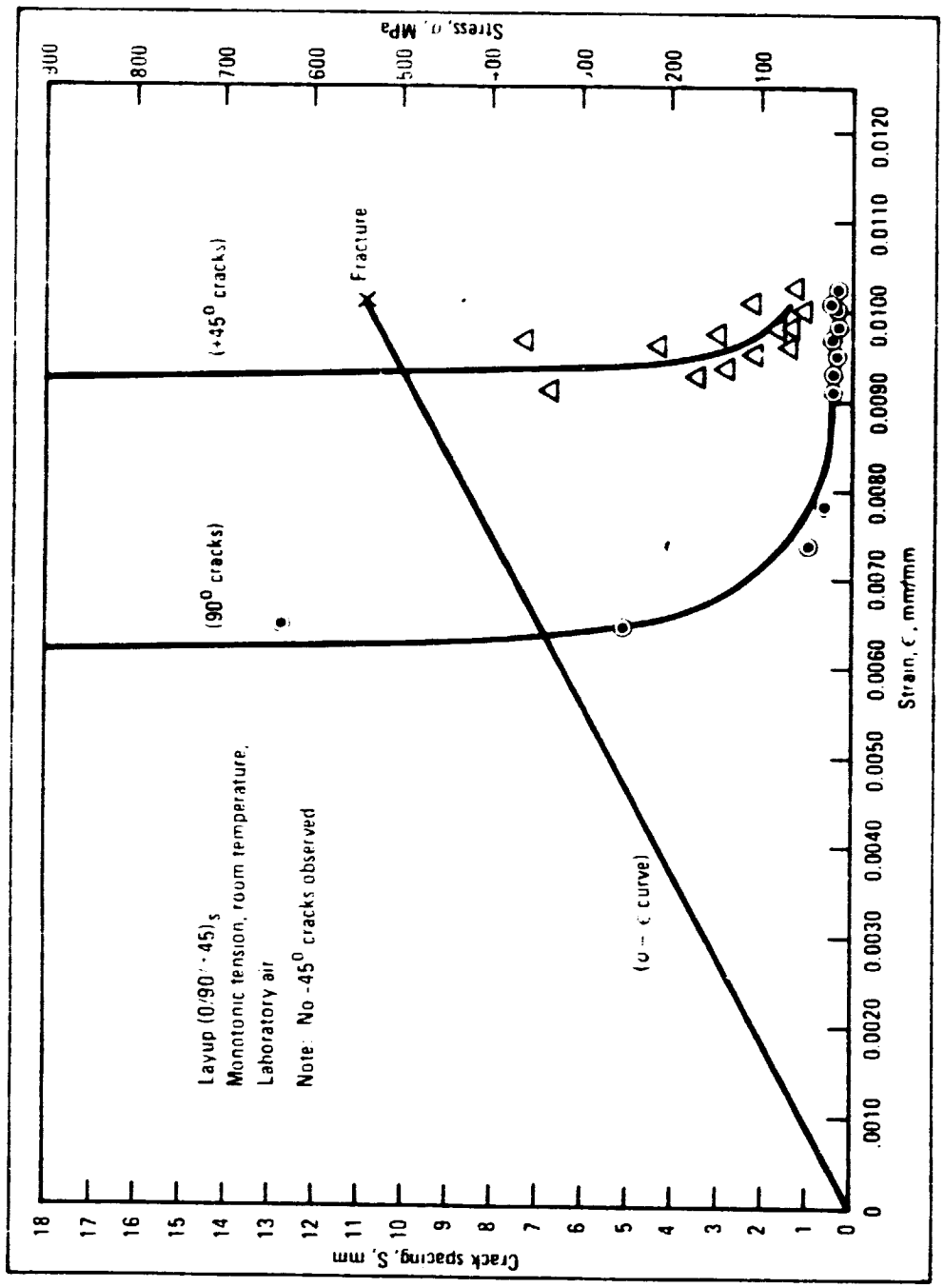

Figure 2: Crack spacing and stress vs. strain

with the computer modeling results of Section 3. The crack spacing in the +45 plies did not appear to reach a plateau prior to coupon failure. Matrix cracking started in the 90° plies above 0.0060 strain and above 0.0093 strain in the +45 plies. The number of matrix cracks was essentially the same in different regions of the gage length, on both edges, and in plies of the same orientation.

The transverse cracks in the 90° plies were perpendicular to the 0° plies while those in the $+45^{\circ}$ plies were usually at approximately a 45° angle to the 0° plies. The $+45^{\circ}$ ply transverse cracks were observed to start at or quite near the end of a 90° ply transverse crack. Delamination could be seen in the edge replicates, starting at the ends of a transverse crack and extending as the strain was increased. Usually the symmetrical delaminations were between the 90/+45 plies, but they were occasionally observed between the +45/-45 plies. As previously noted, these delaminations did not significantly extend into the coupon interiors since they could not be observed by enhanced x-ray photography. Coupon failures all exhibited fracture of the outer 0° plies perpendicular to the fibers and parallel to the 90° plies. Although, the $\pm 45^{\circ}$ plies usually simply pulled apart, they also often fractured along the 90° direction. There were two failure regions in four of the five coupons; these occurred near the ends of the 101.6 mm (4 in.) center gage section. The fifth coupon fractured approximately 12 mm (0.5 in.) away from the coupon centerline.

A summary of the fatigue life data for this laminate is given in Table 6. Stress levels above 448 MPa (65 ksi) would have given lives that were too short to obtain accurate data while stress levels below 379 MPa (55 ksi) would have given lives into and beyond the 10^6 cycle range which was the testing cutoff life for this program. The failure regions did correspond to delaminated regions, but there was no clear correlation to any "most extensive" delaminated region. All coupons fractured within the gage length region, see Table 7. Similar to the monotonic tension loaded coupons, fracture of the 0° fibers occurred along a 90° direction. Even the inner

TABLE 6

SUMMARY OF FATIGUE LIFE DATA
FOR $(0/90/\pm45)_S$ COUPONS

Stress Level MPa	ksi	Coupon ID	Cycles To Failure, Thousands	Remarks
379	55	11-1	198.8	Failure due to Operator Error
		11-3	166.9	
		11-9	298.6	
414	60	11-18	60.0	Failure due to Operator Error
		11-21	212.0	
		11-25	64.5	
		11-45	60.1	
448	65	11-13	29.4	
		11-19	8.0	Failure due to Operator Error
		11-54	8.3	

TABLE 7
FRACTURE LOCATIONS OF
$(0/90/\pm45)_S$ COUPONS SUBJECTED
TO CONSTANT AMPLITUDE
FATIGUE LOADING

Note: Fracture location is relative to the center of the 101.6 mm (4 in.) gage length;+ is towards the upper grip, - is towards the bottom grip.

Coupon ID	Stress Level, MPa	Stress Level, ksi	Fracture Location, mm	Fracture Location, in.
11-3	379	55	+40.6	+1.6
11-9	379	55	+20.3	+0.8
11-21	414	60	-27.9	-1.1
11-25	414	60	-30.5	-1.2
11-45	414	60	+17.8	+0.7
11-13	448	65	- 2.5	+0.1
11-54	448	65	-20.3	-0.8

$\pm 45^{\circ}$ plies often fractured along approximately a 90° line. In other coupons, the $+45^{\circ}$ plies exhibited fiber fracture along approximately a -45° line. In many coupons, the $\pm 45^{\circ}$ plies appeared to essentially be pulled apart without large regions of fractured fibers.

The amount of stiffness loss prior to failure varied considerably from coupon to coupon at each stress level, see Table 8, although the amount of loss prior to failure was naturally higher as the stress level was decreased. The matrix crack spacing within any one ply orientation reached an essentially stable value independent of stress, see Table 9, relatively early in fatigue life (<40 percent of the fatigue life). See Figure 3 for an example at 379 MPa (55 ksi) and Appendix C, Table C2, for the data at other stress levels. The crack spacing was the same for the 90° plies as that reached under monotonic tension load, see Table 9, but was lower for the $\pm 45^{\circ}$ plies.

The matrix crack spacing of all plies thus essentially reached a plateau during fatigue cycling, but not during monotonic tension loading to failure. The plateau spacings observed in fatigue cycling are similar to those calculated by Reifsnider[39]. Certainly, a specific minimum limit to crack spacing appears to exist for this laminate at specific stress levels, but this spacing was not reached under all loading conditions.

The normalized dynamic stiffness loss observed during fatigue loading for these coupons is plotted in Figures 4 to 6. The loss in static stiffness was comparable to the dynamic, but not always exactly the same. The tabulated data and additional associated figures are given in Appendix C, Tables C3 to C22, and Figures C1 to C29. Generally the loss in stiffness was a smooth decrease, but there were occasional deviations of up to $\pm$ 2.5 percent, which occurred after load cycling was continued, for coupons which had been removed for x-ray. However, this deviation in stiffness was less than ± 1 percent as often as it was greater than ± 1 percent.

TABLE 8

SUMMARY OF MAXIMUM PERCENTAGE STIFFNESS LOSS DUE TO FATIGUE LOADING FOR $(0/90/\pm45)_S$ COUPONS

Coupon ID	Stress Level, MPa	Fatigue Cycles (Thousands)	Percent Loss in Dynamic Stiffness	Percent Loss in Monotonic Stiffness	Remarks
11-1	379	198.8	11.1	14	Failure due to operator error
11-3	379	166.9	10.8	--[a]	Failure
11-9	379	290.5	17.3	--[a]	Failure at 298.6K Cycles
11-18	414	60.0	3.3	3.0	Failure due to operator error
11-21	414	212.0	19.4	11.3	Failure
11-25	414	64.5	7.8	--[a]	Failure
11-45	414	58.8	6.1	5.2	Failure at 60.1K Cycles
11-13	448	29.0	5.6	--[a]	Failure at 29.4K Cycles
11-19	448	8.0	1.6	--[a]	Failure due to operator error
11-54	448	7.8	2.0	--[a]	Failure at 8.3K Cycles

TABLE 9

MATRIX CRACK SPACING UNDER
DIFFERENT LOADING CONDITIONS FOR $(0/90/\pm45)_S$

Loading Condition	Range in Average Crack Spacing, mm		
	90°	+45°	-45°
Monotonic Tension	0.28-0.31	1.06-2.17	- a
Fatigue			
379 MPa	0.28-0.32	0.49-0.56	0.91-1.22
413 MPa	0.28-0.59	0.53-0.65	1.06-1.41
448 MPa	0.30	0.53	1.07
Residual Strength			
After Fatigue at 379 MPa	0.25-0.30	0.45-0.61	1.06-1.59
Monotonic Tension	0.25-0.26	0.47-0.48	1.34-1.41

a = No matrix cracks observed

NOTE: Crack spacing values given are those measured just prior to failure or at the end of the loading condition indicated.

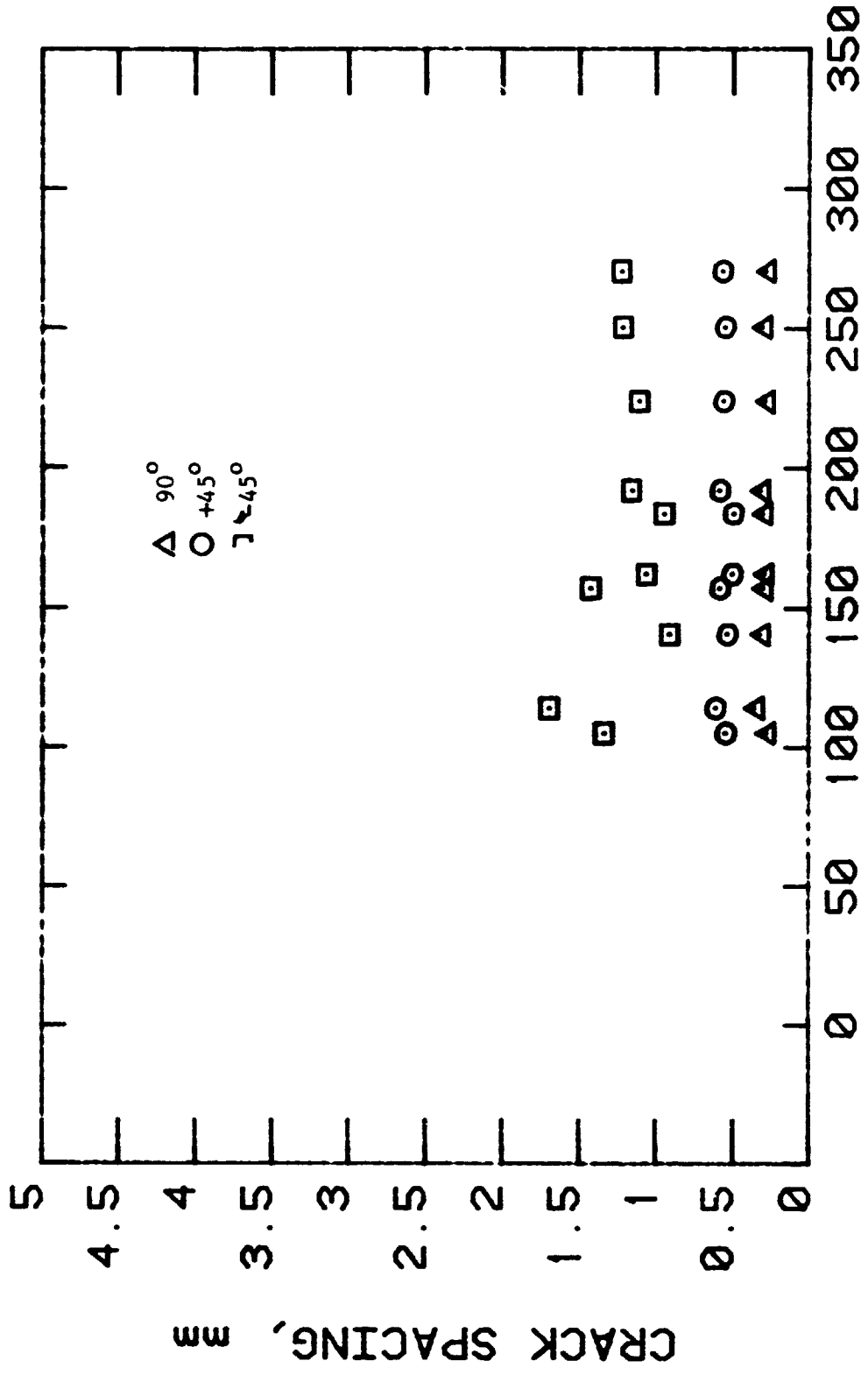

Figure 3: Average crack spacing as a function of fatigue cycles for $(0/90_{\pm}45)_s$ Coupons at σ_{max} = 379 MPa (55 ksi).

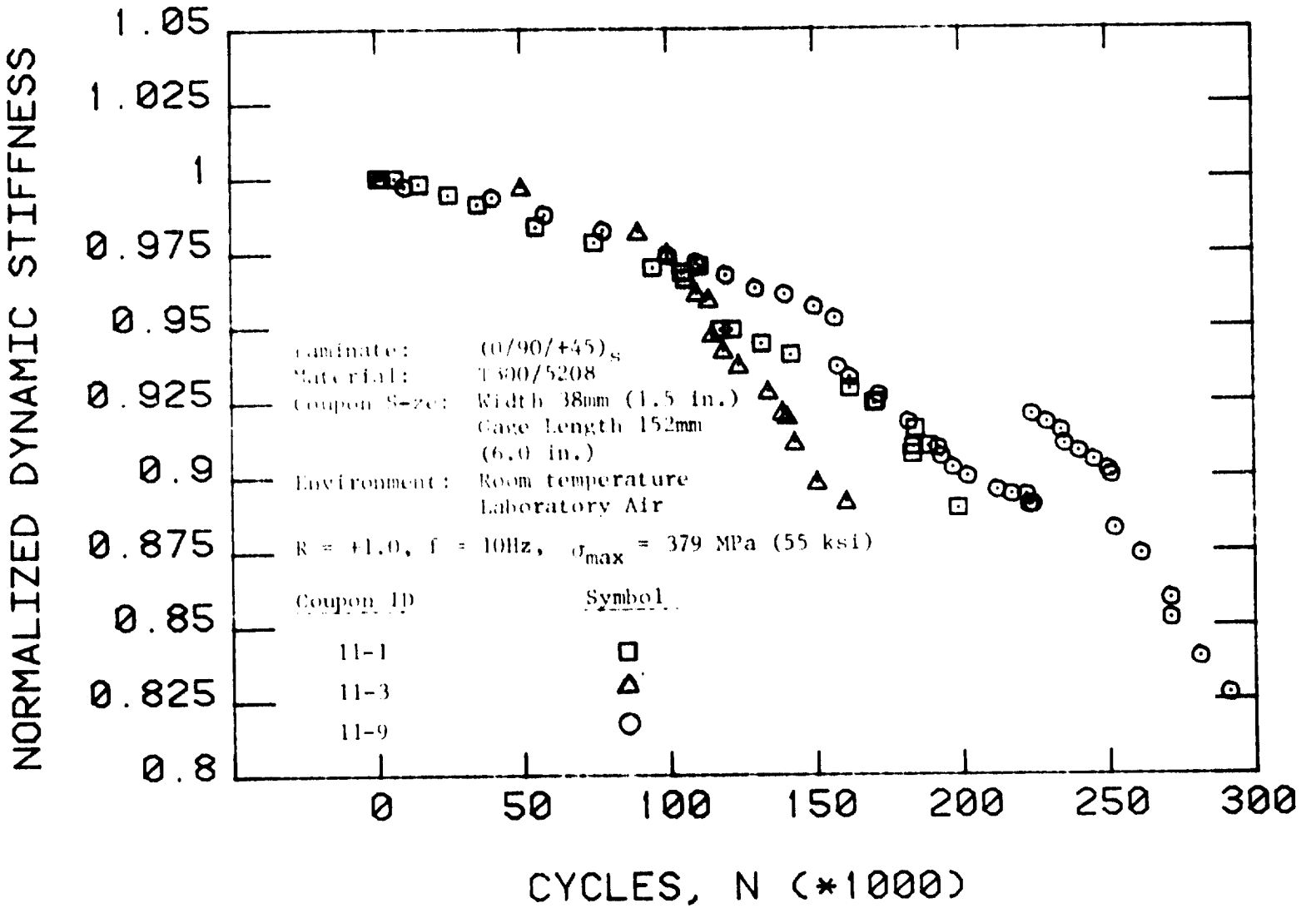

Figure 4: Normalized Dynamic Stiffness vs. constant amplitude fatigue load cycles for $(0/90/+45)_s$ laminate, σ_{max} = 379 MPa (55 ksi)

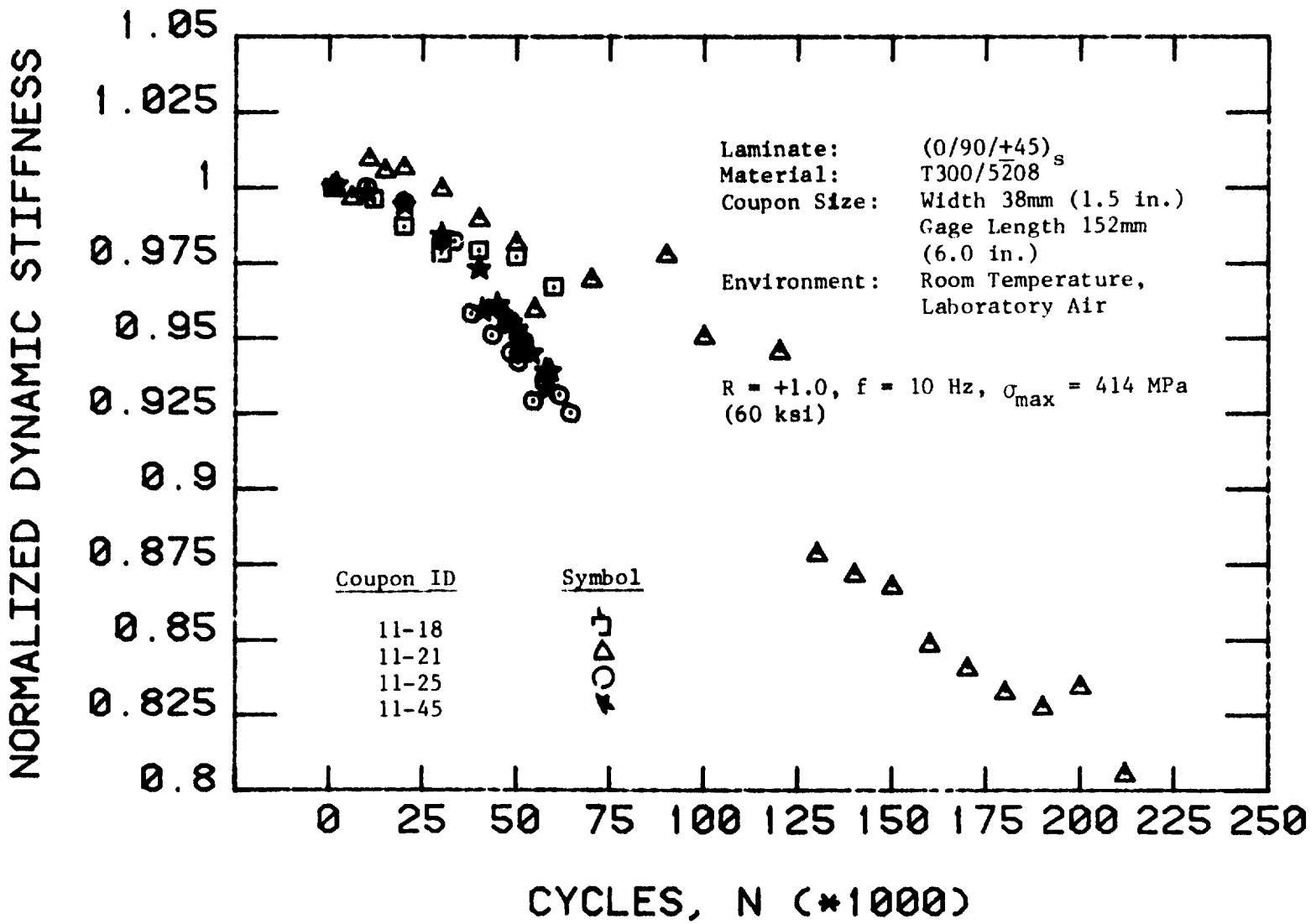

Figure 5: Normalized dynamic stiffness vs. constant amplitude fatigue load cycles for $(0/90/\pm45)_s$ laminate, σ_{max} = 414 MPa (60 ksi)

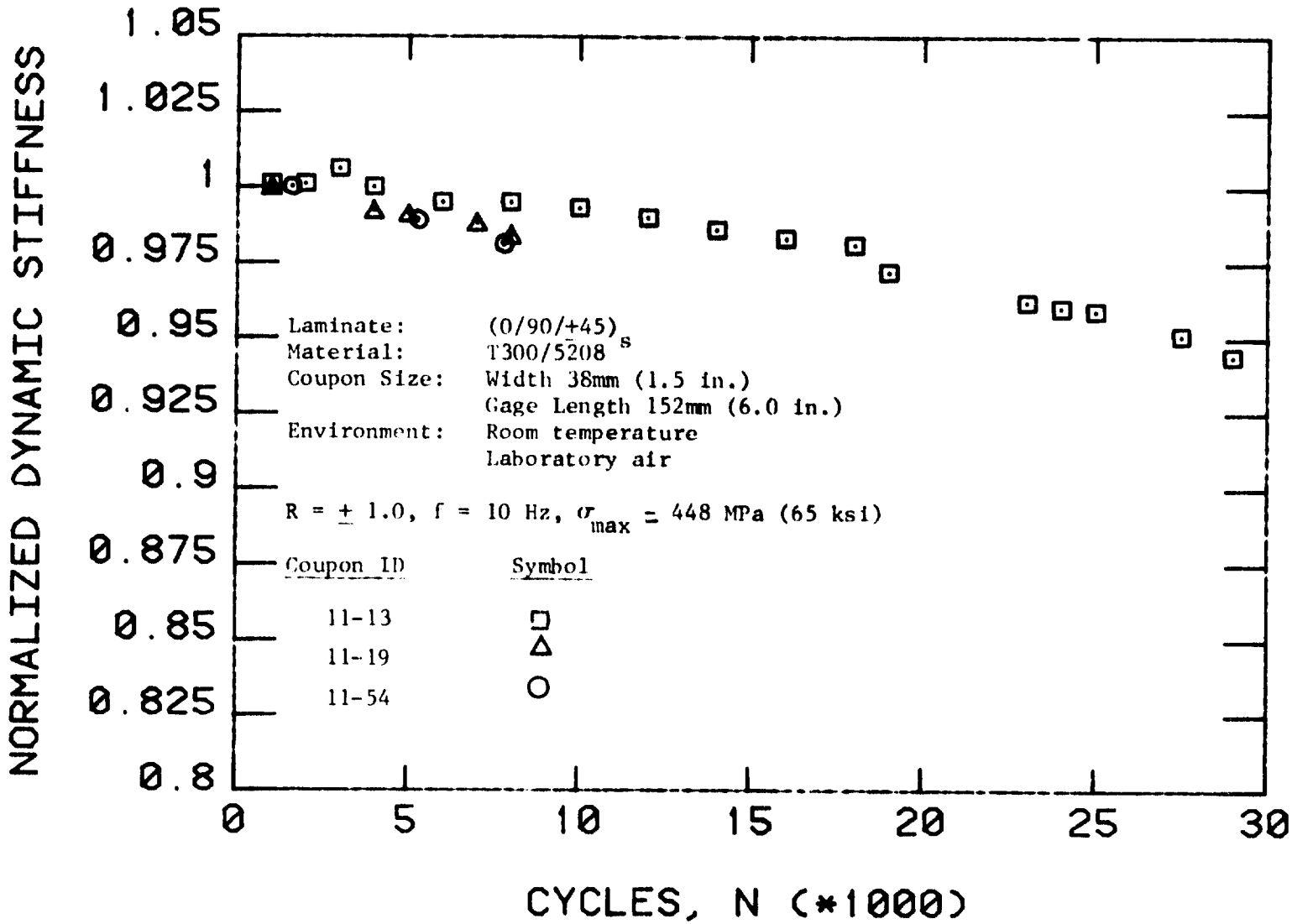

Figure 6: Normalized dynamic stiffness vs. constant amplitude fatigue load cycles for $(0/90/+45)_s$ laminate, σ_{max} = 448 MPa (65 ksi)

Note in Figure 4 that approximately a 2 percent stiffness loss occurred early in fatigue life, followed by an additional 5 tc 9 percent loss over most of the load cycling, and finally by a rapid stiffness loss of up to an additional 7 percent as failure was approached. This pattern was similar to that observed by Jamison and Reifsnider[40] for this same laminate and for the same reasons. The early life region of stiffness loss was primarily due to transverse matrix cracking up to the saturation spacing characteristic of this laminate. Subsequent stiffness loss was due to gradual delamination initiation and growth along the 90/+45 and +45/-45 ply interfaces. The more rapid stiffness loss near failure was apparently due to the linkup of delaminated areas, where delamination in large regions now occurred between the 0/90, 90/+45, and +45/-45 interfaces. In Figure 5, a similar but less clear stiffness loss pattern as in Figure 4 is evident for these coupons cycled at a higher stress level, but in Figure 6 the rapid loss in stiffness near failure is not seen in these coupons cycled at 448 MPa (65 ksi). The reason was attributed to the fact that the early life delamination pattern caused sufficient strain increase in the 0° plies for fracture without the necessity of large stiffness loss due to a more general delamination state. The correctness of these descriptive reasons for the results of Figures 4 to 6 is discussed further in Section 4 where these experimental results are compared to the modeling results of Section 3.

That the observed stiffness loss was primarily due to delamination growth is evident in Figure 7 which shows that matrix crack saturation occurred before 2.5 percent stiffness loss had developed. This is consistent with the computer aided modeling results discussed in Section 3 which indicated the matrix crack saturation should be associated with only a 1 to 3 percent change in stiffness.

Delaminations grew on two interfaces, 90/+45 and +45/-45, but the former interface was dominant in most coupons as shown in Figures 8 to 11 where the extent of 90/+45 delamination was much greater than that of the +45/-45 delamination. The loss in stiffness was thus much more associated with the

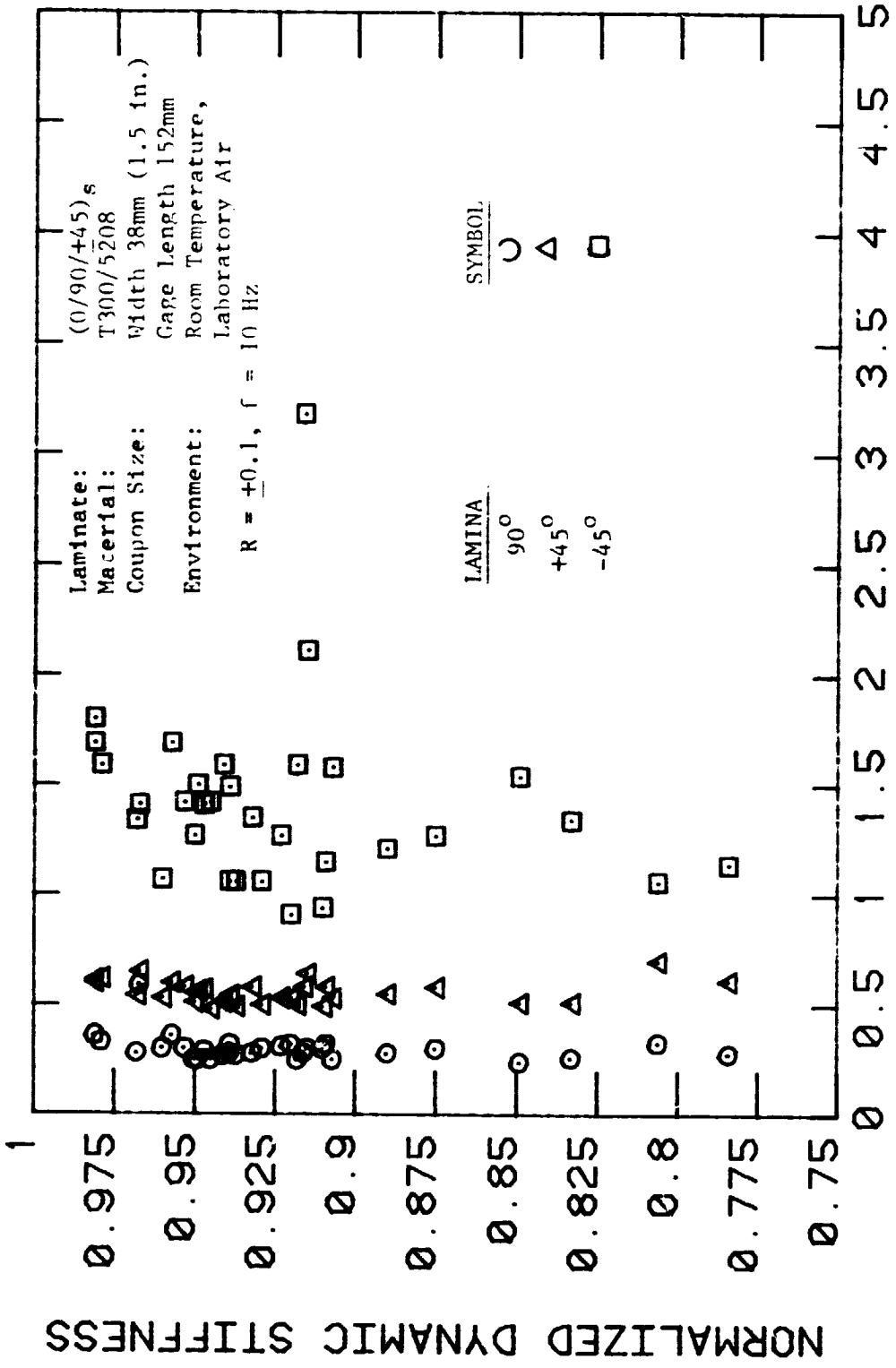

Figure 7: Normalized dynamic stiffness vs. average matrix crack spacing for $(0/90/\pm45)_s$ laminate coupons subjected to constant amplitude fatigue load.

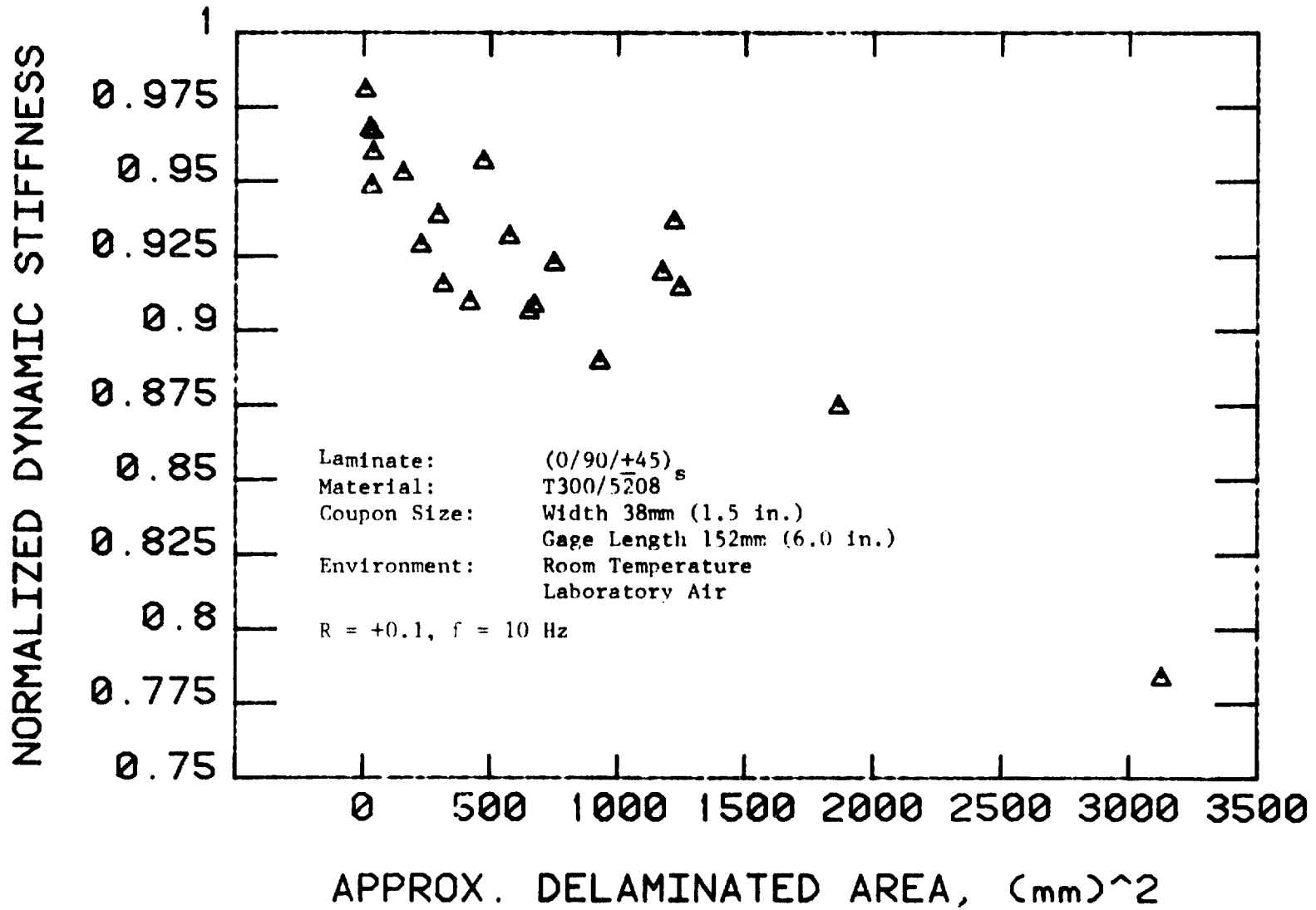

Figure 8: Normalized dynamic stiffness vs. approximate delaminated area, $90^{o}/+45^{o}$ delamination (Type 1), for $(0/90/\pm45)_{s}$ laminate coupons subjected to constant amplitude fatigue load.

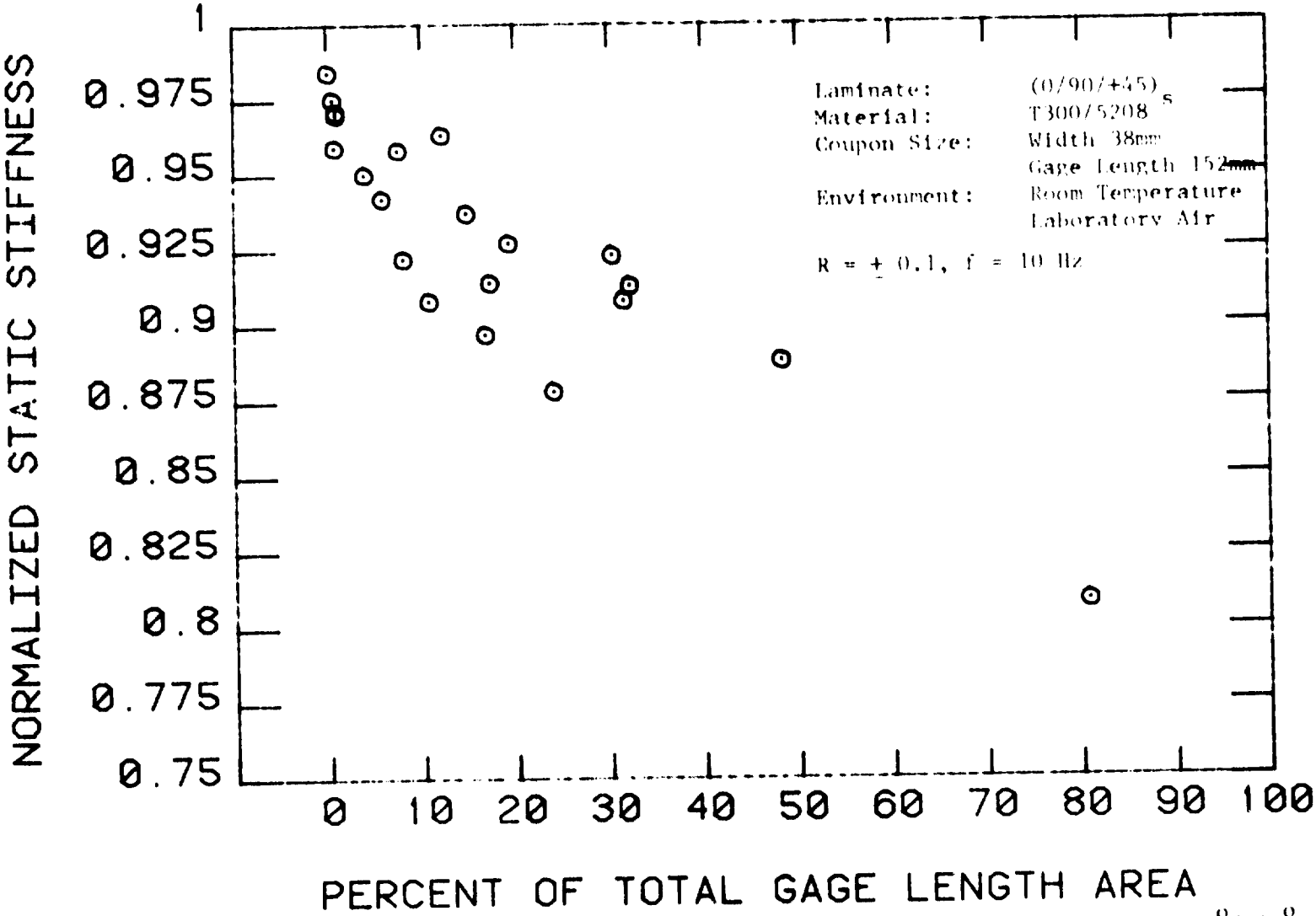

Figure 9: Normalized dynamic stiffness vs. percent of total coupon gage length area, $90^{0}/+45^{0}$ delamination (Type 1) for $(0/90/+45)_{s}$ laminate coupons subjected to constant amplitude fatigue load.

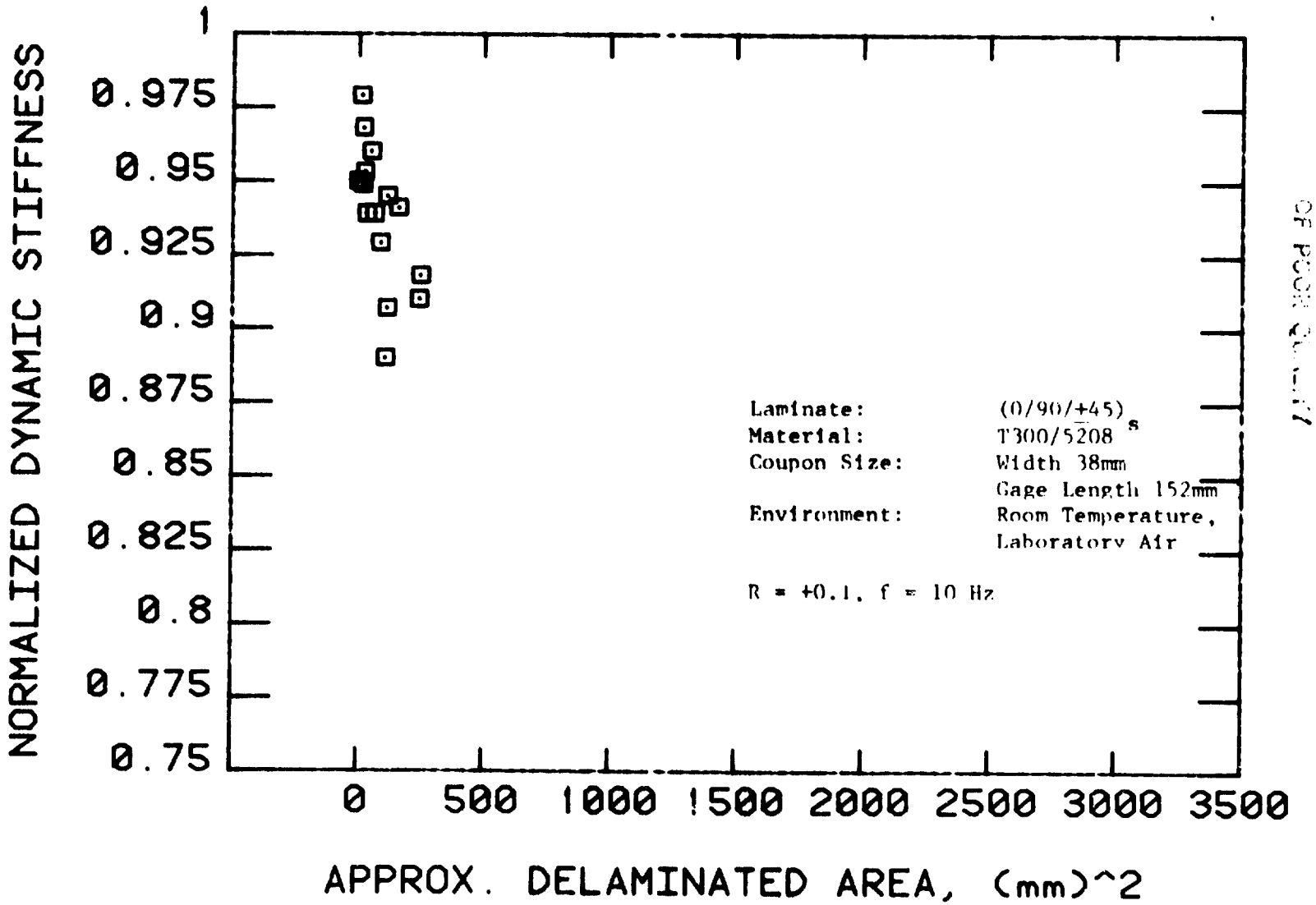

Figure 10: Normalized dynamic stiffness vs. approximate delaminated area, $+45^{o}/-45^{o}$ delamination (Type 2) for $(0/90/\pm45)_s$ laminate coupons subjected to constant amplitude fatigue load.

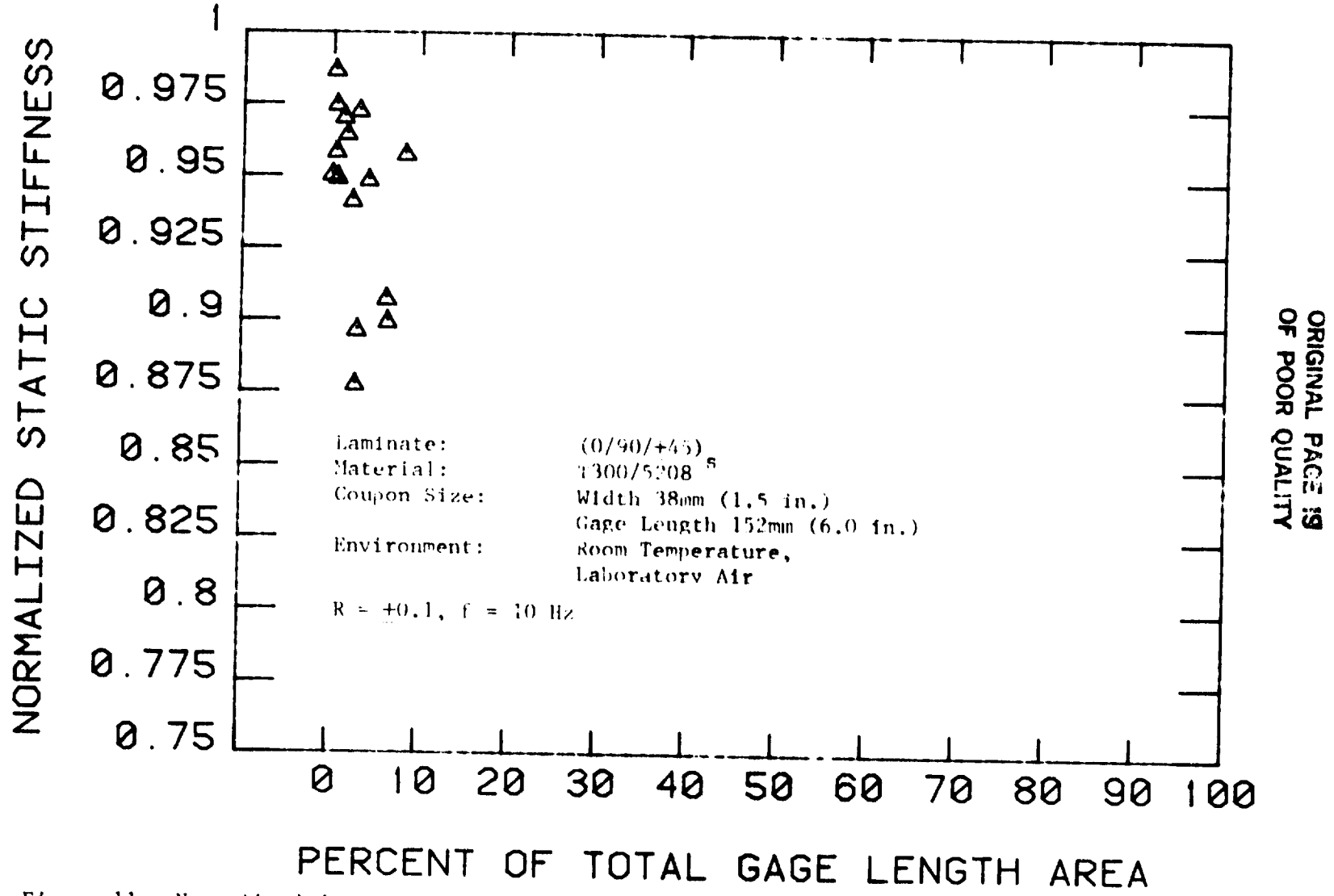

Figure 11: Normalized dynamic stiffness vs. percent of total coupon gage length area, $+45^{o}/-45^{o}$ delamination (Type 2) for $(0/90/+45)_{s}$ laminate coupons subjected to constant amplitude fatigue load.

Type 1, 90/+45 delamination growth than the Type 2, +45/-45 delamination growth. However, the edge replication data indicated that early in fatigue life delamination was more predominant at the +45/-45 interfaces than the 90/+45 interfaces. As load cycling was continued, the 90/+45 interface delaminations became dominant. Delamination at the 0/90 interfaces did occur, but the amount extending from each 90° crack was always observed to be rather short, 0.25 mm (0.01 in.) or less in length.

The pattern of delamination growth was highly irregular in that the growth was not symmetrical from end to end, side to side or extension into the interior of the coupon, see Figures 12 to 15. This was in contrast to the highly symmetrical growth pattern observed in a $(0/45/90/-45)_{2s}$ layup[13], see Figure 16. The dark thumbnail shaped regions in Figures 12 to 16 are 90/+45 interface delaminations while the more faint, trianglar shaped regions are +45/-45 interface delaminations. The irregular patterns of delamination growth were interpreted to mean that stiffness change and residual strength were unlikely to be simple functions of the average delaminated area. That this was indeed true for fatigue cycling is indicated by Figures 8 to 11 where the same amount of stiffness loss corresponded to a considerable variation in delaminated area. The scatter in fatigue life was primarily a reflection of the variations in delamination growth rate.

Figures 12 to 14 clearly show the transverse matrix cracking in addition to the obvious delamination. The darker lines are the transverse cracks in the two ply thick -45° plies. These -45° matrix crack indications were noticed to be quite dark near the coupon edges. Further, with continued cycling the $+45^{\circ}$ transverse indications became progressively darker and wider. These widening indications were assumed to be narrow delaminations growing perpendicular to the transverse cracks at the ply interfaces. Examination of high magnification, stereoscopic pairs of such radiographs of $(0/90/\pm45)_{s}$ coupons by Jamison and Reifsnider[40] revealed tiny matrix cracks perpendicular to the transverse cracks to be the source of the darkening radiograph indications. So many of these cracks eventually occur that they

Figure 12: Enhanced x-ray photograph of delamination pattern in $(0/90/\pm45)_s$ coupon 11-9 due to fatigue loading at R = 0.1, f = 10 Hz for 250 500 cycles, σ_{max} = 379 MPa.

Figure 13: Enhanced x-ray photograph of $90^{\circ}/\pm45^{\circ}$ delamination pattern in $(0/90/\pm45)_{s}$ coupon 11-3 due to fatigue loading at R = +0.1, f = 10 Hz for 140 500 cycles, $\sigma_{max} = 378$ MPa.

Figure 14: Enhanced x-ray photograph of $90^{\circ}/\pm45^{\circ}$ delamination pattern in $(0/90/\pm45)_{s}$ coupon 11-45 due to fatigue loading at R = +0.1, f = 10 Hz for 51 000 cycles, $\sigma_{max} = 414$ MPa.

Figure 15: Enhanced x-ray photograph of $90^{\circ}/+45^{\circ}$ delamination pattern in $(0/90/\pm45)_s$ coupon 11-1, due to fatigue loading at R = +0.1, f = 10 Hz for 198 800 cycles, σ_{max} = 379 MPa.

Figure 16: Enhanced x-ray photograph of delamination pattern in a $(0/45/90/-45)_{2s}$ coupon due to fatigue loading at R = 0.02, f = 10 Hz, σ_{max} = 310 MPa for 200 000 cycles.

essentially are like a delamination if they truly occur at the ply interface. By performing a simple linear elastic fracture mechanics analysis[40], these cracks were attributed to local stress concentration at the transverse crack tips.

In Figure 17, the maximum strain in a coupon during fatigue loading is plotted for five representative coupons, as a function of cycles. Because load was held constant and stiffness decreased, the maximum strain increased. However, as shown in Figure 17, all coupons failed prior to reaching the predetermined monotonic failure strain. The reduction in strain to failure was hypothesized to be due to redistribution of stress into local 0^{o} fiber regions because of the presence of matrix cracking and delamination. O'Brien[41] suggested the strain to failure under fatigue loading could be obtained by considering a simple free body diagram and calculating the local increase in strain due to various possible combinations of matrix cracks and delamination peculiar to a particular laminate. The proper trend in expected strain to failure does result from using such an analysis as discussed in Section 3 and as O'Brien's results indicate[41]. The results of the analysis for several different laminates is given in Section 4.

The coupons selected for residual strength experimentation were load cycled to either a specific amount of stiffness change or to a specific number of fatigue cycles. Because the stiffness loss obtained at or above 414 MPa (60 ksi) was relatively small (and thus delamination small) and the expected fatigue life below 379 MPa (55 ksi) near or greater than 10^{6} cycles, all coupons were cycled at 379 MPa (55 ksi). The tabulated data for these residual strength coupons are given in Appendix C, tables C23 to C40. During load cycling, coupons were inspected for matrix cracking and delamination growth. The extent of damage after load cycling was compared to that observed during the load interruptions of the residual strength tests. The strain levels at which NDI was conducted on the residual strength coupons are given in Table 10. Six coupons were cycled to a specific cycle number (150 000) and three to a specific amount of stiffness loss (approximately 10

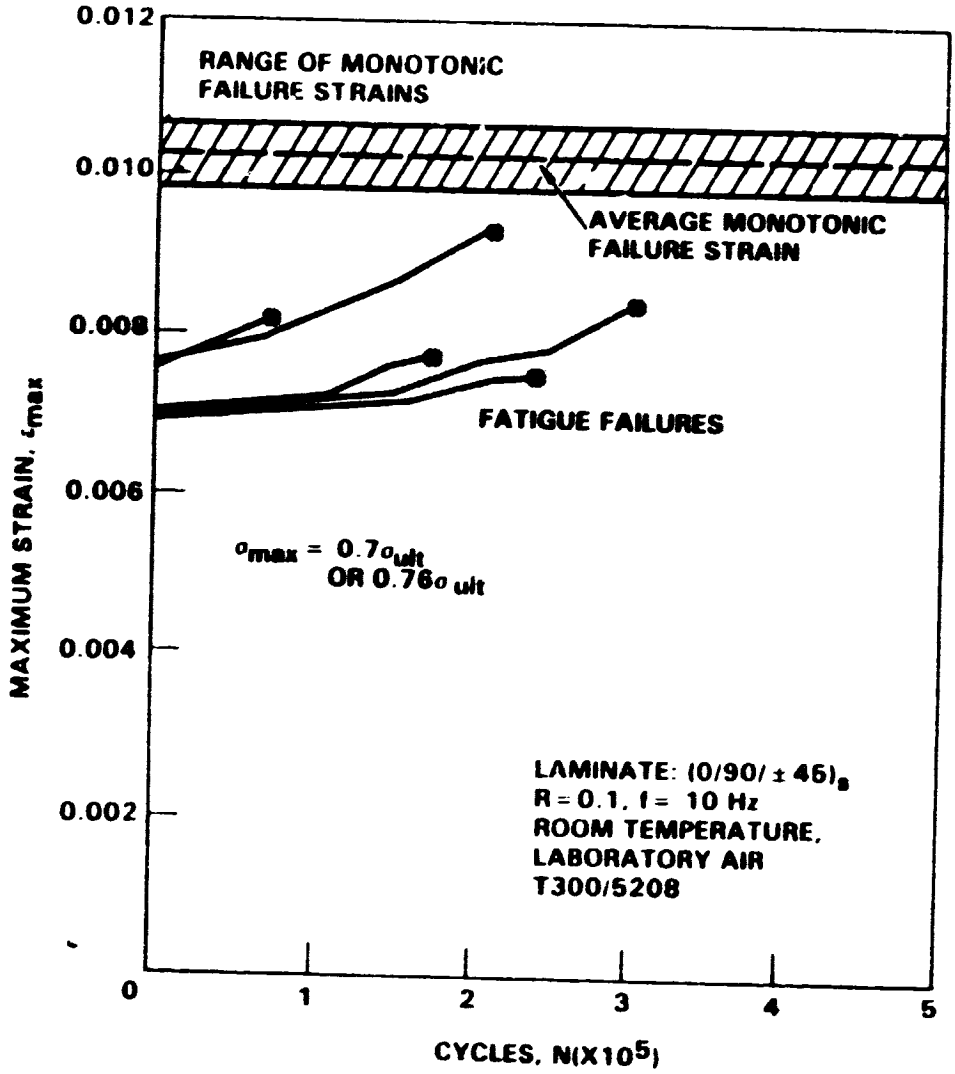

Figure 17: Increase in strain due to fatigue loading of $(0/90/\pm 45)_s$ coupons.

TABLE 10

STRAIN LEVELS AT WHICH
NDI WAS CONDUCTED ON
$(0/90/\pm45)_S$ RESIDUAL STRENGTH COUPONS

Coupon ID	Strain Level for NDI			Failure Strain
	Level 1	Level 2	Level 3	
11-8	0.00825	0.00900	-	0.0095
11-10	0.00900	0.00950	0.01000	0.0106
11-11	0.00825	0.00900	0.00950	0.0096
11-16	0.00850	0.00925	0.00975	0.0098
11-23	0.00875	0.00925	0.001000	0.0107
11-57	0.00875	0.00950	0.001000	0.0109
11-60	0.00900	0.00950	0.001000	0.0109

percent). Of the original nine coupons, one was accidentally overloaded and one failed in fatigue before reaching the planned 150 000 cycles. Table 10 shows that NDI data were obtained quite near to the failure strain of several coupons. In Table 11 the failure locations for the residual strength coupons are listed. The failure locations did roughly correlate with the maximum delamination regions, but these regions were so large as to indeed make the correlation very rough. The possible reason for this is discussed in Section 4. The fracture appearance of these coupons was similar to that of the fatigue loaded coupons.

During the residual strength loading, the number of matrix cracks appeared to be essentially unchanged prior to failure as compared to that observed at the end of fatigue loading. This is shown in Table 9 by the essentially unchanged values for average matrix crack spacing. Measurements of delamination extent observed during residual strength, monotonic tension loading indicated small increases in area occurred (up to a maximum of 5 percent).

Table 12 shows that the amount of stiffness loss in the residual strength coupons correlated well with the extent of delamination, but that strength, although decreased on average, did not correlate. Further, the average strain to failure of the residual strength coupons did not differ from that of the monotonic tension coupons, and the individual coupon strain to failure did not correlate to the percent of delaminated area. These results did not initially appear to be entirely consistent with a gradual increase in strain which occurred during fatigue loading nor with subsequent failure at a strain significantly below the monotonic tension strain which is attributed to increase in local 0° fiber strain due to the presence of delamination. The results are further discussed in Section 4 where they are compared to the modeling results of Section 3.

As an example of the analytical difficulties which are addressed in Section 3 and 4, consider coupon 11-10 of Table 12. At the end of 150 000 fatigue

TABLE 11

FRACTURE LOCATIONS OF $(0/90/\pm45)_S$ RESIDUAL STRENGTH COUPONS

Note: Locations are given relative to the centerline of the 101.6 mm (4 in.) gage length; + is towards the upper grip.

Coupon ID	Fracture Location mm	in.
11-8	-10.2	-0.4
11-10	+38.1	+1.5
11-11	-30.5	-1.2
11-16	-10.2	-0.4
11-23	-38.1	-1.5
11-57	+27.9	+1.1
11-60	-27.9	-1.1

TABLE 12

RESULTS OF RESIDUAL STRENGTH EXPERIMENTS FOR

$(0/90/\pm45)_s$ COUPONS

Coupon ID	Approximate Extent of Delaminated Area %	Monotonic Stiffness at Failure		Percent Loss In Stiffness	Strain To Failure	Stress at Failure		Primary Delamination Region	Number of Prior Fatigue Cycles
		GPa	Msi			GPa	ksi		
11-16	11.3	49.8	7.23	5.1	0.0098	487	70.6	+45/-45	150
11-23	14.7	49.1	7.12	6.3	0.0107	526	76.3	+45/-45	150
11-8	22.5	48.3	7.01	6.3	0.0095	436	63.2	90/+45	150
11-57	30.5	48.2	6.99	9.9	0.0109	525	76.2	90/+45	126
11-60	38.8	48.1	6.98	10.5	0.0109	525	76.1	90/+45	110
11-11	50.0	47.3	6.86	12.0	0.0096	452	65.5	90/+45	150
11-10	89.5	43.4	6.30	19.3	0.0106	461	66.9	90/+45	150
Average		47.8	6.93		0.0103	487	70.7		
Average Undamaged Tension Coupons		53.5	7.74		0.0103	547	79.4		

cycles, stiffness had decreased 19.3 percent. Since load was held constant the strain had increased to approximately 0.0087. According to Figure 17, this coupon was near failure due to fatigue loading. The reduction in strain to failure was hypothesized to have been due to a regional strain increase caused by the presence of delamination and matrix cracking, a situation apparently explainable by the analysis procedure of O'Brien[41] previously mentioned. However, when coupon 11-10 was monotonically loaded to failure, the stiffness remained the same as that recorded at the end of fatigue loading, as expected, but the strain to failure was 0.0106. Thus, strain to failure under fatigue loading occurred at strains of 0.0080 to 0.0090, but if coupons were loaded monotonically to failure with similar amounts of damage, strain to failure is on the average 0.0103; a value unchanged from that for undamaged coupons.

Some quasi-isotropic layups are known to display as much as a 10 percent drop in strain to failure due to changes in loading rate[7]. Hypothetically, the above described discrepency could be due to a difference in loading rates, 10 Hz versus 0.01 Hz, and not to a local strain increase attributed to delamination. However, the extent of the difference was too large to be fully explained by this hypothesis. Alternatively, or additionally, an event may occur in coupons subjected to fatigue loading just prior to (and eventuates in) failure which does not exist earlier. This would be a certain combination of 0° fiber fracture, weak 0° fibers, and local strain increase in a small region. If such an event occurs, the probability of removing a coupon while the event is yet occurring and prior to failure is extremely low. Thus no net effect on strain to failure would occur during residual strength loading. If this scenario is correct the problem remains of determining whether the local strain analysis of O'Brien[41] can account for the observed difference. The generality of this concept of an event unique to fatigue loading will be alluded to throughout Section 2 and discussed in detail in Section 4 as will the correctness of the failure criterion selected to explain the observed phenomenon.

2.3 RESULTS FOR $(0/\pm 45)_s$ COUPONS

In Table 13, the monotonic tension data obtained for the $(0/\pm 45)_s$ coupons are summarized. Coupons 8-6 and 8-19 failed prematurely in the region of 45° direction dimples on the coupon surface. These dimples appeared on several $(0/\pm 45)_s$ coupons which were eliminated from further experimentation in order to reduce the potential of bias in the data. The stress-strain curve of these coupons displayed a slight deviation from a straight line in the form of a gentle upward curve (increasing stiffness). Average strain to failure was essentially the same as that for the $(0/90/\pm 45)_s$ coupons, 0.0106 as compared 0.0103. The stiffnesses recorded at the periodic load interruptions for NDI measurements are given in Table 14. The small variations in stiffness appeared to be essentially random, but an average decrease of approximately 1.4 percent did occur.

Transverse matrix cracks were visible by edge replication in both the $\pm 45^\circ$ plies although more often in the $+45^\circ$ plies. The transverse cracks in both ply orientations were usually at a 45° angle to the loading direction. The matrix cracks did not appear in the enhanced x-ray photographs presumably due to two reasons, the tightness of the cracks in the unloaded condition, and the fact that the transverse cracks in this laminate probably did not extend across the entire coupon width prior to failure. Matrix cracking appeared above a strain level of 0.0045 and remained essentially unchanged above 0.0090.

The number of cracks per 25.4 mm (1 in.) varied from zero to in-excess-of thirty depending on the region of the gage length. The same amount of variation was also found in the same gage length region when comparing the number of cracks in one 45° ply to another. In some regions, matrix cracks only occurred in the -45_2 plies. The variation in the number of matrix cracks observed in the fracture region of different coupons was as great as that found within the gage length of any one coupon. Therefore, no trend curves were used in Figure 18, which shows the matrix crack data for these

TABLE 13

FAILURE STRESSES AND STRAINS
FOR MONOTONIC TENSION EXPERIMENTS
OF $(0/\pm45)_S$ COUPONS

Coupon I.D.	Average Area mm^2	Average Area $in.^2$	Stress at Fracture, MPa	Stress at Fracture, ksi	Strain at Fracture mm/mm in 101.6 mm	Stiffness GPa	Stiffness Msi
8-3	32.0	0.0496	554	80.4	0.00976	56.8	8.24
8-6	32.4	0.0502	492	71.4 [a]	0.00890[a]	55.3	8.02
8-8	31.8	0.0493	585	84.9	0.01030	56.8	8.24
8-14	31.0	0.0481	618	89.6	0.01072	57.6	8.36
8-19	31.8	0.0493	462	67.0 [a]	- -[b]	- - -[b]	
8-25	31.2	0.0484	678	98.4	0.01172	57.9	8.40
		Average	609[c]	88.3 [c]	0.0106[c]	56.9	8.25

a = Coupon failed prematurely due to manufacturing anomaly.

b = Data not recorded.

c = Average value, does not include coupons 8-6 or 8-19.

TABLE 14

STIFFNESS DATA OF $(0/\pm45)_s$ COUPONS
OBTAINED DURING MONOTONIC TENSION EXPERIMENTS

COUPON ID	STRAIN LEVEL mm/mm in 101.6 mm	STIFFNESS. GPA	Msi	
8-3	0.00730	57.1	8.28	
	0.00792	56.7	8.22	
	0.00851	54.8	7.95	
	0.00931	56.5	8.20	
	0.00961	56.1	8.14	
	0.00977	56.7	8.22	Failed on loading
8-8	0.00764	58.7	8.52	
	0.00808	56.9	8.25	
	0.00845	57.0	8.27	
	0.00902	57.8	8.38	
	0.00930	56.4	8.18	
	0.00987	57.4	8.33	
	0.01030	56.7	8.22	Failed on loading
8-14	0.00475	58.3	8.45	
	0.00727	57.2	8.30	
	0.00747	59.2	8.58	
	0.00880	56.5	8.20	
	0.00905	57.4	8.33	
	0.00934	58.0	8.41	
	0.00991	57.7	8.37	
	0.01023	59.5	8.63	
	0.01072	57.6	8.35	Failed on loading
8-25	0.00802	57.8	8.39	
	0.00845	57.0	8.27	
	0.00851	58.6	8.50	
	0.00954	59.0	8.56	
	0.00970	57.4	8.33	
	0.01010	56.9	8.54	
	0.01034	58.5	8.49	
	0.01172	58.0	8.41	Failed on loading

$(0/\pm45)_s$ coupons, because of the large scatter. The data for Figure 18 are tabulated in Appendix C, Table C41. The irregular matrix crack spacing observed in these $(0/\pm45)$s coupons during monotonic tension loading is also indicated in Table 15 which shows the range in spacing observed for various loading conditions. Clearly, matrix crack saturation did not occur prior to failure under monotonic tension load.

Edge replicates revealed regions where delaminations of 25 to 50 mm (1 to 2 in.) in length occurred at the +45/-45 interface. Often, no transverse cracks in the -45° plies were found in these regions. However, no delamination prior to coupon fracture was observed by enhanced x-ray radiographs in these monotonically loaded coupons. Therefore, the delaminations appeared to be primarily an edge phenomenon.

Fracture surfaces of the monotonically loaded coupons were dominated by the $+45^{\circ}$ plies. The outer 0° plies always started to fracture along a $+45^{\circ}$ direction which for half of the fracture surfaces continued across the coupon width and in the others went part way across and then changed to a 90° direction. Thus the strong influence of the underlying ply on the outer 0° plies was again noted as for the $(0/90/\pm45)_s$ coupons and also for the results of other layups previously reported[7,13,32].

A summary of the fatigue life data for the $(0/\pm45)_s$ coupons is given in Table 16. Many $(0/\pm45)_s$ coupons had surface dimple inperfections, as previously mentioned. These coupons were eliminated from the experimental program since their fatigue lives were severely reduced by the presence of the dimples as shown in Table 17. Therefore, for two coupons, 8-13 and 8-15, load cycling was discontinued before failure since they had large dynamic stiffness losses, 9 to 10 percent, and additional coupons were needed for residual strength experimentation.

Fatigue lives exhibited large scatter, as Table 16 shows, therefore a large amount of data was obtained at one stress level, 483 MPa (70 ksi).

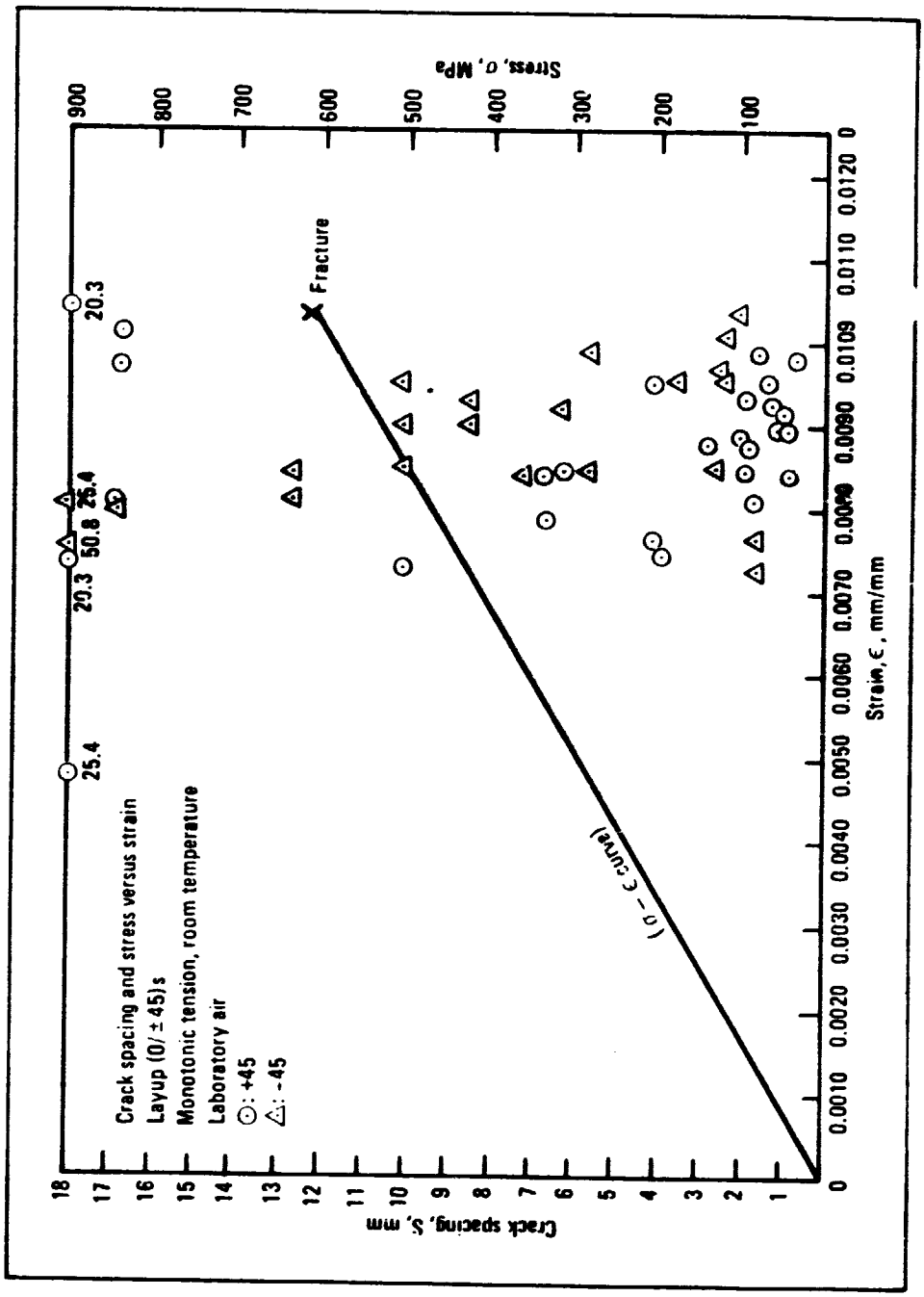

Figure 18 – Crack spacing and stress vs. strain

TABLE 15 - MATRIX CRACK SPACING UNDER DIFFERENT LOADING CONDITIONS FOR (0/±45)s COUPONS

Loading Condition	Range in Average Crack Spacing mm	
	$+45^{o}$	-45^{o}
Monotonic Tension	0.74-20.3	2.12- -[a]
Fatigue at 483 MPa	0.43-0.49	0.74-0.85
Residual Strength		
After Fatigue at 483 MPa	0.43-0.49	0.74-1.16
Monotonic Tension	0.47-0.51	0.75-1.27

a= No matrix cracks observed

NOTE: Crack spacing values given are those measured just prior to failure or at the end of the loading condition indicated.

TABLE 16
SUMMARY OF CONSTANT AMPLITUDE FATIGUE EXPERIMENTS
FOR $(0/\pm45)_s$ COUPONS

R = 0.1, f = 10 Hz, Room Temperature, Laboratory Air

Coupon I.D.	Maximum Stress Level MPa	ksi	No. of Fatigue Cycles
8-45	517	75	125 844
8-12	500	72.5	21 310
8-10	483	70	85 660
8-13	483	70	836 200[a]
8-15	483	70	971 500[a]
8-24	483	70	840
8-27	483	70	1 191 300
8-46	483	70	531 100
8-9	465	67.5	340 000
8-30	448	65	1 000 000[b]

a = Coupon did not fail, removed for residual strength testing

b = Coupon did not fail

TABLE 17
EFFECT OF MATERIAL INPERFECTIONS
ON FATIGUE LIFE OF
$(0/\pm45)_s$ COUPONS

R = +0.1, f = 10 Hz, Fatigue Stress Level = 483 MPa

Coupon Type	Coupon ID	Average Area mm^2	Fatigue Life in Cycles, (Thousands)
Coupons without or with few apparent imperfections	8-10	32.2	61.0[a]
	8-13	30.8	836.2[a]
	8-15	30.7	971.5[a]
	8-27	31.1	1191.3
	8-46	31.8	531.1
Coupons with apparent imperfections	8-2	31.8	2.6
	8-4	31.5	4.7
	8-11	31.6	152.6
	8-16	31.6	6.6[b]
	8-20	32.2	---
	8-22	32.0	12.9
	8-23	31.7	16.9
	8-24	31.4	0.84[c]
	8-32	31.3	129.0

a = Coupons did not fail
b = Coupon failed during monctonic stiffness survey at 474 MPa
c = Coupon reached approximately 98 percent of fatigue load.

Although edge replicates revealed developing delamination at the $\pm 45^{\circ}$ interface, these coupons essentially did not show delamination in the x-ray photographs, except in a few longer life coupons where delamination was minor, less than one percent of the total gage length area. Such delamination consisted of longitudinal regions along the coupon edge. In this region were 0° splits and some 0° fiber fracture as shown in Figure 19. In addition to the usually developed 0° fiber fracture along the edges, such 0° fiber fracture was also occasionally observed on the outer 0° plies, away from the coupon edges.

Fracture locations (Table 18) did not correlate to any worst location matrix crack spacing regions since the crack spacing was regular, see Table 15, in contrast to the irregular spacing observed under monotonic loading. The crack spacing was also considerably shorter after fatigue loading than after monotonic loading, see Table 15. The final crack spacing in the $\pm 45^{\circ}$ plies was essentially the same as that spacing theoretically derived by shear lag analysis, 0.40 mm for the $+45^{\circ}$ plies and 0.73 mm for the -45° plies.[39] However, as the observed range in crack spacing shows (see Table 15) not all coupons or all regions of any one coupon reached the theoretical minimum spacing. The density of the matrix cracks in the -45° plies was essentially the same as that in the $+45^{\circ}$ plies when based upon a normalized thickness basis.

Transverse cracks in both the $+45^{\circ}$ and -45° plies varied between being essentially perpendicular to the 0° plies to approximately a 45° angle. Matrix cracking started at the coupon edges, as the enhanced x-ray photographs showed, and progressed inward as the number of cycles increased, see Figures 20 and 21. Figure 22 shows, as an example, an enlarged picture of coupon 8-15 after 461 000 cycles; the same one shown as the first picture in Figure 21. The $\pm 45^{\circ}$ transverse cracks had not yet fully crossed the coupon width as shown in Figure 22. This observation was typical of the other coupons of this layup. Note in the last photograph in Figure 20 not only the small edge delamination and 0° splitting, but also the 0° splitting near the coupon center. Some delamination and fiber breakage occurred at the ends of this centrally located 0° splitting region.

Figure 19: Coupon 8-30 Fatigue Load Cycled at σ_{max} = 448 MPa (65 ksi); N = 1 000 000 Cycles.

TABLE 18

FRACTURE LOCATIONS OF

$(0/\pm 45)_s$ COUPONS TESTED UNDER

CONSTANT AMPLITUDE LOADING

NOTE: Fracture location is relative to the center line of the 101.6mm (4 in.) gage, + is towards upper grip

	Stress Level		Fracture Location	
Coupon ID	MPa	ksi	mm	in.
8-9	465	67.5	-30.5	-1.2
8-10	483	70	+ 5.1	+0.2
8-24	483	70	+40.6	+1.6
8-27	483	70	-17.8	-0.7
8-46	483	70	-22.9	-0.9
8-12	500	72.5	- 5.1	-0.2
8-45	517	75	-20.3	-0.8

2 OF 6

N84-29978 UNCLAS

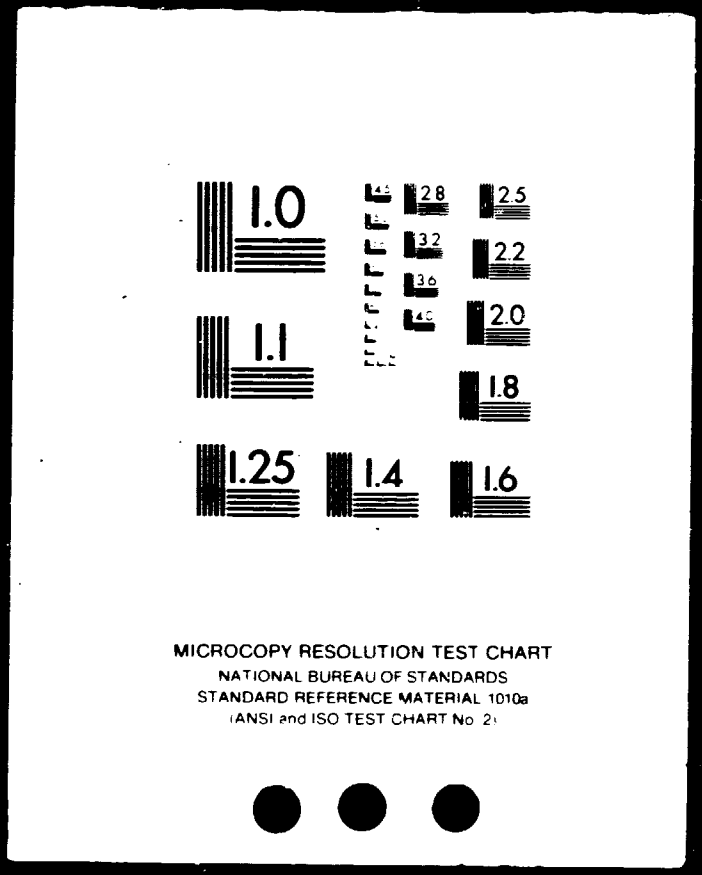

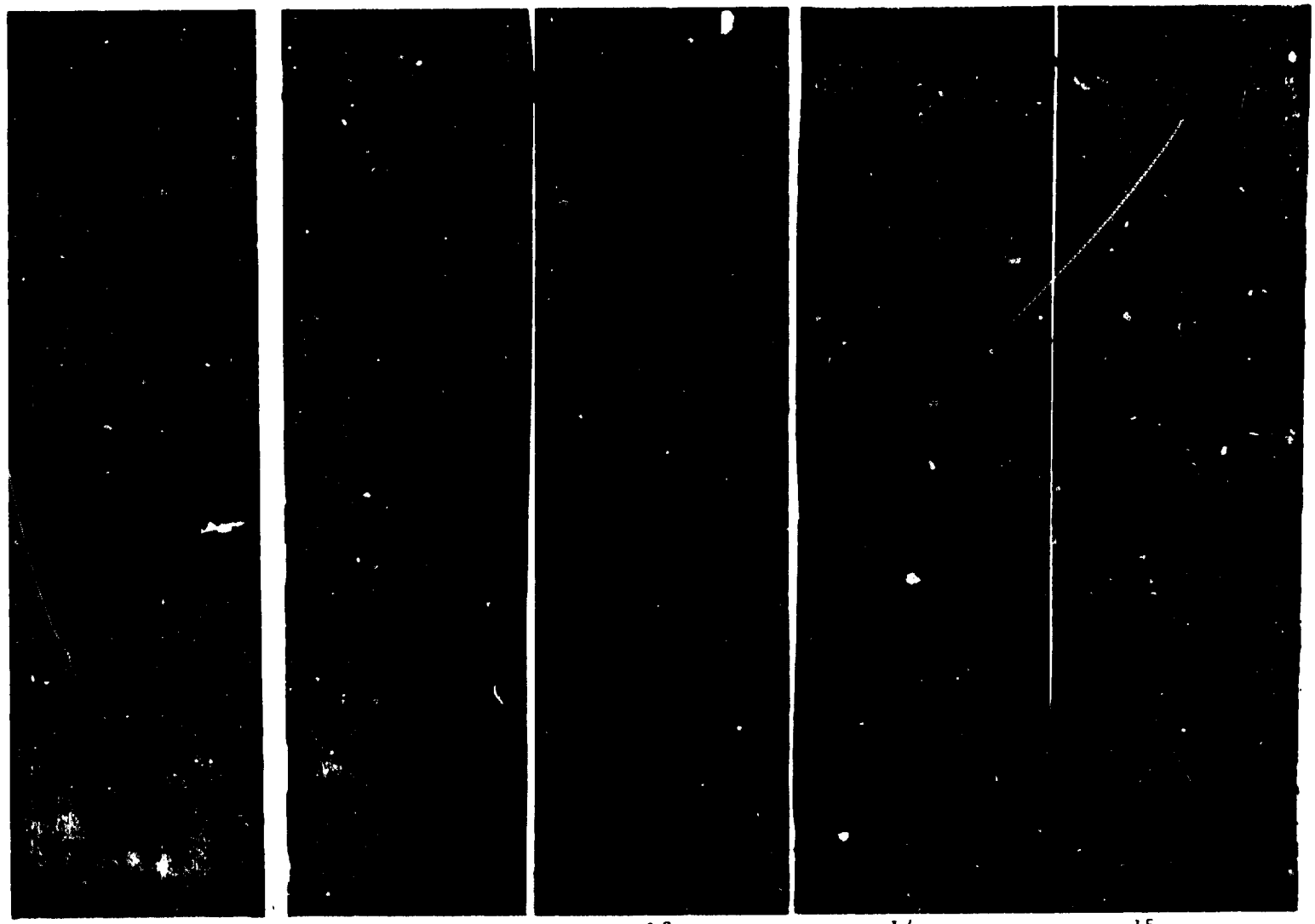

Figure 20: Enhanced x-ray photographs of coupon 8-13, fatigue load cycled at σ_{max} 483 MPa (70 ksi) $(0/\pm45)_s$ laminate - cycles and percent loss in monotonic stiffness are indicated.

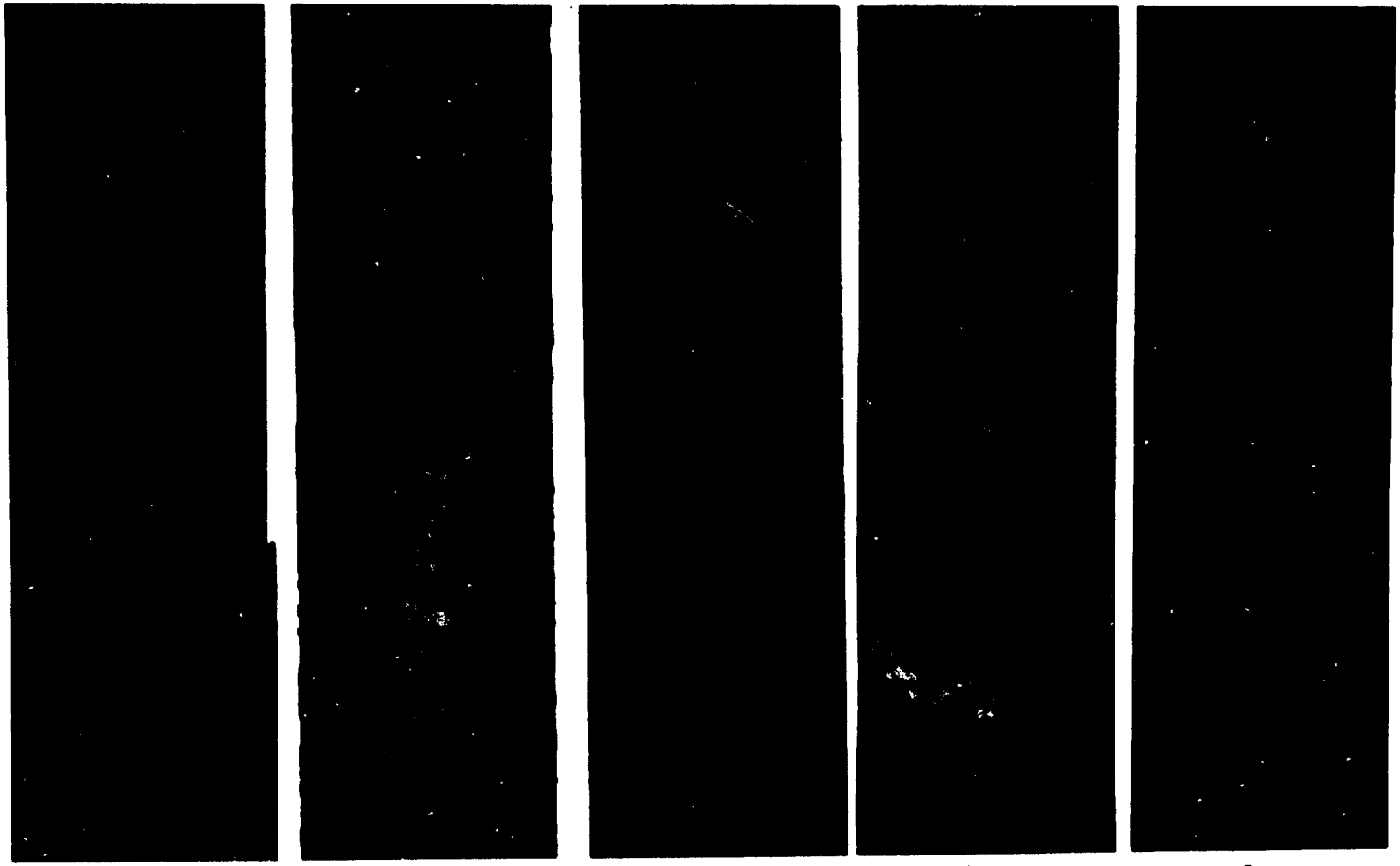

L1	L2	L3	L4	L5
461 000	564 000	754 000	872 000	972 000
2.0	3.9	3.8	5.1	8.8
0.7	1.4	1.5	3.2	5.3

Figure 21: Enhanced x-ray photographs of coupon 8-15, fatigue load cycled at σ_{max} = 483 MPa (70 ksi) $(0/\pm45)_s$ Laminate -- Cycles and percent loss in dynamic and monotonic stiffness are indicated.

Figure 22: Enhanced X-ray photograph of coupon 8-15, after 461 000 cycles, showing that the matrix cracks have not transversed the coupon width.

Throughout Figures 20 to 21, the transverse cracks in the -45° plies are more evident than those in the $+45^{\circ}$ plies. This is due to the fact that the -45° ply is of double thickness and laminate analysis shows this leads to doubling of the crack width. Matrix cracks in the -45° plies appeared, under high magnification, to traverse across the coupon width much sooner than those in the $+45^{\circ}$ plies and to have a much less segmented nature. Transverse crack density continued to increase throughout as much as 50 percent of the coupon fatigue life as shown by the enhanced x-ray photographs of both Figures 20 and 21. Similar to the $(0/90/\pm45)_s$ coupons, short microcracks perpendicular to the $\pm45^{\circ}$ transverse cracks appeared along the major cracks as fatigue cycling progressed. These cracks may essentially constitute a $\pm45^{\circ}$ interface delamination, a point noted also by Jamison and Reifsnider [40].

The fatigue coupons exhibited stiffness loss only roughly correlated with stress level and fatigue life as shown in Table 19. The dynamic stiffness losses were usually somewhat higher than the corresponding monotonic stiffness values. Monotonic stiffness loss of up to 2 percent was attributed to the development of a fully saturated transverse matrix crack pattern. This is shown by Figure 23 (data given in Table C42) which indicates that matrix crack saturation essentially occurred by the time that a 2 percent loss in stiffness had occurred. The additional monotonic stiffness loss was attributed to gradual development of small edge delaminations and to the fine cracking, essentially delamination which slowly developed between the $+45/-45$ interface along the $\pm45^{\circ}$ transverse matrix cracks.

The regularity of stiffness loss is shown in Figures 24 to 28. Additional plots of individual coupons are given in Appendix C, Figures C26 to C37, and all of the data are tabulated in Tables C43 to C53. These figures show that stiffness change was generally a decrease, but often increases of up to two percent occurred prior to any decrease. The gradual nature of the stiffness loss appeared to be due to the slow increase in transverse matrix cracks and the previously mentioned development of the fine $\pm45^{\circ}$ interface cracks. The hypothesized reasons for the observed stiffness loss are discussed further in Sections 3 and 4. The reason for the small initial increase in stiffness is not known.

TABLE 19

SUMMARY OF MAXIMUM PERCENTAGE STIFFNESS LOSS DUE TO FATIGUE LOADING FOR $(0/\pm45)_s$ COUPONS

Coupon ID	Stress Level, MPa	Fatigue Cycles (Thousands)	Percent Loss in Dynamic Stiffness	Percent Loss of Monotonic Stiffness	Remarks
8-30	448	1000.0	8.2	6.0	No failure
8-9	465	335.0	2.2	2.6[a]	Failure at [illegible] cycles
8-10	483	61.0	0.9	--[b]	Failure at 85.7K cycles
8-13	483	836.2	9.6	6.3	No failure
8-15	483	971.5	8.9	5.3	No failure
8-27	483	1107.0	4.6	--[b]	Failure at 1191.3K cycles
8-46	483	530.1	4.6	6.2	Failure at 531.1K cycles
8-12	500	20.0	0.0	--[b]	Failure at 21.3K cycles
8-45	517	125.0	2.9	--[b]	Failure at 125.8K cycles

a = Number is an increase not decrease.

b = monotonic stiffness loss not obtained near failure.

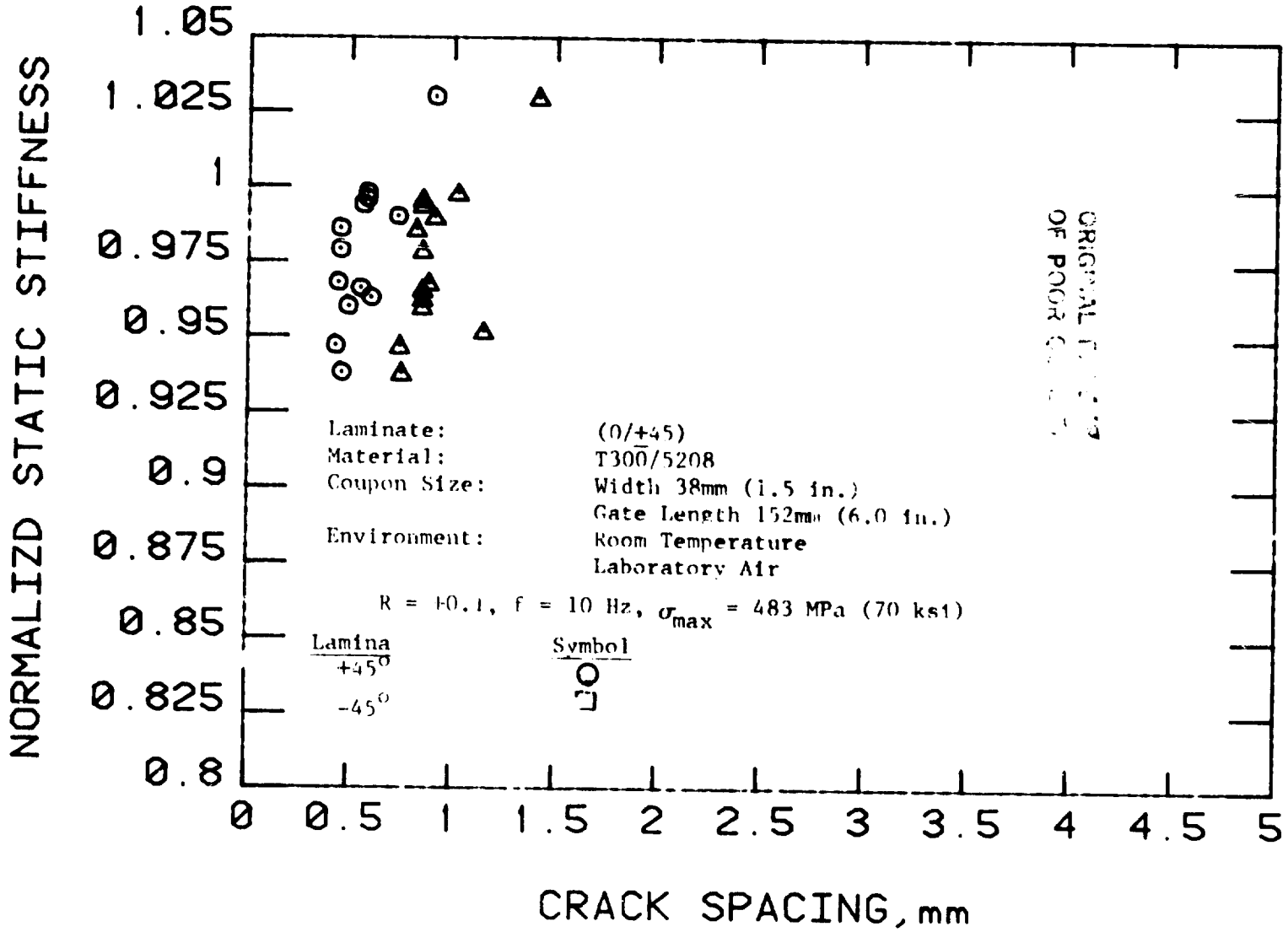

Figure 23: Normalized tensile stiffness vs. average matrix cracking spacing for (0/±45) laminate coupons subjected to [illegible] of constant amplitude tension load, σ_{max} = 483 MPa (70 ksi).

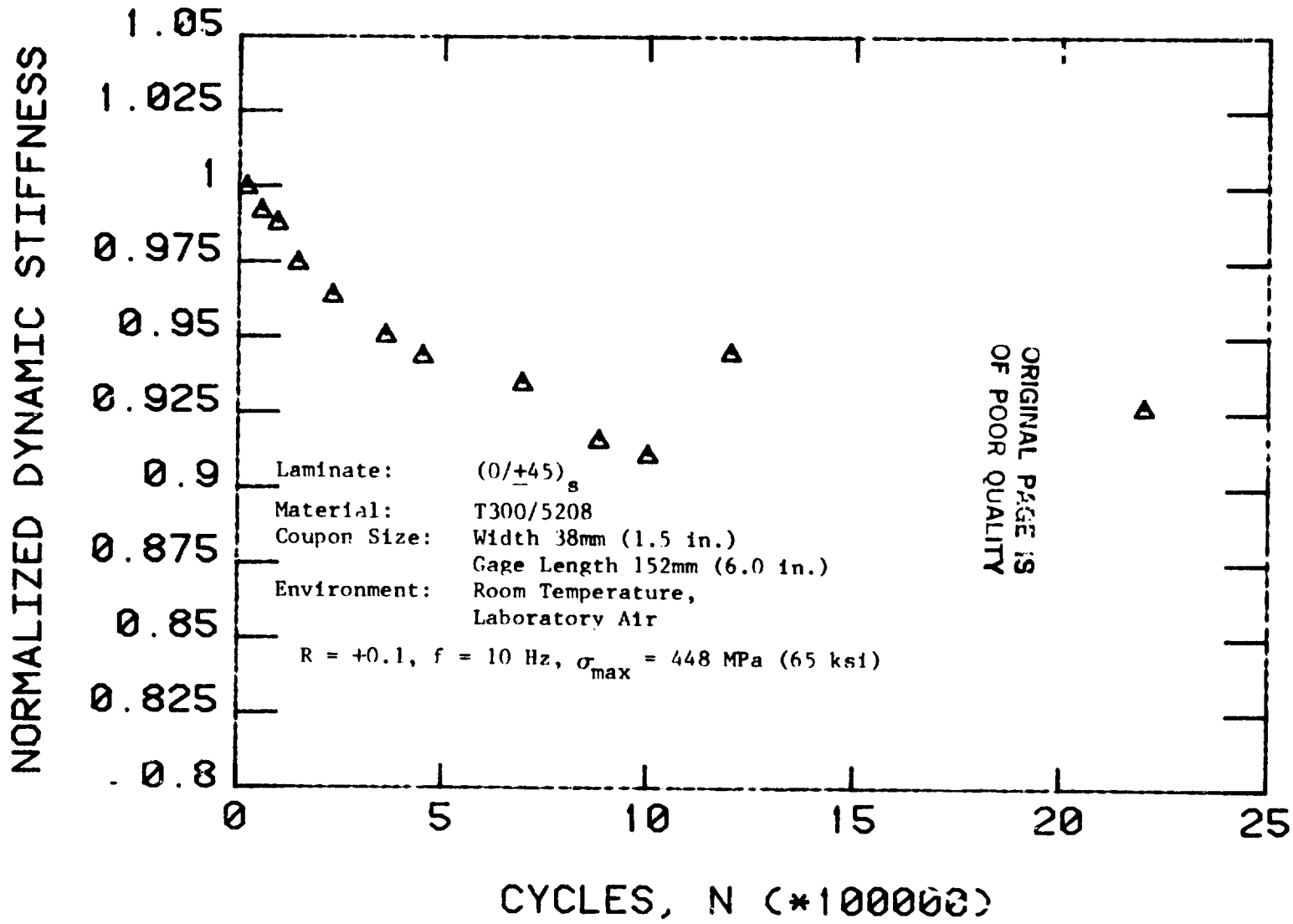

Figure 24: Normalized dynamic stiffness vs. constant amplitude fatigue load cycles for $(0/\pm45)_s$ laminate coupon 8-30, σ_{max} = 448 MPa (65 ksi)

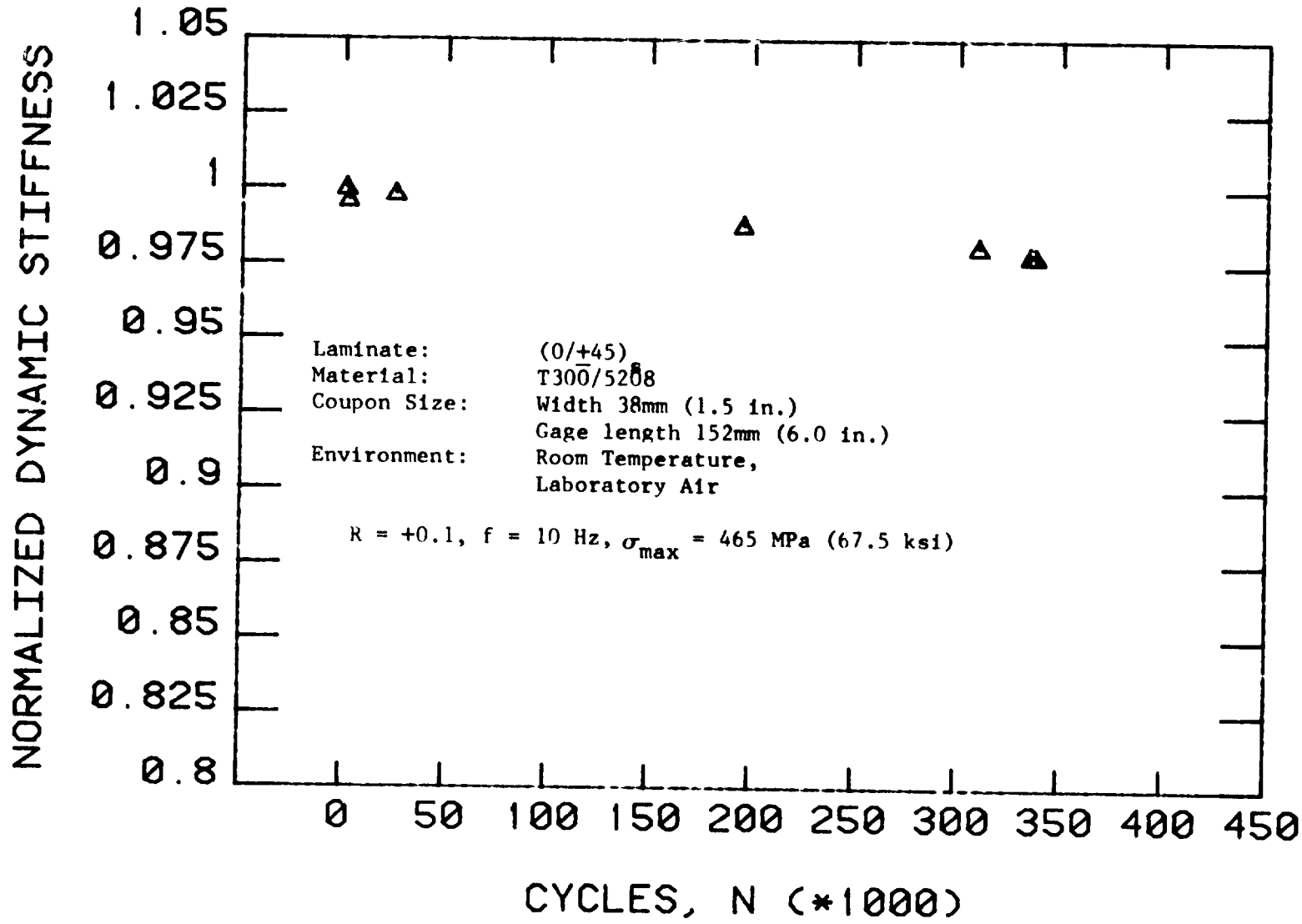

Figure 25: Normalized dynamic stiffness vs. constant amplitude fatigue load cycles for $(0/+45)_s$ laminate coupon 8-9, σ_{max} = 465 MPa (67.5 ksi)

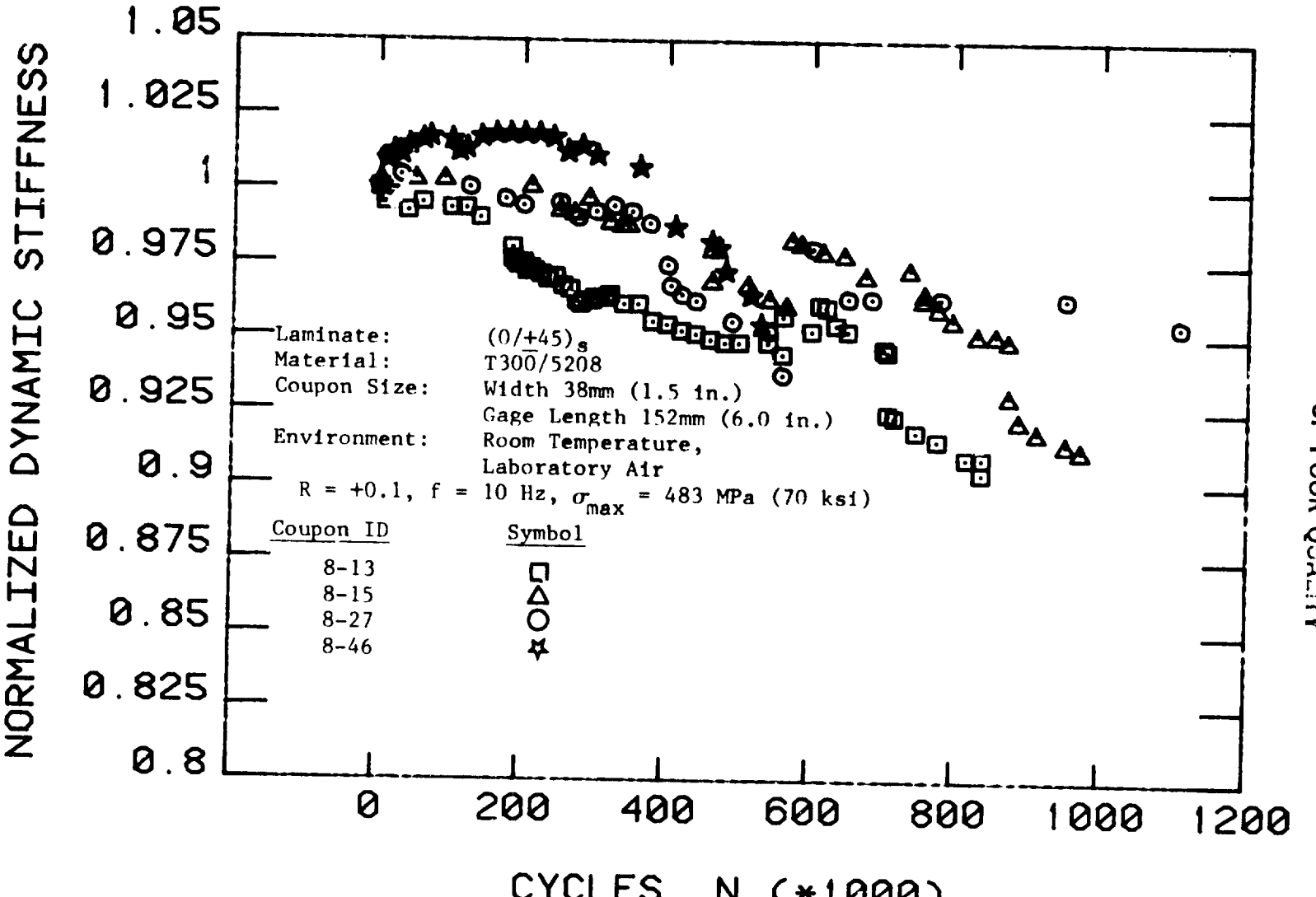

Figure 26: Normalized dynamic stiffness vs. constant amplitude fatigue load cycles for $(0/+45)_s$ laminate, σ_{max} = 483 MPa (70 ksi)

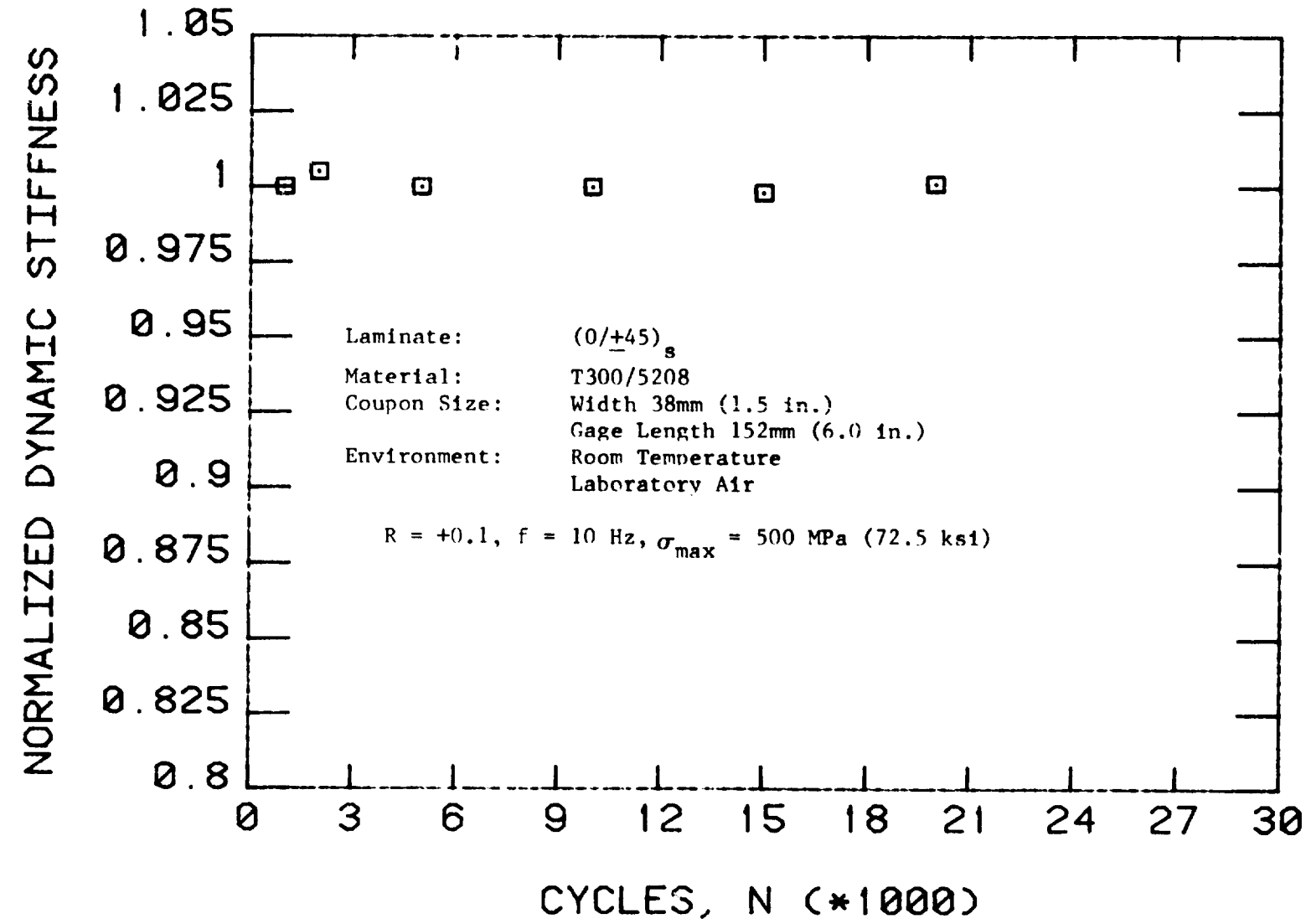

Figure 27: Normalized dynamic stiffness vs. constant amplitude fatigue load cycles for $(0/\pm45)_s$ laminate coupon S-12, σ_{max} = 500 MPa (72.5 ksi).

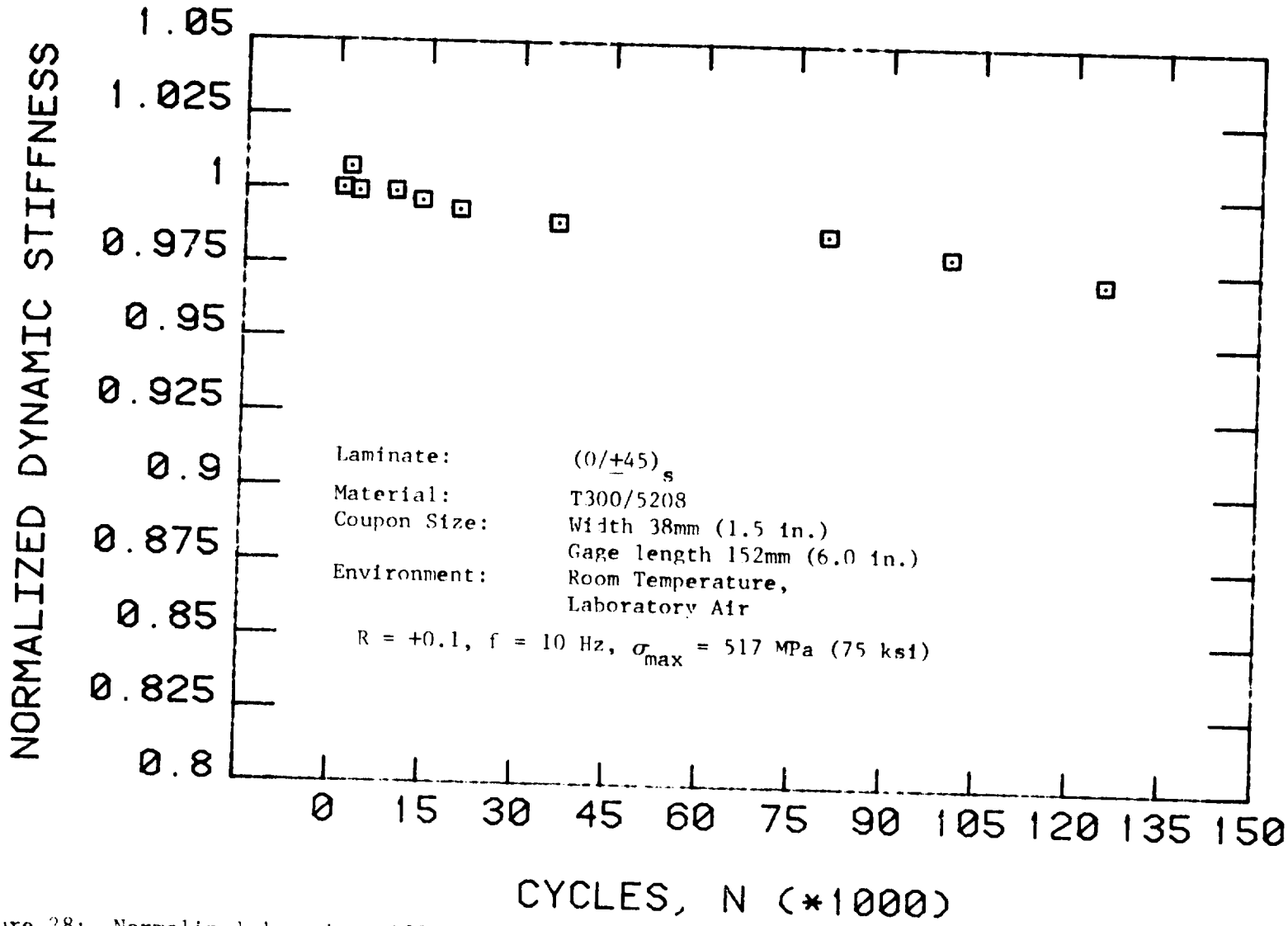

Figure 28: Normalized dynamic stiffness vs. constant amplitude fatigue load cycles for $(0/\pm45)_s$ laminate coupon 8-45, σ_{max} = 517 MPa (75 ksi).

In Figure 29, the maximum strain in a coupon during fatigue loading is plotted for four representative coupons. The numbers in parentheses indicate the amount of dynamic stiffness loss which occurred prior to failure. As for the $(0/90/\pm45)_s$ coupon, these coupons failed under fatigue loading at strain levels significantly below the monotonic strain to failure. The reason for failure at such low strain levels is not immediately obvious because: 1) the coupons did not delaminate on a global scale; 2) the number of matrix cracks saturated before a three percent loss in stiffness occurred; and 3) the total monotonic stiffness loss was under seven percent.

Fracture can be attributed to local load transfer to the 0° fibers because of the matrix cracks and the small delamination like cracks emanating from them. The observations of fiber fracture in the surface 0° plies was considered pertinent. These fibers, recall, would fracture not only at the coupon edges, but also between the edges. A region of broken fibers initially about the wdith of a fiber tow was observed in several coupons just prior to failure. This region of fiber fracture was observed to extend by small, irregular jumps partially across the coupon width due to continued load cycling. Eventually, coupon fracture appeared to occur when sufficient 0° fibers were broken such that fracture of a statistically significant group of fibers could develop. This failure scenario is similar to the fatigue failure event hypothesized for the $(0/90/\pm45)_s$ coupons. As for the monotonically loaded coupons, fracture of the 0° plies generally occurred along a $+45^\circ$ direction. Further discussion is held until Sections 3 and 4.

For the residual strength experiments only three coupons were available because so many had a short fatigue life or were set aside due to the presence of surface dimples. All three coupons were fatigue cycled at 483 MPa (70 ksi) before being loaded in four steps: strains of 0.0085, 0.0090, 0.0095, and to failure. Table 20 shows the results of the residual strength experiments. Detailed data are tabulated in Appendix C, Tables C54 to C56. The results show the previously noted losses in stiffness similar to those

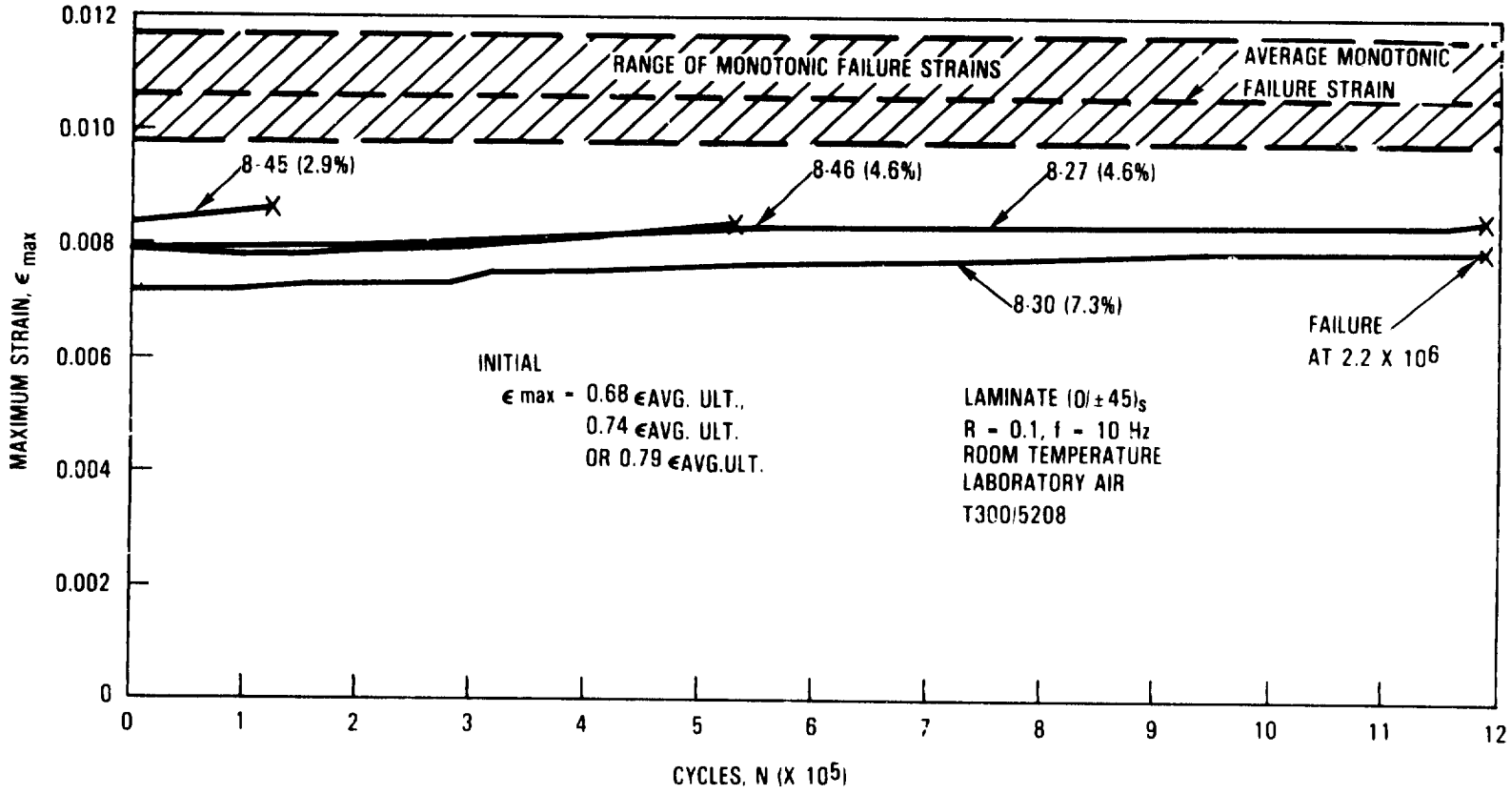

FIGURE 29. INCREASE IN STRAIN DURING FATIGUE LOADING OF $(0/\pm 45)_S$ COUPONS.

TABLE 20
SUMMARY OF MONOTONIC TENSION LOAD RESIDUAL STRENGTH DATA
FOR $(0/+45)_s$ COUPONS
R = +0.1, f = 10 Hz, Fatigue σ_{max} = 483 MPa (70 ksi)

Coupon ID	Number of Prior Fatigue Cycles, Thousands	Stress at Failure MPa	Stress at Failure ksi	Strain at Failure, mm/mm in 101.6 mm	Apparent Modulus of Elasticity GPa	Apparent Modulus of Elasticity Msi	% loss in Initial Modulus[a] at Failure	% loss in Initial Modulus after Fatigue Loading
8-13	836.2	594	86.1	0.0106	56.0	8.12	5.1	6.3
8-15	971.5	592	85.8	0.0109	54.3	7.87	7.3	5.3
8-31	125	558	80.9	0.0102	54.7	7.93	7.8	8.1
Average		581	84.3	0.0106	55.0	7.97		
Average Monotonic Tension		609	88.3	0.0106	56.9	8.25		

a = Modulus values are for monotonic, static, stiffness not dynamic.

observed for $(0/90/\pm45)_s$ coupons. Also similar to that layup, the strain to failure was unchanged from the failure strain obtained under monotonic tension load without prior fatigue damage. The extent of matrix cracking did not appear to change during the residual strength experiments, see Table 15, nor was any new delamination observed to develop or previously observed delamination to extend. Therefore, also like the $(0/90/\pm45)_s$ laminate, $(0/\pm45)_s$ coupons failed under fatigue loading at strains well below the monotonic tension failure strain level, but this effect of damage was not reflected in residual strength coupons despite the loss in stiffness which did occur. Failure locations for these residual strength coupons are given in Table 21. The fracture location of coupon 8-31 is one of the few which occurred outside of the gage length.

2.4 RESULTS FOR $(0/45/0_2/-45/0)_s$ COUPONS

The monotonic tension data obtained for the $(0/45/0_2/-45/0)_s$ coupons are summarized in Table 22. The strain to failure of these coupons was slightly higher than that for the $(0/90/\pm45)_s$, and $(0/\pm45)_s$ layups, which is probably attributable to variation in material batch/lot properties[67]. The comparable results obtained in another research program[32] for a doubly symmetric form of this laminate are also given in Table 22. In Table 23, the stiffness values obtained at the load interruptions for NDI are listed. In general, the stiffness readings slightly increased with strain as is typical for this layup which is known to have an increasing stiffness stress-strain curve[32].

The fracture surfaces of the monotonic tension coupons were dominated by the $+45^\circ$ plies in that fracture of the 0° plies and the -45° plies occurred along a $+45^\circ$ direction. In two coupons, the $+45^\circ$ failure direction only extended part way across the coupon and the remaining fracture was at 90° to the 0° ply orientation.

TABLE 21

FRACTURE LOCATIONS OF
(0/±45)s RESIDUAL
STRENGTH COUPONS

Coupon ID	Fracture Location mm	in.
8-13	+50.8	+2.0
8-15	+35.6	+1.4
8-31	+76.2	3.0

Note: Locations are given relative to the centerline of the 101.6mm (4 in.) gage length; + is towards the upper grip.

TABLE 22
FAILURE STRESSES AND STRAINS FOR MONOTONIC TENSION TESTS
OF $(0/45/0_2/-45/0)_s$ COUPON

Coupon ID	Average Area, mm^2	Average Area, $in.^2$	Stress at Fracture MPa	Stress at Fracture ksi	Strain at Fracture mm/mm in 101.6 mm	Stiffness to Failure GPa	Stiffness to Failure Msi	Fracture[b] Location mm
1ZF1908								
-B1a	63.2	0.0979	1185	171.9	0.01146	103.4	15.0	+56
-B2	64.7	0.1003	1070	155.2	0.01068	100.0	14.5	+46
-B3	63.7	0.0988	1117	162.0	0.01101	101.4	14.7	- 0.2
-B4	62.8	0.0974	1155	167.5	0.01127	102.7	14.9	+58
-B5	64.1	0.0993	1182	171.5	0.01143	103.4	15.0	_[c]
Average			1142	165.6	0.01117	102.0	14.8	

a = Coupon used for damage documentation by in-situ enhanced x-ray.

b = Fracture location is relative to the center line of the 101.6 mm (4 in.) gage length, + is towards the upper grip

c = Coupon exploded.

TABLE 23

STIFFNESS DATA OBTAINED DURING MONOTONIC TENSION EXPERIMENTS OF $(0/45/0_2/-45/0)_s$ COUPONS

Coupon ID	Strain Level mm/mm in 101.6 mm	Stiffness, GPa	Msi	
1ZF1908				
-B1	0.00402	100.7	14.61	
	0.00601	101.2	14.68	
	0.00804	101.9	14.78	
	0.00854	102.2	14.83	
	0.00903	102.5	14.86	
	0.00951	102.7	14.89	
	0.00978	102.2	14.82	
	0.01001	102.5	14.86	
	0.01027	102.9	14.92	
	0.01053	103.1	14.96	
	0.01078	103.1	14.95	
	0.01104	103.3	14.99	
	0.01127	103.2	14.98	
	0.01146	103.4	15.00	Failed on Loading
-B2	0.00402	96.8	14.04	
	0.00804	99.8	14.47	
	0.01002	101.3	14.69	
	0.01052	101.6	14.73	
	0.01068	101.6	14.53	Failed on Loading
-B3	0.00952	100.4	14.56	
	0.01002	100.9	14.63	
	0.01028	100.9	14.64	
	0.01055	100.9	14.64	
	0.01077	101.4	14.70	
	0.01101	101.4	14.71	Failed on Loading

TABLE 23 (continued)

-B4	0.00953	101.1	14.67
	0.01003	101.4	14.70
	0.01028	101.6	14.74
	0.01051	101.8	14.77
	0.01077	102.0	14.79
	0.01105	102.2	14.82
	0.01127	102.5	14.86 Failed on Loading
-B5	0.00504	101.5	14.72
	0.00754	102.0	14.79
	0.01053	103.6	15.03
	0.01077	103.9	15.07
	0.01103	103.9	15.07
	0.01126		15.03 Failed on Loading

This layup is highly dominated by the 0° plies and apparently fracture location is much more sensitive to gripping as shown in the fracture locations of these coupons given in Table 22. However, as discussed in Appendix B, the double symmetric form of this layup showed no significant effect of gripping on the monotonic tension data despite more, apparently, grip influenced failures than statistically expectable based upon a random analysis of fracture in an untapered coupon.[32] Therefore, the strength of these coupons was probably not significantly affected by the increased influence of the grips.

As anticipated, enhanced x-ray photographs showed no delamination occurring during tension loading to failure. In addition, matrix cracks in the ± 45 plies were extremely dfficult to observe by enhanced x-ray even though the radiographs were obtained while coupon B-1 was under a load equal to 80 percent of the previous strain level. Table 24 shows that the number of matrix cracks observed using edge replication was highly irregular, even more so than in the $(0/\pm 45)_s$ coupons, which explains the high probability of not seeing matrix cracks on the enhanced x-ray photographs, since for some coupons cracks were not seen on the edge either. In coupon B2, no matrix cracks were found even by edge replication and in coupon B3 only three -45° ply matrix cracks were observed over the entire 101.6 mm (4 in.) gage length and those only just prior to failure. In coupons B4 and B5, numerous -45° ply matrix cracks were observed, but all in only one of the two -45° plies and not over the entire gage length. Only one to three $+45^{\circ}$ ply matrix cracks per inch were found in coupon B4 and none in B5. Most of the observed matrix cracks were at an angle to the loading direction with many at approximately a 45° angle due to combined in plane normal and shear stresses. The observed matrix cracks usually had no short delamination cracks at their ends between the 0° and 45° plies. The enhanced x-ray evidence was strong that even the few matrix cracks observed by edge replication did not fully cross the coupon width prior to failure, a fact confirmed by microscopic cross sections of coupons.

TABLE 24
MATRIX CRACK SPACING OBSERVED DURING MONOTONIC TENSION LOADING OF $(0/45/0_2/-45/0)_s$ COUPONS

Coupon ID	Strain Level	Average Crack Spacing, mm Ply Level +45	Ply Level -45
1ZF1908-B1	Failed at 0.01146	No cracks observed by x-ray at 13 strain levels, 0.004 to 0.01127.	
-B2	Failed at 0.01068	No cracks observed by edge replication at 4 strain levels, 0.004 to 0.0105.	
-B3	0.00952	--[a]	--
	0.01002	--	--
	0.01028	--	--
	0.01055	--	b
	0.01077	--	b
	Failed at 0.01101		
-B4	0.00953	25.4[c]	0.87[d]
	0.01003	25.4	0.87
	0.01028	8.47	0.85
	0.01077	8.47	0.87
	0.01105	8.47	0.82
	Failed at 0.01127		
-B5	0.00504	--	0.94[d]
	0.00754	--	0.87
	0.01053	--	0.85
	0.01077	--	0.91
	0.01103	--	0.82
	0.01126	--	0.82
	Failed at 0.01143		

a = Indicates that no matrix cracks were observed
b = Only three cracks found, all in a spacing of 1.5 mm and only in one -45° ply
c = One matrix crack observed in one inch in only one +45 ply
d = All matrix cracks found in only one -45 ply

The fatigue life data for this layup are summarized in Table 25. The large scatter in fatigue life was also typical of the doubly symmetric form of this layup[32] and was similar to that of the previously discussed $(0/\pm45)_s$ layup. Coupons of this layup were load cycled from a specific initial strain level. Since all coupons had the same area within a few percent, initial stress was also essentially the same. The stiffness data for these coupons are listed in Appendix C, Table C57. For most coupons, stiffness measurements did not change by even one percent. For a few coupons, apparent changes of one to three percent occurred, but stiffness readings actually increased for as many coupons as those in which a decrease occurred and fluctuations were up and down prior to failure without any discernable pattern. Usually these fluctuations occurred between readings made before and after coupon removal for enhanced x-ray photographs.

An attempt was made using coupon B9 to see if the zinc iodide enhancer affected the stiffness readings, but no effect was found. The reason for the fluctuations is unknown, but their occurrence is especially curious since readings increased as often as they decreased and the rather large fluctuations did not occur for the $(0/90/\pm45)_s$ and $(0_2/90_4)_s$ coupons, but did to a similar extent for the $(0/\pm45)_s$ coupons. Apparently something changes in the $(0/\pm45)_s$ and $(0/45/0_2/-45/0)_s$ layups during the unloaded time periods which does not occur to the same extent in the other two multiaxis layups.

The random nature of the stiffness measurements and the fact that the average value esentially remained unchanged led to the conclusion that the stiffness of these coupons was unaffected by the fatigue cycling. Therefore no stiffness versus cycle plots are shown. Also no strain versus cycle plots were made since strain did not change. However, as with the $(0/90/\pm45)_s$ and $(0/\pm45)_s$ layups, all of these coupons clearly failed in fatigue at strain levels considerably below (20 to 30 percent) the tensile strain to failure region.

TABLE 25
FATIGUE LIVES OF $(0/45/0_2/-45/0)_s$ COUPONS

COUPON ID	STRAIN LEVEL	CYCLES TO FAILURE
1ZF1908-B28	0.0090	11 800
-B7	0.0085	5 674
-B10		101 380
-B11[a]		> 650 000
-B13		144 800
-B17		196 110
-B25		746 500
-B27		4 344
-B9	0.0080	473 880
-B12[b]		300 253
-B14		240 380
-B15		312 540
-B18[b]		> 575 000
-B19[c]		225 180
-B20[b]		> 300 000
-B21[b]		> 300 000
-B26		22 690
-B30[b]		150 720
-B31[b]		> 675 000
-B32		331 040
-B23[b]	0.0075	>1 000 000
-B24[b]		>1 000 000
-B6[b]	0.0070	>1 000 000

a = Coupon failed due to operator error
b = Coupon used for residual strength experimentation
c = Coupon failed while being cycled for residual strength experiment

Table 26 lists the failure location of the fatigue loaded coupons. As for the monotonic coupons, the location of fracture was often outside the extensometer gage length as was also noted[32] for the doubly symmetric form of this laminate. The fracture surfaces of these fatigue loaded coupons were dominated by the $+45^{\circ}$ plies like the monotonic tension coupons. Occasionally the inner 0° plies were fractured for a short distance along the -45° direction, but then returned to the predominant $+45^{\circ}$ direction. Hence, the fracture locations of Table 26 are essentially the centers of the $+45^{\circ}$ angle regions. As noted in the table, occasionally two fracture regions developed and interacted with a final fracture line between them parallel to the 0° ply direction.

The primary form of damage development in the fatigue coupons was matrix cracking in the $\pm 45^{\circ}$ plies. Edge delamination did occur, but this did not always significantly penetrate into the coupon interior as demonstrated by the enhanced x-ray photographs where delamination was often not visible. Most of the delamination was linear in shape and accompanied by 0° splits as shown in Figure 30. Delamination primarily occurred on either side of the $+45^{\circ}$ plies and secondarily, and not on all coupons, on either side of the inner -45° plies. The delamination in Coupon B18 was unusual in being thumbnail in shape as shown in Figure 31. A qualitative summary of the observed matrix cracking and delamination is as follows:

- 0.0070: (up to one million cycles) Edge delamination visible only on edge replicates; irregular matrix crack spacing; number of matrix cracks per unit length considerably less than that observed just prior to failure of monotonic tension coupons.
- 0.0075: (up to one million cycles) Same as 0.0070.
- 0.0080: Highly irregular matrix crack spacing up to 300 000 cycles (0 per 25 mm (in.) up to 125 per 25 mm (in.)), but number per unit length in some plies does exceed that observed prior to failure of monotonic tension coupons; enhanced x-ray visible delaminations normally occurred by 300 000 cycles and sometimes by 150 000 cycles with no significant stiffness loss.

TABLE 26
FRACTURE LOCATION DATA FOR $(0/45/0_2/-45/0)_S$ COUPONS
LOADED IN CONSTANT AMPLITUDE FATIGUE

Coupon ID	Initial Strain Level	Average Fracture Location[a] mm	in.
1ZF1906-B9	0.0080	+4.0	+0.2
-B12		+76.0	+3.0
-B14		+38.0	+1.5
-B15		+84.0	+3.3
-B19		+86.0	+3.4
-B30		-20.0	-0.8
-B32		+15.0 +46.0	+0.6 +1.8
-B7	0.0085	+8.0	+0.3
-B10		+12.0	+0.5
-B13		+76.0	+3.0
-B17		+33.0 -24.0	+1.3 -1.0
-B25		+58.0	+2.3
-B27		-28.0 -46.0	-1.1 -1.8
-B9	0.0090	0.0	0.0

a = A double entry indicates a region of fracture since damage was extensive.

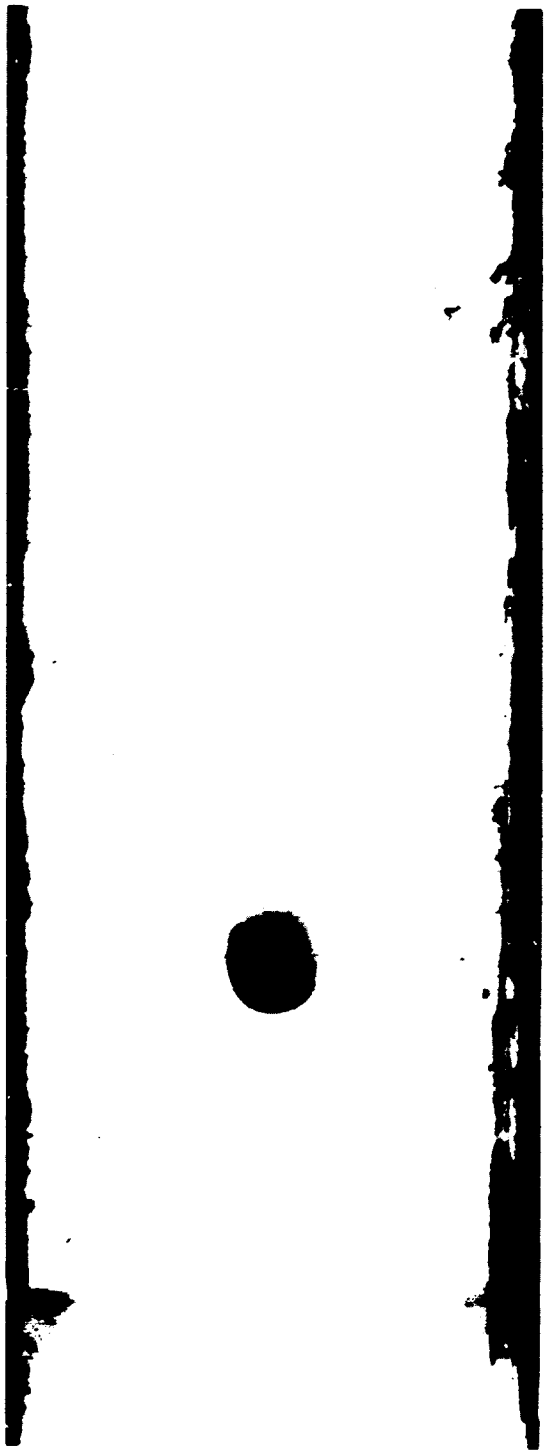

Figure 30: Typical delamination found along the edges of $(0/45/0_2/-45/0)_s$ coupon B14, after 225 000 cycles, by using enhanced x-ray Photography.

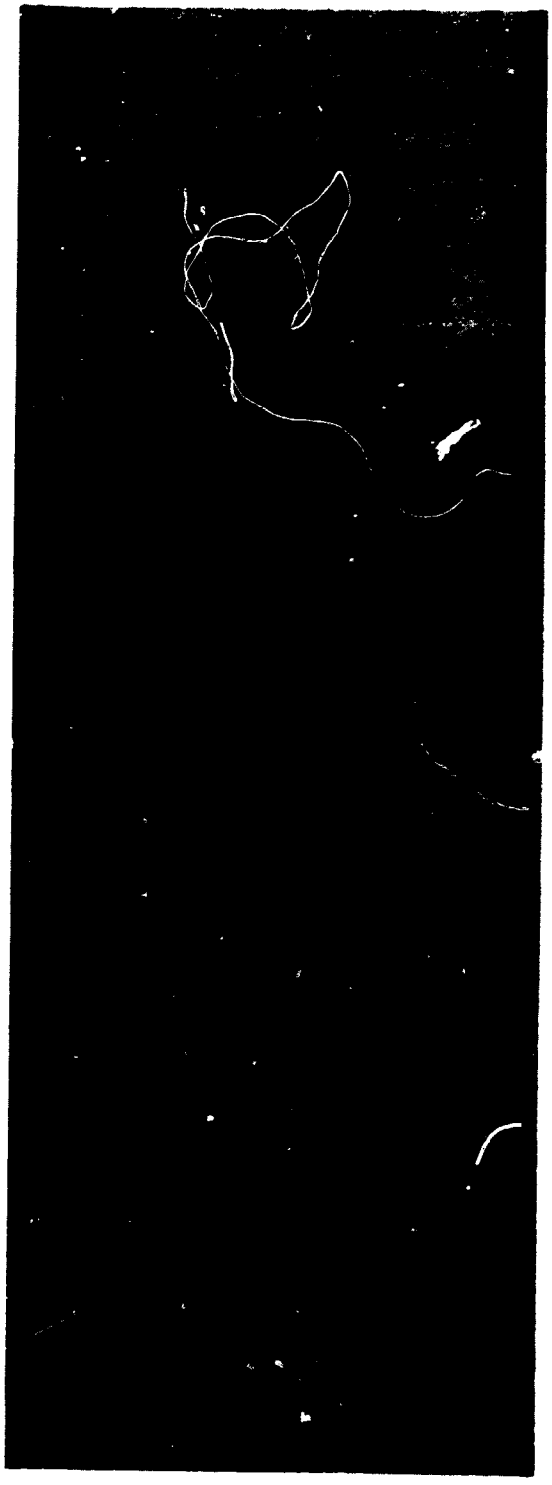

Figure 31: Unusual thumbnail type delamination found in $(0/45/0_2/-45/0)_s$ coupon B18.

- o 0.0085: Similar to observations made for 0.0080 coupons.
- o 0.0090: Little or no delamination confined to edges, and apparently few matrix cracks prior to failure in a few thousand cycles.

The average matrix crack spacing versus cycles in shown in Figures 32 to 34 for coupons fatigue cycled at initial strains of 0.0075, 0.0080 and 0.0085.

Matrix crack spacing did tend to decrease to levels near or below the minimum distance observed under monotonic tension load, see Table 27, but still remained highly irregular with no apparent plateau as Table 27 and Figures 32 to 34 show. The matrix crack data were actually much more irregular than that shown by the average spacing plots of Figures 32 to 34. Regions were found with many matrix cracks, more than 70 per 25 mm, in some plies and none in others, even in the same ply orientation, and even near coupon failure. Other regions, up to 25 to 50 mm in length, had no matrix cracks prior to fracture. The +45 plies were generally, but not always, observed to have considerably more matrix cracks than the -45° plies. Matrix cracks generally were at an angle to the 0° plies, up to 45°. Many of the transverse matrix cracks were not found to ever traverse completely across the coupon width as high magnification examination of the x-ray photographs showed. This was confirmed by taking sections, parallel to the 0° fibers, of two fatigue coupons, 6 mm from the edge and at the centerline, which showed matrix cracks near the edge, but none at the center. These observations on the extent of matrix cracking led to the inference that a saturation plateau was never reached prior to failure under fatigue loading . In fact, the matrix crack states reached prior to failure were apparently far removed from any such saturation plateau state.

Tables 28 and 29 list the results of the residual strength experiments performed on the $(0/45/0_2/-45/0)_s$ coupons. Fracture location data are given in Table 30 which again shows many coupons which fractured outside the extensometer gage length region. These coupons were loaded to failure in several

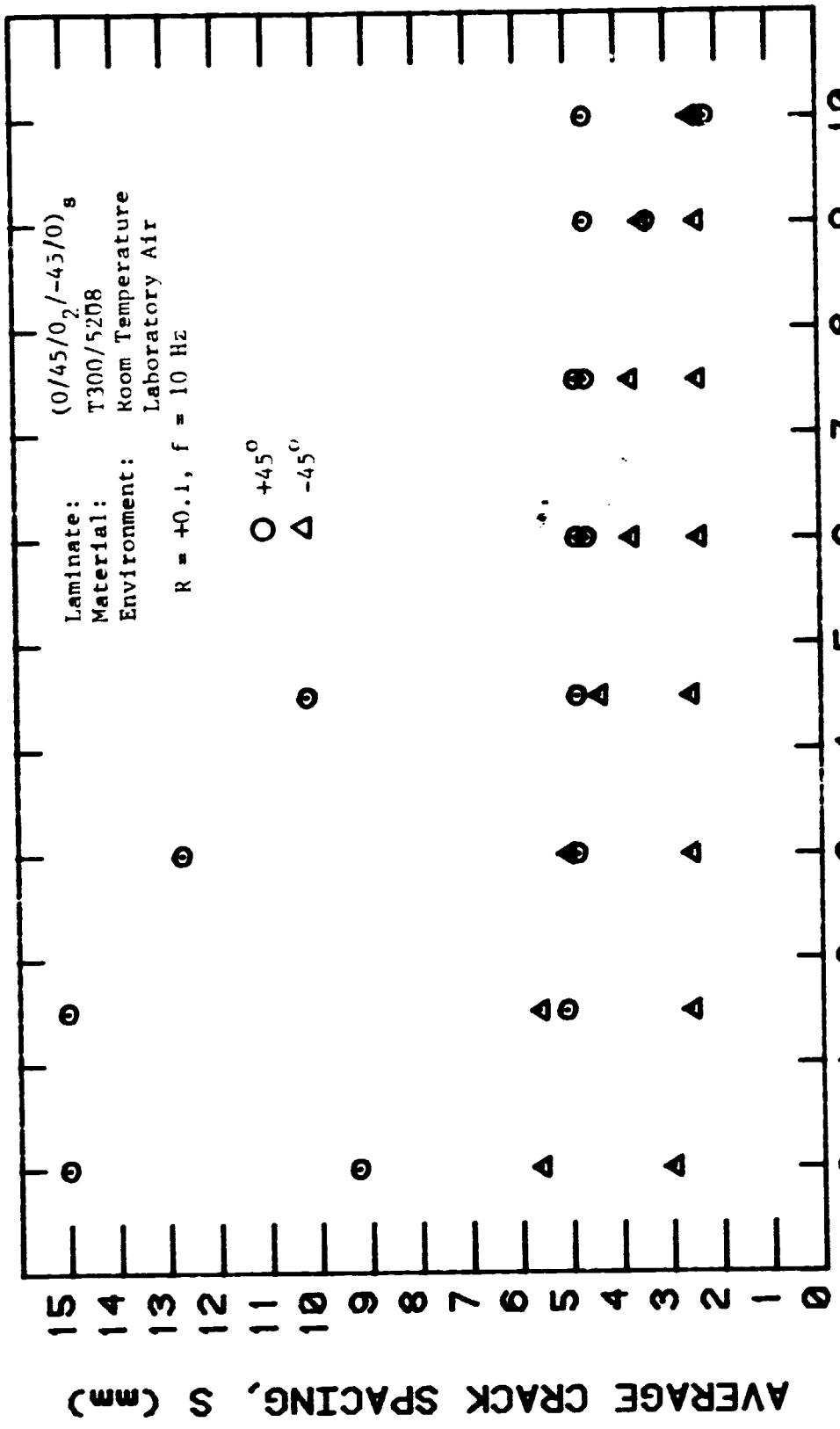

Figure 32: Average crack spacing vs. cycles for $(0/45/0_2/-45/0)_s$ coupons fatigue loaded at an initial strain of 0.0075.

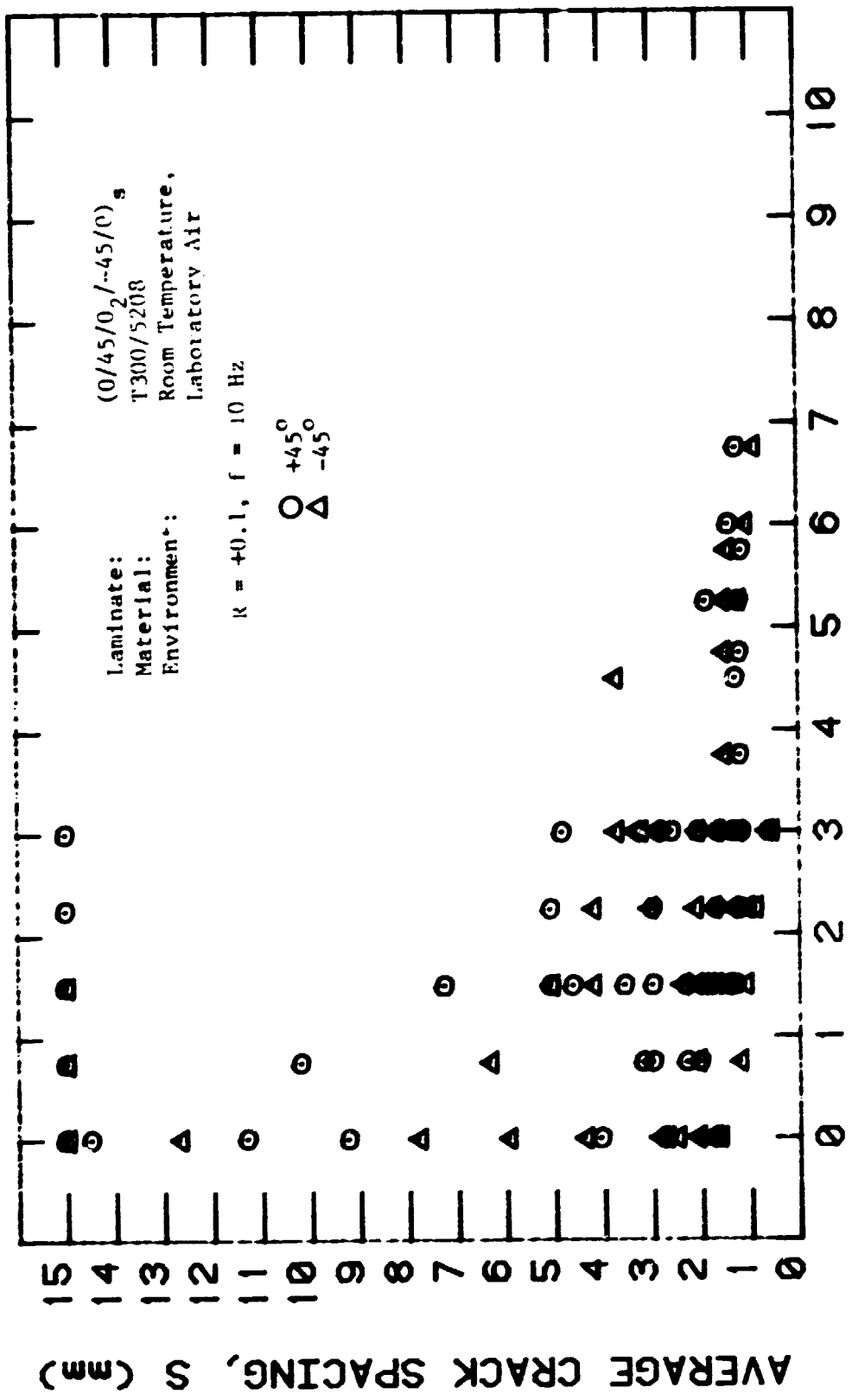

Figure 33: Average crack spacing vs. cycles for $(0/45/0_2/-45/0)_s$ coupons fatigue loaded at an initial strain of 0.0080.

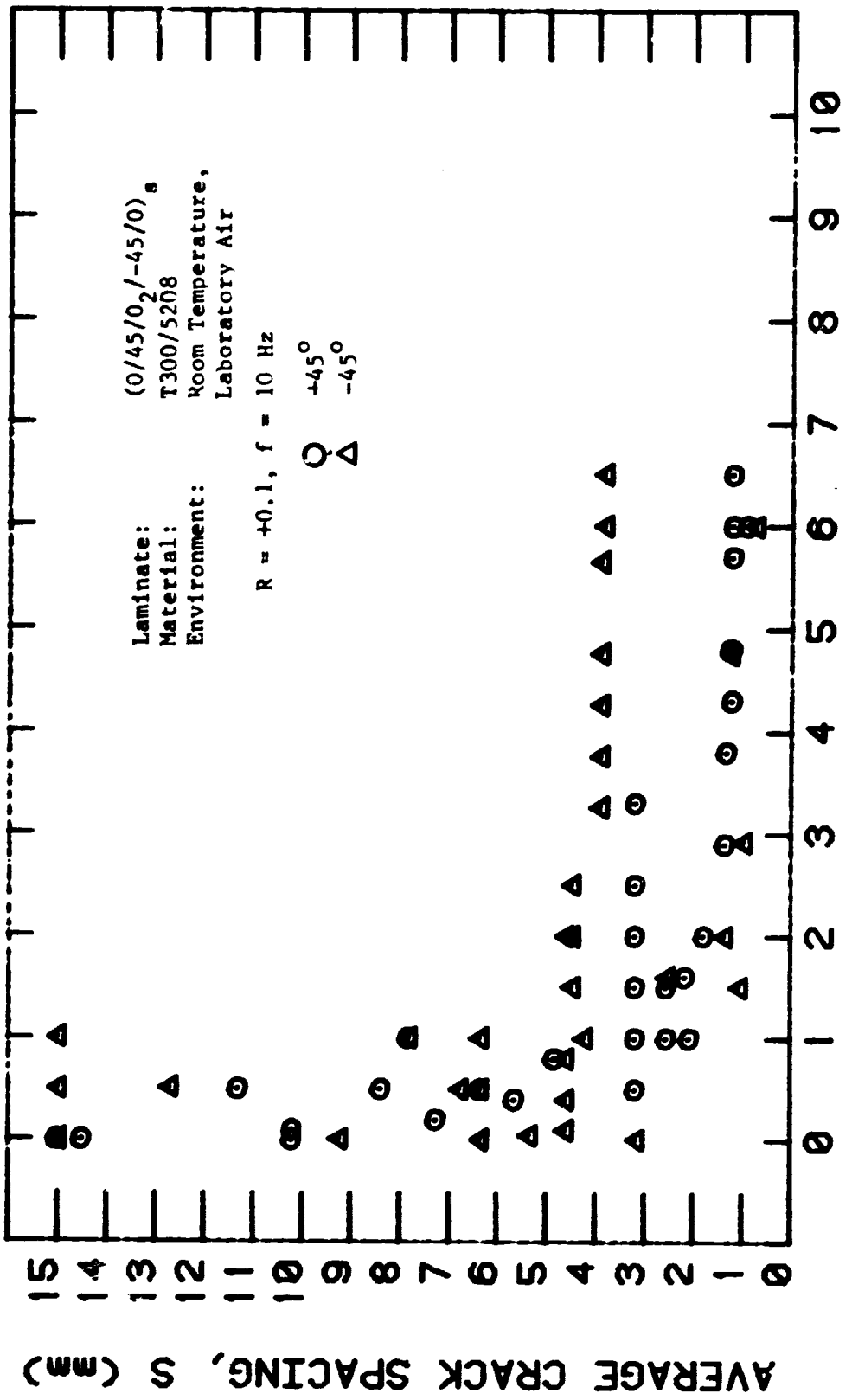

Figure 34: Average crack spacing vs. cycles for $(0/45/0_2/-45/0)_s$ coupons fatigue loaded at an initial strain of 0.0085.

TABLE 27
MATRIX CRACK SPACING UNDER
DIFFERENT LOADING CONDITIONS
FOR $(0/45/0_2/-45/0)_S$ COUPONS

LOADING CONDITION		AVERAGE RANGE IN CRACK SPACING mm $+45^\circ$	-45°
MONOTONIC TENSION		8.47 to -- [a]	0.82 to -- [a]
FATIGUE			
Initial	= 0.0075 [b]	2.21 to 4.62	2.42 to 2.54
	= 0.0080	1.18 to 1.02	0.59 to 3.76
	= 0.0085	0.92 to -- [a]	0.77 to -- [a]
RESIDUAL STRENGTH			
After Fatigue	= 0.0080	0.61 to 4.84	0.69 to 2.99
	= 0.0075	2.21 to 4.62	0.59 to 3.76
Monotonic Tension		0.61 to 5.34	0.69 to 2.99

NOTE: Crack spacing values given were measured just prior to failure or at the end of the loading condition indicated.

a = No matrix cracks observed

b = The two coupons at initial σ of 0.0075 did not fail after 10^6 cycles.

TABLE 28

SUMMARY OF RESULTS FOR FATIGUE AND RESIDUAL STRENGTH LOADING OF $(0/45/0_2/-45/0)_s$ COUPONS

Coupon ID	Initial Maximum Fatigue Strain	Fatigue Cycles (X1000)	Stiffness at End of Fatigue Cycling: Static GPa	Static psi x 10^6	Dynamic GPa	Dynamic psi x 10^6	Extent of Damage	Stress at Fracture MPa	Stress at Fracture ksi	Strain to Failure	Stiffness to Failure GPa	Stiffness to Failure psi x 10^6	Change in Damage State
1ZF1908-86	0.0070	1000	-	-[a]	100.9	14.63	ND[b]	1023	148.4	0.0098	104.3	15.08	None
-B23	0.0075	1000	101.6	14.73	101.1	14.66	ND	1075	155.9	0.0107	100.5	14.57	None
-B24	0.0075	1000	100.9	14.64	101.2	14.67	ND	1098	159.3	0.0108	101.3	14.69	None
-B16	0.0080	300	98.1	14.23	98.9	14.35	D	941	136.5	0.0095	98.7	14.31	None
-B18	0.0080	575	101.1	14.67	96.2	13.95	D	1086	157.5	0.0107	101.3	14.69	None
-B20	0.0080	300	101.7	14.75	101.6	14.73	ND	1076	156.1	0.0107	100.5	14.57	None
-B21	0.0080	300	100.7	14.60	101.4	14.70	ND	1091	158.3	0.0108	101.3	14.69	None
-B29	0.0080	350	-	-[c]	103.1	14.96	D	888	128.8	0.0083	100.1	14.52	None
-B31	0.0080	675	100.1	14.52	101.0	14.65	D	1057	153.4	0.0103	102.6	14.88	None
						Average				0.0102		14.7	
Average of monotonic data for undamaged coupons								1142	165.5	0.0112	102.0	14.8	

a = Fatigue data appears to be incorrect (See Table 1)

b = ND means no delamination visible by enhanced x-ray, matrix cracking only -- D means delamination visible by enhanced x-ray plus matrix cracking.

c = Static stiffness inadvertantly not obtained

TABLE 29

RESULTS OF RESIDUAL STRENGTH LOADING OF $(0/45/0_2/-45/0)_n$ COUPONS

Coupon ID	Average Area, mm^2	Average Area, in^2	Fatigue Cycles (X1000)	Load Level	Strain	Stress, MPa	Stress, ksi	Stiffness, GPa	Stiffness, psi x 10^6	Damage[b] State
1ZF1908-B6	64.0	0.0992	1000	Fatigue	0.0075	--	--	100.9	14.63[a]	ND
				1	0.0085	875	126.9	102.9	14.93	NC
				2	0.0098	1023	148.4	104.0	15.08	F
-B23	63.7	0.0987	1000	Fatigue	0.0075	--	--	101.6	14.73	ND
				1	0.0099	891	129.2	99.0	14.37	NC
				2	0.0100	1003	145.5	100.3	14.54	NC
				3	0.0107	1075	155.9	104.4	15.14	F
-B24	64.0	0.0998	1000	Fatigue	0.0075	--	--	100.9	14.64	ND
				1	0.0090	903	131.0	100.3	14.55	NC
				2	0.0100	1010	146.5	101.1	14.66	NC
				3	0.0105	1065	154.4	101.3	14.69	NC
				4	0.0110	1118	162.2	101.5	14.72	NC
				5	0.0108	1098	159.4	101.3	14.69	F
-B16	64.9	0.1006	300	Fatigue	0.0080	--	--	98.1	14.23	D
				1	0.0090	880	127.7	97.8	14.18	NC
				2	0.0095	941	136.5	98.7	14.31	F
-B18	64.1	0.0994	575	Fatigue	0.0080	--	--	101.1	14.67	D
				1	0.0085	873	126.6	102.0	14.79	NC
				2	0.0090	911	131.1	100.9	14.64	NC
				3	0.0095	967	140.2	101.7	14.75	NC
				4	0.0107	1086	157.5	101.3	14.69	F
-20	63.5	0.0984	300	Fatigue	0.0080	--	--	101.7	14.75	ND
				1	0.0090	898	130.3	99.9	14.49	NC
				2	0.0095	949	137.7	99.9	14.49	NC
				3	0.0100	1001	156.3	100.1	14.52	NC
				4	0.0105	1057	152.9	100.4	14.56	NC
				5	0.1017	1076	156.1	100.5	14.57	F
-21	64.5	0.1000	300	Fatigue	0.0080	--	--	100.7	14.60	ND
				1	0.0090	913	132.4	101.5	14.72	NC
				2	0.0100	1013	146.9	101.2	14.68	NC
				3	0.0105	1063	154.2	101.3	14.69	NC
				4	0.0108	1091	158.3	101.3	14.69	F
-29	63.5	0.0985	350	Fatigue	0.0080	--	--	100.4	14.56	D
				1	0.0085	855	124.0	100.6	14.59	NC
				2	0.0089	888	128.8	100.2	14.54	F
-31	63.9	0.0991	675	Fatigue	0.0080	--	--	100.1	14.52	D
				1	0.0095	857	124.4	100.7	14.60	NC
				2	0.0095	969	137.7	99.9	14.50	NC
				3	0.0103	1057	153.4	102.6	14.88	F

a = Reading taken at 300,000 cycles.
b = ND means no delamination, matrix cracking only -- D means delamination plus matrix cracking -- NC means no change -- F means failure.

TABLE 30
FRACTURE LOCATION DATA FOR $(0/45/0_2/-45/0)_S$ COUPONS
LOADED IN RESIDUAL STRENGTH AFTER CONSTANT AMPLITUDE FATIGUE LOADING

Coupon ID	Initial Strain Level	Average Fracture Location[a] mm	in.
B6	0.0070	0.0	0.0
		+64	+2.5
B23	0.0075	+71	+2.8
		-46	-1.0
B24		0.0	0.0
		+51	+2.0
B16	0.0080	-69	-2.7
		-89	-3.2
B18		-25	-1.0
B20	Test Section Exploded	-	-
B21		+18	+0.7
		+64	+2.5
B29		-66	-2.6
		-81	-3.2
B31	Test Section Exploded	-	-

a = A double entry indicates a region of fracture since damage was extensive.

load steps as shown in Table 29. Detailed stiffness and matrix cracking data obtained during fatigue loadings are given in Appendix C, Tables C57 and C58.

Edge replications were obtained at each load step, but enhanced x-ray photographs were only obtained if edge delamination occurred. Such delamination did not occur prior to failure in five of the coupons. Four coupons contained edge delamination after fatigue testing and enhanced x-ray photographs were obtained at each load step. The damage state at the end of fatigue loading within the non-delaminated coupons consisted only of transverse matrix cracking with short delaminations at their ends. The extent of matrix cracking or delamination did not change during residual strength loading from that observed just prior to fatigue loading, see Table 29. The stiffness in these residual strength coupons was also essentially the same as that of the undamaged monotonic tension coupons.

Strain to failure, and hence strength, was reduced by an average of approximately nine to ten percent below that of the undamaged coupons. However, the strain to failure of some coupons was reduced by as much as 20 percent below the previous average monotonic tension value. Although the strain to failure was reduced in all of the residual strength coupons, the presence of edge delamination, visible by enhanced x-ray, clearly had the most direct correlation to strain at failure, as shown in Table 28. However, the thumbnail like delamination of coupon B18 did not correlate with a large reduction in strain to failure. For all residual strength coupons, strain to failure was again, as for the $(0/90/\pm45)_s$ and $(0/\pm45)_s$ coupons, considerably higher, by 10 to 25 percent, than that of the coupons loaded in fatigue to failure.

Since the presence of fatigue load induced matrix cracking and delamination did not affect stiffness nor reduce strain to failure under residual strength loading to levels equivalent to strain levels at fatigue failure, the cause of the reduction in strain to failure under fatigue loading was of

interest. In essence, something occured under fatigue loading which was not usually encountered under the residual strength monotonic loading. This was attributed to local fiber fracture which was observed not only near the coupon edges, but also on the surface away from the edges, similar to the $(0/\pm45)_s$ coupons. Further discussion of this point will be continued in Section 4 where a comparative summary of the results for all of the layups is given.

2.5 RESULTS FOR $(0_2/\underline{90}_4)_s$ COUPONS

The failure data for the monotonic tension experiments of $(0_2/90_4)_s$ coupons are given in Table 31. Fracture of the $(0_2/90_4)_s$ coupons in monotonic tension occurred in a highly explosive manner. Usually, no specific site of fracture could be discerned. However, the outer 0^o plies fractured along lines parallel to the 90^o plies.

The stiffness of these monotonically loaded coupons usually decreased during each loading, see Table 32, which followed a load interruption to obtain NDI data. The decrease in stiffness was pronounced enough that three additional coupons were fractured in monotonic tension at the same strain rates as before, but without any load interruptions. The results for these three coupons are also given in Table 31. The reason for the low strain to failure of these coupons compared to the other layups of this study is discussed in detail in Section 3, but, in summary, was due to an increase in stress in the 0^o ply adjacent to the end of the 90^o ply transverse matrix cracks. This occurs because a matrix crack in the 8 ply thick 90^o ply induces a stress concentration over a larger region than that due to a single ply thickness and because all of the load in the vicinity of the 8t 90^o ply is essentially dumped into the 0^o ply.

The stiffness (secant modulus to failure) of the three coupons loaded without interruption was the same as the final stiffness value of the previous five coupons used to obtain NDI data, although the average strain

TABLE 31
FAILURE DATA FOR MONOTONIC TENSION EXPERIMENTS
OF $(0_2/90_4)_s$ COUPONS

Coupon ID	Average Area, mm^2	Average Area, $in.^2$	Stress At Fracture, MPa	Stress At Fracture, ksi	Strain At Fracture, mm/mm in 101.6 mm	Stiffness[c] To Failure GPa	Stiffness[c] To Failure Msi	Stiffness To 0.0065 Strain GPa	Stiffness To 0.0065 Strain Msi
COUPONS USED TO OBTAIN NDI DATA									
1ZF1906									
-A1[a]	62.1	0.0963	409	59.3	0.00805	52.2	7.36	51.6	7.48
-A2	63.1	0.0978	689	71.6[b]	0.01027[b]	48.1	6.98	51.2	7.42
-A3	62.4	0.0968	459	66.6	0.00992	46.3	6.72	48.3	7.00
-A4	61.7	0.0957	402	58.3	0.00874[b]	46.0	6.67	48.6	7.05
-A5	63.3	0.0981	456	66.2[b]	0.00951[b]	48.0	6.96	50.0	7.25
COUPONS LOADED WITHOUT LOAD INTERRUPTION OR NDI									
-A7	62.4	0.0968	409	59.3	0.00854	47.7	6.92	52.7	7.64
-A23	62.4	0.0968	372	54.0	0.00767	48.3	7.00	51.0	7.40
-A28	63.6	0.0986	450	65.2	0.00895	50.2	7.28	54.2	7.86
Average			411	62.6	0.00896	48.2	6.99	51.0	7.39

a = Coupon used for damage documentation by in-situ enhanced x-ray.

b = Highest stress and strain values reached, coupon failed on next loading cycle at slightly lower values.

c = Secant modulus values.

d = Secant modulus not recorded at 0.002

TABLE 32

STIFFNESS DATA OBTAINED DURING MONOTONIC TENSION EXPERIMENTS OF $(0_2/90_4)s$ COUPONS

COUPON ID	Strain Level mm/mm in 101.6 mm	Stiffness GPa	Msi	
1ZF1906				
-A1	0.00201	51.6	7.48	
	0.00300	51.7	7.50	
	0.00401	52.3	7.59	
	0.00501	52.3	7.59	
	0.00603	52.3	7.58	
	0.00705	52.2	7.57	
	0.00805	50.8	7.36	Failed on loading.
-A2	0.00202	51.2	7.42	
	0.00303	51.6	7.49	
	0.00782	49.3	7.15	
	0.00803	48.7	7.06	
	0.00855	48.5	7.03	
	0.00903	48.0	6.96	
	0.00928	48.0	6.96	
	0.00953	48.0	6.96	
	0.01000	48.2	6.99	
	0.01027	48.1	6.98	Failed on next loading cycle at slightly lower value.
-A3	0.00304	49.1	7.12	
	0.00601	49.7	7.21	
	0.00703	48.4	7.02	
	0.00752	46.8	6.79	
	0.00804	46.5	6.75	
	0.00880	46.6	6.76	
	0.00928	46.3	6.72	
	0.00979	46.2	6.70	
	0.00992	46.3	6.72	Failed on loading.
-A4	0.00807	47.7	6.92	
	0.00853	46.5	6.74	
	0.00874	46.0	6.67	Failed on loading.
-A5	0.00752	51.0	7.40	
	0.00803	48.5	7.03	
	0.00827	48.0	6.96	
	0.00854	48.0	6.96	
	0.00903	47.8	6.93	
	0.00951	48.0	6.96	Failed on next loading cycle at slight lower value.

to failure was lower perhaps due to a low sample size and hence statistical variation. The generally decreasing stiffness of the coupon load interrupted for NDI could now be understood. The three coupons tested without load interruption exhibited an easily noticeable decrease in stiffness by the time a strain level of 0.0065 was reached. This decreasing stiffness changed more rapidly as failure was approached, due to the increasing number of transverse cracks. The secant stiffness to failure was an average of 6.0 percent less than that up to 0.0050 strain for the last four coupons of Table 32. The amount of stiffness loss prior to failure was the least for coupon A1. Significantly, coupon A1 exhibited the least amount of transverse 90° ply matrix cracks prior to failure.

A plot of the observed matrix crack spacing in the 90° plies versus strain was made and is shown in Figure 35. The previously mentioned 6 percent change in stiffness of these coupons can be seen to correspond to the strain levels where an apparent plateau in the number of transverse 90° ply matrix cracks began to occur. Coupon A1 fractured prior to saturation and thus exhibited little stiffness change. These coupons all had a few 90° ply, transverse matrix cracks prior to loading, approximately 2 to 3 per 25 mm. These manufacture induced cracks were presumably due to thermal stresses which develop during panel cool down. The detailed matrix crack spacing data are tabulated in Appendix C, Table C59.

Damage progression during monotonic tension loading consisted primarily of 90° ply matrix cracks perpendicular to the load direction. Delamination during monotonic loading was not observed by enhanced x-ray, and on the edge replicates delamination extending from the ends of 90° plies was usually short, but obvious and often absent until near coupon failure. At that point, 0/90 delaminations on the coupon edges nearly, but not completely linked together. The spacing of the 90° ply matrix cracks decreased as load increased and tended towards an apparent plateau spacing. However, as in the case of coupon A1, fracture sometimes occurred prior to reaching that

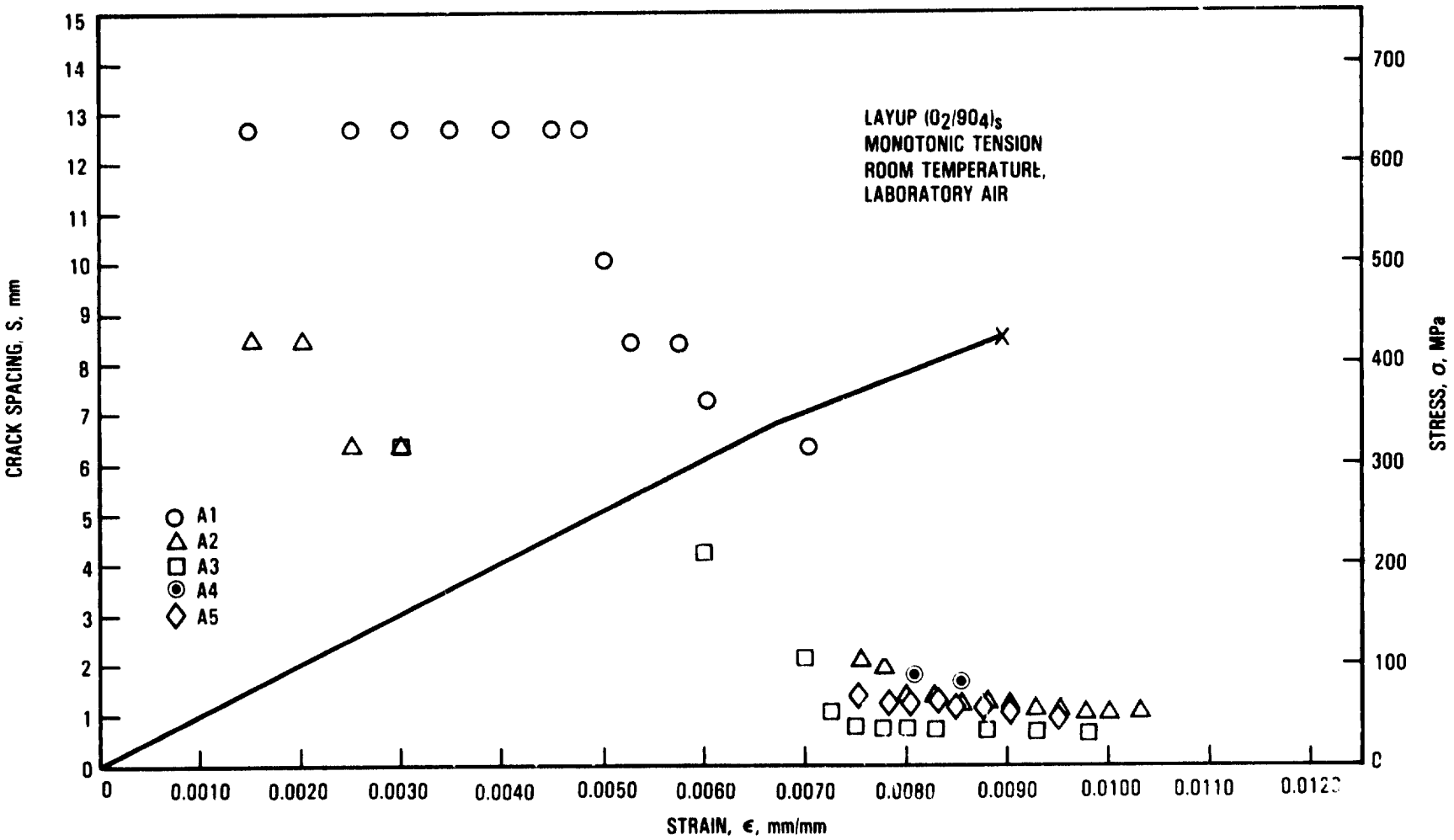

FIGURE 35. CRACK SPACING AND STRESS AS A FUNCTION OF STRAIN FOR $(0_2/90_4)_s$ COUPONS

plateau presumably due to the large stress concentration previously mentioned. A stiffness loss up to 6 percent corresponded to the plateau level matrix crack spacing.

The plotted results of Figure 35 are somewhat misleading since the data shown in Figure 35 do not truly represent the complexity shown in Figure 36. Figure 36 shows three typical, although severe regions of matrix cracking usually found in the monotonically loaded coupons. Most regions of transverse cracking were regular in nature, but regions like that shown in Figure 36 were commonly observed. The 90° matrix crack pattern is clearly appparent in this figure, but so are vertical matrix cracks and complex crack patterns at other angles. For the purposes of analysis, the secondary cracks were assumed to be of less importance than the 90° cracks because these vertical type cracks did not appear to extend significantly into the coupon interior.

These comments on other forms of matrix cracking not withstanding, a pattern of matrix cracks within the 90° plies and perpendicular to the load direction still was the primary form of matrix cracking. Figure 35 showed that crack spacing, hence number of cracks per unit length, did reach an apparent plateau in four coupons prior to failure at around 1 mm between cracks. The results for coupon A4 show that even if only two prior loadings before failure were applied, the crack spacing was about the same. This indicated a lack of a significant influence of the number of prior loadings on final crack spacing, an observation supported by the similarity in stiffness of coupons subjected to and not subjected to load interruption.

Table 33 gives the fatigue life data for the $(0_2/90_4)_s$ coupons. Like the $(0/45/0_2/-45/0)_s$ coupons, these fatigue coupons were loaded to a specific initial strain level, based on initial monotonic modulus, and cycled at constant load to failure. The maximum percent stiffness loss data for these fatigue loaded coupons are given in Table 34. Stiffness losses of up to 18 percent were recorded. The detailed stiffness loss data are tabulated in

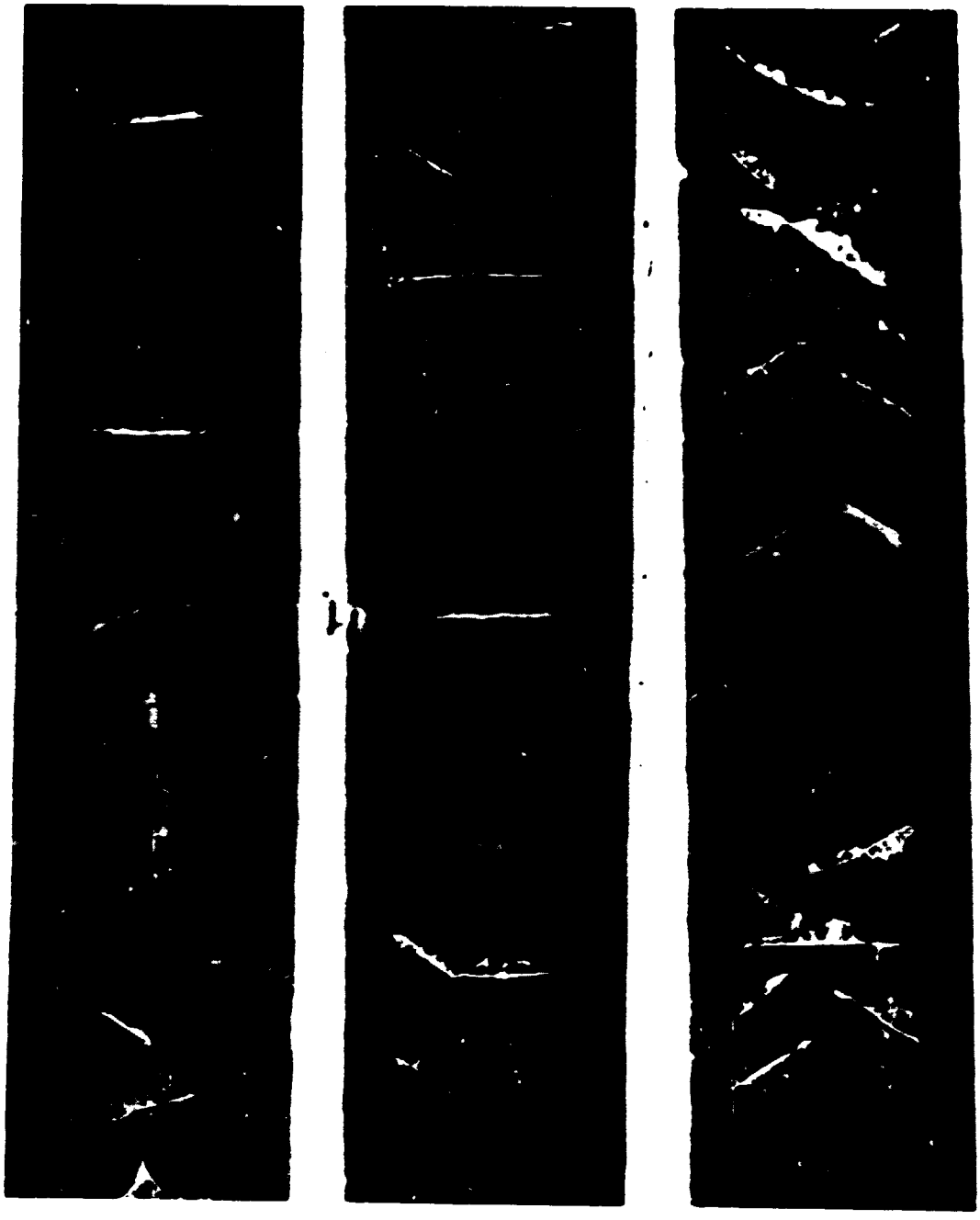

Figure 36: Transverse matrix crack patterns found in Coupon A3 at 0.00975 strain.

TABLE 33

FAILURE LIVES OF $(0_2/90_4)$ COUPONS

COUPON ID	STRAIN LEVEL	CYCLES TO FAILURE
A15	0.0050	445 000
A20		>1 000 000[a]
A21		>1 000 000[a]
A25		>1 000 000[a]
A6	0.0060	> 692 000[b]
A14		28 400
A24		253 600
A31		>1 000 000[a]
A8	0.0065	74 200
A9		14 150
A10		36 960
A27		164 910
A16	0.0075	430
COUPONS USED FOR RESIDUAL STRENGTH EXPERIMENTS		
A12	0.0060	> 68 000
A13		> 30 000
A20		> 690 000
A26		> 35 000
A11	0.0065	> 35 000
A17		>1 000 000
A32		> 25 500

a = Coupon intented for fatigue fatilue, but used for residual strength after reaching 10^6 cycles.

b = Accidentally failed in tension

Appendix C, Table C60. The dynamic stiffness losses appeared to be generally less than the monotonic. However, as shown in Table C60 of Appendix C, dynamic and monotonic moduli were always essentially identical. Therefore the difference in percent stiffness losses were attributed to changes in dynamic stiffness prior to initial recording.

The percent monotonic and dynamic stiffness loss values in Table 34 are based upon the initial monotonic stiffness and the initial dynamic stiffness, taken as early in fatigue life as possible, respectively. The initial dynamic stiffness was recorded as soon as possible because stiffness changed rapidly early in fatigue life due to the rapid saturation of transverse matrix cracking in the 90° plies. Accurate monotonic stiffness changes as representations of the development of damage were difficult to obtain because, as previously discussed, the stress-strain curve of this layup is essentially linear up to approximately 0.0050 strain and noticeably differs by 0.0065 strain. Therefore, the initial monotonic stiffnesses are values somewhat reduced by significant prior damage.

The fatigue loading induced damage which occurred in these coupons was more complex than that observed in the other layups of this investigation. Detailed data are given in Appendix C, Table C61. Matrix cracking consisted of not only 90° ply cracks which went across all 8 plies, see Figure 37, but also of cracks (or delamination if one prefers) parallel to the 0° plies but down the mid plane of the 90° plies. However, as in the monotonically loaded coupons, these midplane cracks did not appear to extend very far into the coupons. In addition there were often regions of a quite complex pattern which contained matrix cracks (delaminations ?) of various other angles such as previously shown in Figure 37. The edge replicates showed that transverse matrix cracking reached an apparent saturation plateau early in the fatigue life of the coupon, in 5 000 cycles or less. This is illustrated in Figure 38 which shows the typical matrix crack pattern, as found by edge replication, for coupon A6. The only difference between 5 000 and 692 000 cycles was in the length of 0/90 interface delamination and the amount of opening of the matrix cracks.

TABLE 34
SUMMARY OF MAXIMUM PERCENTAGE
STIFFNESS LOSS DUE TO FATIGUE LOADING FOR $(0_2/90_4)_s$ COUPONS

Coupon ID	Strain Level	Fatigue Cycles, Thousands	Percent Loss in Monotonic Stiffness	Percent Loss in Dynamic Stiffness	Remarks
A15	0.0050	445 000	9.3	6.6	Failed at 445 100
A21		1 000 000	9.2	8.9	No Failure
A22		1 000 000	8.9	6.9	No Failure
A25		1 000 000	9.3	7.1	No Failure
A6	0.0060	692 000	6.3	6.2	
A14		20 000	-	15.6	Failed at 28 400
A24		238 000	17.1	12.8	Failed at 253 600
A31		1 000 000	12.4	10.7	No Failure
A8	0.0065	50 000	12.0	9.0	Failed at 74 200
A9		14 150	5.9	1.4	
A10		35 000	-	5.0	Failed at 36 960
A27		160 000	7.7	6.7	Failed at 164 910

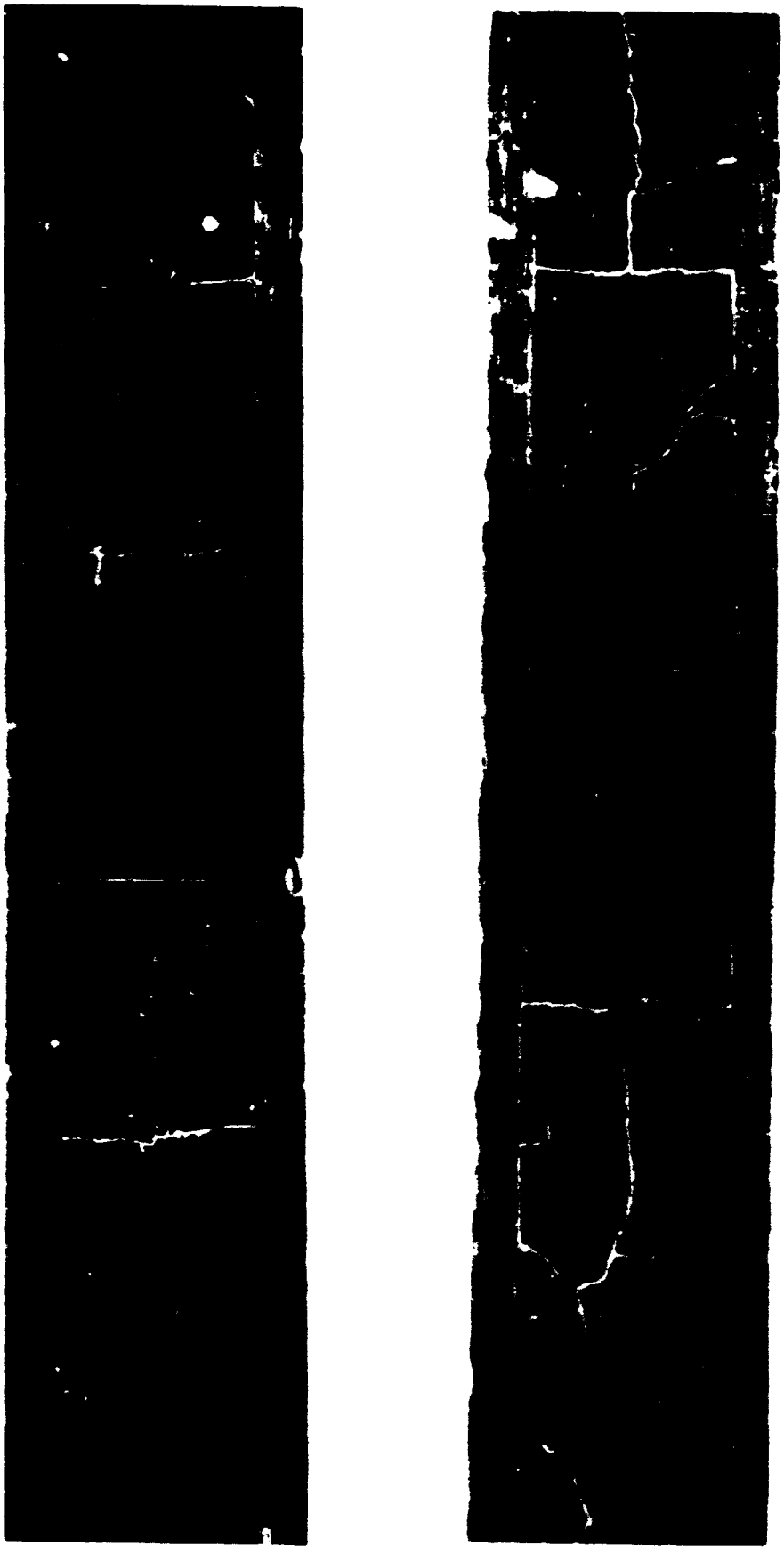

Figure 37: Edge delamination regions found on $(0_2/90_4)_s$ coupon A8 after 50 000 fatigue cycles.

Figure 38: Edge replicates of same location of coupon A6 fatigue cycled at $\epsilon_i = 0.006$.

Enhanced x-ray photographs revealed several interesting features of damage development. They first confirmed that transverse matrix cracking generally saturated by about 5 000 to 10 000 load cycles as shown in Figure 39. The enhanced x-ray photographs, such as that of Figure 39, required higher magnification examination to see this saturation because the width of the transverse cracks varied significantly. Thus, for example, the region in the photograph at 5 000 cycles in Figure 39 which appears to show few matrix cracks was found, on closer inspection, to be essentially saturated with very tight cracks. In other regions, the transverse cracks were much wider and thus appear darker. Additional transverse matrix cracking did occur up to as much as 100 000 cycles.

Another feature was the appearance and growth of longitudinal splits in the 0° plies which started away from the coupon edges eventually growing to the grip region, see Figure 39. Finally, the third damage feature was 0/90 interface delamination which started at the intersections of the 90° transverse matrix cracks and the 0° longitudinal splits. These grew and coalesced as the number of cycles increased, see Figures 39 to 41. The edge stress induced delaminations only extended in the width direction of the coupons a distance about equal to the laminate thickness. Thus, the delaminations which grew from the intersection of the 90° matrix cracks and 0° splits were the dominant delamination mode.

Jamison and Reifsnider[40] rather plausibly attributed the 0° longitudinal splitting to Poisson mismatch between the 0° and 90° plies. They also found that the 0° splits always went completely through the 0° plies. This phenomenon was also observed in this program because when 0° fiber fracture occurred near the grip region, this often resulted in an entire section of a 0° degree ply between splits to separate from the coupon. Finally, Jamison and Reifsnider[40] showed that a rather simple fracture mechanics analysis of crack tip stresses for the 90° cracks implied that the 0° splits should initiate at the matrix crack tips. Further, they[40] postulated that the stresses induced by the 0° splits and the 90° transverse cracks at an

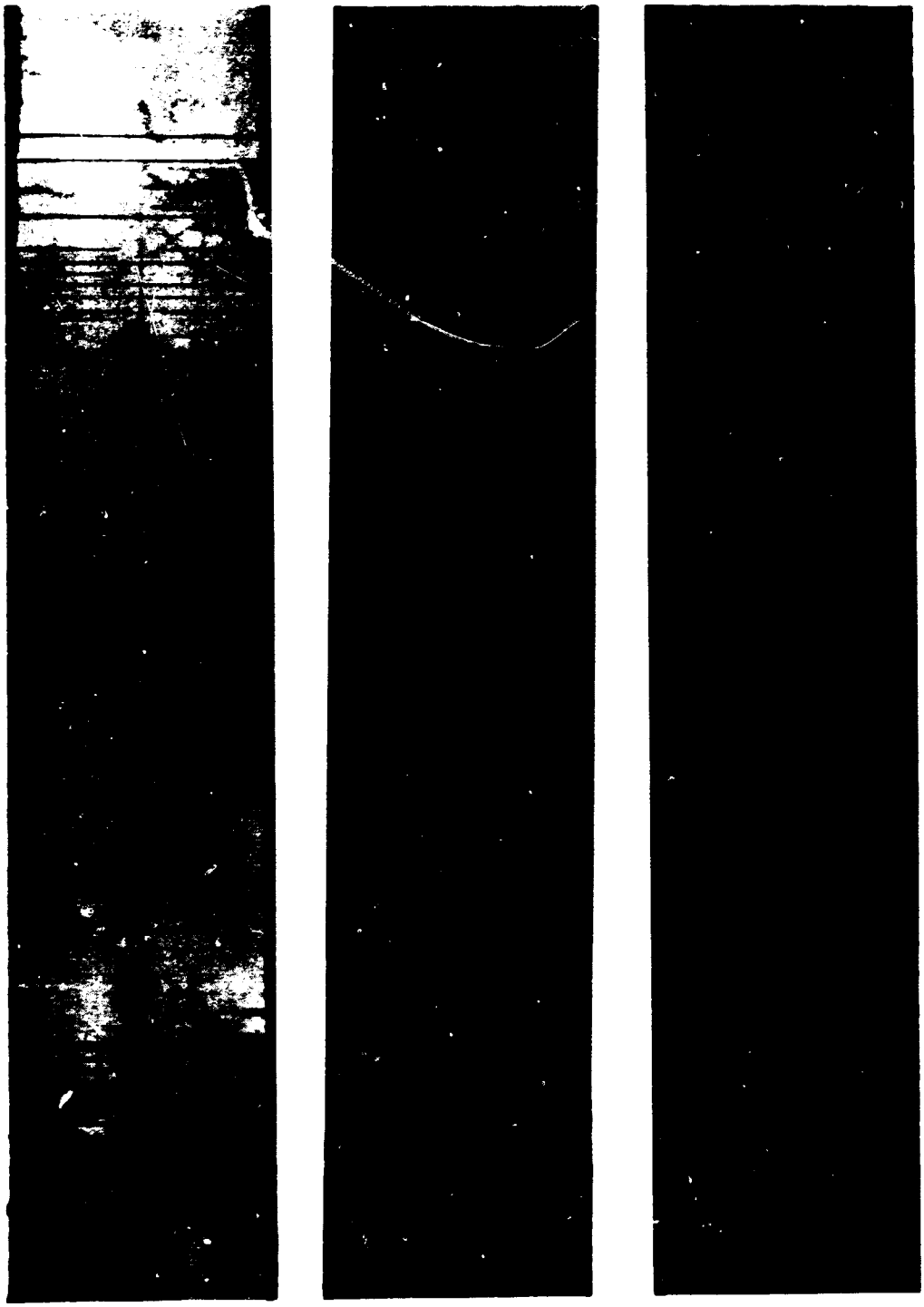

1 000 5 000 692 000

Figure 39: Enhanced x-ray photographs of coupon A6 showing 90^{o} matrix cracking, 0^{o} splits, and delamination; Initial $\epsilon = 0.006$.

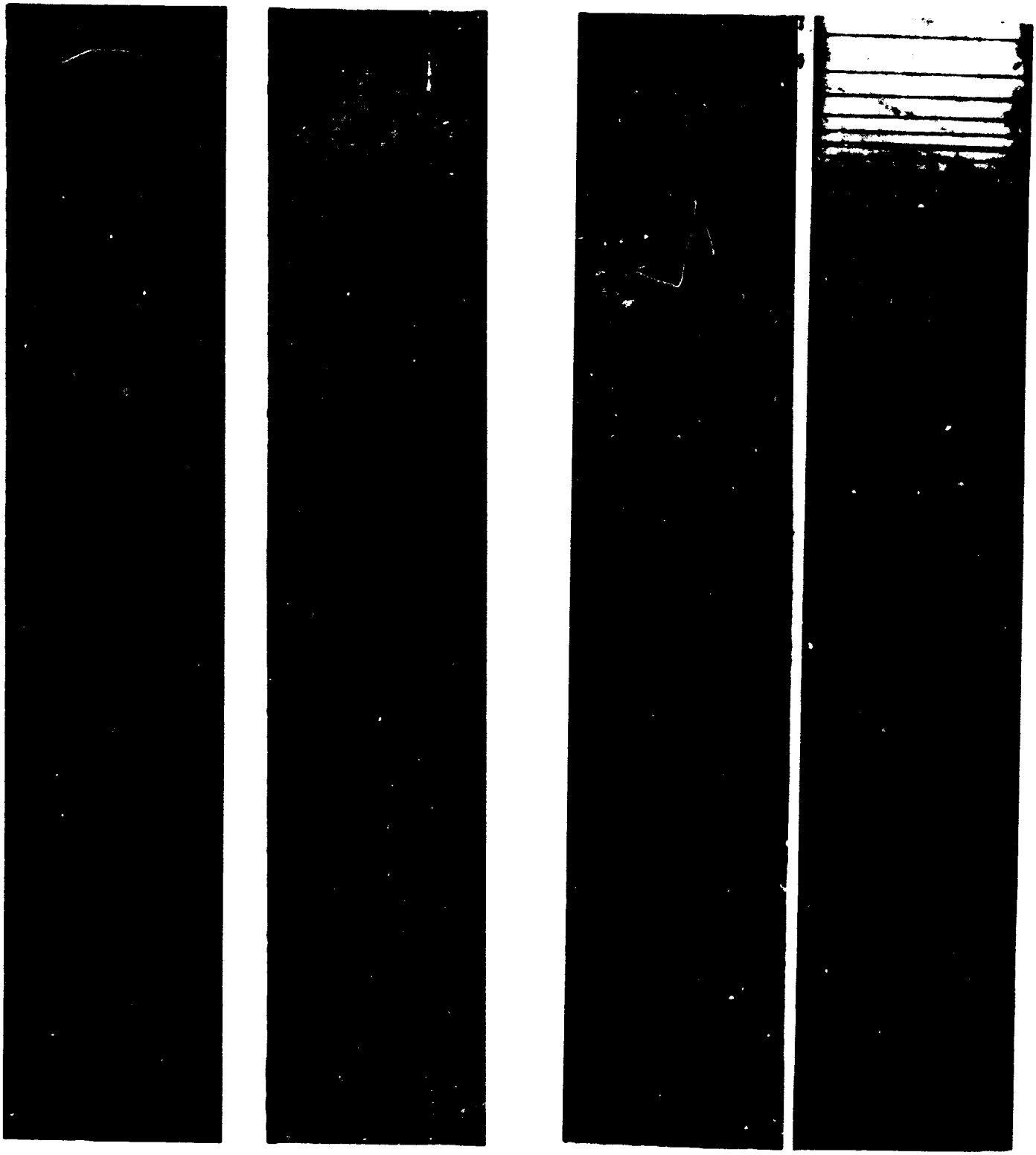

100 000 300 000 600 000 1 000 000

Figure 40: Enhanced x-ray photographs of coupon A22 showing 90° matrix cracking, 0° splits, and delamination; Initial $\epsilon = 0.005$.

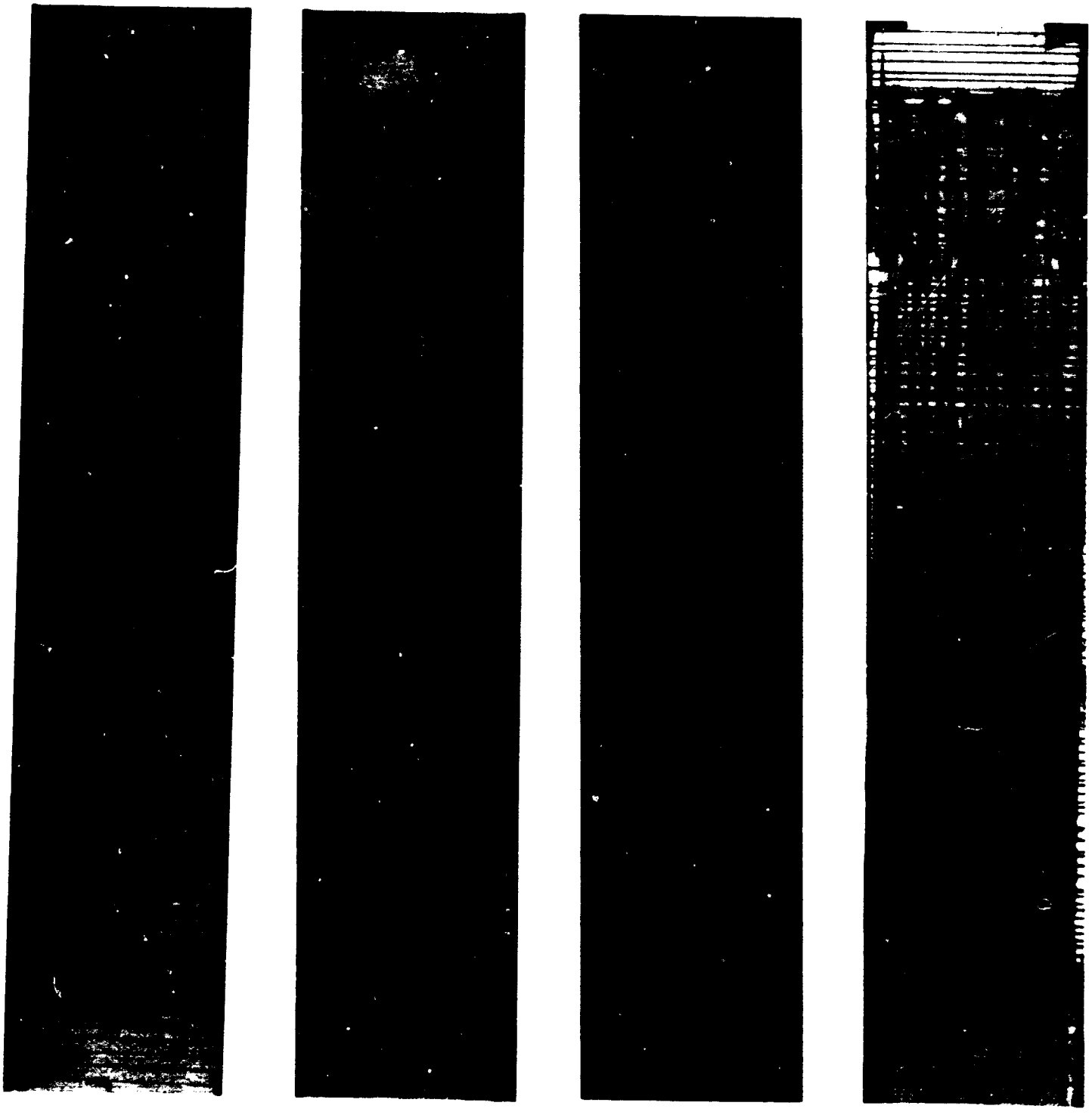

118 000 300 000 682 000 1 000 000

Figure 41: Enhanced x-ray photographs of coupon A31 showing 90^{o} matrix cracking, 0^{o} splits, and delamination; Initial ϵ = 0.006.

intersection should induce delamination, which, in fact, appeared to initiate at those intersections.

The fracture event of these fatigue loaded $(0_2/90_4)_s$ coupons was extremely violent, much like those fractured in monotonic tension. The 0° fibers fractured along a 90° line, but generally not clear across the coupon width because of the 0° longitudinal splits. Multiple fracture regions occurred, some near the grips because of the 0° fiber breaks induced there. Most coupons essentially shattered without a clearly defined failure zone. Notable, numerous 0° fiber fracture regions were observed prior to coupon failure, often long before overall coupon fracture.

Figures 42 to 44 show plots of the transverse matrix crack spacing in the 90° plies versus load cycles. Since study of the enhanced x-ray photographs showed that the 90° transverse cracks usually went across the coupon width, Figures 42 to 44 again indicate that matrix crack saturation occurred early in fatigue life. The saturation levels were similar for each fatigue strain level with some decrease in crack spacing apparent as the strain level increased. The range in observed spacing was more restricted than that seen under monotonic tension load, see Table 35.

Normalized monotonic stiffness is plotted versus crack spacing in Figures 45 to 47 where the normalized value was the initial recorded monotonic stiffness. The data used to plot these three figures plus allowance for stiffness change on initial loading indicate that approximately 5.5 percent of the stiffness loss at 0.0050 strain could be attributed to the development of transverse cracks in the 90° plies. At 0.0060, approximately 6.5 percent of the observed stiffness loss correlated to matrix cracking while at 0.0065 strain, the amount of stiffness loss was closer to 7.0 percent. The differences among the strain levels were attributed to the slightly different matrix crack saturation levels. The 0° longitudinal matrix cracks did not appear to cause a measurable percent stiffness loss as Jamison and Reifsnider discussed[40]. Thus the remaining amount of stiffness loss was attributed to delamination development either from the intersection of the 0° splits and the 90° matrix cracks or along

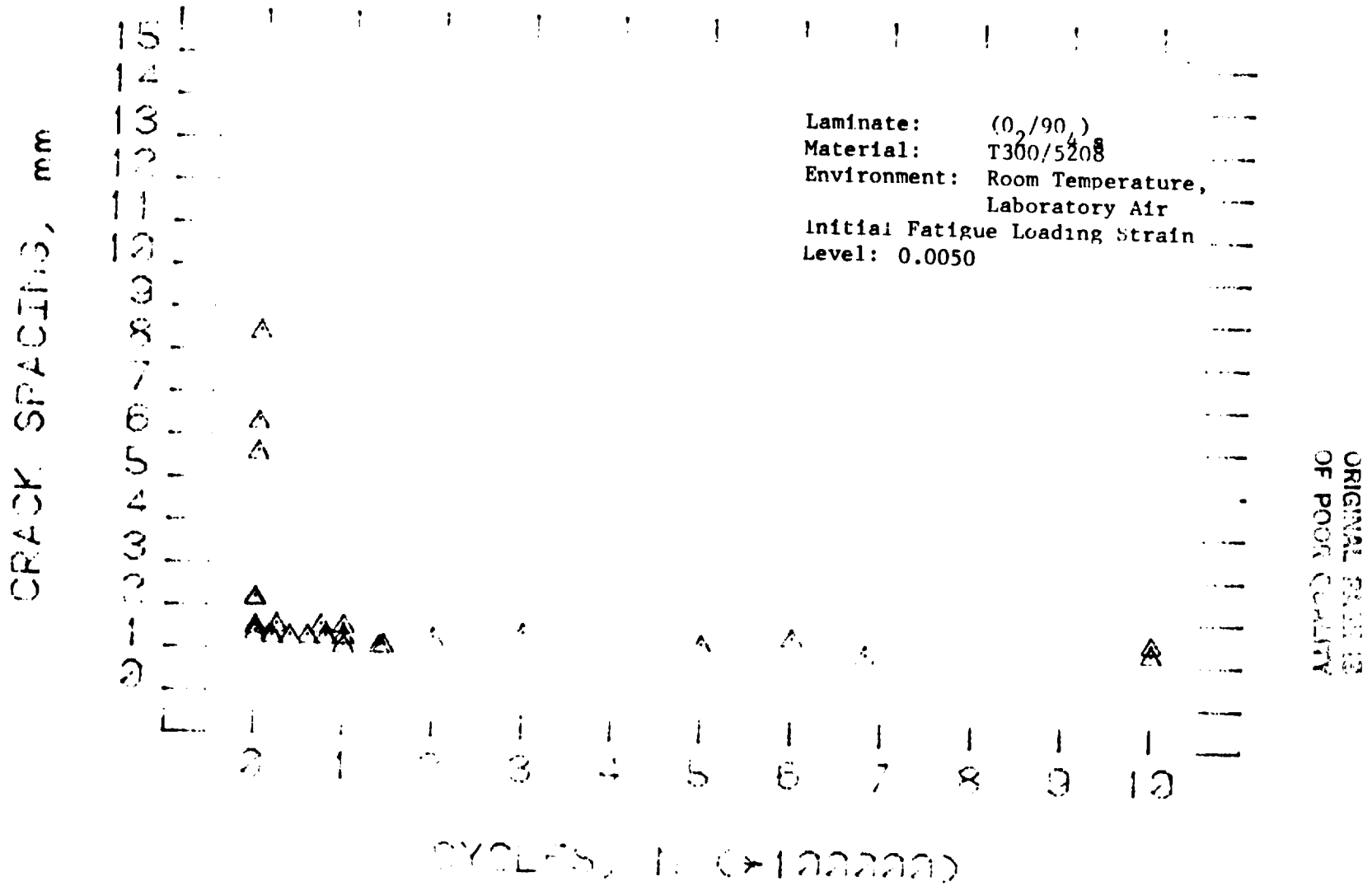

Figure 42: Average matrix crack spacing in the 90° plies vs. cycles for $(0_2/90_4)_s$ coupons fatigue cycled at an initial strain of 0.0050.

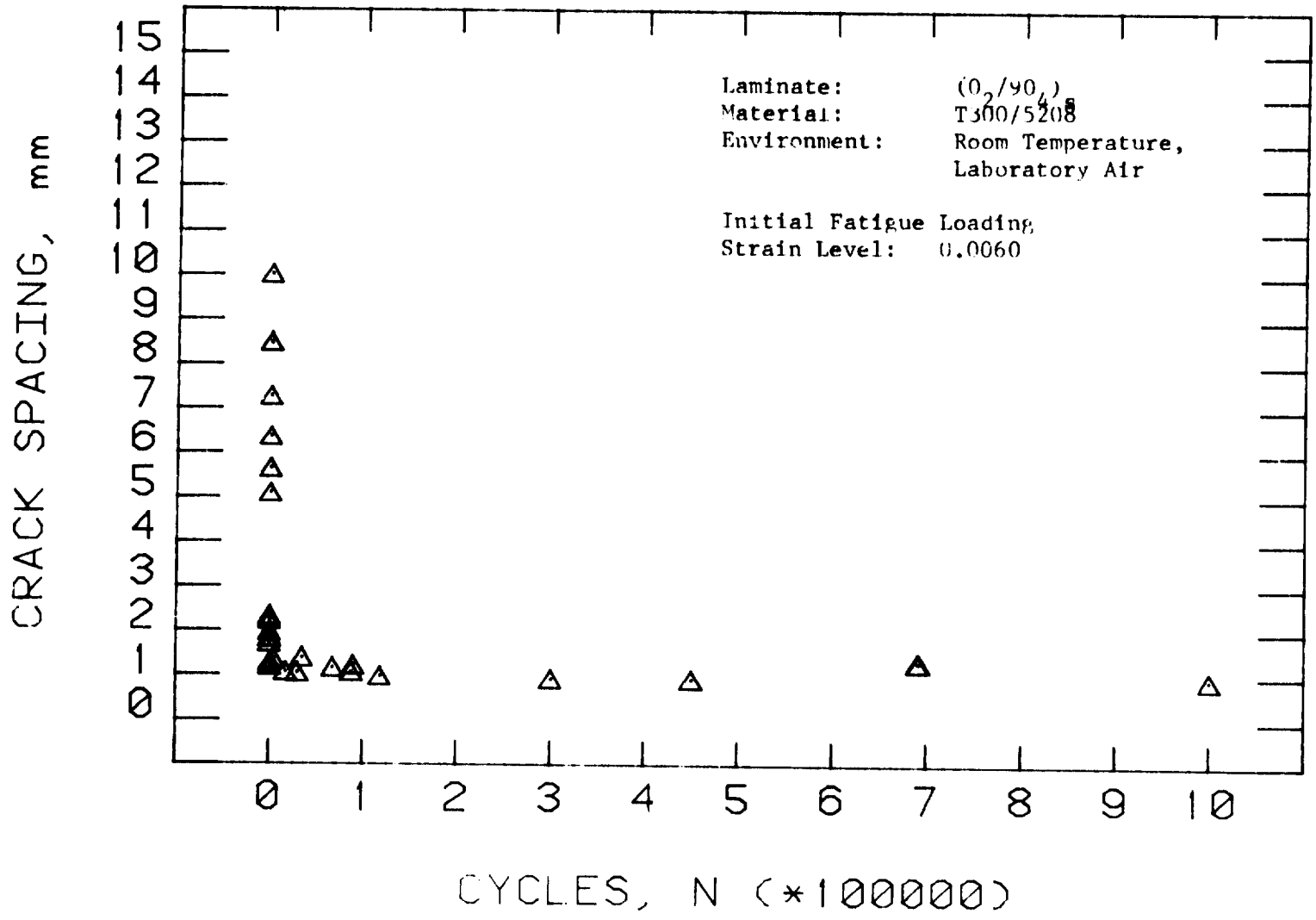

Figure 43: Average matrix crack spacing in the 90° plies vs. cycles for $(0_2/90_4)_s$ coupons fatigue cycled at an initial strain of 0.0060.

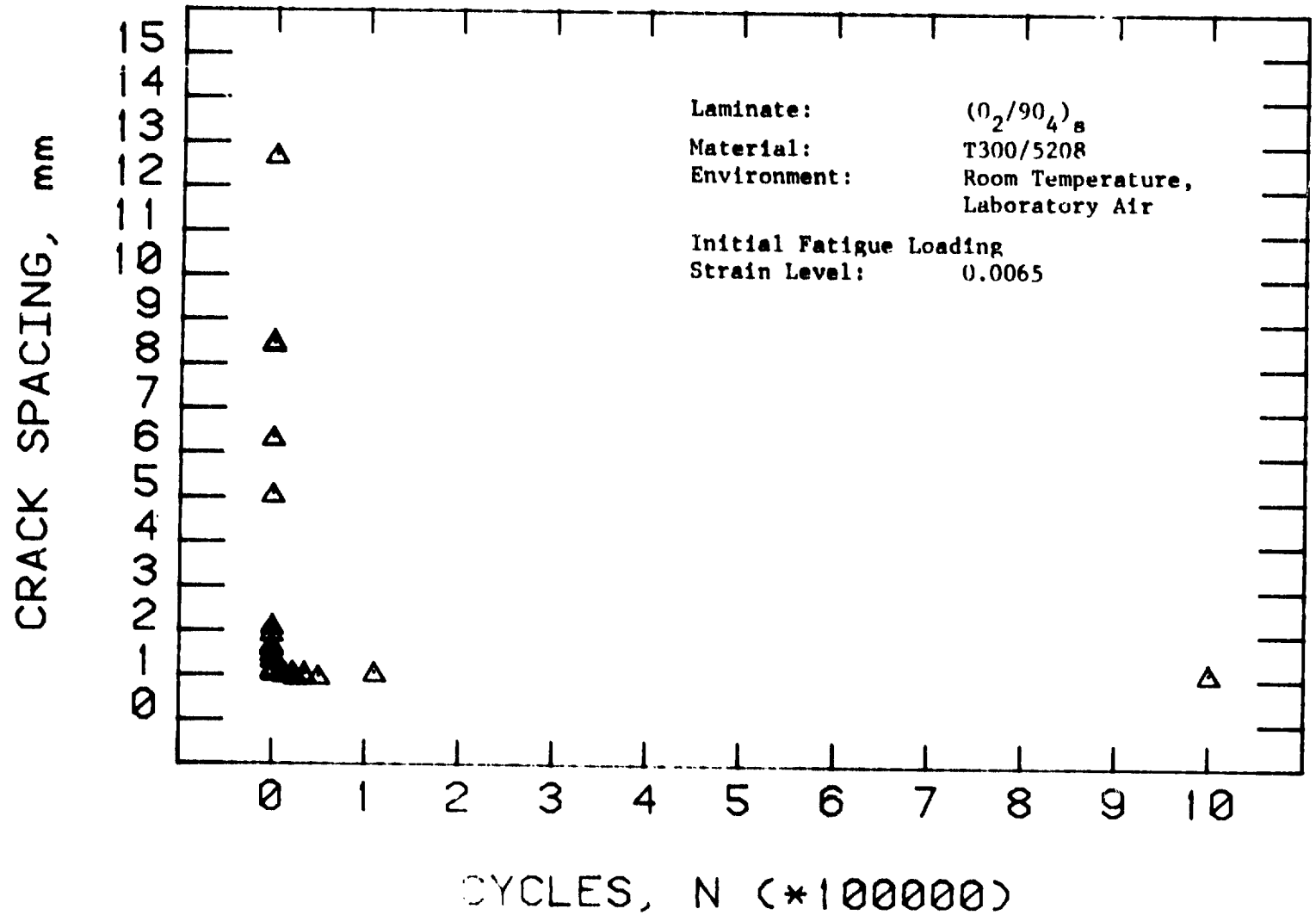

Figure 44: Average matrix crack spacing in the 90° plies vs. cycles for $(0_2/90_4)_s$ coupons fatigue cycled at an initial strain of 0.0065.

TABLE 35
MATRIX CRACK SPACING UNDER DIFFERENT LOADING CONDITIONS FOR $(0_2/90_4)_S$ COUPONS

Note: Crack spacing values given are those measured just prior to failure or at the end of the loading condition indicated

LOADING CONDITION		RANGE IN AVERAGE CRACK SPACING OF 90° CRACKS, mm
MONOTONIC TENSION		0.67 to 6.35
FATIGUE		
Initial	= 0.0050	1.13 to 1.49
	= 0.0060	0.91 to 1.30
	= 0.0065	0.98 to 1.15
RESIDUAL STRENGTH		
After Fatigue		
Initial	= 0.0050	1.13 to 1.49
	= 0.0060	1.04 to 1.37
	= 0.0065	0.98 to 1.13
Monotonic Tension		0.98 to 1.99

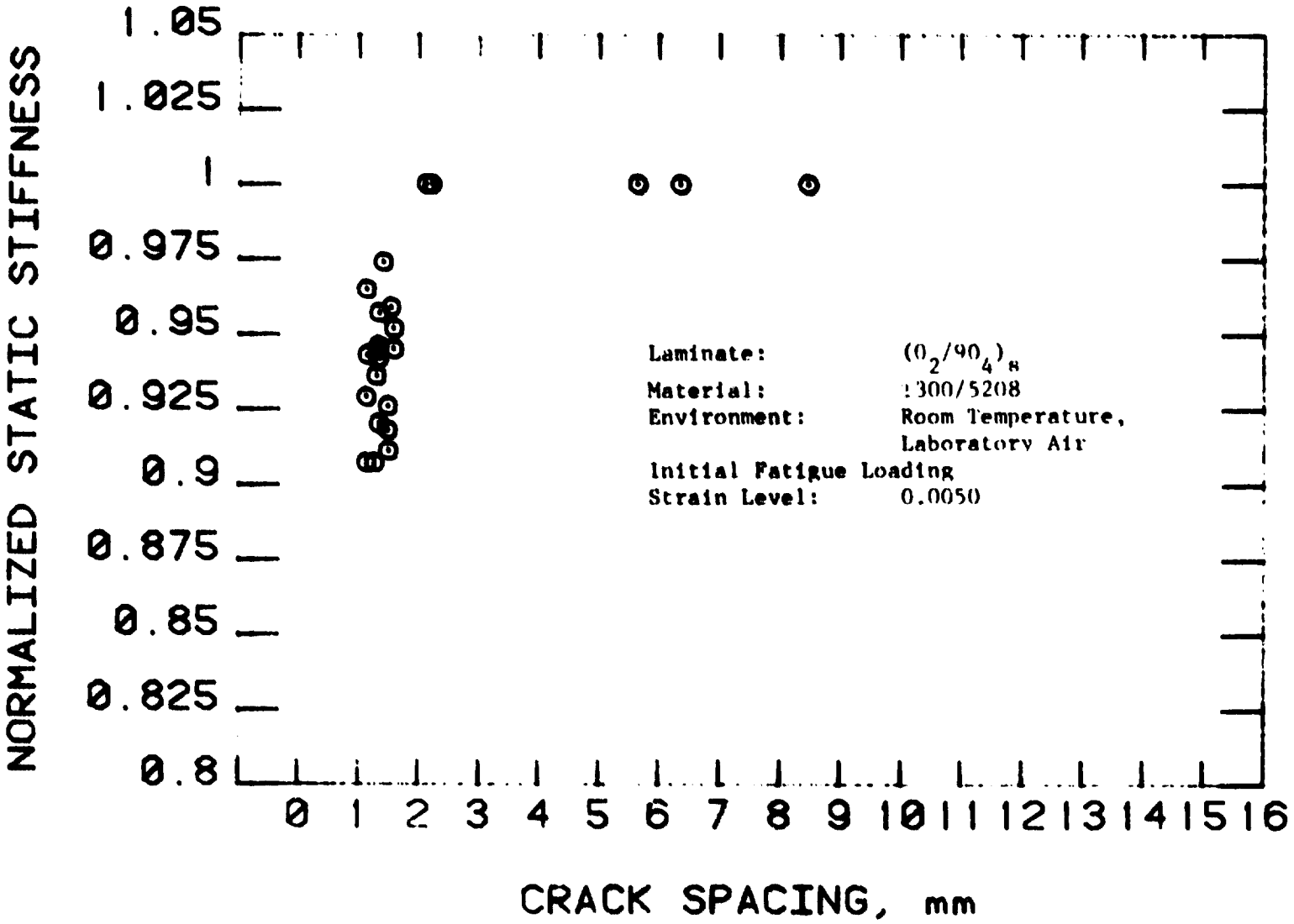

Figure 45: Normalized static stiffness vs. 90^0 matrix crack spacing for $(0_2/90_4)_s$ coupons fatigue cycled at an initial strain of 0.0050.

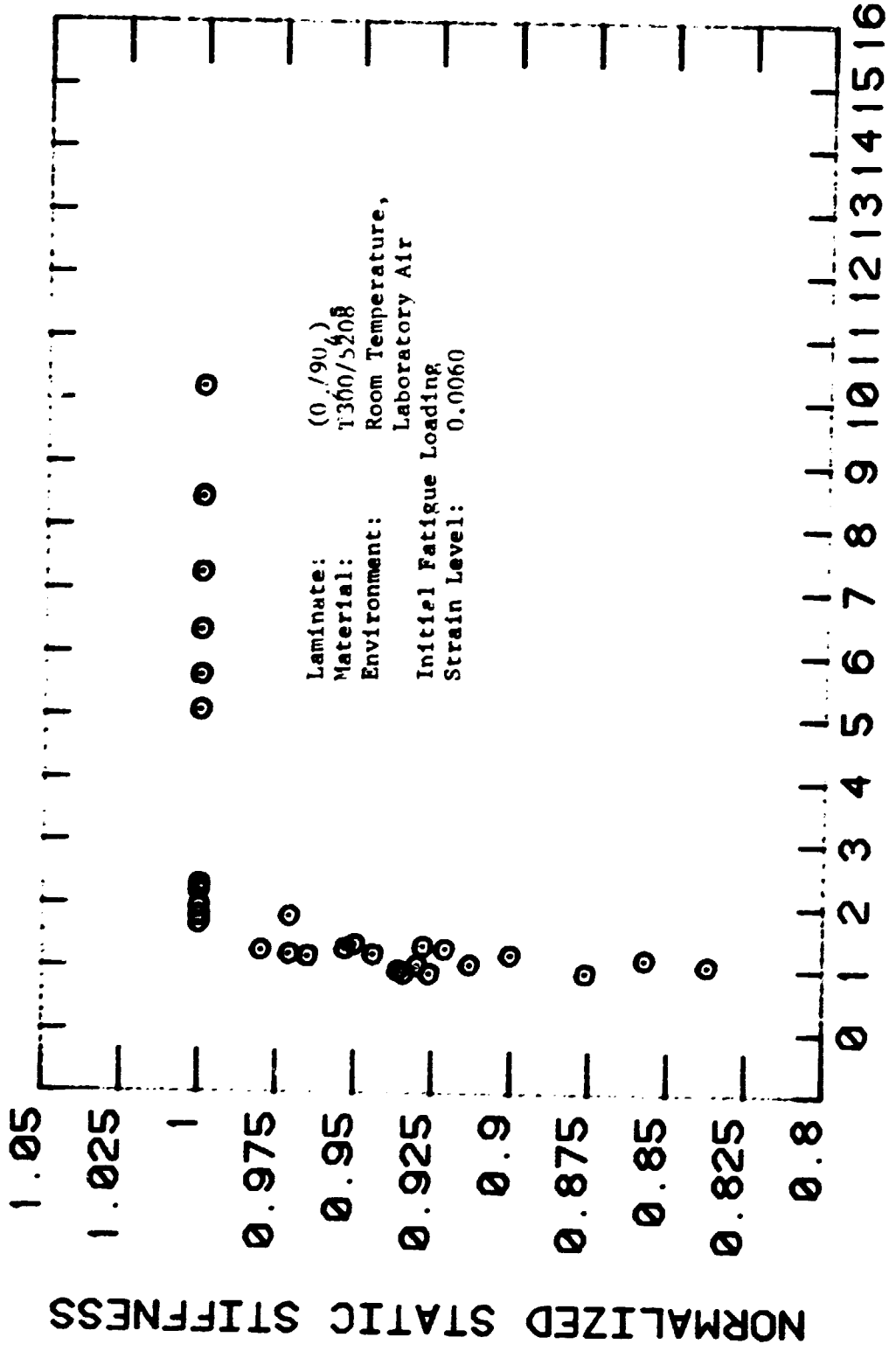

Figure 46: Normalized static stiffness vs. 90° matrix crack spacing for $(0_2/90_4)_s$ coupons fatigue cycled at an initial strain of 0.0060.

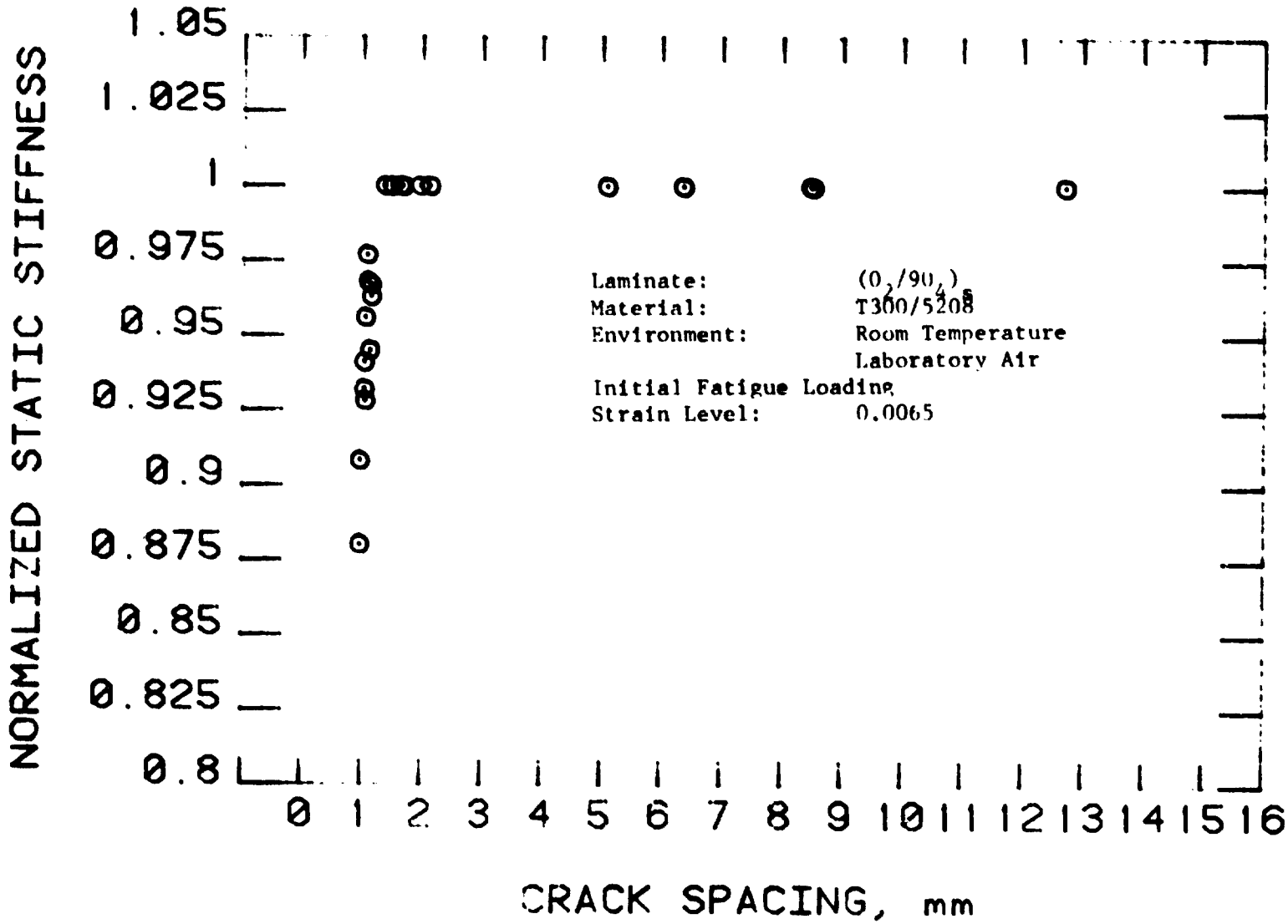

Figure 47: Normalized static stiffness vs. 90^{o} matrix crack spacing for $(0_2/90_4)_s$ coupons fatigue cycled at an initial strain of 0.0065.

the 90^{o} matrix cracks. Normalized monotonic stiffness is plotted versus cycles in Figures 48 to 50. These figures show the gradual progression of stiffness loss due to delamination.

In Figure 51, the maximum strain which occurred in representative fatigue loaded coupons is plotted versus cycles. As in all of the layups of this investigation, the strain at failure was generally 20 to 30 percent below the average monotonic tension failure strain of those coupons not subjected to prior fatigue loading. However, coupon A8 failed at a strain level near to the lowest strain t, failure recorded for a monotonic tension tests.

Coupons used for residual strength experimentation were either those which had reached 10^{6} cycles in prior fatigue loading or had been load cycled to particular percentages of monotonic stiffness loss. Thus coupons A21, A22, A25, A31, and A17 were all cycled to 10^{6} cycles; A13, A20, A26, A11, and A17 were intended to have between 5 and 7 percent stiffness loss; and A12 and A32 to have between 10 and 12 percent stiffness loss. A summary of the residual strength data for this $(0_2/90_4)_s$ laminate is given in Table 36. More detailed data are given in Table 37.

The damage state within the coupons was not observed to change during the residual strength experimentation. The average strain to failure decreased approximately 5.5 percent below the monotonic tension strain to failure of coupons not subjected to fatigue loading. As for the results of the other layups, this average strain to failure was significantly above the observed strain at failure due to fatigue loading. The strain to failure of individual residual strength coupons did not correlate with the extent of delamination. Therefore, as in all of the other layups, the specific failure events which occur during fatigue were concluded not to be present in these residual strength coupons. This conclusion was supported by the failure of two other coupons during a monotonic stiffness survey periodically conducted on each fatigue coupon.

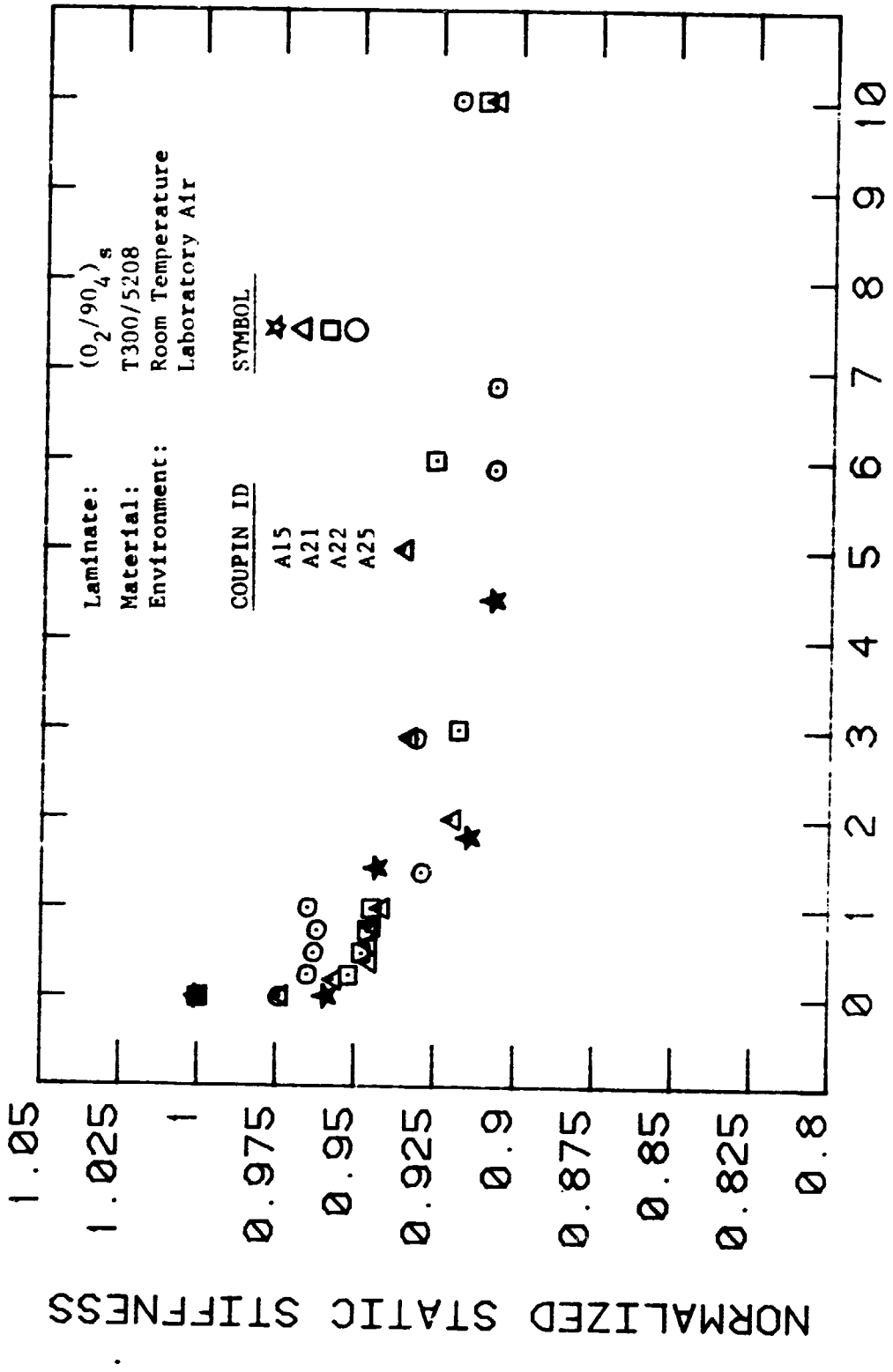

Figure 48: Normalized static stiffness vs. cycles for $(0_2/90_4)_s$ coupons fatigue cycled at an initial maximum strain of 0.0050.

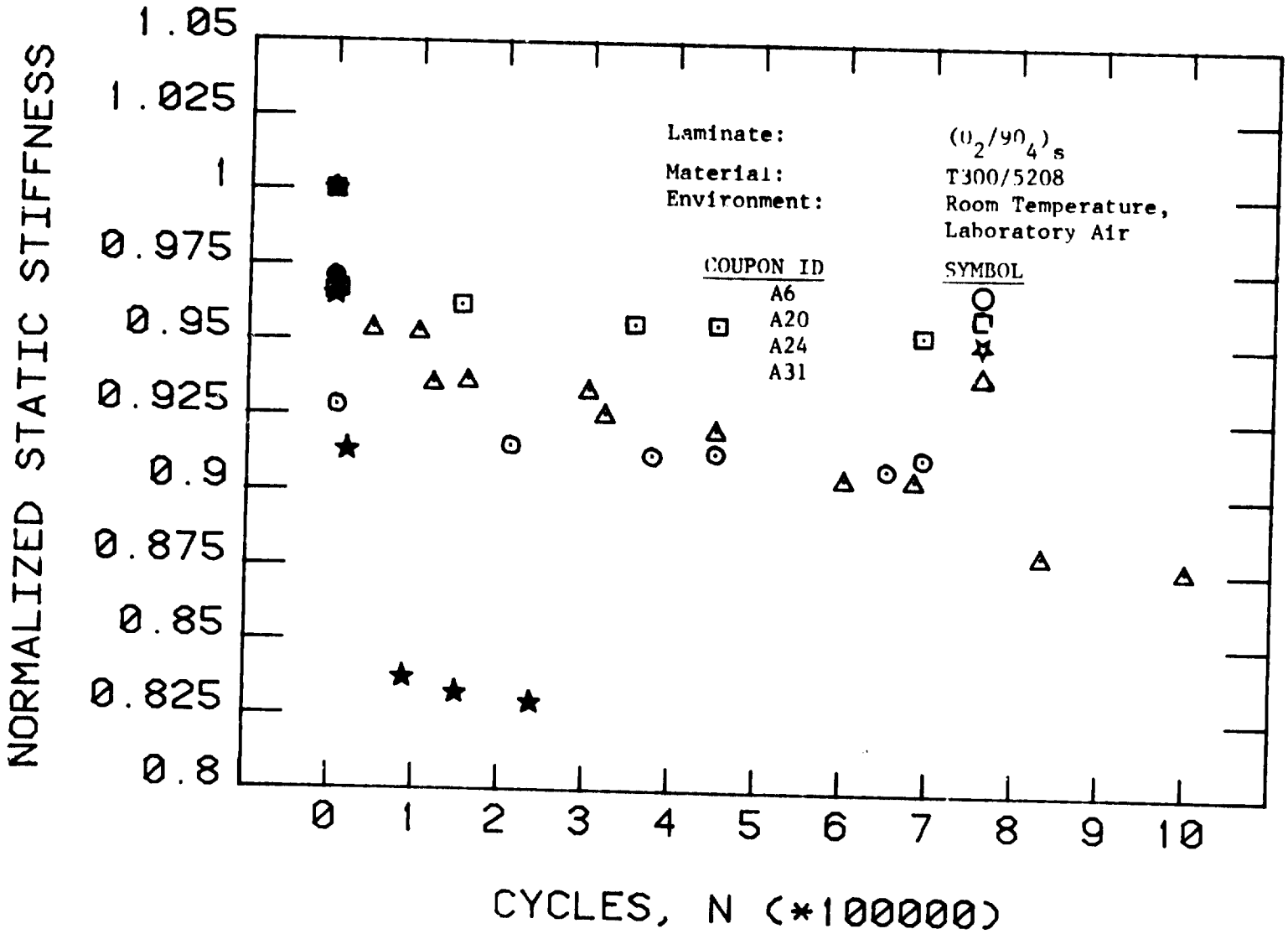

Figure 49: Normalized static stiffness vs. cycles for $(0_2/90_4)_s$ coupons fatigue cycled at an initial maximum strain of 0.0060.

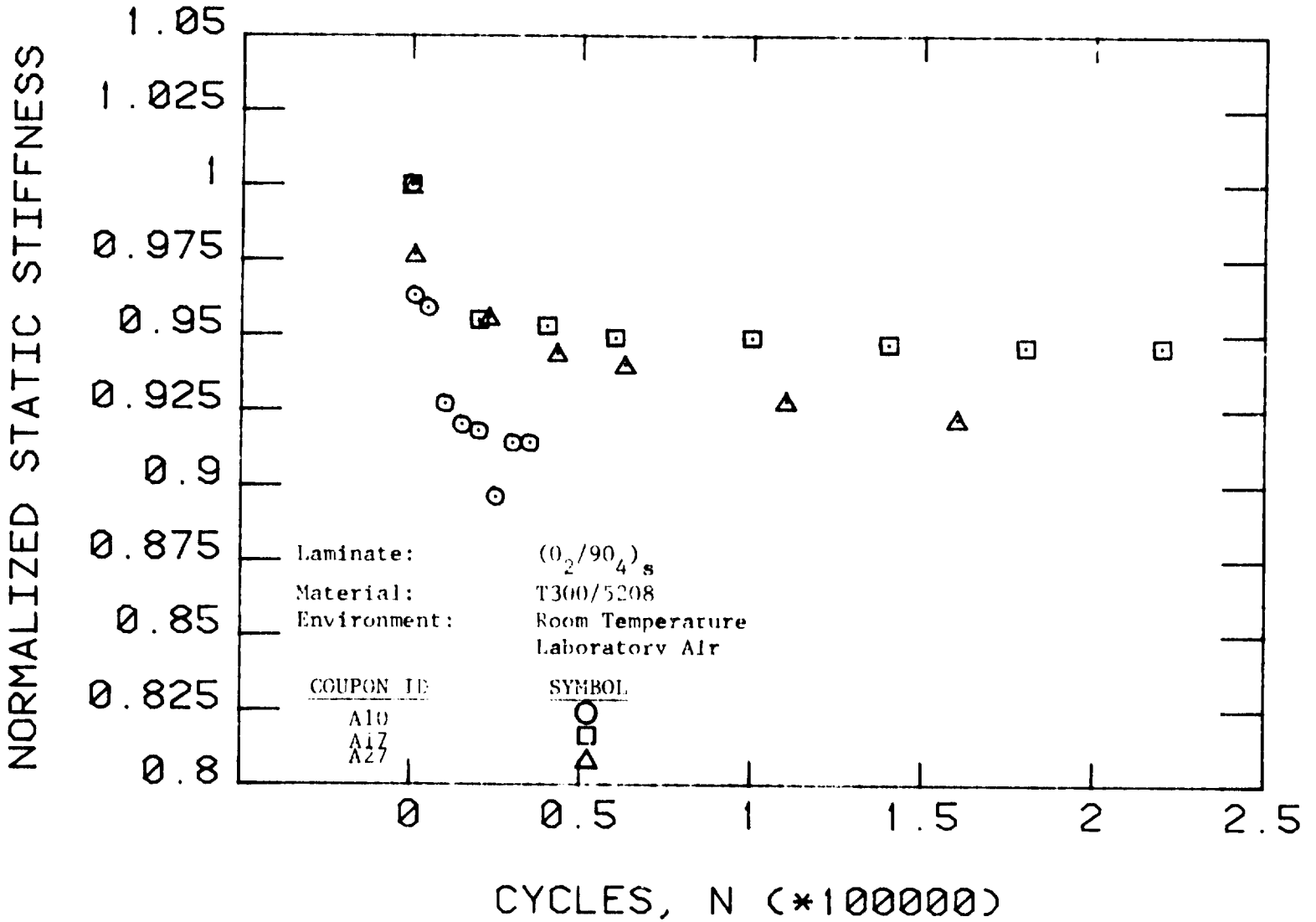

Figure 50: Normalized static stiffness vs. cycles for $(0_2/90_4)_s$ coupons fatigue cycled at an initial maximum strain of 0.0065.

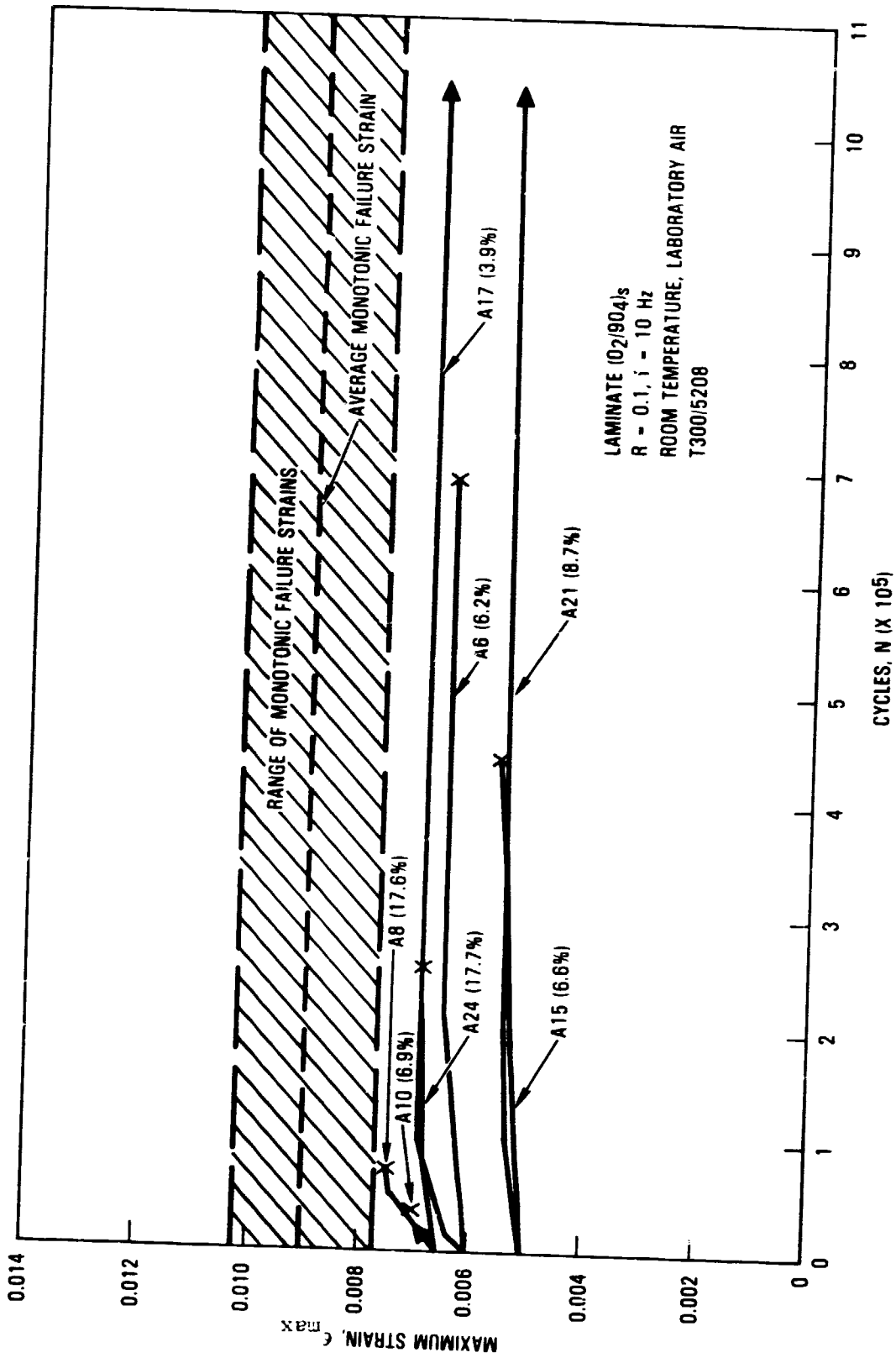

FIGURE 51. INCREASE IN STRAIN DUE TO FATIGUE LOADING IN $(0_2/90_4)_s$ COUPONS.

TABLE 36
SUMMARY OF RESULTS FOR FATIGUE AND RESIDUAL STRENGTH LOADING OF $(0_2/90_4)_S$ COUPONS

COUPON ID	INITIAL MAX. FATIGUE STRAIN	FATIGUE CYCLES X 1000	MONOTONIC STIFFNESS GPA	MONOTONIC STIFFNESS PSI X 10^6	PERCENT DECREASE IN MONOTONIC STIFFNESS	EXTENT[b] OF DAMAGE	STRESS AT FRACTURE MPa	STRESS AT FRACTURE ksi	STRAIN TO FAILURE	STIFFNESS TO FAILURE GPA	STIFFNESS TO FAILURE Msi
A21	0.0050	1600	47.6	6.91	3.2	5,4	431	62.5	0.0098	48.0	6.96
A22	0.0050	1000	48.1	6.98	8.9	9,30	466	67.6	0.0094	49.9	7.20
A25	0.0050	1000	48.5	7.03	8.1	4,10	485	70.4	0.0097	50.4	7.30
A12	0.0060	68	46.0	6.67	14.3	11,40	407	59.0	0.0084	46.3	6.71
A13[a]	0.0060	30	50.0	7.26	7.0	8,15	391	56.7	0.0080	48.6	7.05
A20	0.0060	690	46.1	6.69	4.7	6,20	452	65.5	0.0096	47.0	6.82
A26	0.0060	35	48.4	7.02	5.0	6,10	454	65.9	0.0095	48.9	7.01
A31[a]	0.0060	1000	43.4	6.29	12.4	13,70	340	49.3	0.0078	43.7	6.34
A11	0.0065	35	45.2	6.56	6.8	3,4	361	52.4	0.0079	45.4	6.59
A17	0.0065	1000	49.5	7.18	5.5	2,5	511	74.1	0.0102	49.1	7.11
A32	0.0065	255	47.9	6.95	9.1	6,20	374	54.2	0.0080	47.0	6.82
AVERAGE							425	61.6	0.0089	47.4	6.92
AVERAGE MONOTONIC TENSION TESTS							432	62.6	0.0090	51.0	7.39

a = Failure data are highest values recorded; fractur occurred on next loading at slightly lower values, see Table 37.

b = Damage state at the end of fatigue loading. All coupons had some delamination as well as an essentially saturated matrix crack spacing; the first entry is the number of 0^0 splits while the second is the estimated amount of delamination in percent of gage length area.

TABLE 37
RESULTS OF RESIDUAL STRENGTH LOADING OF $(0_2/90_4)_S$ COUPONS

COUPON ID	AVERAGE AREA mm²	AVERAGE AREA in.²	FATIGUE CYCLES THOUSANDS	LOAD LEVEL	STRAIN[a]	STRESS MPa	STRESS ksi	STIFFNESS GPa	STIFFNESS Msi	DAMAGE[b] STATE
ZF1906										
A21	63.7	0.0987	1000	FATIGUE	0.0050	-	-	47.6	6.91	5,4
				1	0.0075	373	54.1	49.4	7.16	NC
				2	0.0080	401	58.2	50.1	7.26	NC
				3	0.0085	422	61.2	49.4	7.16	NC
				4	0.0090	431	62.5	48.0	6.96	F
A22	63.8	0.0989	1000	FATIGUE	0.0050	-	-	48.1	6.98	9,30
				1	0.0075	368	53.3	48.9	7.09	NC
				2	0.0080	382	55.4	47.6	6.91	NC
				3	0.0085	423	61.4	49.5	7.18	NC
				4	0.0094	466	67.6	49.7	7.20	C
A25	63.9	0.0991	1000	FATIGUE	0.0050	-	-	48.5	7.03	4,10
				1	0.0075	376	54.5	49.9	7.24	NC
				2	0.0080	399	57.8	49.8	7.22	NC
				3	0.0085	423	61.3	49.5	7.17	NC
				4	0.0097	486	70.4	50.4	7.30	F
A12	62.9	0.0975	68	FATIGUE	0.0060	-	-	56.0	6.67	11,40
				1	0.0075	351	50.9	46.6	6.76	NC
				2	0.00825	383	55.5	46.5	6.74	NC
				3	0.0089	407	59.0	46.3	6.71	F
A13	63.4	0.0982	30	FATIGUE	0.0060	-	-	50.0	7.26	8,15
				1	0.00750	371	53.7	49.2	7.13	NC
				2	0.00800	391	56.7	48.6	7.05	NC
				3	0.00792	385	55.9	48.5	7.04	F
A20	62.2	0.0964	690	FATIGUE	0.0060	-	-	46.1	6.69	6,20
				1	0.0075	350	50.8	46.7	6.77	NC
				2	0.00825	385	55.9	46.5	6.75	NC
				3	0.00875	410	59.4	46.7	6.77	NC
				4	0.00961	452	65.5	47.0	6.82	F

TABLE V/ - Continued
RESULTS OF RESIDUAL STRENGTH LOADING OF $(0_2/90_4)_S$ COUPONS

COUPON ID	AVERAGE AREA mm²	AVERAGE AREA in.²	FATIGUE CYCLES THOUSANDS	LOAD LEVEL	STRAIN[a]	STRESS MPa	STRESS ksi	STIFFNESS GPa	STIFFNESS Msi	DAMAGE[b] STATE
A26	63.2	0.0980	35	FATIGUE	0.0066	-	-	49.4	7.16	6,10
				1	0.0075	362	52.6	48.3	7.00	NC
				2	0.00875	407	59.0	48.1	6.42	NC
				3	0.00975	422	61.1	48.0	6.97	NC
				4	0.00931	454	65.9	48.9	7.09	F
A31		0.0977	1000	FATIGUE	0.0060	-	-	43.4	6.29	13,70
				1	0.00775	340	49.3	43.7	6.34	NC
				2	0.00734	317	46.0	43.9	6.37	F
A11	62.2	0.0965	35	FATIGUE	0.0065	-	-	49.2	7.14	4,4
				1	0.0079	361	52.4	45.4	6.59	F
A17	62.7	0.0972	1000	FATIGUE	0.0065	-	-	44.5	7.18	2,5
				1	0.00775	383	55.6	49.4	7.16	NC
				2	0.00825	413	60.0	49.9	7.24	NC
				3	0.00875	428	62.0	48.7	7.06	NC
				4	0.0102	511	74.1	49.1	7.11	F
A32	63.9	0.0991	25.5	FATIGUE	0.0065	-	-	47.9	6.95	6,20
				1	0.00750	364	52.7	47.0	6.91	NC
				2	0.00800	374	54.3	46.5	6.74	NC
				3	0.00805	374	54.2	47.0	6.82	F

a = Strain level is initial strain for fatigue loading.

b = Damage state at the end of indicated fatigue level. All coupons had some delamination as well as essentially saturated matrix crack spacing. The first entry is the number of 0° splits while the second is the estimated amount of delamination. NC means no change in the damage state. F means failure occurred on that loading.

Coupon A6 fractured at 0.0093 strain, due to an inadvertent overload, after an 8.8 percent stiffness loss over 692 000 cycles. Thus for this coupon apparently no damage indicative of final fracture was yet present. However, coupon A9 fractured at a strain of 0.0065 after a 5.9 percent stiffness loss in 14 150 cycles. Apparently, coupon A9 had been stopped during fatigue loading with the failure causing damage present; literally the next load cycle, a monotonic load survey, resulted in a fracture which occurred at a strain of 5.5 percent below that previously reached in fatigue loading. Supporting this inference, the monotonic stiffness in coupon A9 on the last load cycle was five percent below that of the previous cycle while in coupon A6, stiffness was essentially unchanged between the two cycles. Thus the final fracture events in Coupon A9 clearly developed quickly, having significant and large effects.

In the following section, the analysis of the experimental data of this section will be discussed. Further, mathematical based models used to represent that data are presented and evaluated.

SECTION 3
ANALYSIS AND MATHEMATICAL MODELING

Rather extensive analysis of the layups used in this and in other research programs was undertaken. The purpose of this analysis was to resolve the laminates, observed damage states, and associated mechanical properties into their essential elements so that they could be studied critically. Based upon the analysis, a conceptual understanding was hypothesized as to the nature of what transpired within a laminate when subjected to load. The derived description was mathematically modeled in order to articulate and define it in a more detailed manner. Based on these models, expected stiffness, strengths, tendencies to delaminate or matrix crack were quantitatively calculated for some cases and compared to experimental results. In other cases, qualitative inferences were drawn from the model as to expected trends, and these were also compared to experimental results. From these qualitative trends and statements of quantitative precision, a broad range of significant inferences were drawn, which hopefully help clarify and bring added consistency to previously available information. The success, or lack thereof, in developing models properly representative of the mechanics and thereby allowing correct inferences to be drawn was, of course, dependent on the accuracy of the analysis undertaken.

In the initial part of this investigation, the computer software programs, previously developed by Lockheed Missiles and Space Company at the Palo Alto Research Laboratory, were improved and expanded both to further aid the task of modeling and to develop compatability with NASA/Langley computing requirements. Subsequent to this development, computer aided models were developed of various idealized damage states, the results of which are detailed in this section. In addition, thought was given towards developing

a failure criteria and, hence, was concerned with load transfer into and fracture criteria for the 0° plies. These analytically based models of the laminates, plus the experimentally observed damage states, were mathematically represented with the aid of a VAX 11/780 computer.

The following subsections discuss the various aspects of the analytical and mathematical modeling effort. The first subsection presents a summary of an analysis of the data presented in Section 2 and those obtained previously [7,13,21,32,34]. The experimental observations are analyzed for the purposes of selecting those deemed most important for modeling purposes. In the second subsection, some of the historical background to the modeling effort of this study is discussed and a short summary is given of the selected computational procedures. In the following subsections, a detailed description of transverse matrix cracking modeling is given along with associated effects on stiffness and local stress concentrations. In the next subsection, the nature of a failure criterion for the 0° plies is explored which is followed by a subsection in which the results of three dimensional modeling of delamination are discussed. The last subsection presents some results of an investigation into strain to failure under monotonic load. The relationship between these mathematically based results and the experimental results of Section 2 is discussed in Section 4.

3.1 ANALYSIS OF EXPERIMENTAL OBSERVATIONS

A major portion of the large amount of available data concerning tension loading of graphite/epoxy laminates is reviewed in this subsection. A summary description of the state (damage) changes which occurred in each laminate due to loading is given first. This is followed by a discussion of the key experimental observations which were selected for mathematical modeling. Finally, those observations for which satisfactory models have been previously developed are discussed as are those which remained and required further model development.

3.1.1 Experimental Summary

Data obtained from experimental studies in this program and in others are available for a wide range of unnotched, tension loaded graphite/epoxy laminates. The data for some of these laminates are summarized in this section. The summary includes both a description of the damage state development under each loading condition as well as the associated stiffness changes and strain to failure data.

$(0)_4$ Layup

- o Monotonic Loading
  - 0° fiber fractures occurred before failure
  - Stress-strain data exhibited slightly increasing stiffness
  - Strain to failure of 0.0098 was 8 percent less than $(0/90/\pm45)_s$ and $(0/\pm45)_s$ layups
  - Coupons essentially exploded at fracture
- o Fatigue Loading
  - 0° fiber fractures before failure
  - Fatigue life scatter greater than two orders of magnitude
  - Strain at failure was 10 to 20 percent less than that under monotonic tension load
- o Residual Strength
  - No stiffness change
  - Strain to failure same as monotonic tension

$(0/90/\pm45)_s$ Layup (See also References 39,42,43,44 and 45 for a 24-ply version of this layup)

- o Monotonic Loading
  - 90° matrix cracks appeared at approximately 0.0060 strain and saturated at approximately 0.0090; $\pm45^\circ$ matrix cracks

appeared at approximately 0.0093 strain and did not saturate; no -45° matrix cracks; cracks at an angle up to 45° to the 0° plies.

- Delamination between $+45^{\circ}/-45^{\circ}$ interface, followed by $90^{\circ}/+45^{\circ}$ and $0^{\circ}/90^{\circ}$ interfaces; delamination visible only near edges, not visible by enhanced x-ray.

- Stiffness change of less than three percent occurred.

- Average strain to failure 0.0103.

- Fracture of 0° plies along 90° direction, even $\pm 45^{\circ}$ plies often fractured in 90° direction, fracture location within gage length.

o Fatigue Loading

- Matrix crack spacing in 90°, $+45^{\circ}$, and -45° plies saturated in less than 40 percent of fatigue life; spacing in 90° plies same as under monotonic load; crack spacing saturation occurred over first 2 to 3 percent of stiffness loss; cracks at up to 45° angle to 0° plies.

- Short cracks/delamination developed perpendicular to transverse matrix cracks.

- Delamination started at free edge after transverse crack saturation, $90^{\circ}/\pm 45^{\circ}$ interface dominant, then $+45^{\circ}/-45^{\circ}$ and $0^{\circ}/90^{\circ}$ interfaces; $90^{\circ}/+45^{\circ}$ delamination was always irregular and $+45^{\circ}/-45^{\circ}$ interface delaminated first.

- Highly regular and relatively continuous stiffness loss of up to 18 percent occurred.

- Fatigue life scatter approximately one order of magnitude.

- No obvious 0° fiber fracture observed prior to coupon failure.

- Strain at failure was always less than 0.0085. 15 to 25 percent below monotonic strain to failure.

- 0° plies fractured along $+45^{\circ}$ line, fractures within gage length.

o Residual Strength

- No significant further damage state change, slight delamination area increase.

- No further stiffness change.

- Average strain to failure 0.0103, same as in monotonic tension.

- Fracture of 0° plies along 90° direction, fracture within gage length.

$\underline{(0/45/90/-45)_{2s}}$ Layup (See References 7, 13 and 32)

o Monotonic Loading

- 90° matrix cracks appeared by 0.0060 strain and saturated by approximately 0.0090; -45° ply cracks appeared at 0.0080 and saturated at about 0.0095; $+45^{\circ}$ ply crack also appeared by 0.0080, but did not saturate; cracks at an angle up to 45° to 0° plies.

- Just prior to failure long delaminations apparent on coupon edge at ends of transverse cracks; no thumbnail delamination seen by enhanced x-ray; no delamination found in cross sections by microscopy.

- Stiffness change of 3 to 5 percent occurred above 0.0060 strain.

- Average strain to failure of 0.0105.

- Fracture of 0° plies along $+45^{\circ}$ direction, fracture usually within gage length.

o Fatigue Loading

- Matrix crack spacing of off-axis plies saturated early in fatigue life.

- Delamination started at free edges after transverse crack saturation had essentially occurred; order of delamination interfaces was 90/-45, 90/+45, +45/90, -45/90, and 0/+45 with 90/-45 and 90/+45 interface delaminations remaining dominant; delaminations grew symmetrically from both edges.

- Stiffness loss of at least 7 to 15 percent.

- Fatigue life scatter approximately one order of magnitude.

- No obvious 0° fiber fracture observed prior to coupon fracture.

- Strain to failure was always less than 0.0080, 20 to 40 percent below monotonic strain to failure.

- 0° plies fractured along a $\pm 45^{\circ}$ line, fracture usually within gage length.

o Residual Strength

- No further damage state change.

- No further stiffness change.

- Average strain to failure up to six (6) percent below monotonic tension strain to failure; the higher the load during fatigue cycling the less strain to failure decrease exhibited.

- Fracture of 0° plies along $+45^{\circ}$ direction, fracture usually within gage length.

(0/±45)$_s$ Layup (See also Reference 40)

o Monotonic Tension

- Matrix crack spacing highly irregular, no actual saturation, more cracks in $+45^{\circ}$ plies than in -45° plies, cracks at angle up to 45° to 0° plies, cracks appeared above 0.0045 strain level.

- No delamination visible by enhanced x-ray, edge delamination at +45/-45 interface.

- No significant stiffness change, slight upward trend in stress-strain curve.

- Average strain to failure was 0.0106.

- Fracture of the 0° plies was along a $+45^{\circ}$ direction, fracture usually within gage length.

o Fatigue Loading

- Matrix crack spacing saturated in both the $+45^{\circ}$ and -45° plies, cracks were wider in the -45° plies and more discontinuous in the $+45^{\circ}$ plies; cracks often did not cross the coupon width until as much as 50 percent of fatigue life had passed; short cracks/delamination occurred at the ends of the matrix cracks at the ply interface.

- Delamination occurred primarily at the +45/-45 interfaces and secondarily at the 0/+45 interfaces; +45/-45 interface delamination as shown by enhanced x-ray was confined to a narrow edge region which also contained a few 0° ply splits, broken 0° fibers, and even a complete separation from the interior plies; delamination extension in the coupon width direction occurred prior to transverse matrix crack saturation.

- Stiffness loss was irregular, but monotonic stiffness losses of less than 2 percent occurred, apparently due to matrix cracks alone, and up to 7 percent total.

- 0° fiber breaks were commonly observed along the coupon edges and even between the edges in the outer 0° plies.

- Strain to failure was always 15 to 25 percent below monotonic strain to failure.

- Final fracture displayed 0° fibers fractured along a $+45^{\circ}$ direction, fracture usually within gage coupon.

o Residual Strength

- No further damage state change.

- No further stiffness change.

- Average strain to failure of 0.0106, unchanged from previous monotonic tension data.

- Fracture of 0° plies along $+45^{\circ}$ direction, fracture usually within gage length.

$\underline{(0/45/0_2/-45/0)_s}$ Layup

o Monotonic Tension

- Matrix crack spacing highly irregular, no matrix cracks in some coupons prior to failure, usually more cracks in the -45° plies than in the $+45^{\circ}$ plies, no pattern of cracking emerged, cracks at an angle of up to 45° to the 0° plies, matrix cracks apparently did not traverse coupon width.

- Edge replicates revealed no obvious delamination at ends of matrix cracks, no delamination found by enhanced x-ray.

- No significant change in stiffness, slight upward trend in stress-strain curve.

- Average strain to failure was 0.0112.

- Fracture of the 0° plies and usually the -45° plies was primarily at $+45^{\circ}$ direction, this sometimes turned to the 90° direction, fracture location often influenced by grips.

o Fatigue Loading

- Matrix crack spacing much less than for monotonic loading, saturation never occurred, some regions had no matrix cracks prior to coupon fracture, many cracks did not cross coupon width, generally more cracks in $+45^{\circ}$ plies than in -45° plies.

- Edge delamination generally started at the $+45/0_2$ interface followed by the $0/+45$, $0_2/-45$, and $-45/0$ interfaces, the latter often did not develop; enhanced x-ray revealed narrow delamination along the coupon edges, these contained a few 0° fiber splits.

- 0° fiber fractures occurred at the coupon edges and were occasionally observed in the outer 0° plies away from the edges.

- Average stiffness did not change, one to two percent random fluctuation in measurements occurred.

- Fatigue life scatter was in excess of two orders of magnitude.

- Strain to failure was 20 to 35 percent below monotonic strain to failure.

- Fracture of all plies was predominantly along a $+45^{\circ}$ direction, fracture location often influenced by grips.

o Residual Strength

- No further damage state change.

- No stiffness change.

- Average strain to failure of 0.0102 was 9 to 10 percent below previous monotonic tension data.

- Fracture of all plies was predominantly along a $+45^{\circ}$ direction, fracture location was often influenced by grips.

$(0/45/0_2/-45/0)_{2s}$ Layup (See Reference 32)

- o Montonic Tension
  - Same qualitative response as single symmetric form, strain to failure lower because of different material batch.
- o Fatigue Loading
  - Same as single symmetric form except for more extensive 0° fiber fracture prior to failure and often very extensive delamination at long lives ($>1 \times 10^6$ cycles).
- o Residual Strength
  - Same as single symmetric form.

$(0_2/90_4)_s$ Layup (See also References 40 to 46)

- o Monotonic Tension
  - Matrix crack spacing tended towards saturation before fracture, but coupon fracture sometimes occurred prior to saturation; matrix cracking on the edges appeared more complex than in the interior.
  - Short delaminations were found by edge replication at the end of the transverse cracks, no obvious delamination found by enhanced x-ray although cracks widened as strain increased.
  - Stiffness decreased up to 6 percent.
  - Average strain to failure was 0.0090, significantly below that for other layups.
  - Coupons essentially exploded at coupon failure, but fracture of the 0° plies did occur along a 90° direction.
- o Fatigue Loading
  - Transverse matrix cracking saturated in many regions early in fatigue life (5 000 cycles or less) but not in others; the width of transverse cracks appeared to widen in the enhanced x-ray photographs as cycles increased; 0° longitudinal splits developed.
  - $0/90$ interface delamination grew from the intersection of the 0° splits and 90° matrix cracks; edge delamination did not extend significantly in the coupon width direction.

- 0^{o} fiber fracture occurred in large groups both along the coupon edges and within the interior.

- Monotonic stiffness changes of up to 17 percent occurred prior to failure.

- Fatigue life scatter was greater than two orders of magnitude.

- Strain to failure was 20 to 30 percent below the average strain to failure of monotonically loaded coupons.

- At failure, coupons essentially exploded but the 0^{o} plies again fractured along a 90^{o} direction.

o Residual Strength

- No further damage state change.

- No further stiffness change.

- Average strain to failure of 0.0089 was essentially the same as the monotonic load failure strain; one coupon failed in the same strain region as that which occurred due to fatigue load.

- Coupons essentially exploded at failure with 0^{o} fibers fracturing along 90^{o} direction.

3.1.2 Experimental Observations Requiring Modeling

The summary observations given in Section 3.1.1 for each of the layups were combined to give a general picture of the effect of tension load on these unnotched coupons. The combined summary of those observations requiring an explanation is as follows:

o Monotonic Loading

- Strain at which onset and saturation of matrix cracking occurs.

- Saturation spacing of matrix cracks.

- The fact that matrix crack saturation occurs in some layups, but not others.

- Some coupons significantly delaminate and others do not.
- Onset of delamination.
- Change in stiffness, if it occurs, can occur with and without large delamination.
- Strain to failure, essentially the same for all layups containing 0^{o} plies except for unidirectional or 0/90 combinations.
- Extent of scatter.
- Fracture appearance.

o Fatigue Loading

- Matrix crack saturation occurs in some layups, but not others; angle of matrix cracks to 0^{o} load direction.
- Cause of, or lack of, delamination; nature if it occurs; cause of its symmetry in some layups, but not in others; onset of delamination.
- Cause of stiffness change: only a few percent of the change appears to correlate to transverse cracking; does the rest correspond to delamination?; no stiffness change in some layups.
- Failure criterion: influence of transverse matrix cracking, fiber fracture, and other factors; rather sudden fracture events.
- Strain to failure 15 to 35 percent below monotonic strain to failure.
- "Runout" strain at which fatigue life greatly increases.
- Extent of scatter in fatigue life.
- Fracture appearance.
- Shape of S-N curve.

o Residual Strength

- Lack of further damage in all layups.
- Lack of further stiffness change in all layups.

- Average strain to failure unchanged from monotonic strain to failure for many layups, no more than a 5 to 10 percent change in others; this occurs despite often extensive damage and reduced strain to failure under fatigue loading of 15 to 30 percent below monotonic strain to failure.

- Scatter.

- Fracture appearance.

Of the above experimental observations, many are presently understood, at least in principle. For example, the strain for onset of matrix cracking and delamination has been shown to be explainable under monotonic load, at least for a $(\pm 25_n/90_n)_s$ layup based upon a fracture mechanics strain energy analysis[11,12,45-52]. This analysis approach would appear to apply to other layups and for fatigue loadings, although the complexity is much greater. Therefore, this problem was not pursued further in this program. The tendency to edge delaminate can also be approximated by analysis of free edge stresses[53-56]. Saturation of transverse matrix crack spacing has been accurately modeled for cases without delamination using either a shear lag analysis[39,57,58] or a strain energy analysis[48,59]. However, in delaminated regions, at least some layups exhibit an increased transverse crack spacing[12].

The main modeling problems undertaken in this program were those of explaining stiffness changes associated with observed damage states and developing a failure criterion for the 0° fibers given a known damage state. The stiffness problem required analysis of several different matrix cracking and delamination conditions and the calculation of the macroscopic stiffness change associated with each condition. A failure criterion or criteria, must be suitable for explaining the coupon strain to failure which occurs under monotonic load, fatigue load, and in residual strength. The two analysis problems of stiffness change and failure criterion were, therefore, selected because they appeared to be the primary ones requiring further development and would lead to significant insight. The remainder of Section

3 addresses these two problems. The results of the derived models are compared in Section 4 to the experimental observations summarized in this subsection.

3.2 COMPUTATIONAL PROCEDURE

Existing practices for analyzing stress states associated with transverse matrix cracks generally employ a two dimensional laminate analysis and calculate the stresses and strains in the individual laminate; onset of multiple cracks is inferred from the calculated stresses or strains. The approach has not provided a fully satisfactory description of the transverse cracking progress. In a study by Bader, et. al.,[60] cross-ply $(0/90)_s$ graphite/epoxy laminates having different $0^\circ/90^\circ$ thickness ratios were tested under uniaxial tension. The first visible appearance of transverse cracks in the 90° ply was found to occur at distinctly different tensile stress or tensile strain levels, depending on the thickness of the 90° ply. In Reference 60, an energy consideration advanced earlier by Aveston and Kelly[61] was applied to relate the onset of transverse cracking to the available energy release per fully developed crack. Their analysis provided the correct trend of the threshold-strain dependence on the 90° ply thickness. The ply thickness dependence of transverse strength was believed to stem from the ply interactions in the laminate. This supposition has been well supported by the work of Flaggs and Kural[62].

Ply delamination is another mode of matrix dominated failure that involves ply structural interactions in the laminate. Causes of delamination have been attributed generally to the existence of interlaminar stresses usually found near the free edges of the laminate.[53,54] However, delaminations can initiate internally at the intersection of transverse and longitudinal cracks, see Reference 40 and Section 2 of this report. Free edge stresses are highly localized and their sign and magnitude depend on the ply stacking sequence[55,56]; hence, some laminates may be more prone to delamination than others, depending on how the plies are stacked together.[54] In a

manner similar to the transverse cracking phenomenon, onset of free edge ply delamination is found to depend also on the thickness, or the volume of the ply which is stressed interlaminarly. The characteristic of this thickness effect is that the occurrence of ply delamination may be suppressed by a decrease in the ply thickness, or conversely, may be enhanced by an increase in the ply thickness.[11,63]

The applied axial (tensile) stress at the onset of delamination has been shown to vary with the thickness or volume of the plies even though the stacking sequence in all cases is the same.[63] The differences exhibited in the test data for both $(25_n/-25_n/90_n)_s$, n = 1,2[12] and $(45_n/-45_n/0_n/-90_n)_s$, n = 1,2,3[62] laminates indicated that the threshold delamination stress depends inversely on the square root of the thickness of the 90^o layer. The thickness effect on the threshold stress for delamination cannot be adequately explained by a stress analysis alone. Since a stress analysis will determine identical stress magnitudes for each of the two previously mentioned laminate series under the same applied axial stress, a criterion based on the magnitude of stress would necessarily predict the same threshold stress for failure.

Rodini, and Eisemann[63] used a probabilistic argument that a laminate with thick plies contains statistically more defects than laminates with thin plies. Consequently, the thicker ply is likely to fail at a lower stress level. This approach requires the knowledge of the free edge stress distribution, which may become singular, and the strength distribution of the material in a unit volume. In this regard, Wu[28] has recently presented a more general approach based on the Weibull statistical strength theory which takes into account the effect of stress gradient near the site of a stress concentration.

These statistical approaches are certainly plausible; and they do provide an explanation for the thickness effect. However, the observed thickness effect on the threshold stress for ply delamination and transverse cracking

may be explained readily from an energy point of view. In this view, the actual amount of strain energy trapped in the plies of the laminate and the manner of release during a crack process play an important role in the crack initiation and growth behavior. Consequently, the thickness of the plies that contain the crack constitute an important parameter in the cracking process. Furthermore, strain energy release is controlled at least partially by the structural interaction between plies during loading of the laminate. Since this interaction takes into account the kinematics of the crack, the energy release analysis provides not only a criterion for crack growth, but also for kinematic effects such as growth instability. This view point provides a deterministic approach involving the classical fracture mechanics, rather than the statistical approach adopted in References 63 and 28.

In a study by Rybicki, Schmuser, and Fox[64], the free edge delamination problem was described by a crack growth analysis based on the energy release rate concept in classical fracture mechanics. The premise for analysis was that interlaminar flaws or defects existing near the ply-interface/free-edge region cause initiation of ply delamination whenever a certain condition is reached. The growth of the delamination is stable initially, i.e., the applied load must be increased in order to extend the crack. The quantity measuring the material resistance against ply delamination is the critical energy release rate, G_c. During a stable growth process, the stressed plies are hypothesized to release strain energy when a new crack surface is created under the applied load. The rate of the available energy release per unit crack surface, G_F, can be calculated by an elastic stress analysis. The condition $G_F = G_c$ is viewed as a driving force which can extend the crack further. If $G_F < G_c$ the crack will remain stationary until the applied load is increased, whereas the crack growth becomes unstable when $G_F > G_c$. This analysis ignores, of course, the possibility of damage growth under alternating loads.

The available energy release rate, G_F, is generally a complicated function of crack location, crack geometry, ply stacking sequence, ply properties, ply thickness, and applied load. To calculate G_F, Rybicki and Kanninen[65] employed the finite element method in conjunction with a crack-closure procedure. The main assumptions in this method are that edge delamination involves only matrix dominated fracture, which is assumed elastic and brittle, and that the crack path is parallel to the ply-interface. The numerical procedure involves the introduction of a virtual crack of known dimension, and computation of the work done to close the crack. The concept is an extension of Irwin's crack-closure integral[66] via a finite-element representation of the plies. Since the work done in closing the crack is computed directly from the finite-element nodal force and nodal displacement solutions, the procedure bypasses the analysis of the stress field. Hence, the advantage of the energy approach, vis-a-vis a stress approach, is that, for the same level of accuracy, a lower order precision suffices for the energy calculation, based on the product of force and displacement. Furthermore, there is no need to use any singular stress element formulation to obtain a solution for the nodal force and the nodal displacement.

In this research study, the strain energy release rate approach[64] and finite element procedures used were an extension of those developed by Wang and Crossman[11,67] to model the free edge delamination process as well as the transverse cracking process in fiber reinforced composite laminates. In each case, a model was formulated on the basis of conceptual and physical considerations. For a given laminate, a non-dimensional, kinematical energy release rate function was identified which represented the kinematics of the crack process in a given laminate configuration. The mechanics of crack initiation and growth behavior were explained by comparing the calculated energy release rate, based on the function, to the measured material crack-resistance, commonly known as the R-curve of the material.

The development and expansion of previously existing computer software to perform the modeling initially consisted of converting the output of a graphics pre and post processor called GIFTS[68] to the input format required by a finite element program called FREEVIS previously developed at Lockheed (see Appendix D for a detailed description). This enabled finite element models to be generated interactively in the GIFTS processor and subsequently analyzed using FREEVIS. The output of FREEVIS was made compatible with the GIFTS postprocessor to provide contour plotting capability. At the beginning of this research program, only two dimensional modeling of damage states was possible. Three dimensional modeling was carried out with a general purpose finite element call DIAL.

Essentially, the architecture of the GIFTS-FREEVIS interface involves three components. A Command module, a GIFTS-to-FREEVIS module which reformats the mesh data from the GIFTS data base to the FREEVIS card image input file, and a FREEVIS-to-GIFTS module which reformats the results of a FREEVIS analysis from the FREEVIS data base to the GIFTS database. The GIFTS-to-FREEVIS module is capable of reformatting node and element information while the FREEVIS-to-GIFTS module is capable of reformatting element stresses and strains and nodal displacements. The Command module provides interactive control of the data reformatting, as well as comprehensive data checking of the GIFTS-to-FREEVIS module, which was modified to take advantage of the GIFTS generated boundary conditions and material property data. The creation and modification of finite element models and boundary conditions was made as interactive as possible to permit a maximum flexibility in modeling the details of pay cracking and delamination and to provide data output in contour plot and three-dimensional plot formats. A detailed description and example using this highly interactive software system is given in Appendix D. The software system was used as a tool to analyze selected models of damage.

At the start of this study, several models of damage states within a laminate were selected from the viewpoint of establishing bounds on the 0° ply stress state. Figure 52 shows four xz and two yz section models of a quasi-isotropic laminate, selected here as an example for purposes of discussion. Case (a) assumes that the entire load on the laminate is carried by the 0° plies just prior to failure. In the absence of significant stress concentration effects near 90° transverse cracks, this model can be used as a lower bound estimate of laminate strength (or an upper bound estimate of the average 0° ply stress state). Case (a) can be obtained from the ADVLAM laminate code by setting the stiffnesses E_2 and G_{12} to zero in the 90° and 45° plies. Cases (b), (c), and (d) require FREEVIS for xz section analysis. Case (b) uses effective stiffnesses for the 90° and 45° plies based on the observed transverse crack density and an analysis, of E_2 and G_{12} as a function of crack density (see Section 3.3.3). Case (c) models only the transverse cracks adjacent to the 0° ply and uses effective stiffness for the cracked 45° plies. Case (d) models 90° transverse cracks and any surface delamination at (0/90), (90/45), and (45/-45) interfaces, but uses effective stiffness for the 45° cracked plies. Case (e) considers delamination only without transverse cracks while Case (f) considers a region of 0° fibers on the edge having split away.

Figure 53a shows the difficulty in modeling both 90° and 45° ply cracks in a xz section. Only at one point in the entire xz plane do both cracks line up to give the crack trace in the xz plane (shown as the dashed section in Figure 53b). A 45° crack cannot be directly introduced into the xz section because fibers in the 45° ply would be cut, a physically unrealistic model. Furthermore, the 90° ply crack is constrained from extending into the 45° ply by fibers in the latter ply which cross the 90° crack plane, except at the one point in the yz plane where the 90 and 45° transverse cracks intersect. The model in Figure 53b removes the constraint on the 90° crack

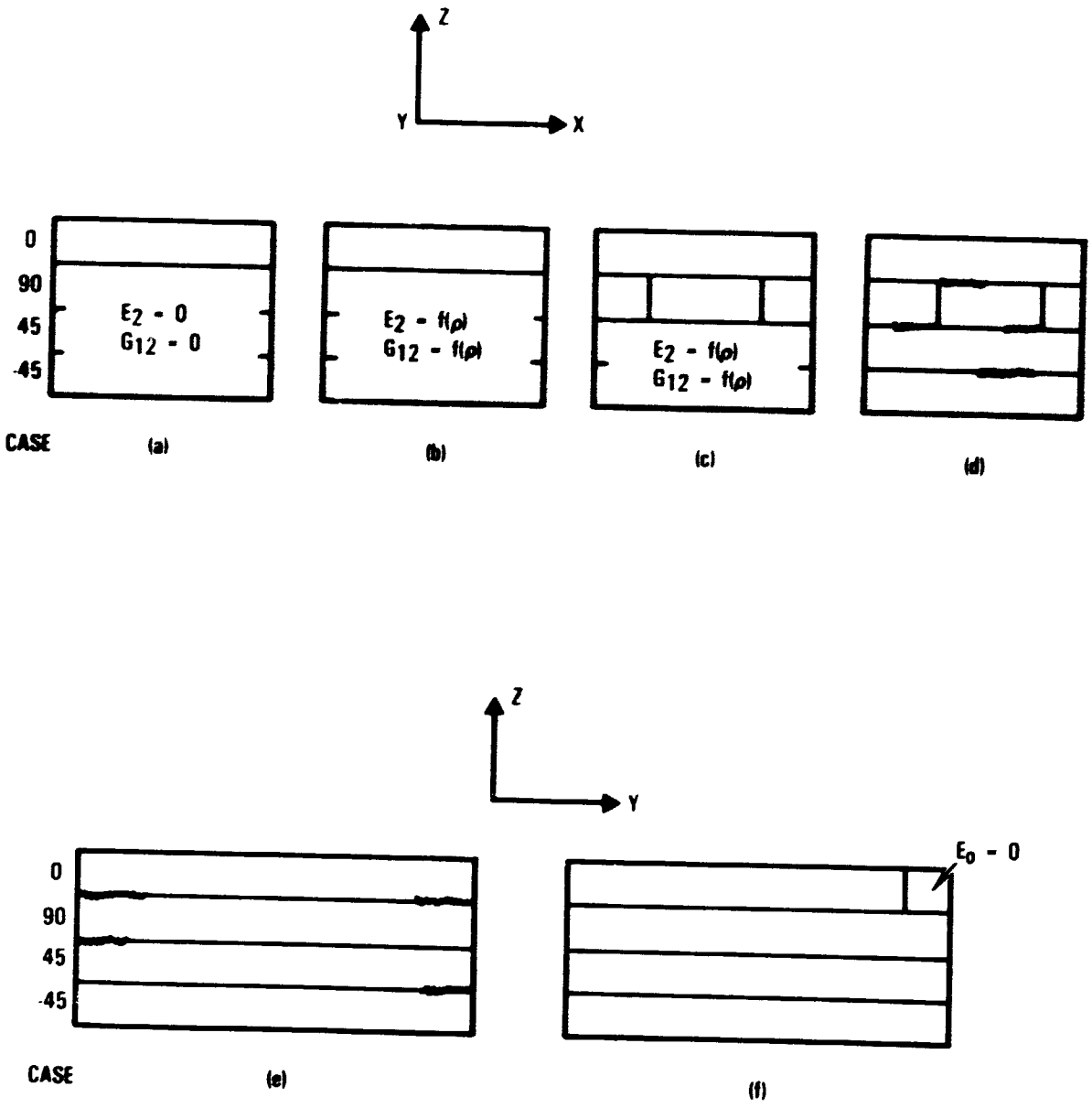

Figure 52: Section models of damage state in a $(0/90/\pm45)_s$ laminate.

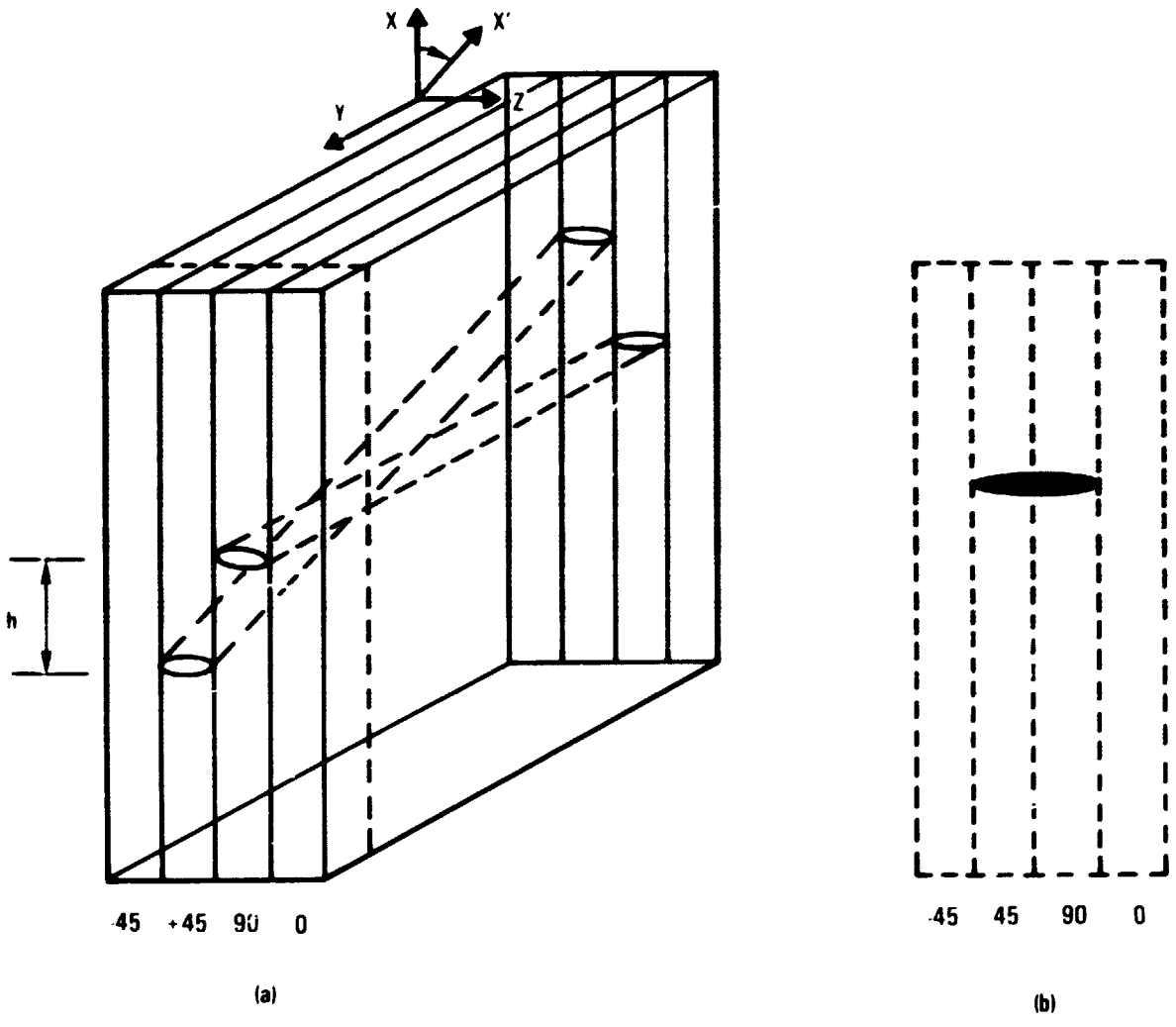

Figure 53: Intersection of 45^{o} and 90^{o} plv matrix cracks.

and will seriously overestimate the effective length of the transverse crack and its influence on the 0° ply stress state. This problem for the 45° plies was solved by substructuring and "smearing" the effect of the 45° ply into an average stiffness value.[69]

If the stress/strain state in the xz plane of the 0° ply is obtained, for example, using the models of Figure 52 (and the yz stress distribution when edge delamination or failure of the 0° ply near the edge is modeled), that stress state can be used to consider failure of the 0° ply. For cases (c) and (d) of Figure 52, the stress state in the 0° ply will vary with position in the ply and certain stress components will approach singular values at the tip of the 90° ply cracks. Essentially, this procedure of analyzing different damage states for the amount of load transferred in some small region to the 0° plies is the same as that previously discussed by O'Brien[41] and by Ryder[7,13].

The two dimensional modeling procedure used in this investigation resulted in cracks in the 90° layers being exactly represented as well as their interaction with the 0° plies. The effect of cracks in the $\pm 45^{\circ}$ layers was averaged with effective moduli because they cannot be directly represented using a two dimentional model. This procedure was based upon the previously mentional concept of modeling by substructuring[69]. Experience with analyzing free-edge stresses by substructuring techniques[69] has indicated that the properties of all layers at least one ply away from the layer or interface of interest can be smeared or averaged into an effective set of stiffnesses without altering the calculated stress state in the region of interest. These results indicated that the use of crack altered effective stiffnesses for the 45° layers was not only accurate, but often easier than direct modeling of transverse cracks in the 45° layer. This technique was thus often used in this study.

3.3 STIFFNESS CHANGE ASSOCIATED WITH TRANSVERSE CRACKS AND DELAMINATION

In the following subsection, the modeling efforts undertaken to determine stiffness changes expected for various aspects of transverse matrix and delamination cracking are discussed.

3.3.1 Effective Laminate Stiffness

In this subsection, the modeling problem of determining the effective stiffness of the 90° and 45° plies associated with multiple transverse cracks is discussed as transverse crack density increases. The analysis was not limited to the "saturation" density characteristics of shear lag or strain energy release rate analysis. Recent studies[12] on $(\pm 25/90_n)_s$ laminates have shown crack densities in regions of delamination which are greater than the saturation density. The mechanics of the formation of this high density of cracks is not sufficiently understood to make quantitative predictions. Therefore, the density of transverse cracks found by actual experimental observation was used in the analysis of stress redistribution within the laminate.

A cross section of a $(0/90)_s$, T300/5208 coupon was modeled by finite elements. The model consisted of 220 elements and 143 nodes. A transverse crack, without delamination at the ends, was introduced in the 90° layer and finite elements were graded from a size of one quarter times the ply thickness near the crack to two times the ply thickness far from the crack at an arbitrary distance, L. A uniform displacement was imposed to simulate tensile loading. The position of L was varied to determine the effect of increased transverse crack density on the tensile modulus of the $(0/90)_s$ laminate. Ratios of L/t (where t is ply thickness) between 1 and 31 were investigated for a ply thickness of 0.13 mm (0.005 in.). This corresponded to a transverse crack density of 1.26 to 39.4 per centimeter In the failure model, a uniform dispersion in the coupon width direction at the L

position was used to determine the in-plane shear modulus of the $(0/90)_s$ laminate as a function of crack density. A Lockheed developed laminate code[70,71] called ADVLAM was employed to determine the effective E_2 and G_{12} moduli of the 90° layer needed to produce the change in stiffness consistent with the desired model of transverse cracking determined by the finite element method.

Using the finite element grid shown in Figure 54 and 55, and the boundary conditions described above, the effective lamina stiffnesses were determined as follows:

1. The reduced laminate stiffness E_x and G_{xy} in the presence of transverse cracks in the 90° layer of a $(0/90)_s$ laminate were determined as a function of crack density. These results are shown in Figures 56 and 57.

2. Next, the moduli E_2 and G_{12} of the "cracked" 90° layer were reduced, and the resulting $(0/90)_s$ laminate stiffness E_x and G_{xy} were determined as a function of level of reduced moduli in the 90° layer.

3. From these analyses, the effective moduli E_{22} and G_{12} of the cracked 90° layer were plotted as a function of crack density as shown in Figures 58 and 59.

Comparison between the laminate stiffnesses (obtained by substitution of effective moduli in the "cracked" 90° layer) determined from the ADVLAM point stress laminate analysis and from the FREEVIS finite element model analysis showed essentially identical results.

The effective modulus plots of E_{22} and G_{12} as a function of crack spacing are presented in Figures 60 and 61. The spacing is normalized to the thickness of the cracked ply which in this analysis of a $(0/90)_s$ laminate was twice the thickness of an individual ply. It can be observed from Figures 60 and 61 that for normalized crack spacings of 5 or greater (i.e., those typically observed in laminates), the effective modulus reduction is no more than 20 - 30 percent from the original value.

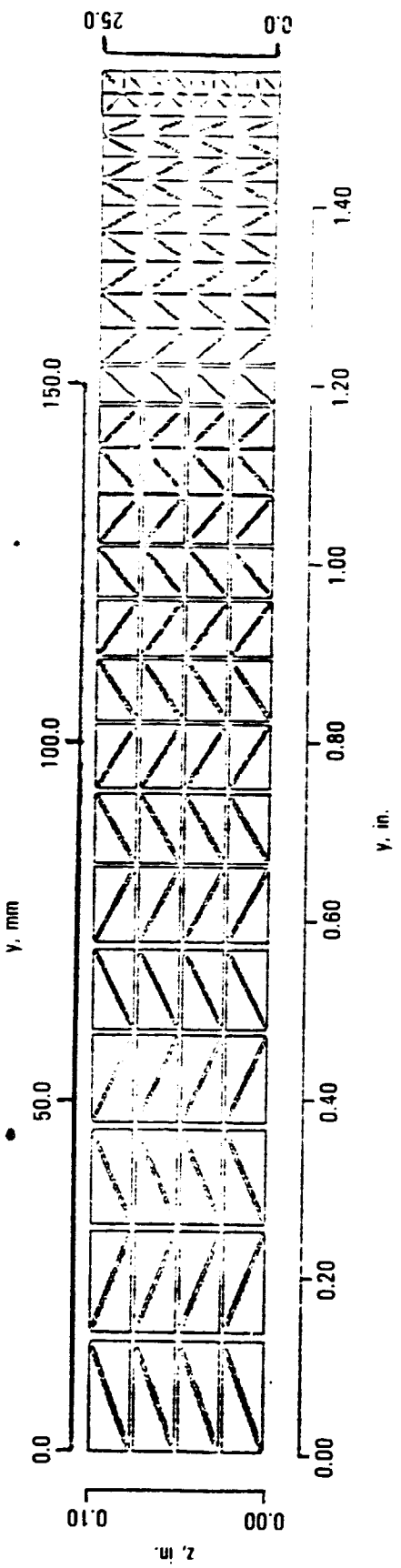

Figure 54: Finite element grid.

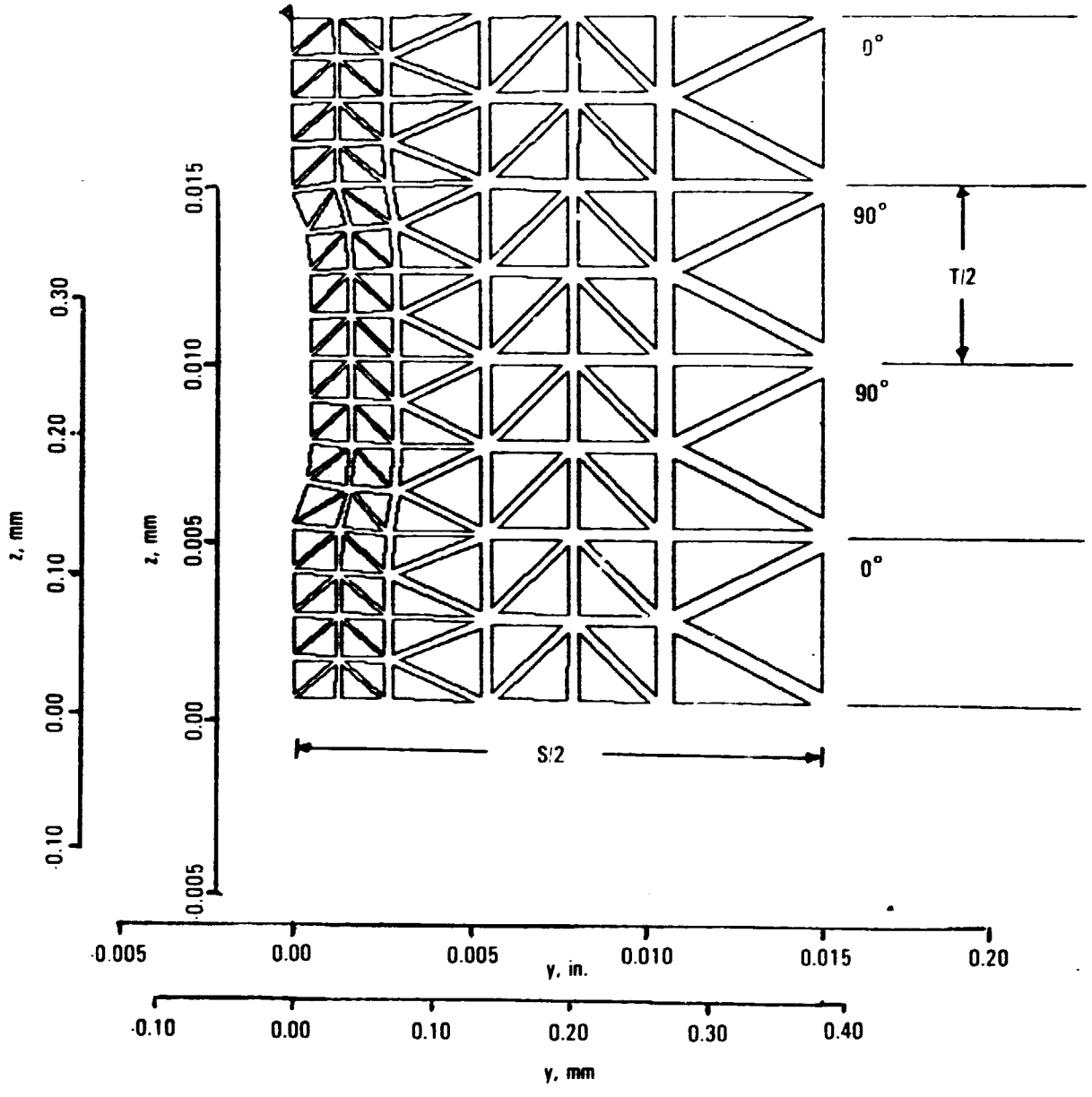

Figure 55: Crack Plane Detail of Finite Element Model Shown in Figure 54.

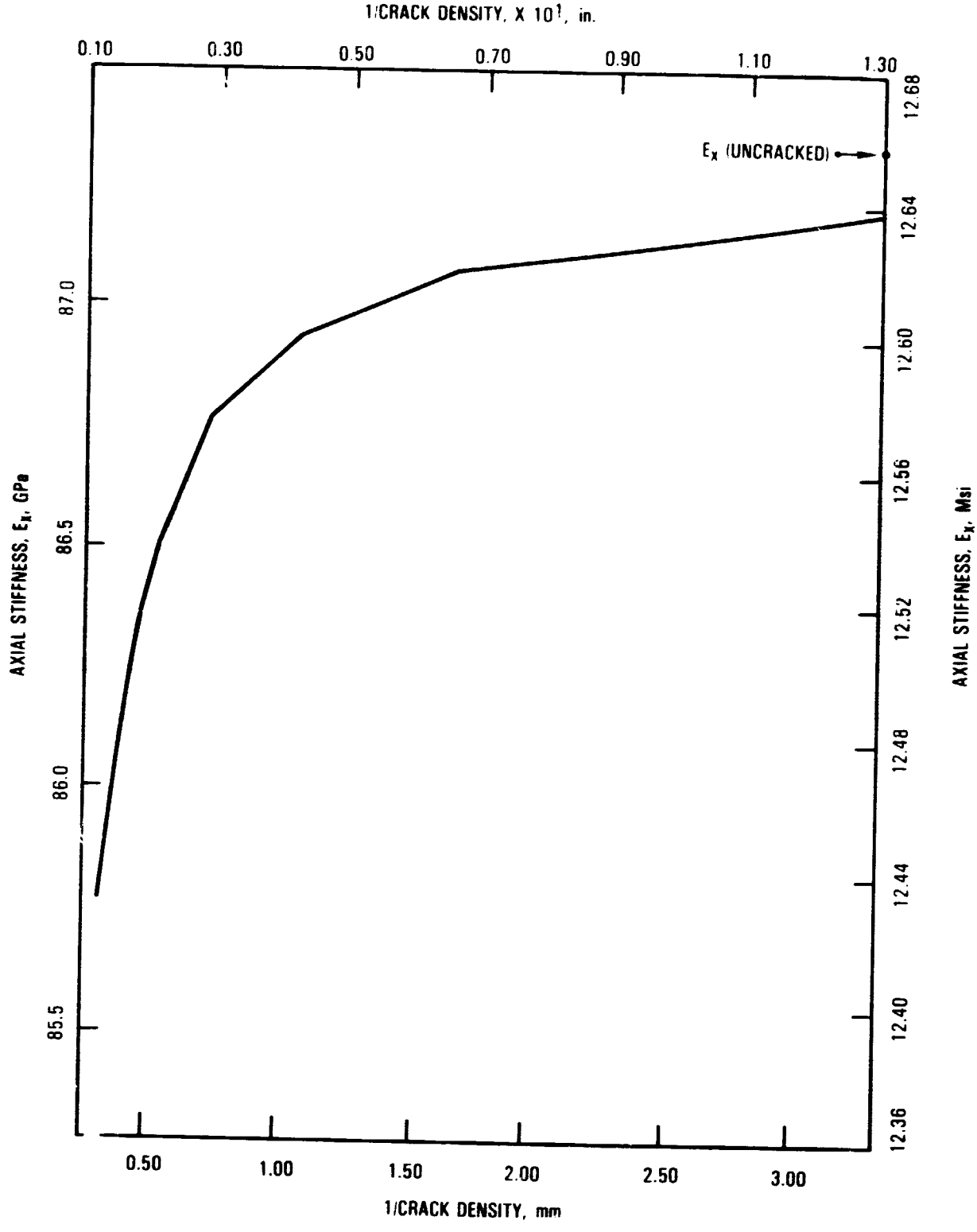

FIGURE 56 $(0/90)_s$ LAMINATE STIFFNESS VS CRACK DENSITY (E_x VS ρ-1)

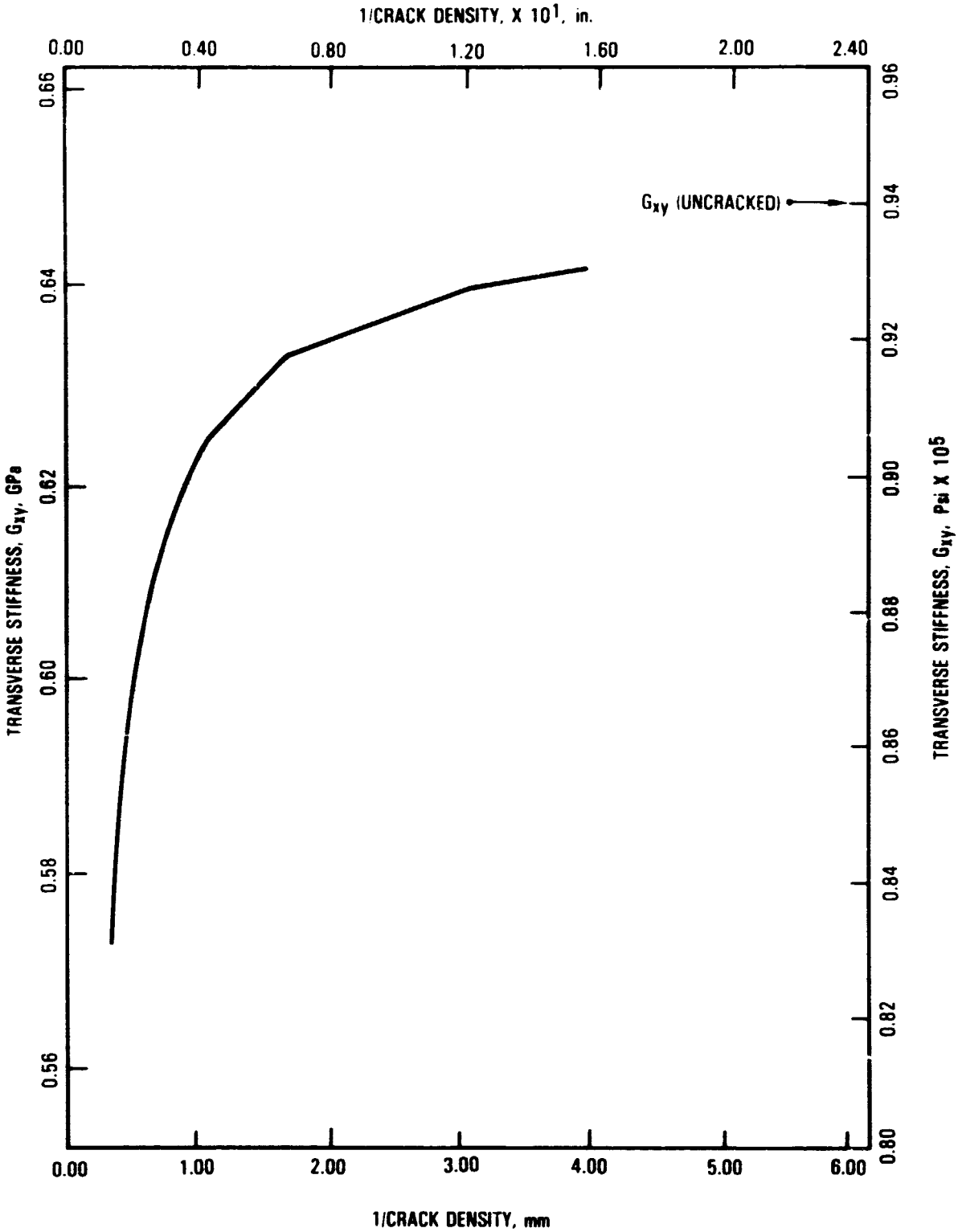

FIGURE 57. $(0/90)_s$ SHEAR STIFFNESS VS CRACK DENSITY (G_{xy} VS ρ^{-1})

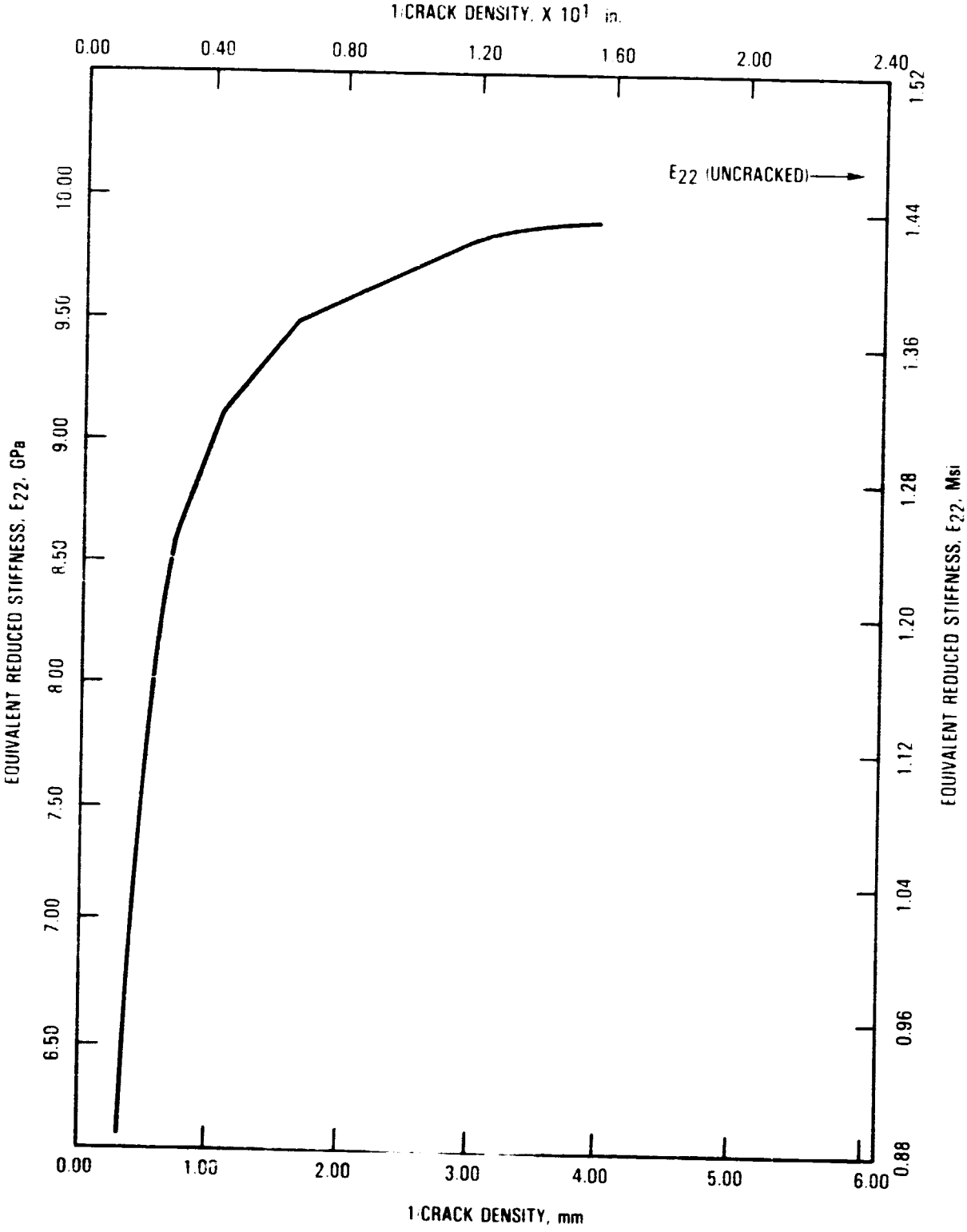

FIGURE 5-. EQUIVALENT STIFFNESS VS CRACK DENSITY E_{22}^{EQUIV} VS P 1)

3 OF 6

N84-29978 UNCLAS

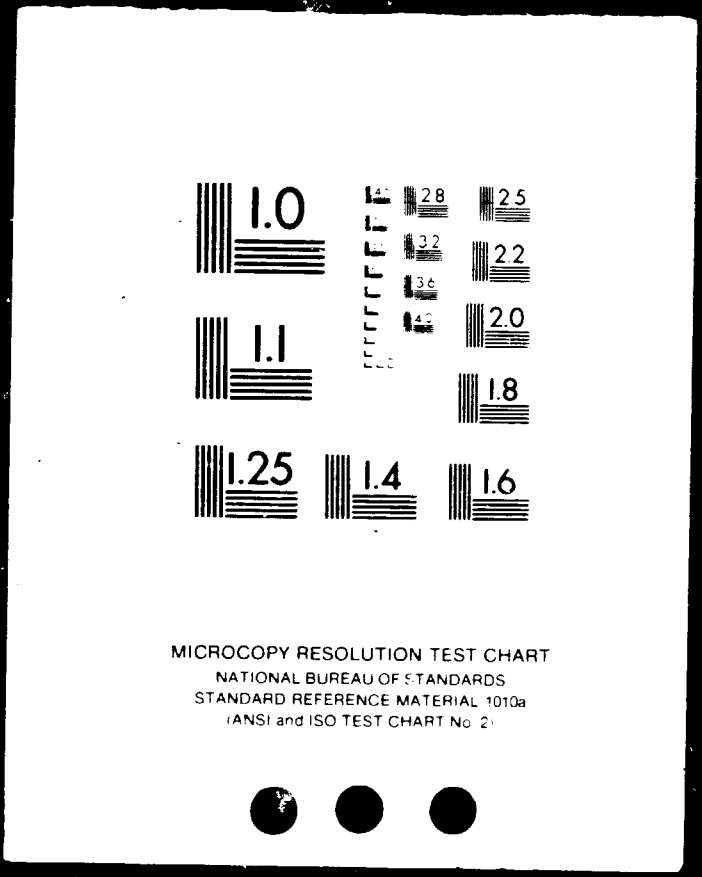

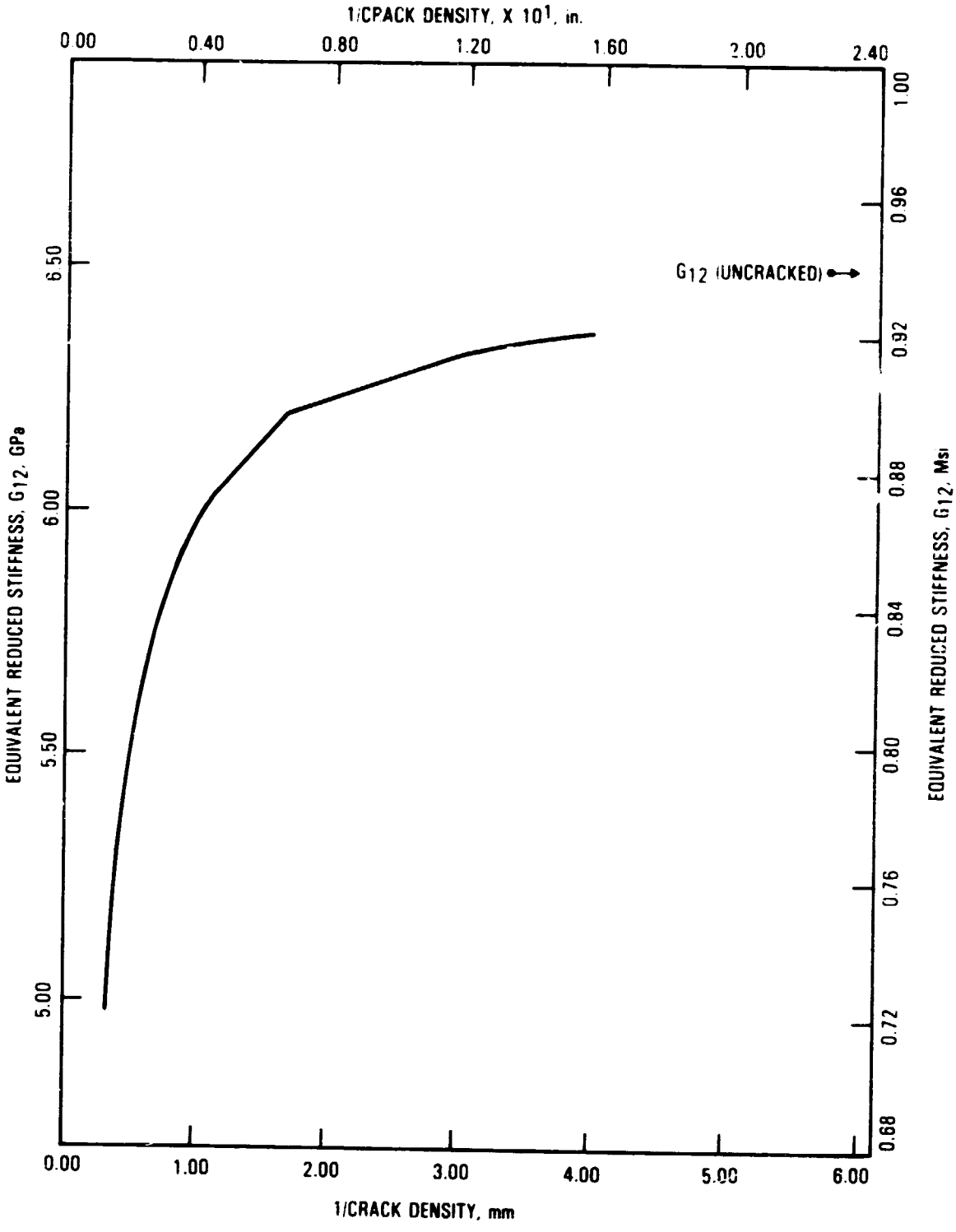

Figure 59: Equivalent stiffness vs property change (G_{12}^{equiv} vs p^{-1})

C-3

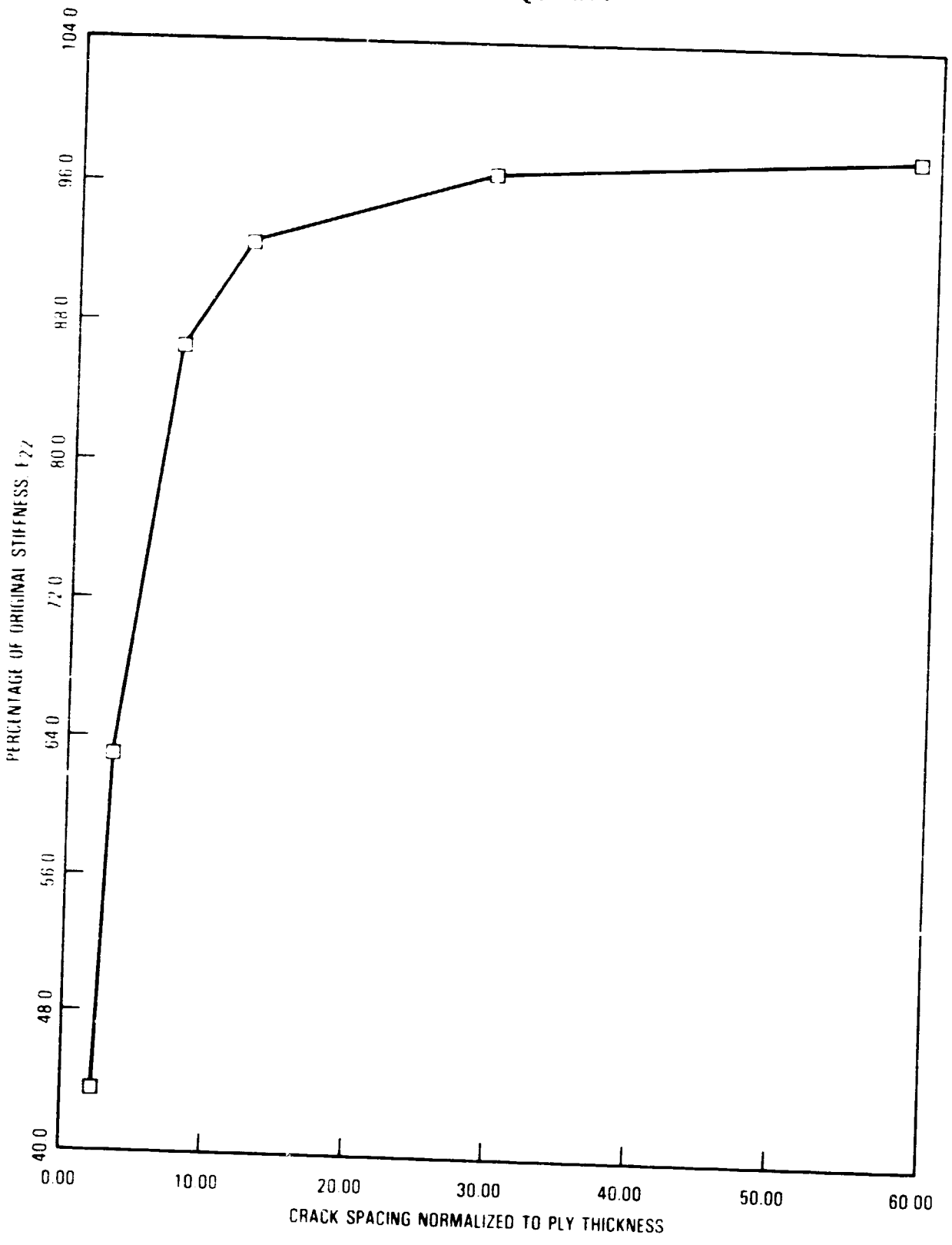

Figure 60: Effective modulus E_y for a $(0/90)_s$ laminate.

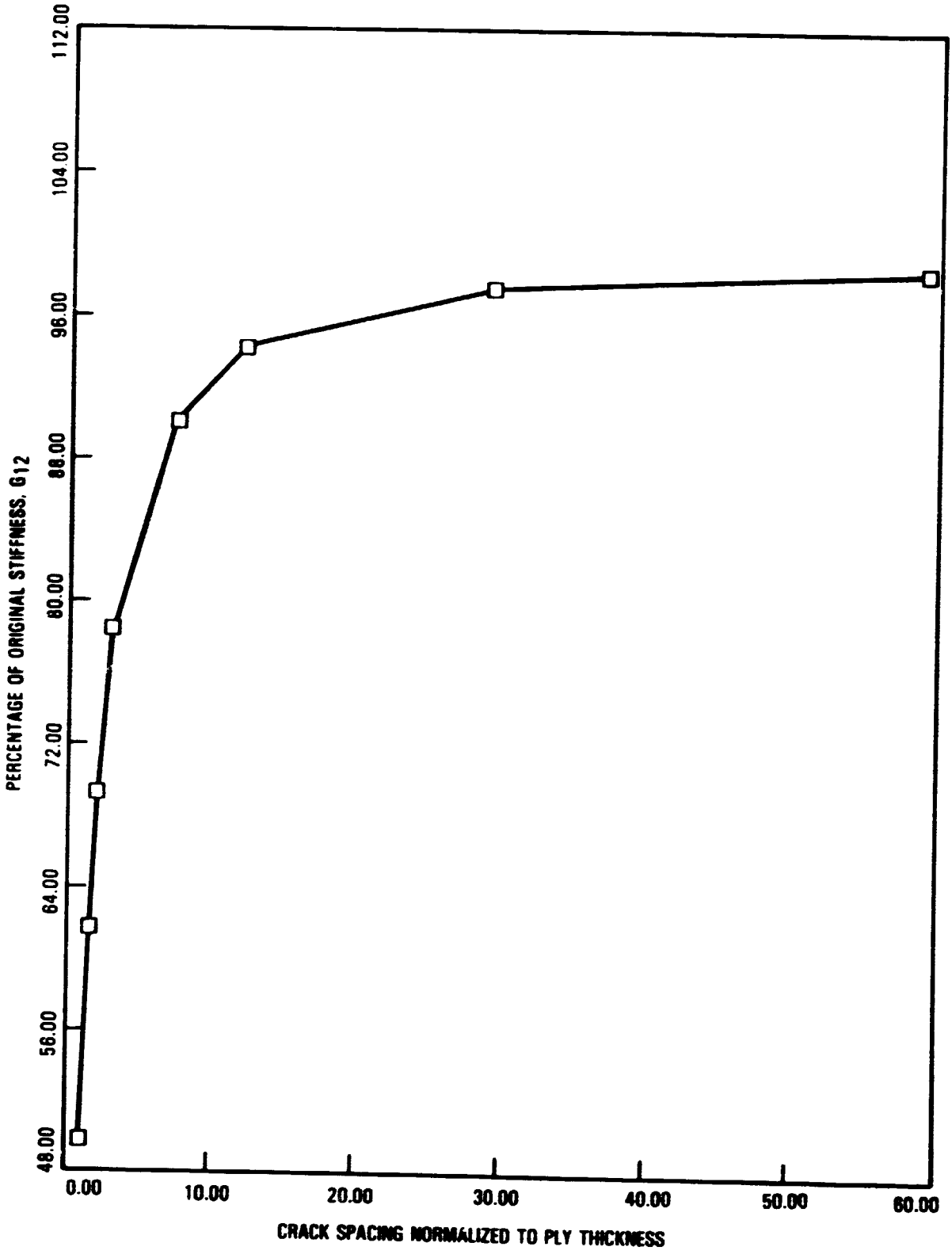

Figure 61: Effective modulus G_{12} for a $(0/90)_s$ laminate.

As an example of the effect of transverse cracking alone, crack spacing data from Reference 1 for tensile loaded $(0/45/90/-45)_s$ laminates are provided in Table 38, and the effective E_{22} and G_{12} moduli for each cracked layer in the laminate were determined from Figures 60 and 61. The results of the analysis, using the ADVLAM laminate code, for the Young's modulus of the laminate with initial (uncracked condition) and effective moduli are summarized in Table 39. Analysis case 1B in Table 39 included a study of the effect of reducing Poisson's ratio of the cracked layer from 0.3 to 0.05. No significant effect on the results was found. Case 1D allowed for a 50% reduction in both E_{22} and G_{12} in all non-0° layers. Such large effective modulus reductions are only possible for a crack spacing, s/t, less than 1, (over 100 cracks per 25 mm) which was not observed in these laminates. Thus the experimentally observed crack densities can account for only a 2% reduction in Young's modulus for the $(0/45/90/-45)_{2s}$ laminate. Similar results were obtained for the other quasi-isotropic layups and for the $(0_n/90_n)_s$ laminates. Case 2 in Table 39 shows that the reduction in axial stiffness in a tension loaded $(45/-45)_s$ laminate on which the ply stresses are shear dominated is due nearly entirely to the reduction of G_{12} and is little influenced by a reduction in the E_{22} term.

3.3.2 Effective Transverse Modulus of Cracked 90° Plies vs Laminate Stiffness

Further mathematical analysis was conducted to see whether the relative stiffness of the constraining plies could play a role in altering the master curves for effective transverse modulus which were presented in Section 3.3.1. The finite element model used for this analysis was the same as that shown in Figures 54 and 55. The definition of crack spacing and cracked ply thickness is evident from Figure 55. The model enabled analysis of high densities of cracks with a crack spacing to thickness ratios (s/t) of 1 to 3 (200 to 66 cracks per 25 mm). The ply thickness was chosen as 0.13 mm (0.005 in.) and the T300/5208 properties from previous analyses were used.

TABLE 38
DATA FOR EFFECTIVE MODULUS CALCULATIONS

Observed Cracks Per 25.4 mm (1 in.)	Crack Spacing Per Ply Thickness s/t	Effective Modulus, Percent E_{22}	Effective Modulus, Percent G_{12}
60 (90^{o} Ply)	3.33	82	90.4
16 ($+45^{o}$ Ply)	12.5	96	97.7
10 (-45^{o} Ply)	20.0	96.5	98.0

E_{11} = 163 GPa (22.7 Msi)
E_{22} = 10.2 GPa (1.48 Msi)
G_{12} = 6.48 GPa (0.94 Msi)
V_{12} = 0.3

TABLE 39
EFFECT OF TRANSVERSE MATRIX CRACKING ON LAMINATE MODULUS

Note: Properties from Table 38 used in this analysis.

Case	Stiffness E_x GPa	Msi	Percent of Original Uncracked Stiffness
Case 1 $(0/45/90/-45)_{2s}$			
A. Uncracked	63.20	9.166	100
B. Cracks Per Table 38	62.08	9.004	98
C. Cracks and Reduced ν	62.05	9.000	98
D. 50% E_{22} and G_{12}	58.85	8.535	93
Case 2 $(45/-45)_s$			
A. Uncracked	27.67	3.288	100
B. 50% G_{12}	12.09	1.754	53
C. 50% E_{22} Only	22.53	3.268	99
D. 50% G_{12} and E_{22}	12.05	1.748	53

Figure 62 shows the relation between the $(0/90)_s$ laminate modulus and the spacing of transverse cracks in the 90° layer. Figure 63 shows a plot of the same laminate modulus as a function of reducing the transverse modulus of the 90° layer. Plots similar to Figures 62 and 63 were generated for $(45/90)_s$ and $(90_{uncracked}/90_{cracked})_s$ laminates.

By cross correlation of the pairs of plots, a master curve was prepared for the effective transverse modulus of the cracked 90° layer as a function of crack spacing for each of the three laminates considered as shown in Figure 64. Clearly the effective modulus of the cracked layer is a function of the stiffness of the uncracked constraining layers. Figure 65 shows the effective laminate modulus as a function of initial laminate modulus. However, since most of the laminates applied in practice have moduli ranging from 55 to 100 GPa (8 to 15 Msi), Figure 65 indicates that the results obtained in Section 3.3.1 for the $(0/90)_s$ laminate were indeed appropriate for purposes of predicting the reduction in laminate stiffness. Figures 66 and 67 provide plots of the effective transverse modulus normalized to the initial value as a function of crack spacing and crack density. The latter plot was normalized to the ply thickness so that it could be used for a variety of other laminate configurations. The original plot of normalized $G_{12\ eff}/G_{12uncracked}$ is presented in Figure 68 in the same format.

3.3.3 Laminate Stiffness Change Associated With Transverse Cracks and Delamination

As described in Sections 3.3.1 and 3.3.2, a generalized plane strain model of a $(0/90)_s$ laminate was used to assess the effective modulus of the cracked 90° layer under both normal and shear loading. A further study was conducted to define the effective transverse and shear modulus of the cracked layers with the additional effect of short delaminations emanating from the tips of the transverse ply cracks called end delaminations. The case of transverse cracks alone was called TC and that with end delaminations HC because the combination of a transverse crack and end

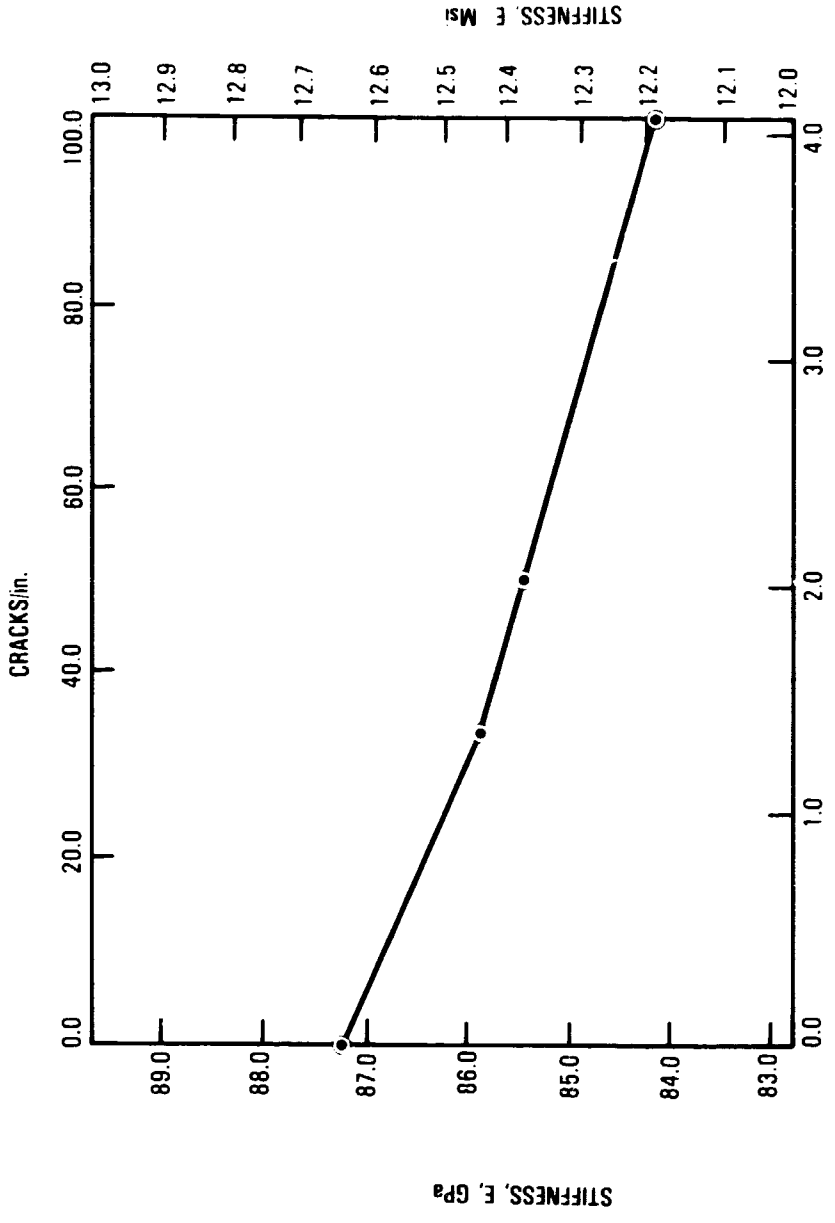

FIGURE 6. $(0/90)_s$ LAMINATE MODULUS VERSUS 90° PLY TRANSVERSE CRACK SPACING.

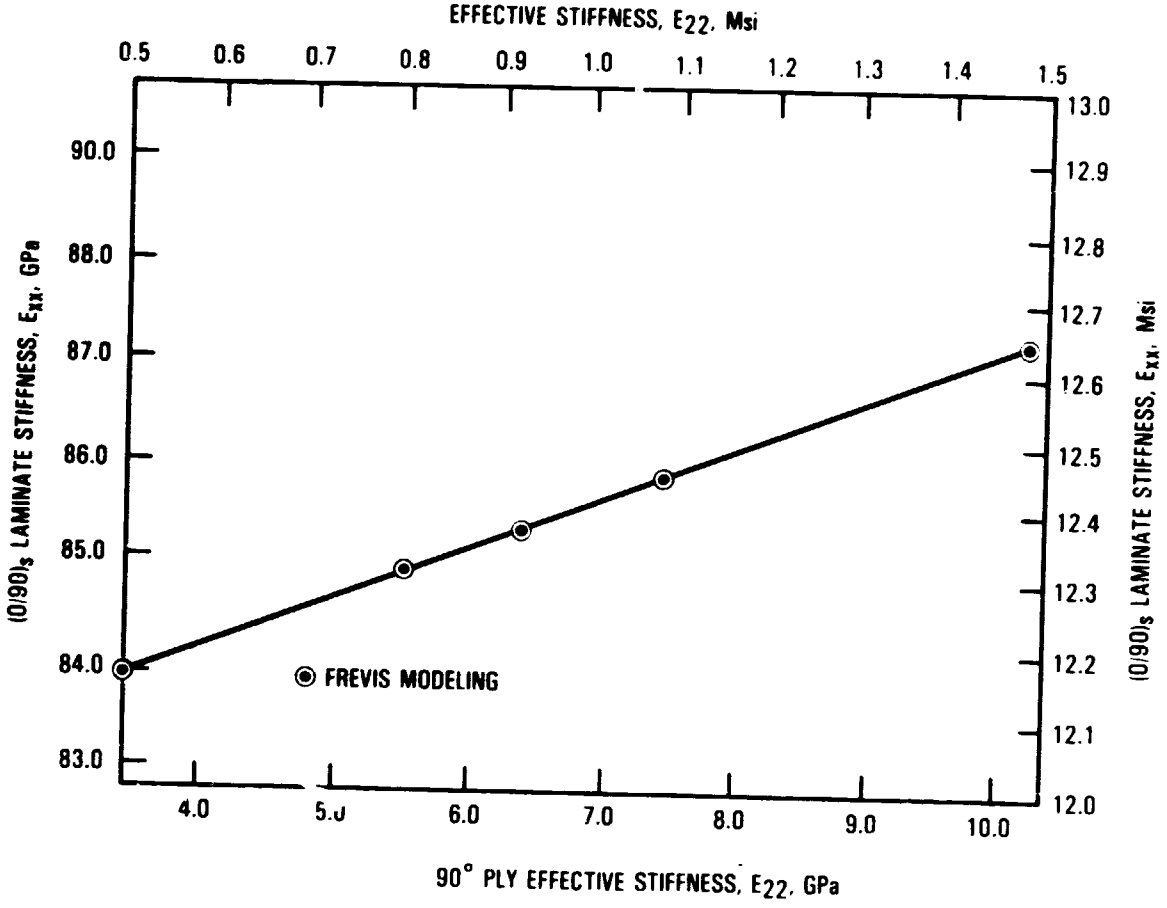

FIGURE 63. LAMINATE MODULUS VERSUS 90° PLY TRANSVERSE MODULUS REDUCTION FOR A $(0/90)_s$ LAMINATE.

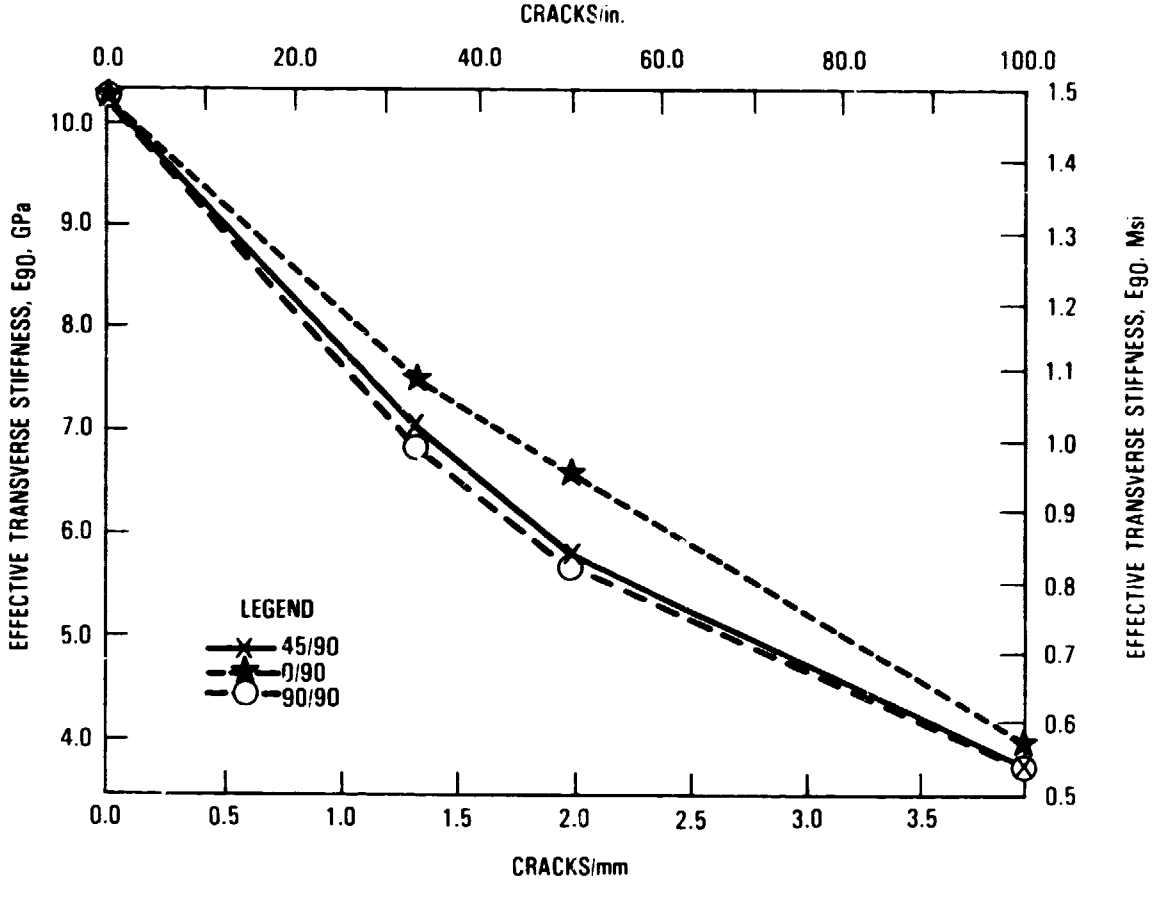

FIGURE 6[illegible]. MASTER CURVES OF EFFECTIVE TRANSVERSE MODULUS VERSUS CRACK SPACING FOR VARIOUS LAYUPS.

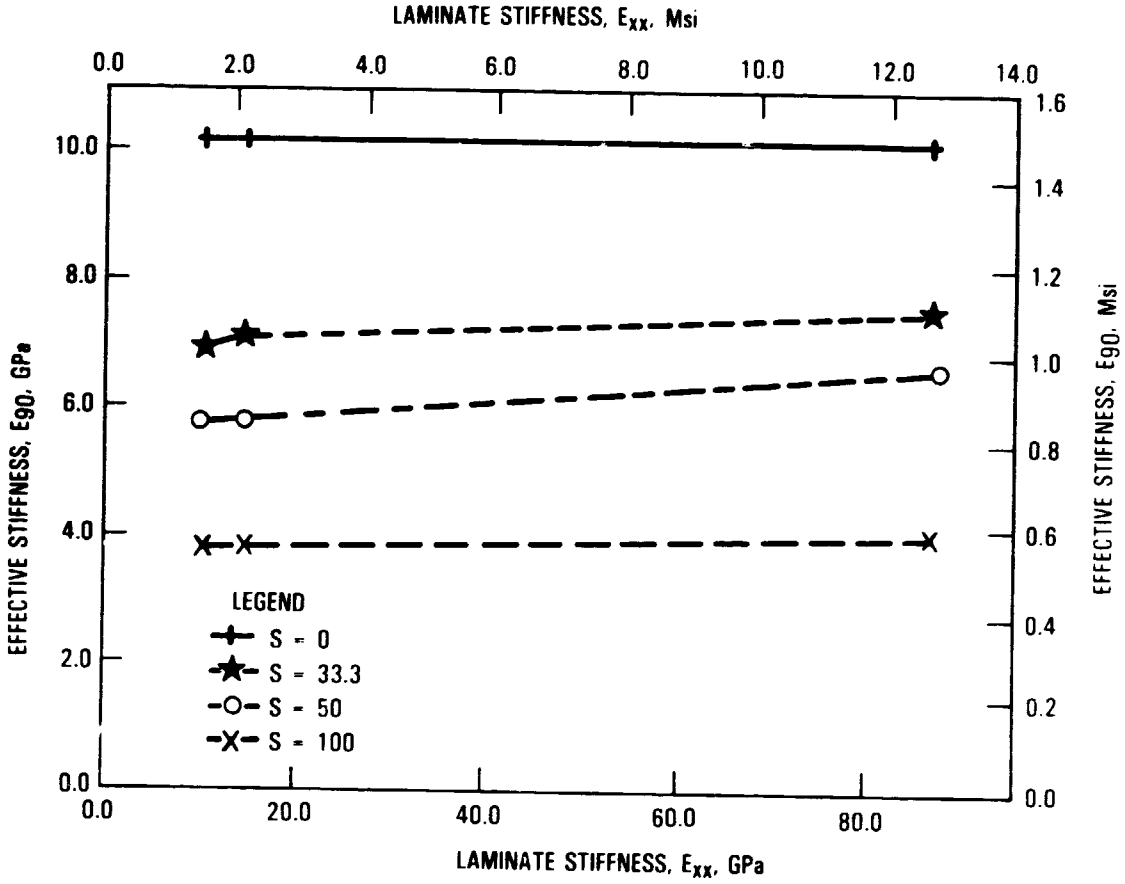

FIGURE 65 . EFFECTIVE STIFFNESS AS A FUNCTION OF INITIAL LAMINATE STIFFNESS

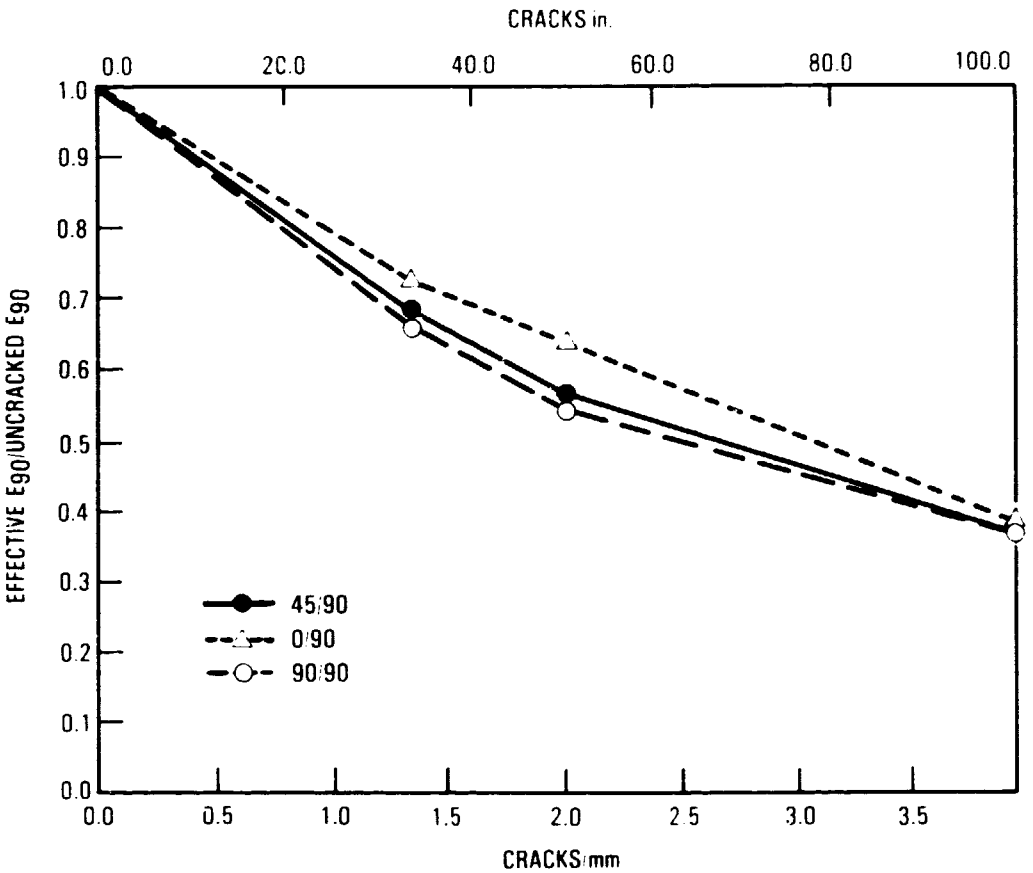

FIGURE · · NORMALIZED EFFECTIVE TRANSVERSE MODULUS VERSUS CRACK SPACING.

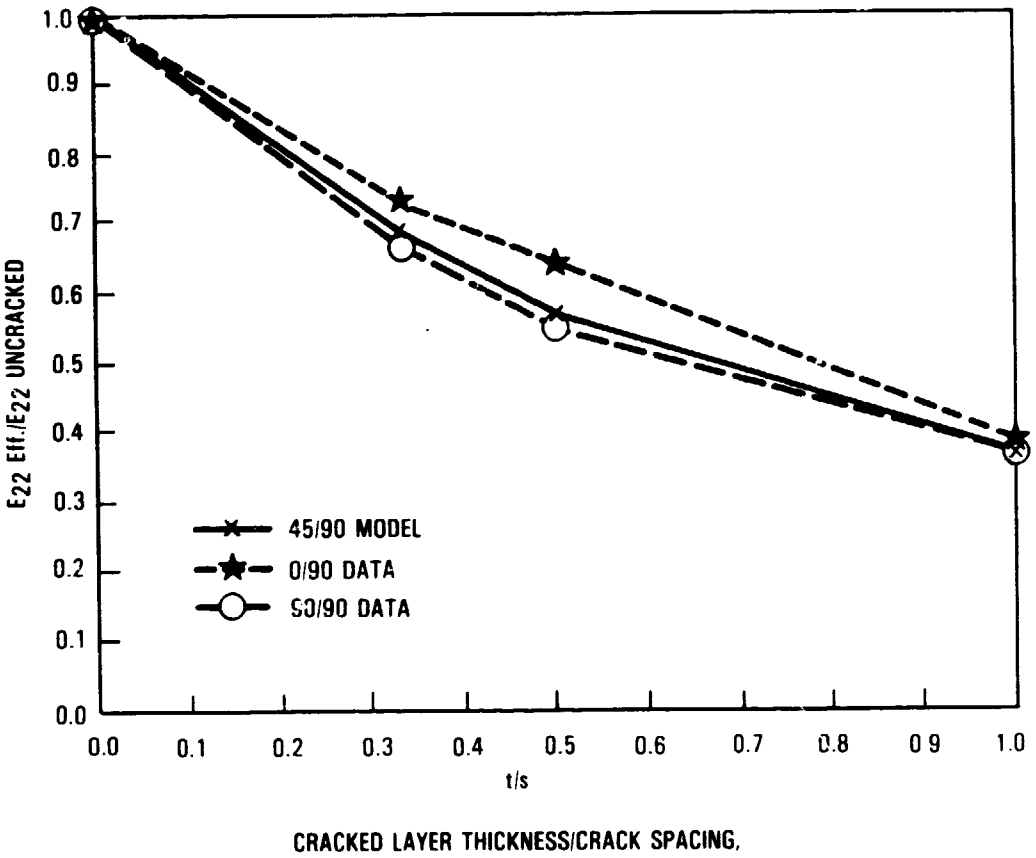

Figure 67: Normalized effective transverse modulus vs. crack density.

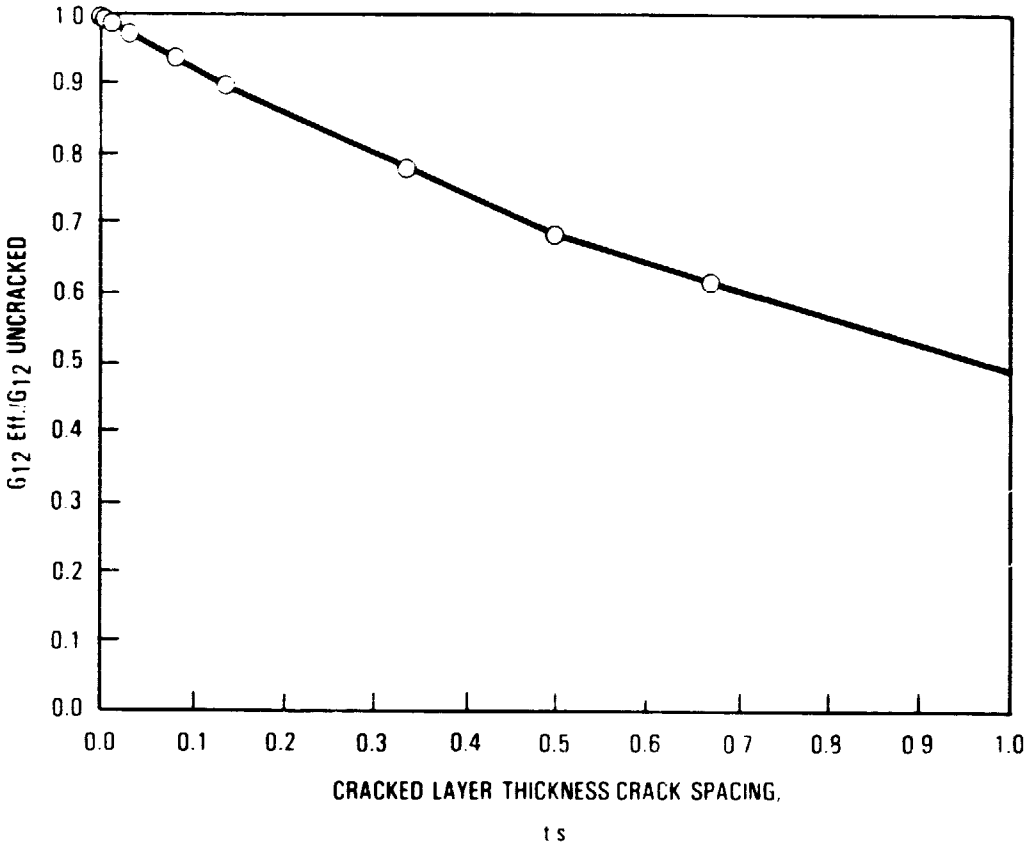

Figure 68: Normalized effective shear modulus vs crack spacing.

delamination exhibits the shape of a letter H when the coupon is held vertically and viewed on edge.

The presence of delamination at the ends of the transverse matrix cracks resulted in a dramatic change in the local deformation of the off-axis ply layer as can be seen by comparing Figure 69 to Figure 55. For modeling purposes, the delamination cracks were assumed to have a length of one ply thickness on each side of the transverse cracks. The reduction of curvature on the transverse crack surface is the result of stress relaxation in the region between the two delamination cracks which effectively unloads the entire zone of the 90° matrix crack that lies vertically between the two delaminations. Using the procedure described in Section 3.3.2, the effective moduli of the HC cracked layer were determined. Figure 70 shows the effective E_{22} and G_{12} moduli (normalized to uncracked layer values) versus the normalized density of transverse cracks (expressed by the thickness of the cracked layer divided by the crack spacing). A significant reduction in effective modulus occurs due to the delamination cracks (about 50% of the total reduction).

Tables 40 to 43 give the calculated reduction in laminate stiffness associated with the experimentally measured density of transverse cracks found for each laminate due to the indicated loading condition. In the calculations, the average crack densities (minimum range values plus maximum range value divided by two) previously shown in Tables 9, 15, 27, and 35 were used. The two values projected from the experimental calculations for each laminate are those anticipated using the moduli data in Figure 70 associated with transverse cracks only (TC's) and those appropriate for "H" cracks (HC's).

Clearly Tables 40 to 43 show that the combination of end delamination and transverse cracks results in significant additional stiffness loss. However, the calculations for HC cases assumed that such delaminations extended across the coupon width and occur at each transverse matrix crack.

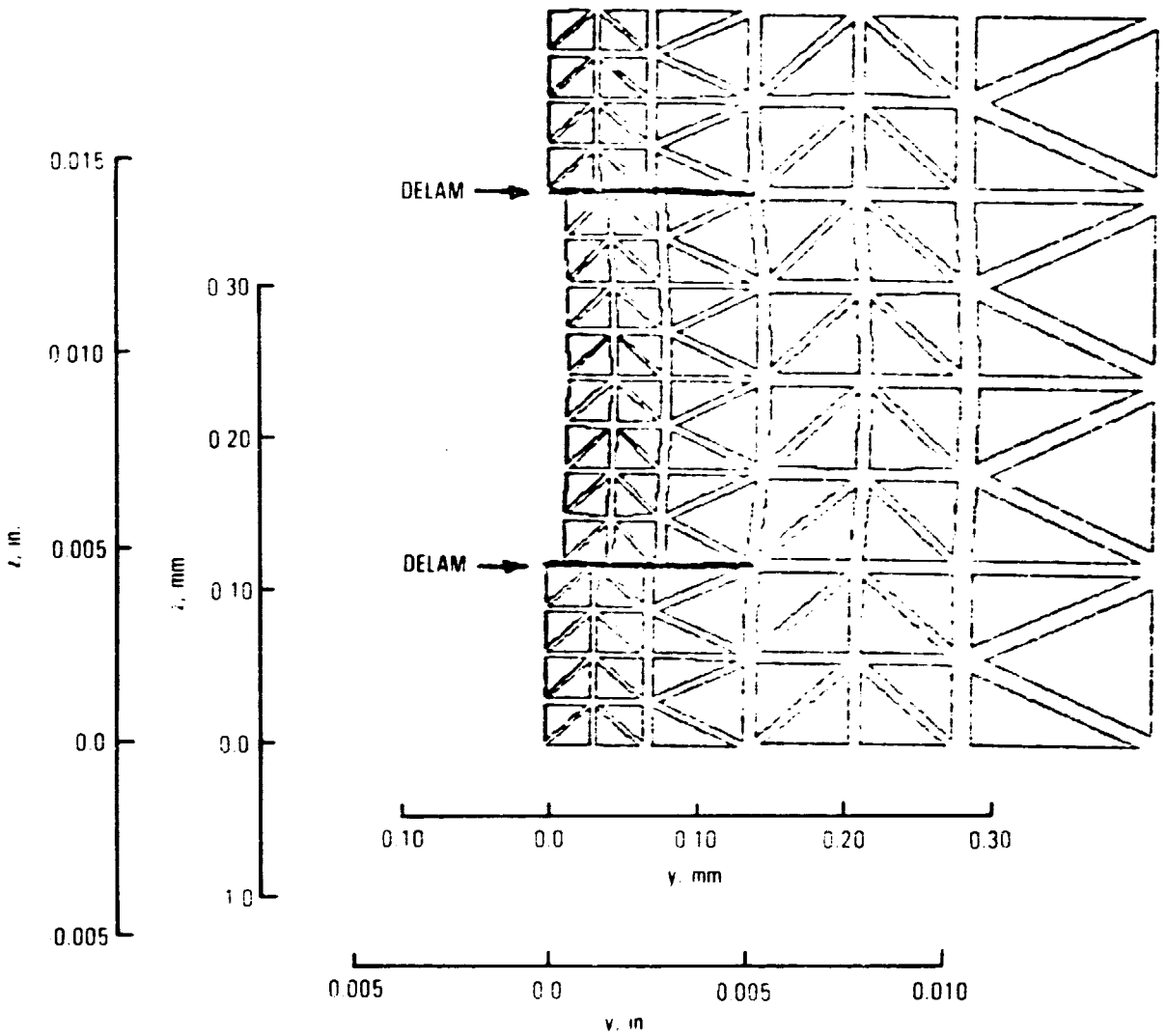

FIGURE 69. FINITE ELEMENT MODEL USED FOR ANALYZING COMBINED EFFECT OF A TRANSVERSE CRACK AND DELAMINATION IN A $(0_2\ 90_4)_s$ LAMINATE

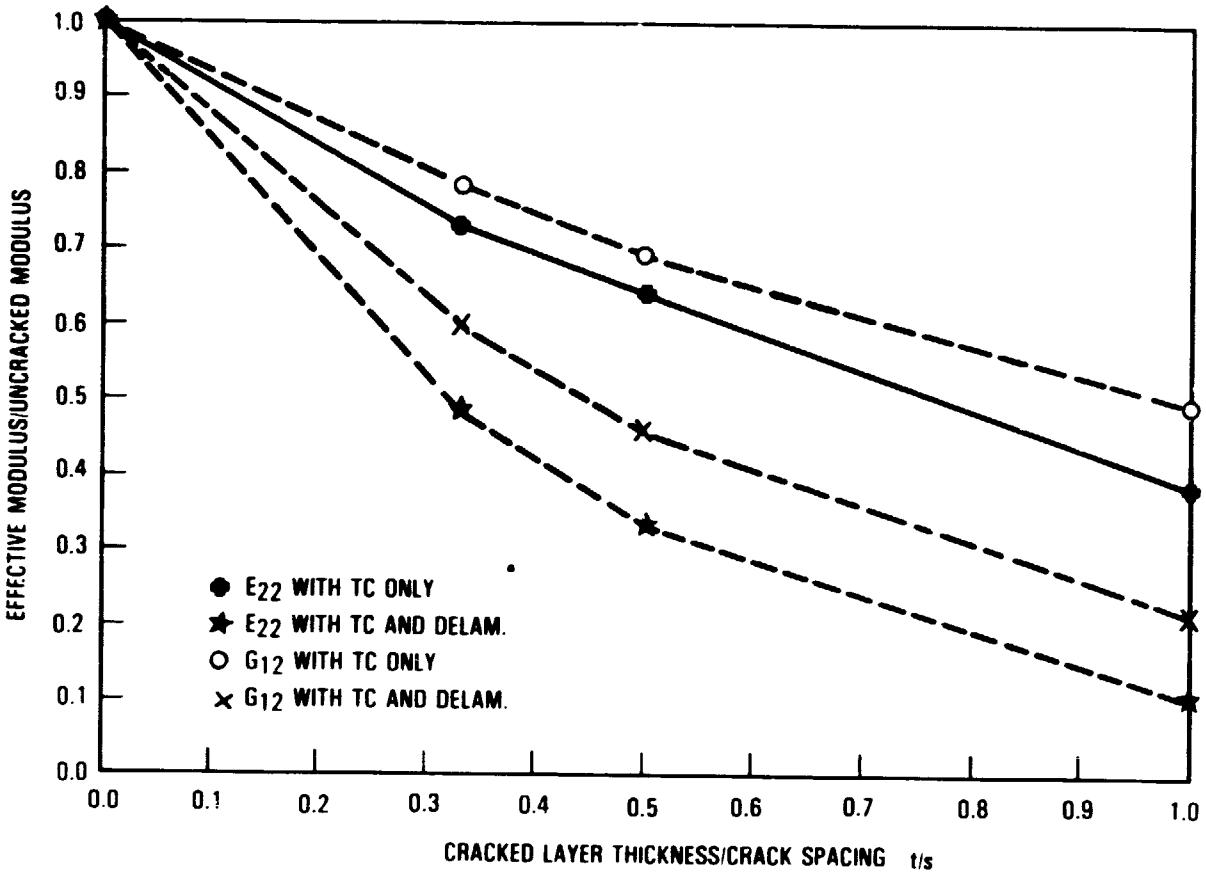

FIGURE 70. NORMALIZED EFFECTIVE MODULUS VERSUS CRACK DENSITY

TABLE 40
LAMINATE STIFFNESS REDUCTION DUE TO TRANSVERSE CRACKING
IN $(0/90/45/-45)_s$ LAMINATE

LOADING CONDITION	AVERAGE CRACK DENSITY IN PLY (PLY THICKNESS/SPACING) (See Table 9)			E_x/E_x (initial) CALCULATED FOR	
	90	45	-45	TC's	HC's
MONOTONIC TENSION	0.43	0.08	0.00	0.986	0.974
FATIGUE					
379 MPa	0.42	0.24	0.12	0.977	0.956
413 MPa	0.29	0.22	0.10	0.980	0.964
448 MPa	0.42	0.24	0.12	0.977	0.956
RESIDUAL STRENGTH					
After Fatigue at 379 MPa	0.46	0.24	0.10	0.977	0.956
Monotonic Tension	0.50	0.27	0.09	0.975	0.953

TABLE 41
LAMINATE STIFFNESS REDUCTION DUE TO TRANSVERSE CRACKING
IN $(0/45/-45)_s$ LAMINATE

LOADING CONDITION	AVERAGE CRACK DENSITY IN PLY (PLY THICKNESS/SPACING) (See Table 15)		E_x/E_x (initial) CALCULATED FOR	
	45	-45	TC's	HC's
MONOTONIC TENSION	0.17	0.12	0.982	0.966
FATIGUE AT 483 MPa	0.28	0.32	0.964	0.932
RESIDUAL STRENGTH After Fatigue at 483 MPa	0.28	0.27	0.967	0.938
Monotonic Tension	0.26	0.25	0.970	0.941

TABLE 42
LAMINATE STIFFNESS REDUCTION DUE TO TRANSVERSE CRACKING
IN $(0/45/0_2/-45/0)_s$ LAMINATE

LOADING CONDITION	AVERAGE CRACK DENSITY IN PLY (PLY THICKNESS/SPACING) (See Table 27) 45	-45	E_x/E_x (initial) CALCULATED FOR TC's	HC's
MONOTONIC TENSION	0.01	0.15	0.998	0.995
FATIGUE				
Initial ϵ = .0075	0.04	0.05	0.998	0.997
Initial ϵ = .0080	0.12	0.06	0.997	0.995
Initial ϵ = .0085	0.14	0.16	0.995	0.991
RESIDUAL STRENGTH				
After Fatigue				
ϵ = .0080	0.05	0.07	0.998	0.997
ϵ = .0075	0.04	0.06	0.998	0.997
Monotonic Tension	0.04	0.07	0.998	0.997

a = Calculated values assume that cracks fully transverse coupon width which did not always occur especially for the monotonic tension experiments.

TABLE 43
LAMINATE STIFFNESS REDUCTION DUE TO TRANSVERSE CRACKING
IN $(0_2/90_4)_s$ LAMINATE

LOADING CONDITION	AVERAGE CRACK DENSITY IN PLY (PLY THICKNESS/SPACING) (See Table 35) 90	E_x/E_x (initial) CALCULATED FOR TC's	HC's
MONOTONIC TENSION	0.90	0.938	0.907
FATIGUE			
Initial ϵ = .0050	0.78	0.945	0.913
Initial ϵ = .0060	0.92	0.938	0.906
Initial ϵ = .0065	0.95	0.935	0.904
RESIDUAL STRENGTH			
After Fatigue			
Initial ϵ = .0050	0.78	0.945	0.913
Initial ϵ = .0060	0.84	0.942	0.910
Initial ϵ = .0065	0.96	0.935	0.904
Monotonic Tension	0.69	0.950	0.919

For the monotonic tension experiments of the laminates of this investigation, the across the coupon width extension of the delaminations did not occur. In the fatigue experiments, matrix cracks with delamination at their ends were not found, by cross sectioning the coupons, to generally extend across the coupon width. However, some delaminations between the ± 45 plies did extend along the matrix cracks for up to 1/4 of the coupon width.

Although small cracks transverse to the matrix cracks were observed by Jamison and Reifsnider[40], in this program they did not appear to form a continuous interface network fully equivalent to delamination. Hence, although delamination extending from the transverse cracks does appear to at least potentially increase stiffness loss associated with matrix cracking, in practice such delamination was not observed in this program or in others [12,41] to occur to any significant extent except along the coupon edges. Thus the effect of delamination emanating from the ends of the transverse matrix cracks on stiffness loss due to transverse matrix cracking was not, in general, expected to be large. However, their effect on fracture of the 0° plies is not insignificant as will be discussed in Section 3.4.5.

3.3.4 Effect of Delamination on Laminate Stiffness

The amount of stiffness change associated only with a delamination between the plies, without transverse matrix cracking, can be reasonably estimated using the procedure suggested by O'Brien[72]. Essentially, the procedure calculates the stiffness change associated with the separation of the plies and the loss of any Poisson contraction type constraint. The undamaged laminate stiffness, E_{LAM}, is first calculated from laminated plate theory. The rule of mixtures assumption is made and the stiffness, E^*, for the fully delaminated case is calculated:

$$E^* = \frac{\sum_{i=1}^{m} E_i t_i}{\sum_{i=1}^{m} t_i} \qquad (1)$$

where

m = Number of sublaminates formed by the delamination

E_i = Laminate stiffness of the ith sublaminate

t_i = Thickness of the ith sublaminate

In general, a laminate is not fully delaminated, thus the actual stiffness, E, is:

$$E = (E^* - E_{LAM})\frac{A}{A^*} + E_{LAM} \qquad (2)$$

where A is the total delaminated area and A* is the total interfacial area.

Using the above procedure, the maximum percent stiffness losses associated with 100 percent delamination in each of the laminates were calculated. The results are given in Table 44. In general, delaminations at 90/45 or 45/-45 interfaces are associated with large stiffness losses while those at 0/90 or 0/45 are associated with small losses. For the quasi-isotropic laminate, 14.0 to 18.5 percent stiffness loss would be expected to be associated with various combinations of full delamination just due to the loss of a Poisson contraction type constraint. The 90/45 interface delamination results in the majority of the stiffness change. The 0/90 interface delaminations are shown in Table 44 only for completeness since significant delamination was not observed at this interface. The extent of stiffness loss associated with the 0/90 delamination is quite small. Notice that for the $(0/\pm 45)_s$ layup no more than 6.3 percent stiffness loss could be expected and for the $(0/45/0_2/-45/0)_s$ layup, less than 2.5 percent stiffness loss would be expected due to the full loss of Poisson contraction type constraint. For the $(0_2/90_4)_s$ layup, the loss in stiffness is even less. Although the effect of delamination alone on stiffness change is small for these laminates, when combined with transverse matrix cracks, a significant local stress concentration occurs, see Section 3.4.5.

TABLE 44
STIFFNESS CHANGES ASSOCIATED WITH 100 PERCENT DELAMINATION AND NO TRANSVERSE CRACKS

NOTE: Brackets between plies indicate delamination

Laminate Type	Calculated Laminate Stiffness GPa	Msi	Percent Stiffness Loss
0/90/+45/-45	53.1	7.70	-
0/90] [45/-45	45.6	6.62	14.0
0] [90] [45/-45	45.4	6.60	14.3
0/90/45] [-45	45.0	6.53	15.2
0/90] [45] [-45	43.4	6.30	18.2
0] [90] [45] [-45	43.3	6.28	18.5
0/45/-45	58.1	8.43	-
0/45] [-45	55.0	7.97	5.5
0] [45] [-45	54.3	7.90	6.3
$0/45/0_2/-45/0$	98.6	14.30	-
$0] [45/0_2/-45/0$	98.5	14.29	0.1
$0/45] [0_2/-45/0$	97.0	14.07	1.6
$0] [45] [0_2/-45/0$	96.7	14.03	1.9
$0] [45] [0_2] [-45/0$	96.4	13.98	2.2
$0] [45] [0_2] [-45] [0$	96.2	13.95	2.4
$0_2/90_4$	52.6	7.63	-
$0_2] [90_4$	52.4	7.60	0.4

The loss of stiffness associated with combined intraply delamination and intraply matrix cracking is also potentially quite large. For example, although the $(0_2/90_4)_s$ coupons would be expected to lose only at most 5 to 7 percent of their stiffness due to transverse cracking alone or 0.4 percent to delamination alone, 12.3 percent would be associated with the complete loss of load carrying capacity within the 90° plies. This would occur by a combination of transverse matrix cracking and delamination which completely isolated the 90° plies from both the 0° plies (due to delamination) and from the gripped end (due to matrix cracks). Similarly complete isolation of the ± 45 plies in the $(0/90/45/-45/)_s$ laminate by delamination between the 90/45 interfaces and matrix cracks in the $\pm 45^\circ$ plies results in a 30 percent stiffness loss. For the $(0/45/-45)_s$ laminate, isolation of the -45° plies results in 13 percent stiffness loss and complete isolation of one 45° ply in the $(0/45/0_2/-45/0)_s$ laminate results in a 3.9 percent loss.

For most laminates, such isolation of plies occurs only in locally confined small regions. Therefore, total possible stiffness loss due to ply isolation prior to failure is rarely, if ever, observed except perhaps for laminates like $(0_2/90_4)_s$. Such local regions of ply isolation also result in large localized increases in strain in adjacent 0° plies. This combined mode of delamination and transverse cracking is treated in further detail in Section 3.4.5 as a possible primary 0° ply failure criterion.

3.3.5 Effect of 0° Splits and Fiber Fracture on Laminate Stiffness

Two other damage modes may have an effect on laminate stiffness. The first of these are the splits which occur in the 0° plies, such as those observed near the edges of the $(0/\pm 45)_s$ and $(0/45/0_2/-45/0)_s$ coupons and across the coupon width in the $(0_2/90_4)_s$ coupons. The second is that due to the fracture of 0° fibers which was observed in both the $(0/\pm 45)_s$ and $(0/45/0_2/-45/0)_s$ and especially in the $(0_2/90_4)_s$ coupons. Jamison and Reifsnider[40] calculated the expected longitudinal stiffness loss

associated with 0° ply splits to be at most 0.5 percent if a total loss of transverse stiffness in the 0° plies is assumed and less than 0.25 percent with a 50 percent transverse stiffness loss assumption. Clearly, therefore, the longitudinal stiffness change associated with the 0° splits is small. As for the effect of fiber fracture on longitudinal stiffness change, Jamison and Reifsnider[40] successfully argued, following the work of Russel[73,74] that for even a one percent stiffness loss, many more fiber breaks (>100 times more) would be required than were actually observed in any laminate prior to fracture. Thus, fiber fracture was also concluded to be associated with little stiffness change.

There is one exception to the above conclusions. If delamination occurs between an outer 0° ply and the adjacent off-axis ply and if longitudinal splits occur in the 0° plies (such as occurs in $(0_2/90_4)_s$ coupons), then loss of load carrying capacity of the entire large sections of 0° fibers will occur if they fracture near a gripped end. Significant stiffness loss would be expected to be associated with these fractured 0° bundles. Such isolated, fractured bundles of 0° fibers were, in fact, often observed in $(0_2/90_4)_s$ coupons.

3.3.6 Summary, Damage State and Stiffness Loss

In the previous five subsections, seven different damage modes were discussed as possibly being associated with changes in coupon stiffness. These were:

1. Transverse matrix cracking without delamination.
2. Interaction of relative stiffness of constraining plies and transverse matrix cracks without delamination.
3. Transverse matrix cracks with end delamination.
4. Delamination between plies without transverse matrix cracking.
5. Ply isolation due to combined delamination and transverse matrix cracking.

6. 0° ply splitting.

7. 0° fiber fracture.

Each of these damage states was associated with some change in coupon stiffness. Table 45 lists each of the damage modes (using the above reference numbers) and the associated expected maximum amount of stiffness change based upon the analyses undertaken in this program or those conducted by other investigators which are referenced in Table 45. Clearly the major change in stiffness are anticipated to be associated with transverse matrix cracks, delamination and ply isolation. Potentially, delamination emanating from the ends of each transverse crack could result in large additional stiffness loss, but such delamination was never observed to any significant extent. All of the remaining damage modes combined are anticipated to be associated with much less than a total of 2 percent stiffness change. The one exception is that large stiffness loss could be associated with fracture of 0° fiber bundles which occurs in the $(0_2/90_4)_s$ laminate. These analytically derived results are compared in Section 4 to the experimental results for each of the laminates.

The amount of stiffness loss associated with ply isolation can be substantial. Such stiffness loss is due to a combination of delamination and transverse cracking such that, either locally, or globally, one or more off-axis plies is completely isolated from the other plies. In such a state, no load will be carried by that region of the off-axis ply. Therefore, the load which would have been carried by the ply is carried by the remaining plies resulting in a strain increase, under constant load control, and an associated stiffness decrease. Stress concentration associated with this mode of stiffness loss is discussed in detail in Section 3.4.5. Further discussion is delayed until that subsection because this type of damage mode was hypothesized to be a primary cause of 0° fiber fracture.

TABLE 45
DAMAGE MODES AND ASSOCIATED
STIFFNESS CHANGES

NOTE: All stiffness changes are decreases

Damage Mode	Estimate of Maximum Amount Of Stiffness Change, Percent
1	2 - 3 in quasi-isotropic laminates; <0.1 to 3 in laminates without 90° plies; up to 8 in $(0_2/90_4)_s$ laminate
2	Less than 1
3	<0.1 and up to 10 depending on laminate type
4	Maximum possible effect: Less than 0.5 and up to 18.5 for the layups of this study; highly layup and delaminated area dependent
5	Potentially large; from a minimum of 3.9 in the $(0/45/0_2/-45/0)_s$ laminate to 35 in the $(0/90/45/-45)_s$ laminate; normally occurs only locally and thus the associated stiffness loss is generally much lower
6	Much less than 0.5 [40]
7	Much less than 1.0 [40] (except if 0° fiber fracture of a bundle occurs as in a $(0_2/90_4)_s$ laminate).

3.4 DEVELOPMENT OF 0° PLY FAILURE CRITERIA

The second major modeling problem was that of developing failure criteria for the 0° plies. Essentially, the strain in these plies must increase sufficiently for global fiber fracture to occur. Several possible means which may account for sufficient strain increase were considered. These were: 1) deterministic strength theories[26-28]; 2) statistical fiber bundle weakness theory[29,30,75-77]; 3) linear elastic fracture mechanics; 4) increased 0° ply stresses due to transverse matrix cracks, and 5) regions of induced strain concentration because of ply isolation due to combined transverse cracks and delamination. Each of these possibilities is explored in this section.

3.4.1 Deterministic Strength Theories

Several deterministic strength theories have been proposed for composite materials[78]. These include the Tsai-Wu[26], Hoffman[27], maximum stress, maximum strain criteria and other such theories[78]. All such theories are fundamentally similar, although they vary, of course, in the basic assumption that is made. Recent investigators have discussed the difficulties and severe inaccuracies that can occur in certain cases when using the theories even for undamaged laminates[79]. For coupons already containing matrix cracking and delamination, such as those tested for residual strength, the deterministic theories are highly inadequate as a 0° ply failure criteria and thus were not really considered further. The only exception was an examination of the approach of Wu[80].

Wu[80] has introduced the concept of applying a deterministic strength criterion at a characteristic distance, r_c from the crack tip singularity. This distance is related to the critical stress intensity factor, K_c, and the tensile strength, X, of a uniformly loaded sample through the equation:

$$r_c = \frac{1}{2}\left(\frac{K_c}{X}\right)^2 \qquad (3)$$

More recently Wu[28] has accounted for statistical variation in tensile strength by assuming a Weibull strength distribution where the probability of survival is given by:

$$P_s = \exp\left[-\int_{v_c}^{v} (\sigma/\sigma_o)^m dv\right] \tag{4}$$

Here v is the sample volume, v_c is the limiting characteristic volume on the order of the smallest flaw size, σ_o is the normalization strength parameter, and m is the Weibull scatter parameter.

Introducing these concepts into the analysis of strength in the presence of stress gradients near crack singularities, Wu postulated a limiting stress gradient above which no stress gradient effect on strength can be measured. On this basis, the limiting characteristic distance from the crack tip at which the strength criterion may be applied was now found to be dependent on the scatter of the tensile strength data by the equation:

$$r_c = \frac{1}{2}\left(\frac{2(1-1/2)^{m+1}}{m+1}\right)^{2/m}\left(\frac{K_Q}{X}\right)^2 \tag{5}$$

There are three major difficulties with this deterministic theory applied in a small local region near a transverse matrix crack tip. First, the magnitude of stress in the ply adjacent to the crack tip is relatively small and extends only over a small region, 1 to 2 fiber diameters. This fact is discussed fully in Section 3.4.4.1 and 3.4.4.2. Second, the magnitude of the stress increase in the adjacent ply is dependent on the relative stiffness of the cracked and uncracked plies, see Section 3.4.4.3. This results in quite small stress concentrations in many layups such as in a quasi-isotropic layup with a crack in a 90° ply next to an uncracked 0° ply. Third, statistical volummetric arguments can be used to show[75 to 77] (see Section 3.7) that the strength of the 0° fibers in such a small volume adjacent to the crack tip, as envisioned in this local deterministic model,

is 20 - 30 percent higher than the average tensile strength value for 0° unidirectional coupons. Although the stress in the 0° fibers is locally increased due to transverse cracking in an adjacent ply, the amount of increase is considerably less than 20 to 30 percent, as discussed in detail in Section 3.4.4. Therefore these three difficulties were used to infer that a deterministic strength criterion modified by statistical considerations for fracture of the 0° plies did not appear to be reasonable since fracture of the 0° plies would not be anticipated.

3.4.2 Statistical Fiber Bundle Theory

A second criterion considered for 0° ply failure was statistical fiber bundle theory[29,30,75-77]. The $(0_2/90_4)_s$ laminates tested in fatigue tend to form 0° ply longitudinal splits which run the length of the specimen from the top to the bottom grip. A cursory examination of the theory of bundle strength was undertaken to determine whether a loss of tensile strength in $(0_2/90_4)_s$ laminates could be attributed a combination of 0/90 interface delamination and to the numerous longitudinal splits which occurred in the 0° plies. In this configuration the 0° layer is essentially broken up into a structure of parallel "n" bundle members which act as smaller 0° tensile specimens. The observed number n was found to range from 1-12 in the various $(0_2/90_4)_s$ coupons.

In the analysis of the strength of bundles, if the weakest bundle breaks, the load that it carried must be transferred to the remaining unfailed members. If we assume that the remaining members share this added load equally, then the bundle will support a higher load L if nL/(n-1) is less than the strength of the second weakest member, nL(n-1+1) is less than the strength of the ith weakest member, ... or if nL is less than the strength of the strongest member, see Reference 77 for details of this analysis.

The analysis of bundle strength requires a cumulative plot of member strength versus frequency of occurence. Discussion with Wang[31] of his analysis using bundle theory strongly indicated that, in general, the number of bundles would have to be large (>100) i.e., statistically significant in a multidirectional laminate for a significant reduction in strength to occur. The number of bundles required for an effect would thus be much larger than the number actually physically observed in this study.

An exception would, however, occur in the case of small n if the assumption is made that the probability is high that the second weakest member would break simultaneously with the first, then the third, simultaneously with the second, and so on until all bundles are broken. The problem of bundle strength prediction now becomes one of determining the probability that the individual strengths of n samples, chosen at random from a given population, will exceed a given value. In a normally distributed population one can use the variance of the population to determine this probability. If the mean and variance of the member strengths were identical to the statistics for larger coupons, this analysis could be carried out to show that the strength of the fatigue loaded coupon would be expected to be less than that of a monotonically loaded coupon with unsplit 0° plies. However, sufficient test data are not available to define the mean and variance to the accuracy needed to prove this hypothesis. Even if the hypothesis is correct, there is little reason to assume that the split members have the same distribution of strength as the 0° tensile coupons.

If the strength of the 0° coupons follows a Weibull strength distribution, the smaller volume of the individual members will actually produce a higher mean strength and a lower variance (higher scatter parameter) by the arguments employed by Phoenix and Harlow[29,30,75-77]. If, for example, the scatter parameter of 18.4, determined by Whitney and Knight [81] for T300/-5208 0° tensile specimens, can be applied to both the split and unsplit 0° layers in our tests, the strength of one member in the split layer is estimated to be equal to the strength of the unsplit layer times the volume

ratio of the unsplit layer to split member raised to the (1/18.4) power. For n = 10 this results in a member mean strength which is 13 percent higher than the unsplit layer strength. Thus while it is possible for a special case of small n to use bundle strength theory to anticipate a reduction of strength in the fatigue loaded $(0_2/90_4)_s$ coupons, Weibull strength theory indicates that this reduction will be partially (or more likely fully) countered by the increase in the mean strength and reduced scatter of the member strength.

A great deal of experimentation on 0° specimens of volume comparable to that of the split members in the laminate would be necessary before the correctness of these suppositions could be rigorously confirmed. However, this examination of bundle theory led to the conclusion that for small n, no significant reduction in strength should occur because of the presence of the bundles. Therefore, the theory did not appear to be adequate for providing a criterion for 0° ply fracture in the $(0_2/90_4)_s$ coupons. The theory was not considered for the other laminates since 0° splits were uncommon.

3.4.3 Application of Linear Elastic Fracture Mechanics

A third criterion for 0° ply failure can be obtained from linear elastic fracture mechanics. Figure 71 shows the application of such a criterion to the analysis of a transversely cracked 90° ply in a $(0/90)_s$ laminate. From experimentally determined measurements of longitudinal and transverse Youngs moduli and Mode I fracture energy, one can calculate the critical size flaw which would grow unstably if the applied stress were equal to the average ultimate strength in both directions. These flaw sizes are obtained from the Griffith-Irwin equation[66]:

$$a_c = \frac{EG_c}{\pi}/(\sigma^{uts})^2 \qquad (6)$$

In this example G_c has been reduced 50% from the experimentally measured value to give an example where the critical flaw size is equal in both

WHEN IS A CRITICAL FLAW NOT CRITICAL?

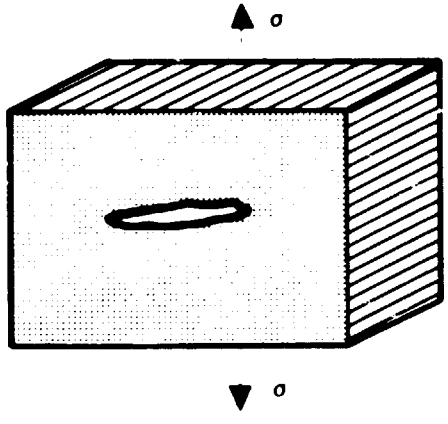

90° UNIDIRECTIONAL

E_{90} = 11.7 GPa (1.7 Msi)
G^C_{90} = 245 J/m^2 (1.4 in.-lb/in.^{2})
σ^{ULT} = 55 MPa (8 ksi)

a^C_{90} = 0.25 mm (0.010 in.)
G = G_C AT ϵ = 0.0047

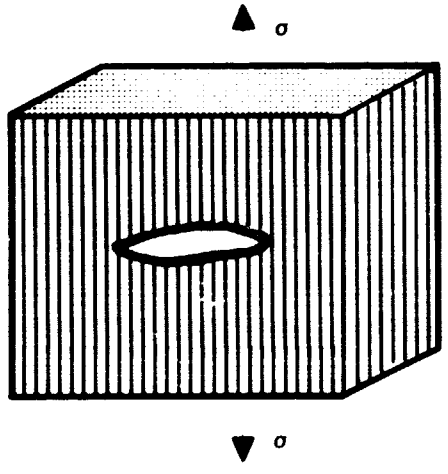

0° UNIDIRECTIONAL

E_0 = 163 GPa (23.7 Msi)
G^C_0 = 9282 J/m^2 (53 in.-lb/in.^{2})
σ^{ULT}_0 = 1379 MPa (200 ksi)

a^C_0 = 0.25 mm (0.010 in.)
G = G_C at ϵ = 0.0084

ANSWER: WHEN IT IS FOUND IN THE LAMINATE.

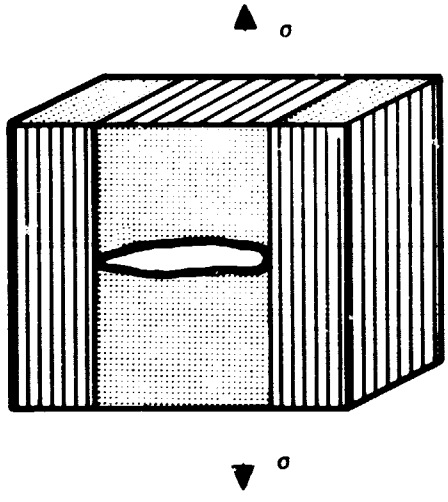

$(0/90)_s$ LAMINATE

G = 1909 J/m^2 (10.9 in.-lb/in.^{2}) < G^C_0
FOR ϵ = 0.0084 AND FAILURE
AND σ_{ULT} = 524 MPa (76 ksi)
G = G_C FOR ϵ = 0.0195
AND σ = 1213 MPa (176 ksi) >> σ_{ULT}

Figure 71: Fracture mechanics analysis of $(0/90)_s$ laminate fracture energy.

directions. The G value in the transversely cracked $(0/90)_s$ laminate in Figure 70 under an applied tensile strain equal to the ultimate strain of a longitudinal coupon was examined by finite element strain energy release rate analysis. As noted in the Figure, G is only 20% of the value needed to propagate the crack through the 0° ply. This example demonstrates that a flaw which may be critical in the unidirectional composite is probably not critical in a multi-directionally reinforced laminate. The result is also a strong indication that a crack in the 90° ply would not release sufficient energy by propagating into the 0° ply in the quasi-isotropic laminate of this program for fracture to occur.

This simple fracture mechanics analysis for flaw criticality showed that unstable extension of a 90° ply transverse matrix crack into the adjacent 0° ply is not predicted. A similar conclusion is reached for a crack in a 45° ply. In fact, such transverse matrix cracks have not been observed to unstably extend into adjacent 0° plies. Therefore, the analytical prediction based upon linear elastic fracture mechanics has been experimentally confirmed. The conclusion is inferred that such fracture mechanics analysis shows that a criterion for failure in the 0° plies cannot be based upon a supposedly unstable extension of adjacent transverse matrix crack. Hence, a failure criterion for the 0° plies must clearly be based on some other principle.

3.4.4 Ply Stresses Due to Transverse Matrix Cracks

Despite the general conclusion of the previous subsection, transverse matrix cracks do induce higher stresses in neighboring plies in the vicinity of the crack tips. These stresses may lead to local fiber fracture in the neighboring plies along the transverse crack angle. Such incipient fracture has been previously observed[7,13,32] and well documented[40]. Therefore, the magnitude of these stresses was estimated. In the modeling procedures, the worst possible case was considered by assuming crack tips without short end delaminations which would reduce the stress concentration. The reason for the development of the short end delaminations, in essence, a turning of the

crack tip, has been discussed by Nair and Reifsnider[82]. The transverse cracks were assumed, for simplicity, to be perpendicular to the 0° ply orientation when in fact they are known to exist at angles up to 45° as mentioned in Section 2. The angles of the transverse cracks are a manifestation of the presence of combined shear and normal ply stresses.

3.4.4.1 Stresses in $(0/90/\pm45)_s$ and $(0/\pm45)_s$ Laminates

Using the modeling procedures discussed in Appendix D, a contour plot of the stress in the loading direction, σ_{yy}, of the $(0/90/45/-45)_s$ laminate containing a 90° crack was obtained. In modeling of the $(0/90/\pm45)s$ laminate, the G_{12} and E_{22} moduli of the 45° layers were reduced to values equivalent to a crack spacing of 8 times the ply thickness, t (approximately 25 cracks per 25 mm). A crack in the 90° layer at the left hand boundary of the model was introduced and a uniform displacement in the loading direction along a y = 8t line was applied, see Figure 72.

As expected, Figure 72 shows that a stress gradient exists at the tip of the 90° crack in both the 0° and 45° layers. However, the stress concentration found at the crack tip element, whose centroid is only 2 - 3 fiber diameters from the crack tip, is only 10% above the average stress in the 0° layer far from the crack. Using a fracture mechanics analysis for an isotropic medium, a stress 1.7 times (see Section 3.4.4.3), the nominal value would be anticipated at this distance. The difference was found not to be due to errors introduced by the coarseness of the grid near the singular point as further modeling with more refined grids showed. The lack of stress concentration caused by the 90° crack in the 0° layer is in fact not surprising when one considers that the 0° layer carries a longitudinal stress approximately 20 times larger than that in the 90° layer before fracture occurs.

For the case where the cracked ply is much thicker, the effect of the crack on the stresses in the adjacent plies can be much larger. Crossman et. al.

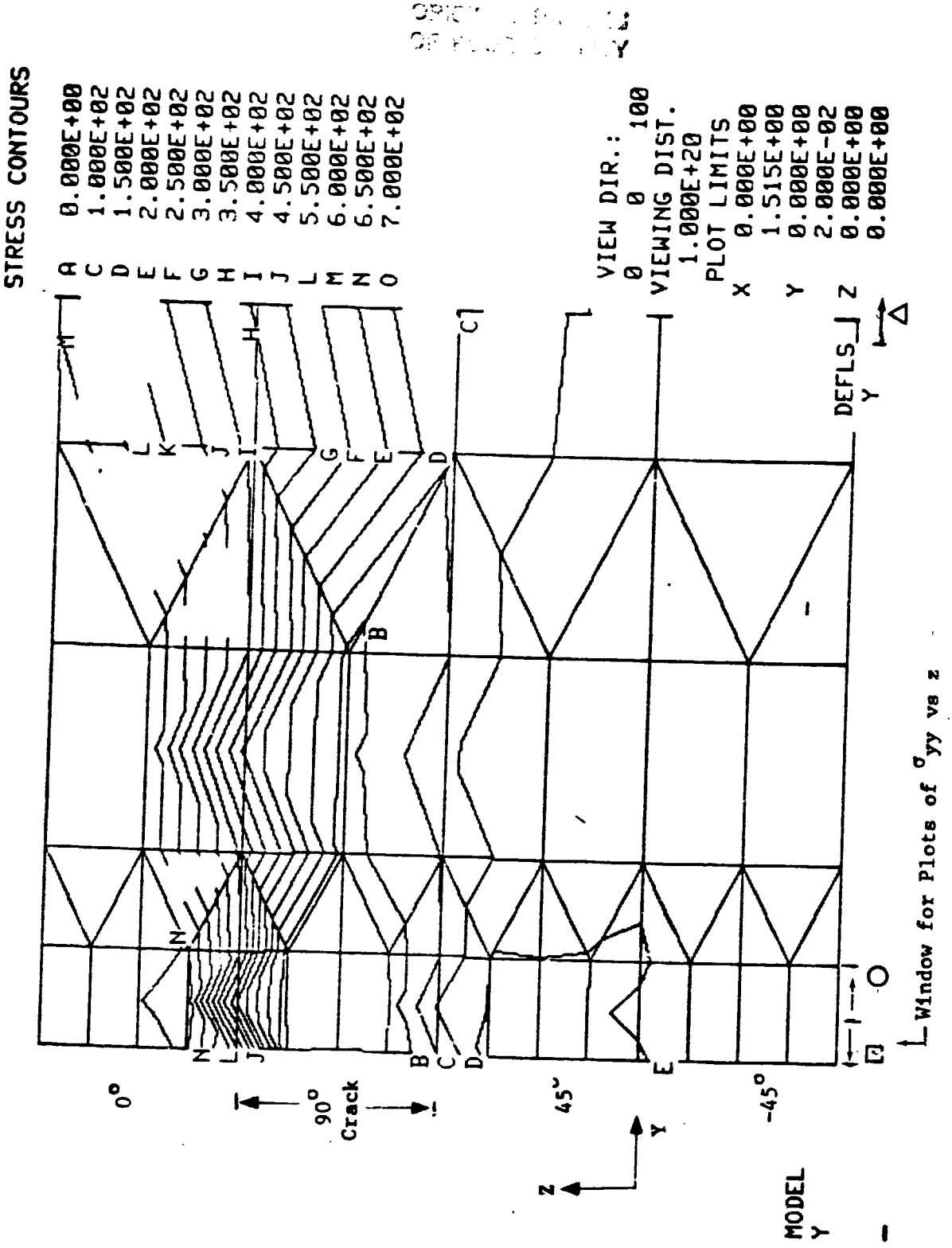

Figure 72: σ_{yy} applied stress model for $(0/90/45/-45)_s$ laminates.

[52] has shown for $(0_2/90_n)_s$ layups that when n becomes greater than 2 (ply thicknesses greater than 4), the 90° ply transverse cracks can induce a stress on the adjacent 0° plies over a considerably larger volume than for the case of a single ply thickness. Thus, this effect was expected to be observed for the $(0_2/90_4)_s$ layup of this investigation.

3.4.4.2 45° Ply Stresses in the Vicinity of a 90° Ply

Consider now the stress state in the 45° plies in the vicinity of a 90° ply transverse crack for the $(0/90/\pm45)_s$ laminate. Figures 73 - 83 summarize the stress state in two 45° plies of the quasi-isotropic laminate loaded parallel to the y or longitudinal, 0° direction, axis under a tensile strain of 0.000026. Ply angles were defined with respect to the Y axis since that was the principal loading direction. Figure 73 shows the finite element grid in the region of interest with deformations magnified to show the position of a 90° ply transverse crack. Figures 77 - 78 plot stress components as a function of z for three windows along the y axis. The square, circle, and triangular symbols in certain elements in Figure 73 indicate which element stresses are plotted. The region A-B-C-D identified in Figure 73 is examined in the contour plots presented in Figures 79 - 83.

As was noted previously for the 0° ply, the stress concentration in the 45° ply adjacent to the 90° ply crack is not large. The normal stress σ_y, in the element directly in front of the crack is only 15% higher than the average value in the 45° plies. The in-plane shear stress, τ_{xy}, peaks at only 10% above the average value. Even these minor stress concentrations are localized in a zone less than one quarter of a ply thickness in radius from the tip of the crack as can be seen in Figures 74 and 75. The z components of stress are found to be much smaller than the in-plane stress components and should not contribute significantly to enhancing the failure of 45° plies in the vicinity of a 90° ply crack.

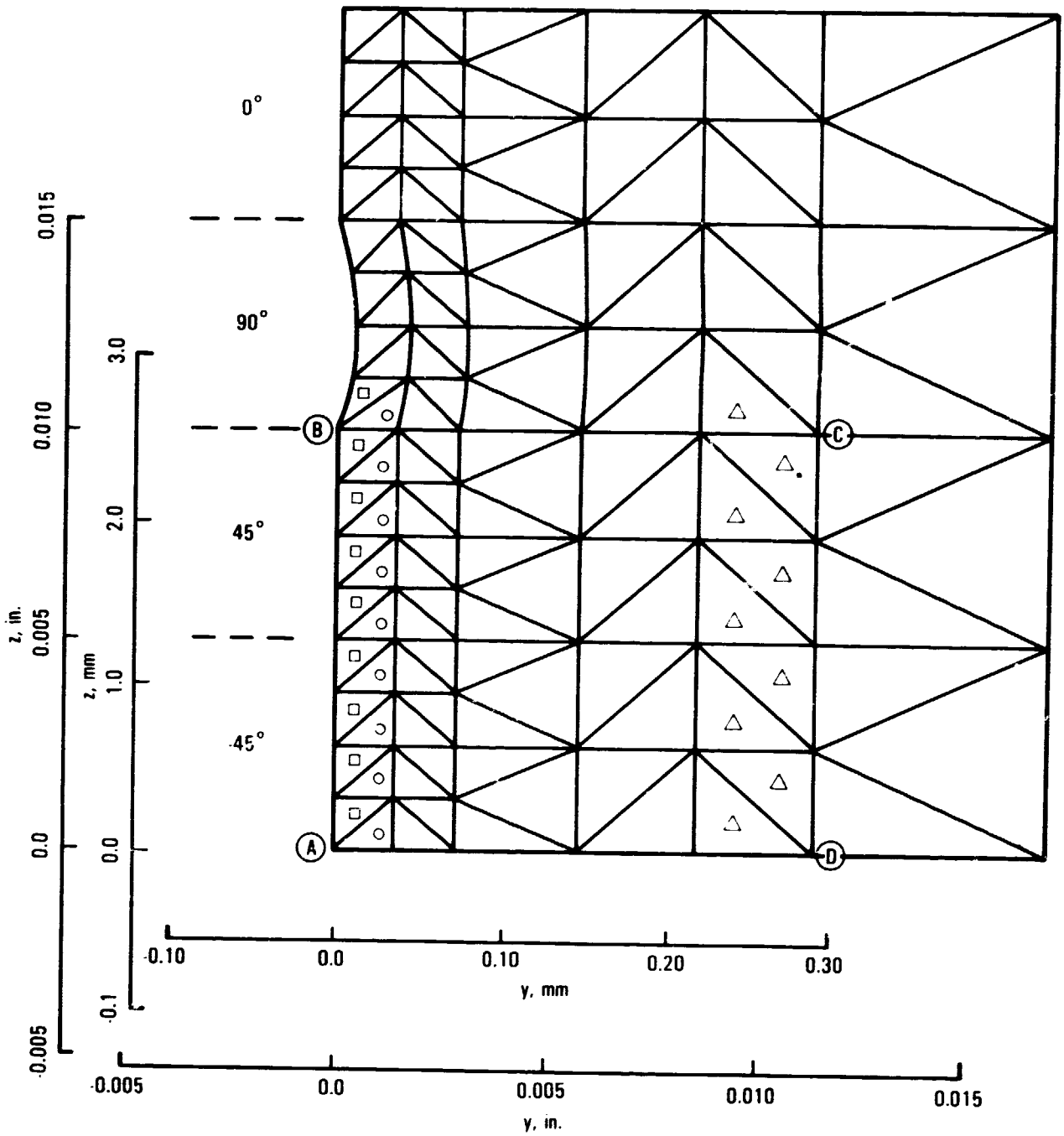

Figure 73: Finite element grid used to model the effect of 90° ply cracks on the stress state in 45° plies of a $(0/90/\pm45)_s$ laminate.

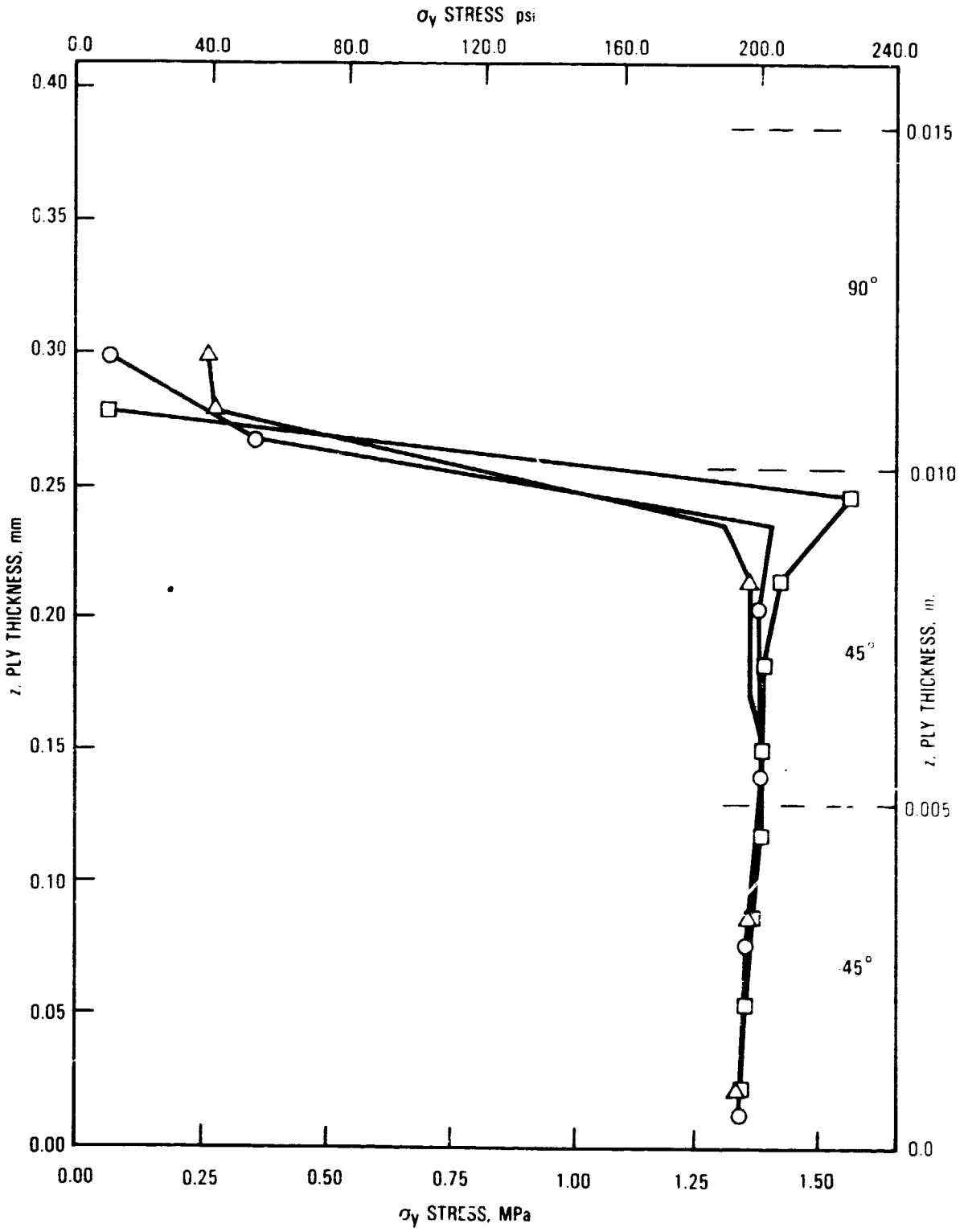

Figure 74: σ_y stress state as a function of Z for model of Figure 73.

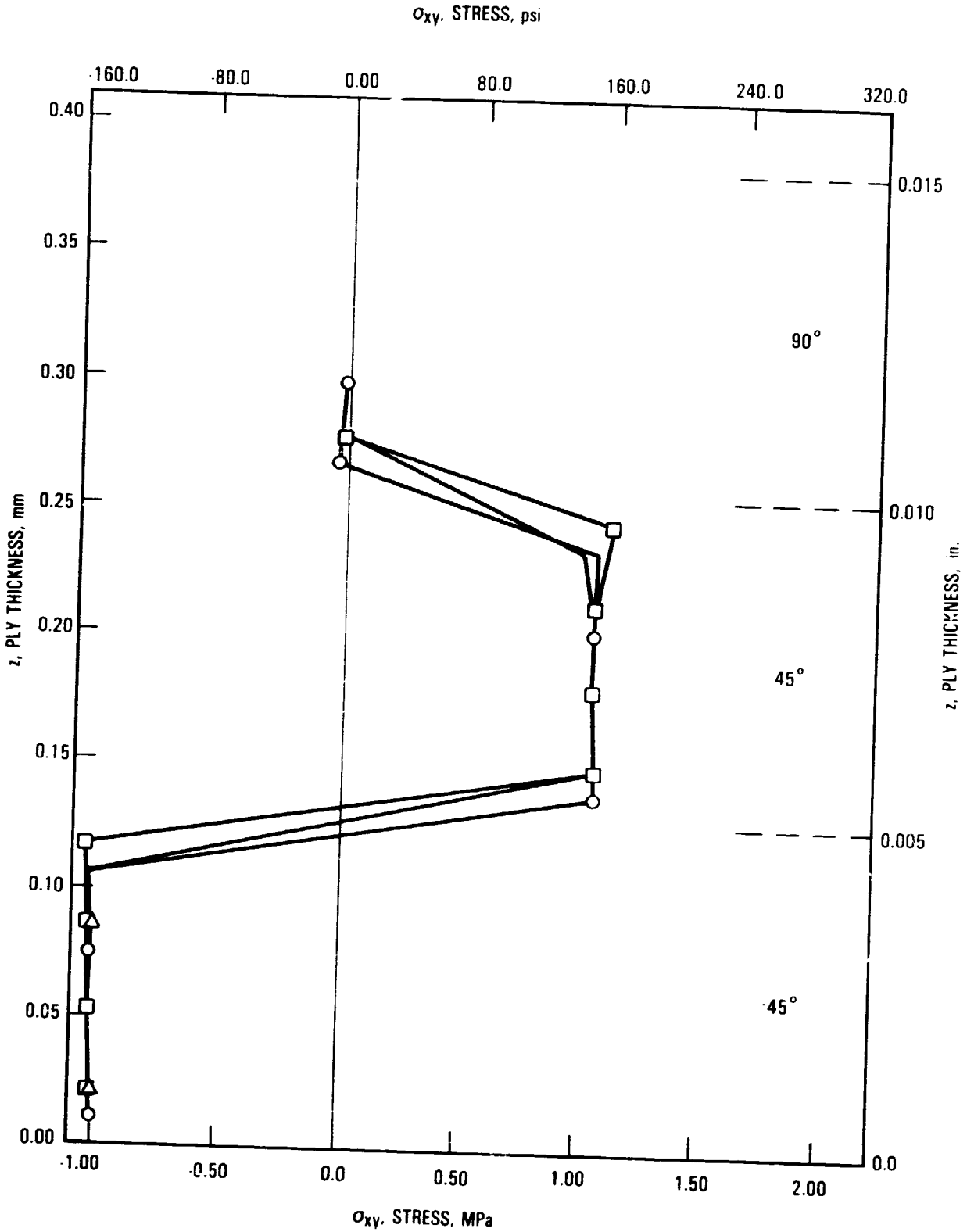

Figure 75: σ_{xy} stress state as a function of Z for model of Figure 73.

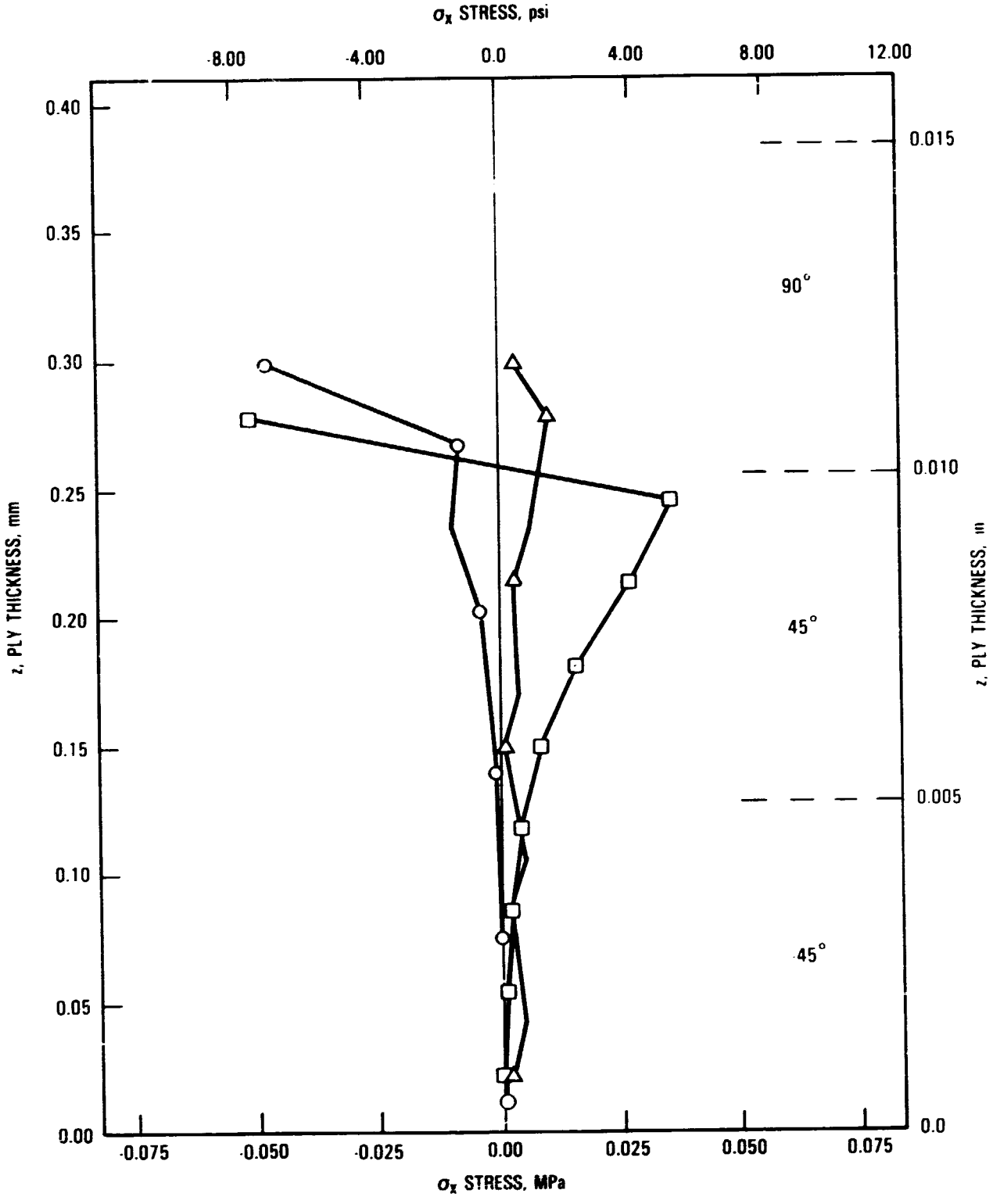

Figure 76: σ_z stress as a function of Z for model of Figure 73.

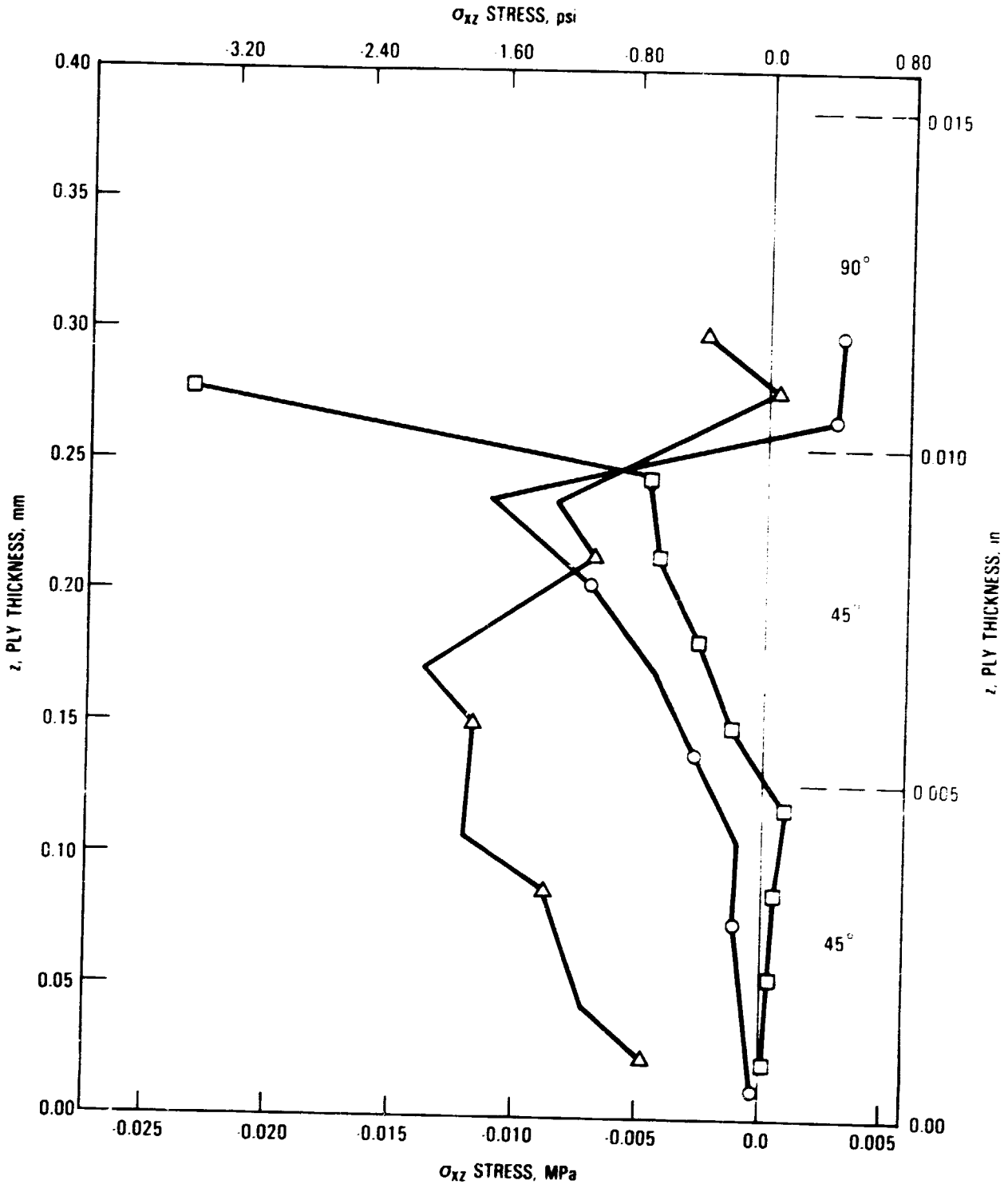

Figure 77: σ_{xz} stress as a function of Z for model of Figure 73.

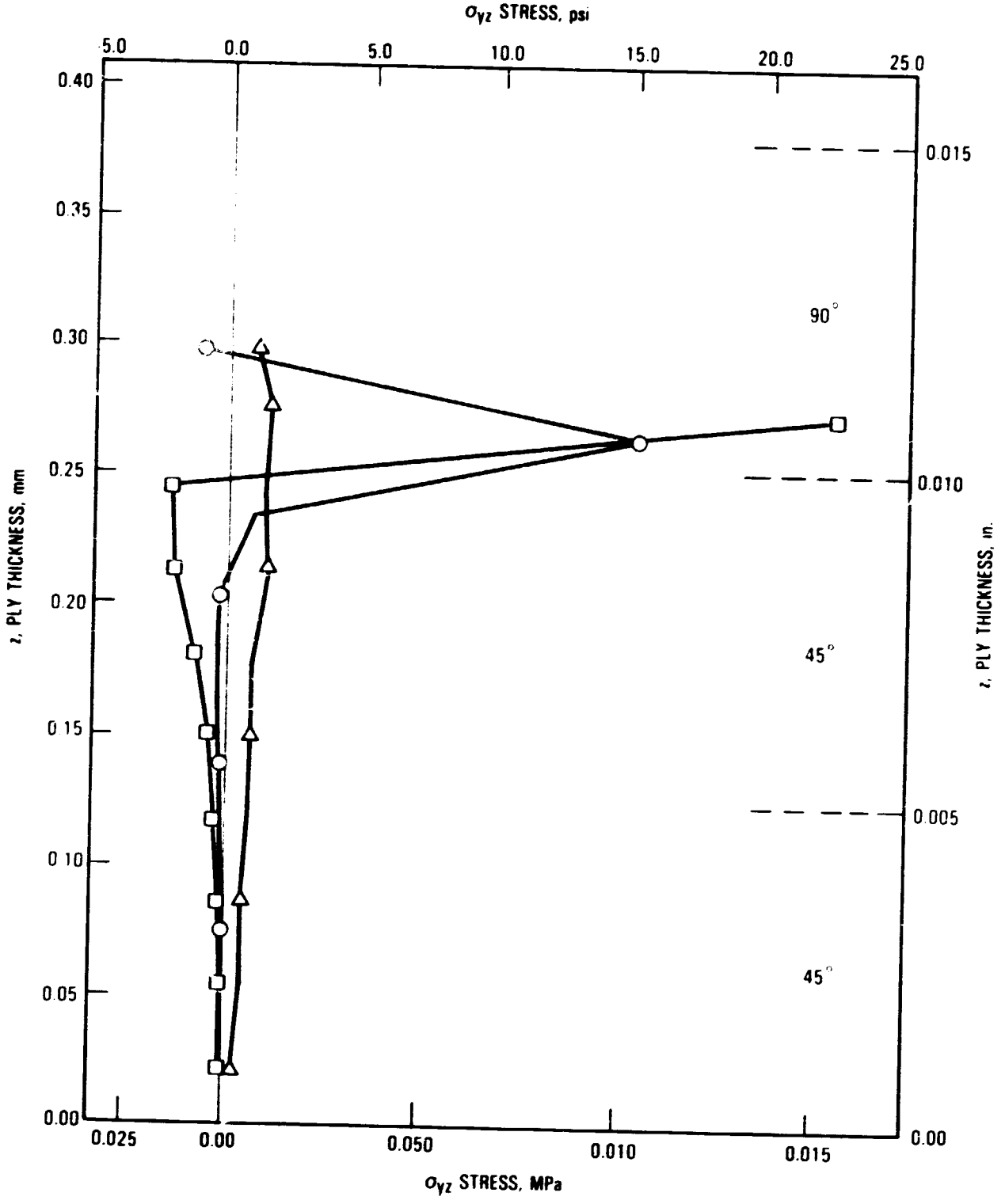

Figure 78: σ_{yz} stress as a function of Z for model of Figure 73.

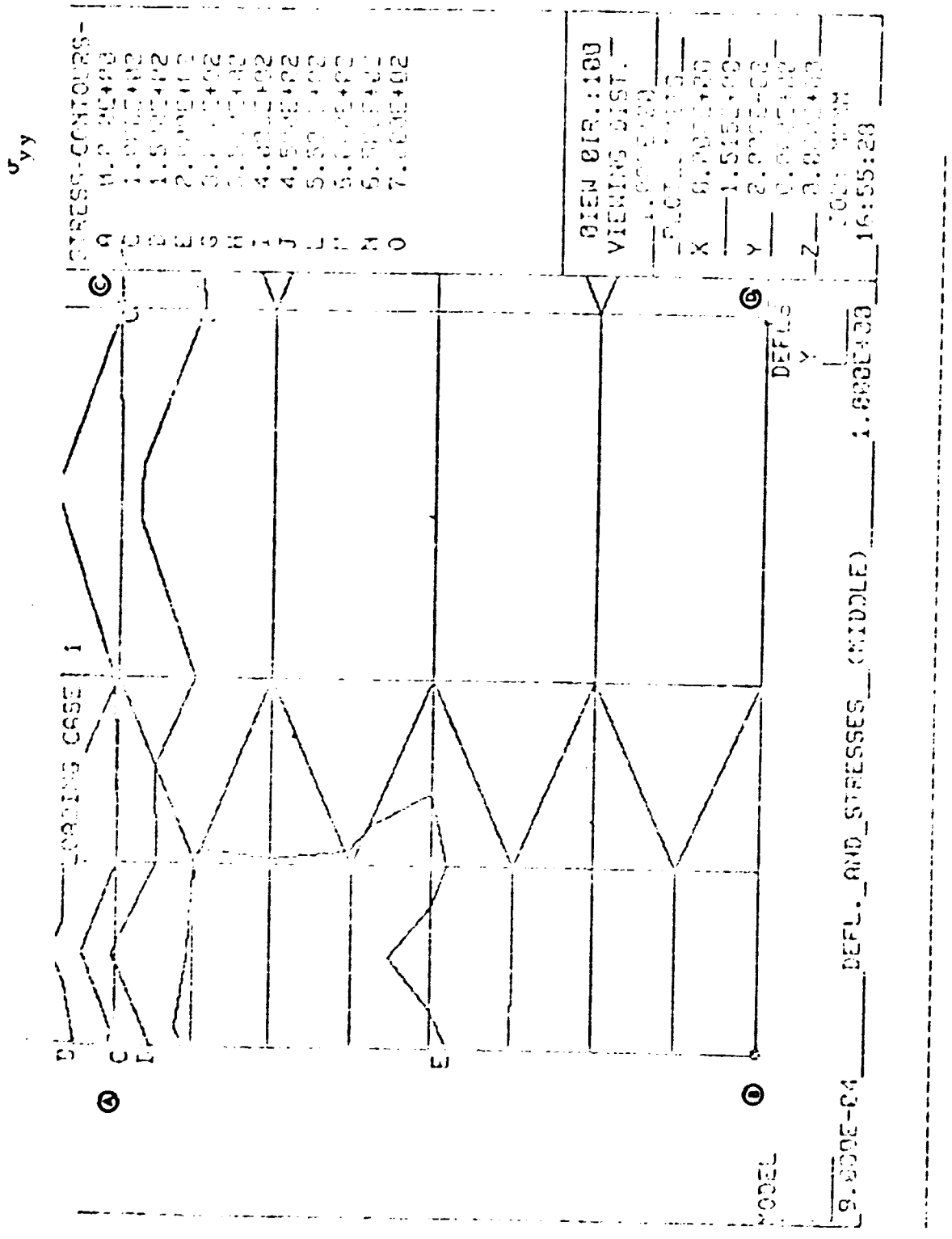

Figure 79. σ_y Stress Contours for Region A-B-C-D of Figure 73.

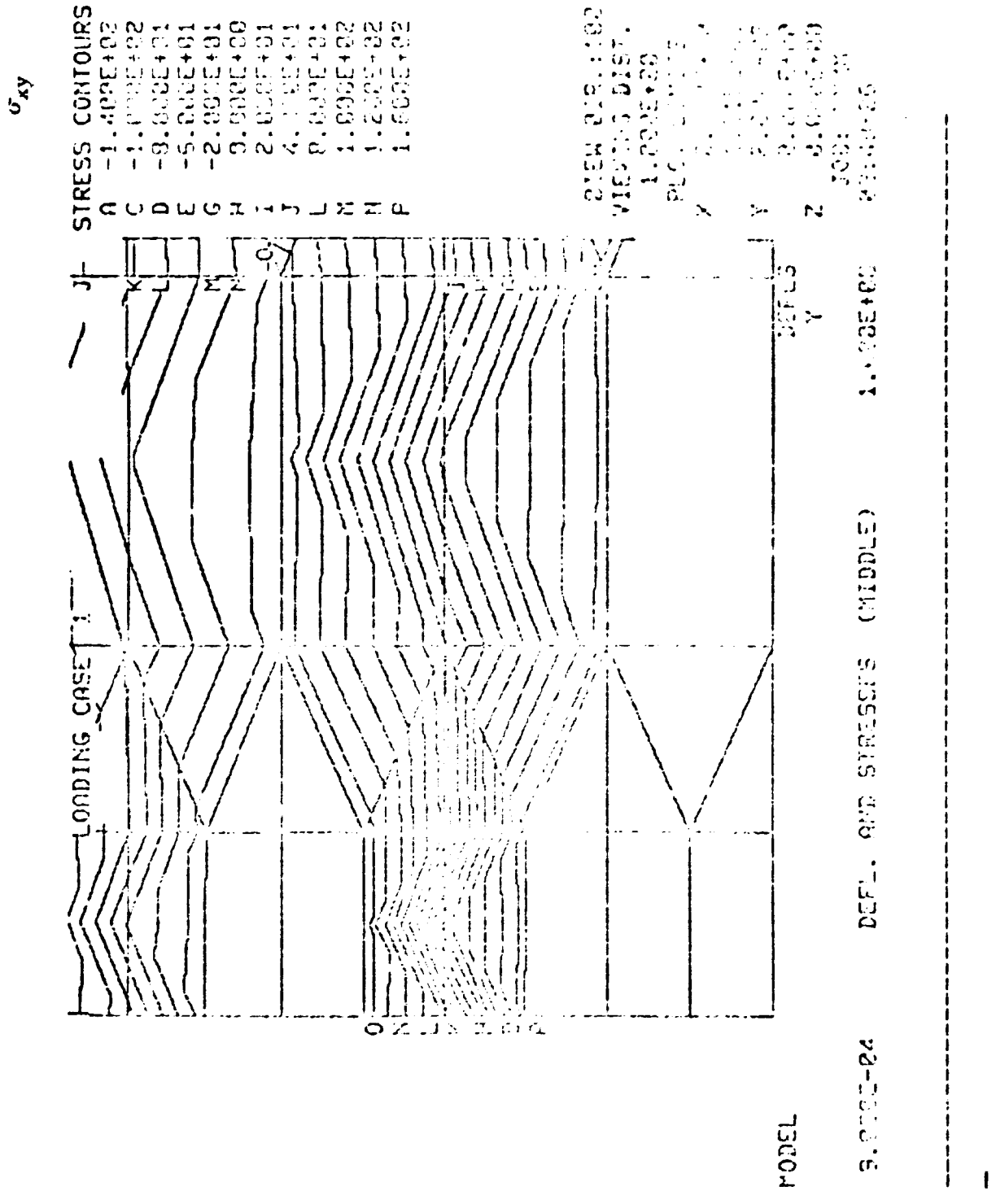

Figure 80: σ_{xy} Stress Contours for Region A-B-C-D of Figure 73.

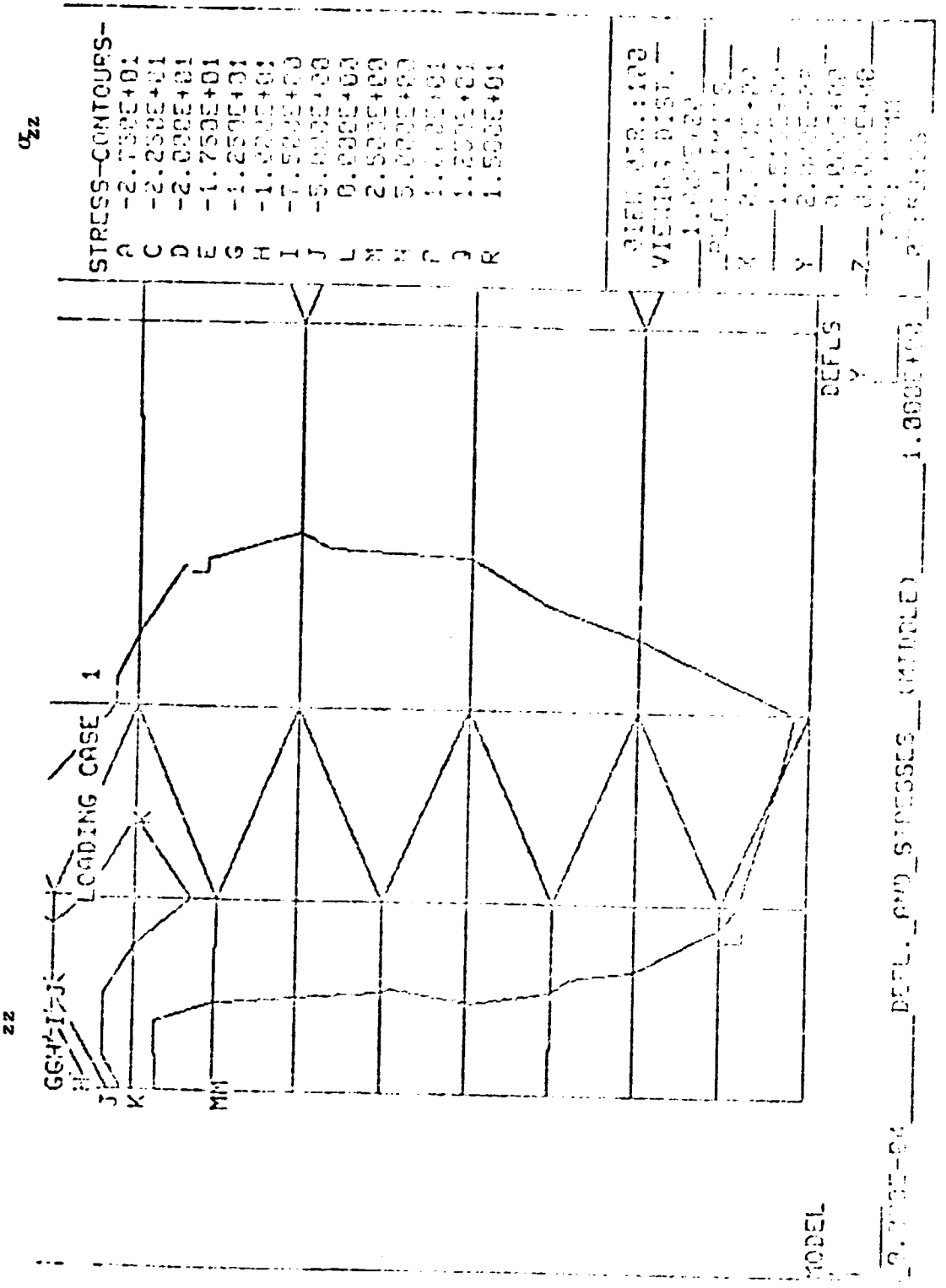

Figure 81: σ_{zz} Stress Contours for Region A-B-C-D of Figure 73.

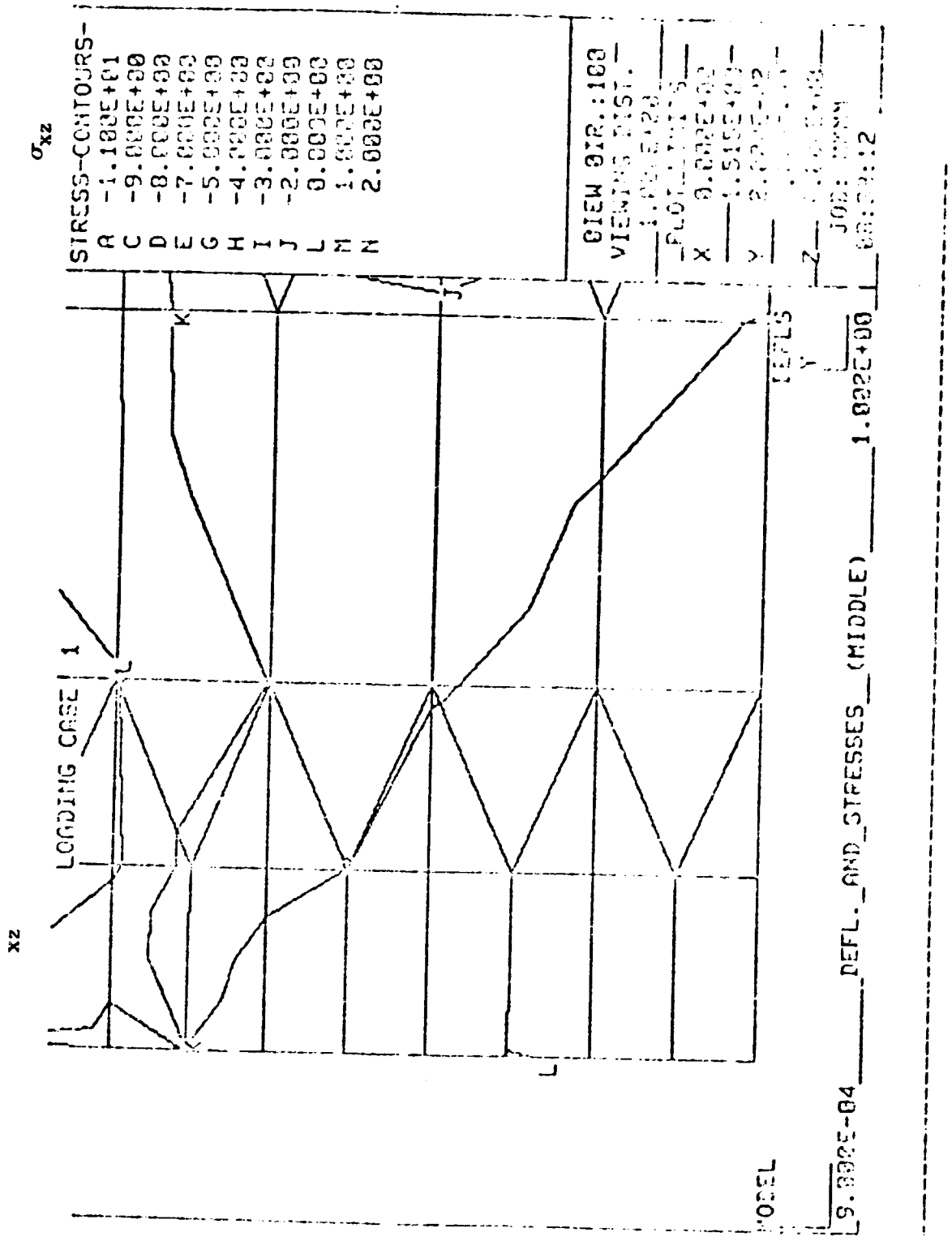

Figure 82: σ_{xz} Stress Contrours for Region A-B-C-D of Figure 73.

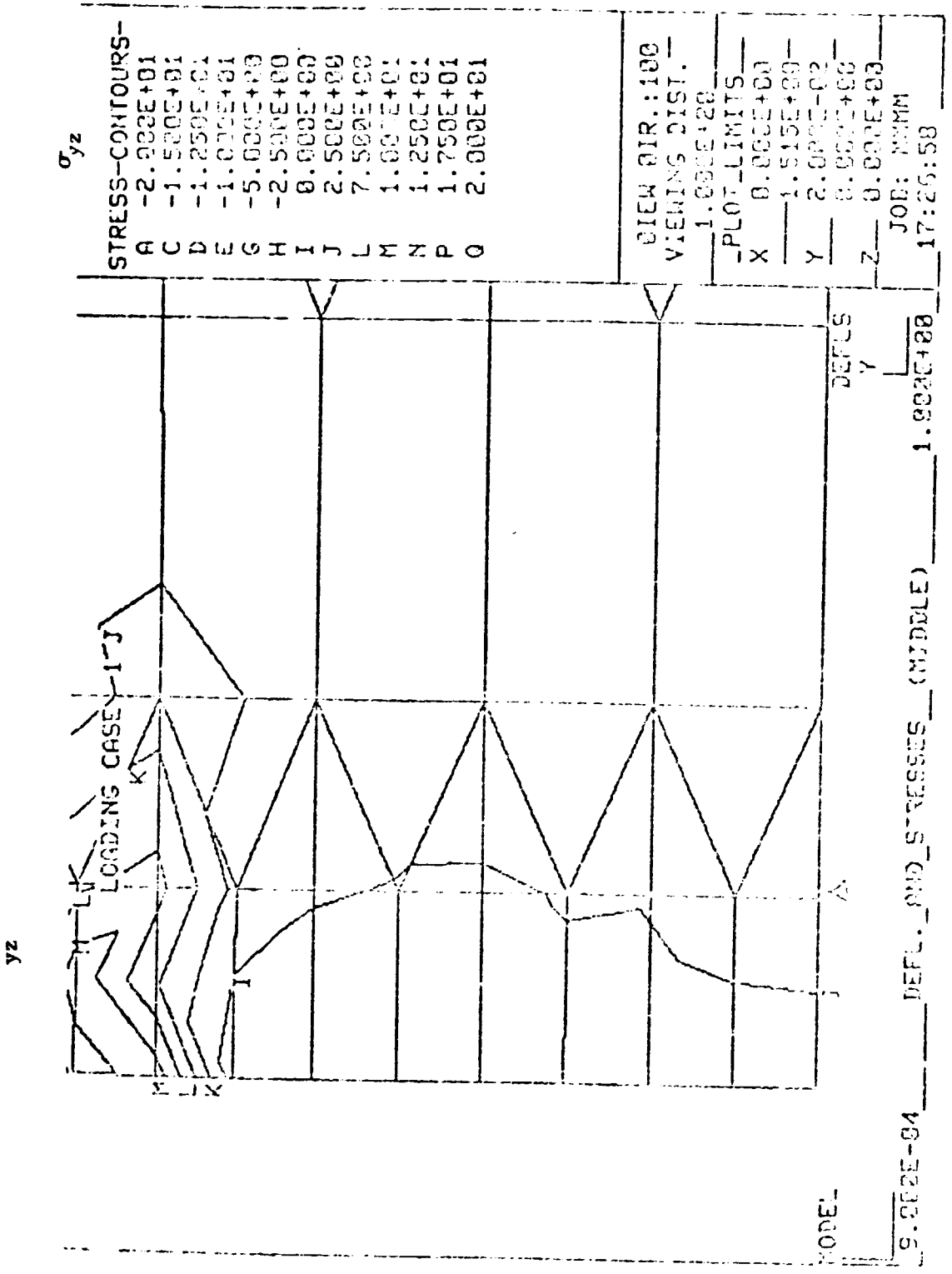

Figure 83: σ_{yz} Stress Contours for Region A-B-C-D of Figure 73.

3.4.4.3 Stress Gradients Near a Ply Transverse Crack -- Effect of Ply Stiffness

This subsection describes the stress analysis in the vicinity of a single ply crack within a $(90)_8$ or $(0)_8$ laminate in order to assess the influence of neighboring ply stiffnesses on the stress gradient near the crack. Figure 84 shows the finite element grid in the vicinity of the ply crack transverse to an applied tensile load in the y direction. Ply angles were thus specified with respect to the y axis. Gradients in the calculated σ_y normal stress near the cracked single ply of a $(0)_8$ and $(90)_8$ laminate are shown in Figures 85 and 86. Element stresses are plotted at the centroids of the elements, as noted in Figure 84, and presented as a function of z at several slices in the y direction in Figures 85 and 86. The stress gradients should be compared to those found near the cracked 90^o ply in a $(0/90/45/-45)_s$ laminate presented in Figure 87 (see Appendix D for a complete analysis of this case).

Comparison of Figures 85, 86, and 87 shows that not only is the peak stress concentration influenced by the relative stiffness of the cracked and uncracked plies, but the distance of significant stress overshoot above the nominal stress within the ply adjacent to the crack is also influenced. The observed peak stress concentration in Figures 85 and 86 is approximately 1.7 and 1.3, respectively, compared to 1.1 in the quasi-isotropic laminate of Figure 87. Note in Figures 85, 86, and especially in Figure 87 that the depth to which the stress concentration penetrates into the adjacent ply is at most 1/4 to 1/2 of the ply thickness. Therefore, this stress concentration at the tip of the crack is only affecting a relatively small local volume.

A calculation was made of the stress concentration expected in an isotropic material at the positions of the two element centroids closest to the crack tip. In order to estimate the stress concentrations at the positions of

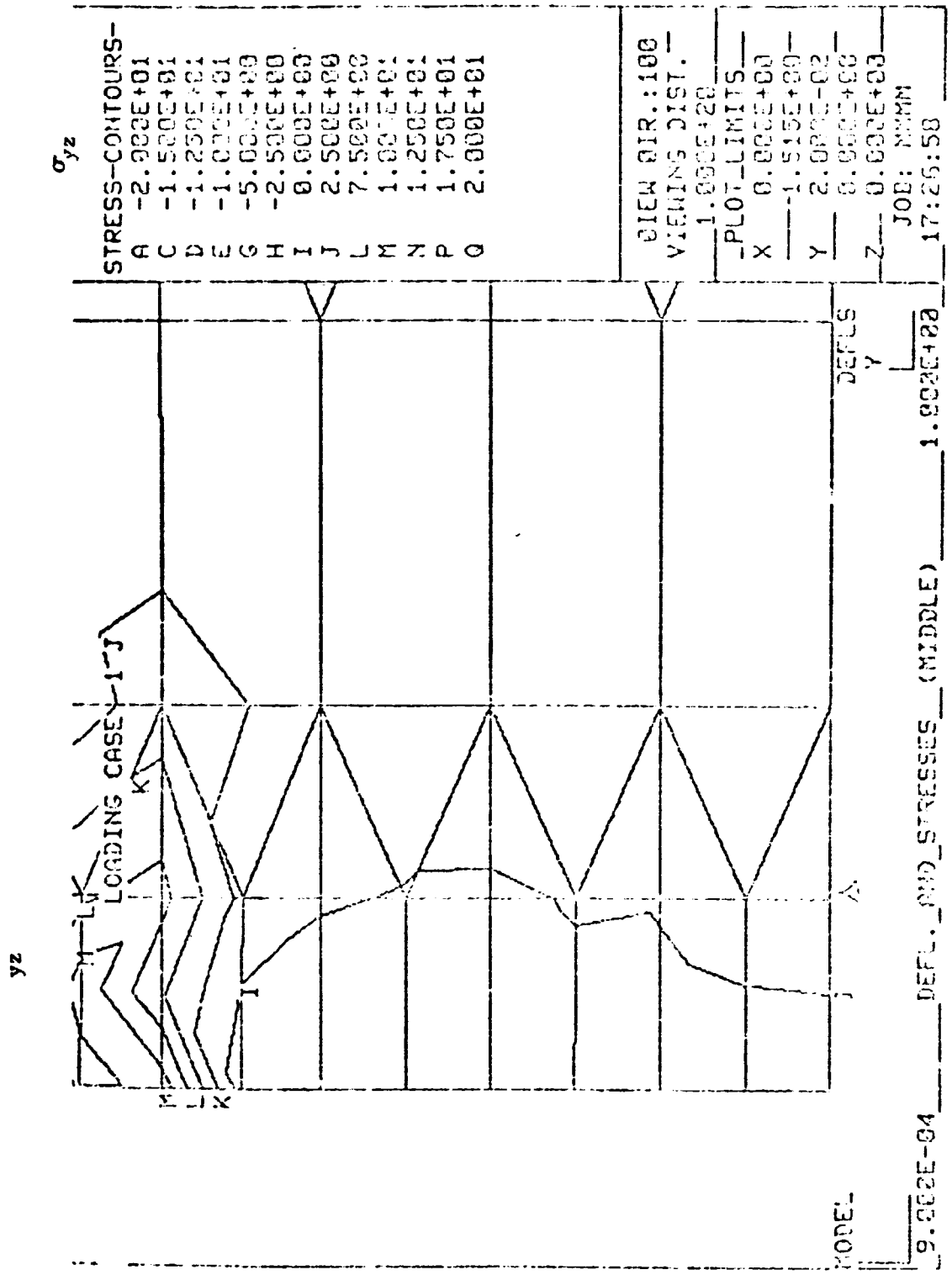

Figure 83: σ_{yz} Stress Contours for Region A-B-C-D of Figure 73.

3.4.4.3 Stress Gradients Near a Ply Transverse Crack -- Effect of Ply Stiffness

This subsection describes the stress analysis in the vicinity of a single ply crack within a $(90)_8$ or $(0)_8$ laminate in order to assess the influence of neighboring ply stiffnesses on the stress gradient near the crack. Figure 84 shows the finite element grid in the vicinity of the ply crack transverse to an applied tensile load in the y direction. Ply angles were thus specified with respect to the y axis. Gradients in the calculated σ_y normal stress near the cracked single ply of a $(0)_8$ and $(90)_8$ laminate are shown in Figures 85 and 86. Element stresses are plotted at the centroids of the elements, as noted in Figure 84, and presented as a function of z at several slices in the y direction in Figures 85 and 86. The stress gradients should be compared to those found near the cracked 90^0 ply in a $(0/90/45/-45)_s$ laminate presented in Figure 87 (see Appendix D for a complete analysis of this case).

Comparison of Figures 85, 86, and 87 shows that not only is the peak stress concentration influenced by the relative stiffness of the cracked and uncracked plies, but the distance of significant stress overshoot above the nominal stress within the ply adjacent to the crack is also influenced. The observed peak stress concentration in Figures 85 and 86 is approximately 1.7 and 1.3, respectively, compared to 1.1 in the quasi-isotropic laminate of Figure 87. Note in Figures 85, 86, and especially in Figure 87 that the depth to which the stress concentration penetrates into the adjacent ply is at most 1/4 to 1/2 of the ply thickness. Therefore, this stress concentration at the tip of the crack is only affecting a relatively small local volume.

A calculation was made of the stress concentration expected in an isotropic material at the positions of the two element centroids closest to the crack tip. In order to estimate the stress concentrations at the positions of

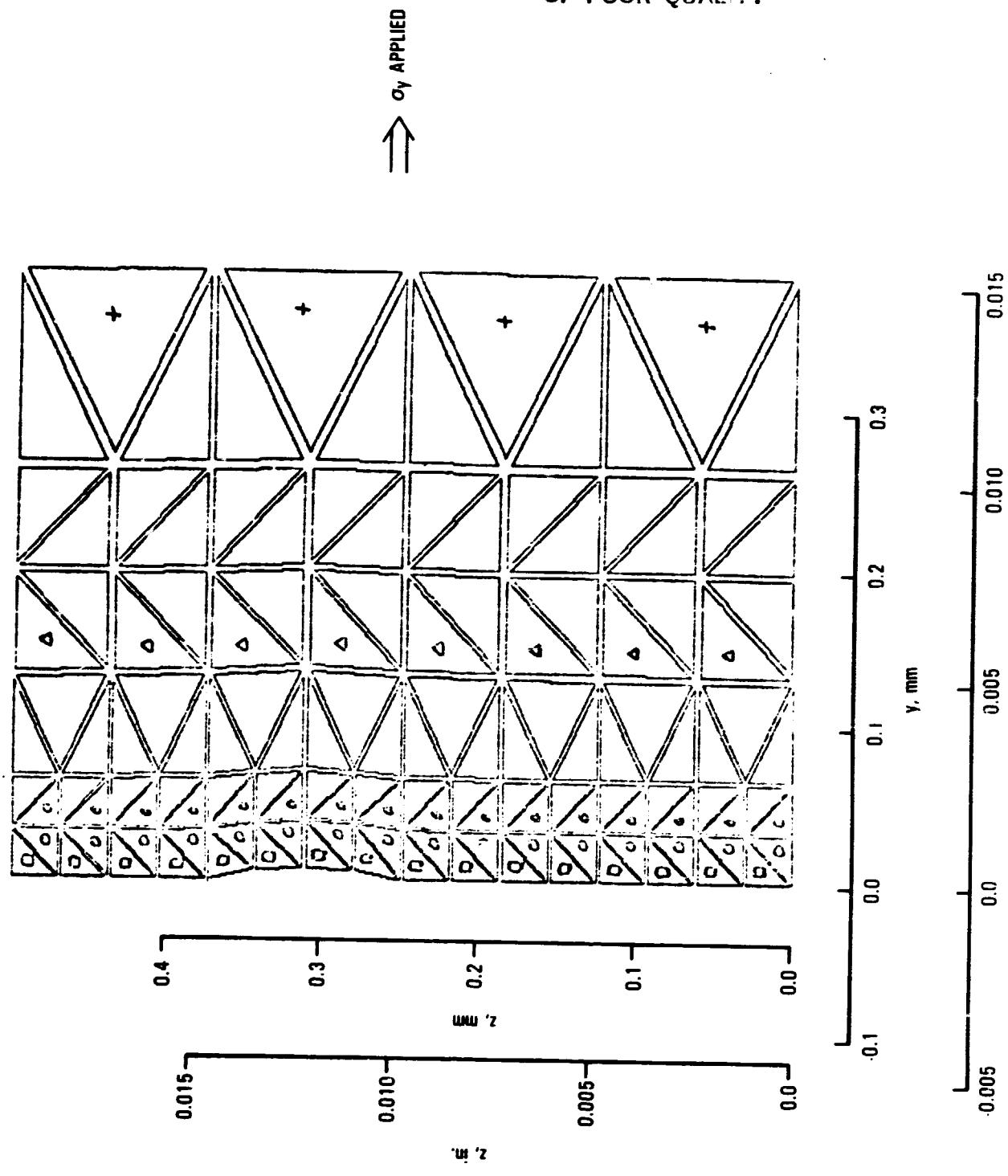

Figure 84. Finite element grid used to model influence of a neighboring ply stiffness on the stress gradient near a crack.

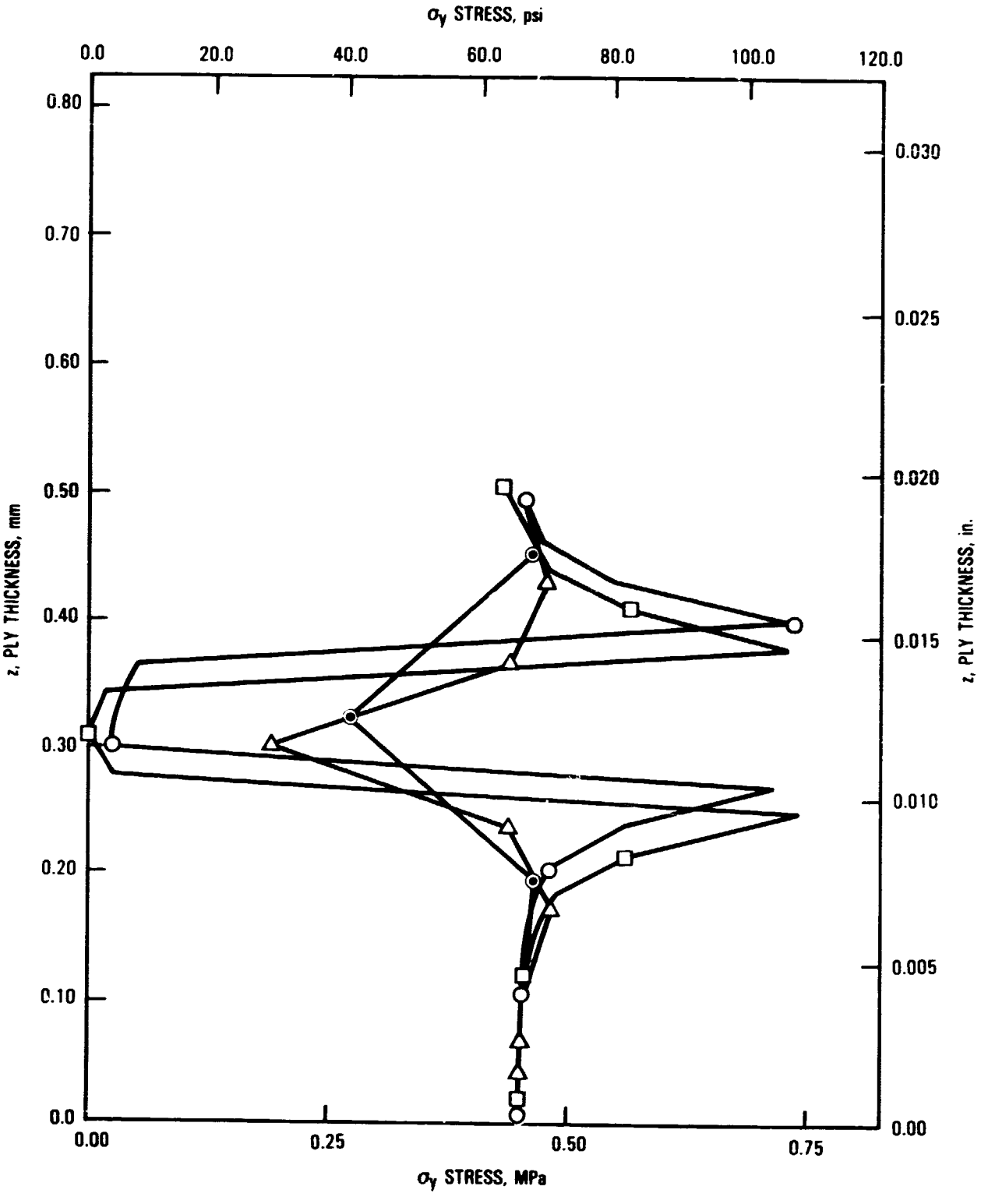

Figure 85: σ_y stress gradients near a crack for $(0)_8$ laminate.

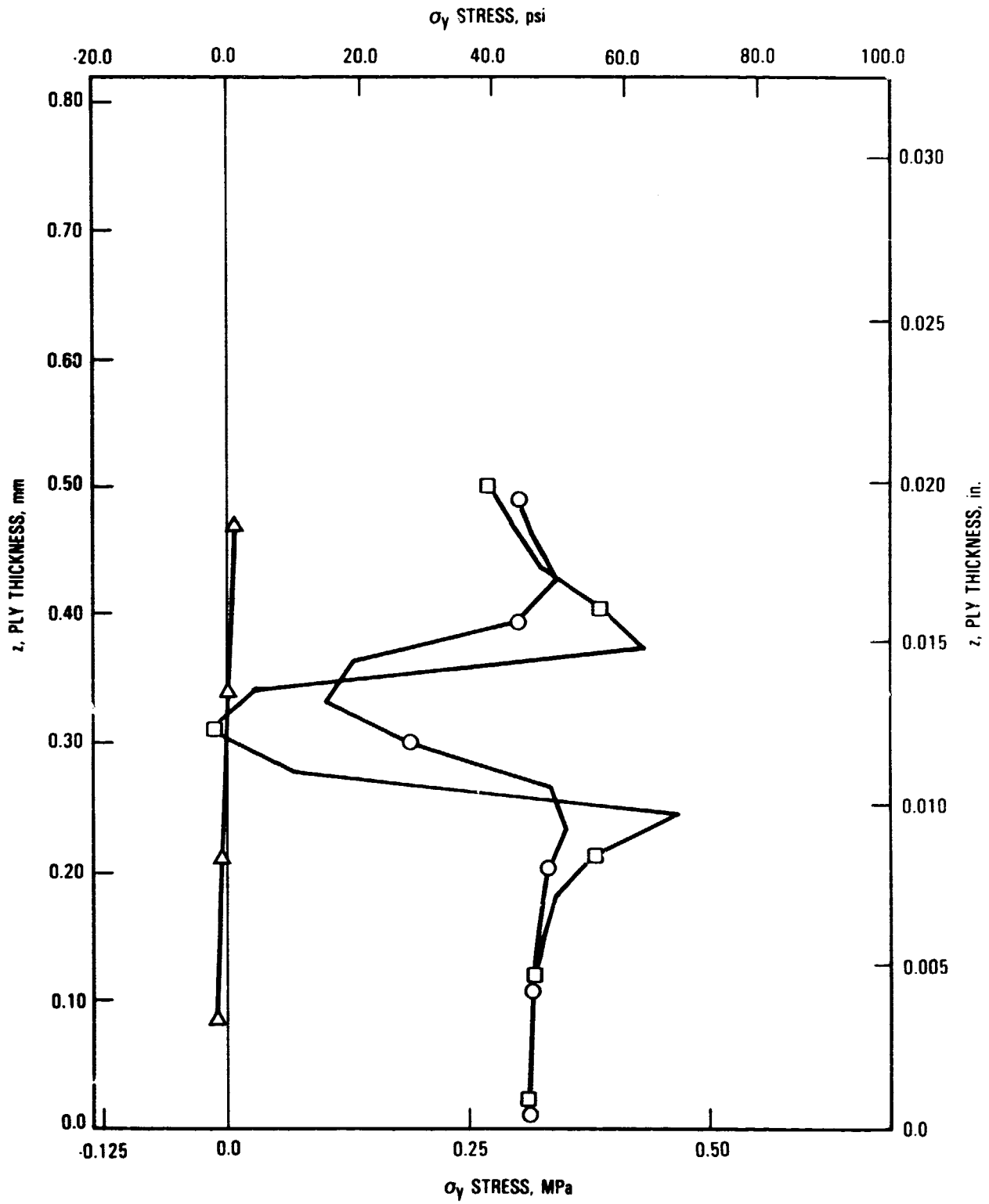

Figure 86: σ_y stress gradients near a crack in a $(90)_8$ laminate.

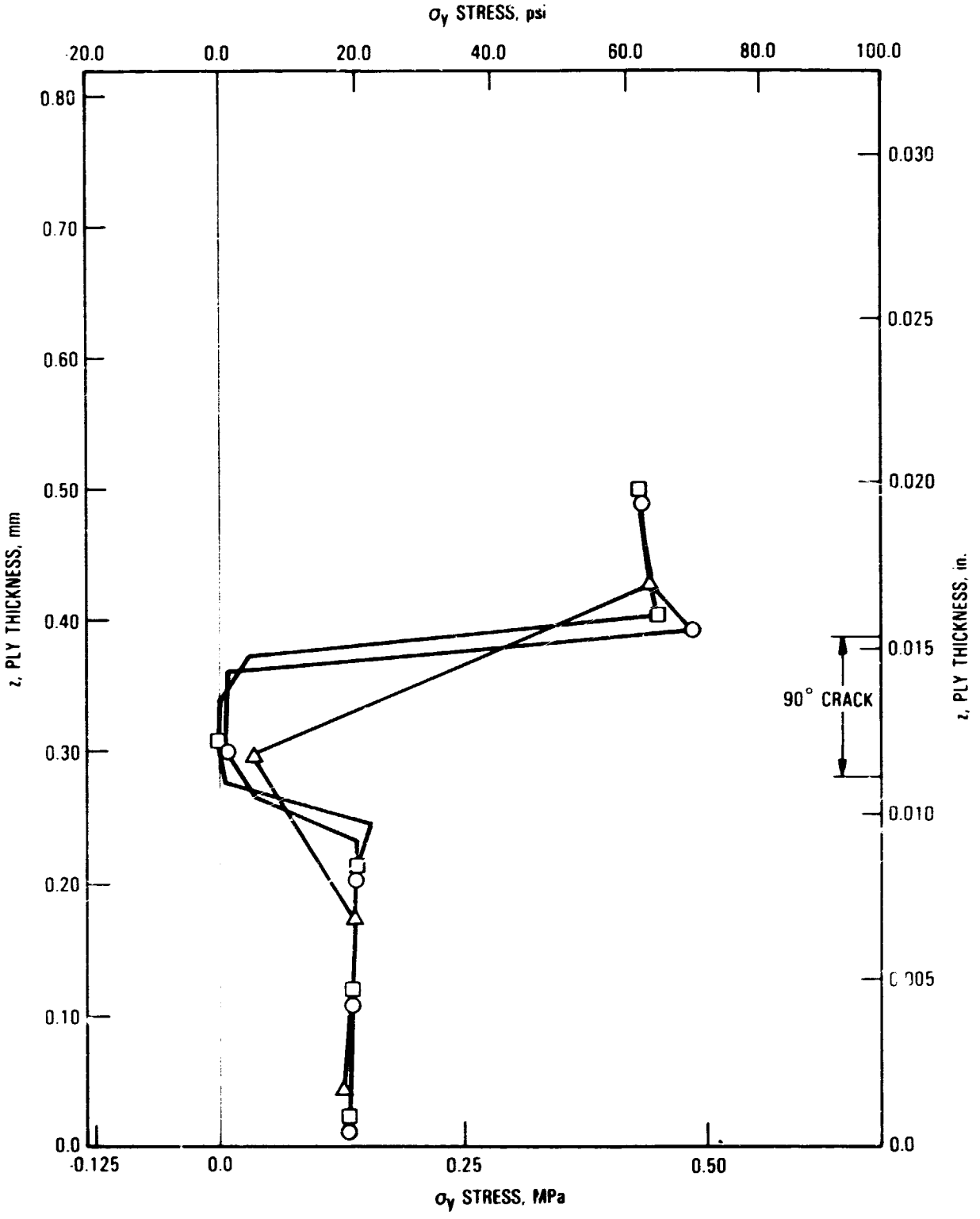

Figure 87 : σ_y stress gradients near a 90° ply crack in a $(0/90/\pm45)_s$ laminate.

the triangular element centroids closest to a 90° crack tip in an isotropic medium, of Figure 84, consider the diagram in Figure 88. In that figure,

$$\phi_1 = 26.57^\circ = \tan^{-1}(1/2) \tag{7}$$

$$\phi_2 = 63.43^\circ = \tan^{-1}(2) \tag{8}$$

and,

$$r_1 = r_2 = (1/3)a/\mathrm{Sin}\ 26.57^\circ = 0.745a. \tag{9}$$

Recall[83] that:

$$\sigma_y = \frac{K}{\sqrt{2\pi r}}\cos(\phi/2)[1+\mathrm{Sin}(\phi/2)\sin(3\phi/2)] \tag{10}$$

$$\sigma_y = \frac{Ya}{\sqrt{2\pi r}}\cos(\phi/2)[1+\mathrm{Sin}(\phi/2)\sin(3\phi/2)] \tag{11}$$

and that for an infinite body,

$$Y = \sqrt{\pi} = 1.77. \tag{12}$$

For a finite width specimen with width w and an imbedded crack of 2a and where 2a/w = 0.5,

$$Y = 2.05, \text{(see Reference 83)} \tag{13}$$

Therefore, for position 1 near the 90° crack,

$$\frac{\sigma_y}{\sigma_{y_\infty}} = 0.73Y \tag{14}$$

which implies a value of 1.29 for an infinite width body and 1.49 for a finite width body. For position 2 near the 90° crack,

$$\frac{\sigma_y}{\sigma_{y_\infty}} = 0.85Y \tag{15}$$

which results in a stress concentration value of 1.50 for an infinite width body and 1.74 for a finite width body.

The calculated stress concentration values of 1.3 to 1.7 agreed reasonably well with the finite element results for the homogeneous $(0)_8$ and $(90)_8$

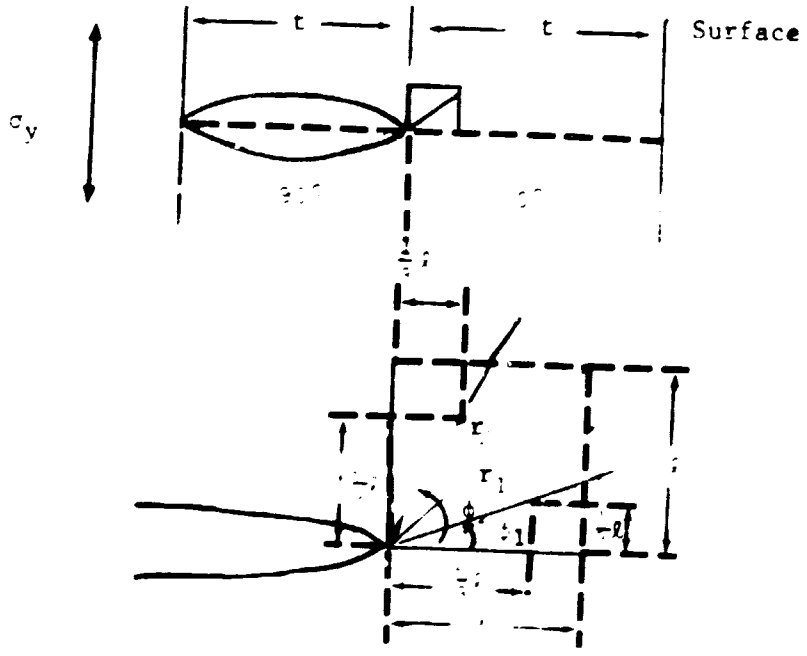

Figure 88: Diagram for analysis of stress concentrations close to a 90^o crack in an isotropic medium.

laminates, but not for the heterogeneous $(0/90/\pm45)_s$ laminate which has large variations in individual ply stiffnesses. This result indicated that the relative stiffness of the cracked and uncracked plies must be accounted for when properly calculating stress concentration due to the presence of matrix cracks.

3.4.4.4 Summary of Stress Concentration Due to Transverse Matrix Cracks

The analysis was undertaken to evaluate the influence of transverse crack tips on stress concentration and hence, fiber fracture in adjacent plies. This analysis was undertaken because fiber breaks have been discerned in the vicinity of transverse crack tips[40] and because the fracture direction in an outer ply is usually along the direction of the adjacent inner ply, see Section 2 and References 7, 13 and 32. The analysis was conducted assuming no short delamination at the ends of the transverse cracks. This allowed a maximum effect to be calculated.

Several interesting results were obtained. First, the stress gradient at a transverse crack was found to extend only a few fiber diameters into an adjacent ply. This led to the supposition that if fiber breakage occurs in an adjacent ply, the region and number of fiber fractures should be small and near the transverse crack tip. Second, by fracture mechanics analysis the strain energy release rate is not sufficient to predict the propagation of transverse cracks into adjacent 0° plies. Third, the relative stiffness of the cracked and uncracked plies must be taken into account. Fourth, a crack in a single thickness 90° ply causes a small stress concentration, of 10 percent or less, in either an adjacent 0° of 45° ply. Thus fiber fracture in quasi-isotropic layups would be anticipated to be rare except near coupon fracture. If a laminate has a thick 90° layer, such as the $(0_2/90_4)_s$ layup, a larger volume of the 0° layer is affected by the transverse cracking leading to possible fiber fracture. Fifth, because the longitudinal stiffness of the 45° ply is higher than in a 90° ply, a transverse crack in that ply could lead to greater load transfer into the adjacent 0° ply leading to possibly greater 0° fiber fracture in adjacent plies than a crack in a 90° ply.

These conclusions must be tempered with the fact that delaminations often exist at the end of transverse cracks, especially when coupons are subjected to fatigue loading. The presence of the delaminations at the ends of the transverse cracks reduces the local stress concentration. However, the analysis did lead to the anticipation that different layups should have significantly different amounts of fiber fracture prior to coupon failure. Essentially, on the basis of this analysis, the quasi-isotropic laminate would be anticipated to exhibit little fiber fracture prior to failure, the $(0/\pm 45)_s$ layups to have more, and the $(0/45/0_2/-45/0)_s$ layups and especially the $(0_2/90_4)_s$ layup to have considerably more fiber fracture. As will be discussed in more detail in Section 4 and as indicated by the results in Section 2 and the study of Jamison and Reifsnider[40], this conclusion was well supported experimentally.

Another possible cause of local fiber fracture would be due to free edge stresses. In fact Jamison and Reifsnider[40] showed that such fiber fracture can indeed occur in regions near transverse cracks. However, they also confirmed the work of Reifsnider, Schulte and Duke[84] that this effect is rapidly deminished within just a few fiber diameters from the free edge. In addition, Jamison and Reifsnider[40] showed that Shulte's[84] proposal that in-plane cracks within the 0° plies may lead to fracture is not, in fact, a major contributor to fiber fracture. A final point is that the stresses induced by the transverse cracks in the 0° ply are not high enough, when acting alone, to result in the 0° ply failure unless the global strain is high. Thus an additional failure criterion is required for many layups, especially quasi-isotropic. This is discussed in the following subsection. When fiber fracture does occur, Harlow and Phoenix[29,30,75-77] have shown that only the fracture of a few fibers in a statistically significant localized region is necessary to precipitate the final 0° ply fracture event. Essentially this statistical concept is based upon the fact that applied load eventually induces fiber fracture in many regions throughout

the 0° plies of an unnotched coupon. There exists, therefore, a statistical distribution of these fiber fractures plus that of the distribution of statistically weak fibers and thus the next likely to fail. The statistical distributions of broken and weak fibers are normally such that general 0° ply failure is not likely to occur. This remains true even when transverse matrix cracks are present in the adjacent plies because the stress induced by them is small. However, an additional group of a few fiber fractures can occur in a localized region such that now a large enough network of broken fibers and weak fibers are adjacent that 0° ply failure takes place. This additional group of fiber fractures is said to take place in a statistically significant region.

3.4.5 Effect of Local Strain Concentrations

O'Brien[41] proposed a method for assessing the strain concentration within a region of 0° plies which occurs due to transverse cracking and local separation of the cracked plies from neighboring plies by delamination, as noted previously[7,13]. Figure 89 illustrates the approach as used to describe the strain concentration in, for example, a $(0/90)_s$ laminate at a plane cut, A-A', across a damage region as compared to a cut made in an uncracked and undelaminated region, B-B'. In the analysis of the model shown in Figure 89, the local damage was assumed to be constant across the width. The strain concentration causes the stresses in the uncracked plies to be higher than those in the undamaged regions, but does not taken into account any highly localized stress concentration due to the tip of the transverse crack. This assumption is consistent with earlier analysis (see Section 3.4.4) which showed that the crack tip stress field was highly localized in a zone only one or two fiber diameters from the interface and failure analysis of this small region would have to proceed from a discrete model of individual fibers. Further, a statistical analysis of the strength in these locally small regions is examined in Section 3.6. The local strength of these small regions was found to be greater than the stress introduced by the transverse crack at distances greater than one fiber diameter.

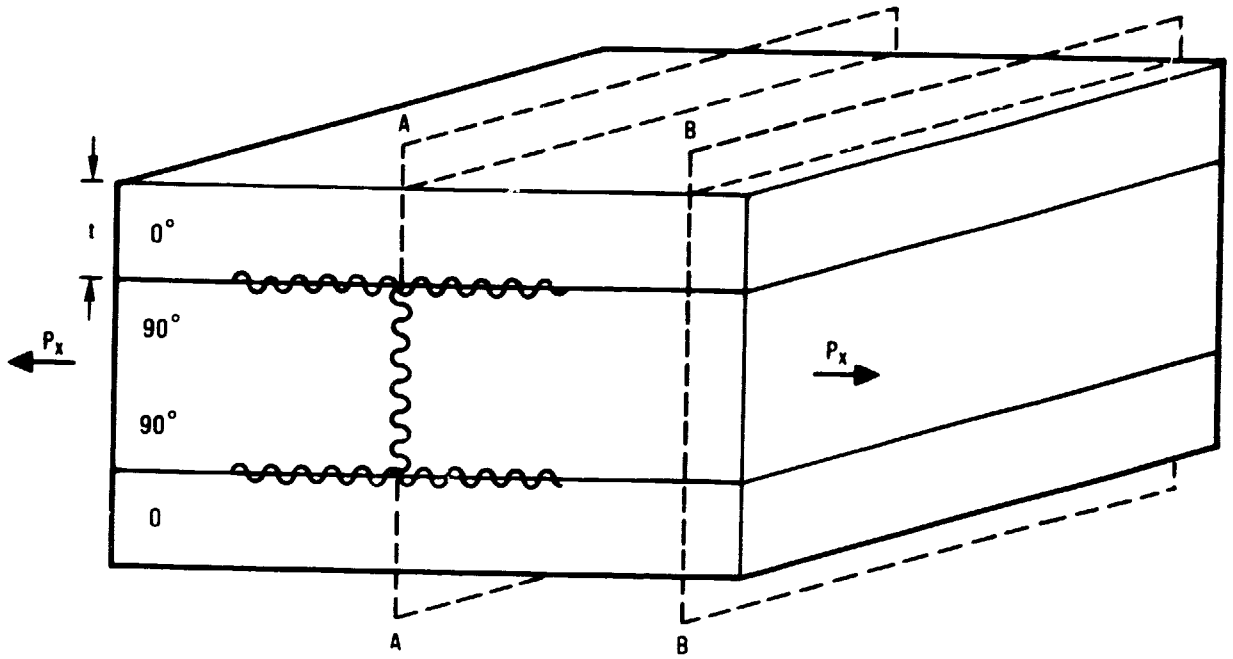

STRAIN CONCENTRATION = $\varepsilon_A/\varepsilon_B$

= $E_B A_B / E_A A_A$

E_A => E_x OF (0_2)

A_A => $2t$

E_B => E_x OF $(0/90)_S$

A_B => $4t$

Figure 89: Model for analyzing effect of matrix cracking and delamination on 0° ply fracture of a $(0/90)_s$ laminate.

O'Brien[41] applied the modeling technique to a $(+45/-45/0/90)_s$ laminate. Figure 90 shows the theoretically possible types of delaminations and the regions selected for modeling. Notice in Figure 90, the two types of delamination previously discussed. The "thumbnail" type of delamination at the 0/90 interface is of large area. This type of delamination may or may not cause significant stiffness loss depending on the interface. In this particular laminate, the 0/90 interface delamination is not associated with any strain concentration. Also shown in Figure 90 are a few +45/-45 interface delaminations which cause little stiffness loss because of their relative rarity, but are associated with large strain concentrations. In Figure 91, a rather straight forward, free body type modeling analysis is shown for the different selected delamination regions. The results of the analysis are given in Figure 92 which shows that the local strain does, at least analytically, increase as the severity of damage increased for this layup. Therefore, this proposal that at least one major contributor to 0^o ply failure is due to the local strain concentration because of combined matrix cracking and delamination was further explored.

To allow for a correlation to be made of experimentally measured and analytically modeled static and fatigue failure strains of the laminates evaluated in this study, a series of laminate stiffness analyses were conducted. The results were used to obtain the necessary stiffness and uncracked ply thicknesses needed to calculate the strain concentration factors for a specific laminate damage state. These laminate analyses were chosen by first categorizing the location of delamination in each laminate in order of appearance. In Figure 93, delamination locations and order of appearance are indicated for several laminates. Although the delamination at the +45/-45 interface in the $(0/90/\pm45)_s$ laminate occurred first, the 90/+45 delamination quickly became dominant, as discussed in Section 2.2.

For certain combinations of various possible delaminations and transverse matrix cracks of Figure 93, local regions of strain concentration within the

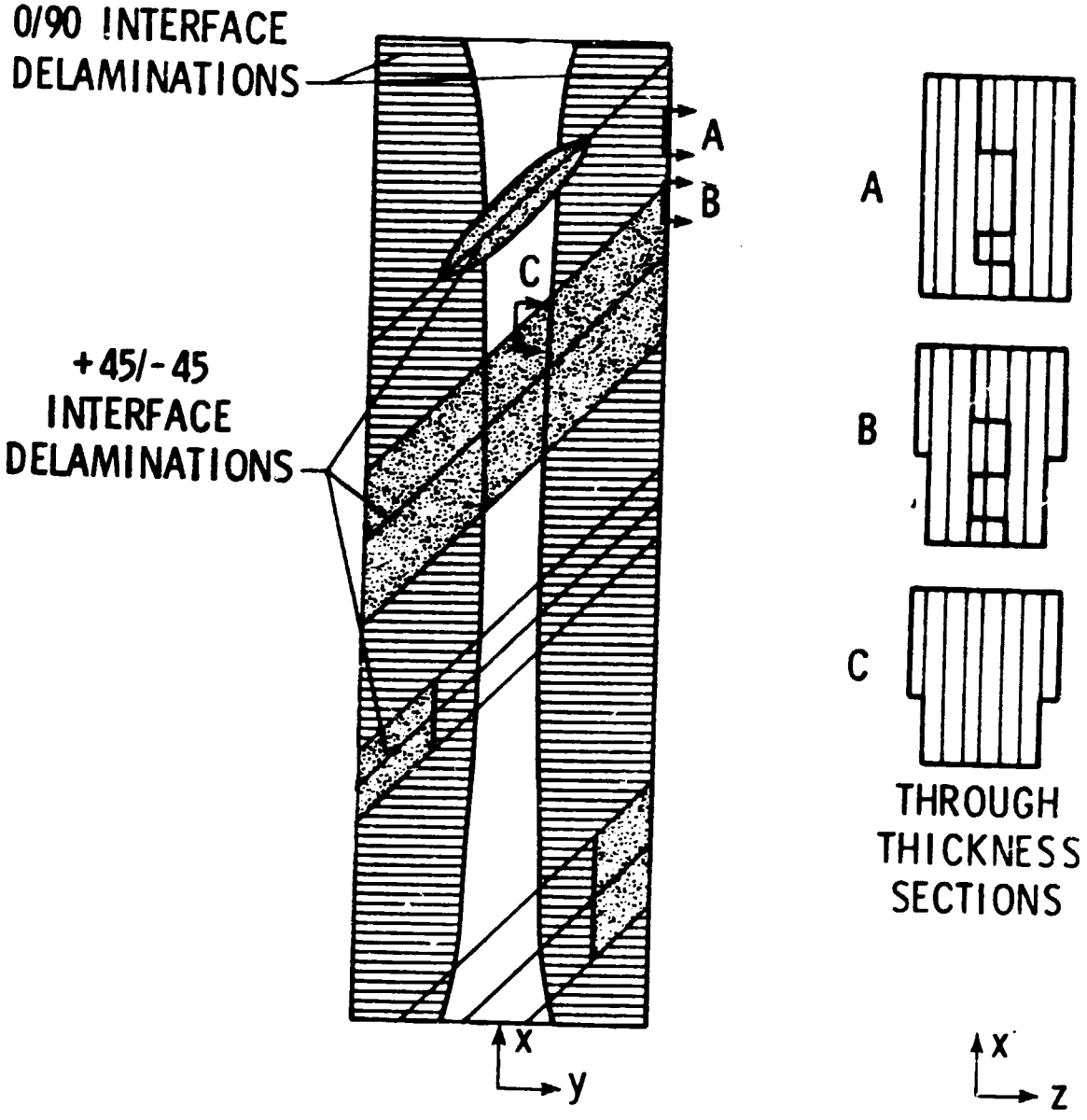

Figure 90: Schematic of Typical Damage Development in $(+45_n/-45_n/0_n/90_n)_s$ Laminates. [41]

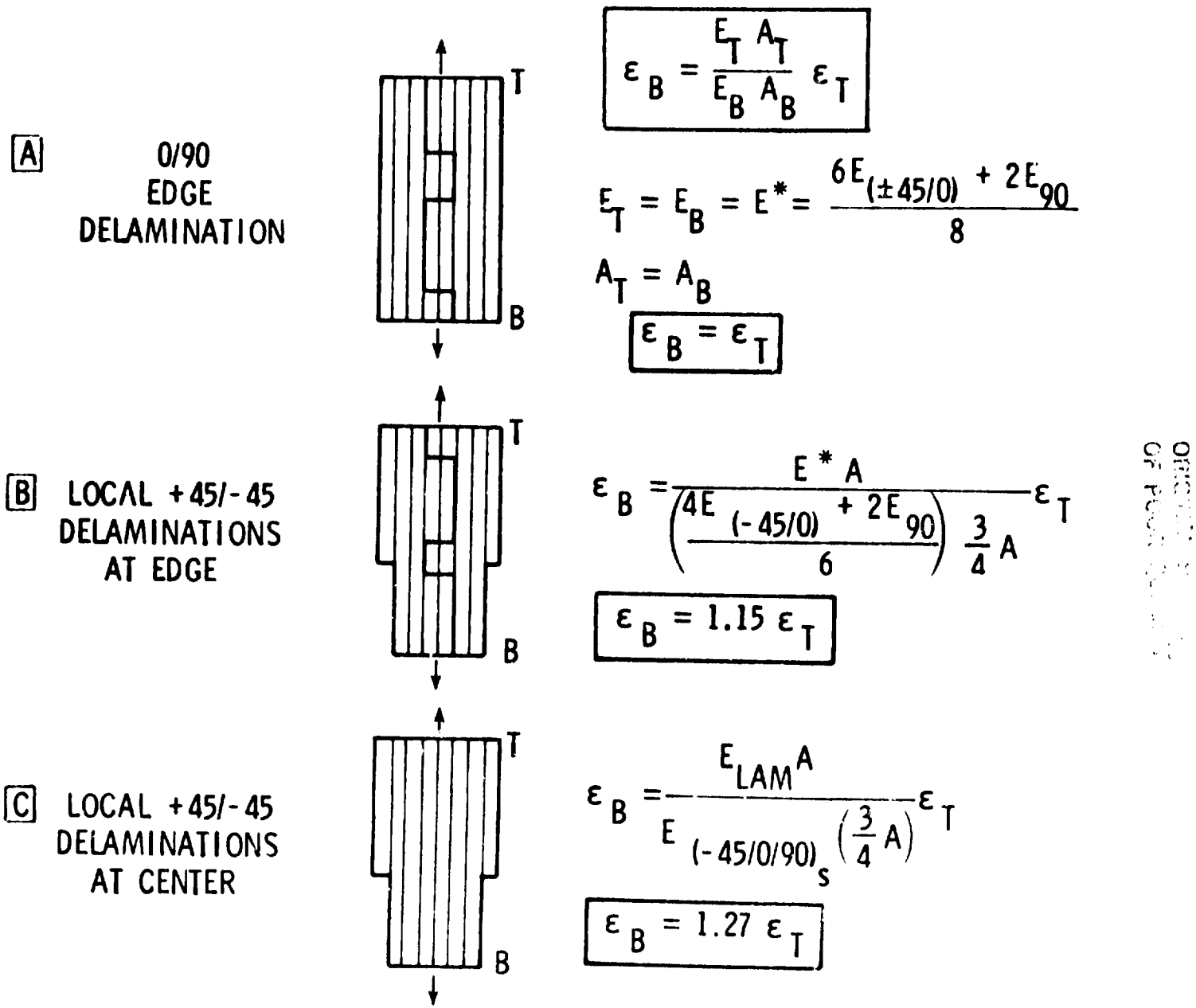

Figure 91 Analysis of Local Strain Concentrations[41]

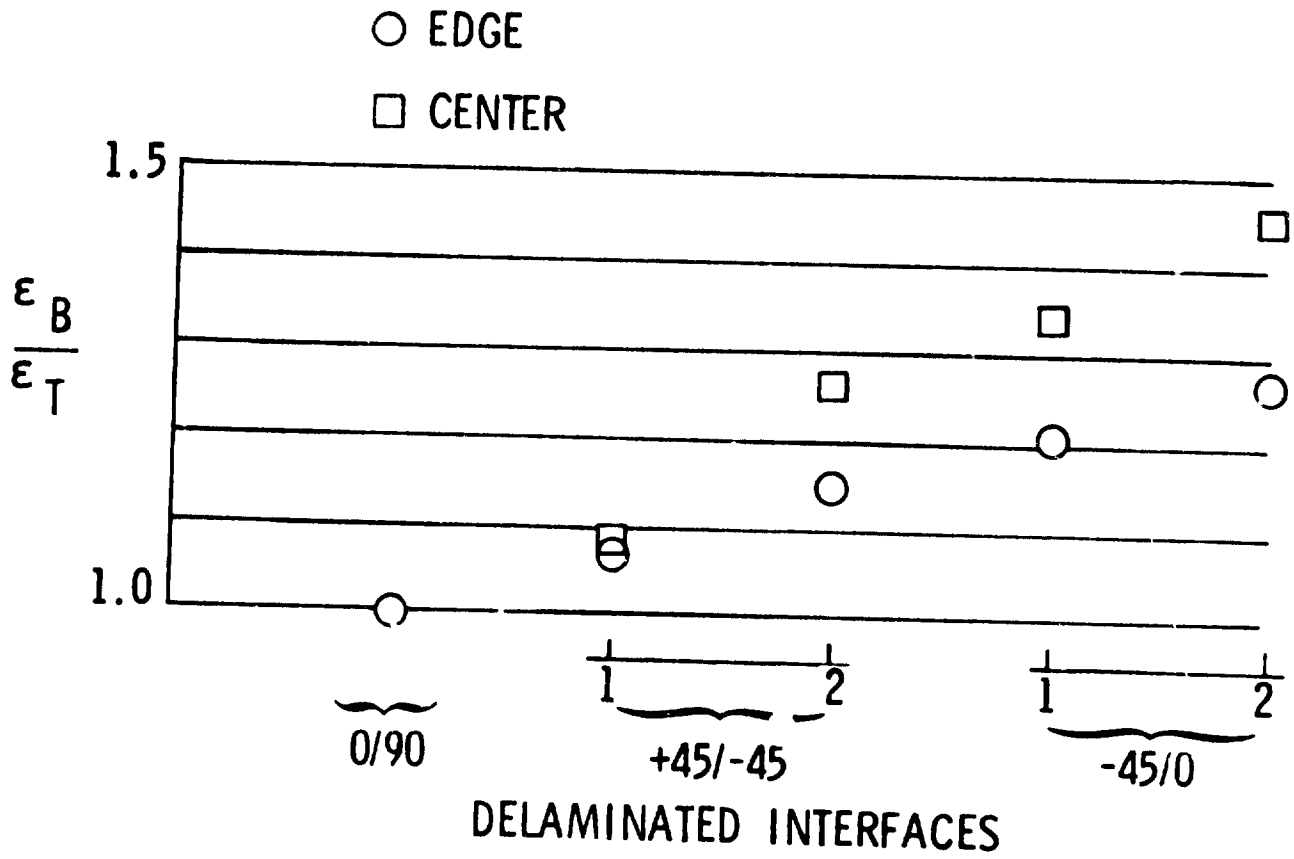

Figure 92 : Local Strain Concentration due to Delamination in $(+45_n/-45_n/0_n/90_n)_s$ Laminates [43]

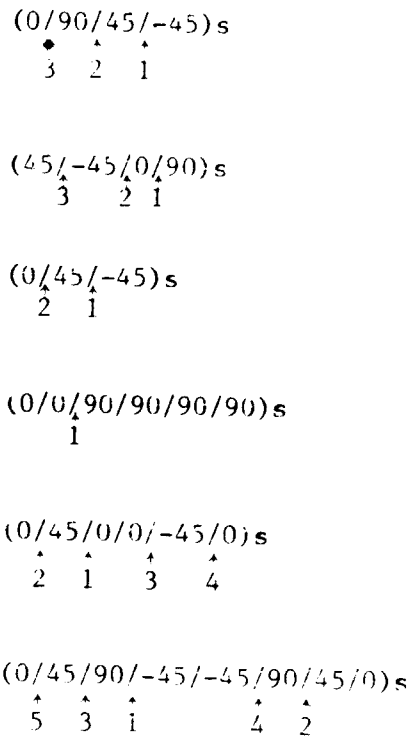

Figure 93 Laminates Chosen for Strain Concentration Analysis; Order of Delamination Appearance is Indicated.

0° plies can occur. For example, consider Figure 94 Case A for the $(0/90/\pm45)_s$ layup. The state of matrix cracking alone is associated with only a few percent stiffness loss, and only a small strain increase, due to the matrix cracks, see Section 3.3.1. There will also be a small local strain concentration in the plies adjacent to the transverse matrix cracks because of the induced stresses at the crack tips. In Case B of Figure 94, further stiffness loss will be associated with the development of delamination, but no large local strain concentration occurs. In fact, the local strain may be decreased because of crack tip blunting due to the presence of the delaminations. In Case C, however, the presence of matrix cracks with delaminations on either side resultes in local stress concentrations, Section AA'; and even an entire region being unable to carry load, specifically the cross hatched $\pm45^\circ$ plies in Section BB'. The load in these plies is locally transfered into the 0° and 90° plies resulting in large local 0° ply strain increases as simple free body modeling of the cuts, similar to that shown in Figures 89 to 91, easily demonstrates. Figure 95 summarizes the influence of the two different types of strain concentration, that due to matrix cracking alone and that due to combined matrix cracking and delamination.

As previously mentioned in Section 3.3.5, if such combinations of transverse cracking and delamination occurred end-to-end and side-to-side within a coupon, the off-axis plies would be totally isolated from the externally applied load. Stiffness loss would occur, very large in some layups, and the stress in the 0° plies would increase. For example, in the 8 ply quasi-isotropic layup, a 43 percent stiffness loss, and hence 43 percent strain increase in the 0° plies, would be associated with complete loss of load carrying capacity in the $\pm45^\circ$ plies due to their isolation. If such ply isolation occurs locally, due to the presence of a local, small region of combined delaminations and matrix cracks, such as at Sections AA' and BB' in Figure 94, significant strain increases in the 0° plies would occur locally and would be associated with some measurable global stiffness decrease. This local region of strain increase is of great interest as a proposed 0° ply failure criterion if strains can be locally increased enough to result in local 0° fiber fracture.

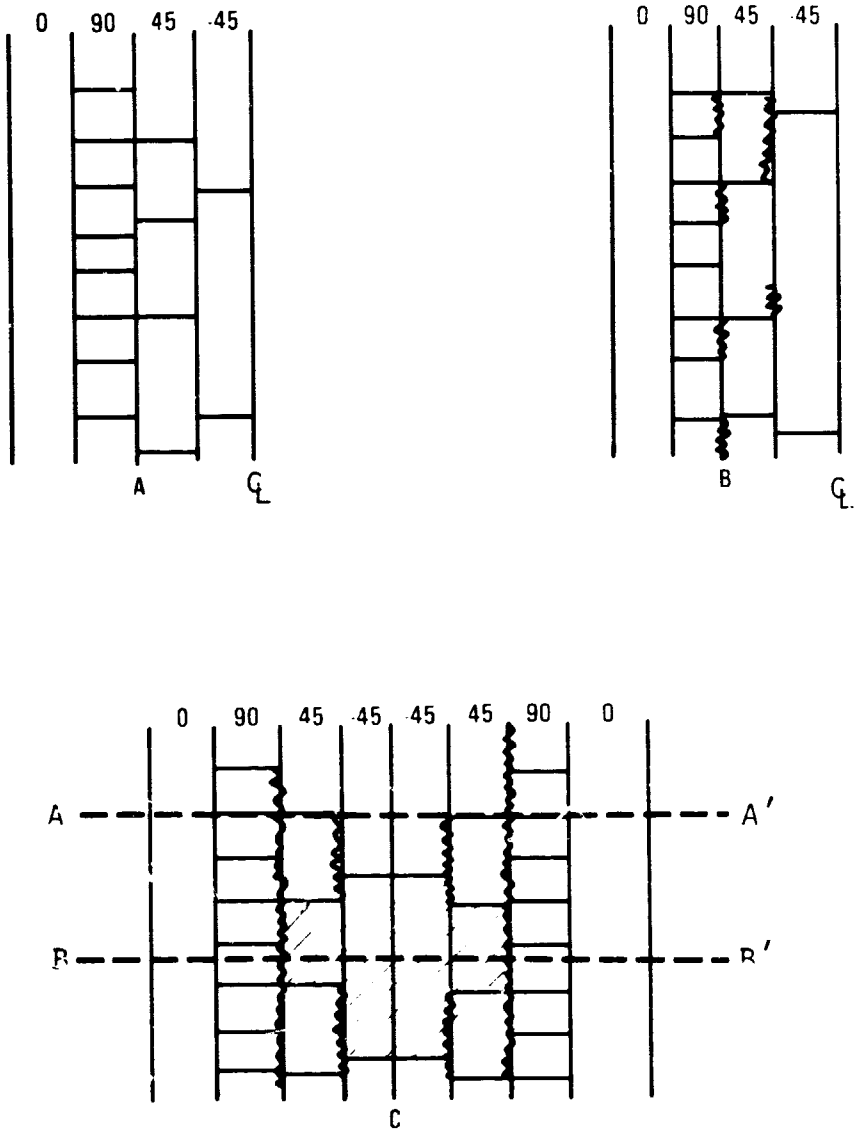

NOTE: "Wiggly" lines indicate delamination, horizontal lines indicate transverse matrix cracking.

Figure 94: Example of various possible damage states in $(0/90/\pm45)_s$ laminate.

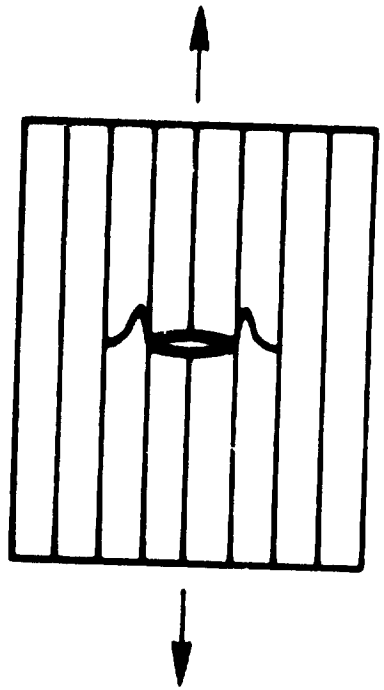

LOCAL STRAIN CONCENTRATION

- IN NEIGHBORING PLY ONLY
- SMALL IN MAGNITUDE
- ACTS ONLY ON SMALL PORTION OF PLY THICKNESS

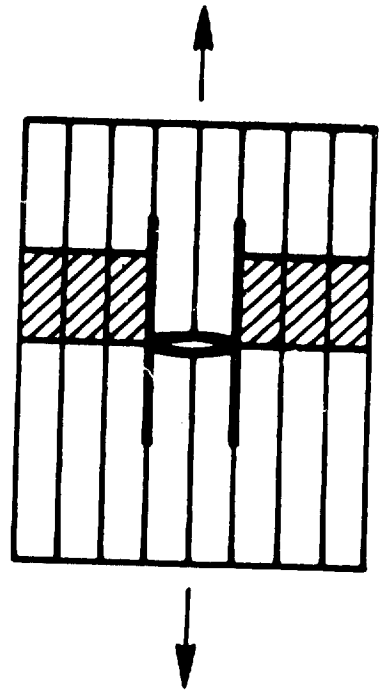

LOCAL STRAIN CONCENTRATION

- UNIFORM THROUGHOUT UNCRACKED SECTION
- MAGNITUDE MAY BE LARGE

Figure 95: Strain concentrations due to local damage in unnotched laminates.

The case of local load transfer to the outer 0° plies which occurs for the $(0/90/\pm45)_s$ quasi-isotropic laminate of this study is similar to the perhaps more subtle case of Figure 90 for the $(\pm45/0/90)_s$ laminate. In that case, transverse cracks in the outer $+45^\circ$ plies which develop a short delamination along the transverse crack in the +45/-45 interface lead directly to a large strain increase because the load carrying capability of the outer +45 plies is immediately locally removed. A similar situation occurs in the $(0/90/\pm45)_s$ layup when delamination develops at both +45/-45 interfaces and there are transverse cracks in the 90° plies, see Section AA' of Figure 94. The key point is that any combination of delamination and transverse matrix cracking that locally isolates one or more plies must be associated with local stress/strain increases in adjacent plies and in global stiffness loss. This ply isolation is potentially of large importance for understanding the mechanical response of these laminated composites. For delamination emanating from the transverse matrix cracks across the coupon width, associated global stiffness loss was shown in Section 3.5.4 to be small because such delamination does not generally occur. However, as shown in this section, local stress concentration is potentially quite large.

The strain concentrations which could occur in the 0° plies, due to ply isolation associated with combined delamination and transverse matrix cracking, were determined for each of the laminates of this study. A table of laminate moduli was constructed using ADVLAM analysis code, the results of which are shown in Table 46. Two cases were run for each laminate. The first analysis put the ply group into a symmetric layup and the modulus associated with this analysis is labeled $E_{x,sym}$. The second analysis considered just the group of plies indicated in column one under uniaxial strain as in the first case, but also allowed for a non-zero curvature about the y axis such that $K_y = 0$. This extra degree of freedom corresponded to the warping up of delamination regions at the free edge and represented a lower bound on the constraint of neighboring plies in inhibiting warping. The actual warping of this delamination region will vary as a function of position and lie between the two extremes that are given in Table 46.

TABLE 46
TENSILE MODULI E_{xy} OF VARIOUS PLY GROUPINGS

Layup	E_x, sym. GPa	E_x, sym. Msi	Number of Plies	E_x, unsym. GPa	E_x, unsym. Msi	K_y, 1/in. x 10^{-5}	1/mm x 10^{-7}
(0)	137.9	20.0	1	----	----	----	----
(0/45)	76.05	11.03	2	75.98	11.02	-1.92	-7.56
(0/90)	74.12	10.75	2	73.98	10.73	2.28	8.98
(45)	12.8	1.85	1	----	----	----	----
(45/-45)	17.2	2.49	2	----	----	----	----
(90)	9.7	1.4	1	----	----	----	----
(0/45/0/0)	107.5	15.59	4	107.5	15.59	0.84	3.31
(0/45/0/0/-45)	90.67	13.15	5	90.53	13.13	-1.13	-4.49
(0/45/90)	55.8	8.09	3	55.0	7.97	3.80	14.96
(0/45/90/-45/-45)	46.8	6.79	5	46.6	6.76	-1.66	-6.54
(45/45/0)	58.1	8.43	3	57.7	8.37	3.57	14.06
(0/90/45)	55.8	8.09	3	53.4	8.03	-3.04	11.97
(0/90/45/-45)	53.1	7.70	4	47.4	6.92	-7.10	27.95

Figure 96 shows the geometry of the stacking sequence in the analysis and the convention used in defining the sign of the K_y curvature.

Except for the (0/90/45/-45) grouping, the inclusion of K_y warping had an insignificant effect on the tensile modulus of the laminate. Given the assumption of damage extending evenly across the width of the laminate, the asymmetry of the group and its influence on the tensile modulus could effectively be ignored in further analyses. However, for many damage states such warping becomes significant and thus cannot be ignored.[85,86]

Table 47 presents the strain concentration factors for different types of ply isolation in each of the laminates studied in this investigation, assuming no warping. The associated strain concentrations, or inversely, stiffness decrease ratios, occur locally and have global effects which depend on the extent of ply isolation. Some of the ply isolation states in Table 47 were not observed in the laminate stacking sequences studied, but are included here for completeness. Note that information on the strain concentration factors of $(0/90/45/-45)_s$ and $(45/-45/0/90)_s$ laminates is found in the same set of analyses because of the independence of the tensile modulus calculations from stacking sequences. In the table a box drawn around a ply or a group of plies indicates the local loss of these plies due to a combination of transverse cracking and delamination, such as in Figure 89, 90, or 94c, where locally a group of plies are isolated.

The results of the strain concentration factor analysis given in Table 47, were used to infer that ply isolation was another primary criterion for 0° ply failure. The results showed that as matrix cracking and delamination developed, strain in the 0° plies would increase in local regions adjacent to the matrix cracking and delamination. Thus the hypothesis was made that when the local strain exceeded the strain capacity of the fibers, local 0° ply fracture would occur and the reduced number of load carrying fibers would lead to coupon fracture.

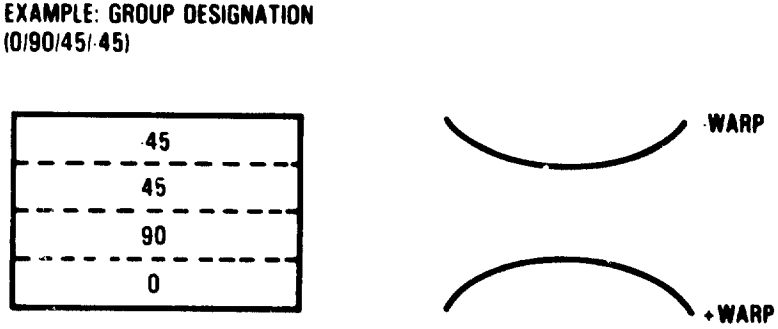

FIGURE 96 EXAMPLE OF STACKING SEQUENCE GEOMETRY AND K_y CURVATURE FOR STRAIN CONCENTRATION ANALYSIS.

TABLE 47
STRAIN CONCENTRATION FACTORS OBTAINED BY
REMOVAL OF PLY GROUPINGS IN BOXES

Layup	Remaining Stiffness GPa (Msi) E_x * Thickness	Strain Conc.
0/90/45/-45	53.1 (7.7) * 4	1.00
0/90/45/-45	74.12 (10.75) * 2	1.43
0/90/45/-45	137.9 (20.0) * 1	1.54
0/90/45/-45	55.8 (8.09) * 3	1.27
0/90/45/-45	58.1 (8.43) * 3	1.22
0/90/45/-45	76.05 (11.03) * 2	1.40
0/45/-45	58.1 (8.43) * 3	1.00
0/45/-45	76.05 (11.03) * 2	1.15
0/45/-45	137.9 (20.0) * 1	1.26
0/0/90/90/90/90	52.5 (7.63) * 6	1.00
0/0/90/90/90/90	137.9 (20.0) * 2	1.14
0/45/0/0/-45/0	98.6 (14.3) * 6	1.00
0/45/0/0/-45/0	107.6 (15.6) * 4+ 137.9 (20.0) * 1	1.04
0/45/0/0/-45/0	137.9 (20.0) * 4	1.07
0/45/90/-45/-45/90/45/0	53.1 (7.7) * 8	1.00
0/45/90/-45/-45/90/45/0	75.8 (11.0) * 2 + 46.8 (6.79) * 5	1.10

3.4.6 Summary of 0° Ply Failure Criteria

The study of possible 0° ply failure criteria led to the conclusion that the problem is primarily one of determining the reasons for fiber fracture in the 0° plies. In this study, the conclusion was that this should primarily occur due to two reasons. First, local stress concentrations due to the presence of the transverse matrix cracks. This should generally be a small effect and be limited to a small region near the crack tip. Second, strain concentration over a local region due to load transfer to the 0° plies because of a combination of matrix cracking and delamination.

In the region of the hypothesized local strain concentration, a statistically based increase in the strength of the 0° fibers can occur. This is due to the smaller volume of fibers compared to the volume in a 0° unidirectional coupon as discussed in detail in Section 3.6. However, this increase in strength is quite small because the volume ratios are similar. This is in contrast to the large statistically based increase in strength which occurs at a transverse crack tip mentioned in Section 3.4.1. In that case, the volume of material is quite small and thus is accompanied by a large increase in strength as demonstrated in Section 3.6. Thus, local strain concentration due to combined delamination and matrix cracking was inferred to be a reasonable failure criteria as opposed to a deterministic failure criteria[80] at the tip of a transverse matrix crack. This is especially true since the delamination at the end of a crack tip greatly reduces the effect of the stress singularity.

The two 0° fiber fracture criteria, when combined, led to several conclusions which are discussed in detail in Section 4. They constitute two of the the primary hypothesized reasons that failure by 0° ply fiber fracture occurs. They must be combined with the fact that even in 0° unidirectional laminates, fiber fracture and coupon failure occur under fatigue load, see Section 2.1. This begins to happen at any strain level above approximately 0.0070[38] and occurs significantly above 0.0080 strain, see Figure 97. Any

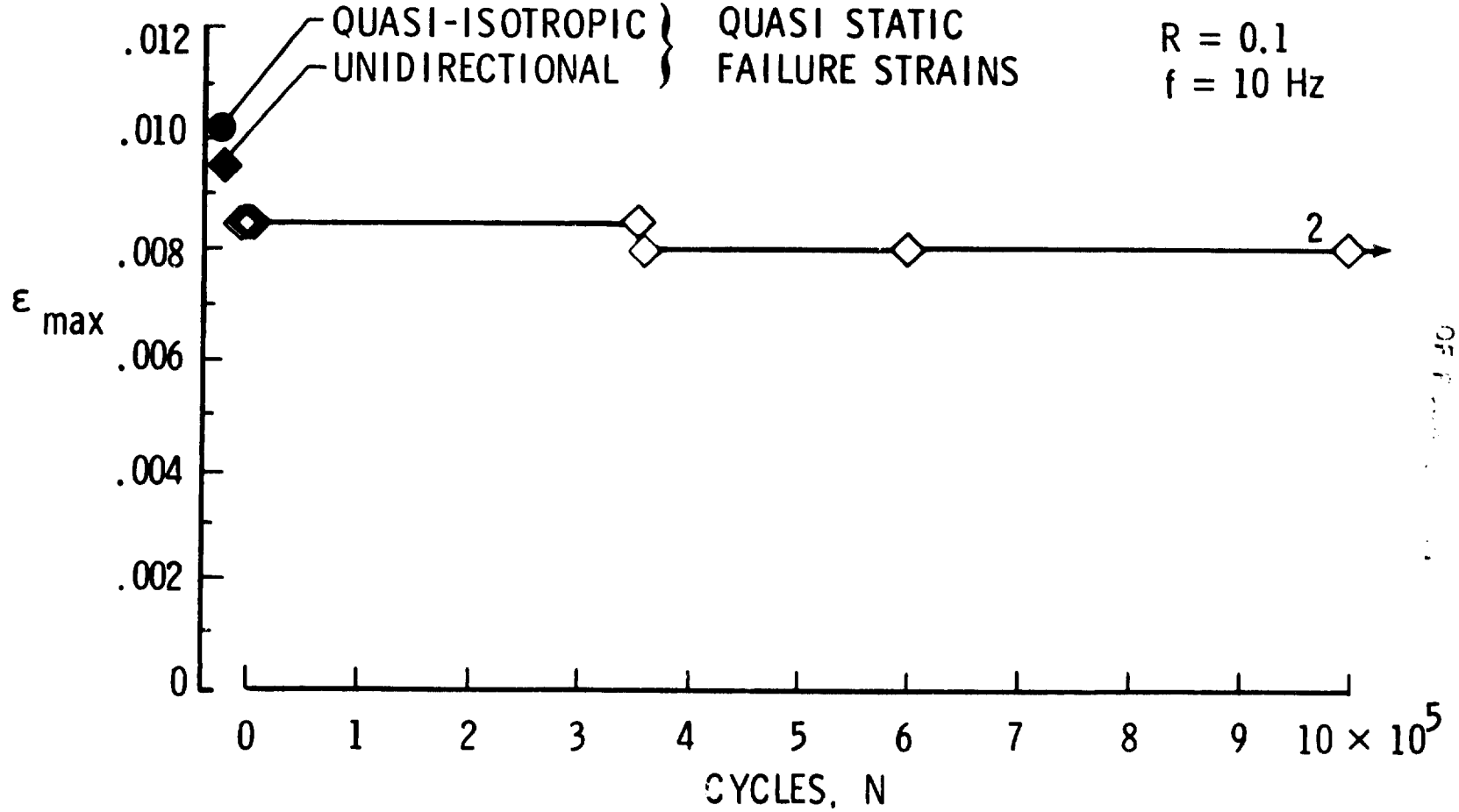

Figure 97: Fatigue behavior of unidirectional $(0)_4$ graphite/epoxy laminates.

damage state which increases the strain in a local 0° ply region above a strain of 0.0070 to 0.0080 can be expected to result eventually in 0° fiber fracture during fatigue loading. In essence, this is a third 0° ply failure criterion.

The limited fatigue data of Figure 97 are those obtained in this investigation. The study by Averbach and Hahn[38] clearly showed that the scatter band for 0° unidirectional data extends both vertically and horizontally. Thus no actual stress-strain curve was exhibited, only a large region, from 0.0070 - 0.0080 to approximately 0.0110 strain and from 0 to at least 10^7 cycles, within which failure under fatigue load cycling can be expected. These fatigue failures apparently occur for similar reasons to those mentioned in Section 3.4.4. Fractures of the weakest coupons occur upon initial load to a strain level above the lower bound of the fiber strength distribution. Subsequent load cycling fractures the next weakest fibers until a distribution of broken fibers exists throughout the coupon. Eventually fibers fracture which form a stastically significant group, one that when combined with other fiber fractures and the distribution in strength of the unbroken fibers results in coupon fracture.[29,30,75-77]

For a multidirectional laminate, the significant fracture of 0° fibers begins if the global strain is above 0.0070 - 0.0080. If a large local strain concentration occurs under fatigue loading dur to combined delamination and matrix (see Section 3.4.5) such that 0° ply strain is above 0.0070 - 0.0080, fiber fracture begins to occur and coupon fracture must eventuate. Similarly, if initial global strains are in the 0.0070 - 0.0080 range, the small local stress increase in the 0° plies due to transverse matrix cracking can also lead to fiber fracture. The amount of fiber fracture in any one small region of the 0° ply does not apparently have to be large for failure to occur. As mentioned for the 0° unidirectional laminate, Harlow and Phoenix[29,30,75-77] have shown that only 4 to 6 fiber fractures in a small statically significant local region are required. Thus the hypothesized reasons for 0° ply failure do not imply that regions of large numbers of broken fibers would generally be found. This fact implies that the final fracture events must be quite sudden.

3.5 EXAMINATION OF THE EFFECT OF FIBER VOLUME ON FAILURE OF 0° PLIES

3.5.1 Strain-to-Failure Differences Between Unidirectional and Multidirectional Laminates

The strain to failure of the unidirectional $(0)_4$ coupons was originally inferred to be similar to that of the $(0/90\pm45)_s$ laminates made from the same batch of material. This was tentatively concluded because of the concern that the lower strain to failure of the $(0)_4$ layup might be due to some unknown prior damage. The correctness of this supposition was, however, somewhat in doubt because there was some evidence that the strain to failure of unidirectional laminates is, in fact, somewhat lower than that for laminates containing off axis plies. Thus perhaps the observed large variation in strain to failure values was due to expected scatter more than to damaged coupons. Table 48 summarizes the strain-to-failure of tensile tested unidirectional composites and laminates of T300/5208 in this current program and in an earlier study conducted for the Air Force[6]. Examination of the strain-to-failure of unidirectional composites and laminates given in Table 48 shows that the laminate failure strains can be on the order of 7 - 10% higher than the unidirectional values. The reason for this possibility was further explored.

None of the laminate constructions of Table 48 exhibit large delamination development or growth under static tensile loading. Therefore, the damage state prior to fiber failure in the 0° plies for the quasi-isotropic and $(0/\pm45)_s$ laminates consists only of transverse ply cracks with small delaminations at the matrix crack ends along the coupon edges. The locations and sizes of the delaminations were such that they could not cause significant stiffness change or local strain concentration, see Section 3.4.3, except ~~very~~ near failure. Based on the results of the stress analysis presented in Section 3.3.6, the strain concentration in the 0° ply caused by

TABLE 48
OBSERVED TENSILE STRAIN-TO-FAILURE
FOR T300/5208 LAMINATES

Laminate	Reference	Average Strain at Failure	Number of Tests	Percent Difference
$(0)_4$	This study	0.0098	5	---[a]
$(0/45/-45)_s$	This study	0.0106	4	8.2
$(0/90/45/-45)_s$	This study	0.0103	5	5.1
$(0)_{16}$	6	0.0095	10	---[b]
$(0/45/90/-45)_{2s}$	6	0.0105	20	10.5
$(0/45/0_2/-45/0)_s$	This study	0.0112	5	---[c]

a = Base strain for comparison to succeeding two entrys, same material batch.

b = Base strain for comparison to subsequent entry, same material batch.

c = Not compared because from different material batch from A or B data.

the adjacent 90° transverse cracks and edge delamination in the $(0/90/45/-45)_s$ laminate was probably sufficient to cause a slight decrease in strain to failure of the 0° ply. The decrease would be slight because the development of delamination and ply isolation are confined to the coupon edge and occur just prior to failure. Further, the 90° ply matrix cracks only cause a small stress increase in a quite restricted volume. Similarly cracks in the adjacent $+45^{\circ}$ ply should be sufficient to somewhat decrease the 0° ply strain to failure in the $(0/45/90/-45)_{2s}$ laminate. For the $(0/\pm 45)_s$ laminate, strain to failure should be much less affected by local strain concentrations because ply isolation essentially does not occur. There should also be virtually no effect in the $(0/45/0_2/-45/0)_s$ laminate. However, the effect of local strain concentration is quite large for the $(0_2/90_4)_s$ laminate[52] as previously discussed, see Section 3.4.4.1. Some of the higher strain to failure values of the $(0/45/0_2/-45/0)_s$ probably reflect variations in material batches.

The local strain concentrations along the coupon edges appears to explain most of the variation in strain to failure among the various multiple axis laminates. However, the differences between the unidirectional and multi-directional laminate strain to failures remained to be explained. Therefore, the question was explored as to whether residual thermal stresses could affect unidirectional fiber strength or whether the difference was a manifestation of volume dependency based on the Weibull strength distribution.

Tables 49 to 51 provide information on the ply stresses in the $(0/45/-45)_s$ and $(0/90/45/-45)_s$ laminates under unit mechanical tensile strain and under a unit change in temperature. The ADVLAM laminate analysis program was used to generate these data. From Reference 87, the effective stress free temperature of $(0_4/90_4)$ T300/5208 laminates was determined to be $171^{\circ}C$ ($340^{\circ}F$) for a test temperature of $24^{\circ}C$ ($75^{\circ}F$), with the appropriate temperature change, ΔT, of $-147^{\circ}C$ ($-265^{\circ}F$). Using the data in Table 47 for the 0° ply, the residual thermal stress, σ_x, in the 0° ply was -39.8 MPa

TABLE 49
T300/5208 LAMINA PLY PROPERTIES USED IN ADVLAM ANALYSIS

E_1 MPa (Msi)	E_2 MPa (Msi)	G_{12} MPa (Msi)	ν	$ALPHA_1$ $10^{-6}/^{\circ}C$ ($10^{-6}/^{\circ}F$)	$ALPHA_2$ $10^{-6}/^{\circ}C$ ($10^{-6}/^{\circ}F$)
16.34	10.2	6.48	.3	-0.36	28.8
(23.7)	(1.48)	(0.94)	.3	(-.2)	(16.0)

TABLE 50
MECHANICAL STRESSES IN $(0/90/45/-45)_s$ LAMINATE UNDER AN APPLIED TENSILE STRAIN OF $\epsilon_s = 10^{**}(-6)$

Ply Layer	σ_x Pa x 10^5	σ_x psi	σ_y Pa x 10^5	σ_y psi	σ_{xy} Pa x 10^5	σ_{xy} psi
0	1.63	23.7	-0.000069	-0.001	0.0	0.0
90	0.093	1.354	-0.463	-6.720	0.0	0.0
45	0.400	5.806	0.232	3.361	0.269	3.907
-45	0.400	5.806	0.232	3.361	-0.269	-3.907

TABLE 51
THERMAL STRESSES IN T300/5208 LAMINATES

Laminate	Ply Layer	σ_x MPa/°C	σ_x psi/°F	σ_y MPa/°C	σ_y psi/°F	σ_{xy} MPa/°C	σ_{xy} psi/°F
$(0/90/45/-45)_s$							
	0	0.271	21.8	-0.271	-21.8	0.0	0.0
	90	0.271	-21.8	0.271	21.8	0.0	0.0
	45	0.0	0.0	0.0	0.0	0.271	21.8
	-45	0.0	0.0	0.0	0.0	-0.271	-21.8
$(0/45/-45)_s$	0	0.0779	-6.28	-0.24	-19.09	0.0	0.0
	45	0.0390	3.141	0.118	9.544	0.338	27.2
	-45	0.0390	3.141	0.118	9.544	-0.338	-27.2

(-5.78 ksi) in the $(0/90/45/-45)_s$ laminate and 11.5 MPa (1.66 ksi) in the $(0/45/-45)_s$ laminate. The mechanical strain, ϵ_x, needed to overcome the thermal stress was determined by dividing the thermal stress by the E_{xx} stiffness. This calculation gave 24 microstrain for the quasi-isotropic laminate and -70 microstrain for the $(0/45/-45)_s$ laminate. This small strain was clearly of little significance and was even of the wrong sign for the $(0/45/-45)_s$ laminate. Therefore, residual thermal stresses did not appear to cause the apparent reduction in unidirectional strain to failure.

The influence of fiber volume was evaluated. In Table 52, taken from Reference 81, the Weibull strength distribution parameters are given for $(0)_8$ and $(0)_{16}$ tensile specimens of T300/5208. The distributions are plotted in Figure 98. Note that the $(0)_8$ coupons were stronger than the $(0)_{16}$ coupons, but had larger scatter. A pooled scatter parameter value of 18.4 was determined for these samples, which were 229 mm (9 in.) long and 12.7 mm (.5 in.) wide. The simple form of the relationship between the characteristic strength, S, of two tensile specimens of different volumes was described[81] by the equation:

$$\frac{S_1}{S_2} = \left(\frac{V_2}{V_1}\right)^{1/a} \qquad (16)$$

where V_1 is the volume of specimen 1, S_1 is the characteristic strength parameter, and "a" is the scatter parameter of the Weibull distribution.

The global volume dependence of strength for a material obeying the Weibull strength distribution of Figure 98 was examined to determine whether this effect can account for the strain-to-failure differential of Table 48. For a scatter parameter value of 18.4, the previously mentioned volume equation was used to project the strength of a single 0° ply to be 1.087 times the strength of an $(0)_4$ laminate and 1.163 times that of a $(0)_{16}$ laminate of the same length and width. This projected increase in strength appears to correlate well with the observed results given in Table 48. The correlation is almost exact for the $(0/\pm45)_s$ layup (8.7 percent versus 8.2 percent).

TABLE 52
WEIBULL STRENGTH PARAMETERS FOR UNIDIRECTIONAL T300/5208 TENSILE TESTS
FROM REFERENCE 87

Laminate	$(0)_8$	$(0)_{16}$
No. Tests	25	20
S(characteristic) MPa (ksi)	1786 (259)	1662 (241)
a(scatter param.)[a]	17.7	18.5
Mean strength MPa (ksi)	1737 (252)	1620 (235)

a = Pooled scatter param. = 18.4

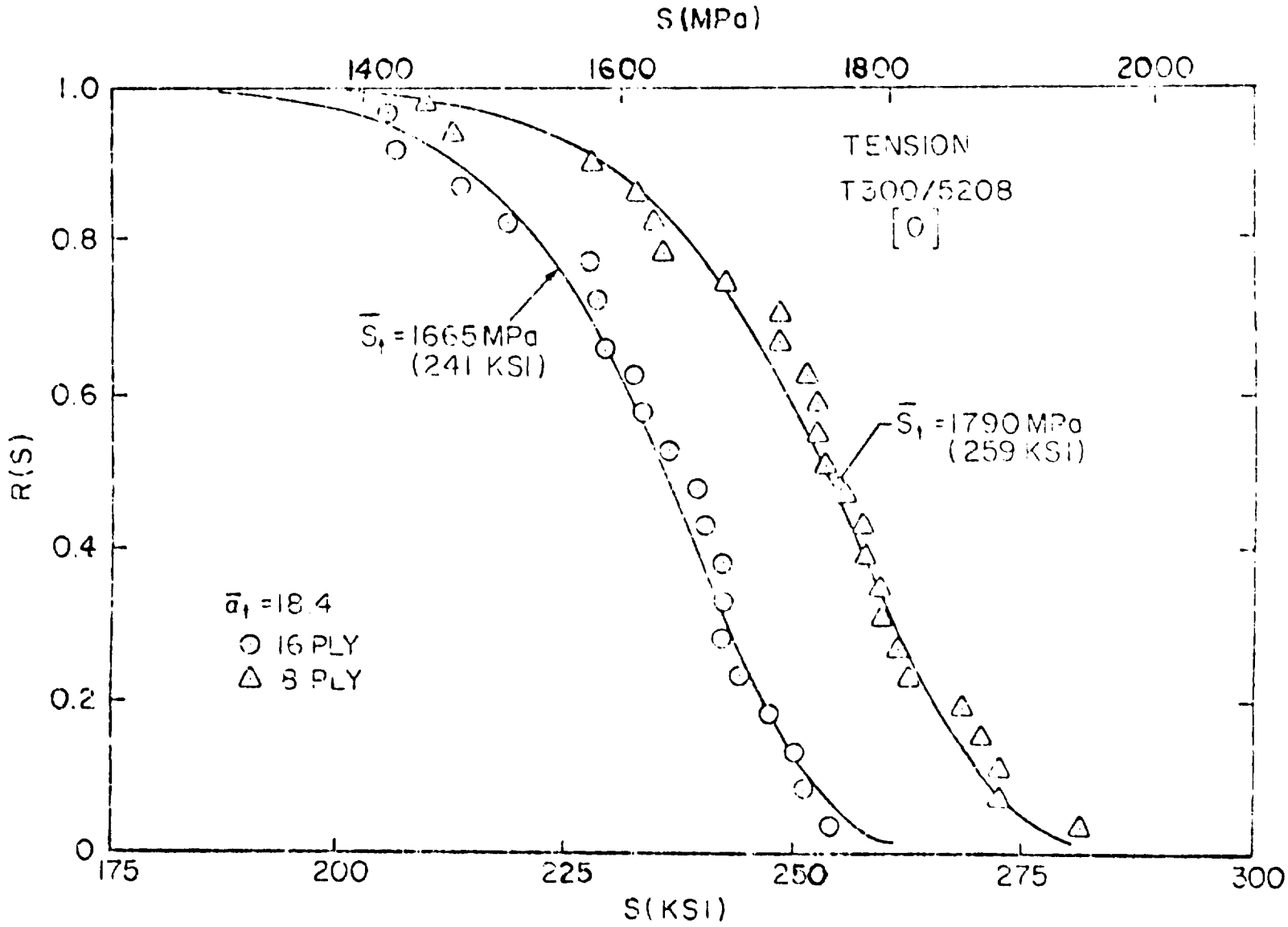

Figure 98: Weibull distribution for tension loading, T300/5208 graphite-epoxy Composites.[87]

For the two quasi-isotropic layups, the amount of increase over their respective $(0)_4$ and $(0)_{16}$ laminates is somewhat less than the expected values: 5.1 percent versus a calculated 8.7 percent for the $(0/90/\pm45)_s$ layup and 10.5 percent versus a calculated 16.3 percent for the $(0/45/90/-45)_s$ layup. These differences are believed to be due to the previously mentioned local stress concentrations resulting from ply isolation.

The calculation of projected strain to failure, recall, assumes that the strain to failure of the 0° plies in the multi-directional ply laminates is unaffected by any local strain concentration associated with delamination and transverse matrix cracking. If such local strain concentration exists, the strain to failure of the multi-directional ply laminate will be less than that anticipated based on the unidirectional strain to failure. For the $(0/45)_s$ laminate, little strain concentration occurs within the coupon along the edge and thus the projected strain to failure value of 0.0106 correlates closely to the actual value of 0.0106. For the $(0/45/90/-45)_s$ laminate, small local strain concentrations can occur and thus the experimentally obtained value of 0.0103 is somewhat lower than the projected value of 0.0106. Much larger strain concentrations occur along the edges of $(0/45/90/-45)_{2s}$ coupons which appears to explain the experimentally determined strain to failure of 0.0105 compared to a projected value of 0.0110. The close agreement between projected and actual strains to failure for these layups, allowing for local strain concentrations, appears to support a conclusion that the strain to failure of 0° unidirectional composites is lower than those containing off axis plies due to a statistical fiber volume effect. A systematic study of laminate strength as a function of 0° ply volume is clearly required to verify this concept.

This discussion on volume dependence of the 0° ply strength is not only pertinent to comparing the strain-to-failure of 0° unidirectional and multidirectional laminates. Recall the 0° ply failure criterion 3 of Section 3.4.6 was stated to be that fatigue failure must eventuate f global

or local strain is avobe 0.0070 - 0.0080. This strain level minimum was based on $(0)_4$ fatigue data. In the multidirectional laminates, the single 0^o ply characteristic strength is increased about 8.5 percent compared to the $(0)_4$ layup because of the volume strength relationship of Equation 16. This relatively small increase in characteristic strain-to-failure is one reason for choosing 0.0080 strain as a limiting value. The other reason is that the scatter in fiber breakage increases as the characteristic strength increases. Thus, the effect of volume on the strain level appropriate for criterion 3 was not considered to be significant.

3.5.2 Effect of Fiber Volume and the Influence of Local Stress Concentration

In Section 3.4.1 a deterministic failure criterion[80] for the 0^o plies which considered the stress gradient at the tip of a transverse crack was shown to be inadequate. This conclusion was reached because although a small stress concentration exists at the tip of a transverse matrix crack, two factors reduce the effect of even the small increase in stress. First, at any place where delamination exists at the crack tip, the local stress concentration is greatly reduced. Second, the stress concentration only influences a small volume of the 0^o ply adjacent to the crack tip. The average strength of 0^o fibers in such a small volume is increased for the same statistical reasons discussed in Section 3.5.1.

The increase in characteristic strength can be calculated by using Equation 16. However, a more accurate procedure is probably preferable. The cumulative distribution function for the strength of a unidirectional coupon containing n fibers in cross section and having a gage length of m times the critical length is given by[75 - 77]:

$$H_{m,n}(X) = 1-[1-l_c(x)]^{mn} \qquad (17)$$

where $l_c(x)$ is the characteristic distribution function which depends on the fiber strength distribution function and the local load redistribution rule chosen when one or several adjacent fibers fail in a coplanar manner.

Phoenix has developed a graphical procedure for estimating the dependence of strength on sample volume[75].

As mentioned in Section 3.4.1, the characteristic strength for the small volume of 0° fibers influenced by stress concentration at the tip of a transverse crack is 20 to 30 percent higher than that for $(0)_4$ coupons. This increase is considerable higher than the increase in stress concentration especially when significantly reduced by the presence of delamination. Thus the effect of a transverse matrix crack on failure of the 0° plies, criterion 1 of Section 3.4.6, is generally quite small unless the initial global strain is large. This increase in characteristic strength does not, however, negate the influence of criterion 2 of Section 3.4.6, stress concentration due to ply isolation. The reasons are: 1) The stress concentration can be much higher for some layups; 2) the stress concentration acts over the entire thickness of the 0° ply since all of the load of the adjacent plies is applied; and 3) the volume of affected 0° plies eventually becomes quite large.

3.6 THREE-DIMENSIONAL ANALYSIS OF DELAMINATION

Three dimensional finite element modeling was conducted of several types of delamination in $(0/90/\pm45)_s$ and $(\pm45/0/90)_s$ laminates. The analysis was undertaken to further examine the stress field in the 0° ply as influenced by delamination and to study the influence of the tensile gripped end tabs on the strain energy release rate of the delamination region. The strain energy release rate during delamination growth was determined for each selected model and the alteration of stresses in the 0° load carrying ply in the presence of these delaminations was examined. A LMSC developed, general purpose, finite element code called DIAL was used for the analysis. Each lamina was modeled with a single layer of 20 node brick elements which could be linked or unlinked at lamina interfaces to simulate a delamination crack. The material properties used in the anslysis were as follows:

$$E_{11} = 163.4 \text{ GPA } (23.7 \text{ Msi})$$
$$E_{22} = E_{33} = 102 \text{ GPa } (1.48 \text{ Msi})$$
$$G_{12} = G_{13} = 6.48 \text{ GPa } (0.94 \text{ Msi})$$
$$G_{23} = 3.79 \text{ GPa } (0.55 \text{ Msi})$$
$$\nu_{12} = \nu_{13} = 0.30$$
$$\nu_{23} = 0.54$$

The coupon model was taken as being 2.54 mm (1 in.) wide with a 50.8 mm (2.0 in.) "gage length" along the z axis loading direction. The load was applied by requiring all nodes on the top boundary of the model to displace by an amount resulting in a strain of unity for the given gage length. The origin of axes was located in the lower right hand corner of the model such that z was the tensile loading direction, x was in the plane of the coupon in the width direction, and y was the through thickness direction as shown in Figure 99. The scalloped free edge delamination was modeled by striking an arc from a position external to the coupon on the z=0 axis. This position served as a reference point for the definition of crack opening mode contribution in the strain energy release rate calculations. In the free-edge delamination models, an attempt was made to ascertain the influence of the proximity of the delamination to the grips by applying z displacements to all nodes located at z = 12.7 mm (0.5 in.), see the line AA' in Figure 99, while maintaining the nominal strain on the 25.4 mm (1 in.) gage length at unity. This analysis is referred to as the short gage length results in the tables which follow.

The analysis of strain energy release rate was accomplished by determining the work done to close up the delamination crack by the amount crosshatched in the figures which will be described, see Figure 99 for an example. The work done at each node located on the delamination crack front is tabulated individually in several accompanying tables. The strain energy release rate of a segment of the crack front area is also presented in the tables. This segment was defined by the midpoints of the lines connecting a given node on the crack front to the two closest neighboring nodes on the front. The

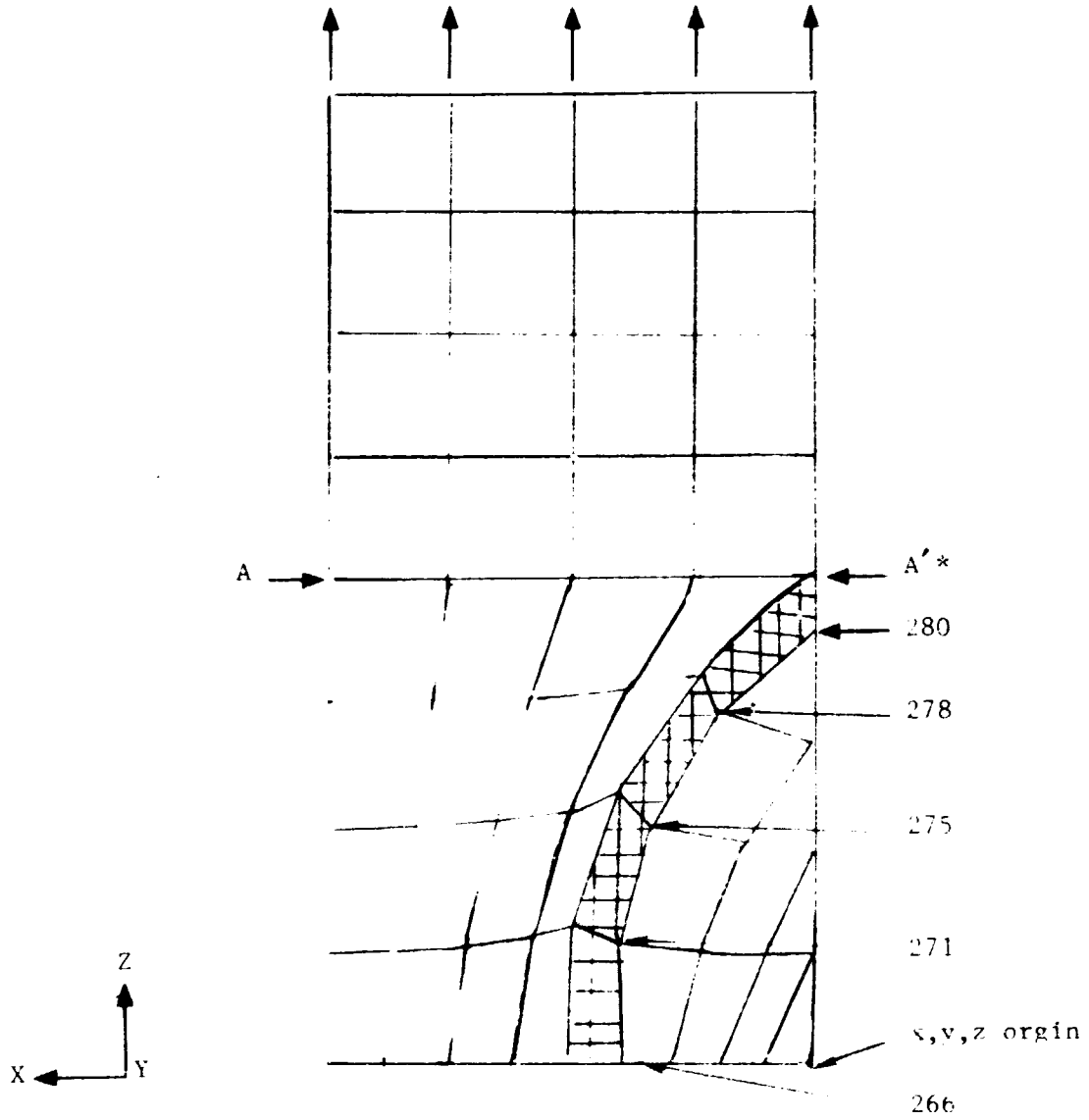

* AA^1 is section for application of short grip B.C.

Figure 99: Plan of $(45/-45/0/90)_s$ Midplane Delamination Model.

choice of crack front shape was made arbitrarily. As a result, the calculated G's at a given location on the crack front are not uniform. They give primarily a qualitative view of the relative contributions of the three crack opening modes under the assumed crack geometry. For each of the three-dimensional models which were examined, the effect of the delamination on the distribution of σ_z stress (longitudinal stress) in the 0° ply of the laminate is presented. The σ_z stresses were calculated at the centroid of the 0° layer elements and are plotted in the succeeding figures.

One should utilize the quantitative information in these studies with a strong measure of caution. The elements employed in the modeling were extremely thin compared to their inplane dimensions. This poor aspect ratio certainly made the accuracy of the out of plane deformation response questionable. However, the degree of element refinement necessary in the inplane direction to be compatible with the ply thickness dimension would make such an analysis prohibitively time-consuming. The analysis conducted without such a complication required approximately four (4) hours of computer processing time for each model. The time and effort needed to develop these models, link or unlink nodes along the delamination front, and check for errors in the boundary conditions and link conditions was not trivial. The authors considered opinion is that such detailed modeling and analysis cannot be conducted routinely during the design of composite components. This type of study must of necessity be reserved for special cases (e.g. failure analyses) for which a semi-quantitative insight must be obtained in order to account for the failure process and to recommend solutions to the problem.

3.6.1 Midplane Free-Edge Delamination of $(45/-45/0/90)_s$ Laminates

Figure 99 shows the plan view of the model and specifies the node pair numbers at which the crack closure analysis was conducted. Figure 100 shows an oblique view of the 90° layer elements in the unloaded and loaded configuration. The Mode I dominance of the delamination crack opening is

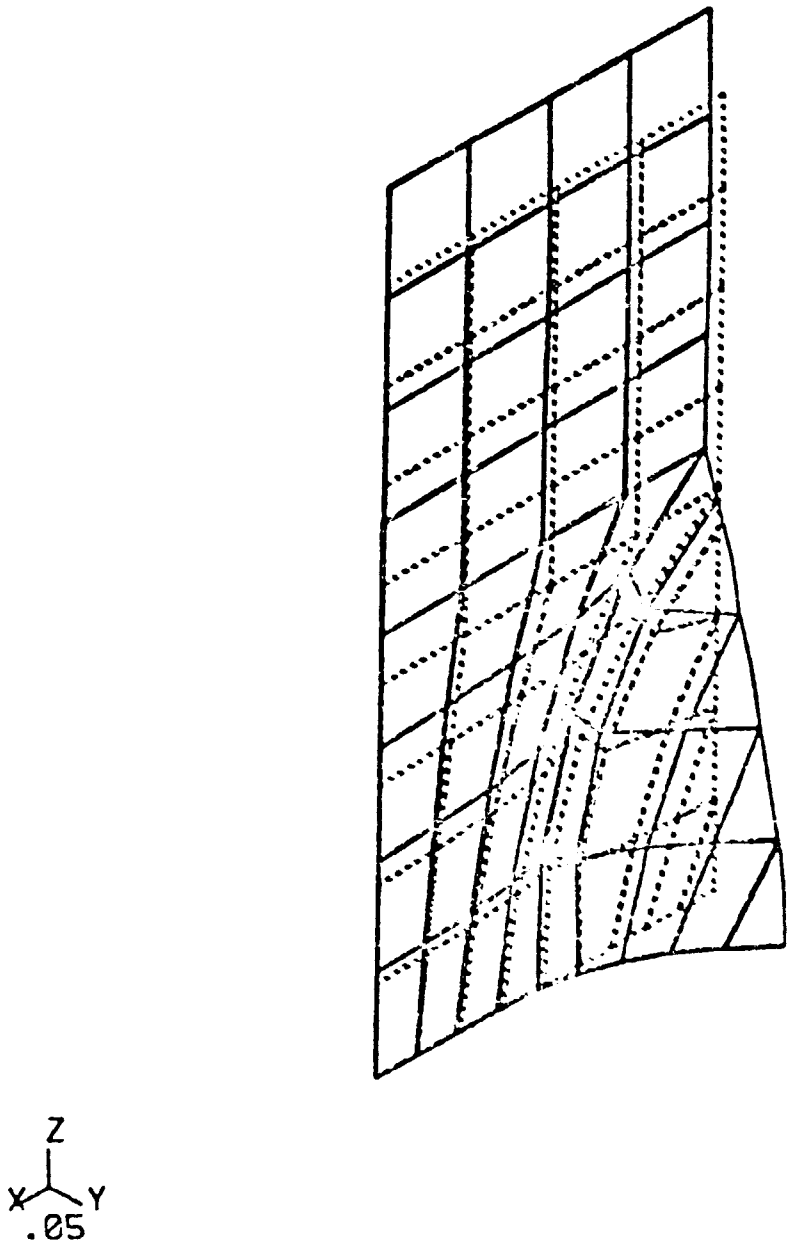

Figure 100: Oblique view of 90^{o} layer elements in unloaded and loaded configuration for $(45/-45/0/90)_{s}$ midplane delamination model.

evident in the figure. Table 53 contains the nodal work done to close the delamination crack front over the cross hatched area of Figure 99 and Table 54 lists the local strain energy release rate in each of the crack segments. There are few surprises in the analysis. The strain energy release rate is Mode I dominated and peaks at nodes 266 and 280 located at the midpoint and end of the delamination crack. When the grip is in closer proximity to the delamination, the strain energy release rate is on the order of 50 percent less; accounting for the experimentally observed scallop shape as the delamination enters the specimen grip region.

In Figure 101, the distribution of longitudinal stresses in the 0° ply is plotted for several positions along the gage length. The longitudinal stress is seen to peak at 10 percent above the nominal value at the z = 0 cross-section and at the tip of the delamination. Notice that the increase in 0° ply stress is quite gradual, without displaying a sharp peak in stress in the vicinity of the delamination crack tip.

3.6.2 90/45 Interface Free-Edge Delamination in a $(0/90/45/-45)_s$ Laminate

Figure 102 shows that the plan view of this model is identical to the previous midplane delamination case. The nodes at which the work and G analysis are calculated are given in the figure. In Figure 103, the deformed shapes of the 90° and 45° layers are plotted. Local interpenetration of the layers is evident in the figure. The distortions indicated that the opening modes are combinations of all three modes. Tables 55 and 56 present the nodal crack closure work and segmental G's. The majority of these terms are negative. By the sign convention employed in this study this is indicative of interpenetration of the delamination surface under tensile loads. Under uniaxial compression the crack would open and the sign of the work terms would be positive.

The crack opening G's are dominated by Mode II shear terms and secondarily by Mode III crack opening instead of Mode I as in the previous model. Interestingly the influence of grip proximity is not large in this model

TABLE 53
CRACK CLOSURE WORK (J)
FOR
MIDPLANE DELAMINATION OF $(45/-45/0/90)_s$ LAMINATE

NODE	COMPONENT x	y	z
Long Gage Length			
280	0.0	26.4	0.0
278	0.0	8.25	0.00145
275	0.00043	5.07	0.0354
271	0.00037	4.54	0.00016
266	0.0	6.78	0.0
Short Gage Length			
280	0.0	14.2	0.0
278	0.0033	18.6	0.0
275	0.00064	4.75	0.0051
271	0.00044	1.82	0.00011
266	0.0	2.85	0.0

TABLE 54
STRAIN ENERGY RELEASE RATE (J/mm^2)
FOR
MIDPLANE DELAMINATION OF $(45/-45/0/90)_s$ LAMINATE

SEGMENT CENTERED ON NODE	G I	G II	G III
Long Gage Length			
280	14.8	0.0	0.0
278	2.19	0.0	0.000038
275	1.25	0.000106	0.0087
271	1.08	0.000088	0.000038
266	3.16	0.0	0.0
Short Gage Length			
280	7.98	0.0	0.0
278	4.34	0.0	0.0
275	1.17	0.00016	0.00121
271	4.31	0.00010	0.000011
266	1.33	0.0	0.0

4 OF 6

N84-29978 UNCLAS

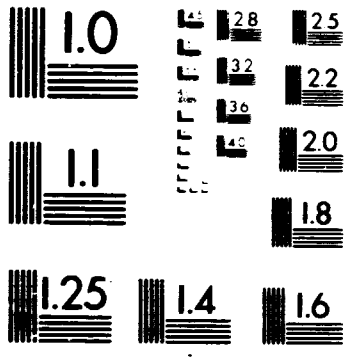

MICROCOPY RESOLUTION TEST CHART
NATIONAL BUREAU OF STANDARDS
STANDARD REFERENCE MATERIAL 1010a
(ANSI and ISO TEST CHART No 2)

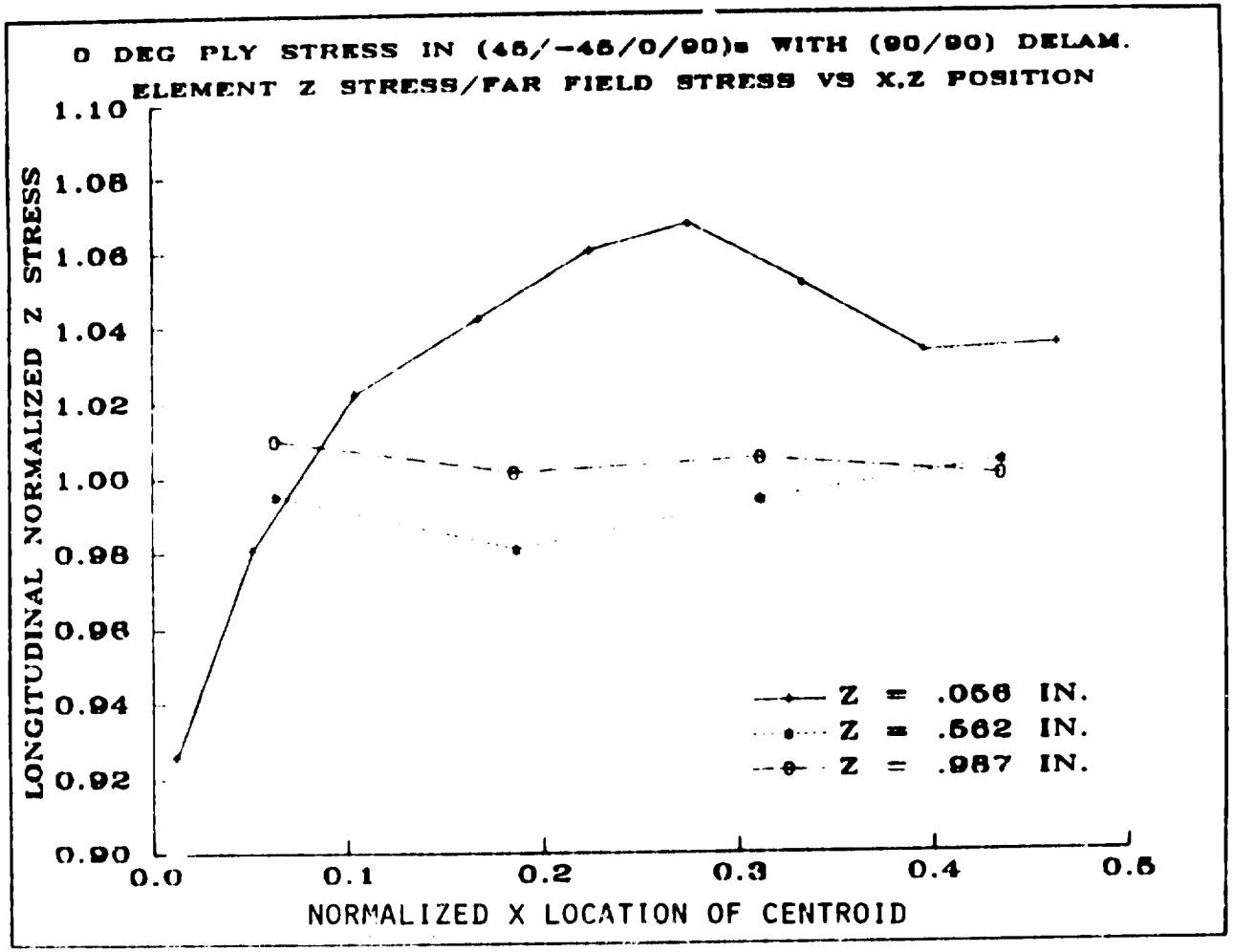

Figure 101 Distribution of longitudinal stresses in the 0^{o} ply for the $(45/-45/0/90/0)_{s}$ midplane delamination model.

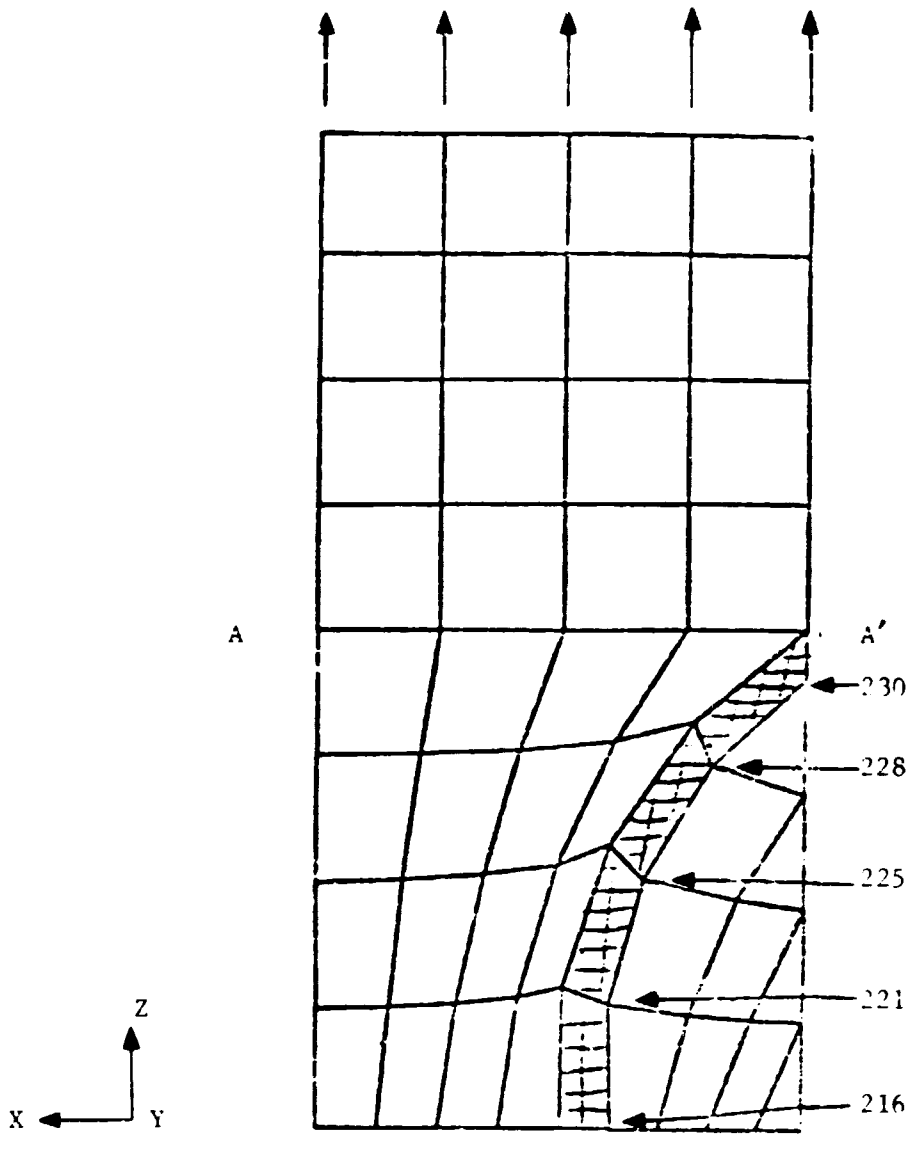

Figure 102: Plan view of $(0/90/45/-45)_s$ 90/45 delamination model.

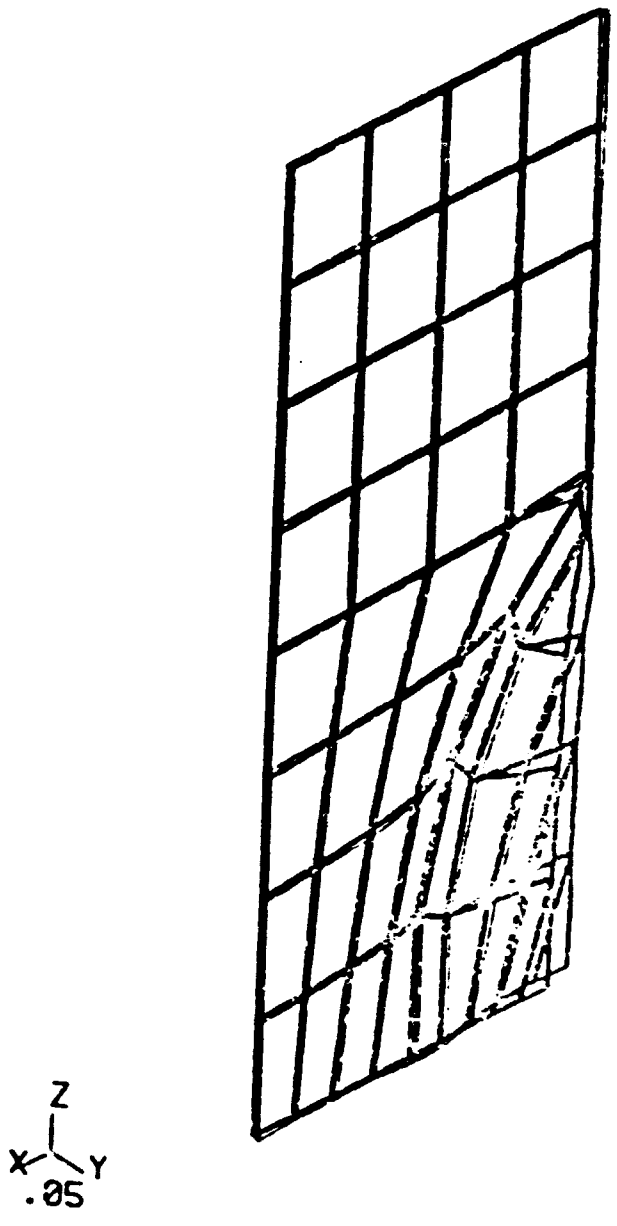

Figure 103: Oblique view of the deformed shape of the 90° and 45° layer elements in the $(0/90/45/-45)_s$ delamination model.

TABLE 55
CRACK CLOSURE WORK (J)
FOR
MIDPLANE DELAMINATION OF $(0/90/45/-45)_s$ LAMINATE

NODE	COMPONENT x	y	z
Long Gage Length			
230	-0.328	-0.0269	-0.337
228	-0.390	-0.00273	-0.025
225	-0.346	-0.00311	-0.013
221	-0.394	-0.00587	-0.00232
216	-0.248	-0.00418	-0.0
Short Gage Length			
230	-0.504	-0.0125	0.00943
228	-0.217	-0.000068	-0.0167
225	-0.286	0.00316	0.00282
221	-0.376	-0.001537	0.00124
216	-0.249	-0.000593	0.0

TABLE 56
STRAIN ENERGY RELEASE RATE (J/mm^2)
FOR
MIDPLANE DELAMINATION OF $(0/90/45/-45)_s$ LAMINATE

SEGMENT CENTERED ON NODE	G I	G II	G III
Long Gage Length			
230	-0.00151	-0.184	-0.0189
228	-0.000718	-0.103	-0.00664
225	-0.00146	-0.0851	0.00322
221	-0.00139	-0.0933	0.000550
216	-0.00198	-0.116	0.0
Short Gage Length			
230	-0.000692	-0.282	0.00557
228	-0.000018	-0.0574	-0.00443
225	0.000771	-0.0704	-0.00723
221	-0.000127	-0.0891	0.000294
216	-0.000275	-0.116	0.0

compared to the previous midplane delamination model of Section 3.5.1. The highest G's are found at node 230 on the free-edge of the coupon. In Figure 104 the distribution of longitudinal stress in the 0° ply is plotted. The tensile stress is greatest on the z = 0 axis above the delamination and peaks at a value 13 percent above the nominal stress in this ply. Again the increase in stress is gradual.

3.6.3 45/-45 Interface Free-Edge Delamination in $(0/90/45/-45)_s$

Figure 105 shows the model, the nodes used in the G analysis, and the location and shape of the delamination. The crack front is parallel to the z (longitudinal) axis of the coupon. The location of nodes for the short gage length case is along the line AA' of element boundaries skewed to the delamination edge as shown in the figure, making this analysis rather artificial. The results for the short gage length case indicate a very large influence of the grip on the ability of this type of delamination crack to grow. Large gage length results indicate Mode I crack opening. The short gage length data indicate interpenetration of the two crack fronts under the tensile loading conditions. Tables 57 and 58 contain the nodal work and G analysis results. Both Mode I and II are significant in the growth of this delamination. The level of energy release rate for this delamination is greater than that obtained for the 90/45 interface of this laminate, but both are significantly less than the level determined for the midplane delamination of the $(45/-45/0/90)_s$ laminate.

Figure 106 shows that the influence of this delamination on the 0° layer was greater than that for the other cases studied. A peak 22 percent increase over the nominal longitudinal stress level was found to occur near the free-edge of the coupon on the z = 0 axis. Notice, again, the lack of any peak singularity stress.

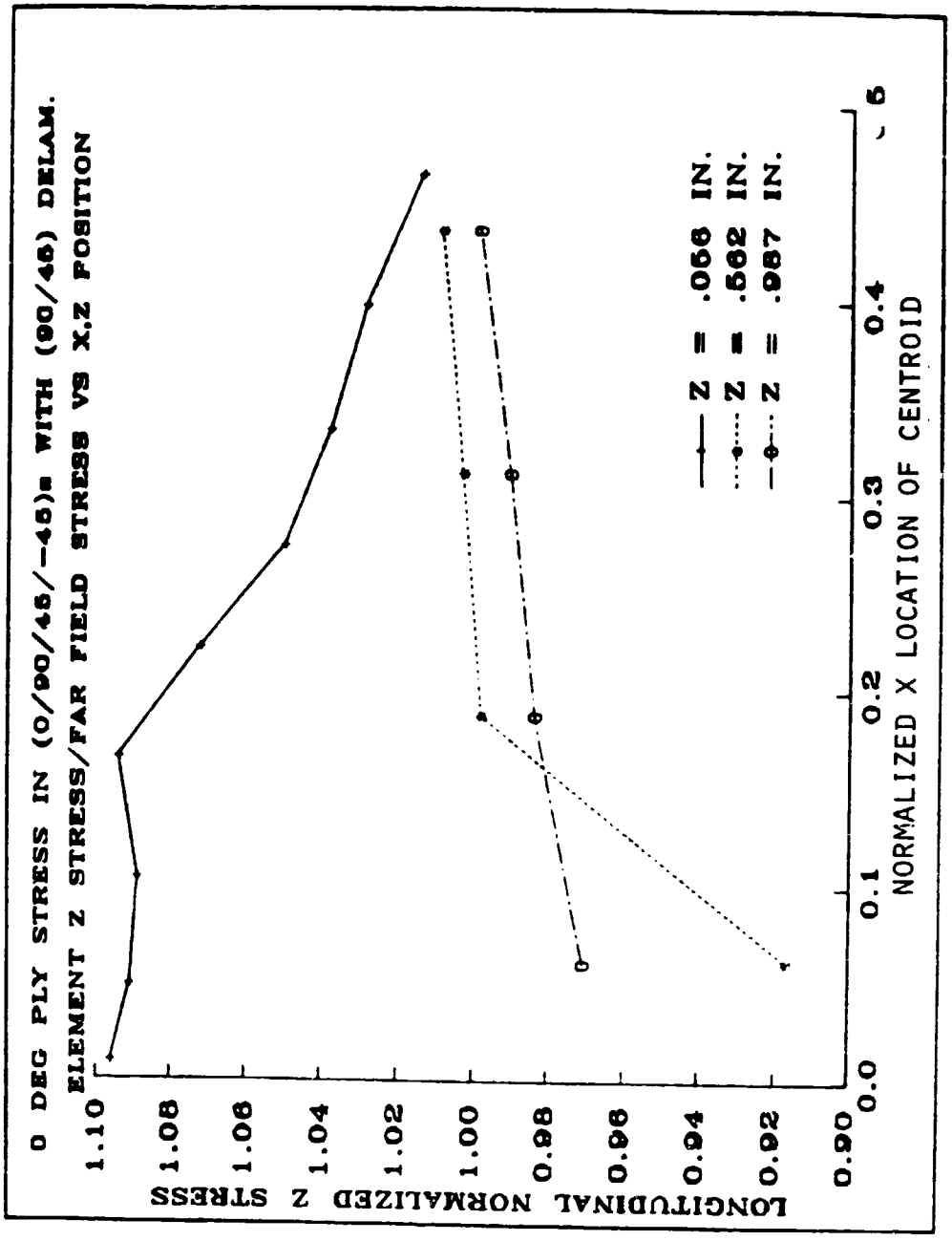

Figure 104: Distribution of longitudinal stress in the 0^{o} ply for the $(0/90/45/-45)_{s}$ 90/45 interface delamination model.

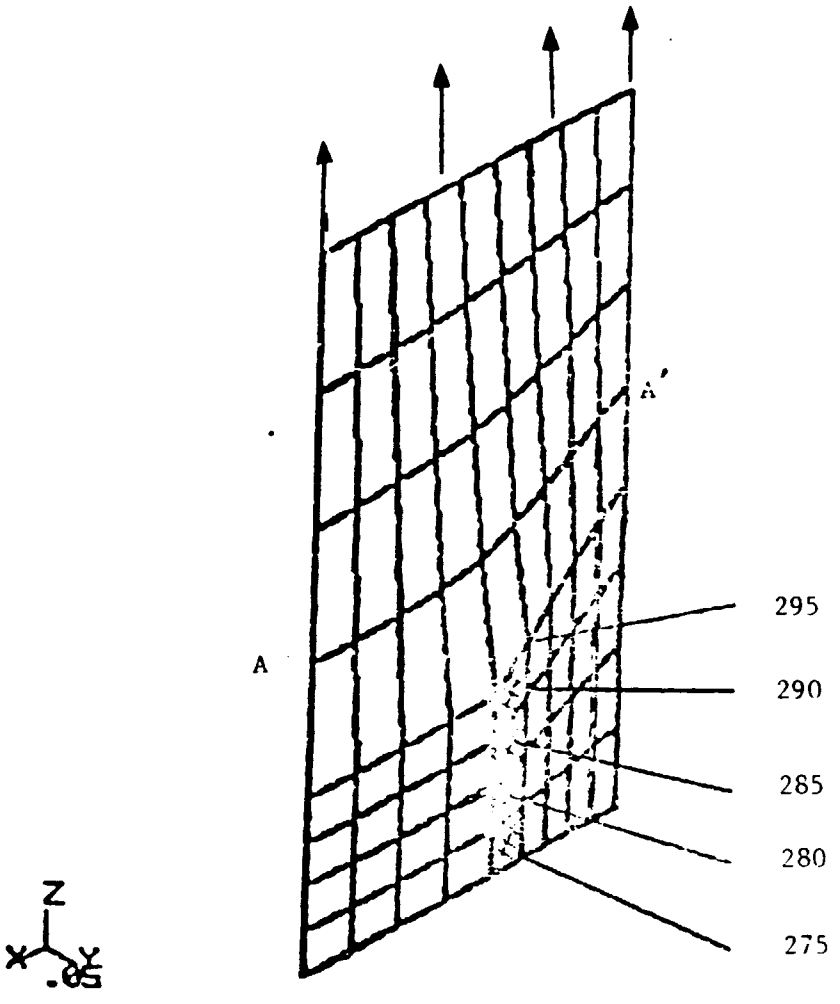

Figure 105: Plan view of $(0/90/45/-45)_s$ 45/-45 delamination model.

TABLE 57
CRACK CLOSURE WORK (J)
FOR
MIDPLANE DELAMINATION OF $(0/90/45/-45)_s$ LAMINATE

NODE	COMPONENT x	y	z
Long Gage Length			
295	0.0221	0.00938	0.103
290	-3.03	0.608	0.828
285	1.57	1.54	-1.51
280	1.53	3.19	-1.07
275	0.340	1.25	0.0
Short Gage Length			
295	-0.055	-0.0185	-0.0852
290	-2.43	-0.784	-2.01
285	-3.03	-2.77	-3.12
280	-1.77	-3.90	-2.52
275	-0.32	-1.56	0.0

TABLE 58
STRAIN ENERGY RELEASE RATE (J/mm^2)
FOR
MIDPLANE DELAMINATION OF $(0/90/45/-45)_s$ LAMINATE

SEGMENT CENTERED ON NODE	G_I	G_{II}	G_{III}
Long Gage Length			
295	0.00420	0.00998	0.00455
290	0.0137	0.683	0.187
285	0.346	0.354	-0.341
280	0.734	0.354	-0.242
275	0.581	0.153	0.0
Short Gage Length			
295	-0.00841	-0.0247	-0.0382
290	-0.178	-0.547	-0.453
285	-0.624	-0.683	-0.703
280	-0.878	-0.400	-0.568
275	-0.705	-0.144	0.0

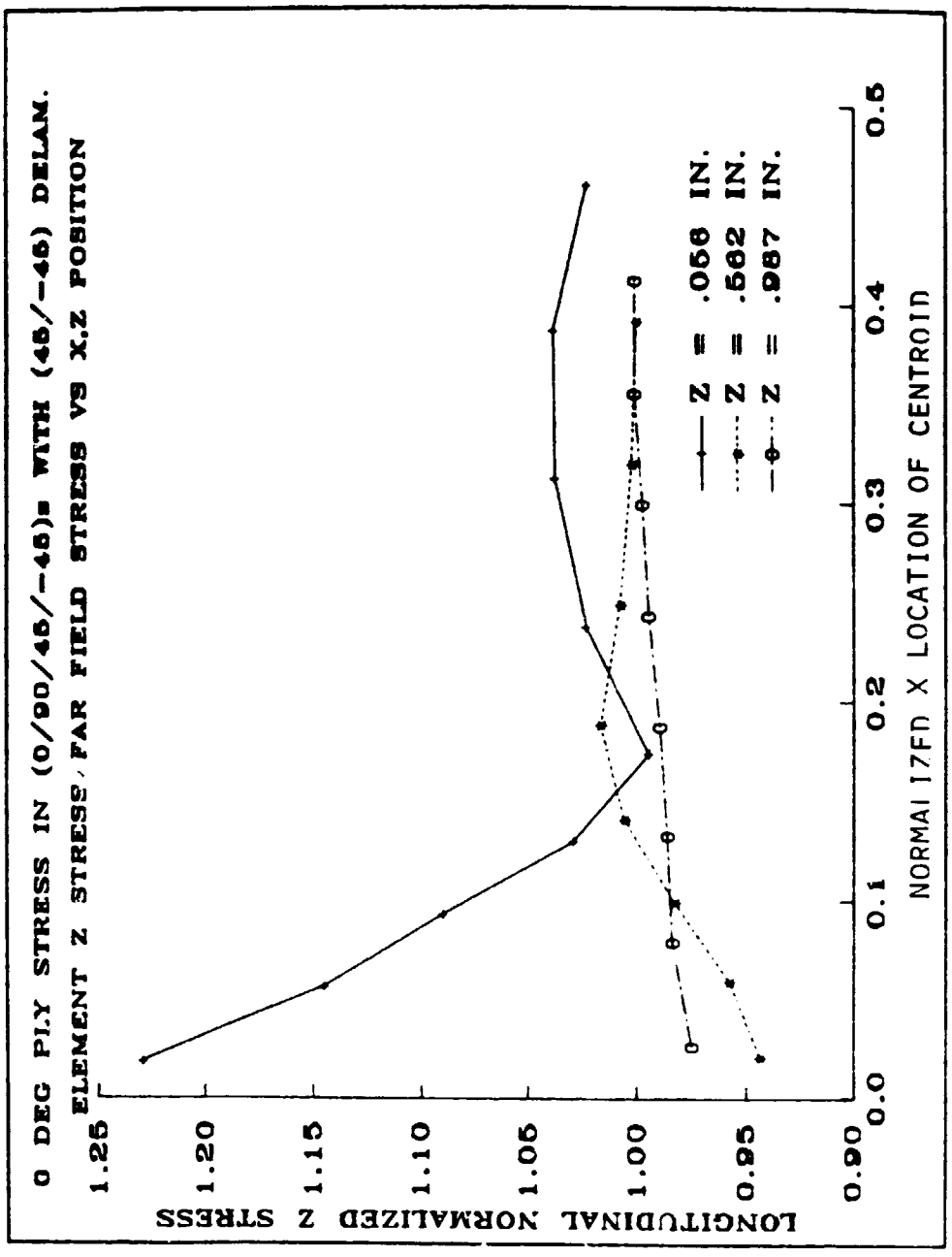

Figure 106: Distribution of longitudinal stress with 0^{o} ply for the $(0/90/45/-45)_{s}$ 45/-45 interface delamination model.

3.6.4 Interaction of 45/-45 Delamination with Transverse Cracks

The last model to be investigated is shown in Figure 107. Two transverse cracks in the 45 and -45° layers intersect at the midpoint of the coupon model on the z = 0 axis. The gage length for this model was only 37.1 mm (1.5 in.) and the coupon width was 25.4 mm (1 in.). The nominal strain applied to this model was 1.33 for all of the data presented in this section.

A delamination was introduced between the 45 and -45 layer with the dimensions shown in the figure. The distortions due to loading on the -45 layer are displayed in Figure 108. The displaced shapes of the 45 and -45 layers in plan view are shown in Figures 109 and 110. Note that the presence of delamination between the 45 layers allows the transverse crack in the -45 layer to open up because that layer is effectively decoupled from the 45 layer in the region of delamination. The node numbers used to calculate delamination growth G's are given in Figure 111. The nodal work and sectional G values are listed in Tables 59 and 60.

Mode I G values are very small for this delamination configuration. Both Mode III and II terms are important during growth of this delamination. The values in Table 60 indicate that the greatest energy release rate occurs in Mode II on the delamination surface perpendicular to the loading direction and is particularly high at the intersection of the delamination crack front with the transverse crack in the -45° layer.

Figure 112 illustrates the positions of several cuts taken across the model to display the spatial variation of longitudinal (z) stress in the 0° layer. The stresses are referenced to the x coordinate of the centroid of the element in which they were calculated. In Figure 113, the 0° longitudinal stress is plotted for the $(0/90/45/-45)_s$ model in the presence of both transverse cracks and delamination. The stress concentration is greatest

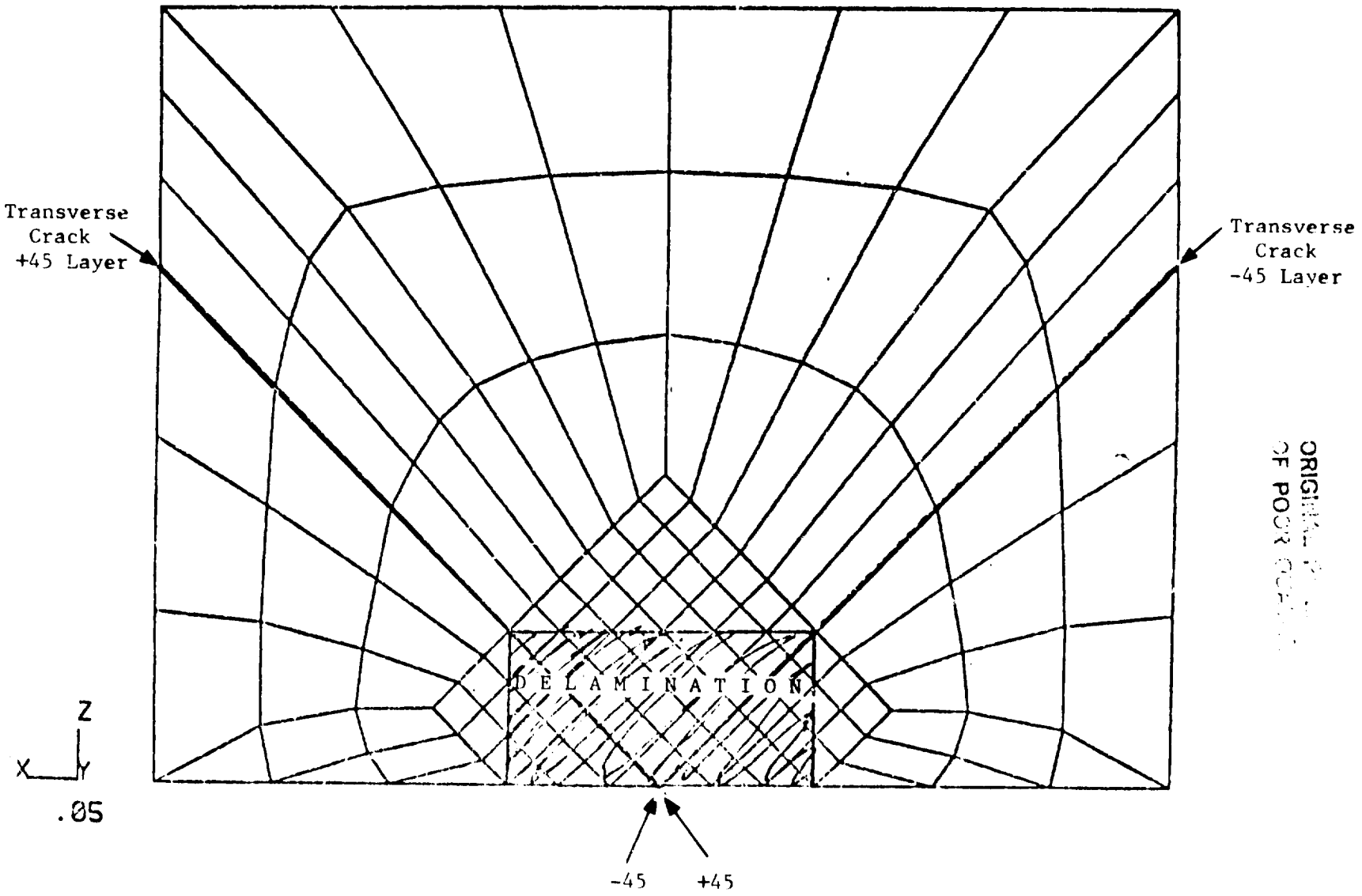

Figure 107: Model of delamination and transverse cracking in 45 and -45 layer of a $(0/90/45/-45)_s$ laminate

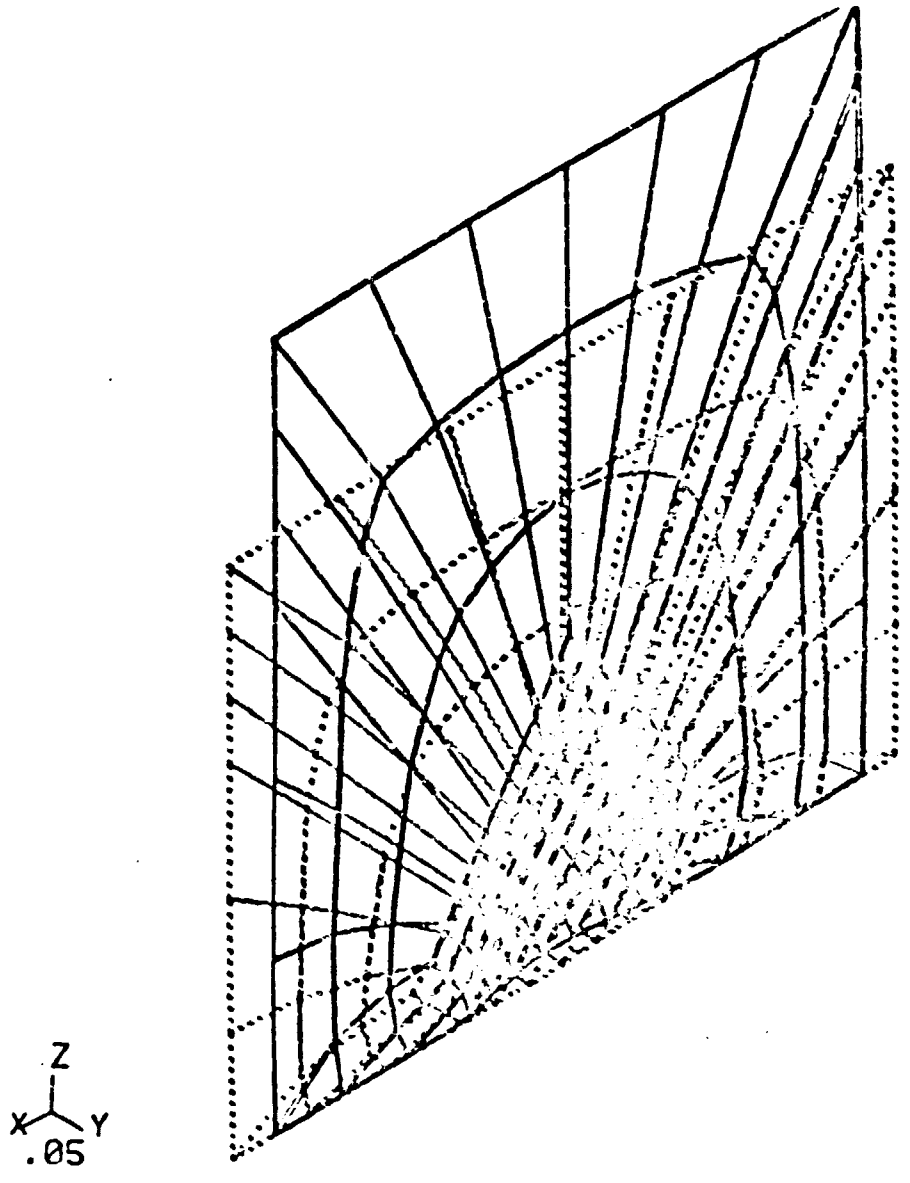

Figure 108: Distortions due to loading on the -45° layer for the model of Figure 107.

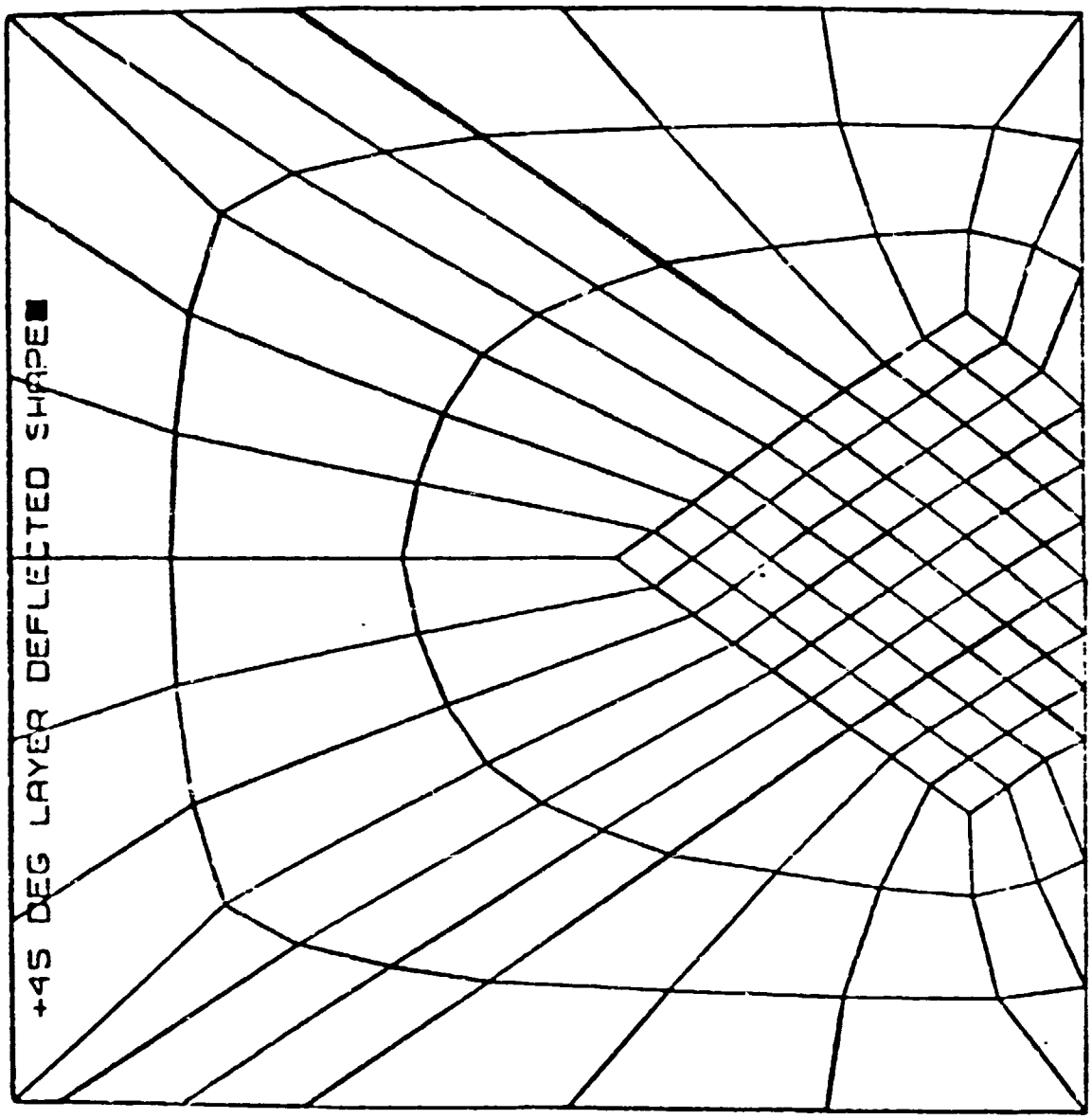

Figure 109. Plan view of displaced shape of $\pm 45^0$ layer for model of Figure 107.

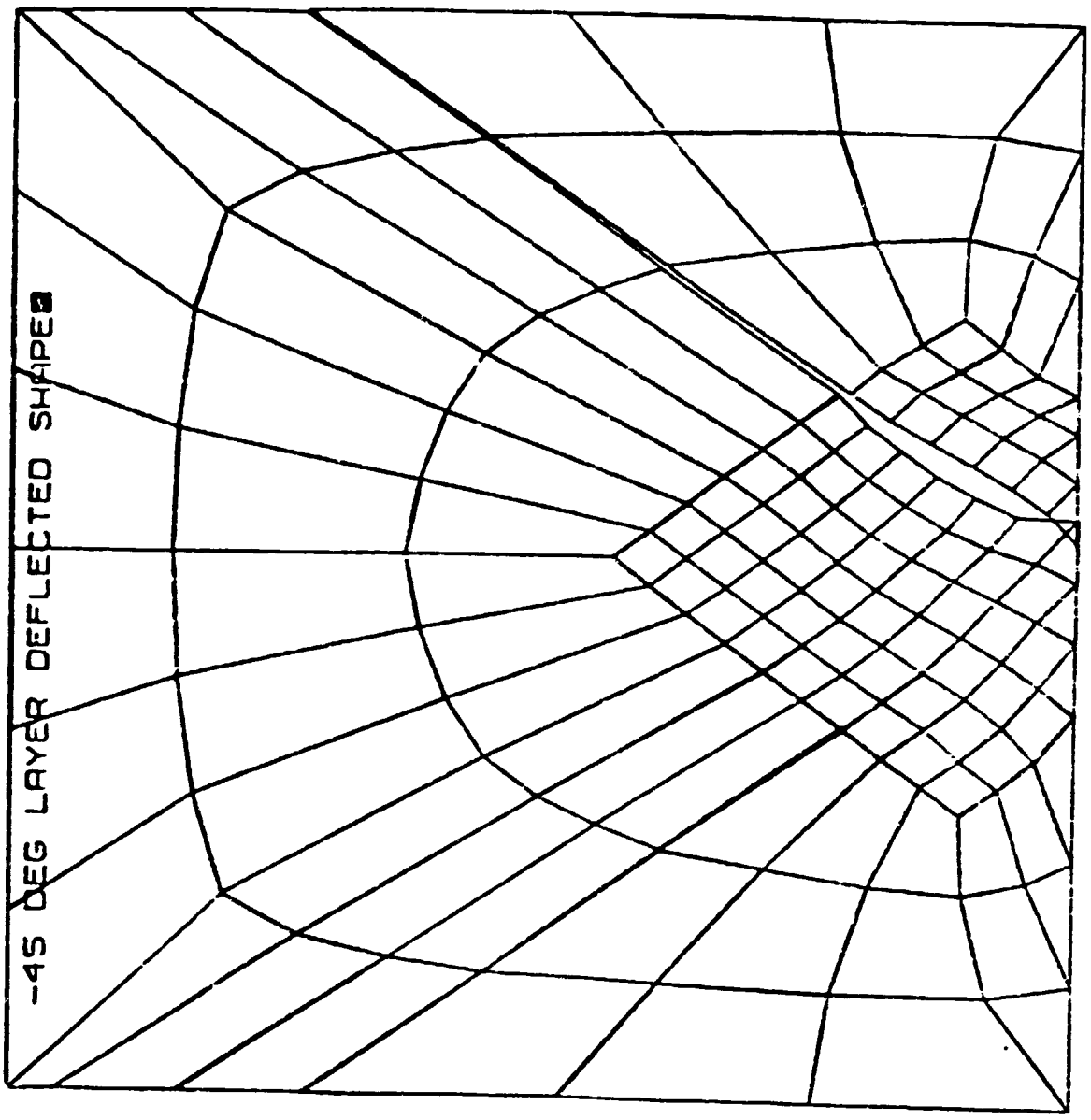

Figure 110: Plan view of displaced shape of -45° layer for model of Figure

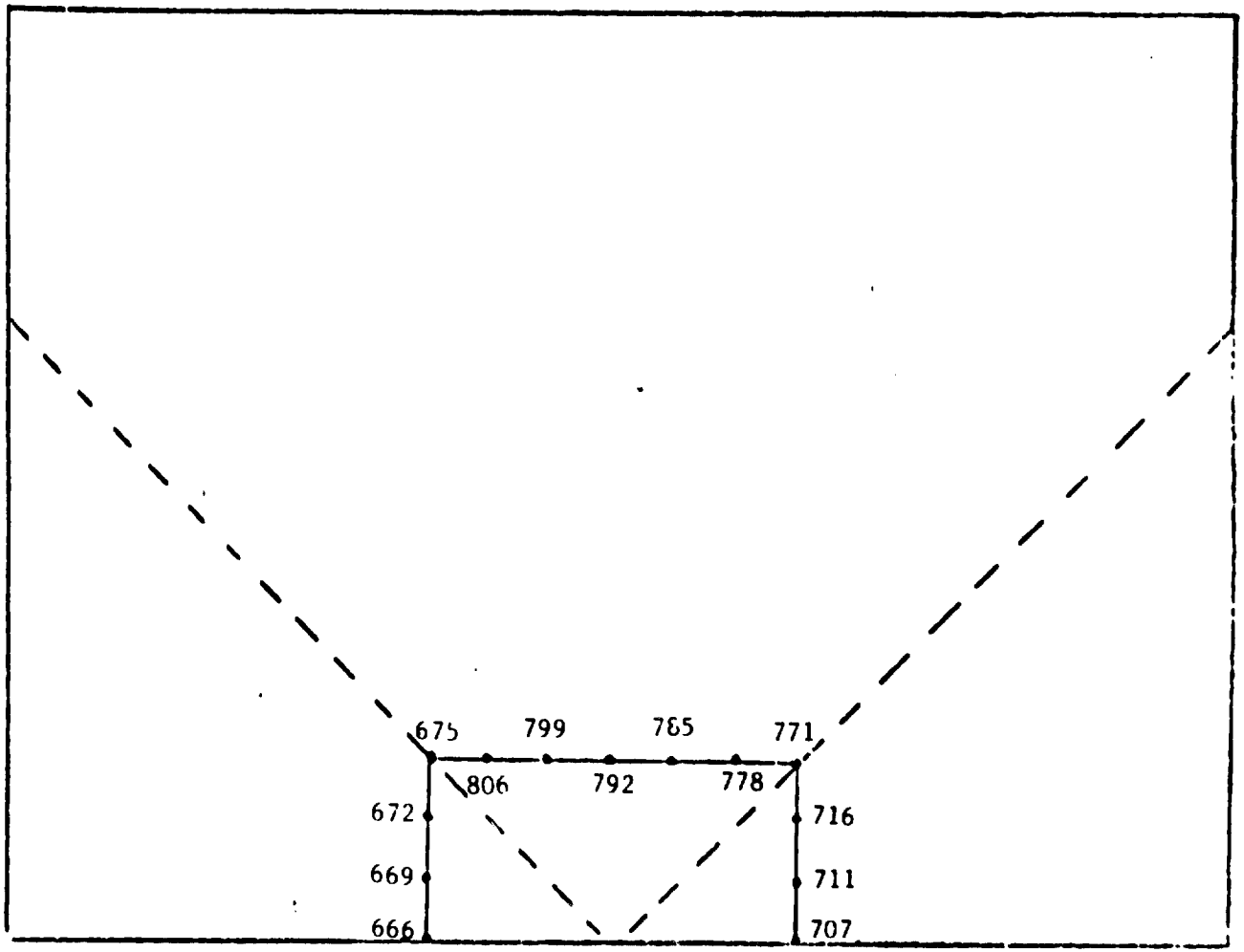

Figure 111: Element node numbers used to calculate delamination growth G values for model of Figure 107.

TABLE 59
CRACK CLOSURE WORK (J)
FOR
MIDPLANE DELAMINATION OF $(0/90/45/-45)_s$ LAMINATE

NODE	COMPONENT x	y	z
Internal Delamination			
666	4.03	0.00203	0.0
669	0.629	0.00395	0.160
672	0.188	0.00203	0.233
675	0.0104	0.00328	0.263
806	0.00564	0.00192	0.139
799	0.0843	0.00271	0.212
792	0.0374	-0.0174	0.459
785	0.0724	-0.0353	1.71
778	0.0269	-0.0258	2.24
771	0.0532	-0.00734	3.04
716	0.209	-0.00757	1.12
711	0.410	-0.0855	0.793
707	1.43	-0.0952	0.0

TABLE 60
STRAIN ENERGY RELEASE RATE (J/mm^2)
FOR
MIDPLANE DELAMINATION OF $(0/90/45/-45)_s$ LAMINATE

SEGMENT CENTERED ON NODE	G I	G II	G III
Internal Delamination			
666	0.00126	2.50	0.0
669	0.00490	0.780	0.198
672	0.00252	0.233	0.289
675	0.00806	0.026	0.653
806	0.00238	0.173	0.00701
799	0.00333	0.262	0.104
792	0.0215	0.569	0.0464
785	0.0438	2.12	0.0898
778	0.0319	2.78	0.0333
771	0.0182	0.132	7.54
716	0.00939	0.259	1.39
711	0.106	0.509	0.983
707	0.236	3.66	0.0

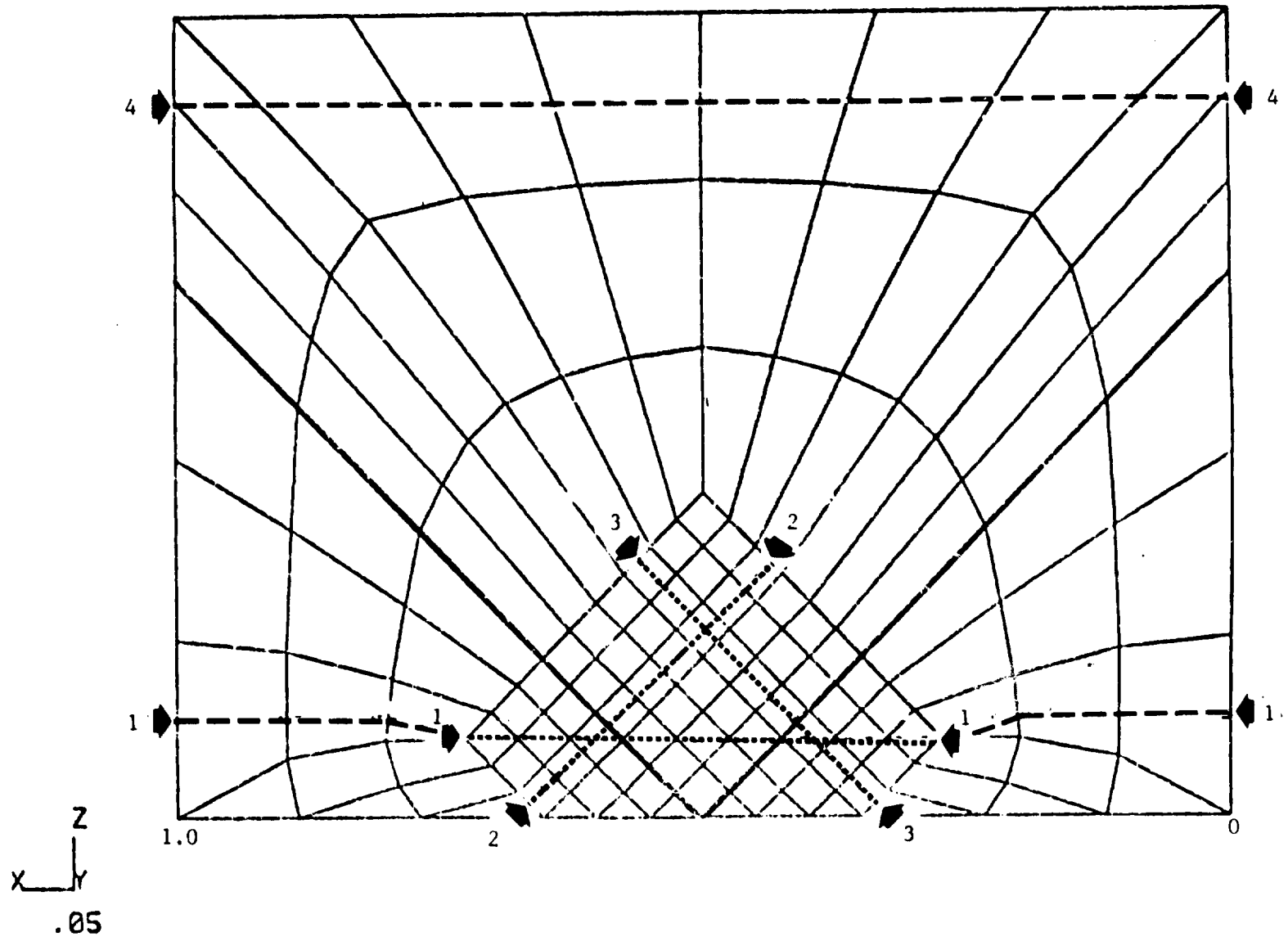

Figure 112: Positions of cuts taken across model of Figure 107 to obtain profiles of 0^{o} ply stresses.

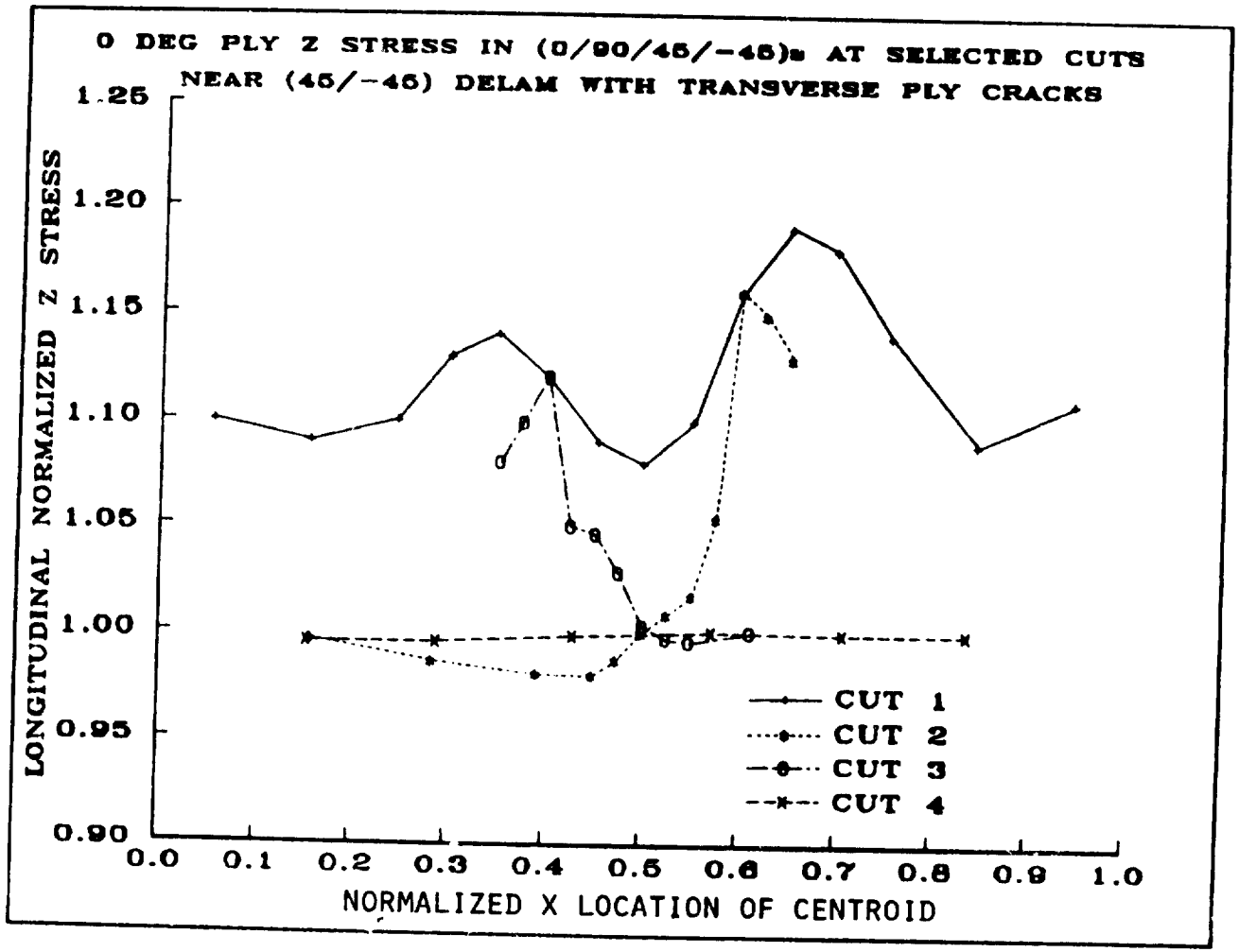

Figure 113: Distribution of longitudinal stresses in the 0° ply for the model of Figure 107 with a delamination.

immediately above the delamination crack front and is as high as 21 percent greater than the nominal value far from the delamination. along cut 1 the longitudinal stress is high in the 0° layer over the entire width of the laminate.

Figure 114 shows the same series of stress cuts in a model containing the transverse cracks in the 45 and -45 layers, but without a delamination between the two plies. In this case the stress concentration in the 0° layer is only about 4 percent at peak value. Thus the presence of a delamination is crucial in causing large stress concentrations in the 0° layer.

3.6.5 Summary of Three Dimensional Delamination Analysis

A tabular comparison of some of the results of the three dimensional delamination analysis study is given in Table 61. The summary shows that rather large localized increases can occur in the 0° ply stresses due to the presence of delamination. However, for all of the models, no large stress concentration was calculated in the 0° ply due to the stress singularity which exists at the delamination crack tip. The small effect of transverse cracks alone on the stress in the 0° ply is again noted here. The amount of 0° ply stress concentration due to delamination alone or matrix cracking alone is thus less than that for ply isolation by combined delamination and transverse cracking. For example, comparison of Tables 61 and 47 shows that 0° ply stresses increased 13 percent due to a 90/45 interface delamination according to the three dimensional analysis of Section 3.5.2 and 22 percent for isolation of the 90° ply according to the analysis of Section 3.4.5. Similarly the 45/-45 delamination resulted in a 22 percent 0° ply stress increase, see Section 3.4.5, while total isolation of the 45° ply produced a 27 percent increase. Therefore, while the complex three dimensional analysis confirmed the expected increase in 0° ply stresses due to delamination alone, the much simpler free body type modeling of Section 3.4.5 provides close agreement to the 3-D analysis. In face since most

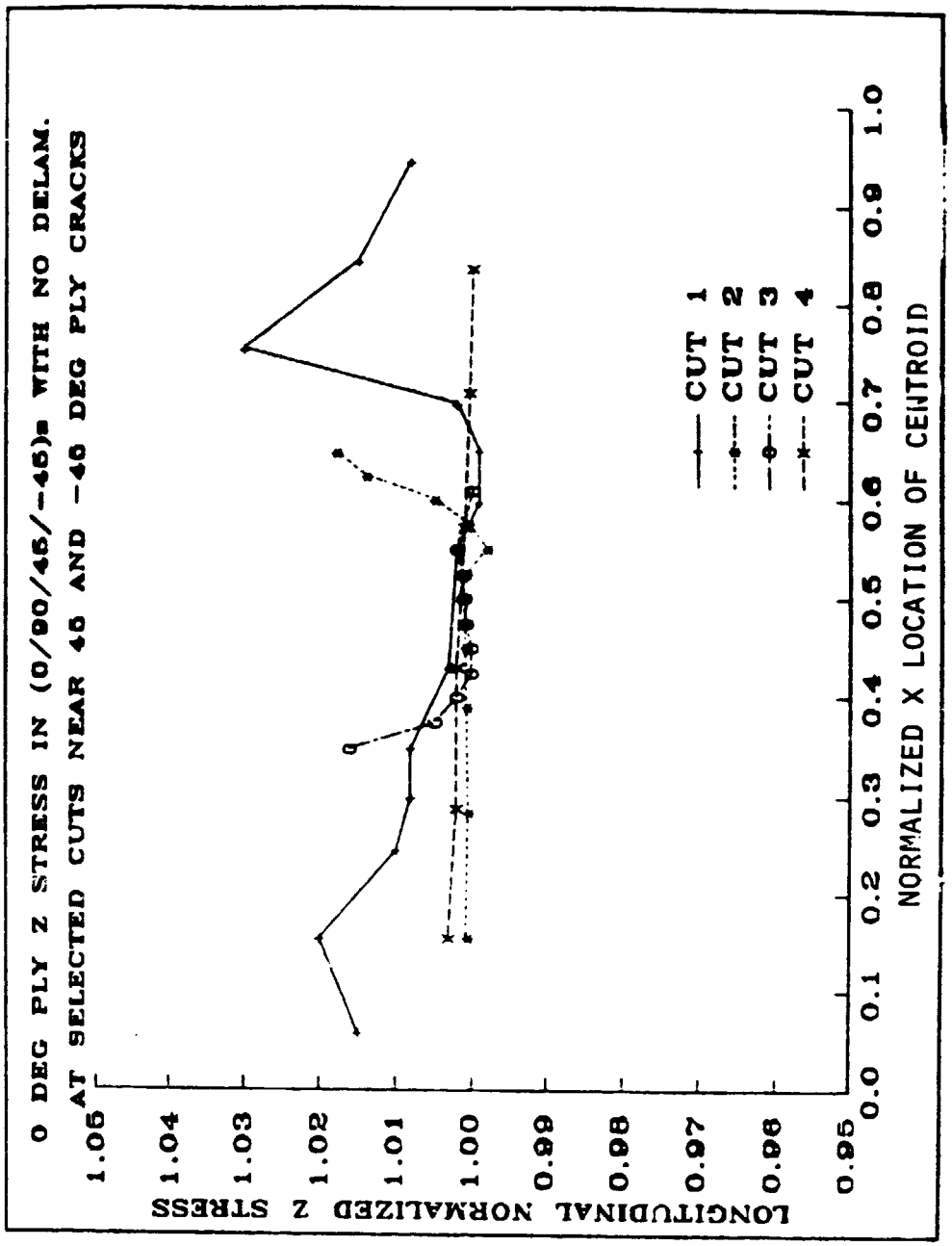

Figure 114 : Distribution of longitudinal stresses in the 0° ply for the model of Figure 107 without a delamination.

TABLE 61

SUMMARY OF THREE DIMENSIONAL DELAMINATION ANALYSIS RESULTS

Laminate	Delamination Interface	Dominant G Mode	Maximum Percent Increase in 0^{o} Ply Stress	Peak $_2$G J/mm^2
$(45/-45/0/90)_s$	90/90	I	10	14.8
$(0/90/45/-45)_s$	90/45	II, III	13	0.184
$(0/90/45/-45)_s$	45/-45	I, II	22	0.734
$(0/90/45/-45)_s$	45/-45 Interior with Transverse Cracks	III, II	21	3.66
$(0/90/45/-45)_s$	45 and -45 Transverse Cracks Without Delamination	-	4	-

coupons delaminate on multiple interfaces and have transverse matrix cracks, ply isolations occur prior to fatigue failure. Thus the free body modeling approach provides both a practical and more realistic technique.

For coupons fatigue loaded at high initial loads, local 0° ply stress increases due to delamination may be sufficient to lead to 0° fiber fracture and coupon failure before ply isolation occurs. However, these coupons have quite short fatigue lives. This fact combined with the more realistic free body type analysis for most other coupons inplies that the detailed and costly three dimensional analysis is not useful for defining the fatigue stress-life curve. Even for failure analysis purposes, the much simpler and more conservative free body type analysis of ply isolation may prove more useful for estimating 0° ply stresses.

The results of this three dimensional analysis also demonstrated that for most practical cases, the anticipation of delamination growth and direction is dependent on G_I, G_{II}, and G_{III}. Each case has a different dominant combination of these modes and is quite complex. Thus, simple laboratory understanding of one mode or another does not necessarily apply to a more complex case. Further, analysis results of practical cases, depend greatly upon the crack shape model selected. That shape, in turn, changes with each growth increment. Thus anticipation of crack growth and direction and subsequent incremental remodeling becomes quite tedious for most complex cases and essentially impractical for design purposes.

Another significant conclusion of the three dimensional analysis study was the deduction that although 0° ply stresses increased due to the presence of delamination, no strong stress concentration were discerned in that ply. The 0° ply stress increases were gradual, rather smooth type reactions. Thus the laminate cracks should be viewed more as resulting in local stress redistributions and not sharp stress concentrations. This implies that fracture mechanics type analysis may prove to be useful for describing onset of transverse cracking or edge delamination and even growth in certain

directions, but may not be useful for more complex, and generally more realistic cases. This clear, but tentataive conclusion casts doubt upon the general usefulness of developing detailed, experimentally based crack growth curves related to different G values.

This is not to imply that fracture mechanics is not of analytical value. In fact fracture mechanics is of extreme value in calculating G and the effect of thickness, laminate concentration, or matrix and fiber properties on G. However, the three dimensional analysis results of this subsection were used to infer that fracture mechanics does not determine the failure event, but determines the effect of geometric scale and "material" properties on the onset of critical events ultimately necessary for failure to eventuate. However, the failure event itself appears to be a property reflective of the structure nature of the laminate. Thus, applicable failure criterion may be primarily of the relatively simple free body type of stress concentration analysis described in Section 3.4.5.

SECTION 4
COMPARISON OF ANALYTICAL AND EXPERIMENTAL RESULTS

The expected response of the coupons based upon the analysis and mathematical modeling described in Section 3 was compared to the experimental results presented in Section 2. That comparison is discussed in this section. The results for each of the three types of experiments are discussed separately followed by a summary subsection. This section attempts to bring together not only many of the results of this study, but also those of other investigations.

4.1 MONOTONIC LOADING

o ONSET STRAIN AND ACCUMULATION OF MATRIX CRACKING

This analysis problem was not examined in this program, but appears to be properly evaluated using a strain energy release type of mathematical approach[11]. The onset of matrix cracking occurs when a critical strain energy release rate is reached, while matrix crack accumulation develops, because of increasing applied strain, as a consequence of the static distribution of transverse strength[46]. Some layups reach a plateau in crack density within certain plies prior to failure while others do not. The reason for this difference has to do with the variations which occur in strain energy release rate for different layups. The expected result for a specific layup can be calculated, using a strain energy release rate analysis, but the technique generally requires extensive effort for any one particular layup. A significant point, however, is that matrix crack saturation should not occur in all layups prior to fracture and not even in all plies. This result was well confirmed for the laminates evaluated in this study.

- ONSET AND EXTENT OF DELAMINATION

Some layups significantly delaminate under monotonic tension prior to failure while others do not. Even in the latter case, however, delamination primarily occurs along the free edge of the coupons. The reason for delamination has been attributed to Poisson mismatch between adjacent plies and large free edge stresses[55,56]. Such delamination can be successfully anticipated using strain energy release rate analysis[11] and by analyzing the free edge stress state. On that basis, for instance, the $(0/90/\pm45)_s$ and $(0/45/90/-45)_{2s}$ quasi-isotropic laminates would not be expected to significantly delaminate under monotonic load while other quasi-isotropic laminates should and do delaminate[34,41]. Likewise, such delamination was not expected under monotonic tensile load for the other three layups studied in this investigation.

- CHANGE IN STIFFNESS

The analysis described in Section 3.3 led to the conclusion that the main contributors to stiffness change would be transverse matrix cracking, delamination, and their combination where they lead to a local loss of load carrying capacity in the off axis plies. O'Brien[39,41,72] has shown that the extent of delamination correlates well with stiffness loss and with a rule of mixtures type approach for those laminates which do delaminate. For the four laminates of this program, no such delamination took place. Thus damage was confined to transverse matrix cracking and the conclusion was made (see Section 3.3.1) that at most, a 2 to 3 percent change in stiffness should take place prior to fracture. Further, that stiffness change should not occur prior to onset of significant matrix cracking and the amount of stiffness loss should be a direct function of the number of transverse cracks.

Table 62 shows that the onset of measurable stiffness change did not occur until after the onset of matrix cracking. The extent of stiffness decrease also correlated well with that expected analytically, see Table 63. Expected stiffness loss for matrix cracks alone was 1.4 percent for the number of transverse cracks observed in the $(0/90/\pm45)_s$ laminate. The experimentally obtained average value of 1.5 $\pm$0.15 percent was essentially identical to the theoretical value. A similar correlation was found for the $(0/\pm45)_s$ laminate. The analytically based conclusion was that no significant stiffness change should be observed for the $(0/45/0_2/-45/0)_s$ layup which was exactly the experimental result. This lack of stiffness change occured because so few cracks developed and their effect is extremely small. The expected stiffness loss is listed as much less than 0.2 percent since that value would result if the observed transverse cracks fully crossed the coupon width. This did not generally occur. Finally, the stiffness change in the $(0_2/90_4)_s$ layup was also understandable analytically. A saturated matrix crack state should result in approximately a 6.2 percent stiffness loss. For the four coupons which essentially reached transverse crack saturation the average value was found to be 6.2 $\pm$0.15 percent which was excellent agreement. The accuracy of the analytically anticipated changes in stiffness due to matrix cracking during monotonic tension loading was clearly well verified by experiment.

For those laminates which tend to delaminate, observed stiffness losses compare well to those calculated using O'Brien's[72] rule of mixtures analysis discussed in Section 3.3.4. Potentially, delamination at the end of transverse matrix cracks plus the cracks themselves is associated with significant stiffness loss. In practice, such delamination is usually confined to the coupon edges, or if extensive in the width direction to at most a few transverse matrix cracks as shown in this program and in References 7, 13, 12, and 39. Thus global stiffness loss associated with delamination running along the transverse matrix crack tips is generally small. The other possible causes of stiffness loss discussed in Section

TABLE 62
CORRELATION BETWEEN EXPECTED
AND ACTUAL STRAINS FOR
ONSET OF STIFFNESS CHANGE
UNDER MONOTONIC LOAD

Laminate	Approximate Strain At Onset of Significant Matrix Cracking	Average Strain At Onset Of Measurable Stiffness Change
$(0/90/\pm45)_s$	0.0060	0.0070
$(0/45/90/-45)_{2s}$	0.0050	0.0056[7,32]
$(0/\pm45)_s$	0.0070	0.0075
$(0/+45/0_2/-45/0)_s$	0.0090	No measurable change
$(0_2/90_4)_s$	0.0050	0.0050

TABLE 63
CORRELATION BETWEEN ACTUAL AND EXPECTED STIFFNESS LOSS FOR COUPONS LOADED IN MONOTONIC TENSION

Laminate	Extent of Matrix Cracking Near Failure	Expected Stiffness Loss, Percent	Average Actual Stiffness Loss, Percent
$(0/90/\pm45)_s$	Near saturation in 90° and 45° plies, No cracks in -45° plies	1.4	1.5
$(0/\pm45)_s$	Number of cracks far less than saturation	1.8	1.7
$(0/45/0_2/-45/0)_s$	Number of cracks far less than saturation	<<0.2	No measurable change
$(0_2/90_4)_s$	Near saturation	6.2	6.0

3.3 were found to be too insignificant to be easily measurable. Therefore, changes in stiffness associated with monotonic tension load induced damage development do appear to be qualitatively understood and quantitatively described using the techniques discussed in Section 3.3.

o STRAIN TO FAILURE

Based on the results of Section 3.3 and except for the $(0_2/90_4)_s$ layup, none of the damage states observed in all of the other multiple axis layups should lead to any local 0° ply strain increases of more than a few percent. Thus all of the layups should exhibit similar strains to failure if the 0° fiber strengths are similar. This result was experimentally confirmed and shown in Table 57 of Section 3.6. O'Brien[72] has shown the same effect for layups which do delaminate, but where again the damage state does not lead to large premature 0° ply fracture due to local strain concentrations. That the strain to failure of layups made from the same material batch is essentially the same is shown in Figure 115, a modification of O'Brien's figure. The only exceptions are the 0° unidirectional layup and the $(0_2/90_4)_s$ layup.

The slight differences among the strain to failure values of Figure 115 can be explained by two reasons. First, different batches of materials do have different 0° fiber strengths[6,7,32]. Thus, for example, the strain to failure of the $(0/45/0_2/-45)_{2s}$[7,13] layup was slightly higher than that of the other layups probably because the coupons were made from different material batches. Second, local strain concentrations due to ply isolation which occur in some layups, primarily quasi-isotropic, along the coupon edges and near ultimate load can somewhat reduce strain to failure. Thus, this was probably the reason that the strain to failure of the $(0/\pm45)_s$ coupons was slightly higher than that of the $(0/90/\pm45)_s$ coupon.

The decreased strain to failure in the $(0_2/90_4)_s$ layup was due to: 1) a much larger stress concentration associated with transverse matrix cracks in an 8 layer thick ply compared to a 1 layer thick ply; 2) a larger volume of

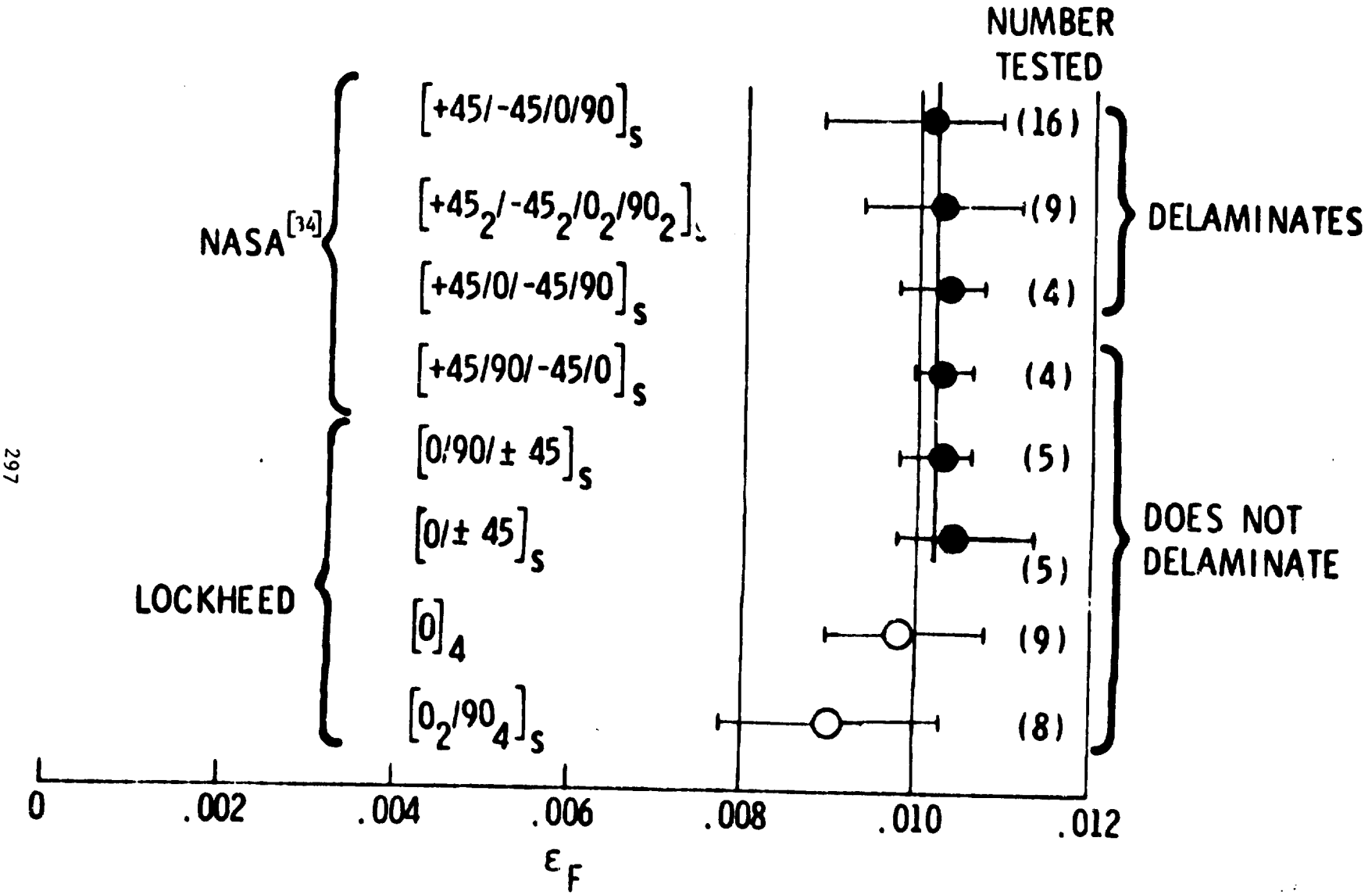

Figure 115: Comparison of average strains to failure under monotonic tension load of various T300/5208 laminates.

the 0° ply being affected by the stress concentration; and 3) the dumping of the load carried by 8 90° layers into the 0° plies[52], an extreme case of local strain concentration attributed to the high local stresses at the matrix crack tips because of the thick 90° ply[83]. The difference between the decreased strain to failure of the unidirectional laminates and that of the multidirectional laminates appears to be understandable based upon a Weibull type statistical effect due to volume differences in the 0° plies as discussed in Section 3.5.1.

- FRACTURE APPEARANCE

In all coupons, the fracture of the 0° plies tended to be along the angle direction of the underlying ply. This was attributed to the matrix crack tip induced stresses which are generally small, but provide a preferred fracture path as the 0° failure strain is approached.

- EXTENT OF SCATTER

The extent of scatter was attributed to four factors. These are:

1. The large variability in fiber strengths.
2. The requirement of only a few 0° fiber fractures in a statistical significant region for ply fracture.
3. The inherent size of microstructure relative to the geometry size.
4. The effect of local strain concentration due to the presence of matrix cracking and delamination.

Not only is fiber strength highly variable, but the average strength also varies significantly from batch to batch. The inherent effect of microstructure was discussed in detail in Section 1. Essentially, this effect is due to the fact that defects must be very large to dominate over the variability due to microstructure.

Harlow and Phoenix[29,30,75-77] have shown that only a few fiber breaks need to occur in a statistically significant region for fracture of the entire 0° ply to occur. The breakage of the minimum necessary number of fibers, however, is dependent on the local matrix crack and delamination state and the local strength distribution of the individual fibers. Both of these factors are statistical distributions, and in the case of fiber strength, are highly variable. Coupon fracture strength reflects the influence of these two variables and the associated scatter. Unidirectional laminates should, therefore, have high variability in strength reflecting fiber distribution, and thus large coefficients of variation (COV) and low scatter parameters.

Multidirectional laminates should have much less scatter which decreases as the effect of the less random local strain concentration, associated with damage, dominates over the variability in fiber strength. For a $(0)_{16}$ laminate, Ryder and Walker[7] obtained a COV of 11.2 percent on strain and a scatter parameter of 17.9. This compares favorably to Whitney's[81] value of 18.4 (see Section 3.6). A $(0/45/0_2/-45/0)_{2s}$ laminate should have reduced scatter compared to a 0° unidirectional laminate because of the presence of matrix cracks in the $\pm 45^{\circ}$ plies. For this layup, Ryder and Walker[7] obtained a COV of 4.84 percent and scatter parameter of 23.2. The scatter in strength of a quasi-isotropic laminate should again be reduced further compared to the $(0/45/0_2/-45/0)_{2s}$ laminate because the less random nature of the local strain concentration along the coupon edges becomes more dominant. Thus the COV for a $(0/45/90/-45)_{2s}$ laminate was found to be 3.80 percent and the scatter parameter 33.9 for the same batch of material used to produce the $(0/45/0/-45/0)_{2s}$ coupons[7]. If local strain concentration does reduce scatter in coupon strength, notched coupons should have less scatter than unnotched coupons. In support of this supposition, Ryder and Walker[32] found a COV of 5.0 percent and scatter parameter of 24.7 for unnotched $(0/45/90/-45)_{2s}$ coupons made from a different material batch and a COV of 3.9 percent and a scatter parameter of 29.2 for notched coupons from the same material batch. Similarly, Langenbeck[88] obtained a COV of 5.5

percent for unnotched $(45/0/-45/90/0)_s$ coupons and 4.4 percent for notched coupons.

This simplified analysis of scatter indicated that at least a qualitative anticipation of scatter in tensile strength properties can be obtained. The scatter in 0^o unidirectional lamina properties provides an upper bound on expected scatter. Calculation of the extent of potential local strain concentration due to transverse matrix cracking and edge delamination provides an estimate of expected reduction in extent of scatter.

4.2 FATIGUE LOADING

o MATRIX CRACKING ONSET AND ACCUMULATION

Essentially this topic was covered under monotonic loading. Detailed strain energy release rate analysis is required for each laminate in order to obtain a high degree of quantitative accuracy. The work of O'Brien[34,41,72] has shown that the critical G level for the onset of matrix cracking is different, and lower, under fatigue loading than under monotonic loading. This phenomenon is interpreted to mean that actual experimental data for G is required under each loading type to accurately anticipate matrix cracking onset. Quasi-isotropic layups tend to reach high densities of matrix cracking rather quickly while in other layups many cycles are required to reach high densities of cracks or they are not reached at all, such as in the $(0/45/0_2/-45/0)_s$ layup. Such differences reflect the fact that laminates which tend to delaminate easily, such as quasi-isotropic, also tend to reach matrix crack density plateaus much earlier.

o DELAMINATION

Again, this analytical problem was essentially covered under monotonic loading. However, precise details for complex layups may require extensive modeling and may not actually be practical because details depend on subtle

strain energy release rate differences involving mixed mode fracture (see Section 3.6) and depend on fatigue versus monotonic loading conditions. Such differences may require extensive experimental verification. Trends for interface delamination order appear to be reasonably well understood[11,12]. The fact that quasi-isotropic layups tend to delaminate more easily than 0/±45 layups, is attributed to the much larger Poisson contraction mismatch which occurs within the quasi-isotropic laminates.

o STIFFNESS CHANGE

The fact that two quite different types of delamination can occur must be kept in mind, see Section 3.4.5. The first of these generally displays a "thumbnail" type delamination and is often characteristic of large Poisson mismatch such as at a 90/45 interface. This type of delamination usually develops over a large area and may or may not be associated with large stiffness loss. The second type occurs between such interfaces as +45/-45 at the end of a transverse matrix crack and extends along the matrix crack in the coupon width direction. Such a delamination can be associated with large stiffness change, but generally is not because the extent of such delamination is generally small. However the effect of this second type of delamination on local stress concentration can be large.

The probable reasons for stiffness change associated with various possible damage states were summarized in Section 3.3.6. Transverse matrix cracking alone was not anticipated to be associated with large percent stiffness loss. The accuracy of the analysis procedures was confirmed for the monotonically loaded coupons as discussed in Section 4.1, see Table 63, and also for the fatigue loaded coupons as shown in Table 64. In the latter table, the anticipated monotonic stiffness losses based upon the observed matrix crack density are shown. The observed stiffness losses are the averages of those measured when a matrix crack density plateau occurred. A range in values is given because matrix crack saturation densities were slightly different at each fatigue stress level with higher densities occurring at higher fatigue stress or strain levels.

TABLE 64
COMPARISON BETWEEN EXPECTED AND ACTUAL MONOTONIC STIFFNESS LOSS
DUE TO MATRIX CRACKING INDUCED BY FATIGUE CYCLING

Laminate	Expected Monotonic Stiffness Loss For Observed Crack Density, Percent	Observed Monotonic Stiffness Loss, Percent
$(0/90/\pm45)_s$	2.0 to 2.3	2.0 to 2.5
$(0/\pm45)_s$	3.6	<4.0
$(0/45/0_2/45/0)_s$	0.2 to 0.5	<0.5
$(0_2/90_4)_s$	5.5 to 7.9	5.5 to 7.5

The onset of delamination was anticipated to lead to further significant stiffness loss, as shown in Section 3.3, both because of the relaxation of stresses near the transverse crack tip, see Section 3.3.3, and the loss of constraint between the plies. This should be, as was observed, a gradual effect for all layups because onset and growth of delamination was a gradual process. Stiffness loss due to the loss of Poisson constraint alone led to the conclusion, Section 3.3.5, that the order of maximum to minimum stiffness loss in the layups should be $(0/90/\pm45)_s$, $(0/\pm45)_s$, $(0/45/0_2/-45/0)_s$, and $(0_2/90_4)_s$. This was indeed the observed order of stiffness loss except for the $(0_2/90_4)_s$ layup, the reasons for which will be explained in more detail later.

For the $(0/90/\pm45)_s$ quasi-isotropic layup, the maximum possible stiffness loss is approximately 16.5 percent for the 90/45 interface fully delaminated, and 22.2 percent due to combined full delamination at both the 90/45 and 45/-45 interfaces and to transverse matrix cracking. Approximately 2.5 percent is due to transverse cracking alone (Section 3.3.3) and the rest to delamination. The maximum stiffness values are somewhat over estimated because the effects of delamination alone and matrix cracking alone are not additive. The development of extensive delamination on either side of a ply containing multiple matrix cracks results in a stiffness loss whose value is decreased by the isolation of the matrix cracks themselves, but increased because the load carried by the isolated ply is transferred to the uncracked adjacent plies. The potential amount of the increase is much greater than the decrease.

In Table 65, observed stiffness loss is compared to that analytically anticipated based upon a summation of that due to transverse matrix cracking alone (approximately 2.5 percent) and delamination alone (Section 3.3.4). The correlation is quite good, but with an increasing error as the percentage stiffness loss increased. This difference was not due to 0° ply splitting or fiber fracture since very little of either phenomenon was observed and their combined effect is much less than one percent, see

TABLE 65
COMPARISON BETWEEN MEASURED
AND ANTICIPATED STIFFNESS LOSS
FOR FATIGUE LOADED $(0/90/\pm45)_s$ COUPONS

Loading Type	Coupon ID	Anticipated Stiffness Loss, Percent	Measured Stiffness Loss, Percent	Dominant Delamination Interface
Fatigue	11-13	2.9	2.9	45/-45
	11-45	3.6	4.2	90/45
	11-3	6.8	7.6	90/45
	11-9	8.3	10.4	90/45
Residual Strength	11-16	4.1	5.1	45/-45
	11-23	4.7	6.3	45/-45
	11-8	5.9	6.3	90/45
	11-57	6.8	9.7	90/45
	11-60	7.9	10.5	90/45
	11-11	9.5	12.0	90/45
	11-10	15.0	19.3	90/45

Section 3.3.6. The difference is primarily to be due to the effect of local ply isolation, see Section 3.4.5. This occurs due to the development of delamination along both sides of a transverse matrix crack either in the width direction parallel to the transverse crack or in a "thumbnail" fashion which is more common. As discussed previously, the first type of delamination was not observed to be particularly common in the laminates of this study. Hence their effect is small. Ply isolation produces a significant effect on stiffness only as that delamination become extensive.

In the $(0/90/\pm45)_s$ layup, isolation of the 45° ply due to 90/45 and 45/-45 interface delaminations easily leads to several percent stiffness loss as delamination increases in area. Thus the difference between observed and anticipated stiffness loss when based only on a simple sum of that due to matrix cracking alone and delamination alone should increase as delamination extent increases. Table 65 shows this to be the case. For low amounts of stiffness loss, anticipated and observed values are quite close while at higher amounts, differences reach 4.3 percent. Thus, the stiffness changes observed during fatigue loading appear to be well understood for this layup.

Monotonic stiffness losses in $(0/\pm45)_s$ coupons were limited to 6.3 percent and were attributed partially to matrix cracking, partially to narrow regions of delamination, and also to transfer of significant load to the 0° plies because of isolation of angle ply regions due to combined transverse cracking and delamination. Observed delamination alone would add only about 0.5 percent to the 3.6 percent stiffness loss due to transverse cracking (see Table 41), thus the combined damage state potentially results in up to 4.1 percent stiffness loss. Complete isolation of the $\pm45^\circ$ plies can result in a 15 percent stiffness loss, according to Table 47 of Section 3.5, while local isolation of 10 percent of the plies along the coupon edge, as observed, results in at least 1.5 percent loss. Local isolation of both the $\pm45^\circ$ plies will add an additional 0.5 to 1 percent stiffness loss. Fiber fracture is associated with much less than even a one percent change.

For the $(0/45/0_2/-45/0)_s$ coupons, no significant stiffness loss was measured. Minor observed fluctuations appeared to be random in nature. These results are consistent with the observation that matrix cracking at coupon fracture was far from saturation and did not fully traverse the coupon width. This matrix cracking would be associated with much less than even the 0.2 to 0.5 percent stiffness loss analytically calculated assuming the transverse crack density was fully saturated and all cracks crossed the coupon width. Further, at most 5 to 10 percent delamination and less than 5 percent associated isolation of the $+45^\circ$ plies were ever observed. According to Tables 44 and 47, this should also result in much less than a 0.2 percent stiffness loss. Fiber fracture in the 0° plies is again associated with much less than a 0.5 percent stiffness loss. Therefore, no observable stiffness loss was analytically expected for this layup and the observed damage states.

In Section 4.1, anticipated stiffness loss in the $(0_2/90_4)_s$ tension loaded coupons due to transverse matrix cracking alone was shown to correlate well with measured stiffness loss. A similar correlation between matrix crack density and stiffness loss was found for fatigue loaded coupons. However, in these experiments delamination at the 0/90 interfaces occurred as did 0° fiber fracture and 0° ply splitting. As indicated in Section 3.3.5, 0° fiber fracture and 0° ply splitting result in less than one percent stiffness loss. In addition, delamination alone can result in only 0.4 percent stiffness loss. Therefore, the measured stiffness losses of up to 17.1 percent in these fatigue loaded $(0_2/90_4)_s$ coupons were attributed not only to matrix cracking, but also to either combined matrix cracking with short delaminations at their ends or to complete ply isolation, or both.

For the $(0_2/90_4)_s$ coupons, matrix cracks with short delaminations at their ends could conceivably be associated with up to a 10 percent stiffness loss if the delaminations extend across the coupon width. However, such extensions beyond a narrow region at the coupon edge were not observed. Instead, delaminations grew from the intersections of the 0° ply splits with

the 90° ply transverse cracks within the interior of the coupons. Such combinations of delamination and 90° ply matrix cracks result in local, but not complete isolation of the 90° plies. If this isolation extends across the coupon, up to 14 percent stiffness loss can occur, see Table 47 in Section 3.4.5. Therefore, the amount of anticipated stiffness loss in these $(0_2/90_4)_s$ coupons was obtained by calculating the expected loss associated with: 1) The measured average matrix crack spacing; and 2) the estimated percent of delaminated area multiplied times the percent of stiffness loss due to ply isolation. The second calculation is not entirely correct because full isolation of the 90° plies is not entirely achieved over the entire delaminated area. However, isolation is complete enough to provide a reasonable estimate.

A comparison between anticipated stiffness loss and measured values for the $(0_2/90_4)_s$ coupons is given in Table 66 for several representative coupons. The correlation appears to be quite good verifying the analytical approach for estimating stiffness loss. The small differences between calculated and measured values appear to be due to possible errors in estimating delamination extent and to the lack of complete 90° ply isolation over the entire delaminated region. Further, the extent of stiffness loss associated with the matrix cracking and with 90° ply isolation is not completely additive, as mentioned previously. Still the correlation does show that the stiffness loss associated with these two phenomena do explain most if not all of the measured values.

- FAILURE CRITERIA

The proposed criteria primarily responsible for inducing 0° fiber fracture are:

1. Local stress concentrations at transverse matrix crack tips,
2. Local transfer of load from the angle plies to adjacent 0° plies due to isolation of the angle plies by combined delamination and transverse matrix cracking,

TABLE 66

COMPARISON BETWEEN MEASURED AND ANTICIPATED STIFFNESS LOSS FOR FATIGUE LOADED $(0_2/90_4)_s$ COUPONS

Coupon ID	Estimated Delaminated Area, Percent	Stiffness Loss Due to Matrix Cracking, Percent	Total Anticipated Stiffness Loss, Percent	Measured Stiffness Loss, Percent
A15	0	6.0	6.0	5.7
A6	40	5.5	11.1	8.8
A22	30	5.0	9.2	8.9
A25	10	6.9	8.3	9.1
A21	10	5.6	7.0	9.2
A9	10	6.7	9.1	9.3
A31	60	5.8	14.2	12.2
A24	70	6.5	16.3	17.1

3. High enough local strain in the 0° plies to result in 0° fiber fracture similar to that which occurs under fatigue load in a 0° unidirectional laminate at high strains, >0.0080.

These three criteria appear to explain all of the observed experimental results. The application of these criteria to each of the layups used in this study is discussed in this subsection. Criterion 1 should not have a major effect unless strains are already high. Further, the analyses of Section 3.4 indicated that the effect of the local transverse crack tip stress concentration should extend only a few fiber diameters into the adjacent ply unless the cracked ply is very thick which has been confirmed by Jamison and Reifsnider[40]. Criterion 3 will apply at or above strain levels of about 0.0070 - 0.0080 strain for these T300 fibers (Section 3.4.6). For global strain levels below approximately 0.0080 strain, Criterion 2, ply isolation, is the primary reason for failure of the 0° plies.

Little fiber fracture should be observed prior to fracture in the $(0/90/\pm45)_s$ quasi-isotropic layup, as confirmed experimentally, see especially Reference 40. Such high strains are induced in the 0° plies by local isolation of the angle plies that a large amount of 0° fiber fracture must immediately occur at most fatigue load levels as soon as ply isolation occurs. Thus, essentially instant coupon fracture takes place. Such strain concentrations range from 1.22 to 1.54 times the nominal strain value (see Table 47). Thus, unless initial strains are quite low in these coupons, development of ply isolation due to combined delamination and matrix cracking requires the application of criterion 2 and criterion 1 is of little importance. Similarly, criterion 3 does not dominate unless initial strains are high. Therefore, at the initial strain levels used in the program, little 0° fiber fracture was expected for this layup. The work of Jamison and Reifsnider[40] confirmed this conclusion.

For the $(0/\pm45)_s$ layup, the effect on local 0° ply strain due to criterion 2 is much less (up to 1.15 due to isolation of the -45° ply, see Table 47),

than for the quasi-isotropic layup. This fact allows much higher strains to be applied under fatigue loading for these coupons without early failure. However, because delamination and associated angle ply isolation are not extensive in this layup, the other two criteria become much more important. In fact, for many initial load levels, the more random nature of criterion 3 dominates, and thus the extent of fiber fracture prior to coupon fracture should be much greater than in a quasi-isotropic layup. This was observed to be true qualitatively in this study and quantitatively by Jamison and Reifsnider[40]. Without significant ply isolation, initial strains must be high, above 0.0080, in these coupons to get failure in less than 10^6 cycles. However, above this strain level the 0° plies themselves have a much shorter life. Hence, any further local strain increases due to ply isolation begin to fracture 0° fibers, since they are now in the same strain range in which 0° fracture occurs in a unidirectional laminate subjected to monotonic load. For this reason, the fatigue life of these coupons at 0.0090 strain or above is very short.

The reasons for failure of the $(0/45/0_2/-45/0)_s$ coupons are exactly the same as for the $(0/\pm45)_s$ coupons except that, as indicated by Table 47, the effect of isolation of the ±45 plies is even less. The local strain concentration in the 0° plies due to isolation of the 45° plies is only 1.04 to 1.07. Thus, once again failure criteria 1 and 3 primarily apply resulting in eventual coupon failure. The extent of fiber fracture possible before coupon failure should be even greater than for the $(0/\pm45)_s$ layup, which has also been verified experimentally[7,32].

Finally, for the $(0_2/90_4)_s$ layup all three proposed criteria again appear to adequately explain the observed results. However, in this layup criterion 1 becomes more important because of the much higher stress concentration associated with an 8-layer thick transverse matrix crack compared to a single layer thick crack (see Section 3.3). In addition, 0° fiber bundles, caused by combined 0/90 interface delamination and 0° ply splitting, fracture near the grips because of high stress concentration, as experimentally described

in Section 2.5. This condition leads to a modified form of criterion 2 since large strain increases in the 0° plies result due to the complete loss of the load carrying capacity of these 0° fiber bundles. Finally, local isolation of the 90° ply because of 0/90 interface delamination leads to a 14 percent increases in local strain.

For all layups, the rather sudden coupon fracture, without any general obvious warning, appears also to be understandable by combining the three failure criteria with the work of Harlow and Phoenix[29,30,75-77]. They showed that only a few fiber fractures, or fractures adjacent to statistically weak fibers, in a small statistically significant region are necessary to cause general 0° ply fracture. Jamison and Reifsnider[40] confirmed this in the $(0/90/\pm45)_s$ and the $(0/\pm45)_s$ laminates by carefully counting single, double, triple, etc., 0° fiber breakage groups. The observed incidence of groups of two broken fibers found prior to coupon fracture was much less than single broken fibers while groups of three were even less than groups of two. Groups of four or more were rarely if ever observed prior to coupon fracture.

Because of the three failure criteria, random fracture of the weakest 0° fibers take place during fatigue loading. This cannot result in observable stiffness change, see Section 3.3.6. Coupon fracture cannot occur until a statistically significant region of broken fibers and unbroken weak fibers developes such that a large region of fibers fracture together. When the correct, small number of 0° fiber fractures eventually occurs in a significantly significant small region, 0° ply fracture occurs and the experimentally observed sudden coupon failure eventuates.

- STRAIN TO FAILURE

Based on the proposed failure criterion for the 0° plies, coupon fatigue life was inferred to be very short if local strains of 0.0080 or higher occur. Therefore, global failure strain in fatigue must always be at least

15 percent below the monotonic failure strain just due to criterion 3. Failure strain in fatigue can even be as much as 30 to 40 percent lower if criterion 2 is substantially involved. This is the case with the $(0/90/\pm45)_s$, $(0/\pm45)_s$ and $(0_2/90_4)_s$ layups. Thus, the 15 to 35 percent difference between strain to failure under fatigue loading and that under monotonic loading is easily understandable.

o FATIGUE LIFE "RUNOUT"

Previous investigations[7,32] have indicated that there may be a strain level below which fatigue failure of unnotched graphite/epoxy laminates will not occur under constant amplitude load. The failure criteria proposed above imply that such limits do exist. By criterion 3, local strains in the 0° plies above 0.0075 to 0.0080 should lead to eventual fatigue failure within 10^6 to 10^7 cycles. Therefore, if criteria 1 and 2 conditions exist and local induced strains are above 0.0080, then fatigue failure must eventually occur. However, if local strain does not increase to at least 0.0075 to 0.0080, fatigue life would probably be longer than the expected life of the structure. This occurs because the fatigue life of the 0° plies themselves becomes extremely long below a strain level of about 0.0075 - 0.0080[38]. The strain level of 0.0080 was somewhat arbitrarily selected as a cutoff strain for long life ($>> 10^7$ cycles) in the 0° plies.

Based upon this analysis, the three 0° ply failure criteria and the results of Table 47, maximum permissible strain levels for long fatigue life ($>>10^7$ cycles) were calculated for each multiangle ply laminate. The "runout" strain was calculated by dividing the long life strain of 0.0080 for the 0° plies by the maximum possible strain concentration due to ply isolation for each laminate. This is equivalent to transferring all load to the 0° plies. Results are shown in Table 67 along with estimated strain levels based on experiment. The strain level for the $(0_2/90_4)_s$ layup was more difficult to estimate because of the 0° ply bundles, caused by 0/90 interface delamination and 0° ply splitting, being removed from load

TABLE 67
COMPARISON BETWEEN ANALYTICALLY DERIVED AND EXPERIMENTALLY BASED ESTIMATES OF FATIGUE LIFE "RUNOUT" STRAINS

Laminate	Analytically Estimated Fatigue Life "Runout" Strain Level	Experimentally Based Fatigue Life "Runout" Strain Level
$(0/90/\pm45)_s$	0.0052	<0.0060
$(0/45/90/-45)_{2s}$	0.0052	~0.0044[7]
$(0/\pm45)_s$	0.0063	<0.0070
$(0/45/0_2/-45/0)_s$	0.0075	<0.0080
$(0_2/90_4)_s$	<0.0060	~0.0050

carrying paths by fracture at the grips. Therefore, a "runout" strain was calculated by taking account of the effect of the 1.14 strain concentration due to ply isolation combined with the reduction due to the 0° fiber "fatigue life threshold" plus the effect of the transverse 90° cracks. This resulted in a slightly unconservative estimate because the effect of 0° fiber bundle fracture was ignored. For the other layups, the hypothesis of a strain below which tension-tension, constant amplitude fatigue life is excessively long appears to be well supported. For the $(0/45/90/-45)_{2s}$ layup, the "runout" strain may be somewhat unconservative. For this layup, coupons were cycled to 10^7 cycles[7] and this data indicated that a 0° ply "runout" strain of 0.0075 may be a better choice than the selected value of 0.0080.

The global "runout" strain hypothesized is a lower bound for the fatigue stress-life curve. Below this strain level, matrix cracking and delamination can initiate and grow. However, sufficient strain concentration cannot occur below the fatigue life "runout" strain to raise the local strain level above 0.0080. Therefore, fracture of the coupon does not eventuate. The strain level above which damage will initiate, but not grow sufficiently to cause coupon fracture, must be calculated using strain energy rate analysis and experimental data for the critical G. This approach allows calculation of such effects as ply thickness. Thus the lower bound on the fatigue life curve is calculated by free body type, strain concentration analysis (see Section 3.4.5), and the lower bound for onset of matrix damage and delamination by strain energy release rate analysis (see Section 3.1 and Reference 41).

- EXTENT OF SCATTER

As discussed in the introduction, laminated, graphite/epoxy composites must inherently exhibit relatively large scatter in fatigue life. This is due to the four reasons listed in Section 4.1. If the layup geometry is such that fracture of the 0° fibers is dominated by failure criterion 2, ply

isolation, then scatter in fatigue life is primarily dominated by the microstructure and not the fiber properties. However, if 0° ply failure criterion 3 dominates, as for the $(0/\pm45)_s$ or $(0/45/0_2/-45/0)_s$ layups, fatigue life is primarily influenced by the scatter in fiber strength, and the randomness of multiple 0° fiber fractures. Since individual 0° fiber strength is highly variable and a statistically significant group of a few adjacent fiber fractures are required for failure, associated fatigue life scatter must be large relative to that dominated by the laminate microstructure. Therefore, quasi-isotropic layups generally have a scatter in fatigue life of about one order of magnitude because failure is dominated by criterion 2. In contrast the $(0/\pm45)_s$, $(0/45/0_2/-45/0)_s$, and $(0_2/90_4)_s$ layups all exhibit a fatigue life scatter much in excess of two orders of magnitude because their failure lives are controlled primarily by criterion 3.

- FRACTURE APPEARANCE

Coupons which failed under fatigue load tended to exhibit 0° ply fracture along the angle of the adjacent ply. Again, as for the monotonically loaded coupons, this appears to occur because the 0° fiber fracture follows along the high strain concentration field induced by the transverse matrix cracks and by local off-axis ply isolation.

- SHAPE OF STRESS (STRAIN) -- LIFE CURVE

Based upon the above discussion of both the effect of monotonic and fatigue loading, the shape of the stress-life curve for tension-tension loads can apparently be estimated without great difficulty. The strength at zero cycles can be calculated based upon the strain to failure under monotonic load, which is generally a constant value easily calculated using Weibull statistics from 0° unidirectional data. Stiffness is calculated using the rule of mixtures modified, if necessary, by the correction for delamination suggested by O'Brien[72] (see Section 3.3.4). The strain at fatigue life "runout" is calculated by determining the maximum possible local strain

concentration due to ply isolation, by a simple rule of mixtures, and dividing this into the maximum strain level below which fatigue life in the 0° unidirectional layup is greater than 10^7 cycles. The fatigue stress-life curve is constructed by first determining the scatter at 10^0 cycles, i.e., under monotonic tension load. Scatter in the monotonic tension properties is determined by free body type strain concentration analysis for discerning whether 0° fiber failure criterion 2 or 3 applies, and adjusting the scatter factor as discussed in Section 4.1. A line drawn between the lower 2σ scatter band at 10^0 cycles to the strain (or stress) at a "runout", arbitrarily selected at 10^6 cycles, provides a lower bound to the fatigue stress-life curve. An upper bound is obtained by connecting a line from the upper 2σ scatter band at 10^0 cycles to a point at "runout" equidistent from the lower bound line on the strain axis. Scatter in fatigue life is automatically given by the two described bounds. As previously mentioned, the lower bound for matrix damage initiation (which does not lead to coupon fracture) can be determined by strain energy release rate analysis.

Estimating the stress (strain) - life curve for laminates containing 0° plies and subjected to tensile load thus appears to be possible based upon: 1) lamina data, for use in the free body type of analysis for calculating strain concentration; 2) fatigue data for the 0° plies, or other reasonable estimate of the maximum strain for "infinite" life in the 0° plies; 3) a rule of mixtures analysis for determination of dominance of criterion 2 or 3 based on the free body type analysis; and 4) calculation of the lower bound of the fatigue life curve by dividing the strain for "infinite" fatigue life of the 0° plies by the strain concentration factor.

4.3 RESIDUAL STRENGTH LOADING

o DAMAGE STATE AND STIFFNESS CHANGE

Neither the damage state nor associated stiffness changed during residual strength loading beyond that observed at the end of fatigue loading. This

result makes analytical sense since a single load cycle cannot cause much change once matrix crack saturation has occurred, which happens early in fatigue life for most layups or never occurs in a few laminates like the $(0/45/0_2/-45/0)_s$ layup. Further, additional delamination growth must be fairly extensive to be reflected in significant stiffness change.

o STRAIN TO FAILURE

The average strain to failure of the $(0/90/\pm45)_s$ coupons subjected to residual strength loading was found to be the same as the monotonic loading despite the presence of often extensive delamination. The reason for this can again be based on criterion 2 of Section 4.2. The effect of a local strain concentration in the 0° plies, due to $\pm45^\circ$ ply isolation by delamination and matrix cracking, is so high (1.43) that coupon failure occurs rapidly. However, if fatigue loading is interrupted prior to failure and the coupon is loaded monotonically to failure, the probability of having that same severe strain concentration condition is so low that the average strain to failure remains unchanged. Thus coupon failure during fatigue loading can be explained for the same reason that residual strain to failure cannot be found to change.

The average residual strength of the $(0/90/\pm45)_s$ coupons was, however, somewhat lower than the original strength due to fatigue load induced stiffness decrease. Although stiffness decrease does correlate well with delaminated area only average residual strength correlates with stiffness change. This is because strain to failure is a highly stochastic processa and residual strength strain to failure is not significantly influenced by the damage state.

Up to a 6 percent decrease in strain to failure during residual strength experimentation has been observed in $(0/45/90/-45)_{2s}$ coupons[32]. In this layup, a common 0° ply strain concentration is that due to local isolation of the 90° ply which results in a ten percent increase in local strain, see

Table 47. This is in contrast to the $(0/90/\pm45)_s$ layup where isolation of the most likely plies, $\pm45^\circ$, results in a 47 percent increase in local strain concentration. Thus if the initial maximum strain under fatigue loading is low enough, local 90° ply isolation can occur without coupon failure in the $(0/45/90/-45)_{2s}$ laminate. Therefore, if a coupon containing local 90° ply isolation is loaded in monotonic tension prior to fatigue failure, some reduction in strain to failure would be observed. However, this effect should lessen as the initial fatigue strain is increased because of the proportionately greater effect of strain concentration. This was indeed observed by Ryder and Walker[33] where the residual strain to failure for this laminate differed by less than 1 percent from the original monotonic strain to failure for coupons at high fatigue load, but by 6 to 7 percent for coupons at a lower fatigue load.

O'Brien[34] observed the same lack of residual strength strain to failure change for a $(\pm45/0/90)_s$ layup loaded at a relatively low fatigue strain level. This case is similar to that for the $(0/90/\pm45)_s$ layup of this study. However, in the $(\pm45/0/90)_s$ layup at higher strain levels, the dominant +45/-45 interface delaminations can significantly extend along the +45 transverse matrix cracks. Such delaminations can also be of large area. This does not generally occur in the $(0/90/\pm45)_s$ laminate where the 90/45 interface delamination is dominant. In the $(\pm45/0/90)_s$ laminate, the 1.37 strain concentration is low enough and the extent of +45/-45 interface delamination usually large enough that under residual strength loading a reduced strain to failure may be exhibited. O'Brien[34] observed that two high strain coupons of a $(45/-45/0/90)_s$ laminate had a reduced strain in residual strength loading and that both coupons indeed did have delamination along the $+45^\circ$ matrix cracks.

For the $(0/\pm45)_s$ layup, initial strains have to be fairly high to induce fatigue failures because the layup tends not to delaminate. However, when delamination occurs and when the $\pm45^\circ$ plies are thereby locally isolated, associated local strain concentrations in the 0° plies are 1.15 to 1.26.

These are high enough to quickly raise local strains to 0.0090 to 0.0100, a range associated with a very short fatigue life for the 0° plies. Hence, once again, if a fatigue loaded coupon is subjected to a residual strength experiment, the probability of observing a strain to failure below the average original monotonic value is low. This is because the probability is remote of interrupting the fatigue load during the time when a significant local strain concentration has occurred and before the fast failure event of, perhaps, a few cycles. Therefore, the average strain to failure in this laminate was unchanged from the original value. However, as for the $(0/90/\pm 45)_s$ coupons, average residual strength was reduced a few percent since stiffness decreased during the prior fatigue loading.

The results of the residual strength experiments for the $(0/45/0_2/-45/0)_s$ layup are again traceable to the damage state and failure criteria 2 and 3 of Section 4.2. Like the $(0/\pm 45)_s$ laminate, this layup does not tend to significantly delaminate. If delamination does develop the combination of delamination and matrix cracking results in 45° ply isolation associated with a local strain concentration of at most 1.07, see Table 47. This low strain concentration is generally not sufficient to result in 0° ply fracture unless initial cyclic strains are quite high, say above 0.0085. Therefore, continued fatigue cycling at strains between 0.0070 - 0.0085 leads to more and more 0° fiber fracture and eventual coupon failure when a statistically significant local concentration of fiber fracture develops (see Section 3.5.2). In contrast to the previous two layups, if cycling of a coupon is interrupted, there is a high probability that large amounts of induced 0° fiber breakage will be present. The additional increase in strain that occurs during a residual strength test will most likely induce a statistically significant combination of fiber breakage rather soon after the maximum fatigue strain is exceeded. This will result in a slightly lower average strain to failure than the original monotonic tension coupons. A 9 percent decrease was found experimentally, see Section 2.4. This failure scenario not only explains why most coupons should have some reduced strain to failure, but also that the amount of decrease should not generally

relate directly to the extent of matrix cracking or delamination. Such damage has only a relatively small effect on fiber breakage in this layup and thus should be only roughly correlated with strain to failure. This was also experimentally observed in Section 2.4, where the strains to failure of all residual strength coupons were decreased below the average monotonic tension value. The largest decrease did roughly correlate with delamination extent, but some delaminated coupons had a relatively high strain to failure and some undelaminated ones, a relatively low value.

Finally, for the $(0_2/90_4)_s$ coupons a rather familiar description applies to the observed average strain to failure in residual strength. The effect of local strain concentration and fracture of 0° fiber bundles results in strain to failure under residual strength loading being essentially the same as that under monotonic loading, 0.0089 versus 0.0090. Initial fatigue strains must be fairly low to obtain a reasonably long fatigue life because of 0° fiber bundle isolation and fracture. The development of local complete ply isolation essentially eliminates the large stress concentration due to the 90° ply transverse matrix cracks. The effect of this is that interrupting a coupon prior to fatigue failure for a residual strength test either results in a strain to failure determined by high stress concentration induced by the presence of complete ply isolation or by that induced by the transverse cracks if no delamination exists. These two effects have essentially the same magnitude, but are not locally additive since only one or the other has an effect. Therefore, the average residual strength strain to failure is close to that of the original monotonic tension coupons which contain only transverse matrix cracks. The fracture of 0° fiber bundles could potentially further reduce the residual strength strain to failure, but clearly this is not a large effect because the residual strength strain to failure is so close to the monotonic tension value. This effect is small because the bundle widths are small (2.5 mm or less) and few of them fracture prior to loading for residual strength. If many bundles fracture, coupons would fail under fatigue loading.

o FRACTURE APPEARANCE

As for the monotonic and fatigue coupons, the 0° plies of the residual strength coupons tended to fracture parallel to the adjacent ply. The reason was the same as that previously discussed in Section 4.1.

4.4 SUMMARY OF ANALYTICAL/EXPERIMENTAL RESULT COMPARISON

A summarizing set of tables and figures was prepared which compare the experimentally obtained results for each laminate and those expectable based upon the analytical results. The material properties shown in Table 68 were used to calculate the analytical results. These lamina data appeared to be reasonably good values, but will of course, lead to slight errors in the laminate results because of batch-to-batch property variations.

Table 69 shows the comparison summary of average values for the monotonic tension experiments. Delamination tendency was anticipated based on the magnitude and sign of the free edge stresses for these layups. This table is a summary of the comparisons discussed in detail in Section 4.1. Stiffness was calculated using the ADVLAM laminate snalysis code. The stiffness loss was calculated using the observed matrix crack spacing and the effective stiffness analysis of Section 3.3.1. Little additional loss would be expected even at full saturation of each ply unless large end delaminations occurred at the crack tips. This was neither a generally anticipated[7,13,40] nor experimentally observed phenomenon. Strain to failure was based upon Weibull statistics and the 0° unidirectional strain to failure properties, see Section 3.6. For the $(0_2/90_4)_s$ laminate, the additional effect of a large strain concentration at the transverse crack tips due to the 8 layer thick 90° ply was qualitatively estimated based upon the study by Crossman et. al.[52]. Strength was calculated by the multiplication of stiffness, reduced by the loss associated with full matrix crack saturation, and the expected strain to failure.

TABLE 68
LAMINA PROPERTIES USED IN
SUMMARY COMPARISON OF ANALYTICAL AND EXPERIMENTAL RESULTS

E_{11} = 163.4 GPa (23.7 Msi)

E_{22} = 10.2 GPa (1.48 Msi)

$G_{12} = G_{13}$ = 6.48 GPa (0.94 Msi)

G_{23} = 3.79 GPa (0.55 Msi)

$\nu_{12} = \nu_{13}$ = 0.30

ν_{23} = 0.54

$(0)_4$ strain to failure = 0.0098

$(0)_{16}$ strain to failure = 0.0095[6]

0° strength Weibull exponent, α, = 18.4[88]

TABLE 69

COMPARISON OF ANALYTICALLY AND EXPERIMENTALLY OBTAINED MONOTONIC TENSION PROPERTIES

NOTE: Average values; first entry is the analytically determined value while the second was experimentally determined.

	$(0/90/45/-45)_s$		$(0/45/90/-45)_{2s}$		$(0/45/-45)_s$		$(0/45/0_3/-45/0)_s$		$(0_3/90)_{4s}$	
Delamination Tendency	low	not observed	low	not observed	low	not observed	low	not observed	low	not observed
Stiffness, GPa (Msi)	53.1 (7.70)	53.0 (7.69)	53.1 (7.70)	53.8 (7.81)	58.2 (8.43)	56.9 (8.25)	98.6 (14.3)	102.1 (14.8)	52.6 (7.63)	51.0 (7.39)
Maximum % Stiffness Loss	1.4	1.5	3 to 5	3 to 5	1.8	1.7	<0.2	<0.2	6.2	6.0
Strain to Failure	0.0106	0.0103	0.0107	0.0105	0.0106	0.0106	0.0106	0.011?	~0.0090	0.0090
Strength, MPa (ksi)	552 (80.0)	548 (79.5)	551 (79.9)	547 (79.3)	604 (87.5)	609 (88.3)	1056 (153)	1145 (166)	445 (64.5)	432 (62.6)
Dominant Fracture Angle	90^o	90^o	$+45^o$	$+45^o$	$+45^o$	$+45^o$	$+45^o$	$+45^o$	90^o	90^o
Weibull Exponent for Strength	35	--	35	34	25	--	25	--	20	--
Strength Coefficient of Variation, Percent	3.5	3	3.5	3.5	5	9	5	4.3	7	9

The remaining three anticipated properties were obtained somewhat more qualitatively. The dominant fracture angle of the entire coupon is essentially that which occurs in the 0° plies and thus is determined by the local stress concentration and the angle of the adjacent ply. An estimate of scatter can be anticipated based upon the Weibull type statistical variation in strength. The limiting scatter case occurs for the 0° unidirectional laminates. Any laminate containing off axis plies reduces the inherent scatter of the 0° plies because of development of local strain concentration due to ply isolation. Thus, the greater the amount of possible strain concentation due to ply isolation. the less the scatter in strength. Such ply isolation occurs under monotonic load only very near failure in these layups and thus does not significantly affect the strain to failure, as discussed in Section 4.1. In fact, for the non quasi-isotropic layups, very little ply isolation was observed to develop under monotonic tension loading. For the $(0/45/0_2/-45/0)_s$ and $(0_2/90_4)_s$ layups no ply isolation was observed.

Scatter in the $(0_2/90_4)_s$ laminate monotonic tension properties is greatly affected by the 90° ply transverse matrix cracks. The high stress concentration due to these transverse cracks not only reduces the average strain to failure, but also can result in coupon fracture long before the matrix crack density becomes large. This occurred in coupons A1 and A23. This effect of the transverse cracks leads to scatter in the $(0_2/90_4)_s$ monotonic tension data being even larger than that for the $(0)_4$ unidirectional coupons.

Based upon the above discussion, the Weibull scatter parameter for the $(0_2/90_4)_s$ layup was qualitatively estimated to be slightly less (higher scatter) than the 0° unidirectional value of 18.0. The scatter in the $(0/45/0_2/-45/0)_s$ and $(0/45/-45)_s$ layups was considered to be qualitatively less than that for the $(0_2/90_4)_s$ layup and thus arbitrarily, but reasonably, put at 25. The parameter for the quasi-isotropic layups was placed at 35 because their scatter should be significantly less than that of the other

layups since local strain concentrations of up to 1.54 can develop. The coefficient of variation values are based upon the Weibull scatter parameters and were included to allow fatigue curves to be drawn as discussed later. All of these values were obtained based on the assumption that some coupons did not have manufacturing induced defects not present in others. Such a situation should lead to significantly increased scatter, as experimentally confirmed[6,7].

The excellent correlation is apparent in Table 69 between the analytically anticipated results and the experimental results. The scatter in strength for the $(0/45/-45)_s$ laminate is higher than anticipated, but this is believed to be due to the manufacturing defect problem with these coupons as discussed in Section 2.3. The experimentally determined strain to failure, hence strength, for the $(0/45/0_2/-45/0)_s$ laminate is approximately five percent higher than that anticipated, but this is believed to be attributable to batch-to-batch variations in material properties. The anticipated Weibull scatter parameters appeared to be reasonable qualitative estimates for coupons without significant anomalies.

In Table 70, analytically anticipated and experimentally determined fatigue properties are compared. The analysis techniques were detailed in Section 3 and their applicability discussed in Section 4.2; Table 70 is simply a summary. The extent of stiffness loss for the $(0/45/90/-45)_{2s}$ layup was not recorded for most coupons, hence the accuracy of the analysis could not be checked. The extent of scatter was estimated qualitatively based upon the nature of the parameters which control scatter as discussed in Section 4.2.

Based upon Tables 69 and 70, fatigue stress-life curves were estimated for each of the five laminates and compared to the experimental results. The fatigue life at 10^0 cycles was estimated using the analytically derived data of Table 69. A "runout" strain, converted to stress, was obtained from Table 70. This runout strain was placed at 10^6 cycles on a logarithmic scale. This was done for two reasons. First, any shorter fatigue life is

TABLE 70

COMPARISON OF ANALYTICALLY AND EXPERIMENTALLY OBTAINED FATIGUE PROPERTIES

	$(0/90/45/-45)_s$		$(0/45/90/-45)_{2s}$ [7,13]		$(0/45/-45)_s$		$(0/45/0_2/-45/0)_s$		$(0_2/90_4)_s$	
Delamination Tendency	high	delam-inates	high	delam-inates	low	small de-lamination	low	small de-lamination	high	delam-inates
Stiffness Change Matrix Cracking	2.0-2.3	2.0-2.5	3 to 5	3 to 5	3.6	<4.0	0.2-0.5	<0.5	5.5-7.9	5.5-7.5
Matrix Cracking & Delamination	2.9-15.0	2.9-19.3	up to 22	>6.7	0.5-7.0	0.5-6.9	0.2-1.0	<1.0	6.0-16.3	5.7-17.1
Strain for "Short" Fatigue Life	>0.0080	>0.0080	>0.0080	>0.0080	>0.0080	>0.0080	>0.0080	>0.0080	>0.0070	>0.0070
Strain at "runout"	0.0052	0.0060	0.0052	0.0044	0.0067	0.0070	0.0075	0.0075	<0.0061	<0.0050
Estimated Scatter (Order of Magnitude)	1 to 1	1 to 2	1 to 2	1 to 2	>2	>2	>2	>2	>2	>2
Dominant Failure Angle	90^o	90^o	45^o	45^o	45^o	45^o	45^o	45^o	90^o	90^o

not traditionally considered as a "runout", long fatigue life. Second, selecting any longer life does not significantly affect the curve boundaries and 10^6 does provide a convenient, conservative fatigue life estimate. Thus a lower boundary for the fatigue stress-life curve was drawn as a straight line between the lower scatter boundary estimate at 10^0 cycles and the fatigue "runout" stress at 10^6 cycles. An upper bound was selected as a constant vertical width above the lower bound with the width being equal to the static scatter band. This rather simplistic approach gives a straight line fatigue stress-life curve. The more traditional S shape would be more realistic because the scatter in fatigue life for coupons loaded near the static ultimate strength is still quite large. However, the simplified approach did not prove to be particularly unrealistic. Prediction of a lower bound for damage development with eventual coupon fracture requires a strain energy release rate analysis as previously discussed.

In Figures 116 to 120, the analytically derived fatigue stress-life curves are compared to the actual fatigue data. In the calculation of the fatigue curves, no allowance was made for the effect of stress range. This is known to affect the fatigue curve and thus cannot be ignored[6]. For the fatigue load experiments conducted at R = +0.1 in this program, the effect is small[6] but the curves would generally be raised somewhat making them even closer to the actual data. For the $(0/90/\pm45)_s$ layup, Figure 116, the analytical curve is somewhat conservative compared to the actual data, although a more realistic and traditional S shaped curve combined with accounting for the R = +0.1 stress ratio would almost completely correct this conservatism. In Figure 117, the analytically based curve and the experimental data agree extremely well partially due to the fact these data were obtained at R = 0.0 and not +0.1 as for the other layups. The "runout" strain has been observed[7] to be slightly lower than that theoretically anticipated in Table 70, but that may possibly again be due to batch-to-batch variations. In addition, the assumption of a long life at 0.0080 strain for 0^0 unidirectional coupons is somewhat unconservative. The $(0/\pm45)_s$ data in Figure 118 again shows a good fit to the analysis curve as

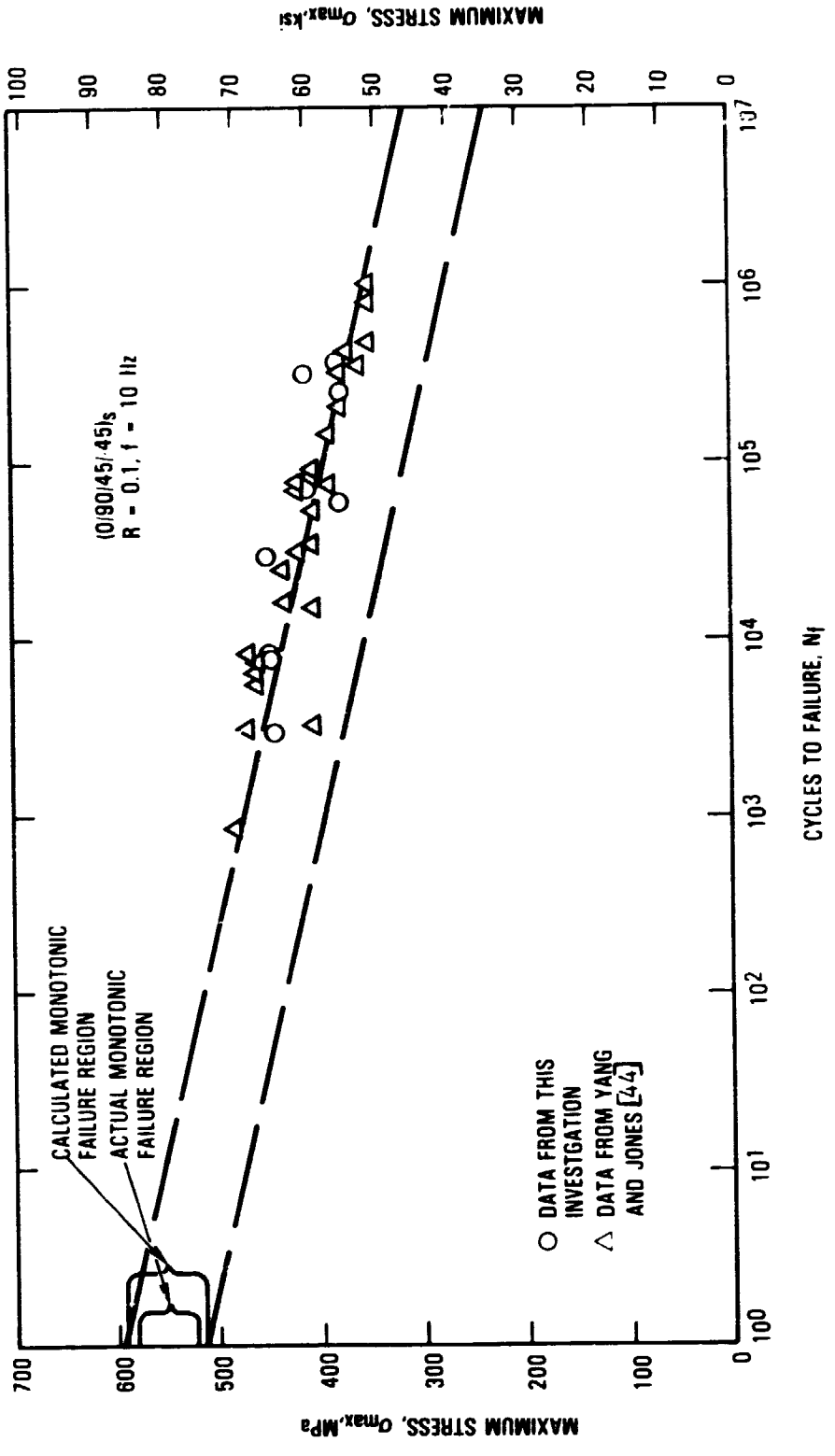

Figure 116. Comparison between analytically derived stress-life relation and experimental data for $(0/90/45/-45)_s$ coupons.

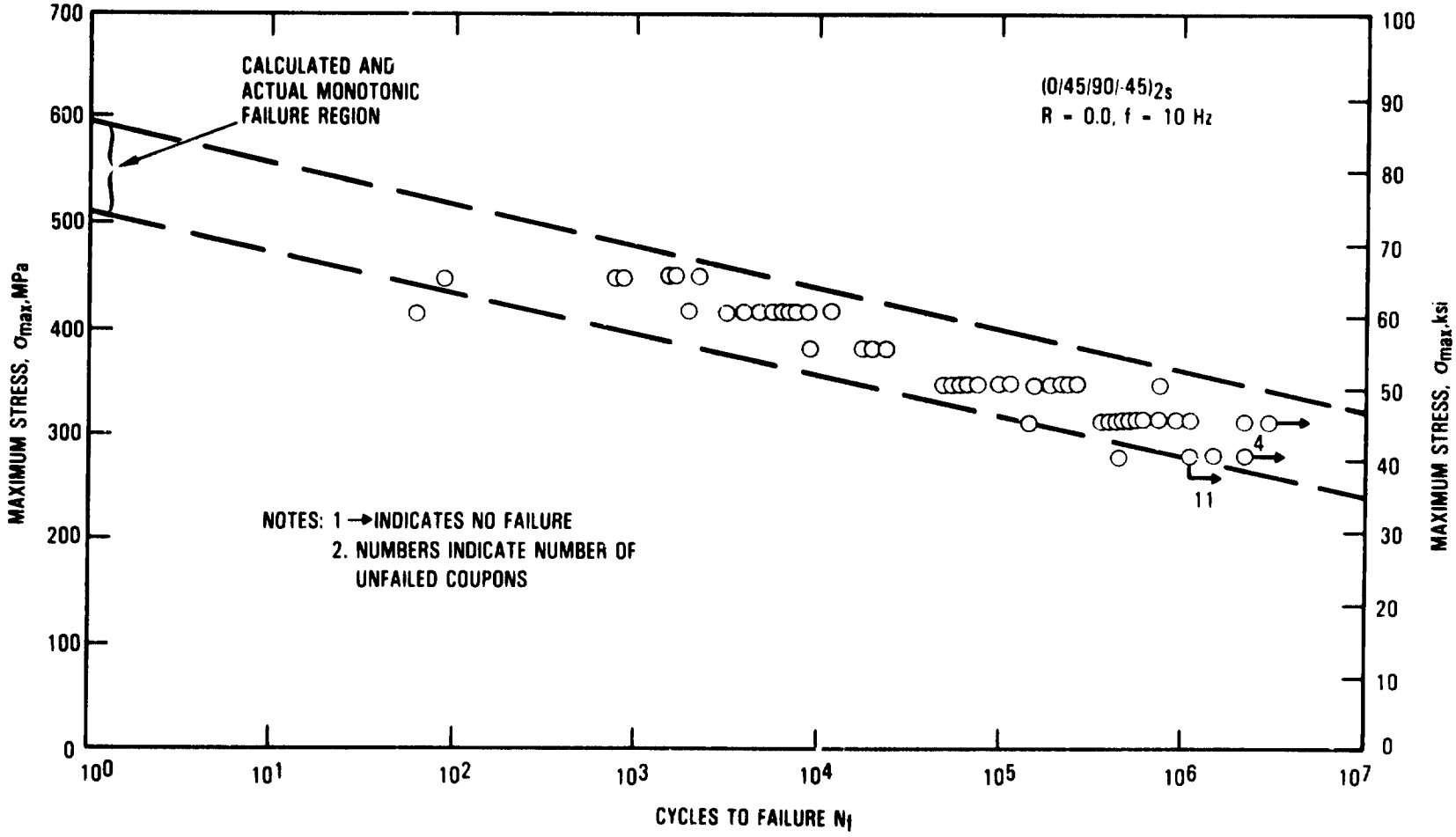

Figure 117: Comparison between analytically derived stress-life relation and experimental data for $(0/45/90/-45)_{2s}$ coupons.

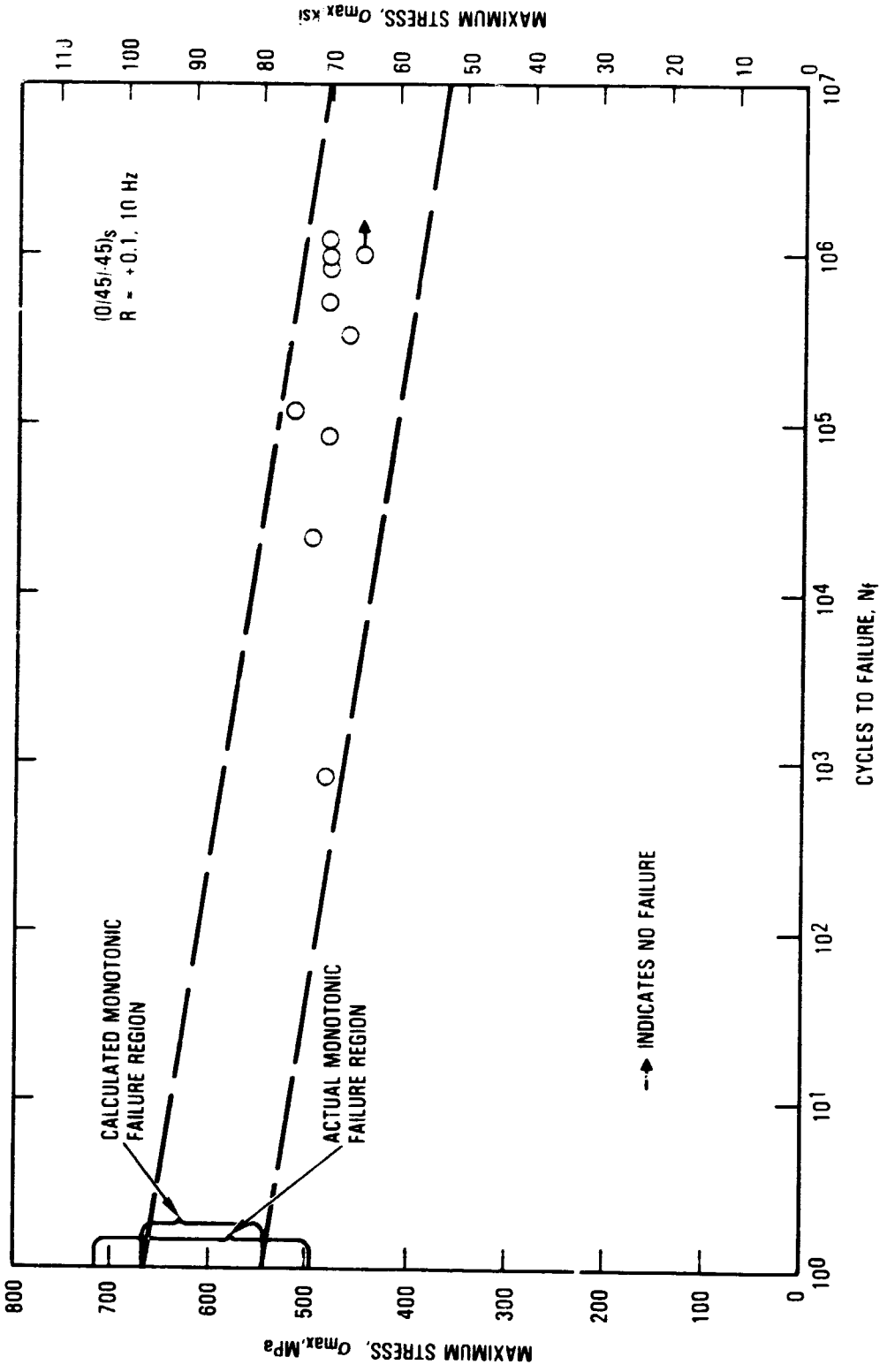

Figure 118: Comparison between analytically derived stress-life relation and experimental data for $(0/45/-45)_s$ coupons.

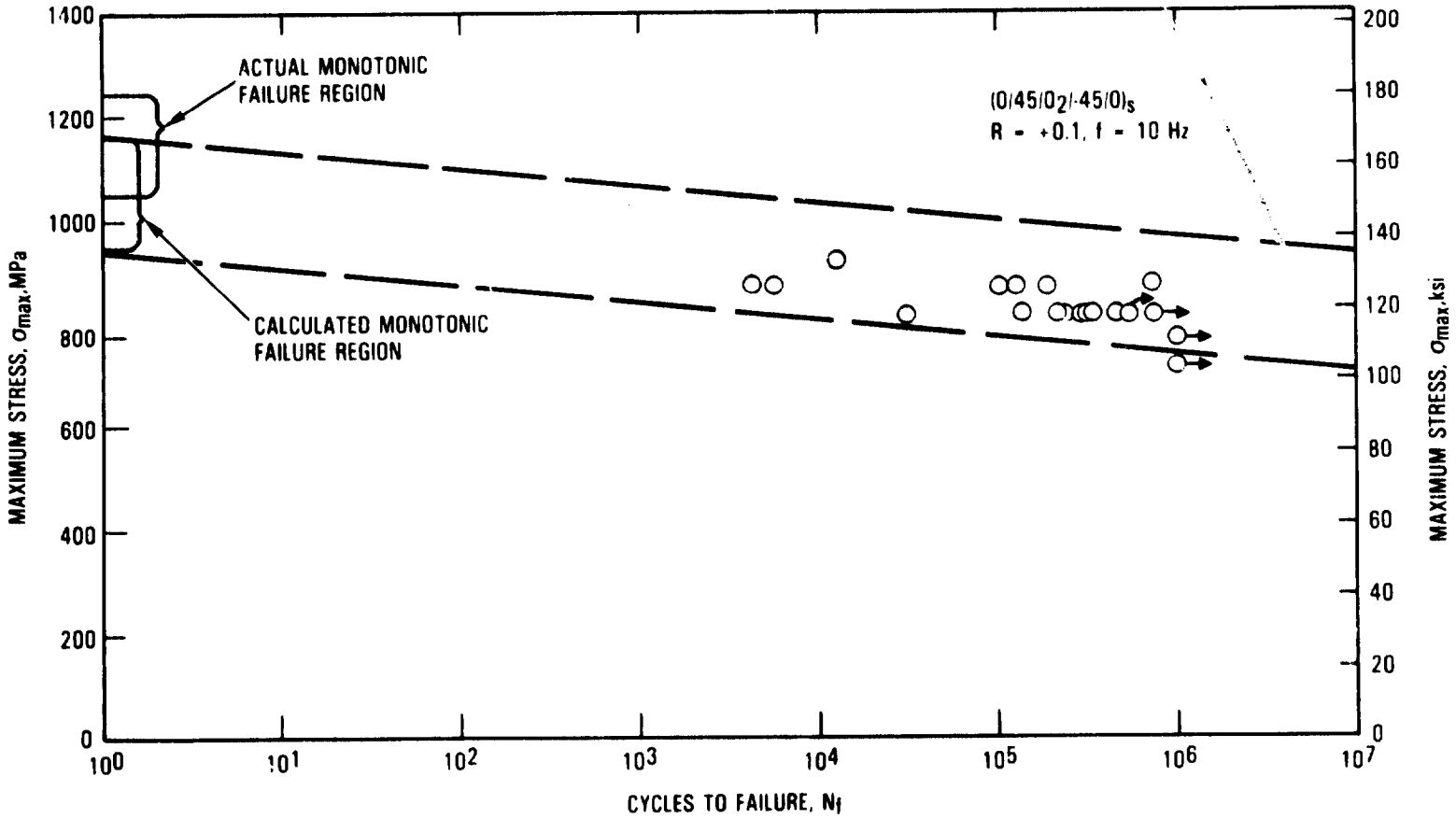

Figure 119: Comparison between analytically derived stress-life relation and experimental data for $(0/45/0_2/-45/0)_s$ coupons.

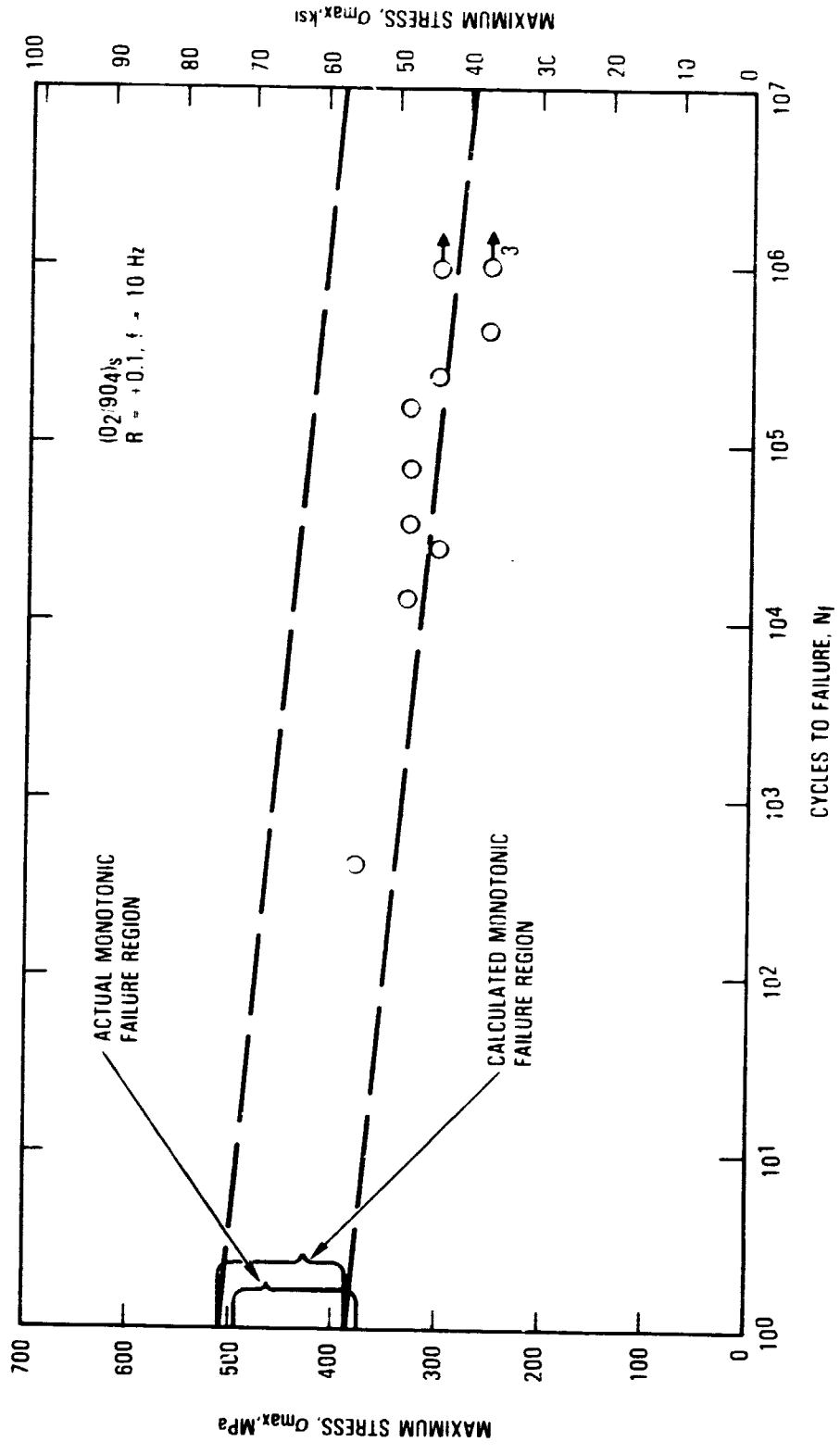

Figure 120 : Comparison between analytically derived stress-life relation and experimental data for $(0_2/90)_4{}_s$ coupons.

do the $(0/45/0_2/-45/0)_s$ data in Figure 119. If the effect of R ratio were accounted for, they would be in even closer agreement. For the $(0_2/90_4)_s$ data, Figure 120, the analytical curve is not conservative although the data still fit well. The error in conservatism was expected because the effect of the 0° fiber bundle breakage was not taken into account. Note, however, that Figure 120 indicates that this effect is small because the analytical and experimental results are in close agreement.

A summary comparison of analytical and experimental results for the residual strength experiments is given in Table 71. The lack of any analytically anticipated further significant changes in damage state and stiffness change was based upon the previously mentioned fact that one additional cycle for these layups cannot have a large effect since the majority of the possible changes have already occurred. The reasons for the observed average strain to failures were discussed in Section 4.3. For the $(0/90/45/-45)_s$ laminate, no change in strain to failure compared to the monotonic tension value was expected and none was observed. A similar result occurred for the $(0/45/-45)_s$ and the $(0_2/90_4)_s$ laminates. The maximum analytically anticipated percent change in the strain to failure of the $(0/45/90/-45)_s$ laminate was 11 percent as compared to an observed value of 9 percent. For the $(0/45/0_2/-45/0)_s$ laminate, the initial fatigue load strains were high enough to lead to significant 0° fiber fracture and thus a potentially reduced strain to failure in residual strength. The analytical estimate of an 11 percent decrease in strain to 0.0010 was based upon a qualitative evaluation. Residual strength was estimated by multiplying the range of analytically expected stiffness values, those decreased by matrix cracking and delamination, and the anticipated strain to failure. The comparisons again appear to be reasonable.

4.5 SUMMARY

The results of the analytical part of this investigation appeared to compare extremely well to the experimental results. Two important conclusions were

TABLE 71

COMPARISON OF ANALYTICALLY AND EXPERIMENTALLY OBTAINED
RESIDUAL STRENGTH PROPERTIES

	$(0/90/45/-45)_s$		$(0/45/90/-45)^{[7,13]}_{2s}$		$(0/45/-45)_s$		$(0/45/0_2/-45/0)_s$		$(0_2/90_4)_s$	
Damage State change from fatigue	none	very small	none	none	none	none	none	none	none	none
Stiffness change from fatigue	none	none	none	none	none	none	none	none	none	none
Average Strain to Failure	0.0106	0.0103	0.0096	0.0092	0.0106	0.0106	0.0010	0.0102	0.0090	0.0089
Strength Range MPa (ksi)	479 (69.4) 546 (79.2)	452 (65.5) 526 (76.3)	--[a]	--[a]	573 (83.1) 614 (89.0)	558 (80.9) 594 (86.1)	986 (143)	1035 (150)	397 (57.5) 445 (64.5)	361 (52.4) 511 (74.1)
Dominant Fracture Angle	90^o	90^o	45^o	45^o	45^o	45^o	45^o	45^o	90^o	90^o

a = Experimental data on strength are from different material batches where stiffness data were not obtained, hence no comparison was possible.

based upon the comparison. First, a relatively simple procedure exists for estimating monotonic strength, fatigue life, and residual strength properties of multi-angle ply laminates based only on lamina properties. Second, given a known damage state, stiffness and strength can be accurately calculated. However, remaining fatigue life for a particular coupon is a highly stochastic variable and cannot be reliably estimated knowing the damage state. The procedure for estimating strength, fatigue life and residual strength consists of the following steps:

1. Calculation of strain to failure based upon 0° unidirectional strain to failure along with a calculation of the effect of volume;

2. Calculation of stiffness by simple laminate analysis using lamina properties;

3. Calculation of reduced stiffness by accounting for effect of saturated matrix cracking (and delamination, if necessary);

4. Calculation of strength by multiplying reduced stiffness by estimated strain to failure;

5. Estimation of scatter based upon statistical scatter of 0° unidirectional laminate monotonic tension failure data and qualitative adjustment for effect of ply isolation;

6. Calculation of a lower bound strain for the fatigue curve by determining the largest strain concentration due to ply isolation and dividing this into the lower bound fatigue strain for a 0° unidirectional laminate;

7. Construction of an S-N curve as per the procedure described in Section 4.2;

8. Estimate of strain to failure under residual strength loading by calculating possible types of ply isolation;

9. Estimate of range of possible stiffness values during residual strength experimentation by allowing for transverse matrix cracking, delamination, and ply isolation.

10. Calculation of range of residual strength by multiplying estimated strain to failure by estimated range in stiffness.

This procedure is simple and straight forward and requires no complex analysis. The general validity of the procedure requires further verification by calculating anticipated results for new layups followed by experimental verification or refutation.

SECTION 5

CONCLUSIONS, IMPLICATIONS, RECOMMENDATIONS

In this section, a summary is given of each of the major conclusions drawn from this study, followed by a discussion of some of the implications, and finally by a list of recommendations for future research.

5.1 CONCLUSIONS

The principal conclusions reached during this investigation are listed below in the order in which they were discussed in the first four sections. The number in parenthesis after each conclusion refers to the section in which the relevant idea is primarily discussed.

- If a damage state is known, stiffness and strength can be relatively simply calculated (4).
- Residual strength is not directly related to fatigue life (4).
- Exclusive of external impact, changes in laminate stiffness are associated with seven possible damage conditions. These are:
  1. Transverse matrix cracking.
  2. Interaction of relative stiffness of adjacent constraining plies and transverse cracks.
  3. Transverse matrix cracks with end delaminations
  4. Interply delamination.
  5. Isolation of an off axis ply from the loading.
  6. Ply splitting.
  7. Fiber fracture.

- Change in stiffness is primarily associated with: 1) transverse matrix cracking; 2) interply delamination; and 3) local ply isolation due to combined matrix cracking and delamination (3.3, 3.4, 4.1, 4.2).

- Relative stiffness of constraining plies, 0° ply splitting and fiber fracture combined have only a small effect on stiffness change (3.3.2).

- Small delaminations at the end of transverse matrix cracks are potentially associated with significant stiffness change, but since they do not generally extend into the coupon interior they do not usually have a large effect (3.3.3).

- Of the many theories discussed as possible criteria for inducing 0° fiber and ply fracture, three were found to be compatable with experimental results (3.4). These are:

  1. **Local stress concentrations at transverse crack tips;**

  2. **Local stress concentration due to isolation of adjacent plies because of delamination and transverse matrix cracking calculated by free body type analysis;**

  3. 0° ply stress above threshold of 0° unidirectional fatigue failure.

- Other possible theories of 0° ply fracture did not appear to be reasonable (3.4). These were:

  1. Deterministic strength theories,

  2. Statistical fiber bundle theory,

  3. Linear elastic fracture mechanics,

  4. Free edge stresses,

  5. In-plane cracks within the 0° plies.

- Complex, costly, and time consuming 3-D finite element analysis of damage states does not necessarily lead to great improvements in accuracy of estimated stress concentrations (3.5). Relatively simple two dimensional free body type models of damage state, which can be used to bound a problem, appear to be of more value than complex three dimensional models which actually may only be providing conservative estimates of stress concentration.

- Stress concentrations do occur due to the presence of damage, but generally sharp stress concentrations do not occur in the primary load carrying 0° ply. Hence, fracture toughness concepts do not lead to useful failure criteria for laminates (3.4, 3.6).

- Damage growth (both direction and rate) generally depends on complex relations among G_I, G_{II}, and G_{III}. In addition, assumed models must be constantly altered to accomodate growth. This renders the use of such complex 3-D models questionable (3.5).

- The strain to failure of a 0° ply is dependent upon volume and thus the strain to failure under monotonic load of a 0° unidirectional laminate can be related to those laminates containing off axis plies by a Weibull type statistical analysis of volume ratios (3.6).

- Statistical scatter in properties is primarily believed to be due to: 1) the intrinsic size of the microstructure relative to the geometric dimensions; 2) the variability in fiber strength; 3) the requirement of only a few adjacent statistically significant fiber fractures to trigger general failure of a 0° ply; 4) local strain concentration due to combined delamination and matrix cracking.

- A relatively simple procedure exists for anticipating monotonic, fatigue, and residual strength loading properties of unnotched, laminated graphite/epoxy coupons (containing at least some 0° plies) based only upon lamina properties (4).

- The relation between damage state and fatigue life of a particular coupon is highly stochastic. Thus the fatigue life of individual coupons is quite difficult to predict. Instead, anticipation of the population life is a more reasonable undertaking (4).

5.2 IMPLICATIONS

Based upon the results of the experiments and the analysis, the success of the analytical and experimental comparison, and upon the conclusions of Section 5.1, several implications were drawn. These implications are conclusions in a sense, but not as well demonstrated as those in Section 5.1.

- The analytical study resulted in an explanation of disparate experimental results from many different investigations. For many, if not most layups, residual strength does not decrease except just before fatigue failure. The "sudden death" representation of residual strength degradation[15] is correct for these layups. For some quasi-isotropic layups, residual strength does decrease, although not in a smooth fashion. Thus representations which assume residual strength degradation[14,16,19] are partially correct.

- The simplified procedure for estimating monotonic, fatigue, and residual strength properties provides a basis for comparing one laminate to another in a design type format.

- The empirically based awareness that thick plies lead to potential difficulties can be analytically understood and anticipated based on the results of this study combined with that of other investigations (see, for example, Reference 83).

- This investigation has shown that relatively simple analysis procedures exist for estimating strength, constant amplitude fatigue, and residual strength properties under tension load of unnotched laminated graphite/epoxy composites. The implication is that not only do such techniques exist for the unnotched case, but also for the notched case.

  Further understanding and anticipation of the fatigue properties of notched coupons could be studied as an extension of the tension loaded case. For example, consider a quasi-isotropic laminate. First, the notched strength can be estimated by well known simple approaches[100]. Second, the lower bound of the fatigue curve can be estimated using the reasonable assumption that fatigue loading leads to local ply isolation at the notch. Hence, any global applied strain less than approximately 0.0080 divided by the maximum stress concentration (1.54 for quasi-isotropic laminates) leads to excessively long "infinite" fatigue life. Allowance must, of course, be made for the effect of the reduced section size of the notch. As a first approximation, this might be estimated by dividing the ratio of the areas into the lower bound strain estimate giving a further reduction. Naturally a more rigorous analysis is required to support such a simple supposition, but the fit to experimental data is quite reasonable as shown in Figure 121.

  The difference between the calculated lower bound fatigue life "runout" strain and that due to a circular notch is

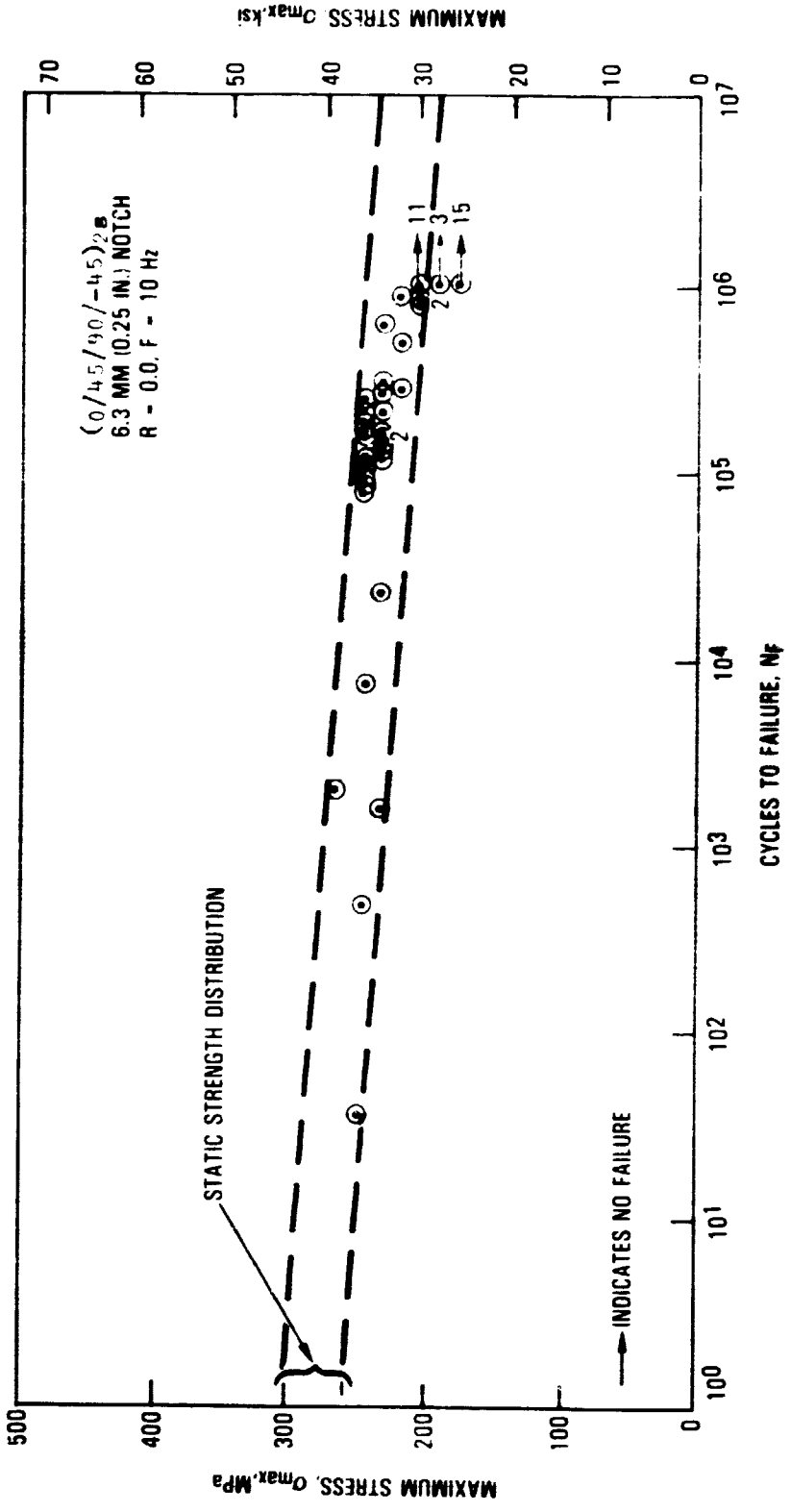

Figure 121: Notched tension-tension fatigue test results for a $(0/45/90/-45)_{2s}$ laminate, R = 0.0.

relatively small. Further, any higher globally applied strains lead to high local strains due to ply isolation. This leads to large scatter in fatigue life since local strains in the 0° are then above 0.0080. At this strain level the scatter in the fatigue life is now determined by the 0° plies. In addition, before significant delamination develops notch acuity may greatly reduce the life of a few "weak" coupons. Therefore, the fatigue stress-life curve should be narrowly bounded and have large scatter. This type of data is shown in Figure 121.

- Perhaps, even for the case of spectrum fatigue loading, relatively simple procedures exist for estimating response. In Reference 13, indications are given that rather simple rules may apply.

5.3 RECOMMENDATIONS FOR FUTURE RESEARCH

Based upon the conclusions of this investigation and the implications, several recommendations for future research are offered.

- **Confirm the reliability of the analytically based predictive procedure for anticipating strength for laminates which tend to delaminate under monotonic load.**
- Develop anticipated results for other laminates, manufacture the laminates and obtain experimental confirmation of the analytical results.
- Develop analysis techniques which anticipate the effect of R ratio.
- Confirm and further develop the procedure proposed in Section 5.2 for anticipating the effect of notches on fatigue life.
- Investigate the hypothesis of using Weibull type statistical analysis, based on volume, to anticipate the strain to failure of 0° plies.
- Develop analytical models for compression dominated fatigue; investigate the possibility of bounding the fatigue curves by a buckling analysis which primarily considers the geometric constraint conditions.
- Investigate the feasibility of analyzing complex damage states, such as those induced by impact, by simple models of damage, such as partially through-the-thickness holes for non-penetrating impact damage.

REFERENCES

1. Ryder, J.T., and Lauraitis, K.N., "Towards a Qualitative Interpretation of the Response of Laminated Composites to Mechanical Load: Structure and Significance", Presented at the Second United States - Japan Conference on Composite Materials, American Society for Testing and Materials, NASA-Langley Research Center, Hampton, Virginia, June 6 - 8, 1983.

2. Standard Recommended Practice for Constant-Amplitude Axial Fatigue Tests of Metallic Materials, ANSI/ASTM E466-76.

3. Standard Recommended Practice for Constant-Amplitude Low-Cycle Fatigue Testing, ASTM E606-78.

4. Raske, D.T., and Morrow, Jo Dean, "Mechanics of Materials in Low Cycle Fatigue Testing", Manual on Low Cycle Fatigue Testing, ASTM STP 465, American Society for Testing and Materials, 1969, pp. 1-25.

5. Pettit, D.E., Ryder, J.T., and Lautaitis K.N., "Effects of Line Discontinuity in Composite Laminates on Static and Fatigue Strength Distribution", Presented at the 34th National Sampe Symposium, San Francisco, California, May 8 - 10, 1979, published in the Conference Proceedings.

6. Ryder, J.T., "Effect of Load History on Fatigue Life - Task I", AFWAL-TR-80-4044, June 1980.

7. Ryder, J.T., and Walker, E.K., "The Effect of Compressive Loading on the Fatigue Lifetime of Graphite/Epoxy Laminates", AFML-TR-79-4128, October 1979.

8. Kim, R.Y., "Prevention of Free-Edge Delamination", Proceedings of the 28th National SAMPE Symposium and Exhibition, Vol. 28, Material and Processes - Continuing Innovations, Anaheim, California, April 12 - 14, 1983, pp. 200 - 209.

9. Lauraitis, K.N., Ryder, J.T., and Pettit, D.E., "Advanced Residual Strength Degradation Rate Modeling for Advanced Composite Structures, Volume II - Tasks II and III", AFWAL-TR-79-3095, July 1981.

10. Reifsnider, K.L., and Talug, A., "Analysis of Fatigue Damage in Composite Materials", Int. J. Fatigue, January 1980, pp. 3 -11.

11. Wang, A.S.D. and Crossman, F.W., "Initiation and Growth of Transverse Cracks and Edge Delamination in Composite Laminates - Part I An Energy Method", J. Composite Materials, June 1980, also Drexel U. Report, October 1979.

12. Crossman, F.W., Warren, W.J., Wang, A.S.D., and Law, G.L., "Initiation and Growth of Transverse Cracks and Edge Delamination in Composite Laminates - Part II - Experimental Correlation", J. Composite Materials, June 1980, also Drexel U. Report, October 1979.

13. Ryder, J.T., and Lauraitis, K.N., "Effect of Load History on Fatigue Life - Task II", AFWAL-TR-81-4155, December, 1981.

14. Hahn, H.T., and Kim, R.Y., "Proof Testing of Composite Materials", J. Composite Materials, Vol. 9, July 1975, pp. 297 - 311.

15. Chow, P.C., and Croman, R., "Degradation and Sudden-Death Models of Fatigue of Graphite/Epoxy Composites", Composite Materials: Testing and Design (Fifth Conference), ASTM STP 674, S. W. Tsai, Ed., American Society for Testing and Materials, 1979, pp. 431-454.

16. Yang, J.N. and Lice, M.D., "Residual Strength Degradation Model and Theory of Periodic Proof Tests for Graphite/Epoxy Laminates", J. Composite Materials, Vol. 11, April 1977, pp. 431 - 454.

17. Yang, J.N., and Jones, D.L., "Load Sequence Effects on the Fatigue of Unnotched Composite Materials", Fatigue of Fibrous Composite Materials, ASTM STP 723, American Society for Testing and Materials, 1981, pp. 213 - 232.

18. Hahn, H.T., "Fatigue Behavior and Life Prediction of Composite Laminates", Composite Materials: Testing and Design (Fifth Conference) ASTM STP 674, S.W. Tsai, Ed., American Society for Testing and Materials, 1979, pp. 383-417.

19. Halpin, J.C., Waddoups, M.E., and Johnson, T.A., "Kinetic Fracture Models and Fracture Stability", Int. J. Fracture Mechanics, Vol. 8, 1972, pp. 465 - 468.

20. Kulkarni, S.V., McLaughlin, P.V., Pipes, R.B., and Rosen, B.W., "Fatigue of Notched Fiber Composite Laminates: Analytical and Experimental Evaluation", Composite Materials: Testing and Design (Fourth Conference), ASTM STP 617, American Society for Testing and Materials, 1977, pp. 70 - 92.

21. O'Brien, T.K., "The Effect of Delamination on the Tensile Strength of Unnotched, Quasi-Isotropic, Graphite/Epoxy Laminates", Proceedings of the SESA/JSME International Conference on Experimental Mechanics, Honolulu, Hawaii, May, 1982.

22. Ratwani, M.M. and Kan, H.P., "Compression Fatigue Analysis of Fiber Composites", NADC-78049-60, September 1979.

23. Kitagawa, H., Fujita, T., and Miyazawa, K., "Small Randomly Distributed Cracks in Corrosion Fatigue", Proc. 2nd Intl. Conf. on Mech. Behavior of Materials, Boston, 1976.

24. Beaumont, P., "Fracture Strength and Fatigue of Fibrous Composites", Failure Modes in Composites, AIME, 1973, p. 49.

25. Konish, H.J., Jr., Swedlow, J.L., and Cruse, T.A., "Experimental Investigation of Fracture on an Advanced Composite", J. Composite Materials, Vol. 6, January 1972, p. 114 - 124.

26. Tsai, S.W. aand Wu, E.M., "A General Theory of Strength for Anisotropic Materials", AFML-TR-71-12, August 1972.

27. Hoffman, O., "The Brittle Strength of Orthotropic Materials", J. Composite Materials, Vol. I, 1967, p. 200

28. Wu, E.M., "Failure Analysis of Composites with Stress Gradient", Fracture of Composite Materials, Ed. G.C. Sih and V.P. Tamuzs, Sighoff and Noordhoff, Netherlands, 1979, p. 63.

29. Phoenix, S.L., "Statistical Aspects of Failure of Fibrous Materials", Composite Materials: Testing and Design (Fifth Conference), ASTM STP 674, S. W. Tsai, Ed., American Society for Testing and Materials, 1979, pp. 455 - 483.

30. Harlow, D.G., "Properties of the Strength Distribution for Composite Materials", Composite Materials: Testing and Design (Fifth Conference), ASTM STP 674, S. W. Tsai, Ed., American Society for Testing and Materials, 1979, pp. 484 - 501.

31. Wang, A.S.D., Private Communication, July, 1983.

32. Ryder, J.T. and Walker, E.K., "Ascertainment of the Effect of Compressive Loading on the Fatigue Lifetime of Graphite/Epoxy Laminates for Structural Applications", AFML-TR-76-241, December 1976.

33. Grimes, G.C., "Structural Design Significance of Tension - Tension Fatigue Data on Composites", Composite Materials: Testing anad Design (Fourth Conference), ASTM STP 617, American Society for Testing and Materials, 1977, pp. 106 - 119.

34. O'Brien, T.K., "Tension Fatigue Behavior of Quasi-Isotropic Graphite/-Epoxy Laminates", Proceedings of the Third International Symposium on Metallurgy and Materials Science: Fatigue and Creep of Composite Materials, H. Lilholt and R. Tarega Eds., September 1982, Roskilde, Denmark, pp. 259 - 264.

35. Lauraitis, K.N., and Sandorff, P.E., "The Effect of Environment on the Compressive Strength of Laminated Epoxy Matrix Composites", AFML-TR-79-4179, December 1979.

36. Von Druemel, WIM H.M., and Kamp, John L.H., "Non Hookeon Behavior in the Fibre Direction of Carbon-Fibre Composites and the Influence of Fibre Waviness on the Tensile Properties", J. Comp. Materials, Vol. 11, October 1977, pp. 461 - 469.

37. Curtis, G. T., "Non-Hookeon Behavior of Strong Carbon Fibres", Nature, Vol. 220, December, 1968.

38. Averbach, J., and Hahn, H.T., "Fatigue and Proof Testing of Unidirectional Graphite/Epoxy Composites", Fatigue of Filamentary Composites, ASTM STP 636, K.L. Reifsnider and K.N. Lauraitis, Eds., American Society for Testing and Materials, 1977, pp. 248 - 266.

39. Reifsnider, K.L., "Some Fundamental Aspects of the Fatigue and Fracture Response of Composite Materials", Proceedings of the Fourteenth Meeting of the Society of Engineering Science, Lehigh University, November, 1977.

40. Jamison, R.D., and Reifsnider, K.L., "Advanced Fatigue Damage Development in Graphite/Epoxy Laminates", AFWAL-TR-82-3103, Interim Report for Period 1 April 1981 to 1 December 1982, December 1982.

41. O'Brien, T.K., "Analysis of Local Delaminations and their Influence on Composite Laminate Behavior", Presented at the Symposium on Delamination and Debonding of Materials, Sponsored by the American Society for Testing and Materials, Pittsburgh, Pennsylvania, 9-10 November, 1983.

42. Kim, R.Y., "Experimental Assessment of Static and Fatigue Damage of Graphite/Epoxy Laminates", Advances in Composite Materials, ICCM3 3rd International Conference on Composite Materials, Paris, 26 - 29 August, 1980, Vol. 2, Pergamon Press, pp. 1015 - 1028.

43. Kim, R.Y., "Improved Materials for Composites and Adhesives", AFWAL-TR-80-4132, October 1980.

44. Yang, J.N., and Jones, D.L., "Fatigue of Graphite/Epoxy (0/90/45/-45)$_s$ Laminates Under Dual Stress Levels", Comp. Tech. Rev., Vol. 4, No. 3, Fall 1982, pp. 63 - 70.

45. "Cumulative Damage Model for Advanced Composite Materials", prepared by General Dynamics, Fort Worth Division, Fort Worth, Texas, on AFML contract No. F33615-81-C-5049, Semi-Annual Progress Reports No. 1 (Dec. 1, 1981), No. 2 (March 1982) and No. 3 (October 1982).

46. Chou, P.C., Wang, A.S.D., and Mitlar, H., "Cumulative Damage Model for Advanced Composite Materials", AFWAL-TR-82-4083, September 1982.

47. Wang, A.S.D., and Law, G.E., "Interlaminer Failure in Epoxy-Based Composite Laminates", Proceedings 29th Symposium: Failure Modes in Composites, NBS, 1979.

48. Wang, A.S.D., Law, G.E., and Warren, W.J., "An Energy Method for Multiple Transverse Cracks in Graphite/Epoxy Laminates", Modern Development in Composite Materials and Structures, Ed. J. R. Vinson, Procedures of 1978 ASTM Winter Annual Meeting Symposium, 1979, p. 17.

49. Wang, A.S.D., "Growth Mechanisms of Transverse Cracks and Ply Delamination in Composite Laminates", Proc. 3rd Intl. Conf. Composite Materials, Paris, August 1980.

50. Wang, A.S.D., and Crossman, F.W., "Fracture Mechanics of Transverse Cracks and Edge Delamination in Graphite/Epoxy Composite Laminates", Technical Report F 49620-79-C-0206 AFSOR, 1982.

51. Crossman, F.W., and Wang, A.S.D., "The Dependence of Transverse Cracking and Delamination on Ply Thickness in Graphite-Epoxy Laminates", Damage in Composite Materials, ASTM STP 775, American Society for Testing and Materials, June 1982, pp. 118 - 139.

52. Crossman, F.W., Warren W. J., and Wang, A.S.D., "Influence of Ply Thickness on Damage Accumulation and Final Fracture", Presented at the ASME WAM Aerospace Division Technical Sessions, November 13 - 18, 1983. Bostom, MA, Published in Symposium Volume on Composite Fatigue and Fracture, U. Yuceoglu Ed., ASME, 1983.

53. Reifsnider, K.L., Henneke, E.G., and Stinchcomb, W.W., "Delamination of Quasi-Isotropic Graphite/Epoxy Laminates", Composite Materials-Testing and Design (Fourth Conference), ASTM STP 617, American Society for Testing and Materials 1977, p. 63.

54. Bjeletich, J.G., Crossman, F.W., and Warren, W.J., "The Influence of Stacking Sequence on Failure Modes in Quasi-Isotropic Graphite/Epoxy Laminates", Failure Modes in Composites-IV, AIME, 1979.

55. Pipes, R.B., and Pagano, N.J., "Interlaminar Stresses in Composite Laminates Under Uniform Axial Extension", J. Composite Materials, Vol. 4, 1979, p. 538.

56. Wang, A.S.D., and Crossman, F.W., "Some New Results on Edge Effects in Symmetric Composite Laminates", J. Composite Materials, Volume 11, 1977, p. 92.

57. Reifsnider, K.L., Henneke, E.G., II, and Stinchcomb, W.W., "Defect Property Relationships in Composite Materials", AFML-TR-76-81 Part IV, June 1979.

58 ibid, AFML-TR-76-81 Part III, June 1978.

59. Wang, A.S.D., Crossman, F.W., and Law, G.W., "Interlaminar Failure in Epoxy Based Composite Laminates", Proc. NBS Conf. on Fracture, April 1979.

60. Bader, M.C., Bailey, J.E., Curtis, P.T., and Parvizi, A., "The Mechanisms of Initiation and Development of Damage in Multiaxial Fiber-reinforced Plastic Laminates", Proc. 3rd Intl. Symp. Mech. Behavior of Materials, 3, 1978, p. 227.

61. Aveston, J. and Kelly, A., "Theory of Multiple Fracture of Fibrous Composites", J. Material Science, Vol. 8, 1973, p. 352.

62. Flaggs, D.L., and Kural, M.H., "Experimental Determination of the In-Situ Transverse Lamina Strength in Graphite/Epoxy Laminates", J. Composite Materials, Vol. 16, March 1982, pp. 103 - 115.

63. Rodini, B.T., and Eisenmann, J.R., "An Analytical and Experimental Investigation of Edge Delamination in Composite Laminates", Proc. 4th Conf. Fibers and Composites, San Diego, November 1978.

64. Rybicki, E.F., Schmueser, D.W., and Fox. J., "An Energy Release Rate Approach for Stable Crack Growth in the Free Edge Delamination Problem", J. Composite Materials, Vol. 11, 1977, p. 470.

65. Rybicki, E.F., and Kanninen, M.F., "A Finite Element Calculation of Stress Intensity Factors by a Modified Crack Closure Integral", Engr. Fracture Mechanics, Vol. 9, 1977, p. 931.

66. Irwin, G.R., "Fracture", Handbuch der Physik, Vol. 6, Springer-Verlag, 1958, p. 551.

67. Wang, A.S.D., and Crossman, F.W., "Edge Effects on Thermally Induced Stresses in Composite Laminates", J. Composite Materials, 1977, p. 330.

68. CIFTS System, Contact Prof. H.A. Kamel, University of Arizona, College of Engineering, Tucson, Arizona, 1983.

69. Wang, A.S.D., and Crossman, F.W., "Calculation of Edge-Stresses in Multilayer Laminates by Substructuring", J. Comp. Mat., Vol. 11, 1978, p. 92.

70. Crossman, F.W., and Flaggs, D.L., "Dimensional Stability of Composite Laminates During Environmental Exposure", Proc. 24th SAMPE Symposium, San Francisco, May 1979.

71. Crossman, F.W., and Flaggs, D.L., "ADV*LAM - An Advanced Laminate Code for Visco-elastic Analysis", Composite Technology Review, June 1979, pp. 8 - 10.

72. O'Brien, T.K., "Characterization of Delamination Onset and Growth in a Composite Laminate", Damage in Composite Materials, ASTM STP 775, American Society for Testing and Materials, June 1982, pp. 140 - 167, also NASA TM-81940, 1981.

73. Russel, W.B., "On the Effective Moduli of Composite Materials: Slender, Rigid Inclusions at Dilute Concentrations", Journal of Applied Mathematics and Physics, (ZAMP), Vol. 23, 1972.

74. Russel, W.B., "On the Effective Moduli of Composite Materials: Effect of Fiber Length and Geometry at Dilute Concentrations, Journal of Applied Mathematics and Physics, (ZAMP), Vol. 24, 1973.

75. Phoenix, S.L., "Asymptotic Distributions for the Strength of Fibrous Materials Under Local Load-sharing Among Fibers", Cornell University, School of Mechanical and Aerospace Engineering Report MSD 81-01, January 1981.

76. Harlow, D.G., and Phoenix, S.L., "Probability Distributions for the Strength of Composite Materials II: A Convergent Sequence of Tight Bounds", Int. Journal of Fracture, Vol. 17, 1981, pp. 601 - 630. See also references 1 to 4 of this paper.

77. Phoenix, S.L., "Statistics for the Strength of Bundles in Fibers in a Matrix", Encyclopedia of Materials Science and Engineering, Pergamon Press, 1981.

78. Whitney, J.M., Daniel, I.M., and Pipes, R.B., Experimental Mechanics of Fiber Reinforced Composite Materials, SESA Monograph No. 4, 1982.

79. Owens, J., and Rice, J.S., "Flexural Strength Behavior of Glass Fabric Reinforced Polyester Resins", presented at the Sixth Conference on Composite Materials: Testing and Design, May 16-17, 1981, Phoenix, Arizona, to be published in 1982 by American Society for Testing and Materials as an STP.

80. Wu, E.M., "Strength and Fracture of Composites", Composite Materials, Academic Press, 1974, ed. L. J. Broutman.

81. Whitney, J.M. and Knight, M., "The Relationship Between Tensile Strength and Flexure Strength in Fiber Reinforced Composites", AFWAL-TR-80-4104, December 1980.

82. Nair, P., and Reifsnider, K.L., "A Stress Function Formulation and Approximate solution of the Unsymmetric Deformation Problem for Cracks in Non-Uniform Materials", VPI-E-73-31 Report, September 1973.

83. Hertzberg, R.W., Deformation and Fracture Mechanics of Engineering Materials, John Wiley and Sons, 1976.

84. Reifsnider, K.L., Schulte, K., and Duke, J.C., "Long-Term Fatigue Behavior of Composite Materials", Presented at the ASTM Conference on Long-Term Behavior of Composites, Williamsburg, Virginia, March 1982.

85. Ho, T., and Schapery, R.A., "The Effect of Environment on the Mechanical Behavior of AS/3501-6 Graphite/Epoxy Material - Phase IV", Department of the Navy, NAVAIR Contract No. N00019-81-C-0179, Vought Corporation, ATC Report No. R-80700/2CR-9, Final Report for Period of August 1981 - November 1982, February 1983.

86. Whitcomb, J. D., and Raju, I.S., "Analysis of Free-Edge Stresses in Thick Composite Laminates", Presented at the Symposium on Delamination and Debonding of Materials, Sponsored by the American Society for Testing and Materials, Pittsburgh, Pennsylvania, November 9-10, 1983.

87. Crossman, F.W., Mauri, R.E., and Warren, W.J., "Hygrothermal Damage Mechanisms in Graphite-Epoxy Composites", NASA CR 3189, December 1979.

88. Langenbeck, S.L., "Advanced Composite Aileron- Additional Design Allowables Test Results on T300/5208 Graphite/Epoxy Fabric", Lockheed-California Company Report EL/80-71-143 on NASA Contract NAS1-15069, 18 July 1980.

89. Cunningham, M.E., Schoultz, S.V., and Toth, Jr., J.M., "Effect of End Tab Design on Tensile Stress Concentrations", presented at the Second United States-Japan Symposium on Composite Materials, American Society for Testing and Materials, NASA-Langley Research Center, Hampton, Virginia, June 6 - 8, 1983.

90. Kural, M.H., and Flaggs, D.L., "A Finite Element Analysis of Composite Tension Specimens", Composite Technology Review, Vol. 5, No. 1, Spring 1983, pp. 11 - 17.

91. Sendeckyj, G., Unpublished AFFDL report, private communication, May 1983.

92. Standard Test Method for Tensile Properties of Oriented Fiber Composites, ANSI/ASTM D3039-76.

93. Pagano, N.J., Private communication on unpublished research, AFML, May 1983.

94. Micro-Measurements, "Tech-Note, Fatigue of Strain Gages", TN-130-3, and private communication, April 1980.

95. Stalnaker, D.O., and Stinchcomb, W.W., "An Investigation of Edge Damage Development in Quasi-Isotropic Graphite-Epoxy Laminates", Interim Report, AFML Contract F33615-75-C-5119, Virginia Polytechnic Institute and State University Report, VPI-E-77-24, September 1977.

96. Crossman, F.W., and Wang, A.S.D., "Stress Field Induced by Transient Moisture Sorption in Finite Width Composite Laminates", J. Composite Materials, Vol. 12, 1978, p.2.

97. Flaggs, D.L. and Crossman, F.W., "Viscoelastic Response of a Bonded Joint Due to Transient Hygrothermal Exposure".

98. Crossman, F.W., and Flaggs, D.L., "Development of Computer Software to Predict Viscoelastic Response of Composite Laminates Based on Fibers and Matrix Data", Final Report on Navy Contract N60921-79-M-4271, January 1980.

99. Kriz, R.D., Stinchcomb, W.W., and Tenney, D.R., "Effects of Moisture Residual Thermal Curing Stresses and Mechanical Load on the Damage Development in Quasi-Isotropic Laminates", VPI-E-80-5, February 1980.

100 Nuismer, R.J., and Whitney, J. M., "Uniaxial Failure of Composite Laminates Containing Stress Concentrations", Fracture Mechanics of Composites, ASTM STP 593, American Society for Testing and Materials, 1975, pp. 117 - 142.

APPENDIX A
MATERIAL AND COUPON MANUFACTURE

All of the coupons used in this program were obtained from panels manufactured of T300/5208 graphite/epoxy materials. Coupons of the $(0)_4$, $(0/90/\pm45)_s$, and $(0/\pm45)_s$ layups were supplied by NASA while those of the $(0/45/0_2/-45/0)_s$ and $(0_2/90_4)_s$ layups were manufactured by Lockheed. All coupons were of nominal dimensions 254 mm (10 in.) long by 38.1 mm (1.5 in.) wide. The NASA supplied coupons were manufactured by MacDonald-Douglas Aircraft Company, Long Beach, on December 10, 1979 from Narmco batch No. 1443, rolls 2 and 10. The Lockheed manufactured panels were cured on September 27, 1982 from Narmco batch 1890, Roll No. 21. C-scans of the Lockheed panels showed no void indications. Widths of coupons within a coupon varied by at most ±0.4 percent and thicknesses by at most $\pm$ 1.0 percent. Approximate fiber volumn fractions of the different layups were as follows:

Layup	Percent Volume Fracture
$(0)_4$	58
$(0/90/\pm45)_s$	61
$(0/\pm45)_s$	60
$(0/45/0_2/-45/0)_s$	59
$(0_2/90_4)_s$	60

APPENDIX B
EXPERIMENTAL PROCEDURES

B.1 LOADING PROCEDURES

Both the monotonic tension and constant amplitude fatigue experiments were conducted at room temperature, in laboratory air in two closed-loop, 22 kip MTS test systems. The strain measuring devices were a MTS 25.4 mm (1 in.) gage length extensometers with attached 76.2 mm (3 in.) extenders giving an effective gage length of 101.6 mm (4 in.). The extensometer knife edge points rested on aluminum pads of approximately 3 x 3 mm (1/8 by 1/8 in.) dimensions which were bonded with epoxy glue to the coupons. The extensometer knife edge points were held in place with specially designed aluminum clips which went around the specimen. The experimental set-up is shown in Figure B1. Load and deflection were digitally read by computer and load or stress versus strain displayed on a CRT from which video copies were made. Coupon width was measured in three places within the gage length and thickness in six places. These values were averaged to obtain coupon area.

Coupons were loaded using MTS type hydraulic grips. Bonded tabs were used on the $(0)_4$ coupons because of potential damage to these delicate coupons. For all other coupons, unbonded 1.5 mm (0.060 in.) thick plexiglass tabs were employed. These tabs, suggested by the program manager O'Brien, were found to work exceedingly well, however, difficulties can be encountered if hydraulic grips are not used. Failure of $(0/90/\pm45)_s$ and $(0/\pm45)_s$ coupons were within the gage length while even for the $(0/45/0_2/-45/0)_s$ layup, failures were often within the gage length and usually away from the end tab. The $(0_2/90_4)_s$ coupons more often than not simply shattered. A recent research report[89] analytical supported the concept that unbonded tabs would probably give the lowest stress concentration at the end tab.

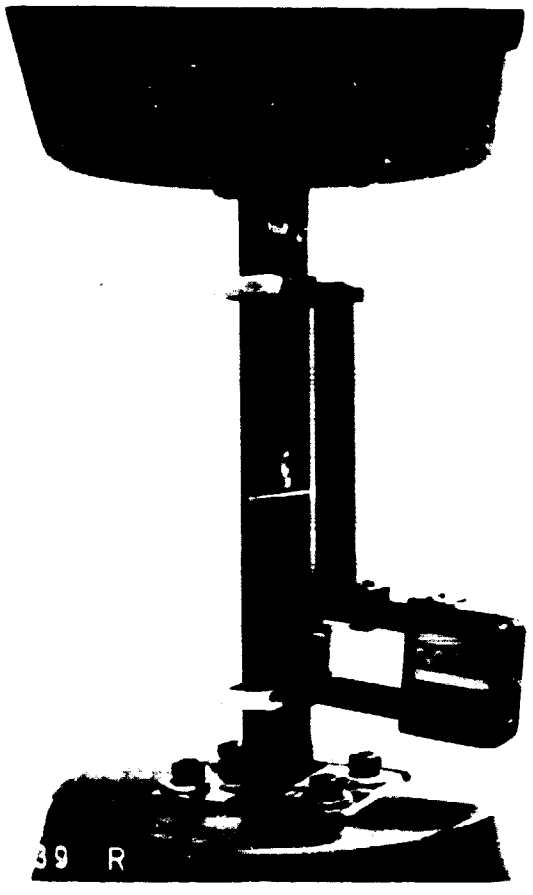

Figure B1: Experimental set-up for monotonic and fatigue experimentation.

The tabs used in this program were square ended, not tapered and were griped to the end of the tab. The untappered tab design was selected because an analysis of previously obtained data[6,7] showed no significant effect of a square ended tab on strength. The analysis of this data was as follows:

16 ply T300/5208 layup $(0/45/90/-45_2/90/45/0)_s$

- o 55 straight tabbed coupons.
- o 30.25 mm (5.5 in.) gage length, 267 mm (10.5 in.) long; 25.4 mm (1 in.) wide
- o any failure in the center 108 mm (3.5 in.) was considered as "independent" of the tab/grip ends, all other failure locations were considered as possibly being influenced by the tab/grip.
- o coupons gripped by hydraulic grips to the end of the tab (critical importance)
- o Results
  - If no end effect, number of coupons expected to fail in center length was 35; number of coupons failed in center length was 35.
  - Average strength of 35 center failed coupons was 568 MPa (82.4 ksi); average strength of 20 end failed coupons was 566 MPa (82.1 ksi); a 0.36 percent difference

24-Ply T300/5208 layup $(0/45/0_2/-45/0)_{2s}$

- o 25 straight tabbed coupons
- o Geometry and other conditions same as previous data
- o Results
  - 8 center failed coupons
  - 17 end failed coupons (the reverse of the unaffected ratio).
  - Average strength of 8 center failed coupons was 1113 MPa (161.4 ksi); average strength of 17 end

failed coupons was 1109 MPa (160.8 ksi); a 0.37 percent difference.

A study by Kural and Flaggs[90] indicated a possible advantage of tapered over straight tabs for coupons tested in mechanical hand-tightened grips. However, the advantage is less than 2% difference in failure load, and even then all loading conditions must be essentially perfect.

In an unpublished study by Sendeckyj[91], $\pm 45^{\circ}$ specimens having a tapered tab on one side and a square ended tab on the other were tested in tension. The square-ended tabs had an undercut produced by a teflon insert and were gripped to the end of the tabs. The tapered tabs had a 30 degree taper per ASTM D3039[92]. Data were evaluated based on location and direction of failure. Results were somewhat inconclusive due to the small sample size (approximately 10 coupons). However, there appeared to be no difference between square-ended and tapered tabs with the square-ended perhaps fairing slightly better. The observation was made that the gripping to the end of the tab was an important fact which is supported by the finite element analysis of Kural and Flaggs[90]. Pagano[93] (AFWAL) did a study on tapered and square-ended tabs of fatigue test coupons and found that if the tapered region was not supported an edge delamination would occur near the taper.

Coupons used for monotonic tension to failure experiments were loaded in several steps. At preselected strain levels, the load was reduced approximately 20 percent, edge replicates were obtained, the coupon was unloaded and removed, finally, enhanced x-rays were obtained. This procedure was repeated to failure. For one monotonic coupon of each of the $(0/45/0_2/-45/0)_s$ and $(0_2/90_4)_s$ layups, the enhanced x-ray photographs were obtained at the reduced load without coupon removal or full unloading. Load interruption strain levels were varied for each coupon of the same layup so that damage data over a wide range of strain levels could be obtained thus avoiding the possibility of not recording pertinent damage conditions.

All fatigue cycling experiments were conducted at constant amplitude at a load range of R = 0.1. Coupons were brought to maximum load, upon initial loading, in approximately 100 cycles in order to prevent premature dynamic load induced failure which is often a problem, especially with unidirectional layups. Coupons were cycled under constant load, not strain, to insure that failures occurred and to allow the initial strain level to increase if any stiffness decrease eventuated. This permitted an evaluation of whether the strain at fatigue failure would increase to the monotonic tension failure strain. Before fatigue cycling, the monotonic (static) stiffness and an edge replicate were obtained for each coupon. The dynamic stiffness was obtained soon after starting the load cycling, usually at 1000 cycles since little dynamic stiffness change was shown to occur beforehand. However, for the $(0_2/90_4)_s$ coupons, dynamic stiffness was obtained as soon as possible after cycling was started because stiffness could rapidly change in these coupons. Dynamic stiffness was defined as the slope of a line down the center of a hysteric slope as shown in Figure B2. This slope was automatically obtained using the computer system.

Dynamic stiffness was recorded periodically during load cycling. After an appropriate amount of stiffness loss had occurred or cycles were applied, dynamic stiffness was obtained and cycling stopped. A static stiffness was obtained by loading up to approximately 80 percent of the fatigue load. The load was held at the 80 percent value while edge replications were obtained. Subsequently the coupon was unloaded, removed, and an enhanced x-ray photograph obtained. The coupon was reinserted in the test machine and cycled to another stopping point where the procedure was repeated. Coupons were cycled to failure, to 10^6 cycles, or to a preset amount of stiffness loss or cycles and used for residual strength experimentation. The number of cycles between NDI intervals was varied in such a manner as to insure that damage initiation and development throughout the fatigue life could be well documented by comparing data obtained from several coupons cycled at the same stress level.

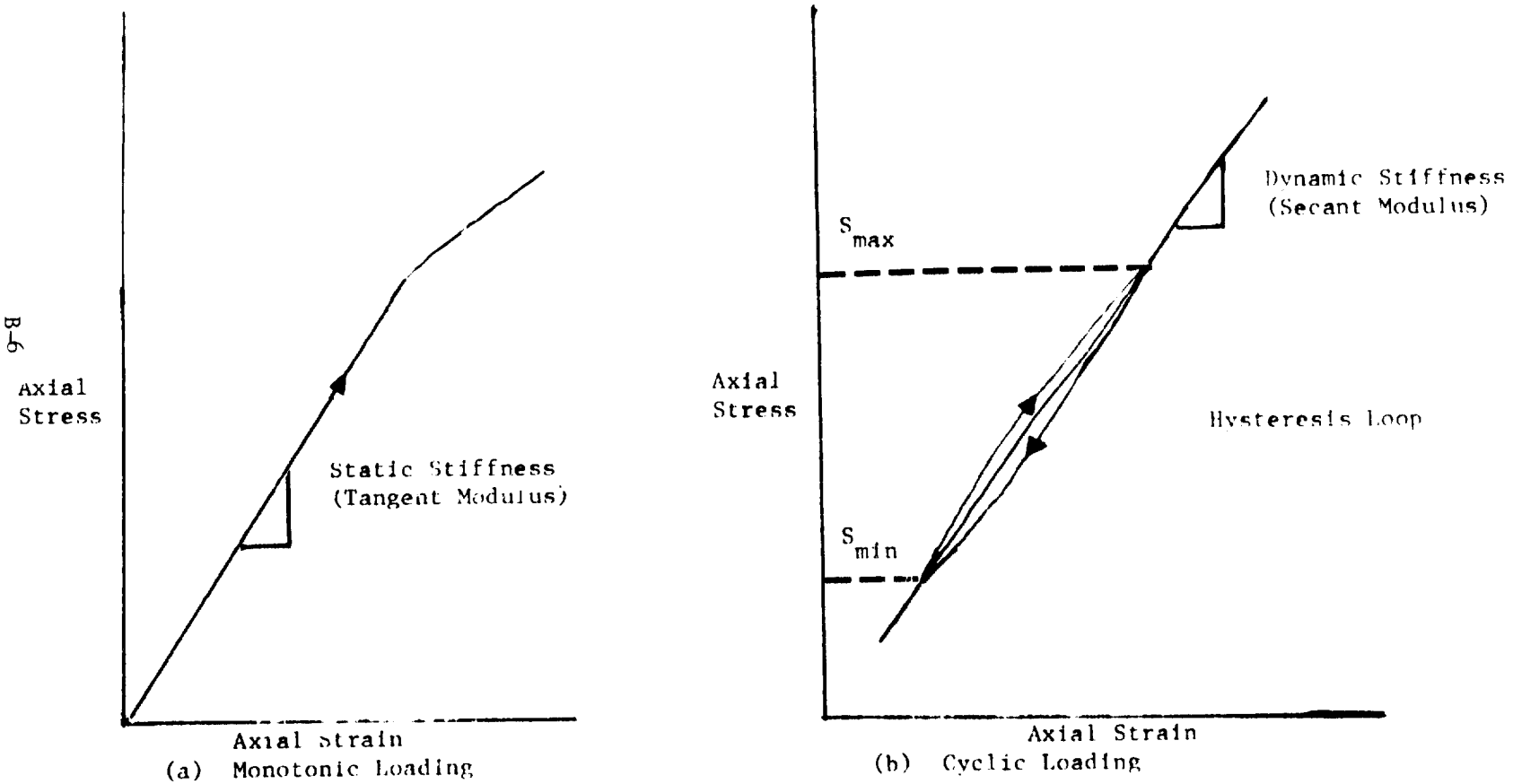

Figure B2: Examples of stiffness measurement.

Coupons intended for residual strength experimentation were cycled in fatigue in the same manner as other coupons. At the end of fatigue cycling, static and dynamic stiffness were obtained as were edge replicates and enhanced x-ray photographs. These coupons were subsequently loaded to failure with several load interruptions to obtain NDI data similar to the monotonic tension experiments of undamaged coupons.

B.2 STIFFNESS MEASUREMENTS AND ANALYSIS OF EXPERIMENTAL ERROR

Coupon stiffness, both static and dynamic, was measured, as previously mentioned, over a 101.6 mm (4 in.) gage length using instrumentation which consisted of an MTS type low mass, clip gage attached to the coupon. The repeatable accuracy of removing and reattaching the clip gage on composite coupons was found to be extremely good as will be discussed in detail later. This system of strain measurement for obtaining stiffness was selected instead of strain gages for two reasons. First, strain gages can give strain measurement only over a short length of the coupon gage length. Use of the clip gage reduces the possible bias introduced by local strain perturbations by giving an average value representative of overall damage progression. Second, the best strain gages commercially available for use in fatigue loading, for instance those from Micro-Measurements, have a fatigue life of approximately 10^5 cycles at a strain range of 0 to 5400 $\mu\epsilon$. However, the measurement error is as much as 10 percent[94]. This strain range of 0 - 5400 μ is approximately that required to give lives between 10^5 and 10^6 cycles for the quasi-isotropic laminate used in this program. Shorter lives for the quasi-isotropic layup and all lives less than 10^6 cycles for the other layups require a much higher strain range (>0 to 6000 or 7000 $\mu\epsilon$). Presently available strain gages are inadequate for such conditions. Thus, strain gages were not used for obtaining static and dynamic stiffness over the entire cycle life range of interest in this program.

An analysis and experimental verification was performed of expected errors in the stress, strain, and stiffness measurements obtained during the program. This study included two aspects. The first was determination of expected absolute accuracy in the measurements as limited by the measuring apparatus itself and by the calibration procedure and equipment. The second aspect involved determining the repeatable measurement accuracy due to removal and reapplication of the strain measuring device or due to variations in successive dynamic modulus measurements.

During an experiment the stress and strain values were obtained as voltage outputs of the appropriate transducers. These values were sampled and converted to digital readings at a scan rate of 1500 per second for dynamic tests and at 15 per second for static. Thus, for example, on each cycle, at 10 Hz frequency, 150 readings were obtained for forming a single hysterisis loop and 1500 points for 10 successive cycles. These sampled voltage values were converted to units of stress and strain and plotted by the computer. Stiffness was calculated by:

$$E + Er\% = \frac{(V \quad + Er\%)\ (SF \quad + Er\%)}{(V_e \pm Er\%)\ (SF \quad \pm Er\%)} \qquad (B1)$$

E is stiffness, Er % is the error for the indicated value, and where V and SF are the load cell output voltages and corresponding scale factor relating voltage to stress. Similarly, V and SF are the extensometer (clip gauge) output voltages and corresponding scale factor which relates voltage to strain. The worst possible error in absolute stress measurement was found to be $\pm$ 0.2% and in strain $\pm$ 0.3%. These values were due to calibration, computer, and instrumentation limitations. An analysis of worst case possible error in stiffness gave a result of $\pm$0.50%

The repeatable accuracy was defined as the worst possible error in stiffness reading due to removal and reattachment of the clip gauge or due to successive readings under dynamic conditions during one attachment. This error was experimentally determined by measuring the stiffness of a 16-ply quasi-isotropic coupon of T300/5208 material with a geometry of 25.4 mm

5 OF 6

N84-29978 UNCLAS

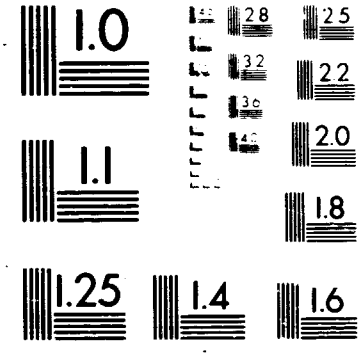

(1 in.) width and 152.4 mm (6 in.) length between the grips. A 6.35 mm (1/4-in.) gauge length strain gauge was bonded to the center of the coupon for comparison purposes. Five successive measurements of stiffness were obtained while removing and reattaching the clip gauge between each measurement.

Stiffness measurements taken during static loadings of the coupon to 248 MPa (36 ksi) at a strain rate 0.01 min are shown in Table B1. Stress was held to this value in order to remain well below the "knee" in the stress-strain curve (which occurs at approximately 345 MPa(50 ksi)) and thus allows repeatable measurements. Representative stress-strain curves are shown in Figures B3 and B4. The average strain gauge and 25.4 mm (1-in.) clip gauge readings agreed with each other within 0.3%. While for the 101.6 mm (4-in.) gauge length using the same clip gage (used in this program), the difference was about 2% as expected when measuring stiffness over such different lengths. The repeatable accuracy of the 101.6 mm (4 in.) clip guage was $\pm$ 0.10%, the same as the strain gauge, see Table B1.

Dynamic repeatable accuracy measurements are shown in Table B2 and representative curves are given in Figures B5 and B6. Table B2 shows that repeatable accuracy under dynamic conditions was at worst $\pm$ 0.12% for the 101.6 mm (4 in.) clip gauge. This was true under both removal and reattachment conditions and for any five cycles selected from a group of ten with the clip gauged not removed. In addition, comparison of Tables B1 and B2 shows that the static and dynamic moduli as measured by the 101.6 mm (4 in.) clip gauge agreed within 0.25%. Also both Tables B1 and B2 show that the 101.6 mm (4 in.) clip gauge was as accurate as the strain gauge as far as repeatability is concerned.

B.3 NDI PROCEDURES

The methods most commonly used for the inspection of composites are ultra-sonic C-scan, x-ray, Moire, brittle lacquer, acoustic imaging,

Table B1
Stiffness Measurements for
Repeatable Accuracy
Static Survey

16-Ply Quasi-Isotropic Coupon, [illegible] ksi,
0.01 in./in./min. Values are psi x 10^6

Index	Measurement Type	
	Strain Gauge	1-in. Clip Gauge
1	7.860 - 0.04%	7.897 + 0.15%
2	7.858 - 0.06%	7.881 - 0.05%
3	7.873 + 0.12%	7.905 + 0.25%
4	7.859 - 0.06%	[illegible]
5	7.866 + 0.02%	7.902 + 0.22%
Average	7.863 + 0.12%	[illegible]
	- 0.06%	- 0.58%
	Strain Gauge	4-in. Clip Gauge
1	7.832 - 0.08%	8.041 - 0.10%
2	7.836 - 0.04%	8.045 - 0.05%
3	7.838 - 0.01%	8.057 + 0.10%
4	7.847 + 0.10%	8.058 + 0.10%
5	7.842 + 0.04%	8.043 - 0.07%
Average	7.839 + 0.10%	8.049 ± 0.10%
	- 0.08%	

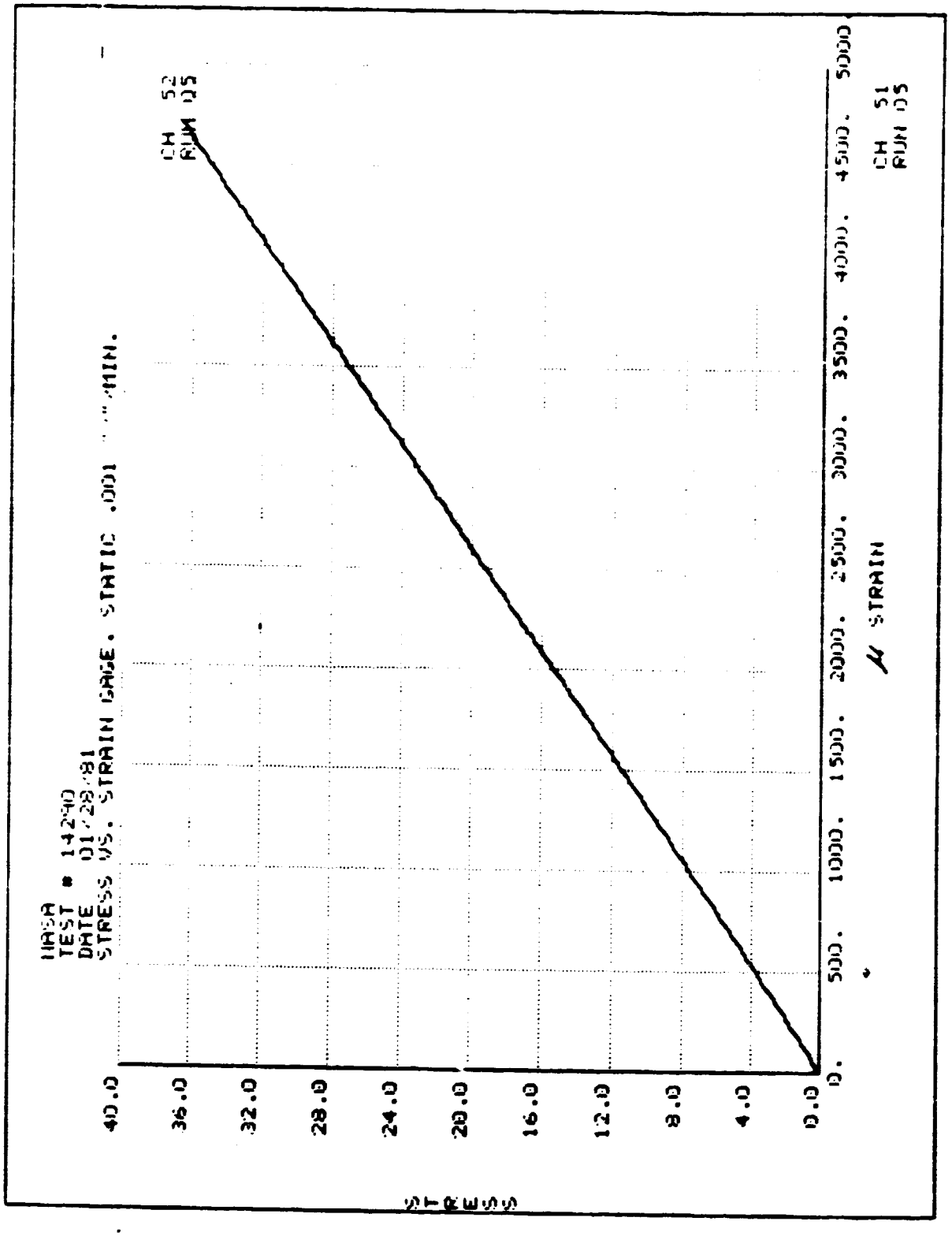

Figure B3: Static load stress-strain plot of a bi-axial quasi-isotropic coupon obtained with a strain gauge.

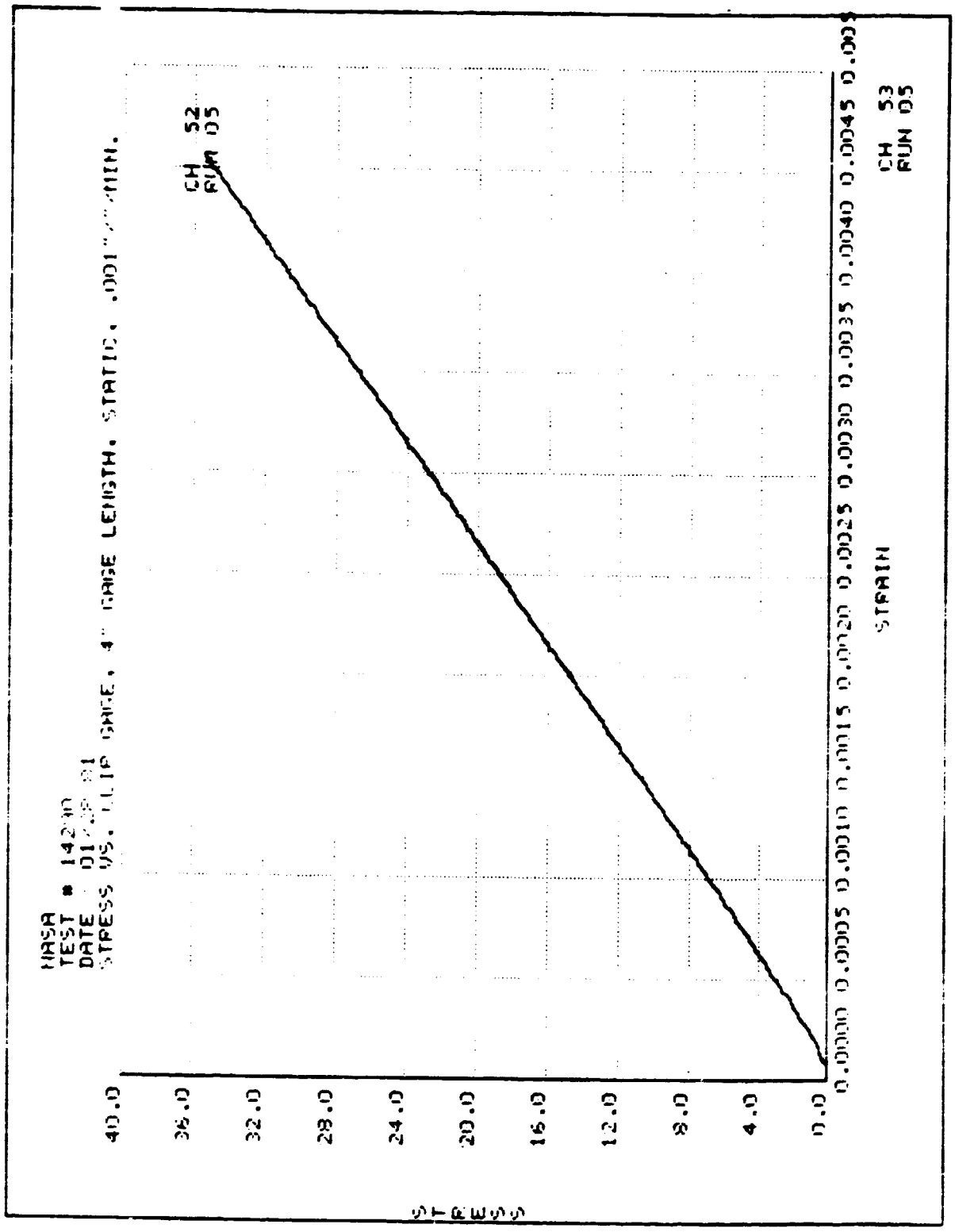

Figure B6: Static load stress strain [illegible] for common obtained with a [illegible] extensometer.

Table B2
Stiffness Measurements For
Repeatable Accuracy
Dynamic Survey

16-Ply Quasi-Isotropic Coupon, 3.6 to 36 ksi, 10 Hz

Index	Measurement Type	
	Strain Gauge	4-in. Clip Gauge
1	7.883 + 0.03%	8.071 - 0.01%
2	7.884 + 0.04%	8.064 - 0.07%
3	7.858 - 0.30%	8.070 0.00%
4	7.875 - 0.08%	8.080 + 0.12%
5	7.907 + 0.33%	8.066 - 0.05%
Average	7.881 + 0.30%	8.070 + 0.12%
	- 0.33%	-0.07%

Measurement of Five Cycles
Taken From Group of Ten Without Clip Gauge Removal

	Strain Gauge	4-in. Clip Gauge
1	7.885 + 0.03%	8.066 + 0.12%
2	7.878 - 0.06%	8.058 + 0.02%
3	7.884 - 0.01%	8.064 + 0.10%
4	7.890 + 0.09%	8.047 - 0.11%
5	7.880 - 0.04%	8.046 - 0.12%
Average	7.883 - 0.09%	8.056 ± 0.12%
	- 0.06%	

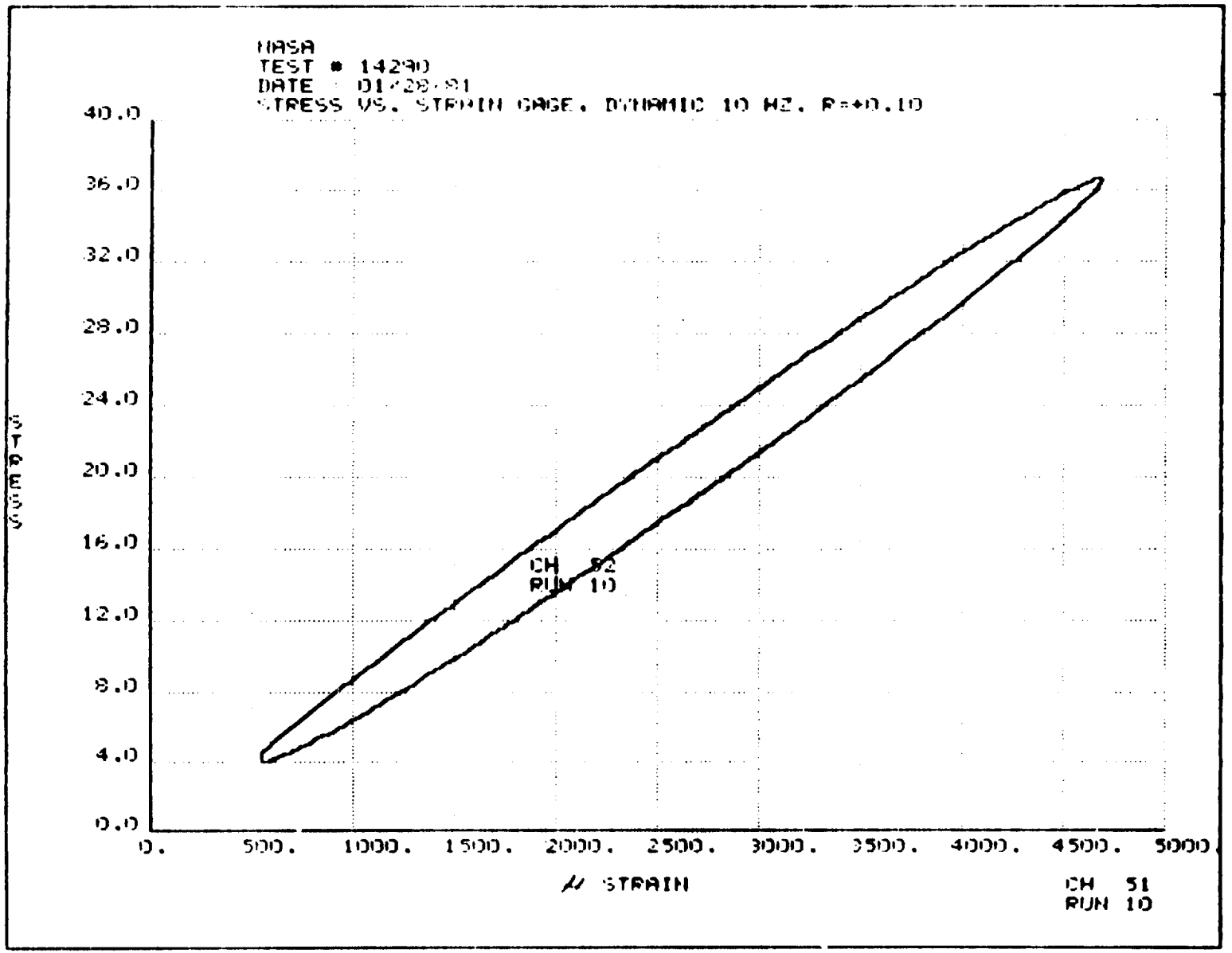

Figure B5: Dynamic load stress-strain plot of a lo-ply quasi-isotropic coupon obtained with a strain gage.

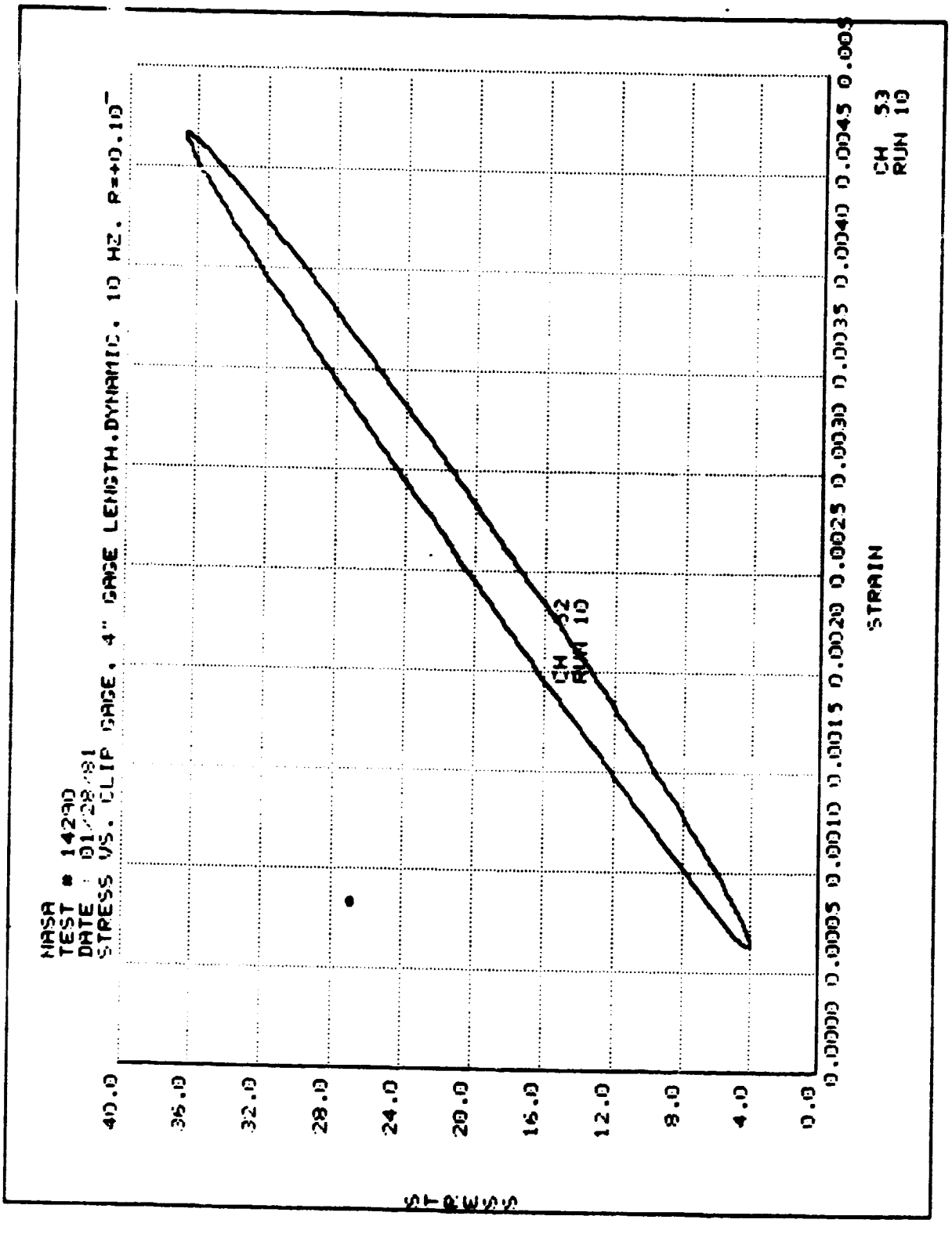

Figure B6: Dynamic load stress-strain plot of a 16-ply quasi-isotropic coupon obtained with a 4 inch extensometer.

photoelastic casting, penetrant, thermography, acoustic emission, and laser holography. In addition, some methods are being used to measure specific parameters, such as ultrasonics to measure moisture level, eddy current to monitor fiber volume, and radiography and thermal neutron mass absorption to determine resin content. A review of the literature[6] showed that of the variety of NDI methods available, few provided detailed information on the type of damage present. Based on that survey, the edge-replication technique was selected to determine ply damage location. The enhanced x-ray technique was selected to give a quick and simple observation of delamination extent. The two methods are complimentary in that edge replication does not reveal interior delamination and x-ray does not easily show the ply loction of delamination. The combination of the two procedures helped insure that all pertinent information was preserved for analysis.

Ultrasonic C-scan was eliminated because of the inability to determine the ply level of damage. Acoustic imaging was not selected because no system was available at the program inception with the required attributes. a pulse-echo, ultrasonic system such as Holoscan has severe geometric restrictions when used on small coupons and available systems lacks definitiveness for determining ply level damage. Moire, brittle lacquer, and laser holography also fail to detect the level of ply damage. This same problem exists for thermography. Simple penetrant inspection was eliminated because of the lack of definitiveness of damage detection and lack of knowledge as to the potential damage to the graphite/epoxy composite material.

•

The pastic-cast edge replication technique used for this program is a modification of the original method of Stalnaker and Stinchcomb.[95] A strip of acetate tape, 5 mil thick, is softened by acetone and placed on the edge of a specimen being held under load. A fresh acetate strip is placed over the first tape and pressed firmly to ensure good contact at the tape with the specimen edge and to remove aira bubbles from between the two tapes. After drying for fifteen minutes, the replica is removed from the

specimen edge and placed between two glass slides to maintain flatness. Photographs of selected portions of a replica can be made by using the replica as a negative in a microfiche reader. Prints up to 24X magnification are made and permanent negatives made from them.

At each inspection interval, both edges of the coupon were examined using the edge replication technique. Such a technique clearly shows inter and intralamina cracking. This technique allowed the location of cracks within layers to be easily discerned which was especially important for interply delamination type cracking. The edge replicates extended over the entire gage length region of the $(0/90/\pm45)_s$ and $(0/\pm45)_s$ coupons. The extent of matrix cracking was determined for the center 25.4 mm (1 in.) region on both left and right replicates, and for the upper 25.4 mm (1 in.) region of the left replicate and similarly for the lower region of the right replicate, both just inside the end of the gage length boundary. The number of matrix cracks for each ply type in each of the four regions were averaged together. Other regions were looked at to discern if the selected regions were truely representative, which was found to be the case. For the $(0/45/0_2/-45/0)_s$ and $(0_2/90_4)_s$ coupons, only the two left and right center 25.4 mm (1 in.) regions were used for crack counting. This was done because other regions displayed essentially the same information thus a decision was made to reduce the amount of labor effort in data tabulation. To discern the ply location of a delamination, the entire region of an edge replicate would be reviewed.

Enhanced x-ray of damaged coupons was conducted using a Norelco MG 150 constant potential radiographic x-ray system with a 150 Kv Beryllium window tube used in conjunction with the radio-opaque penetrant Zinc iodide. Zinc iodide was selected because of nontoxicity and apparent non damage to the coupons. The enhancer was applied to the specimen edges, allowed to penetrate, and the surface residue removed. A microfocus x-ray tube with a 0.7 mm focal spot was used to produce the x-ray on Kodak Type R film. This low grain, high contrast negative was selected in order that large

magnification of the negatives was possible thus allowing more accurate inspection of matrix and delamination. Exposures were made at 25 kvp, 5 ma for 150 sec. at a focal distance of 183 cm (72 in.). X-ray negatives were usually, but not always, made at the same time as edge replicates were obtained.

APPENDIX C
EXPERIMENTAL DATA

This Appendix contains tables of the detailed data used in a summary manner in Section 2. Various additional plots are also given of some of the data for completeness purposes.

TABLE C1
SUMMARY OF MATRIX CRACK DATA
FOR (0/90/±45)s MONOTONIC TENSION COUPONS

Coupons 11-2, 11-6, 11-15, 11-22, 11-29

Note: No -45° Ply Matrix Cracks Were Observed

Strain mm/mm	Average Crack Spacing in mm $+90^{\circ}$ Plies	$+45^{\circ}$ Plies
0.00394	$\rightarrow\infty$ [a]	$\rightarrow\infty$
0.00641	5.08	$\rightarrow\infty$
0.00648	12.7	$\rightarrow\infty$
0.00737	0.98	$\rightarrow\infty$
0.00782	0.66	$\rightarrow\infty$
0.00881	0.83	$\rightarrow\infty$
0.00909	0.32	6.77
0.00912	0.48	$\rightarrow\infty$
0.00925	0.39	$\rightarrow\infty$
0.00923	0.34	3.40
0.00937	0.36	2.75
0.00953	0.29	2.12
0.00958	0.32	4.23
0.00968	0.48	7.26
0.00973	0.37	2.90
0.00983	0.28	1.75
0.00983	0.30	1.69
0.00984	0.31	1.34
0.01003	0.29	1.06
0.01009	0.39	2.17
0.01025	0.28	1.19

a = The symbols $\rightarrow\infty$ indicate that matrix cracks were not observed in the regions examined.

TABLE C2

SUMMARY OF PERCENT STIFFNESS LOSS COMPARED TO DELAMINATED AREA AND MATRIX CRACK SPACING FOR $(0/90/\pm45)_s$ FATIGUE COUPONS

Percent of Initial Dynamic Stiffness	Percent of Initial Monotonic Stiffness	Approx. Delaminated Area mm^2	Percent of Total Gage Length Area	Delamination Type: 90/+45=1 +45/-45=2	Average Crack Spacing, mm 90	+45	-45	Coupon ID	Fatigue Stress Level MPa	Fatigue Cycles, Thousands
-	-	100.0	0.0	None	1.80	a	a	at 0.0071 Strain[b]		
-	-	100.0	0.0	None	0.80	a	a	at 0.0078 Strain[b]		
-	-	100.0	0.0	None	0.50	a	a	at 0.0084 Strain[b]		
98.1	98.4	6.4	0.16	1	0.36	0.61	1.80	11-13	448	18.0
98.1	-	-[c]	-	-	0.36	0.60	1.69	11-21	414	50.0
97.9	98.7	12.9	0.33	2	0.33	0.62	1.59	11-25	414	33.5
96.8	97.5	25.8	0.67	1	0.28	0.54	1.34	11-1	379	105.0
		19.4	0.50	2						
96.7	97.0	38.7	1.00	1	0.59	0.65	1.41	11-18	414	60.0
96.0	97.1	38.7	1.00	1	0.30	0.53	1.07	11-13	448	24.0
		51.6	1.33	2						
95.7	96.3	471.0	12.2	1	0.36	0.60	1.69	11-3	379	114.0
95.3	95.0	155.0	4.00	1	0.30	0.58	1.42	11-9 5	379	157.0
		25.8	0.67	2						

TABLEC2(Continued)
SUMMARY OF PERCENT STIFFNESS LOSS COMPARED TO DELAMINATED AREA AND MATRIX CRACK SPACING FOR $(0/90/\pm45)_s$ FATIGUE COUPONS

Percent of Initial Dynamic Stiffness	Percent of Initial Monotonic Stiffness	Approx. Delaminated Area mm^2	Percent of Total Gage Length Area	Delamination Type: 90/+45=1 +45/-45=2	Average Crack Spacing, mm 90	+45	-45	Coupon ID	Fatigue Stress Level MPa	Fatigue Cycles, Thousands
95.0	95.1	0.0	0.0	2	0.25	0.51	1.27	11-16	379	125.0
94.9	95.9	32.0	0.83	1	0.25	0.56	1.50	11-8	379	125.0
		19.0	0.49	2						
94.7	[illegible].0	--c	-	-	0.29	0.57	1.41	11-21	414	70.0
94.5	97.3	116.0	3.00	2	0.25	0.48	1.42	11-16	379	150.0
94.1	94.9	161.0	4.16	2	0.27	0.51	1.59	11-23	379	150.0
93.9	96.5	64.5	1.67	2	0.28	0.53	1.49	11-25	414	60.0
93.9	95.8	294.0	7.59	1	0.32	0.54	1.06	11-45	414	58.2
		32.3	0.83	2						
93.7	90.8	1219.0	31.5	1	0.27	0.49	1.06	11-60	379	100.0
93.2	93.7	574.0	14.8	1	0.28	0.58	1.35	11-11	379	125.0
92.9	94.2	226.0	5.84	1	0.30	0.50	1.06	11-1	379	162.0
		90.3	2.33	2						
92.3	92.7	749.0	19.3	1	0.31	0.53	1.27	11-57	379	101.0

TABLE C2-(Continued)
SUMMARY OF PERCENT STIFFNESS LOSS COMPARED TO DELAMINATED AREA AND MATRIX CRACK SPACING FOR $(0/90/\pm45)_s$ FATIGUE COUPONS

Percent of Initial Dynamic Stiffness	Percent of Initial Monotonic Stiffness	Approx. Delaminated Area mm^2	Percent of Total Gage Length Area	Delamination Type: 90/+45=1 +45/-45=2	Average Crack Spacing, mm 90	+45	-45	Coupon ID	Fatigue Stress Level MPa	Fatigue Cycles, Thousands
92.0	92.3	1174.0	30.3	1	0.32	0.53	0.91	11-3	379	140.0
91.8	90.0	250.0	6.46	2	0.25	0.50	1.59	11-23	379	150.0
91.6	92.2	313.0	8.08	1	0.28	0.58	3.18	11-17	379	125.0
91.5	91.3	1245.0	32.2	1	0.30	0.64	2.11	11-10	379	125.0
91.0	90.8	419.0	10.8	1	0.30	0.49	0.94	11-1	379	184.0
		245.0	6.33	2						
90.9	91.4	671.0	17.3	1	0.32	0.58	1.15	11-9	379	192.0
90.7	89.7	652.0	16.8	1	0.25	0.53	1.58	11-8	379	150.0
		116.0	3.00	2						
89.0	87.8	929.0	24.0	1	0.28	0.55	1.21	11-9	379	224.0
		110.0	2.84	2						
87.5	88.8	1864.0	48.2	1	0.30	0.58	1.27	11-11	379	150.0
85.9	84.7	--[d]	--	1	0.26	0.56	1.22	11-9	379	270.5
84.9	92.4	--[e]	--	--	0.24	0.51	1.54	11-21	414	160.0

TABLE C2-(Continued)
SUMMARY OF PERCENT STIFFNESS LOSS COMPARED TO DELAMINATED
AREA AND MATRIX CRACK SPACING FOR $(0/90/\pm45)_s$ FATIGUE COUPONS

Percent of Initial Dynamic Stiffness	Percent of Initial Monotonic Stiffness	Approx. Delaminated Area mm^2	Percent of Total Gage Length Area	Delamination Type: 90/+45=1 +45/-45=2	Average Crack Spacing, mm			Coupon ID	Fatigue Stress Level MPa	Fatigue Cycles, Thousands
					90	+45	-45			
83.3	90.9	--c	--	--	0.26	0.51	1.34	11-21	414	180.0
80.6	88.7	--c	--	--	0.33	0.70	1.06	11-21	414	212.0
78.4	80.8	3125.0	80.7	1	0.28	0.61	1.14	11-10	379	150.0

a = No cracks detected

b = Estimated average crack spacings which occur during initial loading of the fatigue coupons for monotonic stiffness determination

c = Delamination location and area not obtained for this coupon.

d = Delamination area data not obtained, coupon failed in static stiffness survey.

TABLE C3

FATIGUE TESTING OF $(0/90/\pm45)_s$ COUPONS AT 379 MPa, MODULUS AND EDGE REPLICATION DATA

R = +0.1, f = 10 Hz

Coupon ID	Initial[a] Moduli, GPa	Cycles (Thousands)	Dynamic Modulus GPa	Percent of Initial Modulus	Monotonic Modulus, GPa	Percent of Initial Modulus	Average Crack Spacing mm/Crack 90	+45	-45
11-1	E_d = 54.6	105.0	52.9	96.8	51.9	97.5	0.279	0.540	1.336
	E_m = 53.3	162.0	50.8	92.9	50.2	94.2	0.295	0.498	1.058
		183.8	49.7	91.0	48.4	90.8	0.302	0.489	0.941
		198.8	48.6	88.9	45.7	86.0	-	-	-
		198.8+	Failure due to operator error						
11-3	E_d = 54.1	114.0	51.9	95.9	51.0	96.3	0.358	0.605	1.693
	E_m = 53.0	140.5	49.8	92.0	48.9	92.3	0.318	0.529	0.907
		166.9	48.2	89.2	-	-	-	-	-
		166.9+	Coupon failed						
11-9	E_d = 54.5	157.0	51.9	95.3	50.8	95.0	0.302	0.577	1.422
	E_m = 53.5	192.0	49.5	90.9	48.9	91.4	0.318	0.577	1.154
		224.0	48.5	89.0	47.0	87.8	0.285	0.552	1.104
		250.5	49.0	90.0	48.0	89.6	0.302	0.540	1.210
		270.5	46.8	85.9	45.3	84.7	0.279	0.559	1.219
		299.2	Coupon failed						

a = E_d amd E_m are dynamic and monotonic moduli, respectively; E_d obtained at 2000 cycles except for 11-1 which was obtained at 6500 cycles.

TABLE C4

FATIGUE TESTING OF $(0/90/\pm45)_s$ COUPONS AT 414 MPa, MODULUS AND EDGE REPLICATION DATA
R = +0.1, f = 10 Hz

Coupon ID	Initial[a] Moduli, GPa	Cycles (Thousands)	Dynamic Modulus GPa	Percent of Initial Modulus	Monotonic Modulus, GPa	Percent of Initial Modulus	Average Crack Spacing mm/Crack 90	+45	-45
11-18	E_d = 54.3	60.0	52.5	96.7	51.8	97.0	0.591	0.651	1.411
	E_m = 53.4	Failure due to operator error							
11-21	E_d = 54.6	50.0	53.6	98.1	--	--	0.36	0.60	1.69
	E_m = 53.2	70.0	51.7	94.7	51.6	97.0	0.29	0.57	1.41
		160.0[b]	46.3	84.9	49.2	92.4	0.24	0.51	1.54
		180.0	45.5	83.3	48.4	90.9	0.26	0.51	1.34
		212.0	44.0	80.6	47.2	88.7	0.33	0.70	1.06
11-25	E_d = 54.6	33.5	53.6	97.9	52.0	98.7	0.330	0.620	1.588
	E_m = 52.7	50.5	51.5	93.9	50.8	96.5	0.285	0.529	1.494
		64.5	50.5	92.2	--	--	--	--	--
		65.2	Coupon failed						
11-45	E_d = 54.6	40.0	53.1	97.3	51.6	97.1	0.339	0.552	1.588
	E_m = 53.2	58.2	51.0	93.9	51.0	95.8	0.318	0.540	1.058
		58.8	51.3	93.9	--	--	--	--	--
		60.1	Coupon failed						

a = E_d and E_m are dynamic and monotonic moduli, respectively; E_d obtained at 1000 cycles except for 11-21 which was obtained at 1500 cycles.

b = R ratio after 130 000 cycles was between 0.12 and 0.15.

TABLE C5

FATIGUE TESTING OF $(0/90/\pm45)_s$ COUPONS AT 448 MPa, MODULUS AND EDGE REPLICATION DATA

R = +0.1, f = 10 Hz

Coupon ID	Initial[a] Moduli, GPa	Cycles (Thousands)	Dynamic Modulus GPa	Percent of Initial Modulus	Monotonic Modulus, GPa	Percent of Initial Modulus	Average Crack Spacing mm/Crack 90	+45	-45
11-13	E_d = 54.7	18.0	53.6	98.1	52.7	98.4	0.355	0.610	1.803
		24.0	52.5	96.0	52.0	97.1	0.305	0.533	1.067
	E_m = 53.5	29.0	51.6	94.4	--	--	--	--	--
		29.4	Coupon failed						
11-19	E_d = 55.0	8.0	54.2	98.4	Coupon failure due to operator error				
	E_m = 54.1								
11-54	E_d = 54.2	7.8	53.1	98.0	51.7	97.8	No NDI Data Obtained		
		8.3	Coupon failed						
	E_m = 52.9								

a = E_d amd E_m are dynamic and monotonic moduli, respectively; initial E_d obtained at 1000 cycles except for 11-54 which was obtained at 1600 cycles.

TABLE C6
COUPON 11-1, FATIGUE TESTING, STIFFNESS DATA
R = +0.1, f = 10 Hz. Fatigue Stress Level = 379 MPa

NDI Level	Number of Fatigue Cycles (Thousands)	Monotonic Stiffness, GPa	Percent of Initial Stiffness	Dynamic Stiffness GPa	Percent of Initial Stiffness
1	0	53.3	100.0	--	--
	0.75			54.6	100.0
	6.50			54.6	100.0
	15.00			54.5	99.8
	25.00			54.3	99.4
	35.00			54.2	99.1
	55.00			53.7	98.4
	75.00			53.4	97.8
	95.00			53.0	97.0
	105.00	51.9	97.5	52.9	96.8
2	106.00			52.0	96.6
	111.00			53.0	97.0
	118.00			51.9	94.9
	122.00			51.8	94.9
	132.00			51.6	94.4
	142.00			51.4	94.0
	162.00	50.2	94.2	50.8	92.9
3	170.25			50.5	92.4
	171.00			50.5	92.5
	183.15			49.6	90.7
	183.75	48.4	90.8	49.7	91.0
4	184.25			50.0	91.6
	188.75			49.7	91.0
	198.75	45.7	86.0	48.6	88.9
	198.75	FAILURE			

TABLE C7
COUPON 11-1 FATIGUE TESTING, DELAMINATION DATA

R = +0.1, f = 10 Hz, Fatigue Stress Level = 55 ksi
Initial Moduli, E_d = 7.92, E_m = 7.72[a]

Loading Condition	Geometric Loc. of Delamination, in.	Delamination Length		Delamination Depth		Delamination Area		Total Delaminated Area		Apparent Major Ply Interface
		in.	mm	in.	mm	$in.^2$	mm^2	$in.^2$	mm^2	
105 K Cycles E_d = 7.67[a] E_m = 7.53	R-2.02 to -1.63[b]	0.39	9.9	0.11	2.8	0.04	26			90/+45
	R-0.09 to +0.29	0.38	9.6	0.07	1.8	0.03	19			+45/-45
162 K Cycles E_d = 7.36 E_m = 7.28	R-2.37 to -1.60	0.77	19.6	0.16	4.1	0.04	26	0.06	39	90/+45
	R-0.87 to +0.55	1.42	36.1	0.28	7.1	0.30	194			90/+45
	R+1.15 to +1.44	0.29	7.4	0.09[c]	2.3	0.01	6			90/+45[e]
	L+0.11 to +1.96	--	--	0.04[c]	1.0	0.14	90			90/+45[e]
	L+2.15 to +3.02	0.87	22.1	0.21	5.3	--	--	0.11	71	90/+45[e]
184 K Cycles E_d = 7.21 E_m = 7.01	R-3.17 to -1.53	1.64	42.2	0.40	10.2	0.13	84	0.47	303	90/+45
	R-1.30 to +0.46	1.76	45.0	0.41	10.4	0.52	335			90/+45
	R[d]									
	L-0.25 to +0.93	1.18	30.0	0.17	4.3	0.13	84			+45/-45
	L+2.10 to +3.13	1.03	26.7	0.24	6.1	--	--	0.17	110	f
	L+0.78 to +2.31	1.53	39.4	0.29	7.4	0.25	161	0.34	219	+45/-45
199 K Cycles E_d = 7.05 E_m = 9.65	FAILURE DUE TO OPERATOR ERROR									

a = E_d and E_m are dynamic and monotonic moduli, respectively, units of 10^6 psi
b = L and R indicate left and right side of coupon
c = Maximum of three small delaminations
d = Delamination does not appear in photograph
e = Dominant delamination, but +45/-45 delamination is clearly evident
f = Delamination occurred outside of edge replication region

TABLE C8
COUPON 11-3, FATIGUE TESTING, STIFFNESS DATA
R = +0.1, F = 10 Hz, Fatigue Stress Level = 379 MPa

NDI Level	Number of Fatigue Cycles (Thousands)	Monotonic Stiffness, GPa	Percent of Initial Stiffness	Dynamic Stiffness GPa	Percent of Initial Stiffness
1	0.00	53.0	100.0	--	--
	2.00			54.1	100.0
	50.00			53.9	99.7
	90.00			53.1	98.2
	100.00			52.8	97.5
	110.00			52.0	96.1
	114.00	51.0	96.3	51.9	95.9
2	115.00				
	119.00			51.3	94.8
	124.00			51.0	94.2
	134.00			50.7	93.7
	139.00			50.2	92.8
	140.50	48.9	92.4	49.9	92.2
3	143.10			49.8	92.0
	150.50			49.3	91.1
	160.50			48.6	89.8
	166.90	FAILURE		48.2	89.2

TABLE C9
COUPON 11-3 FATIGUE TESTING, DELAMINATION DATA

R = +0.1, f = 10 Hz, Fatigue Stress Level = 55 ksi
Initial Moduli, E_d = 7.85, E_m = 7.68[a]

Loading Condition	Geometric Loc. of Delamination, in.	Delamination Length		Delamination Depth		Delamination Area		Total Delaminated Area		Apparent Major Ply Interface
		in.	mm	in.	mm	$in.^2$	mm^2	$in.^2$	mm^2	
114 K Cycles E_d = 7.53[a] E_m = 7.40	L-2.22 to +0.41[b]	2.63	66.8	0.39	9.9	0.73	471	0.77	497	90/+45
140 K Cycles E_d = 7.22 E_m = 7.10	L-2.33 to +1.85	4.18	106.2	0.59	15.0	1.82	1174	1.88	1213	90/+45
167 K Cycles E_d = 7.00	FAILURE, LOCATION CENTER LINE +1.6 in.									

a = E_d and E_m are dynamic and monotonic moduli, respectively, units of 10^6 psi
b = L and R indicate left and right side of coupon

TABLE C10
COUPON 11-9, FATIGUE TESTING, STIFFNESS DATA
R = +0.1, f = 10 Hz, fatigue Stress Level = 379 MPa

NDI Level	Number of Fatigue Cycles (Thousands)	Monotonic Stiffness, GPa	Percent of Initial Stiffness	Dynamic Stiffness GPa	Percent of Initial Stiffness
1	0.00	53.5	100.0	--	--
	2.00			54.5	100.0
	10.00			54.3	99.7
	40.00			54.1	99.3
	58.00			53.8	98.8
	78.00			53.5	98.2
	100.00			53.1	97.4
	110.00			52.9	97.1
	120.00			52.7	96.7
	130.00			52.4	96.3
	140.00			52.3	96.1
	150.00			52.1	95.7
	157.00	50.8	95.0	51.9	95.3
2	158.00			51.0	93.6
	162.00			50.8	93.3
	172.00			50.5	92.7
	182.00			50.0	91.8
	192.00	48.9	91.4	49.5	90.9
3	193.03			49.4	90.6
	197.00			49.2	90.3
	202.00			49.0	89.9
	207.00			48.8	89.5
	212.00			48.8	89.5
	217.00			48.7	89.4
	222.00			48.7	89.3
	223.01			48.4	89.0
	224.09	47.0	87.8	48.5	89.0
4	224.29			50.1	92.0
	229.00			50.0	91.8
	234.09			49.8	91.5
	235.89			49.6	91.0
	240.89			49.5	90.8
	245.00			49.3	90.5
	250.00			49.1	90.2
	251.00	48.0	89.6	49.0	90.0

TABLE C10 (Continued)
COUPON 11-9, FATIGUE TESTING, STIFFNESS DATA
R = +0.1, f = 10 Hz, fatigue Stress Level = 379 MPa

NDI Level	Number of Fatigue Cycles (Thousands)	Monotonic Stiffness, GPa	Percent of Initial Stiffness	Dynamic Stiffness GPa	Percent of Initial Stiffness
5	252.00			48.1	88.2
	261.00			47.6	87.4
	271.00	45.3	84.7	46.8	85.9
6	271.10			46.4	85.2
	281.00			45.7	83.9
	291.00			45.0	82.7
	299.15			FAILURE	

TABLE C11
COUPON 11-9 FATIGUE TESTING, DELAMINATION DATA

R = +0.1, f = 10 Hz, Fatigue Stress Level = 55 ksi
Initial Moduli, E_d = 7.90, E_m = 7.76[a]

Loading Condition	Geometric Loc. of Delamination, in.	Delamination Length		Delamination Depth		Delamination Area		Total Delaminated Area		Apparent Major Ply Interface
		in.	mm	in.	mm	$in.^2$	mm^2	$in.^2$	mm^2	
157 K Cycles E_d = 7.53[a] E_m = 7.37	L-0.39 to +1.06[b] R-1.09 to -0.46	1.45 0.63	36.8 16.5	0.25 0.07	6.4 1.8	0.24 0.04	155 26			90/+45 +45/-45
192 K Cycles E_d = 7.18 E_m = 7.09	L-0.42 to +3.06 R-2.00 to +2.00[c]	3.48 --	88.4 --	0.49 --	12.4 --	1.04 0.14	671 90	1.29	832	90/+45 +45/-45
224 K Cycles E_d = 7.03 E_m = 6.82	L-0.80 to +3.12 L-1.59 to -1.01 R-2.00 to +2.00	3.92 0.58 4.00	99.6 16.0 101.6	0.73 0.11 0.11	18.5 2.8 2.8[d]	1.39 0.05 0.12	897 32 77	1.85	1194	90/+45 90/+45 +45/-45
250 K Cycles E_d = 7.11 E_m = 6.96	L-0.87 to +3.38 L-1.59 to -0.96 L-2.00 to -1.65 L-2.69 to -0.08 R-2.00 to +2.00	4.25 0.63 0.35 2.61 4.00	108.0 16.0 8.9 13.7 101.6	0.85 0.16 0.06 0.14 0.14	21.6 4.1 1.5[d] 3.5 3.5[d]	2.03 0.05 0.02 -- 0.33	1310 32 13 -- 213	2.70 0.06	1742 39	90/+45 90/+45 +45/-45 e +45/-45
271 K Cycles E_d = 6.78 E_m = 6.57	DELAMINATION DATA NOT OBTAINED									
299.2 K Cycles	FAILURE, LOCATION CENTER LINE +0.8 in.									

a = E_d and E_m are dynamic and monotonic moduli, respectively, units of 10^6 psi
b = L and R indicate left and right side of coupon
c = Several small delaminations
d = Not thumbnail shape
e = Out of edge replication area

TABLE C12

COUPON 11-18, FATIGUE TESTING, STIFFNESS DATA

R = +0.1, f = 10 Hz, Fatigue Stress Level = 414 MPa

NDI Level	Number of Fatigue Cycles (Thousands)	Monotonic Stiffness, GPa	Percent of Initial Stiffness	Dynamic Stiffness GPa	Percent of Initial Stiffness
1	0.00	53.4	100.0	--	--
	1.00			54.3	100.0
	12.00			54.1	99.6
	20.00			53.6	98.7
	30.00			53.1	97.8
	40.00			53.2	97.9
	50.00			53.1	97.7
	60.00	51.8	97.0	52.5	96.7
	60.00	FAILURE, OPERATOR ERROR			

TABLE C13
COUPON 11-18 FATIGUE TESTING, DELAMINATION DATA

R = +0.1, f = 10 Hz, Fatigue Stress Level = 60 ksi
Initial Moduli, E_d = 7.88, E_m = 7.75[a]

Loading Condition	Geometric Loc. of Delamination, in.	Delamination Length		Delamination Depth		Delamination Area		Total Delaminated Area		Apparent Major Ply Interface
		in.	mm	in.	mm	$in.^2$	mm^2	$in.^2$	mm^2	
60 K Cycles E_d = 7.62[a] E_m = 7.52	-0.46 to +0.12[b] L+0.51 to +0.96 L+1.72 to +2.29	0.58 0.45 0.57	14.7 11.4 14.5	0.02 0.02 0.02	0.5 0.5 0.5	0.02 0.02 0.02	13 13 13			+45/-45 +45/-45 +45/-45
60+ K Cycles	FAILURE DUE TO OPERATOR ERROR									

a = E_d and E_m are dynamic and monotonic moduli, respectively, units of 10^6 psi
b = L and R indicate left and right side of coupon

TABLE C14
COUPON 11-21, FATIGUE TESTING, STIFFNESS DATA
R = +0.1, f = 10 Hz, Fatigue Stress Level = 414 MPa

NDI Level	Number of Fatigue Cycles (Thousands)	Monotonic Stiffness, GPa	Percent of Initial Stiffness	Dynamic Stiffness GPa	Percent of Initial Stiffness
a	0.00	53.2	100.0	--	--
	1.50			54.6	100.0
	6.00			54.4	99.7
	10.80			55.1	101.0
	15.00			54.9	100.6
	20.00			54.9	100.7
	30.00			54.6	100.0
	40.00			54.0	99.0
	50.00			53.6	98.2
	55.00			52.4	96.0
	70.00	51.6	97.0	51.7	94.7
	90.00	52.0	97.8	--	--
	100.00	50.6	95.1	--	--
	120.00	50.3	94.6	--	--
	130.00			48.0[b]	87.9
	140.00			47.6	87.2
	150.00			47.4	86.8
	160.00	49.2	92.4	46.3	84.9
	170.00			45.9	84.1
	180.00	48.4	90.9	45.5	83.3
	190.00			45.2	82.8
	200.00			45.6	83.5
	212.00	47.2	88.7	44.0	80.6
	212.00	--	--	FAILURE	

a = No NDI taken
b = R ratio at 130 000 and subsequent cycles was approximately +0.15 instead of +0.1

TABLE C15
COUPON 11-25, FATIGUE TESTING, STIFFNESS DATA
R = +0.1, f = 10 Hz, Fatigue Stress Level = 414 MPa

NDI Level	Number of Fatigue Cycles (Thousands)	Monotonic Stiffness, GPa	Percent of Initial Stiffness	Dynamic Stiffness GPa	Percent of Initial Stiffness
1	0	52.7	100.0	--	--
	10.00			54.6	100.0
	20.00			54.3	99.5
	30.00			53.6	98.2
	33.50	52.0	98.7	53.6	98.2
2	38.00			52.3	95.8
	43.50			51.9	95.1
	48.50			51.6	94.5
	50.50	50.8	96.5	51.5	94.2
3	51.00			51.8	94.8
	51.50			51.7	94.6
	52.00			51.8	94.9
	52.50			51.6	94.5
	54.50			51.3	92.9
	57.50			51.1	93.6
	61.50			50.8	93.1
	64.50			50.5	92.5
	65.20			FAILURE	

TABLE C16
COUPON 11-25 FATIGUE TESTING, DELAMINATION DATA

R = +0.1, F = 10 Hz, Fatigue Stress Level = 60 ksi
Initial Moduli, E_d = 7.94, E_m = 7.64[a]

Loading Condition	Geometric Loc. of Delamination, in.	Delamination Length		Delamination Depth		Delamination Area		Total Delaminated Area		Apparent Major Ply Interface
		in.	mm	in.	mm	$in.^2$	mm^2	$in.^2$	mm^2	
34 K Cycles E_d = 7.78[a] E_m = 7.55	R-0.72 to -0.39	0.33	8.4	0.04	1.0	0.02	13			+45/-45
50 K Cycles E_d = 7.46 E_m = 7.37	R-2.00 to +2.00 L-2.00 to +2.00	NUMEROUS SMALL DELAMINATIONS OVER ENTIRE GAGE LENGTH								+45/-45 +45/-45
64 K Cycles E_d = 7.33										
65 K Cycles		FAILURE, LOCATION CENTER LINE - 1.2 in.								

a = E_d and E_m are dynamic and monotonic moduli, respectively, units of 10^6 psi
b = L and R indicate left and right side of coupon

TABLE C17
COUPON 11-45, FATIGUE TESTING, STIFFNESS DATA
R = +0.1, f = 10 Hz, Fatigue Stress Level = 414 MPa

NDI Level	Number of Fatigue Cycles (Thousands)	Monotonic Stiffness, GPa	Percent of Initial Stiffness	Dynamic Stiffness GPa	Percent of Initial Stiffness
1	0	53.2	100.0	--	--
	1.00			54.6	100.0
	2.00			54.7	100.1
	10.00			54.5	99.8
	20.00			54.3	99.4
	30.00			53.7	98.4
	40.00	51.6	97.1	53.1	97.3
2	41.00			52.4	95.9
	45.00			52.5	96.1
	47.00			52.2	95.7
	47.50			52.2	95.6
	48.50			52.2	95.6
	50.00			52.0	95.3
	54.00			51.6	94.5
	58.00			51.3	93.9
	58.20	51.00	95.8	51.0	93.3
3	59.00			51.3	93.9
	60.10	FAILURE			

TABLE C18
COUPON 11-45 FATIGUE TESTING, DELAMINATION DATA

R = +0.1, f = 10 Hz, Fatigue Stress Level = 60 ksi
Initial Moduli, E_d = 7.70, E_m = 7.71[a]

Loading Condition	Geometric Loc. of Delamination, in.	Delamination Length		Delamination Depth		Delamination Area		Total Delaminated Area		Apparent Major Ply Interface
		in.	mm	in.	mm	$in.^2$	mm^2	$in.^2$	mm^2	
40 K Cycles E_d = 7.70[a] E_m = 7.49	L+2.41 to +3.07[b]	0.66	16.8	0.13	3.3			0.05	32	---
58 K Cycles	L+2.08 to +3.38	1.30	33.0	0.29	7.4			0.23	148	+45/-45
E_d = 7.44	L-1.70 to -0.46	1.24	31.5	0.05	1.3[c]	0.05	32			+45/-45
E_m = 7.39	R-2.24 to -1.50	0.74	18.8	0.05	1.3[c]	0.03	19	0.04	26	90/+45
	R+0.25 to +1.91	1.66	42.2	0.32	8.1	0.41	265			90/+45
59 K Cycles E_d = 7.43										
60 K Cycles	FAILURE, LOCATION CENTER LINE +0.7 in.									

a = E_d and E_m are dynamic and monotonic moduli, respectively, units of 10^6 psi
b = L and R indicate left and right side of coupon
c = Not a thumbnail shape

TABLE C19
COUPON 11-13, FATIGUE TESTING, STIFFNESS DATA
R = +0.1, f = 10 Hz, Fatigue Stress Level = 448 MPa

NDI Level	Number of Fatigue Cycles (Thousands)	Monotonic Stiffness, GPa	Percent of Initial Stiffness	Dynamic Stiffness GPa	Percent of Initial Stiffness
1	0	53.5	100.0	—	—
	1.00			54.7	100.0
	2.00			54.8	100.1
	3.00			55.0	100.6
	4.00			54.7	100
	6.00			54.4	99.5
	8.00			54.4	99.5
	10.00			54.3	99.3
	12.00			54.2	99.0
	14.00			53.9	98.6
	16.00			53.8	98.3
	18.00	52.7	98.4	53.6	98.1
2	19.00			53.2	97.2
	23.00			52.6	96.2
	24.00	52.00	97.1	52.5	96.0
3	25.00			52.4	95.9
	27.50			52.0	95.1
	29.00			51.6	94.4
	29.40	FAILURE			

TABLE C20
COUPON 11-13 FATIGUE TESTING, DELAMINATION DATA

R = +0.1, f = 10 Hz, Fatigue Stress Level = 65 ksi
Initial Moduli, E_d = 7.93, E_m = 7.76[a]

Loading Condition	Geometric Loc. of Delamination, in.	Delamination Length		Delamination Depth		Delamination Area		Total Delaminated Area		Apparent Major Ply Interface
		in.	mm	in.	mm	$in.^2$	mm^2	$in.^2$	mm^2	
18 K Cycles E_d = 7.78[a] E_m = 7.64	R-0.29 to -0.11[b]	0.18	4.6	0.04	1.0	0.01	6			90/+45
24 K Cycles E_d = 7.62 E_m = 7.54	R-0.37 to +0.29	0.66	16.8	0.11	2.8	0.06	39			90/+45
	R-2.10 to -1.88	0.22	5.6	0.05	1.3	0.01	6			+45/-45
	R-1.74 to -1.51	0.23	5.8	0.06	1.5	0.01	6			+45/-45
	R-1.29 to -0.74	0.55	14.0	0.12	3.0	0.03	19			+45/-45
	L-1.62 to -1.18	0.45	11.4	0.10	2.5	0.03	19			+45/-45
29 K Cycles E_d = 7.49	FAILURE, LOCATION CENTER LINE +0.1 in.									

a = E_d and E_m are dynamic and monotonic moduli, respectively, units of 10^6 psi
b = L and R indicate left and right side of coupon

TABLE C21
COUPON 11-19, FATIGUE TESTING, STIFFNESS DATA
R = +0.1, f = 10 Hz, Fatigue Stress Level = 448 MPa

NDI	Number of Fatigue Cycles (Thousands)	Monotonic Stiffness, GPa	Percent of Initial Stiffness	Dynamic Stiffness GPa	Percent of Initial Stiffness
a	0	54.1	100.0	--	--
	1.00			55.0	100
	4.00			54.6	99.2
	5.00			54.6	99.1
	7.00			54.4	98.8
	8.00			54.2	98.4
	8.00	FAILURE OPERATOR ERROR			

a = No NDI taken

TABLE C22
COUPON 11-54, FATIGUE TESTING, STIFFNESS DATA
R = +0.1, f = 10 Hz, Fatigue Stress Level = 448 MPa

NDI Level	Number of Fatigue Cycles (Thousands)	Monotonic Stiffness, GPa	Percent of Initial Stiffness	Dynamic Stiffness GPa	Percent of Initial Stiffness
a	0	52.9	100.00	--	--
	1.60			54.2	100.0
	5.30			53.6	98.9
	7.80			53.1	98.1
	8.30	51.7	97.8	FAILURE	

a = No NDI taken

TABLE C23
COUPON 11-8 RESIDUAL STRENGTH TESTING, DELAMINATION DATA

R = +0.1, f = 10 Hz, Fatigue Stress Level = 55 ksi
Initial Monotonic Modulus = 7.48 x 10^6 psi

Loading Condition	Geometric Loc. of Delamination, in.	Delamination Length		Delamination Depth		Delamination Area		Total Delaminated Area		Apparent Major Ply Interface
		in.	mm	in.	mm	$in.^2$	mm^2	$in.^2$	mm^2	
Fat. L1	L-1.06 to -0.18[a]	0.88	22.4	0.06	1.5	0.03	19			+45/-45
125 K Cycles	L+1.52 to +1.91	0.39	9.9	0.12	3.0	0.03	19			90/+45
E = 7.17[b]	R+1.76 to +2.04	0.28	7.1	0.07	1.8	0.02	13			90/+45
Fat. L2	L-2.12 to +0.54	2.66	67.6	0.15	3.8	0.18	116			+45/-45
150 K Cycles	L+1.36 to +2.03	0.67	17.0	0.18	4.6	0.09	58			90/+45
E = 6.71	R[d]									90/+45
	R-2.43 to +0.27	2.70	68.6	0.50	12.7	0.91	587	1.00	645	90/+45
Res. Str. 1	L-2.28 to +0.52	2.80	71.1	0.16	4.1	0.20	129			+45/-45
ϵ_1 = 0.00825[c]	L+1.39 to +2.04	0.65	16.5	0.20	5.1	0.09	58			90/+45
E = 6.87	R+1.44 to +2.14	0.70	17.8	0.21	5.3	0.08	52	0.10	65	90/+45
	R-2.48 to +0.31	2.79	70.9	0.54	13.7	1.04	671	1.14	735	90/+45
	R+0.47 to +1.22	0.75	19.0	0.19	4.8	0.11	71			90/+45
	R+2.25 to +2.56	0.31	7.9	0.07	1.8	--	--	0.03	19	90/+45
Res. Str. 2	L-2.36 to +0.51	2.87	72.9	0.14	3.6	0.20	123	0.22	142	+45/-45
ϵ_2 = 0.00900	L+1.36 to +2.03	0.67	17.0	0.17	4.3	0.08	52			90/+45
E = 6.78	R+1.47 to +2.16	0.69	17.5	0.20	5.1	0.09	45	0.09	58	90/+45
	R-2.48 to +0.28	2.76	70.1	0.52	13.2	1.00	645	1.09	703	90/+45
	R+0.47 to +1.20	0.73	18.5	0.18	4.6	0.09	58			90/+45
	R+2.30 to +2.59	0.29	7.4	0.08	2.0	--	--	0.02	13	e
Res. Str. 3	FAILURE, LOCATION CENTER LINE -0.4 INCH, σ_f = 63.2 ksi, ϵ_f = 0.0095, E_f = 7.01 x 10^6 psi									

a = L indicates left edge of coupon, R indicates right edge
b = Monotonic load moduli at end of fatigue loading level or during residual strength loading, units of 10^6 psi
c = Strain level reached during residual strength loading
d = Delamination too faint to record dimensions.
e = Delamination region outside replication length

TABLE C24
COUPON 11-8 RESIDUAL STRENGTH TESTING, MATRIX CRACK DATA

R = +0.1, f = 10 Hz, Fatigue Stress Level = 55 ksi[a]
Initial Moduli, E_d = 7.63, E_m = 7.48

Loading Condition	Average No. of Cracks Cracks/in.			Average Crack Spacing in.			Average Crack Spacing mm		
	90	+45	-45	90	+45	-45	90	+45	-45
Fat. L1 125 K Cycles E_d = 7.24[a] E_m = 7.17	97	46	17	0.010	0.022	0.059	0.25	0.56	1.50
Fat. L2 150 K Cycles E_d = 6.92 E_m = 6.71	96	47	16	0.010	0.021	0.062	0.25	0.53	1.58

a = E_d and E_m are the moduli obtained at the end of fatigue (dynamic) and monotonic loading level, units of 10^6 psi

TABLE C25
COUPON 11-10 RESIDUAL STRENGTH TESTING, DELAMINATION DATA

R = +0.1, f = 10 Hz, Fatigue Stress Level$_6$ = 55 ksi
Initial Monotnic Modulus = 7.81 x 10^6 psi

Loading Condition	Geometric Loc. of Delamination, in.	Delamination Length		Delamination Depth		Delamination Area		Total Delaminated Area		Apparent Major Ply Interface
		in.	mm	in.	mm	in.^{2}	mm^2	in.^{2}	mm^2	
Fat. L1	L-2.02 to +1.83[a]	3.85	97.8	0.56	14.2	1.57	1013			90/+45
125 K Cycles	L+2.21 to +2.66	0.45	11.4	0.08	2.0	0.03	19			d
E = 7.13	R-2.79 to -1.08	1.71	43.4	0.27	6.6	0.13	84	0.33	213	90/+45
	R-0.53 to +0.72	1.25	31.8	0.24	6.1	0.20	129			90/+45
Fat. L2	L-2.45 to +3.11	5.56	141.2	0.76	19.3	2.98	1922	3.46	2232	90/+45
150 K Cycles	L e									
E = 6.31	R-3.42 to +1.49	4.91	124.7	0.66	16.8	1.88	1213	2.37	1529	90/+45
	R e									
	R+1.86 to +2.52	0.72	18.3	0.19	4.8	0.02	13	0.08	52	d
	R+1.86 to +2.52	0.66[c]	16.8	1.00[c]	25.4	0.07[c]	45	0.64[c]	413	d
Res. Str. 1	L-2.36 to +3.13	5.49	139.4	0.83	21.1	3.03	1955	3.54	2284	90/+45
ϵ_1= 0.00900[c]	R-3.41 to +1.51	4.92	125.0	0.70	17.8	2.20	1419	2.76	1781	90/+45
E = 6.30	R+1.86 to +2.52	0.66[c]	16.8	1.00[c]	25.4	0.07[c]	45	0.64[c]	413	d
Res. Str. 2	L-2.31 to +3.14	5.45	138.4	0.81	20.6	3.00	1935	3.51	2264	90/+45
ϵ_2= 0.00950	R-3.42 to +1.50	4.92[c]	125.0	0.73	18.5	2.16[c]	1394	2.69[c]	1735	90/+45
E = 6.26	R+1.84 to +2.56	0.72[c]	18.3	0.98	24.9	0.07[c]	45	0.64[c]	413	d
Res. Str. 3	L-2.36 to +3.16	5.52	140.7	0.80	20.3	3.06	1974	3.55	2290	90/+45
ϵ_3= 0.01000	R-3.43 to +1.54	4.97	126.2	0.71[c]	18.0	2.24[c]	1445	2.82	1819	90/+45
E = 6.15	R+1.86 to +2.55	0.69[c]	17.5	1.00[c]	25.4	0.07[c]	45	0.64	413	d
Res. Str. 4	FAILURE, LOCATION CENTER LINE +1.5 INCH, σ_f = 66.9 ksi, ϵ_f = 0.0106, E_f = 6.30 x 10^6 psi									

a = L indicates left edge of coupon, R indicates right edge
b = Monotonic load moduli at end of fatigue loading level or during residual strength loading, units of 10^6 psi
c = Strain level reached during residual strength loading
d = Delamination region outside edge replication length
e = Edge delamination merger
f = Mid-bay failure

TABLE C26
COUPON 11-10 RESIDUAL STRENGTH TESTING, MATRIX CRACK DATA

R = +0.1, f = 10 Hz, Fatigue Stress Level = 55 ksi
Initial Moduli, E_d = 7.90, E_m = 7.81 [a]

Loading Condition	Average No. of Cracks Cracks/in.			Average Crack Spacing in.			Average Crack Spacing mm		
	90	+45	-45	90	+45	-45	90	+45	-45
Fat. L1 125 K Cycles E_d = 7.23[a] E_m = 7.13	84	40	12	0.012	0.025	0.083	0.30	0.64	2.11
Fat. L2 150 K Cycles E_d = 6.49 E_m = 6.31	89	42	22	0.011	0.024	0.045	0.28	0.61	1.14

a = E_d and E_m are the moduli obtained at the end of fatigue (dynamic) and monotonic loading level, units of 10^6 psi

TABLE C27
COUPON 11-11 RESIDUAL STRENGTH TESTING, DELAMINATION DATA

R = +0.1, f = 10 Hz, Fatigue Stress Level = 55 ksi
Initial Monotonic Modulus = 7.80 x 10^6 psi

Loading Condition	Geometric Loc. of Delamination, in.	Delamination Length		Delamination Depth		Delamination Area		Total Delaminated Area		Apparent Major Ply Interface
		in.	mm	in.	mm	$in.^2$	mm^2	$in.^2$	mm^2	
Fat. L1	L-2.53 to +0.60[a]	3.13	79.5	0.46	11.7	0.89	574	0.96	619	90/+45
125 K Cycles	L+2.52 to +3.16	0.64	16.3	0.14	3.6	--	--	0.06	39	d
E = 7.31[b]										
Fat. L2	L-2.56 to +3.11[e]	5.67	144.0	0.76	19.3	2.89	1864	3.45	2226	90/+45
150 K Cycles										
E = 6.93										
Res. Str. 1	L-2.56 to +3.13	5.69	144.5	0.78	19.8	2.90	1845	3.40	2194	90/+45
ϵ_1 = 0.00825[c]	R-0.24 to +0.17	0.41	10.4	0.06	1.5	0.03	19			+45/-45
E = 6.99										
Res. Str. 2	L-2.56 to +3.15	5.71	145.0	0.78	19.8	2.90	1852	3.44	2219	90/+45
ϵ_2 = 0.00900	R-0.18 to +0.15	0.33	8.4	0.08	2.0	0.04	26	--	--	+45/-45
E = 6.92										
Res. Str. 3	L-2.60 to +3.15	5.75	146.0	0.79	20.1	2.96	1910	3.56	2297	90/+45
ϵ_3 = 0.00950	R-0.47 to +0.16	0.63	16.0	0.07	1.8	0.04	26	--	--	+45/-45
E = 6.82										
Res. Str 4	FAILURE, LOCATION CENTER LINE -1.2 INCH, σ_f = 65.5 ksi, ϵ_f = 0.0096, E_f = 6.86 x 10^6 psi									

a = L indicates left edge of coupon, R indicates right edge
b = Monotonic load moduli at end of fatigue loading level or during residual strength loading, units of 10^6 psi
c = Strain level reached during residual strength loading
d = Delaminated region was outside of the edge replication length
e = Two delamination merger

TABLE C28
COUPON 11-11 RESIDUAL STRENGTH TESTING, MATRIX CRACK DATA

R = +0.1, f = 10 Hz, Fatigue Stress Level = 35 ksi
Initial Moduli, E_d = 7.98, E_m = 7.80[a]

Loading Condition	Average No. of Cracks Cracks/in.			Average Crack Spacing in.			Average Crack Spacing mm		
	90	+45	-45	90	+45	-45	90	+45	-45
Fat. L1 125 K Cycles E_d = 7.44[a] E_m = 7.31	87	43	19	0.011	0.023	0.053	0.28	0.58	1.35
Fat. L2 150 K Cycles E_d = 6.98 E_m = 6.93	82	43	20	0.012	0.023	0.050	0.30	0.58	1.27

a = E_d and E_m are the moduli obtained at the end of fatigue (dynamic) and monotonic loading level, units of 10^6 psi

TABLE C29
COUPON 11-12 RESIDUAL STRENGTH TESTING, DELAMINATION DATA

R = 0.1, f = 10 Hz, Fatigue Stress Level = 55 ksi
Initial Monotonic Modulus = 7.72×10^6 psi

Loading Condition	Geometric Loc. of Delamination, in.	Delamination Length in.	Delamination Length mm	Delamination Depth in.	Delamination Depth mm	Delamination Area $in.^2$	Delamination Area mm^2	Total Delaminated Area $in.^2$	Total Delaminated Area mm^2	Apparent Major Ply Interface
Fat. L1 125 K Cycles E = 7.45[a]	NO VISABLE DELAMINATION									b
Fat. L2	COUPON WAS ACCIDENTALLY OVERLOADED BEFORE REACHING 150 000 CYCLES									

a = L indicates left edge of coupon, R indicates right edge
b = Delamination too faint to record dimensions.

TABLE C30
COUPON 11-12 RESIDUAL STRENGTH TESTING, MATRIX CRACK DATA

R = +0.1, f = 10 Hz, Fatigue Stress Level = 55 ksi
Initial Moduli, E_d = 7.93, E_m = 7.71[a]

Loading Condition	Average No. of Cracks Cracks/in.			Average Crack Spacing in.			Average Crack Spacing in.		
	90	+45	-45	90	+45	-45	90	+45	-45
Fat. L1 125 K Cycles E_d = 7.55 E_m = 7.45	92	26	12	0.011	0.038	0.083	0.28	0.96	2.11
Fat. L2 150 K Cycles	COUPON ACCIDENTALLY OVERLOADED BEFORE REACHING 150 000 CYCLES								

a = E_d and E_m are the moduli obtained at the end of fatigue (dynamic) and monotonic loading level, units of 10^6 psi

TABLE C31
COUPON 11-16 RESIDUAL STRENGTH TESTING, DELAMINATION DATA

R = +0.1, F = 10Hz, Fatigue Stress Level = 55 ksi
Initial Monotonic Modulus = 7.62×10^6 psi

Loading Condition	Geometric Loc. of Delamination, in.	Delamination Length		Delamination Depth		Delamination Area		Total Delaminated Area		Apparent Major Ply Interface
		in.	mm	in.	mm	$in.^2$	mm^2	$in.^2$	mm^2	
Fat. L1 125 K Cycles E = 7.25[b]	NO VISABLE DELAMINATION									
Fat. L2 150 K Cycles E = 7.41	L-2.69 to -0.32[a] R-1.94 to -1.52	2.37 0.42	60.2 10.7	0.10 0.09	2.5 2.3	0.14 0.04	90 26	0.20	129	+45/-45 +45/-45
Res. Str. 1 ϵ_1 = 0.00850[c] E = 7.39	L-3.01 to +2.27 R-1.99 to -0.28	5.28 1.71	134.1 43.4	0.18 0.15	4.6 3.8	0.40 0.11	258 71	0.50 0.13	323 84	+45/-45 +45/-45
Res. Str. 2 ϵ_2 = 0.00925 E = 7.44	L-3.41 to +0.38 R-1.96 to -0.31	3.79 1.65	96.3 41.9	0.14 0.13	3.6 3.3	0.18 0.17	116 110	0.27	174	+45/-45 +45/-45[d]
	L+0.68 to +1.74 R+0.10 to +2.89	1.06 2.99	26.9 76.0	0.08 0.18	2.0 4.6	0.09 0.14	58 90	0.19	123	90/+45 +45/-45 +45/-45
Res. Str. 3	FAILURE LOCATION, CENTER LINE -0.4, σ_f = 70.6 ksi, ϵ_f = 0.0098, E_f = 7.23×10^6 psi									

a = L indicates left edge of coupon, R indicates right edge
b = Monotonic load moduli at end of fatigue loading level or during residual strength loading, units of 10^6 psi
c = Strain level reached during residual strength loading
d = Two separate delaminations, -1.96 to -1.48 is 90/+45

TABLE C32
COUPON 11-16 RESIDUAL STRENGTH TESTING, MATRIX CRACK DATA

R = +0.1, f = 10 Hz, Fatigue Stress Level = 55 ksi
Initial Moduli, E_d = 7.82, E_m = 7.62[a]

Loading Condition	Average No. of Cracks Cracks/in.			Average Crack Spacing in.			Average Crack Spacing mm		
	90	+45	-45	90	+45	-45	90	+45	-45
Fat. L1 125 K Cycles E_d = 7.43[a] E_m = 7.25	96	51	20	0.010	0.020	0.050	0.25	0.51	1.27
Fat. L2 150 K Cycles E_d = 7.39 E_m = 7.41	96	53	18	0.010	0.019	0.056	0.25	0.48	1.42
Res. Str. 1 ϵ_1 = 0.00850[b] E_m = 7.39	94	51	18	0.010	0.019	0.055	0.27	0.50	1.41
Res. Str. 2 ϵ_2 = 0.00925 E_m = 7.44	100	54	19	0.010	0.018	0.053	0.25	0.47	1.34
Res. Str. 3	FAILURE, LOCATION CENTER LINE -0.4, σ_f = 70.6 ksi, ϵ_f = 0.0098, E_f = 7.23 x 10^6 psi								

a = E_d and E_m are the moduli obtained at the end of fatigue (dynamic) and monotonic loading level, units of 10^6 psi

b = Strain level reached during residual strength loading

TABLE C33
COUPON 11-17 RESIDUAL STRENGTH TESTING, DELAMINATION DATA

R = +0.1, f = 10 Hz, Fatigue Stress Level = 55 ksi
Initial Monotonic Modulus = 7.67×10^6 psi

Loading Condition	Geometric Loc. of Delamination, in.	Delamination Length		Delamination Depth		Delamination Area		Total Delaminated Area		Apparent Major Ply Interface
		in.	mm	in.	mm	$in.^2$	mm^2	$in.^2$	mm^2	
Fat. L1 125 K Cycles E = 7.07[b]	L-0.13 to +2.10[a]	2.23	56.6	0.23	5.8	0.33	213			90/+45
Fat. L2 139 K Cycles	FAILURE, LOCATION CENTER LINE -0.6									

a = L indicates left edge of coupon, R indicates right edge
b = Monotonic load moduli at end of fatigue loading level, units of 10^6 psi

TABLE C34
COUPON 11-17 RESIDUAL STRENGTH TESTING, MATRIX CRACK DATA

R = +0.1, f = 10 Hz, Fatigue Stress Level = 55 ksi
Initial Moduli, E_d = 7.96, E_m = 7.67[a]

Loading Condition	Average No. of Cracks Cracks/in.			Average Crack Spacing in.			Average Crack Spacing mm		
	90	+45	-45	90	+45	-45	90	+45	-45
Fat. L1 125 K Cycles E_d = 7.29[a] E_m = 7.07	89	44	8	0.011	0.023	0.125	0.28	0.58	3.18
Fat. L2	COUPON FAILED AT APPROXIMATELY 139 000 CYCLES								

a = E_d and E_m are the moduli obtained at the end of fatigue (dynamic) and monotonic loading level, units of 10^6 psi

TABLE C35
COUPON 11-23 RESIDUAL STRENGTH TESTING, DELAMINATION DATA

R = +0.1, f = 10 Hz, Fatigue Stress Level = 55 ksi
Initial Monotonic Modulus = 7.60 x 10^6 psi

Loading Condition	Geometric Loc. of Delamination, in.	Delamination Length		Delamination Depth		Delamination Area		Total Delaminated Area		Stacking Sequence Ply Orientation
		in.	mm	in.	mm	in^2	mm^2	in^2	mm^2	
Fat. L1 130 K Cycles E = 7.21[b]	L-2.00 to +2.00[a]	--	--	0.05	1.3	0.25	161			+45/-45
Fat. L2 162 K Cycles E = 6.84	L-2.00 to +2.00 R-2.00 to +2.00	d d	d d	d d	d d	d d	d d	d d	d d	+45/-45 +45/-45
Res. Str. 1 ϵ_1 = .00875[c] E = 7.18	L-3.33 to -0.58 L+0.07 to +1.66 R-2.14 to +2.83	2.75 1.59 4.97	69.9 403.9 126.2	0.28 0.23 0.26	7.1 5.8 6.7	0.24 0.16 0.48	155 103 310	0.47 0.61	303 394	+45/-45 +45/-45 +45/-45
Res. Str. 2 ϵ_2 = .00925 E = 7.08	L e e R e R e	5.0[e] -- 5.4[e] --	127[e] -- 140[e] --	0.28[e] -- 0.18[e] --	7.0[e] -- 4.5[e] --	-- -- -- --	-- -- -- --	0.59[e] -- 0.45[e] --	33 -- 29[e] --	+45/-45 +45/-45 +45/-45 +45/-45
Res. Str. 3 ϵ_3 = 0.01000 E = 7.07	L e L e R e R e	f f f f		f f f f						+45/-45 +45/-45 +45/-45 +45/-45
Res. Str. 4	FAILURE, LOCATION CENTER LINE -1.5, σ_f = 76.3 ksi, ϵ_f = 0.0107, E_f = 7.12 x 10^6 psi									

a = L indicates left edge of coupon, R indicates right edge
b = Monotonic load moduli at end of fatigue loading level or during residual strength loading, units of 10^6 psi
c = Strain level reached during residual strength loading
d = Small numerous delaminations connected together
e = Estimate, delaminated area not well defined, enhancing agent stains on front and back surfaces
f = Not well defined, visual comparison shows level 3 less "damaged" than level 2

TABLE C 36
COUPON 11-23 RESIDUAL STRENGTH TESTING, MATRIX CRACK DATA

R = +0.1, f = 10 Hz, Fatigue Stress Level = 55 ksi
Initial Moduli, E_d = 7.75, E_m = 7.60[a]

Loading Condition	Average No. of Cracks Cracks/in.			Average Crack Spacing in.			Average Crack Spacing mm		
	90	+45	-45	90	+45	-45	90	+45	-45
Fat. L1 130 K Cycles E_d = 7.29[a] E_m = 7.21	94	50	16	0.011	0.020	0.062	0.27	0.51	1.59
Fat. L2 161 K Cycles E_d = 7.11 E_m = 6.84	99	51	16	0.010	0.020	0.062	0.25	0.50	1.59
Res. Str. 1 ϵ_1 = 0.00875 E_m = 7.18	96	52	16	0.010	0.019	0.062	0.26	0.49	1.59
Res. Str. 2 ϵ_2 = 0.00925 E_m = 7.08	95	52	17	0.010	0.019	0.059	0.27	0.49	1.49
Res. Str. 3 ϵ_3 = 0.01000 E_m = 7.07	96	53	18	0.010	0.019	0.056	0.26	0.48	1.41
Res. Str. 4	FAILURE, LOCATION CENTER LINE -1.5, σ_f = 76.3 ksi, ϵ_f = 0.0107, E_f = 7.12 x 10^6 psi								

a = E_d and E_m are the moduli obtained at the end of fatigue (dynamic) and monotonic loading level, units of 10^6 psi

TABLE C37
COUPON 11-57 RESIDUAL STRENGTH TESTING, DELAMINATION DATA

R = +0.1, f = 10 Hz, Fatigue Stress Level = 55 ksi
Initial Monotonic Modulus = 7.76 x 10^6 psi

Loading Condition	Geometric Loc. of Delamination, in.	Delamination Length		Delamination Depth		Delamination Area		Total Delaminated Area		Apparent Major Ply Interface
		in.	mm	in.	mm	$in.^2$	mm^2	$in.^2$	mm^2	
Fat. L1	L-0.50 to +3.03[a]	3.53	89.7	0.57	14.5	1.10	710	1.41	910	90/+45
101 K Cycles	R-1.12 to +3.02	0.62	15.8	0.13	3.3	0.06	39			90/+45
E = 7.19[b]	R+2.31 to +3.02	0.71	18.0	0.11	2.8	0.06	39			d
Fat. L2										
124 K Cycles	e									
E = 7.11										
Res. Str. 1	L-0.78 to +3.25	4.03	102.4	0.71	18.0	1.62	1045	2.11	1361	90/+45
ϵ_1 = 0.00875[c]	R-1.09 to -0.29	0.80	20.3	0.18	4.6	0.09	58			90/+45
E = 7.04	R+1.58 to +3.09	1.51	38.4	0.31	7.9	0.04	26	0.28	181	90/+45
	R-0.51 to +0.28	0.79	20.1	0.17	4.3	0.09	58			90/+45
	R+0.19 to +0.51	0.32	8.1	0.09	2.3	0.02	13			90/+45
	R+0.43 to +0.94	0.51	13.0	0.13	3.3	0.04	26			90/+45
Res. Str. 2	L-0.80 to +3.22[f]	4.02	102.1	0.68[g]	17.3	1.50[g]	968	1.95	1258	90/+45
ϵ_2 = 0.00950	R-1.14 to +0.91[f]	2.05	52.1	0.19[g]	4.8	0.26[g]	168			90/+45
E = 6.94	R+1.57 to +3.10	1.53	38.9	0.31	7.9	0.03	19	0.28	181	90/+45
Res. Str. 3	L-0.74 to +3.22	3.96	100.6	0.70	17.8	1.55	1000	2.28	1471	90/+45
ϵ_3 = 0.01000	R-1.13 to +0.90	2.03	51.5	0.19	4.8	0.23	148			90/+45
E = 6.89	R+1.50 to +3.08	1.58	40.1	0.30	7.6	0.05	32	0.27	174	90/+45
Res. Str. 4	FAILURE, LOCATION CENTER LINE +1.1, σ_f = 76.2 ksi, E_f = 6.99 x 10^6 psi, ϵ_f = 0.0109									

a = L indicates left edge of coupon, R indicates right edge
b = Monotonic load moduli at end of fatigue loading level or during residual strength loading, units of 10^6 psi
c = Strain level reached during residual strength loading
d = Delaminated region was outside of the edge replication length
e = Data inadvertently not taken at 150 K Cycles
f = Not thumbnail shape
g = Four delaminations from Res. Str. 1 merged into one

TABLE C38
COUPON 11-57 RESIDUAL STRENGTH TESTING, MATRIX CRACK DATA

R = +0.1, f = 10 Hz, Fatigue Stress Level = 55 ksi
Initial Moduli E_d = 7.91, E_m = 7.76

Loading Condition	Average No. of Cracks Cracks/in.			Average Crack Spacing in.			Average Crack Spacing		
	90	+45	-45	90	+45	-45	90	+45	-45
Fat. L1 101 K Cycles E_d = 7.30 E_m = 7.19	83	48	20	0.012	0.021	0.050	0.31	0.53	1.27
Fat. L2 124 K Cycles E_d = 7.08 E_m = 7.11	80	49	22	0.012	0.020	0.045	0.31	0.51	1.14

a = E_d and E_m are the moduli obtained at the end of fatigue (dynamic) and monotonic loading level, units of 10^6 psi

TABLE C39
COUPON 11-60 RESIDUAL STRENGTH TESTING, DELAMINATION DATA

R = +0.1, f = 10 Hz, Fatigue Stress Level = 55 ksi
Initial Monotonic Modulus = 7.80 x 10^6 psi

Loading Condition	Geometric Loc. of Delamination, in.	Delamination Length		Delamination Depth		Delamination Area		Total Delaminated Area		Apparent Major Ply Interface
		in.	mm	in.	mm	$in.^2$	mm^2	$in.^2$	mm^2	
Fat. L1 100 K Cycles E = 7.08	R-1.99 to +2.25[a] R-3.27 to -1.41[d]	4.24 1.86	107.7 47.2	0.59 0.32	15.0 8.1	1.80 0.09	1161 58	0.38	245	90/+45 90/+45
Fat. L2 110 K Cycles E = 7.06	[e]									
Res. Str. 1 ϵ_1 = 0.00900[c] E = 6.95	R-2.56 to +2.24 R-3.33 to -1.45	4.80 1.88	122.0 48.0	0.70 0.32	18.0 8.0	2.29 0.11	1477 71	2.40 0.40	1548 258	90/+45 90/+45
Res. Str. 2 ϵ_2 = 0.00950 E = 6.81	R-3.37 to +2.28[f]	5.65	143.5	0.67	17.0	2.30	1483	2.63	1697	90/+45
Res. Str. 3 ϵ_3 = 0.01000 E = 6.81	R-3.36 to +2.34	5.70	144.8	0.71	18.0	2.33	1503	2.67	1723	90/+45
Res. Str. 4	FAILURE, LOCATION CENTER LINE -1.1, σ_f = 76.1 ksi, ϵ_f = 0.0109, E_f = 6.98 x 10^6 psi									

a = L indicates left edge of coupon, R indicates right edge
b = Monotonic load moduli at end of fatigue loading level or during residual strength loading, units of 10^6 psi
c = Strain level reached during residual strength loading
d = Delaminated areas overlapped
e = Data inadvertently not taken at 150 K Cycles
f = Delamination merger

TABLE C40
COUPON 11-60 RESIDUAL STRENGTH TESTING, MATRIX CRACK DATA

R = +0.1, f = 10 Hz, Fatigue Stress Level = 55 ksi
Initial Moduli, E_d = 7.95, E_m = 7.80[a]

Loading Condition	Average No. of Cracks Cracks/in.			Average Crack Spacing in.			Average Crack Spacing mm		
	90	+45	-45	90	+45	-45	90	+45	-45
Fat. L1 100 K Cycles E_d = 7.20 E_m = 7.08	94	52	24	0.011	0.019	0.042	0.27	0.49	1.06
Fat. L2 110 K Cycles E_d = 7.10 E_m = 7.06	92	56	24	0.011	0.018	0.042	0.28	0.45	1.06

a = E_d and E_m are the moduli obtained at the end of fatigue (dynamic) and monotonic loading level, units of 10^6 psi

TABLE C41
SUMMARY OF MATRIX CRACK DATA
FOR (0/±45)s MONOTONIC TENSION COUPONS

Coupons 8-3, 8-8, 8-14, 8-25

Strain mm/mm	Average Crack Spacing in mm $+45^{o}$ Plies	-45^{o} Plies
0.00475	25.40	→ ∞ a
0.00727	20.32	→ ∞
0.00730	10.16	1.69
0.00750	2.90	→ ∞
0.00764	4.23	1.69
0.00792	6.77	16.93
0.00803	16.93	25.4
0.00808	1.81	12.70
0.00845	0.99	12.70
0.00845	6.77	5.64
0.00850	6.35	2.67
0.00851 b	1.99	10.16
0.00880 b	2.90	→ ∞
0.00880	1.92	→ ∞
0.00890 b	2.12	→ ∞
0.00902 b	1.00	8.47
0.00902	1.25	10.16
0.00918	1.06	6.35
0.00931	1.35	8.47
0.00934 b	1.95	→ ∞
0.00954 b	4.23	3.63
0.00954	25.4	2.42
0.00956	1.49	10.16
0.00970	16.9	2.54
0.00987	0.74	5.64
0.00991	1.69	→ ∞
0.01010	16.93	2.42
0.01034	20.32	2.12

a = The symbols → ∞ indicate that matrix cracks were not observed in the regions examined.

b = The two different values obtained at the same strain levels were found in different regions of the edge replications.

TABLE C42
SUMMARY OF PERCENT STIFFNESS LOSS COMPARED
TO MATRIX CRACK SPACING FOR $(0/\pm45)_s$ FATIGUE COUPONS

Percent of Initial Dynamic Stiffness	Percent of Initial Monotonic Stiffness	Average Crack Spacing, mm		Coupon ID	Fatigue Stress Level, MPa	Fatigue Cycles, Thousands
		+45	-45			
--	100.0	1-17	2-15 at 0.0085 Strain[a]			
98.3	103.0	0.91	1.41	8-9	465	335
98.0	96.3	0.60	0.85	8-46	483	470
97.9	99.0	0.73	0.91	8-13	483	185
97.9	99.4	0.56	0.85	8-15	483	461
97.4	99.8	0.58	1.02	8-27	483	400
96.1	98.6	0.45	0.82	8-15	483	564
95.9	99.6	0.58	0.85	8-13	483	295
95.4	93.8	0.46	0.75	8-46	483	530
95.2	96.6	0.55	0.85	8-13	483	600
94.9	96.8	0.44	0.88	8-15	483	872
94.8	97.9	0.45	0.85	8-27	483	560
94.5	96.0	0.49	0.85	8-13	483	705
91.1	94.7	0.43	0.74	8-15	483	972
90.3	-	0.47	1.15	8-31	483	125

a = estimated average crack spacings which occur during initial monotonic loading of the fatigue coupons.

TABLE C43

FATIGUE TESTING OF $(0/\pm45)_s$ COUPONS, MODULUS AND EDGE REPLICATION DATA

R = +0.1, f = 10 Hz

Coupon ID	Fatigue Stress Level, MPa	Initial[a] Moduli, GPa	Cycles, Thousands	Dynamic Modulus, GPa	Percent of Initial Modulus	Monotonic Modulus, GPa	Percent of Initial Modulus	Average Crack Spacing, mm +45	Average Crack Spacing, mm -45
8- 9	465	E_d = 59.8	335.0	58.5	97.8	57.1	102.6	0.907	1.411
		E_m = 55.6	340.0	Coupon failed, location centerline -30.5 mm					
8-13	483	E_d = 61.8	185.0	60.6	98.0	58.4	99.1	0.726	0.907
			295.0	59.5	96.2	58.7	99.6	0.577	0.847
		E_m = 59.0	600.0	58.9	95.2	57.0	96.7	0.552	0.847
			705.0	58.4	94.5	56.6	96.1	0.488	0.847
			836.2	55.9	90.4	55.2	93.7		
		Coupon removed for residual strength determination.							
8-15	483	E_d = 61.4	461.0	60.2	98.0	58.3	99.3	0.564	0.847
			564.0	59.0	96.1	57.8	98.6	0.446	0.819
		E_m = 58.7	754.0	59.1	96.2	57.8	98.6	0.438	0.747
			871.5	58.2	94.9	56.8	96.8	0.438	0.876
			971.5	56.0	91.2	55.6	94.7	0.432	0.737
		Coupon removed for residual strength determination.							
8-27	483	E_d = 61.3	400.0	59.7	97.4	58.6	99.8	0.577	1.016
			560.0	57.4	93.7	57.1	97.3	0.454	0.847
		E_m = 58.7	1107.0	58.5	95.4				
			1191.3	Coupon failed, location centerline - 17.8 mm					

a = E_d and E_m are dynamic and monotonic moduli, respectively; E_d obtained at 1000 cycles.

TABLE C43 - Continued

FATIGUE TESTING OF $(\pm 45)_s$ COUPONS, MODULUS AND EDGE REPLICATION DATA

R = +0.1, f = 10 Hz

Coupon ID	Fatigue Stress Level, MPa	Initial[a] Moduli, GPa	Cycles, Thousands	Dynamic Modulus, GPa	Percent of Initial Modulus	Monotonic Modulus, GPa	Percent of Initial Modulus	Average Crack Spacing, mm +45	-45
8-46	483	E_d = 60.7	470.0	59.5	98.0	57.8	96.3	0.605	0.847
		E_m = 60.0	530.1	57.9	95.4	56.2	93.8	0.462	0.747
			531.1	Coupon failed, location centerline -22.9 mm					

a = E_d and E_m are dynamic and monotonic moduli, respectively; E_d obtained at 1000 cycles.

TABLE C44
COUPON 8-30, FATIGUE TESTING, STIFFNESS DATA
R = +0.1, f = 10 Hz, Fatigue Stress Level = 448 MPa

NDI Level	Number of Fatigue Cycles (Thousands)	Monotonic Stiffness, GPa	Percent of Initial Stiffness	Dynamic Stiffness GPa	Percent of Initial Stiffness
a	3.22[b]	59.0	100.0	62.4	100.0
	7.50	59.1	100.0	62.4	100.0
	9.00			62.6	100.3
	15.00			62.9	100.8
	25.00			62.8	100.6
	35.00			62.5	100.1
	75.00			62.3	99.8
	95.00			62.1	99.5
	115.00			61.7	98.9
	125.00			61.5	98.6
	145.00			61.3	98.2
	150.00	58.2	98.7	—	—
	160.00	58.3	98.8	61.2	98.0
	230.00			60.6	97.2
	280.00			60.1	96.3
	320.00			59.8	95.8
	400.00			59.4	95.2
	458.00	55.2	93.6	—	—
	545.00			58.9	94.3
	760.00			58.4	93.5
	880.00			57.6	92.3
	948.00			57.3	91.8
	952.00	55.5	94.0	—	—
	1000.00			57.3	91.8

a = No NDI taken

b = Initial monotonic stiffness survey inadvertently not obtained at zero cycles

TABLE C45
COUPON 8-9 FATIGUE TESTING, STIFFNESS DATA
R = +0.1, f = 10Hz, Fatigue Stress Level = 465 MPa

NDI Level	Number of Fatigue Cycles (Thousands)	Monotonic Stiffness, GPa	Percent of Initial Stiffness	Dynamic Stiffness GPa	Percent of Initial Stiffness
1	0.0	55.6	100.0	--	--
	1.00			59.8	100.0
	2.00			59.6	99.6
	25.00			59.7	99.8
	195.00			59.1	98.8
	310.00			58.7	98.1
	335.00	57.1	102.6	58.5	97.8
2	337.50			58.5	97.8
	337.50			FAILURE	

TABLE C46
COUPON 8-10, FATIGUE TESTING, STIFFNESS DATA
R = +0.1, f = 10 Hz, Fatigue Stress Level = 483 MPa

NDI Level	Number of Fatigue Cycles (Thousands)	Monotonic Stiffness, GPa	Percent of Initial Stiffness	Dynamic Stiffness GPa	Percent of Initial Stiffness
a	0.00	56.7	100.0	—	—
	1.00			60.0	100.0
	21.00			60.2	100.3
	41.00			60.1	100.1
	61.00			59.5	99.1
	85.66			FAILURE	

a = No NDI taken

TABLE C47
COUPON 8-13, FATIGUE TESTING, STIFFNESS DATA
R = +0.1, f = 10 Hz, fatigue Stress Level = 483 MPa

NDI Level	Number of Fatigue Cycles (Thousands)	Monotonic Stiffness, GPa	Percent of Initial Stiffness	Dynamic Stiffness GPa	Percent of Initial Stiffness
1	0.00	59.0	100.0	--	--
	1.00			61.8	100.0
	8.00			61.5	99.5
	14.00			61.6	99.7
	40.00			61.3	99.2
	60.00			61.5	99.5
	100.00			61.4	99.3
	120.00			61.4	99.3
	140.00			61.2	99.0
	185.00	58.4	99.1	60.6	98.0
2	186.00			60.4	97.6
	190.00			60.3	97.5
	193.00			60.2	97.4
	200.00			60.3	97.5
	205.00			60.1	97.2
	210.00			60.1	97.3
	215.00			60.1	97.2
	225.00			60.0	97.1
	235.00			59.9	96.9
	245.00			60.0	97.0
	255.00			59.8	96.7
	265.00			59.7	96.6
	275.00			59.5	96.2
	280.00			59.4	96.1
	295.00	58.7	99.6	59.5	96.2
3	300.00			59.5	96.3
	305.00			59.5	96.3
	315.00			59.5	96.3
	320.00			59.6	96.4
	340.00			59.4	96.1
	360.00			59.4	96.1
	380.00			59.0	95.5
	400.00			59.0	95.4
	420.00			58.8	95.2
	440.00			58.8	95.1

TABLE 47 (Continued)
COUPON 8-13, FATIGUE TESTING, STIFFNESS DATA
R = +0.1, f = 10 Hz, fatigue Stress Level = 483 MPa

NDI Level	Number of Fatigue Cycles (Thousands)	Monotonic Stiffness, GPa	Percent of Initial Stiffness	Dynamic Stiffness GPa	Percent of Initial Stiffness
3	460.00			58.7	94.9
	480.00			58.6	94.8
	500.00			58.6	94.8
	540.00			58.6	94.8
	560.00			58.4	94.4
	560.30			59.2[a]	95.7
	600.00	57.0	96.7	58.9	95.2
4	610.00			59.4	96.1
	620.00			59.4	96.0
	633.33			59.0	95.4
	650.00			58.9	95.2
	700.00	56.6	96.1	58.4	94.5
5	705.00	56.0	95.1	—	—
	706.00	56.7	96.2	57.1	92.4
	715.00			57.0	92.3
	745.00			56.7	91.8
	775.00			56.6	91.5
	815.00			56.2	90.9
	836.00	55.6	94.4	56.2	90.9
	836.20	55.2	93.7	55.9	90.4

COUPON REMOVED FOR RESIDUAL STRENGTH DETERMINATION

a = Extensometer recalibrated

TABLE C48
COUPON 8-15, FATIGUE TESTING, STIFFNESS DATA
R = +0.1, f = 10 Hz, Fatigue Stress Level = 483 MPa

NDI Level	Number of Fatigue Cycles (Thousands)	Monotonic Stiffness, GPa	Percent of Initial Stiffness	Dynamic Stiffness GPa	Percent of Initial Stiffness
1	0.0	58.7	100.00	--	--
	1.00			61.4	100.0
	50.00			61.6	100.3
	90.00			61.6	100.3
	210.00			61.4	100.1
	250.00			61.0	99.3
	270.00			60.9	99.2
	290.00			61.2	99.7
	320.00			60.7	98.9
	336.00			60.6	98.8
	346.00			60.7	98.8
	461.00	58.3	99.3	60.2	98.0
2	462.00			59.5	96.9
	511.00			59.4	96.8
	541.00			59.1	96.3
	564.00	57.8	98.6	58.9	96.1
3	571.00			60.4	98.3
	584.00			60.3	98.2
	614.00			60.1	97.9
	644.00			60.0	97.8
	674.00			59.6	97.1
	734.00			59.7	97.3
	754.00	57.8	98.5	59.1	96.3
4	755.00			59.2	96.5
	774.00			58.9	96.0
	794.00			58.7	95.6
	829.00			58.4	95.1
	854.00			58.4	95.1
	871.50	56.8	96.8	58.2	94.9
5	871.50	56.6	96.5	--	--
	872.50			57.1	93.0
	886.50			56.6	92.2
	911.50			56.4	91.8
	951.50			56.2	91.4
	971.50	55.6	94.7	56.0	91.2

COUPON REMOVED FOR RESIDUAL STRENGTH DETERMINATION

TABLE C49
COUPON 8-24, FATIGUE TESTING, STIFFNESS DATA
R = +0.1, f = 10 Hz, Fatigue Stress Level = 483 MPa

NDI Level	Number of Fatigue Cycles (Thousands)	Monotonic Stiffness, GPa	Percent of Initial Stiffness	Dynamic Stiffness GPa	Percent of Initial Stiffness
1	0.00	57.2	100.0	--	--
	0.84[a]	--	--	--	--

a = Coupon failure, did not reach maximum-minimum of fatigue cycle.

TABLE C50
COUPON 8-27, FATIGUE TESTING, STIFFNESS DATA
R = +0.1, f = 10 Hz, Fatigue Stress Level = 483 MPa

NDI Level	Number of Fatigue Cycles (Thousands)	Monotonic Stiffness, GPa	Percent of Initial Stiffness	Dynamic Stiffness GPa	Percent of Initial Stiffness
1	0.0	58.7	100.0	--	--
	1.00			61.3	100.0
	10.00			61.9	101.0
	30.00			61.6	100.4
	125.00			61.3	100.0
	175.00			61.1	99.6
	200.00			61.0	99.4
	250.00			61.0	99.5
	275.00			60.7	99.0
	300.00			60.8	99.2
	325.00			61.0	99.4
	350.00			60.8	99.2
	375.00			60.6	98.8
	400.00	58.6	99.8	59.7	97.4
2	405.00			59.3	96.7
	420.00			59.1	96.4
	440.00			59.0	96.2
	490.00			58.6	95.5
	540.00			58.4	95.2
	560.00			58.2	94.9
	560.04	57.4	97.9	--	--
3	560.84			59.3	96.7
	620.04			58.8	95.9
	649.74			59.0	96.2
	778.14			59.0	96.3
	950.04			59.0	96.3
	1021.04			58.6	95.6
	1067.04			58.5	95.4
	1109.04			58.5	95.4
	1160.04			58.5	95.4
	1191.38			FAILURE	

TABLE C51
COUPON 8-46, FATIGUE TESTING, STIFFNESS DATA
R = +0.1, f = 10 Hz, Fatigue Stress Level = 483 MPa

NDI Level	Number of Fatigue Cycles (Thousands)	Monotonic Stiffness, GPa	Percent of Initial Stiffness	Dynamic Stiffness GPa	Percent of Initial Stiffness
1	0.0	60.0	100.0	--	--
	1.00			60.7	100.0
	10.00			61.3	100.9
	20.00			61.5	101.2
	30.00			61.4	101.1
	40.00			61.6	101.4
	60.00			61.7	101.6
	70.00			61.8	101.7
	100.00			61.7	101.6
	110.00			61.5	101.2
	120.00			61.5	101.3
	140.00			61.7	101.7
	160.00			61.8	101.8
	180.00			61.8	101.8
	200.00			61.8	101.8
	220.00			61.8	101.8
	240.00			61.8	101.7
	260.00			61.5	101.2
	280.00			61.6	101.4
	300.00			61.4	101.1
	360.00			61.2	100.7
	410.00			60.0	98.7
	460.00			59.6	98.2
	470.00	57.8	96.3	59.5	98.0
2	480.00			59.0	97.2
	515.00			58.6	96.4
	530.00	56.2	93.8	57.9	95.4
3	531.10			FAILURE	

TABLE C52
COUPON 8-12 FATIGUE TESTING, STIFFNESS DATA
R = +0.1, f = 10 Hz, Fatigue Stress Level = 500 MPa

NDI Level	Number of Fatigue Cycles (Thousands)	Monotonic Stiffness, GPa	Percent of Initial Stiffness	Dynamic Stiffness GPa	Percent of Initial Stiffness
a	0.00	58.0	100.0	--	--
	1.00			60.2	100.0
	2.00			60.5	100.5
	5.00			60.2	100.0
	10.00			60.2	100.0
	15.00			60.0	99.8
	20.00			60.2	100.1
	21.31			FAILURE	

a = No NDI taken

TABLE C53
COUPON 8-45, FATIGUE TESTING, STIFFNESS DATA
R = +0.1, f = 10 Hz, Fatigue Stress Level = 517 MPa

NDI Level	Number of Fatigue Cycles (Thousands)	Monotonic Stiffness, GPa	Percent of Initial Stiffness	Dynamic Stiffness GPa	Percent of Initial Stiffness
a	0.00	58.4	100.0	--	--
	1.00			61.7	100.0
	2.10			62.2	100.7
	3.50			61.6	99.9
	9.50			61.7	99.9
	13.80			61.5	99.6
	20.00			61.3	99.3
	36.00			61.0	98.9
	80.00			60.9	98.6
	100.00	57.7	98.8	60.4	97.9
	125.00			59.9	97.1
	125.84			FAILURE	

a = No NDI taken

TABLE C54

8-13, RESIDUAL STRENGTH EXPERIMENTS, MODULUS AND EDGE REPLICATION DATA

R = +0.1, f = 10 Hz, FATIGUE STRESS LEVEL = 483 MPa

INITIAL MODULI[a], E_d = 61.8 GPa , E_m = 59.0 GPa

Loading Condition	Dynamic Modulus, GPa	Percent of Initial Modulus	Monotonic Modulus, GPa	Percent of Initial Modulus	Average Crack Spacing mm +45	-45
Fat. 1 185.0[b]	60.6	98.0	58.4	99.1	0.726	0.907
Fat. 2 295.0	59.5	96.2	58.7	99.6	0.577	0.847
Fat. 3 600.0	58.9	95.2	57.0	96.7	0.552	0.847
Fat. 4 705.0	58.4	94.5	56.6	96.1	0.488	0.847
Fat. 4 836.2	55.9	90.4	55.2	93.7	-	-
Res. Str. 1 ϵ = 0.0085[c]	-	-	56.0	94.9	-	-
Res. Str. 2 ϵ = 0.0090	-	-	55.9	94.7	0.470	0.747
Res. Str. 3 ϵ = 0.0095	-	-	55.0	93.2	-	-
Res. Str. 4	Failure, Location Centerline + 50.8mm, σ = 594 MPa, ϵ_f = 0.0106, E_f = 56.0 GPa					

a = E_d and E_m are dynamic and monotonic moduli, respectively; E_d obtained at 1000 cycles.

b = Cycles in thousands.

c = Strain level to which coupon was loaded in monotonic tension.

TABLE C55

8-15, RESIDUAL STRENGTH EXPERIMENTS, MODULUS AND EDGE REPLICATION DATA

R = +0.1, f = 10 Hz, FATIGUE STRESS LEVEL = 483 MPa

INITIAL MODULI[a], E_d = 61.4 GPa, E_m = 58.7 GPa

Loading Condition	Dynamic Modulus, GPa	Percent of Initial Modulus	Monotonic Modulus, GPa	Percent of Initial Modulus	Average Crack Spacing, mm +45	-45
Fat. 1 461.0[b]	60.2	98.0	58.3	99.3	0.564	0.847
Fat. 2 564.0	59.0	96.1	57.8	98.6	0.446	0.819
Fat. 3 754.0	59.1	96.2	57.8	98.6	0.438	0.747
Fat. 4 871.5	58.2	94.9	56.8	96.8	0.438	0.876
Fat. 5 971.5	56.0	91.2	55.6	94.7	0.432	0.737
Res. Str. 1 ϵ = 0.0085[c]	-	-	55.8	95.0	-	-
Res. Str. 2 ϵ = 0.0090	-	-	55.9	95.2	0.446	0.794
Res. Str. 3 ϵ = 0.0095	-	-	55.3	94.4	-	-
Res. Str. 4	Failure, location centerline +35.6mm, σ_f = 592 MPa, ϵ_f = 0.0109, E_f = 54.3 GPa					

a = E_d and E_m are dynamic and monotonic moduli, respectively; E_d obtained at 1000 cycles.

b = Cycles in thousands.

c = Strain level to which coupon was loaded in monotonic tension.

TABLE C56

8-31, RESIDUAL STRENGTH EXPERIMENTS, MODULUS AND EDGE REPLICATION DATA

R = 0.1, f = 10 Hz, FATIGUE STRESS LEVEL = 483 MPa

INITIAL MODULI[a], E_d = 61.6 GPa, E_m = 59.3 GPa

Loading Condition	Dynamic Modulus, GPa	Percent of Initial Modulus	Monotonic Modulus, GPa	Percent of Initial Modulus	Average Crack Spacing mm +45	-45
Fat. 1 125.0[b]	55.7	90.3	-	-	0.470	1.155
Res. Str. 1 ϵ = 0.0085[c]	-	-	54.5	91.9	0.508	1.209
Res. Str. 2 ϵ = 0.0090	-	-	55.4 "	93.4	0.508	1.270
Res. Str. 3 ϵ = 0.0095	-	-	54.4	91.8	0.498	1.270
Res. Str. 4	Failure, location centerline +76.2mm, σ_f = 558 MPa, ϵ_f = 0.0102, E_f = 54.7 GPa					

a = E_d and E_m are dynamic and monotonic moduli, respectively; E_d obtained at 1000 cycles.

b = Cycles in thousands.

c = Strain level to which coupon was loaded in monotonic tension.

TABLE C57
STIFFNESS MEASUREMENTS OBTAINED DURING FATIGUE LOADING
OF $(0/45/0_2/-45/0)_s$ COUPONS
NOTE: Edge replications taken at every interval unless otherwise indicated

Coupon ID	Initial Strain Level	Cycles	Modulus, Static GPa	Modulus, Static psi_6 x 10^{-6}	Modulus, Dynamic GPa	Modulus, Dynamic psi_6 x 10^{-6}
CF1905-B6	0.0070	0	98.7	14.30	-	-
		1 000	-	-	100.0	14.50
		520 000	-	-	99.7	14.45[e]
		570 000	-	-	100.7	14.61[e]
		620 000	-	-	100.8	14.62[e]
		850 000	-	-	100.7	14.61[e]
		920 000	-	-	100.7	14.61[e]
		970 000	-	-	100.7	14.60[e]
		1 000 000	84.1	12.20	100.3	14.63
		Removed for residual strength, expermentation, no visible delaminations				
-23	0.0075	0	100.9	14.63	-	-
		1 000	-	-	100.3	14.55[e]
		75 000	100.8	14.62	100.5	14.57[e]
		150 000	101.1	14.66	100.8	14.62
		225 000	101.1	14.66	101.0	14.65[e]
		300 000	101.0	14.65	101.0	14.65
		375 000	101.4	14.71	100.9	14.63[e]
		450 000	101.2	14.67	101.0	14.65
		525 000	101.2	14.68	100.9	14.63[e]
		600 000	101.4	14.70	101.1	14.66
		675 000	102.1	14.81	101.2	14.68[e]
		750 000	101.8	14.76	101.5	14.72
		825 000	102.5	14.86	101.2	14.67[e]
		900 000	101.6	14.74	101.1	14.66
		1 000 000	101.6	14.73	101.1	14.66
		Removed for residual strength experimentation, no visible delaminations				
-B24[d]	0.0075	0	100.6	14.59	-	-
		1 000	-	-	101.2	14.68[e]
		75 000	-	-	101.6	14.73[e]
		150 000	100.0	14.51	101.0	14.65
		235 000	-	-	101.2	14.67
		300 000	100.6	14.59	101.0	14.65
		375 000	100.4	14.56	101.2	14.67[e]
		450 000	100.5	14.58	101.4	14.70
		525 000	100.6	14.59	100.9	14.63

TABLE C57 (Continued)
STIFFNESS MEASUREMENTS OBTAINED DURING FATIGUE LOADING
OF $(0/45/0_2/-45/0)_s$ COUPONS
NOTE: Edge replications taken at every interval unless otherwise indicated

Coupon ID	Initial Strain Level	Cycles	Modulus, Static GPa	Static psi x 10^{-6}	Dynamic GPa	Dynamic psi x 10^{-6}
-B24[d] (Cont)		600 000	100.7	14.60	101.2	14.67
		675 000	100.8	14.62	101.2	14.67[e]
		750 000	100.5	14.58	101.2	14.67
		825 000	101.1	14.66	101.1	14.66[e]
		900 000	100.9	14.63	101.3	14.69
		975 000	101.4	14.71	101.1	14.66[e]
		1 000 000	100.9	14.64	101.2	14.67
		Removed for residual strength experiments, no visible delaminations				
-B9	0.0080	0	99.6	14.45	-	-
		1 000	-	-	100.3	14.55
		75 000	100.6	14.59	100.4	14.56
		150 000	99.8	14.47	100.3	14.55
		No visible delamination, continued cycling after coupon removal for two weeks				
		150 000	101.8	14.76	100.2	14.53
		Coupon submitted ZnI_2 enhancer and x-ray, reason for modulus reduction unclear				
		150 000	102.7	14.89	96.2	13.95
		300 000	99.7	14.46	94.3	13.68
		Removed for x-ray, visible delamination				
		300 000	98.7	14.31	99.6	14.44
		450 000	98.3	14.26	99.2	14.38
		Removed for x-ray, visible delamination				
		300 000	98.7	14.31	99.6	14.44
		450 000	98.3	14.26	99.2	14.38
		Removed for x-ray, visible delamination				
		450 000	99.5	14.43	99.6	14.45
		473 800	Failure			
-B12[d]	0.0080	0	97.6	14.15	-	-
		1 000	-	-	100.3	14.55[e]
		150 000	99.0	14.37	100.7	14.60
		225 000	99.3	14.40	100.9	14.64
		300 000	98.7	14.32	100.5	14.58
		300 253	Failed			

TABLE C57 (Continued)
STIFFNESS MEASUREMENTS OBTAINED DURING FATIGUE LOADING
OF $(0/45/0_2/-45/0)_s$ COUPONS

NOTE: Edge replications taken at every interval unless otherwise indicated

Coupon ID	Initial Strain Level	Cycles	Modulus, Static GPa	Static x 10^6 psi	Modulus, Dynamic GPa	Dynamic x 10^6 psi
-B14	0.0080	0	99.5	14.43	-	-
		1 000	100.0	14.50	100.3	14.54
		75 000	99.4	14.41	99.5	14.43
		150 000[a]	99.6	14.39	99.2	14.39
		Removed for x-ray, visible delaminations				
		150 000[b]	101.2	14.67	100.7	14.61
		225 000	101.7	14.75	100.9	14.63
		Removed for x-ray, visible delaminations				
		225 000[b]	97.7	14.17	95.5	14.09
		240 380	Failure			
-B15	0.0080	0	97.1	14.09	-	-
		1 000	97.5	14.14	100.4	14.56
		75 000	96.5	13.99	100.3	14.54
		150 000[a]	99.6	14.44	100.7	14.60
		No visible delamination, continued cycling				
		150 000[b]	100.9	14.63	101.7	14.75
		225 000	102.7	14.89	101.9	14.78
		300 000[a]	102.8	14.91	102.1	14.80
		Removed for x-ray, visible delaminations				
		300 000[b]	100.5	14.57	100.6	14.59
		312 540	Failure			
-B16[d]	0.0080	0	101.6	14.74	-	-
		1 000	-	-	101.8	14.76[c]
		150 000	100.2	14.54	100.3	14.62
		Removed for x-ray, visible delaminations				
		150 000	99.5	14.43	100.1	14.52
		225 000	99.0	14.36	99.8	14.48
		300 000	98.1	14.23	99.0	14.35
		Removed for x-ray and residual strength experiment, visible delaminations				
-B18	0.0080	0	97.1	14.08	-	-
		1 000	98.4	14.27	100.7	14.60
		75 000	96.9	14.03	99.8	14.47

TABLE C57 (Continued)
STIFFNESS MEASUREMENTS OBTAINED DURING FATIGUE LOADING
OF $(0/45/0_2/-45/0)_s$ COUPONS
NOTE: Edge replications taken at every interval unless otherwise indicated

Coupon ID	Initial Strain Level	Cycles	Modulus, Static GPa	Static psi x 10^{-6}	Dynamic GPa	Dynamic psi x 10^{-6}
-B18 (Cont.)		150 000[a]	97.4	14.13	100.0	14.51
		Removed for x-ray, no visible delaminations				
		150 000[b]	100.3	14.55	101.7	14.75
		225 000	100.5	14.57	101.6	14.73
		300 000[a]	100.4	14.56	101.4	14.70
		Removed for x-ray, visible delaminations				
		300 000[b]	102.0	14.80	102.0	14.79
		375 000	102.1	14.81	102.0	14.80
		Removed for x-ray, visible delaminations				
		475 000	99.5	14.43	100.6	14.56
		Removed for x-ray, visible delaminations				
		475 000	98.9	14.34	100.2	14.54
		525 000	99.3	14.40	100.2	14.54
		Removed for x-ray, visible delaminations				
		525 000	101.6	14.74	97.6	14.15
		575 000	101.1	14.67	96.2	13.95
		Removed for x-ray and residual strength experiment, visible delamination				
-B19[d]	0.0080	0	103.6	15.02	-	-
		1 000	-	-	102.6	14.88[e]
		150 000	104.2	15.12	102.7	14.89
		Removed for x-ray, visible delaminations				
		150 000[b]	100.2	14.53	100.7	14.60
		225 000	-	-	100.5	14.58
		225 180	Failure			
-B20[d]	0.0080	0	100.1	14.52	-	-
		1 000	-	-	100.2	14.54[e]
		150 000	100.9	14.63	101.4	14.71
		225 000	101.5	14.72	101.7	14.75
		300 000	101.7	14.75	101.6	14.73
		Removed for residual strength experiment, no visible delaminations				

TABLE C57 (Continued)
STIFFNESS MEASUREMENTS OBTAINED DURING FATIGUE LOADING
OF $(0/45/0_2/-45/0)_s$ COUPONS
NOTE: Edge replications taken at every interval unless otherwise indicated

Coupon ID	Initial Strain Level	Cycles	Modulus, Static GPa	Static psi x 10^{-6}	Dynamic GPa	Dynamic psi x 10^{-6}
-B21[d]	0.0080	0	100.6	14.59	-	-
		1 000	-	-	101.4	14.70[e]
		150 000	100.3	14.55	101.3	14.69
		225 000	100.4	14.56	101.4	14.70
		300 000	100.7	14.60	101.4	14.70
		Removed for residual strength experiment				
-B26[d]	0.0080	0	99.3	14.40	-	-
		1 000	-	-	100.6	14.59
		22 690	Failure			
-B29[d]	0.0080	0	100.8	14.62	-	-
		1 000	-	-	102.5	14.87
		75 000	101.2	14.68	102.5	14.86
		150 000	101.1	14.66	102.3	14.84
		300 000	101.1	14.56	102.0	14.79
		Removed for residual strength experimentation, no visible delaminations				
		300 000[b]	103.7	15.04	103.1	14.95
		350 000	-	-	103.1	14.95
		Removed for x-ray and residual strength experiment				
-B30[d]	0.0080	0	98.7	14.32	-	-
		1 000	-	-	100.7	14.61
		150 000	99.2	14.38	100.3	14.55
		Small amount of delamination				
		150 720	Failure			
-B31[d]	0.0080	0	100.0	14.51	-	-
		1 000	-	-	100.7	14.61[e]
		75 000	100.5	14.57	101.2	14.67[e]
		150 000	100.5	14.58	101.2	14.68[e]
		225 000	100.7	14.60	101.2	14.68[e]
		300 000	100.7	14.60	101.4	14.71[e]
		375 000	100.5	14.58	101.2	14.67[e]
		450 000	100.5	14.57	101.1	14.66[e]
		525 000	100.9	14.63	101.3	14.69

TABLE C57 (Continued)
STIFFNESS MEASUREMENTS OBTAINED DURING FATIGUE LOADING
OF $(0/45/0_2/-45/0)_s$ COUPONS
NOTE: Edge replications taken at every interval unless otherwise indicated

Coupon ID	Initial Strain Level	Cycles	Modulus, Static GPa	Static psi_{-6} x 10^{-6}	Dynamic GPa	Dynamic psi_{-6} x 10^{-6}
B31d (Cont.)		600 000	100.9	14.63	101.4	14.70
		675 000	100.1	14.52	101.0	14.65
		Removed for x-ray and residual strength experiment, no visible delaminations				
-B32	0.0080	0	98.5	14.29	-	-
		1 000	99.2	14.39	101.1	14.67
		75 000	98.7	14.31	101.3	14.69
		150 000[a]	99.2	14.39	101.4	14.70
		Removed for x-ray, no visible delaminations				
		150 000[b]	102.2	14.82	102.6	14.88
		225 000	103.1	14.96	102.1	14.81
		300 000	102.2	14.82	102.0	14.80
		Removed for x-ray, visible delaminations				
		300 000	102.7	14.90	102.5	14.87
		331 040	Failure			
-B7	0.0085	0	101.7	14.75	-	-
		1 000	101.2	14.68	101.0	14.65
		5 674	Failure			
-B10	0.0085	0	99.9	14.49	-	-
		1 000	101.0	14.65	101.8	14.77[e]
		50 000	102.4	14.85	102.2	14.83[e]
		100 000	100.1	14.52	102.1	14.81
		101 380	Failure			
-B11	0.0086	0	101.2	14.68	-	-
		1 000	100.9	14.64	102.0	14.79
		51 000	101.1	14.66	102.4	14.85
		100 000	100.7	14.60	102.4	14.79
		149 800	-	-	101.9	14.78[e]
		150 000	100.7	14.61	-	-
		Removed for x-ray, no delaminations visible				
		150 000	100.1	14.52	100.8	14.76
		200 000	100.4	14.56	102.0	14.79
		250 000[a]	100.5	14.57	102.0	14.79

TABLE C57 (Continued)
STIFFNESS MEASUREMENTS OBTAINED DURING FATIGUE LOADING
OF $(0/45/0_2/-45/0)_s$ COUPONS
NOTE: Edge replications taken at every interval unless otherwise indicated

Coupon ID	Initial Strain Level	Cycles	Modulus, Static GPa	Static psi, x 10^{-6}	Dynamic GPa	Dynamic psi, x 10^{-6}
-B11 (Cont.)		Removed for x-ray, visible delaminations				
		250 000[b]	102.7	14.90	102.7	14.[illegible]
		326 000	102.3	14.84	102.5	14.[illegible]
		376 000	101.5	14.72	102.0	14.80
		426 000	101.7	14.75	102.1	14.81
		476 000	101.8	14.76	101.7	14.75
		526 000	101.9	14.78	102.2	14.82[e]
		565 000	101.9	14.78	101.9	14.78
		Removed for x-ray, visible delaminations				
		565 000	100.2	14.53	100.9	14.63
		600 000	100.0	14.51	100.8	14.62
		Removed for x-ray, visible delaminations				
		600 000	99.8	14.47	100.7	14.60
		650 000	100.5	14.58	100.9	14.64
		Removed for x-ray, visible delaminations				
		Coupon failed during subsequent static curvey due to operator overload error				
-B13	0.0085	0	98.7	14.31	-	-
		1 000	98.7	14.31	101.3	14.69
		50 000	97.8	14.19	101.2	14.68
		100 000	99.0	14.36	101.0	14.65
		144 800	Failure			
-B17	0.0085	0	104.2	15.11	-	-
		1 000	103.6	15.02	103.9	15.[illegible]
		50 000	103.0	14.94	103.6	15.02
		100 000	103.6	15.02	103.4	15.[illegible]
		150 000[a]	103.3	14.98	103.3	14.[illegible]
		Removed for x-ray, visible delaminations				
		150 000[b]	106.2	15.40	103.9	15.07
		196 110	Failure			
-B25[c]	0.0087	0	96.5	14.0	-	-
		1 000	-	-	99.7	14.46
		20 000	96.7	14.02	99.8	14.47
		80 000	97.8	14.18	99.7	14.46

TABLE C57 (Continued)
STIFFNESS MEASUREMENTS OBTAINED DURING FATIGUE LOADING
OF $(0/45/0_2/-45/0)_s$ COUPONS
NOTE: Edge replications taken at every interval unless otherwise indicated

Coupon ID	Initial Strain Level	Cycles	Modulus, Static GPa	Static psi_{-6} x 10	Dynamic GPa	Dynamic psi_{-6} x 10
-B17	0.0085	0	104.2	15.11	-	-
		1 000	103.6	15.02	103.9	15.07
		50 000	103.0	14.94	103.6	15.02
		100 000	103.6	15.02	103.4	15.00
		150 000[a]	103.3	14.98	103.3	14.98
		Removed for x-ray, visible delaminations				
		150 000[b]	106.2	15.40	103.9	15.07
		196 110	**Failure**			
-B25[c]	0.0087	0	96.5	14.0	-	-
		1 000	-	-	99.7	14.46
		20 000	96.7	14.02	99.8	14.47
		80 000	97.8	14.18	99.7	14.46
		160 000	97.1	14.09	99.1	14.37
		200 000	96.7	14.03	98.9	14.35[e]
		250 000	96.7	14.02	98.4	14.28[e]
		333 000	96.4	13.98	98.5	14.29[e]
		413 000	95.7	13.88	98.0	14.22[e]
		500 000	95.2	13.81	97.3	14.11[e]
		550 000	95.1	13.79	97.2	14.10
		600 000	95.0	13.78	97.1	14.09
		640 000	95.1	13.80	97.7	14.17[e]
		685 000	94.9	13.77	96.8	14.04[e]
		710 000	94.6	13.72	96.3	13.97[e]
		735 000	94.4	13.70	96.1	13.94
		746 500	**Failure**			
-B27	0.0086	0	99.5	14.43	-	-
		1 000	99.8	14.48	101.6	14.73
		4 344	**Failure**			

TABLE C57 (Continued)
STIFFNESS MEASUREMENTS OBTAINED DURING FATIGUE LOADING
OF $(0/45/0_2/-45/0)_s$ COUPONS
NOTE: Edge replications taken at every interval unless otherwise indicated

Coupon ID	Initial Strain Level	Cycles	Modulus, Static GPa	Static psi x 10^{-6}	Dynamic GPa	Dynamic psi x 10^{-6}
-B28	0.0091	0	14.5	-	-	
		100.0	-	-	102.7	14.9
		1 000	-	-		
		11 800	Failure			

a = Data obtained before x-ray
b = Data obtained after x-ray, reason for stiffness change is being investigated
c = Approximately 40 percent of the readings are listed in order to show trends.
d = Coupon intended for residual strength experimentation
e = Edge replication not obtained

TABLE C58
SUMMARY OF MATRIX CRACK AND DELAMINATION
DATA FOR $(0/45/0_2/-45/0)_s$ COUPONS

COUPON ID	INITIAL CONDITIONS	LOADING CONDITIONS	AVERAGE CRACK SPACING IN mm +45	-45	DELAMINATION STATE
B-6	ϵ=0.0070	Fatigue			None
	σ=695[a]	1,000[b]	16.9	4.23	
		Residual Strength			
		ϵ=0.0085[c]	2.60	2.36	
		Failure-Location from Centerline 0.0 and 6.4			
		σ_f=1023 MPa; ϵ_f = 0.0098; E_f = 104.0 GPa			
B-23	ϵ=0.0075	Static	9.24	2.99	None
	σ=758[a]	Fatigue			
		150.0[b]	5.08	2.60	
		300.0	4.84	2.60	
		450.0	4.84	2.60	
		600.0	4.62	2.42	
		750.0	4.62	2.42	
		900.0	4.62	2.42	
		1000.0	4.62	2.42	
		Residual Strength			
		ϵ=0.0090[c]	4.42	2.21	
		ϵ=0.0100	4.06	2.26	
		Failure-Location from Center +7.1 and -4.6			
		σ_f=1075 MPa; ϵ_f = 0.0107; ϵ_f = 100.5 GPa			
B-24	ϵ=0.0075	Static	——[d]	5.64	None
	σ=756[a]	Fatigue			
		150.0[b]	50.8	5.64	
		300.0	12.7	5.08	
		450.0	10.2	4.42	
		600.0	4.83	3.76	
		750.0	4.83	3.76	
		900.0	3.38	3.50	
		1000.0	2.21	2.54	
		Residual Strength			
		ϵ=0.0090[c]	2.31	2.42	

Table C-58 - Continued

COUPON ID	INITIAL CONDITIONS	LOADING CONDITIONS	AVERAGE CRACK SPACING IN mm +45	-45	DELAMINATION STATE
B-24 (continued)		ε=0.0100	2.31	2.36	
		ε=0.0105	2.31	2.36	
		ε=0.0110	2.31	2.36	
		Failure - Location from Centerline +2.5 cm			
		σ_f-1099 MPa; ε_f=0.01085; ε_f = 101.3 GPa			
B-9	ε=0.0080	Static	____[d]	____[d]	
	σ=797[a]	Fatigue			
		75.0[b]	2.03	33.9	
		150.0	1.88	33.9	
		300.0	1.34	3.76	None
		450.0	1.29	3.76	Some
		473.8	Failure, Location 0.4 cm		
B-12	ε=0.0080	Static	____[d]	5.98	None
	σ=782[a]	Fatigue			
		150.0[b]	102	5.08	
		225.0	102	4.23	
		300.0	102	3.39	
		300.253	Failure, location +7.6 cm		
B-14	ε=0.0080	Static	____[d]	____[d]	
	σ=798[a]	Fatigue			
		1[b]	____[d]	25.4	
		75	____[d]	18.1	
		150	25.4	18.1	Some
		225	Illegible[e]	Illegible[e]	Large Edge
		240.38	Failure, location +3.8 cm		
B-15	ε=0.0080	Static	____[d]	____[d]	
	σ=780[a]	Fatigue			
		1[b]	____[d]	____[d]	
		75	3.18	____[d]	
		150	1.29	____[d]	Some
		225	1.21	1.41	Increased
		300	1.18	1.30	"
		312.54	Failure, location +8.4 cm		

Table C58 - Continued

COUPON ID	INITIAL CONDITION	LOADING CONDITIONS	AVERAGE CRACK SPACING IN mm +45	-45	DELAMINATION STATE
B-16	ε=0.0080	Static	25.4	2.75	
	σ=789[a]	Fatigue			
		150[b]	1.43	1.75	Some
		225	0.92	1.10	Increased
		300	0.61	0.69	Increased
		Residual Strength			
		ε=0.0090[c]	0.61	0.69	Severe Edge
		Failure - Location from Centerline - 7.9 cm			
		σ_f=941 MPa; ε_f = 0.0095; ε_f = 99.1 GPa			
B-18	ε=0.0080	Static	2.75	2.12	
	σ=773[a]	Fatigue			
		1[b]	2.75	2.12	
		75	2.30	2.11	Some
		150	2.30	1.92	No Change
		225	1.20	1.78	Increased
		300	1.20	1.78	Increased
		375	1.20	1.56	No Change
		475	1.20	1.56	Increased
		525	1.20	1.56	Increased
		575	1.15	1.49	No Change
		Residual Strength ε=0.0085[c]	1.52	1.49	No Change
		ε=0.0090	1.52	1.49	No Change
		ε=0.0095	1.52	1.49	No change
		Failure - Location - 2.5 cm			
		σ_f = 1086 MPa; ε_f = 0.0107; ε_f = 101.3 GPa			
B-19	ε=0.0080	Static	9.23	1.67	None
	σ=828[a]	Fatigue			
		150[b]	5.08	1.54	
		225.18	Failure, location +8.6 cm		

Table C58 - Continued

COUPON ID	INITIAL CONDITIONS	LOADING CONDITIONS	AVERAGE CRACK SPACING IN mm +45	-45	DELAMINATION STATE
B-20	ε=0.0080	Static	——— [d]	12.7	None
	σ=800[a]	Fatigue			
		150.0[b]	3.56	4.23	
		225.0	2.49	3.08	
		300.0	2.82	2.99	
		Residual Strength			
		ε=0.0090[c]	2.67	2.99	
		ε=0.0095	2.67	2.99	
		ε=0.0100	2.67	2.99	
		ε=0.0105	2.67	2.99	
		Failure - Location Test Section Exploded			
		σ_f=1076 MPa; ε_f = 0.01071; E_f = 100.5 GPa			
B-21	ε=0.0080	Static	——— [d]	4.42	None
	σ=805[a]	Fatigue			
		150.0[b]	7.25	2.42	
		225.0	5.08	2.16	
		300.0	4.84	2.12	
		Residual Strength			
		ε=0.0090[c]	5.34	2.12	
		ε=0.0100	5.34	1.99	
		ε=0.0105	5.34	2.03	
		Failure-Location from Centerline +1.8 and +6.4 cm			
		σ_f=1091 MPa; ε_f = 0.0108; E_f = 101.3 GPa			
B-29	ε=0.0080	Static	102	7.82	
	σ=808[a]	Fatigue			
		75[b]	10.2	6.35	
		150	4.62	5.08	
		300	2.07	3.28	Some
		350	2.07	2.99	No Change
		Residual Strength			

Table C58 - Continued

COUPON ID	INITIAL CONDITIONS	LOADING CONDITIONS	AVERAGE CRACK SPACING IN mm +45	-45	DELAMINATION STATE
		ε=0.0085[c]	2.07	2.99	
		Failure - Location from Centerline -7.4 cm			
		σ_f=888 MPa; ε_f = 0.00886; E_f=100.2 GPa			
B-30	ε=0.0080	Static	4.06	2.90	None
	σ=794[a]	Fatigue			
		150[b]	1.72	2.03	Some
		150.72	Failure, location -2.0 cm		
B-31	ε=0.0080	Static	____[d]	2.54	
	σ=796[a]	Fatigue			
		150.0[b]	7.26	2.16	None
		300.0	2.60	1.72	Some
		525.0	1.88	1.24	Increased
		600.0	1.41	1.09	Increased
		675.0	1.25	0.93	Heavy
		Residual Strength			
		ε=0.0085[c]	1.25	0.93	Heavy
		ε=0.0095	Illegible[e]	Illegible[e]	Heavy
		Failure-Location from Centerline +8.4 and -6.4 cm			
		σ_f=1057 MPa; ε_f = 0.0103; E_f = 102.6 GPa			
B-32	ε=0.0080	Static	14.5	1.89	
	σ=790[a]	Fatigue			
		1[b]	11.3	1.78	Some
		75	2.99	1.24	Some
		150	2.99	1.13	Some
		225	1.69	0.93	Increased
		300	1.64	0.59	Increased
		331.04	Failure-Location +3.0 cm		
B-7	ε=0.0085	Static	____[d]	____[d]	
	σ=855[a]	Fatigue			
		1[b]	102	____[d]	Some
		5.674	Failure-Location + 0.8 cm		

Table C58 - Continued

COUPON ID	INITIAL CONDITIONS	LOADING CONDITIONS	AVERAGE CRACK SPACING IN +45	AVERAGE CRACK SPACING IN -45	DELAMINATION STATE
B-10	ε=0.0085	Static	____[d]	____[d]	
	σ=851[a]	Fatigue			
		1[b]	____[c]	9.24	Some
		50	11.3	6.77	No Change
		100	7.82	4.23	No X-Ray Available
		101.38	Failure-Location +1.3 cm		
B-11	ε=0.0085	Static	____[d]	____[d]	
	σ=866[a]	Fatigue			
		1[b]	14.5	____[d]	
		51	3.18	12.7	
		100	3.18	6.35	Some
		150	3.18	4.48	Some
		200	3.18	4.48	Increased
		250	3.18	4.48	"
		326	3.18	3.91	"
		376	1.32	3.91	"
		426	1.22	3.91	"
		476	1.22	3.91	Heavy Edge
		565	1.21	3.91	"
		600	1.21	3.85	"
		650	1.21	3.85	"
		Failure (Oper. error)			
B-13	ε=0.0085	Static	____[d]	____[d]	
	σ=841[a]	Fatigue			
		1[b]	____[d]	____[d]	
		30	6.35	____[d]	
		100	2.07	____[d]	Some
		144.8	Failure-Location -1.3 cm		
B-17	ε=0.0085	Static	____[d]	____[d]	
	σ=882[a]	Fatigue			
		1[b]	33.9	____[d]	Some
		50	8.38	6.35	Increased

Table C58 - Continued

COUPON ID	INITIAL CONDITIONS	LOADING CONDITIONS	AVERAGE CRACK SPACING IN mm +45	-45	DELAMINATION STATE
B-17 (continued)		100	2.54	7.81	Increased
		150	2.54	1.06	No Change
		196.1 Failure, Location +3.3 and -2.5 cm			
B-25	ε=0.0085	Static	16.9	6.35	
	σ=839[a]	Fatigue			
		1[b]	16.9	6.35	
		5	10.2	5.35	
		10	10.2	4.62	
		20	7.25	4.62	
		40	5.64	4.62	
		80	4.83	4.62	
		160	2.16	2.54	Some
		200	1.78	1.37	Increased
		292	1.35	0.98	"
		475.8	1.27	1.27	Illegible[e]
		600	0.92	0.77	"
		735 (Illegible due to delamination)[e]			
		746.5 Failure, location +5.8cm			
B-27	ε=0.0085	Static			No X-Ray
	σ=851[a]	Fatigue			
		1[b]	——[d]	3.18	
		4.344 Failure, location -3.7 cm			
B-28	ε=0.0090	Static	3.90	4.62	
	σ=907[a]	Fatigue			No Data
		11.8[b] Failure, location +0.0 cm			

FOOTNOTES:

a = Maximum Fatigue Stress in MPa
b = Cycles in Thousands
c = Strain Level Reached in Monotonic Tension Loading
d = A - indicates no matrix cracks observed
e = Edge Replicate illegible due to severe edge delamination

TABLE C59
MATRIX CRACK SPACING OBSERVED DURING MONOTONIC TENSION LOADING OF $(0_2/90_4)_s$ COUPONS

Coupon ID	Strain Level	Average Crack Spacing in 90° Ply, mm
1ZF1906-A1[a]	0.00150	12.7
	0.00250	12.7
	0.00300	12.7
	0.00351	12.7
	0.00400	12.7
	0.00451	12.7
	0.00478	12.7
	0.00501	10.2
	0.00527	8.47
	0.00575	8.47
	0.00603	7.26
	0.00705	6.35
	Failed at 0.00805	
-A2	0.00152	8.47
	0.00202	8.47
	0.00252	6.35
	0.00303	6.35
	0.00756	2.12
	0.00782	1.95
	0.00803	1.34[b]
	0.00826	1.34
	0.00855	1.27[c]
	0.00877	1.27
	0.00903	1.21[d]
	0.00929	1.10
	0.00953	1.10
	0.00979	1.06
	0.01000	1.06
	0.01027	1.06
	Failed at 0.00988	

Continued on next page

TABLE C59 - Continued
MATRIX CRACK SPACING OBSERVED DURING MONOTONIC TENSION LOADING OF $(0_2/90_4)_s$ COUPONS

Coupon ID	Strain Level	Average Crack Spacing in 90° Ply, mm
-A3	0.00304	6.35[d]
	0.00601	4.23
	0.00703	2.12
	0.00726	1.06
	0.00752	0.79
	0.00778	0.77
	0.00804	0.77
	0.00828	0.72
	0.00880	0.70
	0.00928	0.70
	0.00979	0.67
	Failed at 0.00992	
-A4	0.00807	1.81[e]
	0.00853	1.69[f]
	Failed at 0.00874	
-A5	0.00752	1.49
	0.00776	1.27
	0.00803	1.21
	0.00827	1.21
	0.00854	1.15
	0.00879	1.10
	0.00903	1.10
	0.00951	1.10
	Failed at 0.00918	

a = All cracks detected using enhanced x-ray.

b = Three short cracks running parallel to 0° ply through center of 90° plies

c = A few additional vertical cracks observed

d = Some cracks are at a 45° direction, often in right angle pairs

e = Two vertical cracks, 2-3 mm long, in center of 90° plies

f = Small amount of delamination between 0° and 90° plies

TABLE C60
STIFFNESS MEASUREMENTS TAKEN DURING
FATIGUE LOADING OF $(0_2/90_4)_s$ COUPONS

Coupon ID	Initial Strain Level	Cycles, Thousands	Modulus Static GPa	Static Msi	Dynamic GPa	Dynamic Msi
A15		0	50.5	7.32	-	-
	0.0050	0.13	-	-	49.0	7.10
		1.0	48.4	7.02	48.7	7.06
		Removed for x-ray				
		30.0	-	-	48.0	6.97
		145.0	47.6	6.90	47.6	6.90
		Removed for x-ray				
		180.0	46.1	6.69	45.9	6.66
		445.0	45.8	6.64	45.7	6.63
		445.1		Failure		
A21	0.0050	0	52.5	7.61	52.4	7.60
		1.0	51.1	7.41	50.9	7.38
		20.0	50.2	7.28	49.9	7.24
		40.0	49.6	7.20	49.4	7.17
		60.0	49.6	7.20	49.4	7.17
		80.0	49.6	7.19	49.3	7.15
		100.0	49.4	7.17	49.1	7.14
		Removed for x-ray				
		200.0	48.3	7.00	48.5	7.04
		Removed for x-ray				
		291.0	49.0	7.11	49.0	7.11
		500.0	49.1	7.12	48.8	7.08
		Removed for x-ray				
		1000.0	47.6	6.91	47.8	6.94
		Removed for x-ray and residual strength experimentation				
A22	0.0050	0	52.8	7.66	51.6	7.49
		25.0	50.3	7.29	50.0	7.25
		100.0	49.9	7.24	49.6	7.20
		Removed for x-ray				
		300.0	48.5	7.03	48.6	7.05
		Removed for x-ray				

TABLE C60- Continued
STIFFNESS MEASUREMENTS TAKEN DURING
FATIGUE LOADING OF $(0_2/90_4)_s$ COUPONS

Coupon ID	Initial Strain Level	Cycles, Thousands	Modulus Static GPa	Static Msi	Dynamic GPa	Dynamic Msi
A22-Cont.		600.0	48.9	7.09	48.5	7.04
		1000.0	48.1	6.98	48.1	6.98
		Removed for x-ray and residual strength experimentation				
A25	0.0050	0	52.7	7.65	-	-
		0.19	52.7	7.65	52.5	7.61
		1.0	51.4	7.45	51.5	7.47
		25.0	50.9	7.38	50.6	7.34
		100.0	50.9	7.38	50.6	7.34
		Removed for x-ray				
		140.0	49.0	7.11	49.2	7.14
		Removed for x-ray				
		290.0	49.1	7.12	49.2	7.13
		590.0	47.8	6.94	49.0	7.11
		682.0	48.0	6.97	48.7	7.07
		Removed for x-ray				
		682.0	47.1	6.83	48.6	7.05
		1000.0	48.5	7.03	48.7	7.07
		Removed for x-ray and residual strength experimentation				
A6	0.0060	0	52.6	7.63	51.0	7.40
		1.0	51.1	7.41	49.7	7.21
		Removed for x-ray				
		5.0	48.8	7.08	48.8	7.08
		Removed for x-ray				
		210.0	48.1	6.98	48.0	6.96
		373.0	48.0	6.96	48.0	6.96
		450.0	48.0	6.97	48.0	6.97
		650.0	47.8	6.93	47.8	6.94
		692.0	48.0	6.96	47.8	6.94
		Failed in static tension				
A12	0.0060	0	53.6	7.78	-	-
		0.10	-	-	51.6	7.49
		68.0	46.0	6.67	46.0	6.67
		Removed for x-ray and residual strength experimentation				

TABLE C60 -- Continued
STIFFNESS MEASUREMENTS TAKEN DURING
FATIGUE LOADING OF $(0_2/90_4)_s$ COUPONS

Coupon ID	Initial Strain Level	Cycles, Thousands	Modulus Static GPa	Static Msi	Dynamic GPa	Dynamic Msi
A13	0.0060	0	53.8	7.81	-	-
		0.10	-	-	53.6	7.78
		1.0	-	-	51.6	7.48
		30.0	50.0	7.26	50.1	7.27
		Removed for x-ray and residual strength experimentation				
A14	0.0060	0	51.6	7.48	51.7	7.50
		1.0	48.7	7.06	48.6	7.05
		10.0	-	-	44.7	6.48
		20.0	-	-	43.6	6.33
		28.4	Failure			
A20	0.0060	0	48.4	7.02	-	-
		0.10	-	-	48.2	6.99
		6.0	-	-	46.8	6.79
		150.0	46.5	6.75	46.5	6.74
		353.0	46.3	6.71	46.2	6.70
		450.0	46.3	6.71	46.2	6.70
		690.0	46.1	6.69	46.1	6.69
		Removed for x-ray and residual strength experimentation				
A24	0.0060	0	53.8	7.80	-	-
		0.30	-	-	50.7	7.36
		1.0	51.9	7.53	50.5	7.32
		5.0	-	-	49.1	7.12
		18.0	49.1	7.12	47.8	6.94
		Removed for x-ray				
		88.0	45.0	6.53	44.6	6.47
		Removed for x-ray				
		150.0	44.7	6.49	44.4	6.44
		238.0	44.6	6.47	44.3	6.42
		253.6	Failure			
A26	0.0060	0	51.0	7.39	-	-
		0.10	-	-	50.7	7.36
		19.0	-	-	49.1	7.12

TABLE C60 - Continued
STIFFNESS MEASUREMENTS TAKEN DURING
FATIGUE LOADING OF $(0_2/90_4)_s$ COUPONS

Coupon ID	Initial Strain Level	Cycles, Thousands	Modulus Static GPa	Static Msi	Dynamic GPa	Dynamic Msi
A26-Cont.		27.0	-	-	48.4	7.02
		30.0	-	-	48.3	7.01
		35.0	48.4	7.02	48.2	6.99
		Removed for x-ray and residual strength experimentation				
A31	0.0060	0	49.5	7.18	-	-
		0.10	-	-	48.9	7.09
		1.0	48.1	6.97	48.5	7.03
		46.0	-	-	47.4	6.88
		100.0	-	-	47.3	6.86
		118.0	46.3	6.72	46.5	6.74
		Removed for x-ray				
		158.0	-	-	46.5	6.75
		218.0	-	-	46.3	6.71
		300.0	46.3	6.71	46.1	6.68
		Removed for x-ray				
		450.0	45.8	6.65	45.8	6.64
		600.0	-	-	45.0	6.52
		682.0	44.8	6.50	94.7	6.49
		Removed for x-ray				
		682.0	44.7	6.33	44.7	6.48
		832.0	43.8	6.36	43.8	6.36
		1000.0	43.6	6.48	43.6	6.33
		Removed for x-ray and residual strength experimentation				
A8	0.0065	0	51.8	7.51	-	-
		1.0	50.1	7.26	49.9	7.24
		50.0	45.9	6.61	45.4	6.59
		74.2	Failure			
A9	0.0065	0	51.6	7.48	-	-
		0.15	-	-	49.3	7.15
		1.0	49.9	7.24	48.7	7.07
		Removed for x-ray				
		14.15	48.5	7.04	48.6	7.05
		Removed for x-ray				
		14.15	46.0	6.67	-	-
		Failed during static survey				

TABLE C60 - Continued
STIFFNESS MEASUREMENTS TAKEN DURING
FATIGUE LOADING OF $(0_2/90_4)_s$ COUPONS

Coupon ID	Initial Strain Level	Cycles, Thousands	Modulus Static GPa	Static Msi	Dynamic GPa	Dynamic Msi
A10	0.0065	0	52.0	7.54	-	-
		1.0	50.1	7.26	50.0	7.25
		5.0	-	-	49.8	7.23
		10.0	-	-	48.2	6.99
		15.0	-	-	47.8	6.94
		20.0	-	-	47.7	6.92
		25.0	-	-	46.6	6.76
		30.0	-	-	47.5	6.89
		35.0	-	-	47.5	6.89
		36.96	Failure			
A11	0.0065	0	48.5	7.04	-	-
		0.20	-	-	47.6	6.91
		20.0	-	-	46.1	6.69
		35.0	45.2	6.56	45.2	6.55
		Removed for x-ray and residual strength experimentation				
A17	0.0065	0	52.4	7.60	-	-
		0.10	-	-	51.5	7.47
		20.0	-	-	50.2	7.28
		40.0	-	-	50.1	7.26
		100.0	-	-	49.8	7.23
		140.0	-	-	49.8	7.22
		180.0	-	-	49.7	7.21
		300.0	49.6	7.19	49.6	7.19
		460.0	49.6	7.19	49.5	7.18
		1000.0	49.5	7.18	49.5	7.18
		Removed for x-ray and residual strength experimentation				
A27	0.0065	0	47.2	6.84	-	-
		0.15	-	-	46.6	6.76
		1.0	46.1	6.68	46.3	6.72
		Removed for x-ray				
		23.0	45.1	6.54	45.1	6.52
		Removed for x-ray				
		23.0	44.8	6.50	45.0	6.53

TABLE C60 - Cont.
STIFFNESS MEASUREMENTS TAKEN DURING
FATIGUE LOADING OF $(0_2/90_4)_s$ COUPONS

Coupon ID	Initial Strain Level	Cycles, Thousands	Modulus Static GPa	Static Msi	Dynamic GPa	Dynamic Msi
A27 - Cont		43.0	-	-	44.5	6.43
		63.0	-	-	44.3	6.43
		110.0	43.8	6.35	43.6	6.32
		Removed for x-ray				
		110.0	43.5	6.31	43.4	6.30
		160.0	-	-	43.5	6.31
		164.9	Failure			
A32	0.0065	0	52.7	7.65	-	-
		0.10	-	-	51.1	7.41
		20.0	-	-	49.4	7.16
		24.0	-	-	48.6	7.05
		25.5	47.9	6.95	47.8	6.94
		Removed for x-ray and residual strength experimentation				

a = Except where noted, the initial dynamic modulus was obtained within the first 100 fatigue cycles.

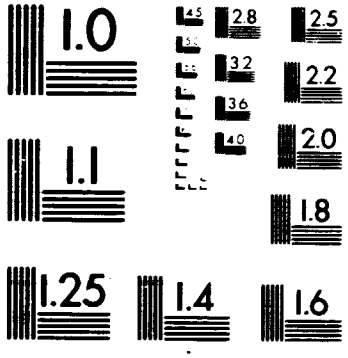

TABLE C61
SUMMARY OF MATRIX CRACKING AND DELAMINATION
DATA FOR $(0_2/90_4)_S$ COUPONS

COUPON ID	INITIAL STRAIN	LOADING CONDITION	AVERAGE CRACK SPACING IN 90° PLIES (mm)	AVERAGE[b] NUMBER OF VERTICAL CRACKS	EDGE[c] DELAMINATION STATE	DAMAGE[d] STATE BY X-RAY
A-15	0.0050	Unloaded	8.47	0	None	
		Static	2.21	0	None	
		Fatigue[a]				
		1.0	1.54	3	Short	0,0
		145.0	1.15	3	Medium	3S,0
		445.0	Failure			
A21	0.0050	Unloaded	6.35	2	None	
		Static	2.12	7	Short	
		Fatigue[a]				
		1.0	1.41	7		
		20.0	1.34	7		
		60.0	1.34	7		
		80.0	1.34	7		
		100.0	1.34	7		4,0
		200.0	1.34	Long	Medium	5,3
		500.0	1.30	Long		5,4
		1000.0	1.27	Long		5,10
		Residual Strength				
		ε = 0.0075	1.27	Long	Medium	5,10
		ε = 0.0080	1.27	Long	Medium	5,10
		ε = 0.0085	1.27	Long	Medium	5,10
		σ_f = 431 MPa; ε_f = 0.0090; E_f = 48.0 GPa				
A-22	0.0050	Unloaded	5.64	4	None	
		Fatigue[a]				
		25.0	1.59	11	Short	
		75.0	1.59	11	Short	
		100.0	1.59	11	Short	9,3
		300.0	1.49	11	Long	9,10
		1 000.0	1.49	Long	Long	9,30
		Residual				

C-6

TABLE C61 - Continued
SUMMARY OF MATRIX CRACKING AND DELAMINATION DATA FOR $(0_2/90_4)_S$ COUPONS

COUPON ID	INITIAL STRAIN	LOADING CONDITION	AVERAGE CRACK SPACING IN 90° PLIES (mm)	AVERAGE[b] NUMBER OF VERTICAL CRACKS	EDGE[c] DELAMINATION STATE	DAMAGE[d] STATE BY X-RAY
		Strength				
		ε = 0.0075	1.49	Long	Long	9,30
		ε = 0.0080	1.49	Long	Long	9,30
		ε = 0.0085	1.49	Long	Long	9,30
		σ_f = 466 MPa; ε_f = 0.0094; E_f = 49.7 GPa				
A-25	0.0050	**Unloaded**	**Data Unavailable**			
		Static	**Data Unavailable**			
		Fatigue[a]				
		100.0	1.13	4	Short	3S,0
		140.0	1.13	4	Medium	1,0
		682.0	1.13	4	Long	4,10
		1 000.0				4,10
		Residual Strength				
		ε = 0.0075	1.10	4	Long	4,10
		ε = 0.0080	1.10	4	Long	
		ε = 0.0085	1.04	4	Long	4,10
		σ_f = 486 MPa; ε_f = 0.0097; E_f = 50.4 GPa				
A-6	0.0060	Unloaded	8.47	0	None	
		Fatigue[a]				
		1.0	1.81	4	Short	3S,0
		5.0	1.34	4	Long	7,2
		692.0	1.30	4	Long	7,40
		692.0	Failure			
A-12	0.0060	Unloaded	8.46	0	None	
		Static	1.95	2	None	
		Fatigue[a]				
		68.0	1.15	3	Long	11,40
		Residual Strength				
		ε = 0.0075	1.13	3	Long	11,40

TABLE C61 - Continued
SUMMARY OF MATRIX CRACKING AND DELAMINATION DATA FOR $(0_2/90_4)_S$ COUPONS

COUPON ID	INITIAL STRAIN	LOADING CONDITION	AVERAGE CRACK SPACING IN IN 90° PLIES (mm)	AVERAGE[b] NUMBER OF VERTICAL CRACKS	EDGE[c] DELAMINATION STATE	DAMAGE[d] STATE BY X-RAY
		ε = 0.00825	1.10	3	Long	11,40
		σ_f = 407 MPa; ε_f = 0.0088; E_f = 46.3 GPa				
A-13	0.0060	Unloaded	8.46	0	None	
		Static Fatigue[a]	2.21	1	None	
		30.0 Residual Strength	1.04	1	Medium	8,15
		ε = 0.0075	1.02	1	Medium	8,15
		ε = 0.0080	0.98	2	Medium	8,15
		σ_f = 385 MPa; ε_f = 0.00792; E_f = 48.5 GPa				
A-14	0.0060	Unloaded	10.2	0	None	
		Static Fatigue[a]	1.69	2	None	
		1.0	1.21	2	Short	
		28.4	Failure			
A-20	0.0060	Unloaded	5.64	3	None	
		Fatigue[a] 690.0 Residual Strength	1.30	6	Long	6,20
		ε = 0.0075	1.30	7.5	Long	6,20
		ε = 0.00825	1.24	7.5	Long	6,20
		ε = 0.00875	1.24	7.5	Long	6,20
		σ_f = 452 MPa; ε_f = 0.00961; E_f = 47.0 GPa				
A-24	0.0060	Unloaded	7.26	0	None	
		Static Fatigue[a]	1.81	4	None	
		1.0	1.18	4	Short	
		18.0	1.06	5	Short	15,2

TABLE C61 - Continued
SUMMARY OF MATRIX CRACKING AND DELAMINATION
DATA FOR $(0_2/90_4)_S$ COUPONS

COUPON ID	INITIAL STRAIN	LOADING CONDITION	AVERAGE CRACK SPACING IN IN 90° PLIES (mm)	AVERAGE[b] NUMBER OF VERTICAL CRACKS	EDGE[c] DELAMINATION STATE	DAMAGE[d] STATE BY X-RAY
		88.0	1.06	5	Long	10,70
		253.6	Failure			
A-26	0.0060	Unloaded	6.35	0	None	
		Fatigue[a]				
		35.0	1.37	2	Long	6,10
		Residual Strength				
		ε = 0.0075	1.37	2	Long	6,10
		ε = 0.00825	1.37	2	Long	6,10
		ε = 0.00875	1.34	2	Long	6,10
		σ_f = 454 MPa; ε_f = 0.00931; E_f = 48.9 GPa				
A-29	0.0060	Unloaded	5.08	2	None	
		Static	2.31	4	None	
		Fatigue[a]				
		1.0	1.27	5	None	
		90.0	1.21	6	Short	4,25
		Failed due to equipment malfunction.				
A-31	0.0060	Unloaded	5.64	0	None	
		Static	1.81	4	Short	
		Fatigue[a]				
		1.0	1.21	5	Short	
		118.0	0.96	5	Delaminations	9,4
		300.0	0.91	6	are linking up	13,60
		500.0	0.91	5	Large	13,60
		682.0	-	-		13,60
		1 000.0	0.93	5	Long	13,60
		Residual Strength				
		ε = 0.00775	0.92	5	Long	13,60
		σ_f = 317 MPa; ε_f = 0.00734; E_f = 43.9 GPa				

TABLE C61 - Continued
SUMMARY OF MATRIX CRACKING AND DELAMINATION DATA FOR $(0_2/90_4)_S$ COUPONS

COUPON ID	INITIAL STRAIN	LOADING CONDITION	AVERAGE CRACK SPACING IN IN 90° PLIES (mm)	AVERAGE[b] NUMBER OF VERTICAL CRACKS	EDGE[c] DELAMINATION STATE	DAMAGE STATE BY X-RAY
A-8	0.0065	Unloaded	8.51	2	None	
		Static Fatigue[a]	1.95	2	None	
		1.0	1.15	10	Short	
		50.0	0.98	11	Longer	
		74.2	Failure			
A-9	0.0065	Unloaded	8.47	2	None	
		Static Fatigue[a]	1.69	4	Short	
		1.0	1.10	4	Short	2,0
		14.2	1.04	14	Long	4,10
		14.2	Failure			
A-10	0.0065	Unloaded	12.7	1	None	
		Static Fatigue[a]	1.64	7		
		1.0	1.15	8	Short	
		36.96	Failure			
A-11	0.0065	Unloaded	8.47	0	None	
		Static Fatigue[a]	2.12	4	None	
		35.0	1.04	4	Long	3S,4
		Residual Strength				
		σ_f = 361 MPa; ϵ_f = 0.0079 E_f = 45.4 GPa				
A-17	0.0065	Unloaded	6.35	2	None	
		Static Fatigue	1.37	4	Medium	
		1 000.0[a]	1.13	4	Long	2,5
		Residual				

TABLE C61 - Continued
SUMMARY OF MATRIX CRACKING AND DELAMINATION
DATA FOR $(0_2/90_4)_S$ COUPONS

COUPON ID	INITIAL STRAIN	LOADING CONDITION	AVERAGE CRACK SPACING IN IN 90^o PLIES (mm)	AVERAGE[b] NUMBER OF VERTICAL CRACKS	EDGE[c] DELAMINATION STATE	DAMAGE[d] STATE BY X-RAY
		Strength				
		ε = 0.00775	1.08	5	Long	2,5
		ε = 0.00825	1.08	5	Long	2,5
		ε = 0.00875	1.04	5	Long	2,5
		σ_f = 511 MPa; ε_f = 0.0102 ; E_f = 49.1 GPa				
A-27	0.0065	Unloaded	6.35	0	None	
		Static	1.49	2	Short	
		Fatigue[a]				
		1.0	1.08	3	Short	1,0
		23.0	1.06	3	Medium	3,3
		110.0	1.06	3	Long	10,40
		164.91	Failure			
A-32	0.0065	Unloaded	5.08	2	None	
		Static	1.64	4	None	
		Fatigue[a]				
		25.5	0.98	5	Short	6,20
		Residual Strength				
		ε = 0.0075	0.98	5	Medium	6,20
		ε = 0.0080	0.96	5	Medium	6,20
		σ_f = 374 MPa; ε_f = 0.00805; E_f = 47.0 GPa				

a = Cycles in thousands

b = Vertical cracks lie between or connect the 90^o matrix cracks. A number indicates average number of transverse crack pairs connected; Long, indicates essentially all pairs on edge are connected.

c = Estimated amount of delamination found by edge replication; Short, means matrix cracks have short delaminated ends; Medium, that cracks have ends connecting; Long, that 0/90 interface is fully delaminated.

d = First entry refers to the number of 0^o longitudinal splits, an S means the splits are short and not full length; the second entry is a visual estimate of the amount of delamination in percent.

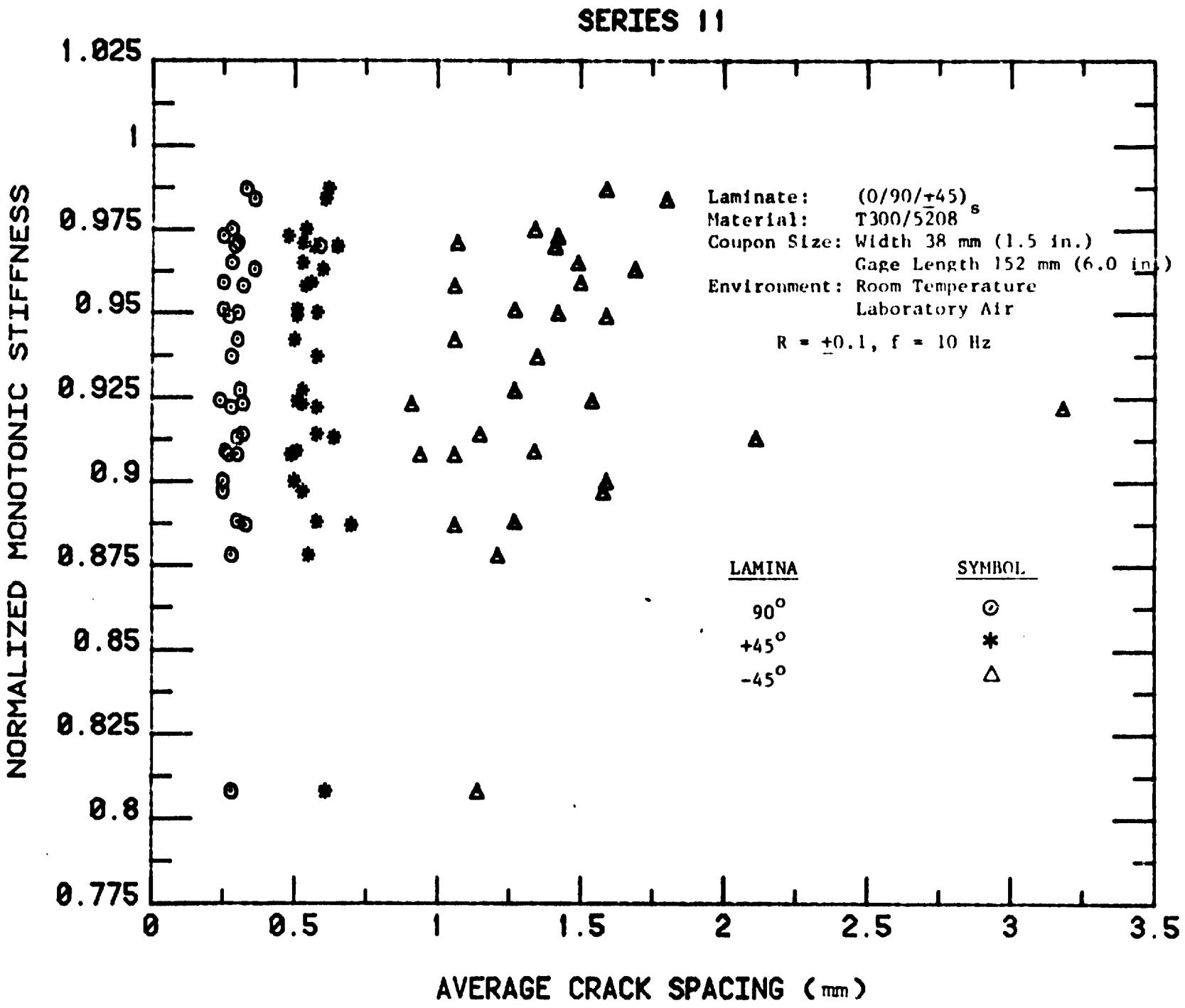

Figure C1: Normalized Monotonic Stiffness vs. Average Matrix Crack Spacing for $(0/90/\pm45)_s$ Laminate Coupons Subjected to Constant Amplitude Fatigue Load.

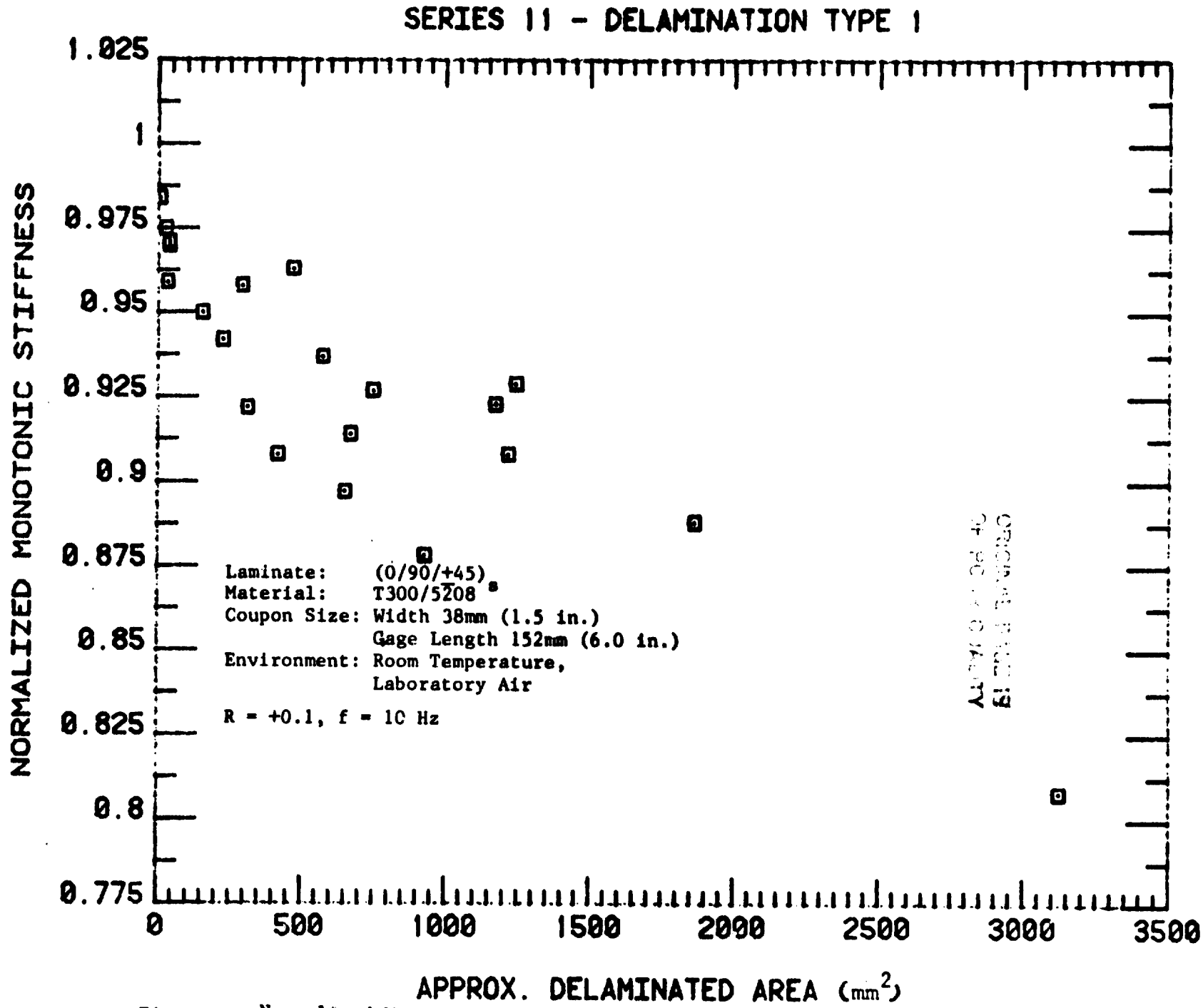

Figure C2: Normalized Monotonic Stiffness vs. Approximate Delaminated Area, $90^{o}/\pm45^{o}$ Delamination (Type 1), for $(0/90/\pm45)_{s}$ Laminate Coupons Subjected to Constant Amplitude Fatigue Load.

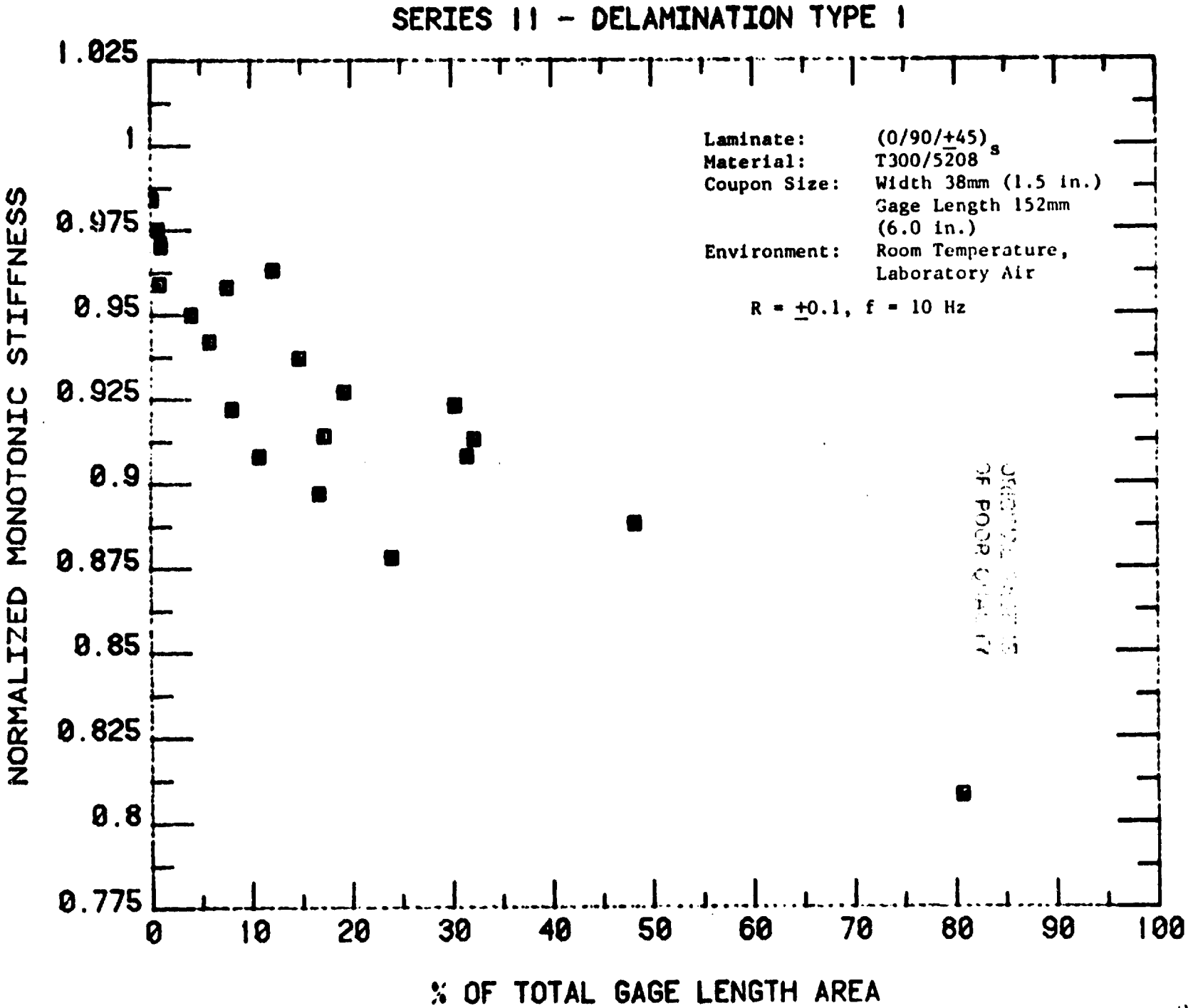

Figure C3: Normalized Monotonic Stiffness vs. Percent of Total Coupon Gage Length Area, $90^{0}/45^{0}$ Delamination (Type 1) for $(0/90/\pm45)_{s}$ Laminate Coupons Subjected to Constant Amplitude Fatigue Load.

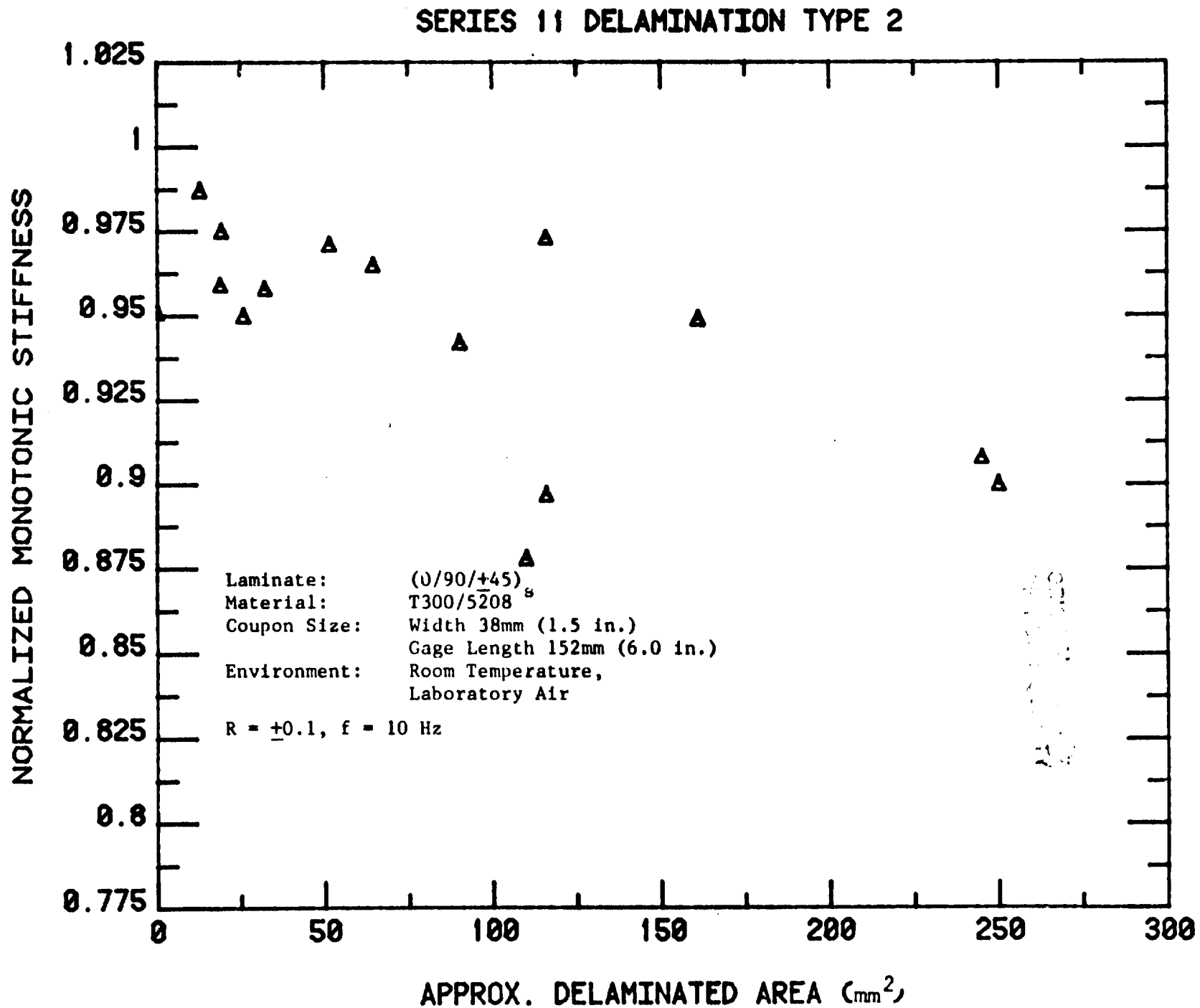

Figure C4: Normalized Monotonic Stiffness vs. Approximate Delaminated Area, $+45^{\circ}/-45^{\circ}$ Delamination (Type 2) for $(0/90/\pm45)_s$ Laminate Coupons Subjected to Constant Amplitude Fatigue Load.

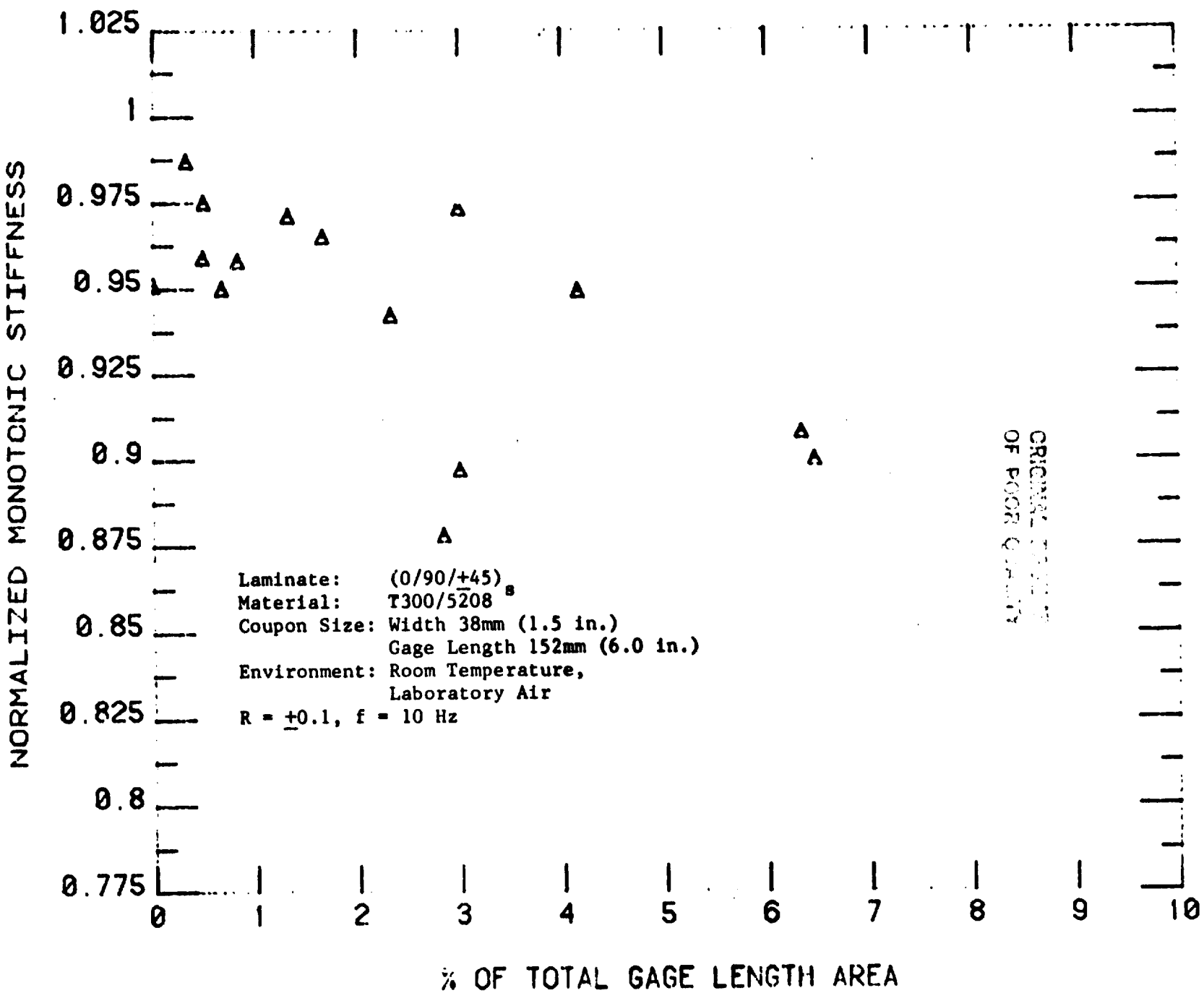

Figure: C5: Normalized Monotonic Stiffness vs. Percent of Total Coupon Gage Length Area, $+45^{0}/-45^{0}$ Delamination (Type 2) for $(0/90/\pm45)_{s}$ Laminate Coupons Subjected to Constant Amplitude Fatigue Load.

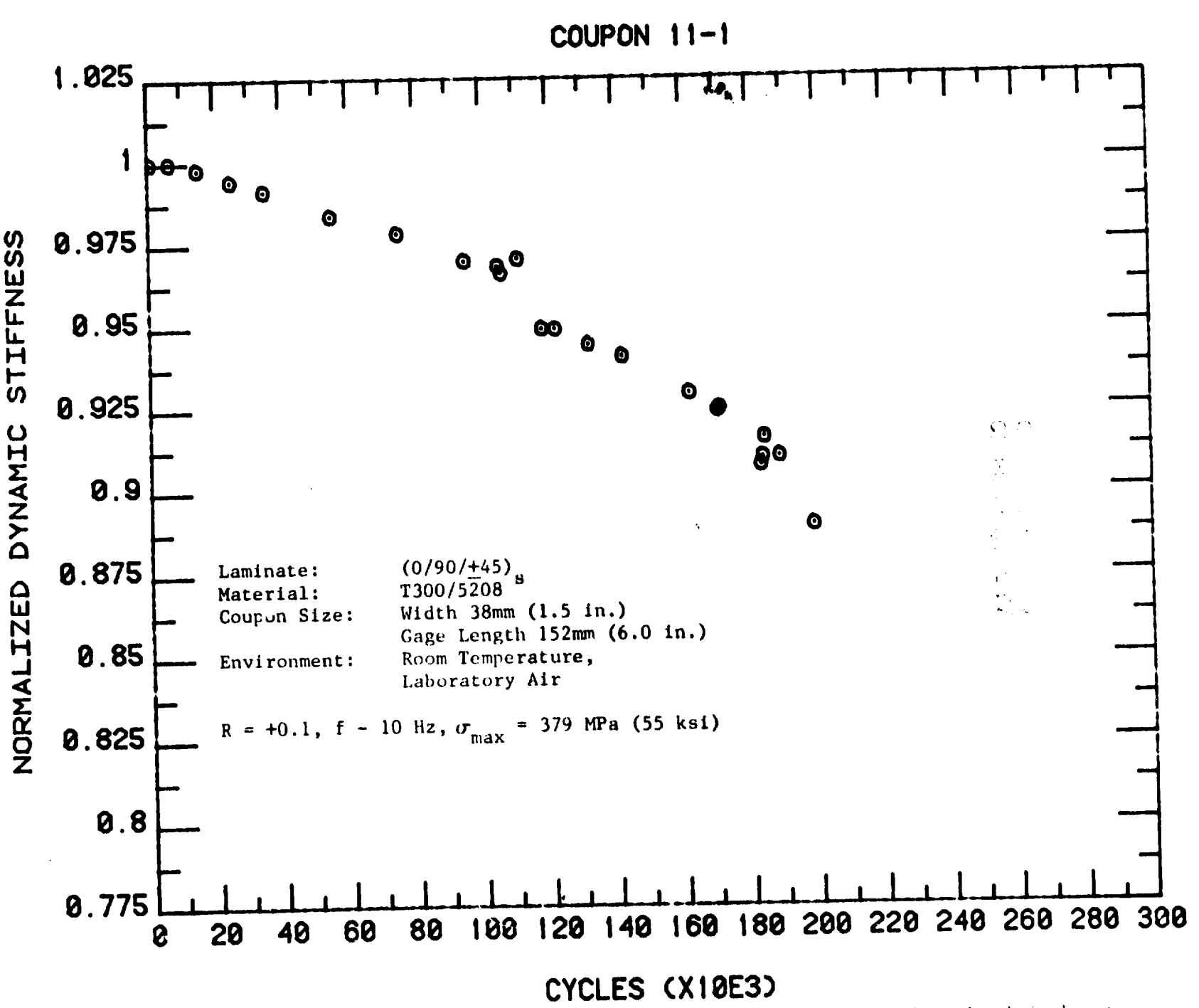

Figure C6: Normalized Dynamic Stiffness vs. Constant Amplitude Fatigue Load Cycles for $(0/90/\pm45)_s$ Laminate Coupon 11-1, σ_{max} = 379 MPa (55 ksi).

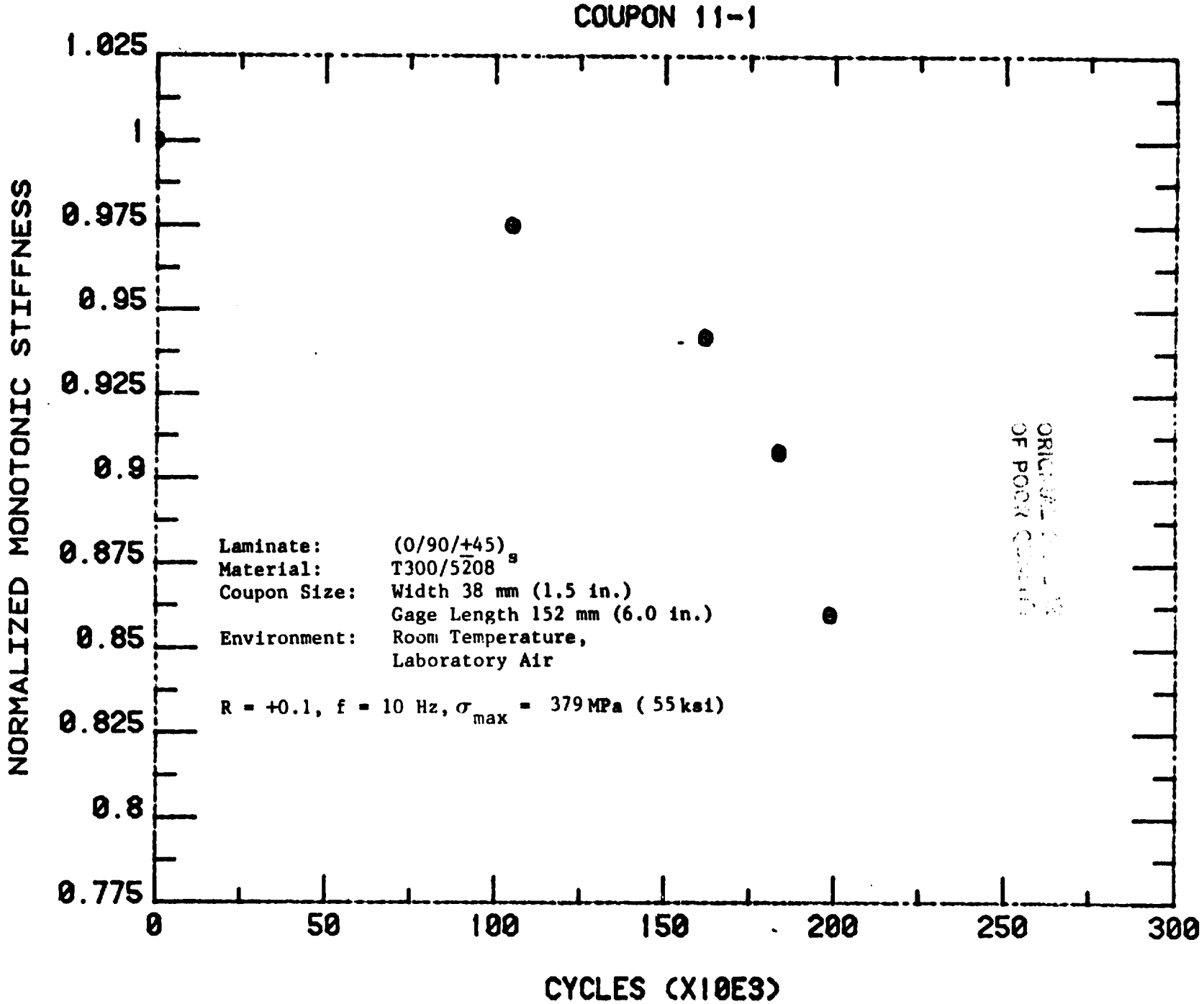

Figure C7: Normalized Monotonic Stiffness vs. Constant Amplitude Fatigue Load Cycles for $(0/90/\pm45)_s$ Laminate Coupon 11-1, σ_{max} = 379 MPa (55 ksi)

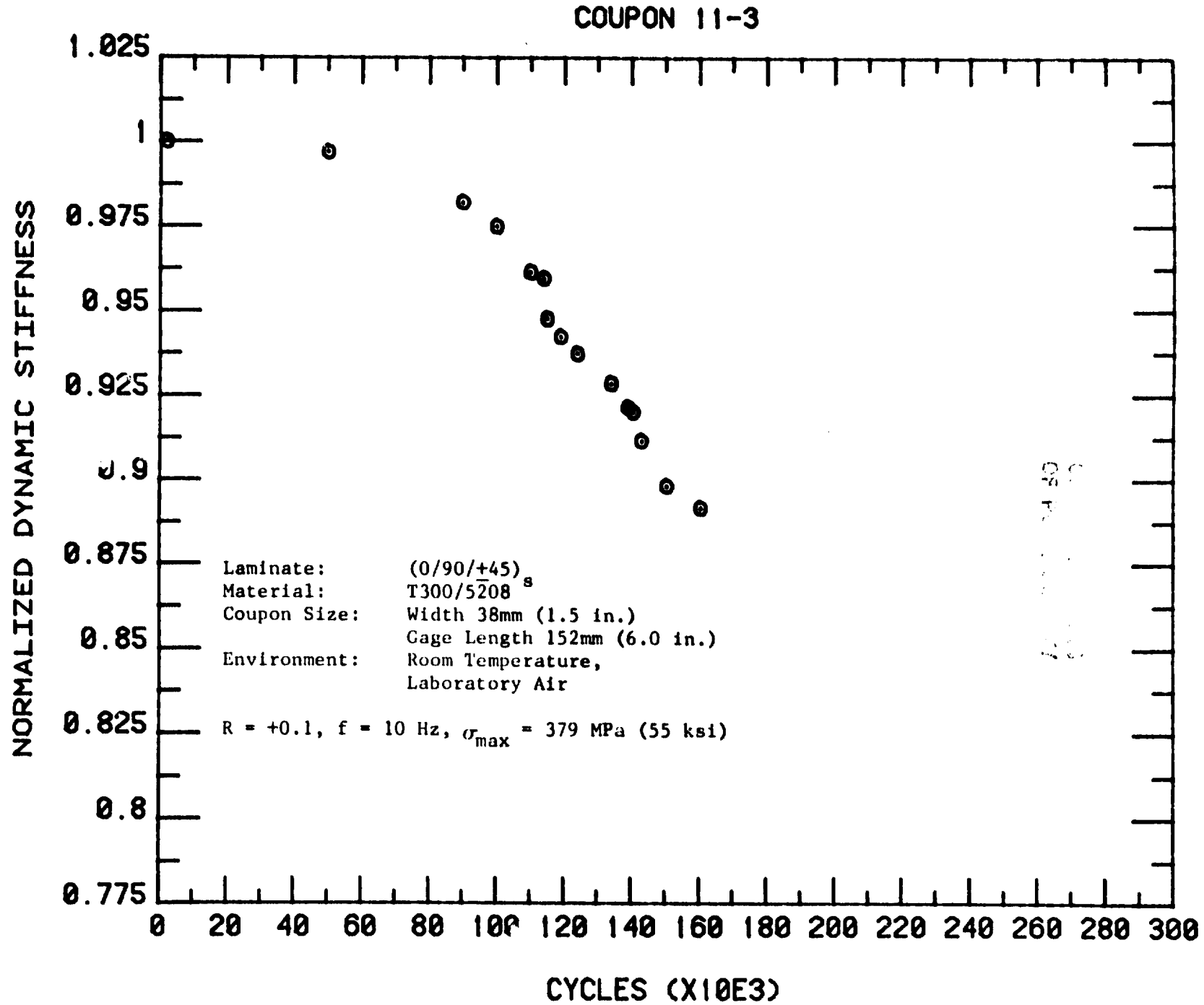
COUPON 11-3
NORMALIZED DYNAMIC STIFFNESS
1.025
1
0.975
0.95
0.925
0.9
0.875
0.85
0.825
0.8
0.775
0 20 40 60 80 100 120 140 160 180 200 220 240 260 280 300
CYCLES (X10E3)
Laminate: (0/90/+45)s
Material: T300/5208
Coupon Size: Width 38mm (1.5 in.)
Gage Length 152mm (6.0 in.)
Environment: Room Temperature,
Laboratory Air
R = +0.1, f = 10 Hz, σmax = 379 MPa (55 ksi)

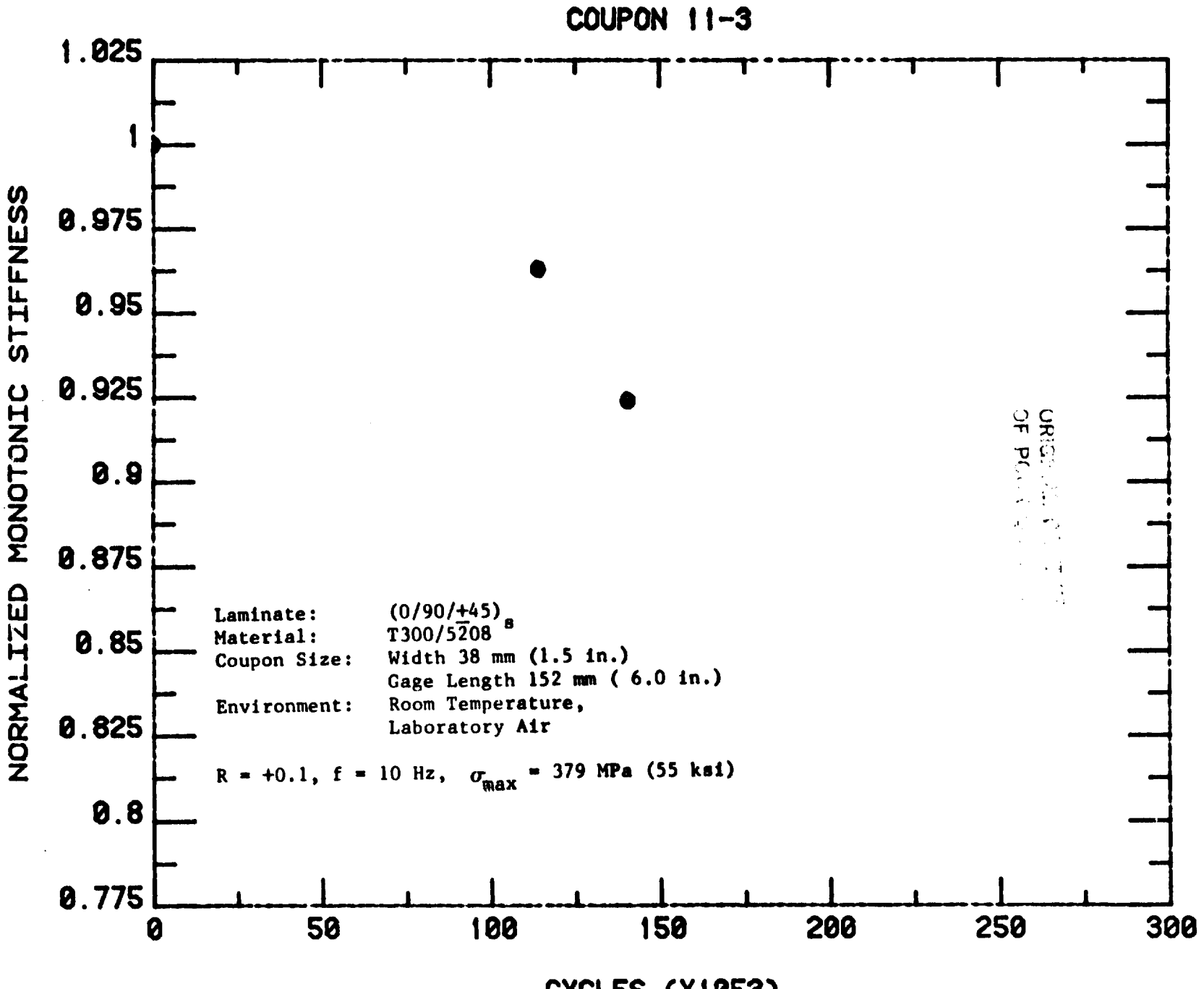

Figure C9: Normalized Monotonic Stiffness vs. Constant Amplitude Fatigue Load Cycles for $(0/90/\pm45)_s$ Laminate Coupon 11-3, σ_{max} = 379 MPa (55 ksi)

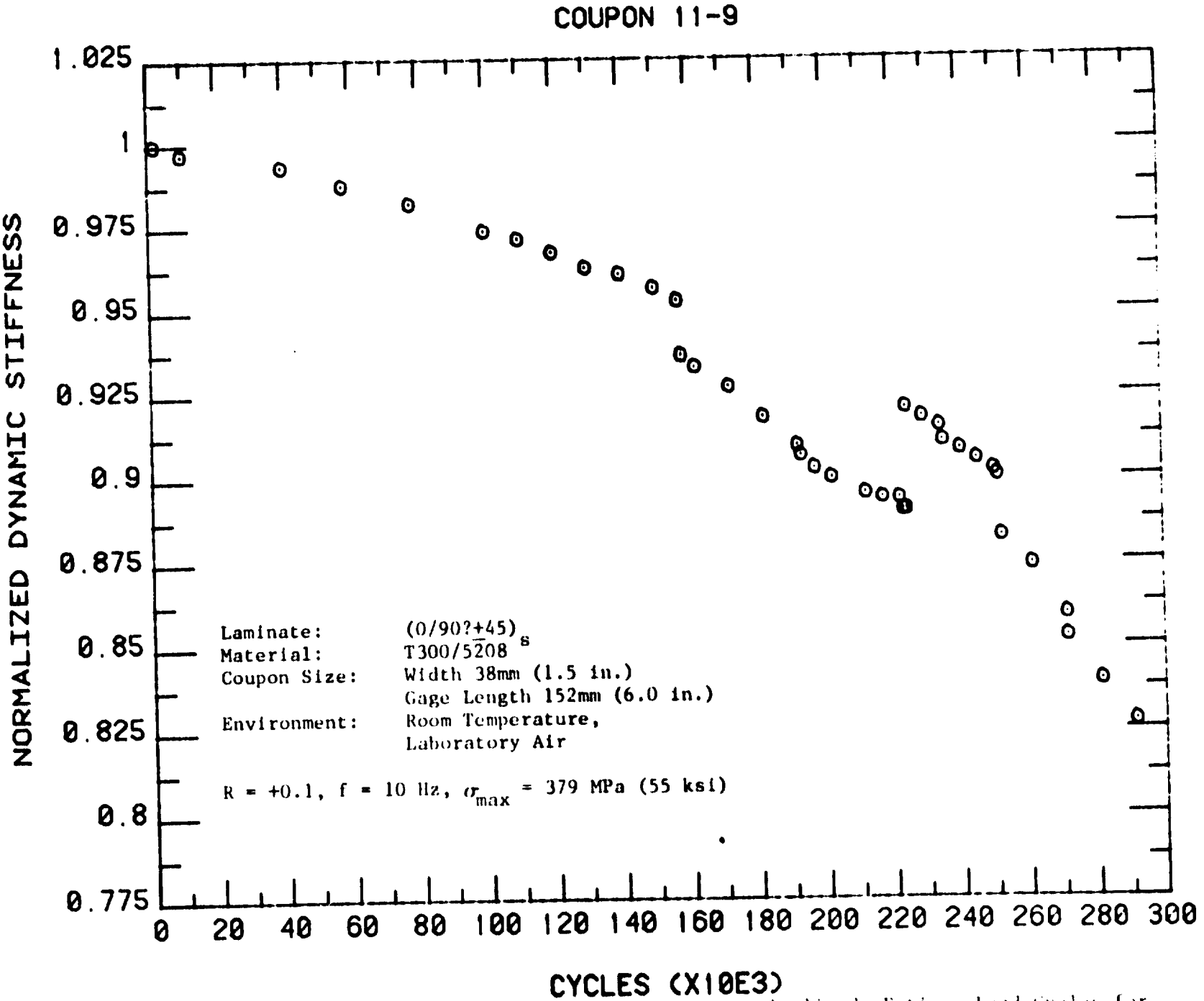

Figure C10 Normalized Dynamic Stiffness vs. Constant Amplitude Fatigue Load Cycles for $(0/90/\pm45)_s$ Laminate Coupon 11-9, σ_{max} = 379 MPa (55 ksi)

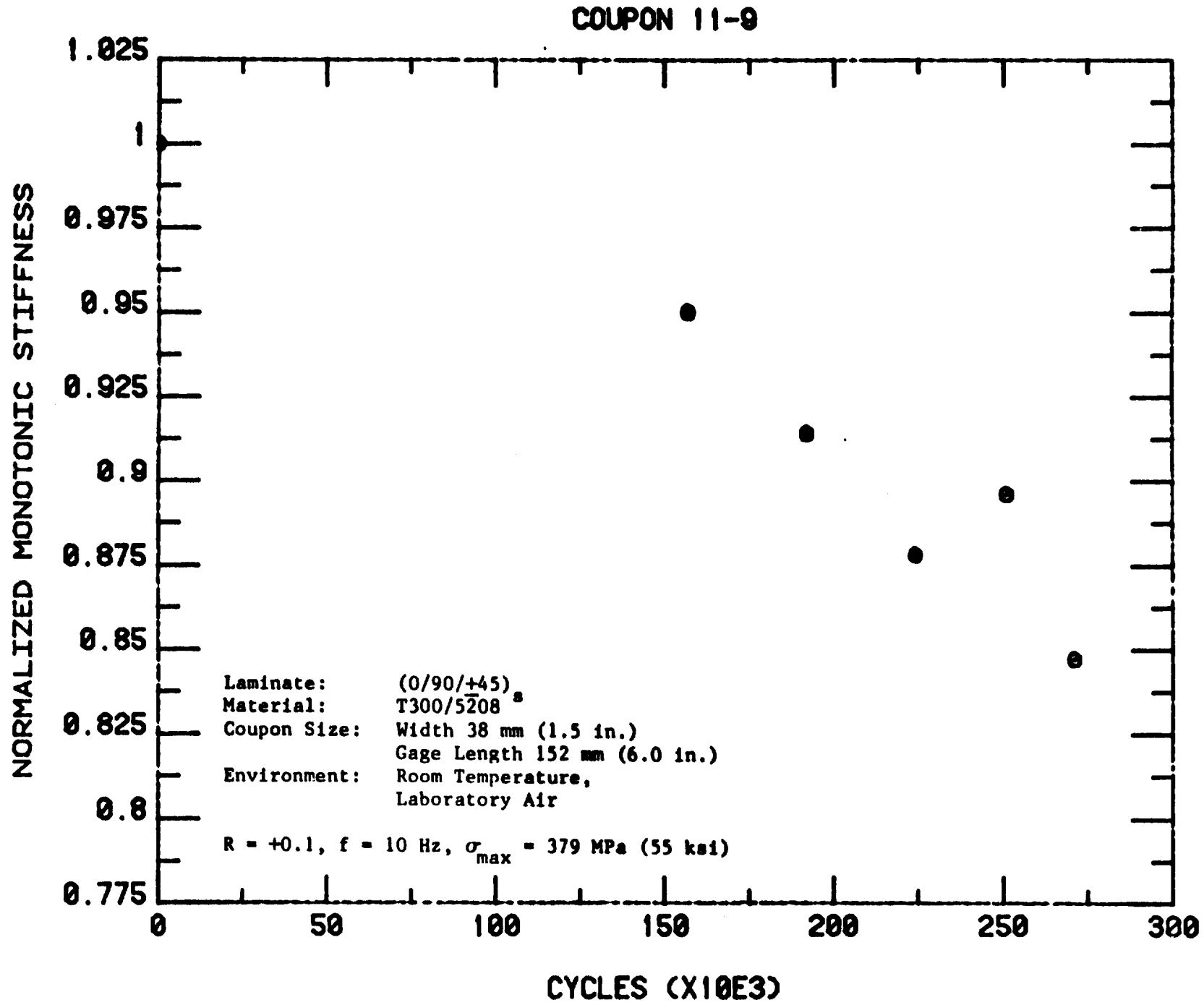

Figure C11: Normalized Monotonic Stiffness vs. Constant Amplitude Fatigue Load Cycles for $(0/90/\pm45)_s$ Laminate Coupon 11-9, σ_{max} = 379 MPa (55 ksi)

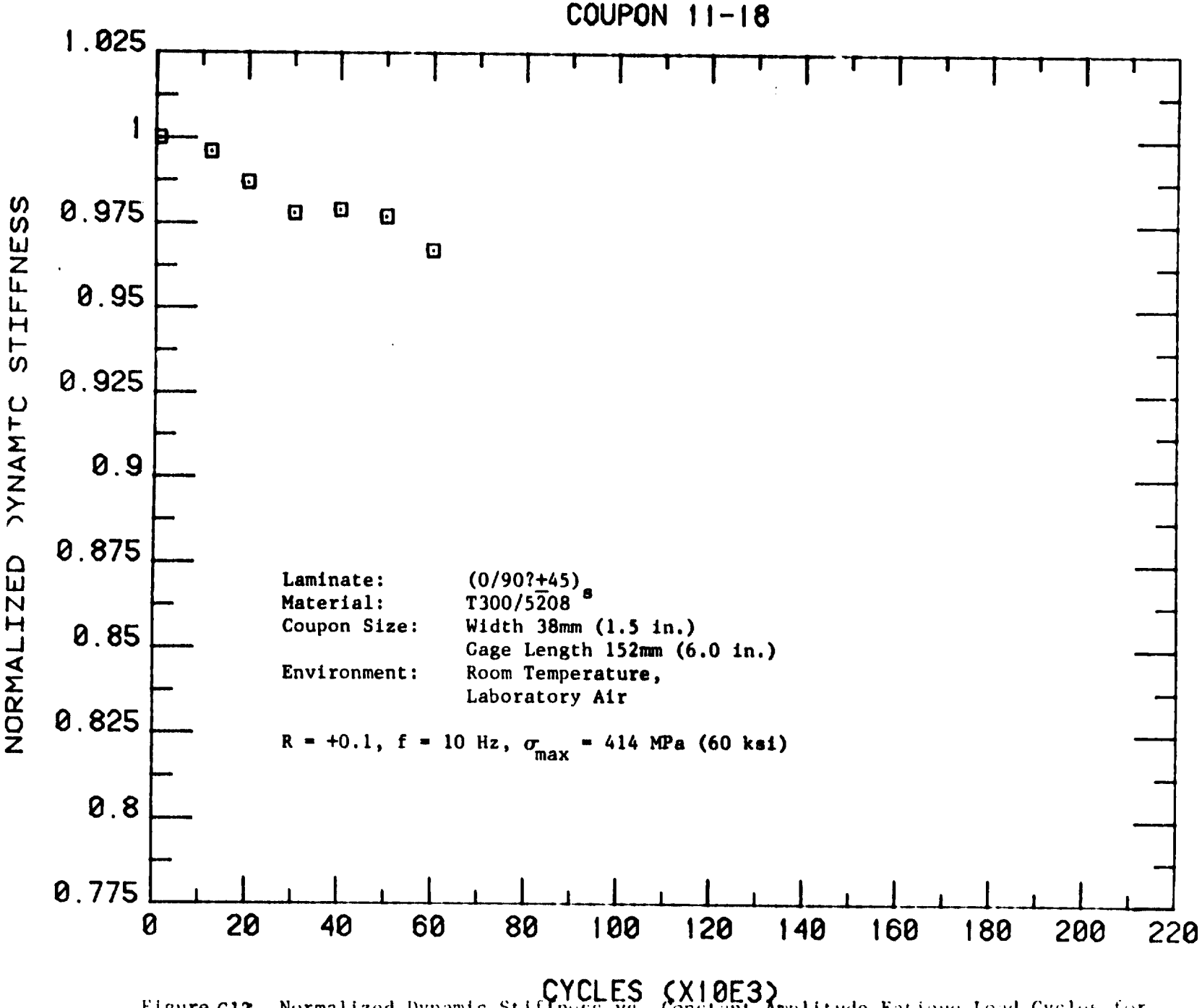

Figure C12 Normalized Dynamic Stiffness vs. Constant Amplitude Fatigue Load Cycles for $(0/90/\pm45)_s$ Laminate Coupon 11-18, σ_{max} = 414 MPa (60 ksi)

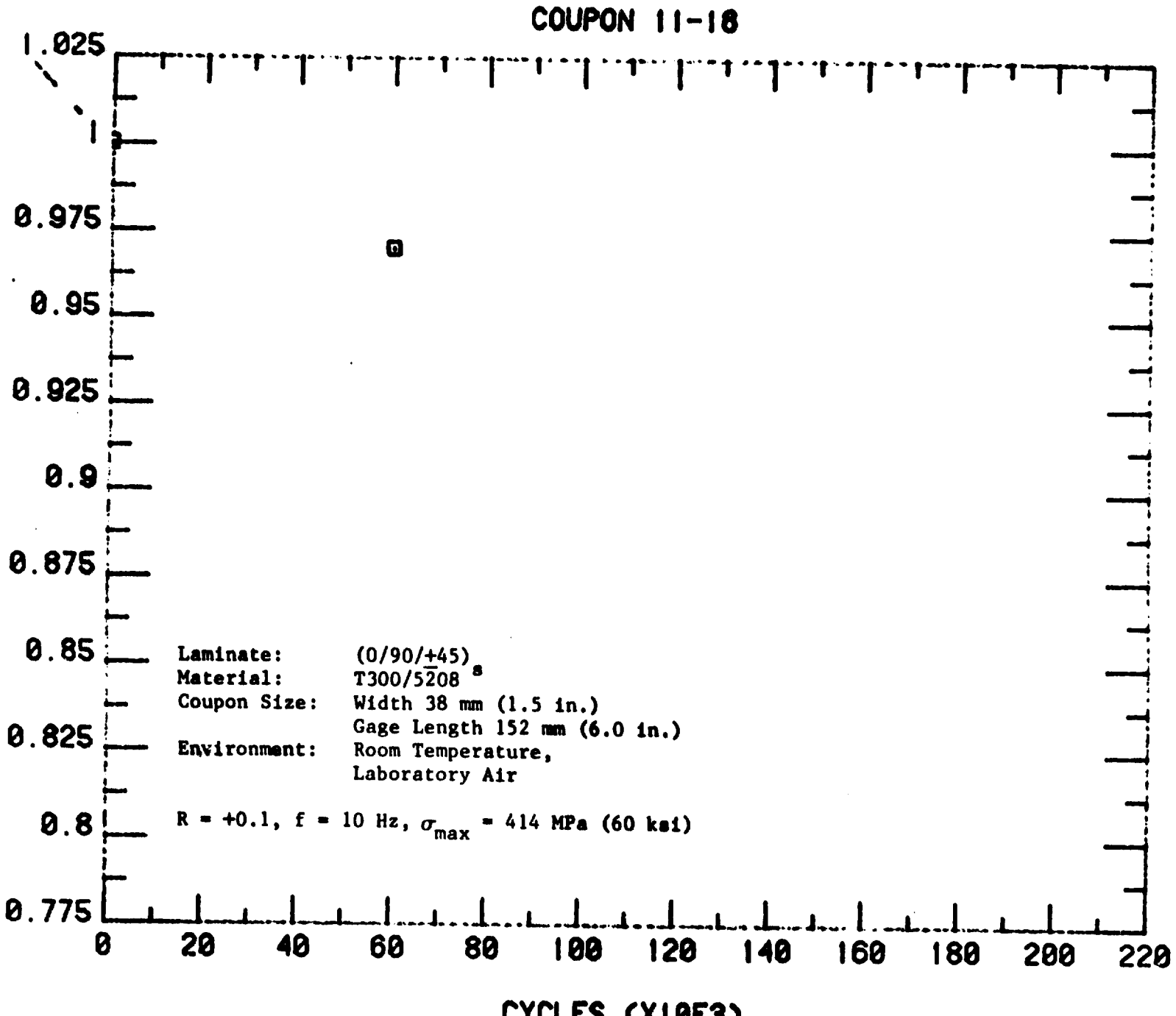

Figure: C13 Normalized Monotonic Stiffness vs. Constant Amplitude Fatigue Load Cycles for $(0/90/\pm45)_s$ Laminate Coupon 11-18, σ_{max} = 414 MPa (60 ksi).

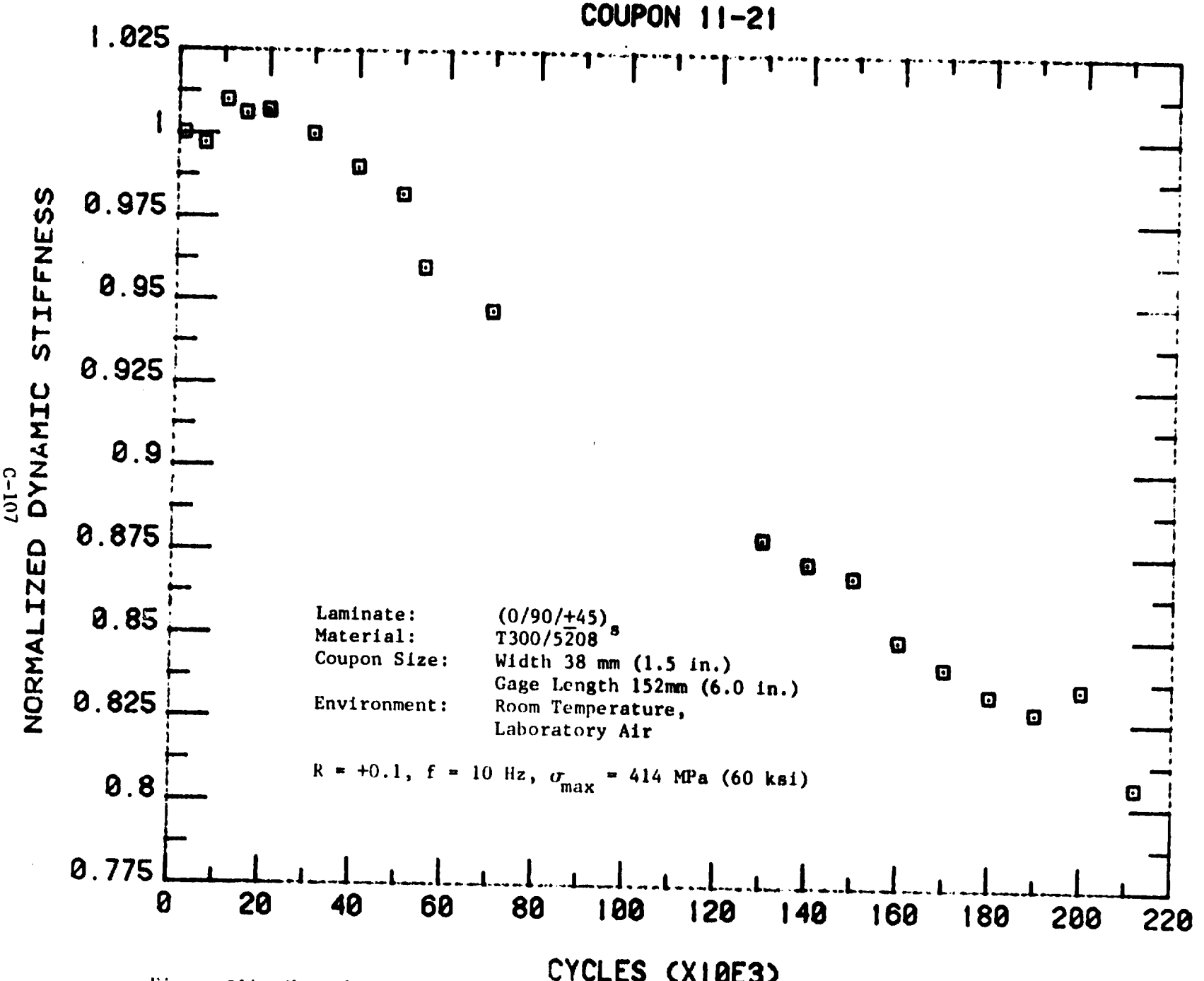

Figure C14 Normalized Dynamic Stiffness vs. Constant Amplitude Fatigue Load Cycles for $(0/90/\pm45)_s$ Laminate 11-21, σ_{max} = 414 MPa (60 ksi)

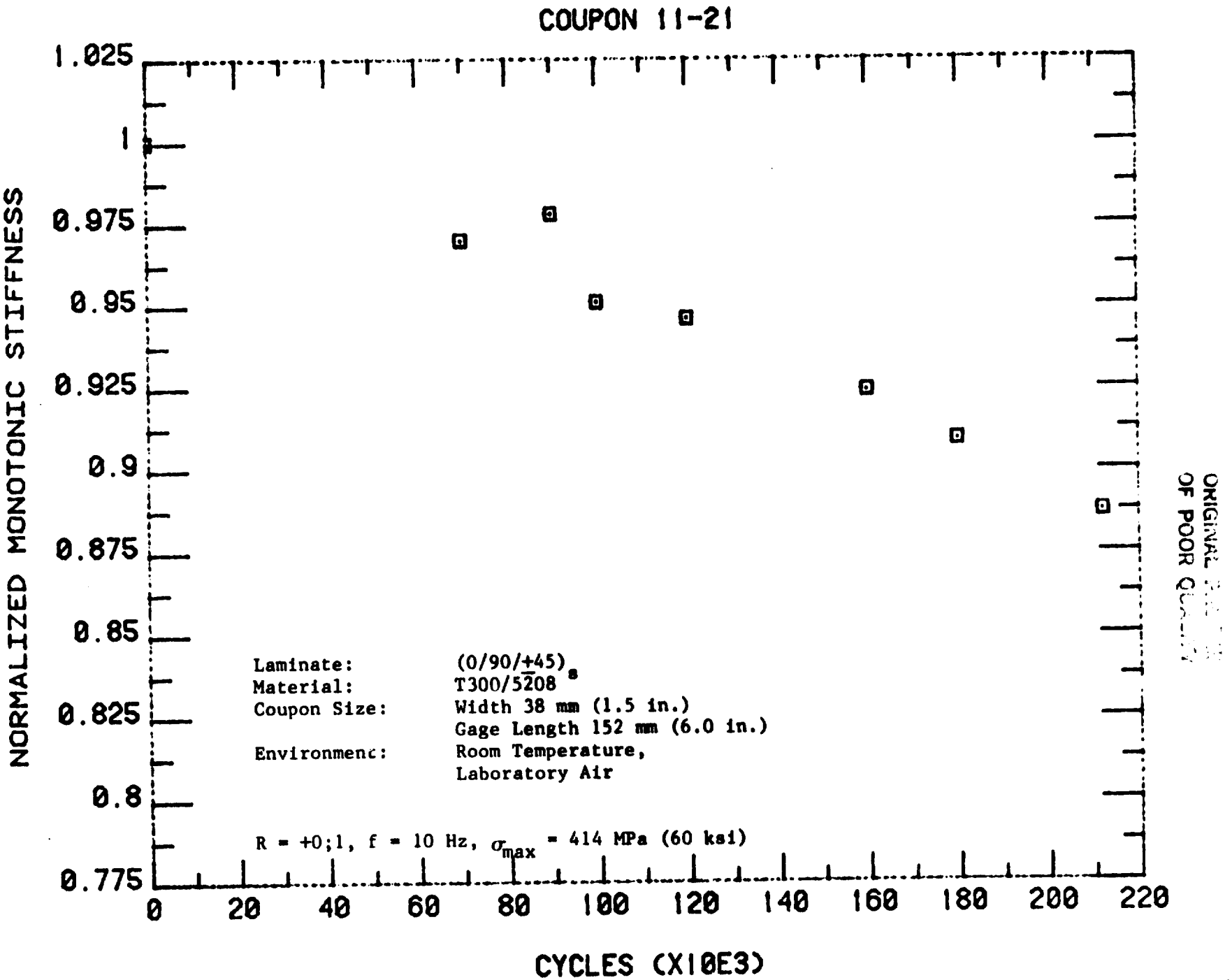

Figure C15: Normalized Monotonic Stiffness vs. Constant Amplitude Fatigue Load Cycles for $(0/90/\pm45)_s$ Laminate Coupon 11-21, σ_{max} = 414 MPa (60 ksi).

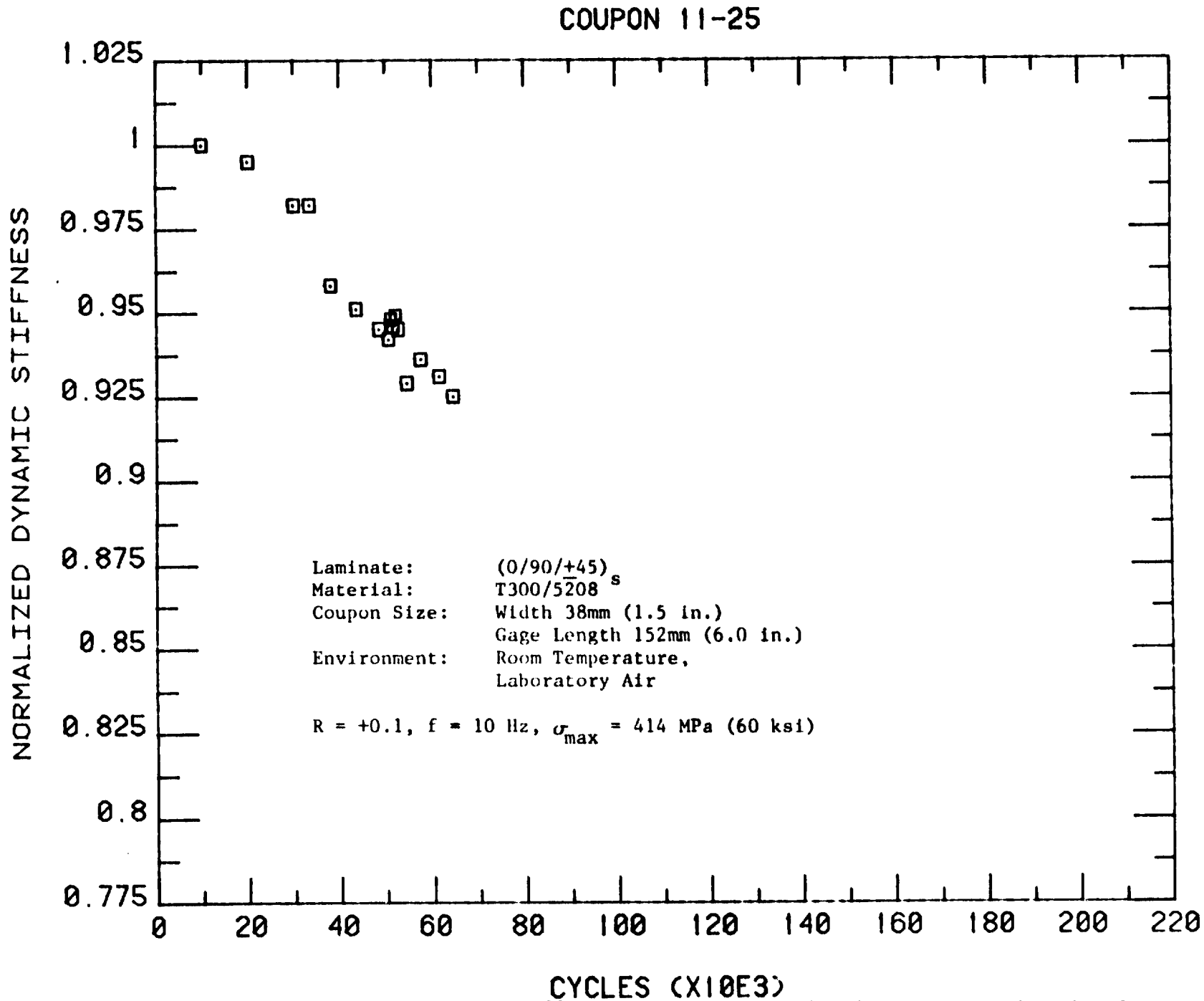

Figure C16 Normalized Dynamic Stiffness vs. Constant Amplitude Fatigue Load Cycles for (0/90/±45) Laminate 11-25 σ_{max} = 414 MPa (60 ksi)

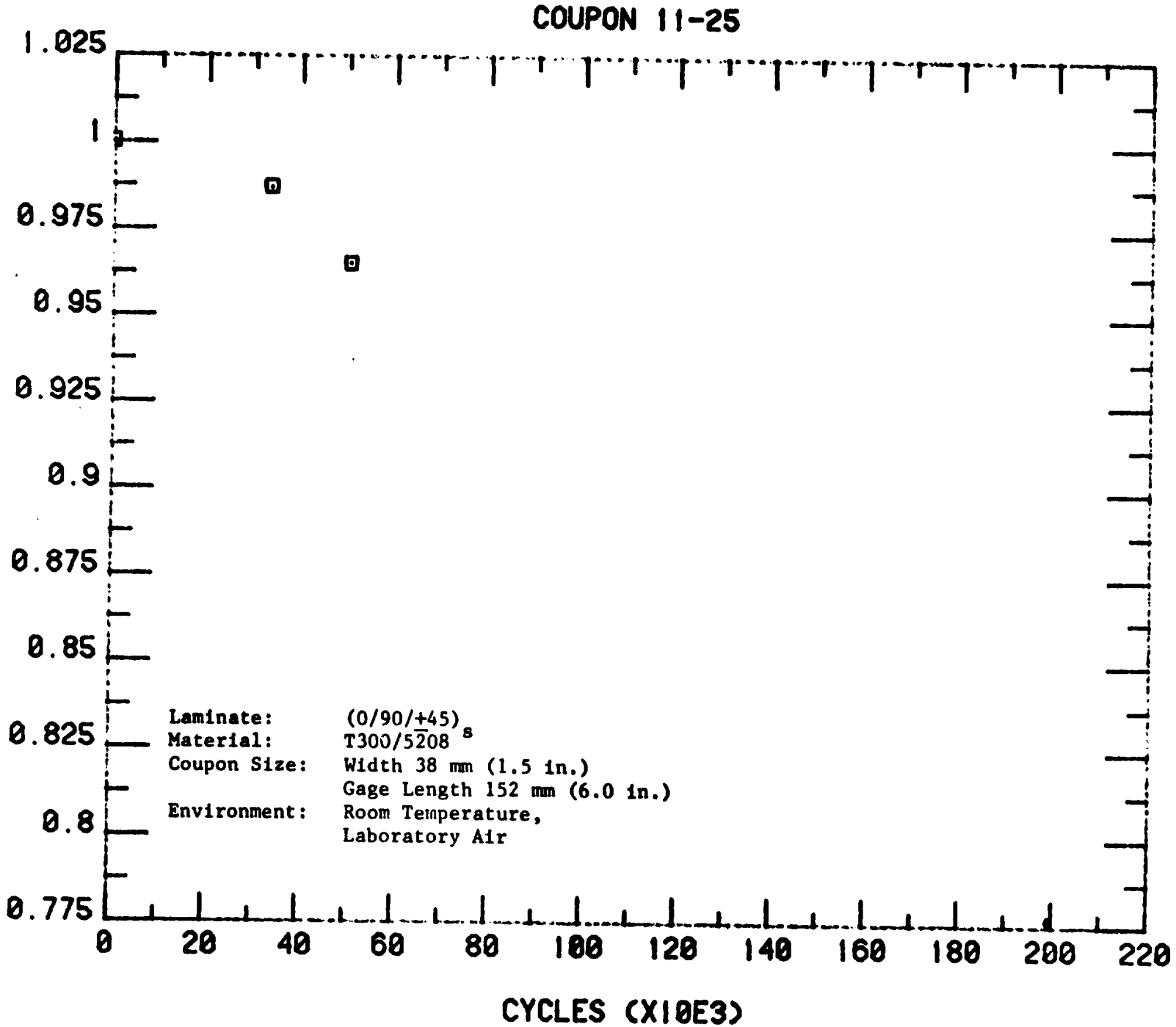

Figure C17 Normalized Monotonic Stiffness vs. Constant Amplitude Fatigue Load Cycles for $(0/90\pm45)_s$ Laminate Coupon 11-25, σ_{max} = 414 MPa (60 ksi)

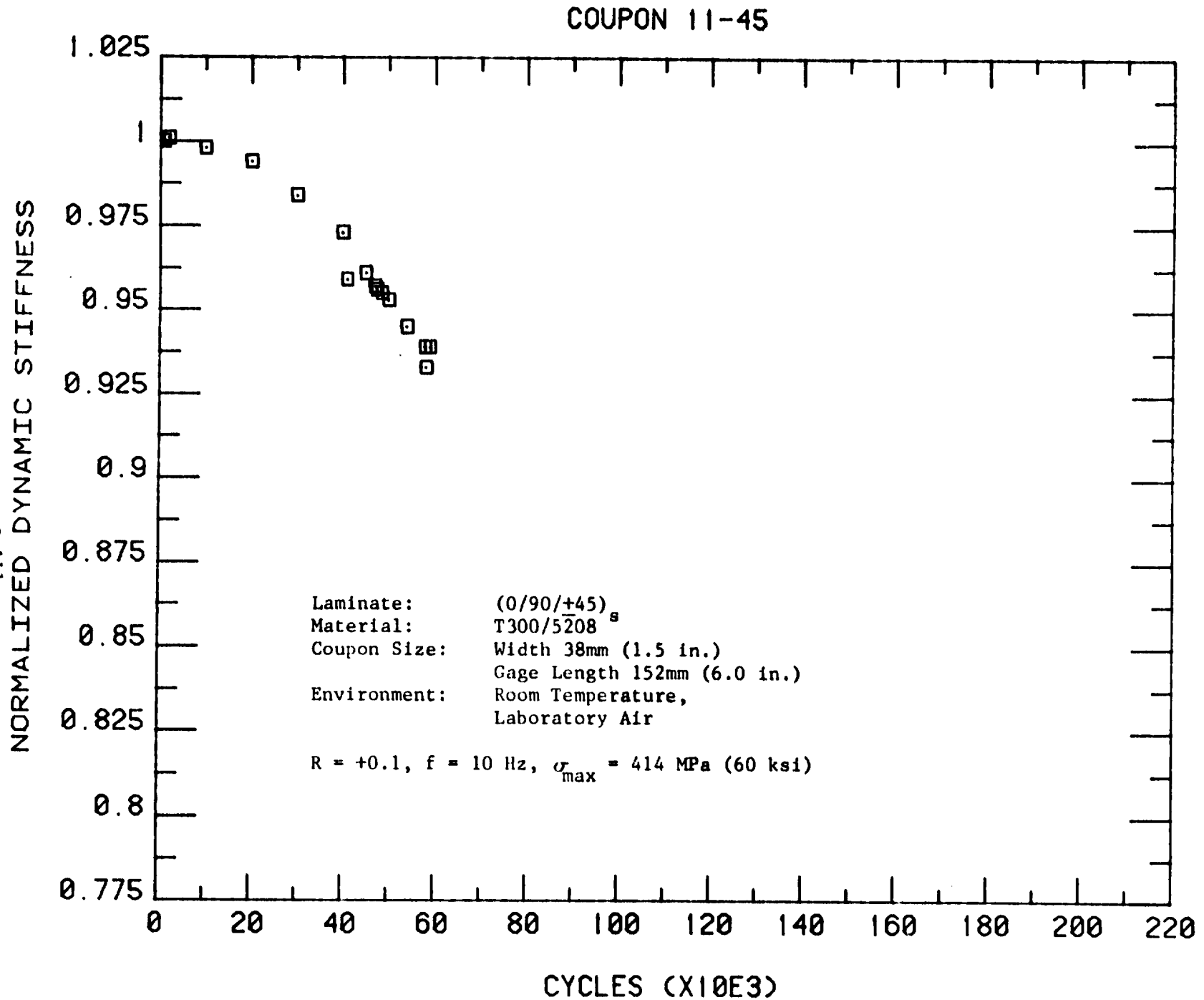

Figure C18 Normalized Dynamic Stiffness vs. Constant Amplitude Fatigue Load Cycles For $(0/90/\pm45)_s$ Laminate 11-45, σ_{max} = 414 MPa (60 ksi)

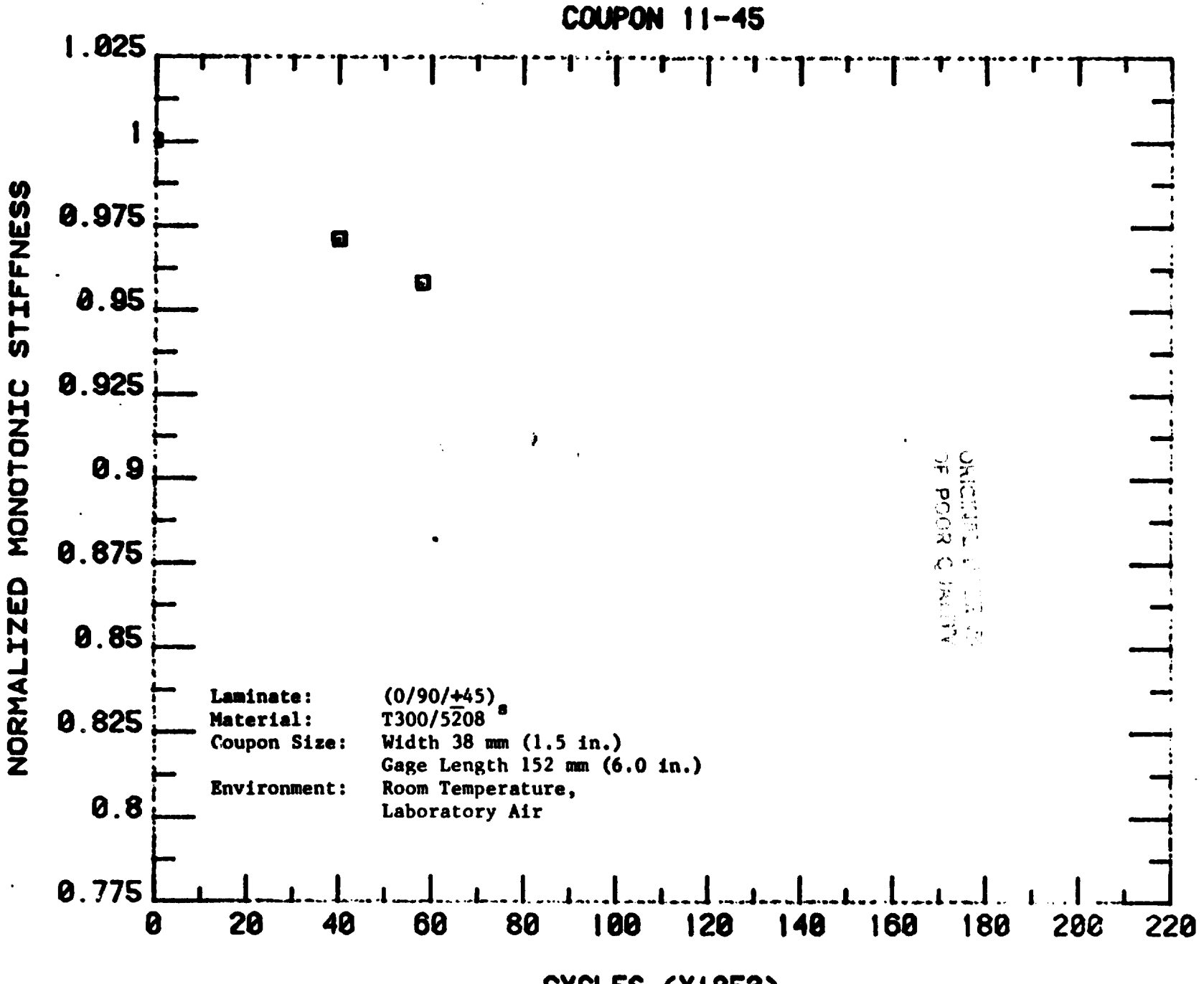

Figure C19 Normalized Monotonic Stiffness vs. Constant Amplitude Fatigue Load Cycles for $(0/90/\pm45)_s$ Laminate Coupon 11-45, σ_{max} = 414 MPa (60 ksi)

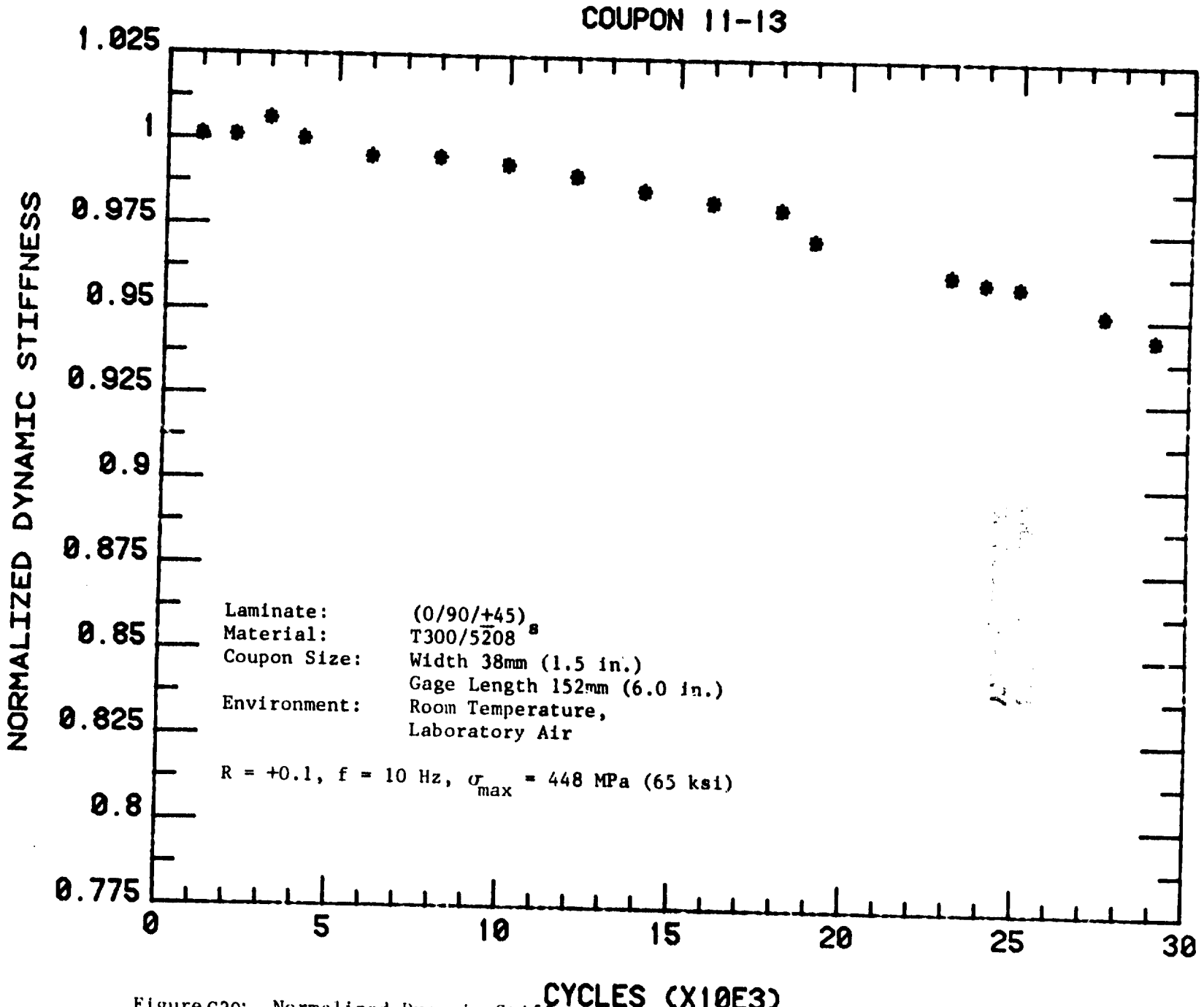

Figure C20: Normalized Dynamic Stiffness vs. Constant Amplitude Fatigue Load Cycles for $(0/90/\pm45)_s$ Laminate Coupon 11-13, σ_{max} = 448 MPa (65 ksi)

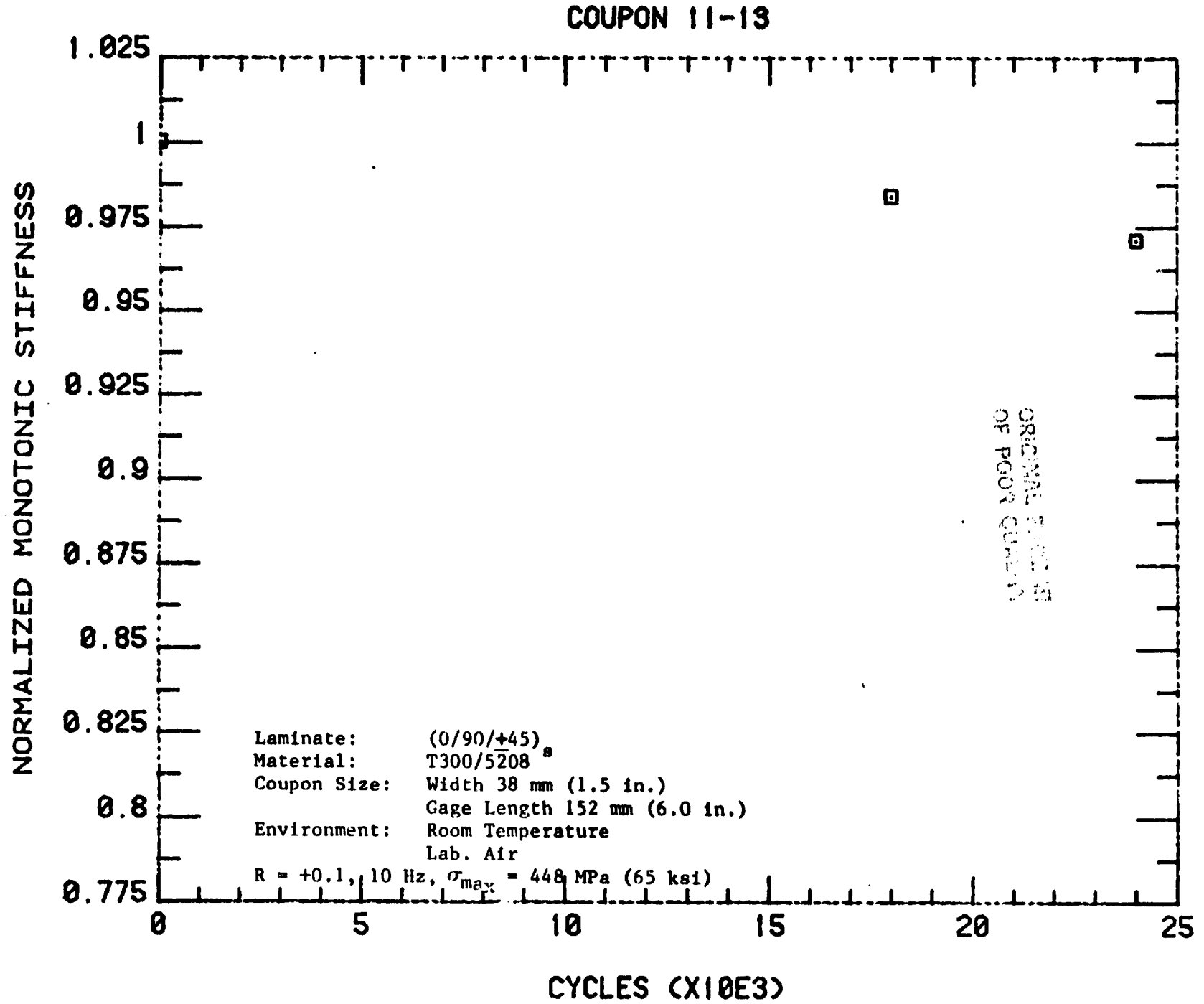

Figure C21 Normalized Monotonic Stiffness vs. Constant Amplitude Fatigue Load Cycles for $(0/90/\pm45)_s$ Laminate Coupon 11-13, σ_{max} = 448 MPa (65 ksi)

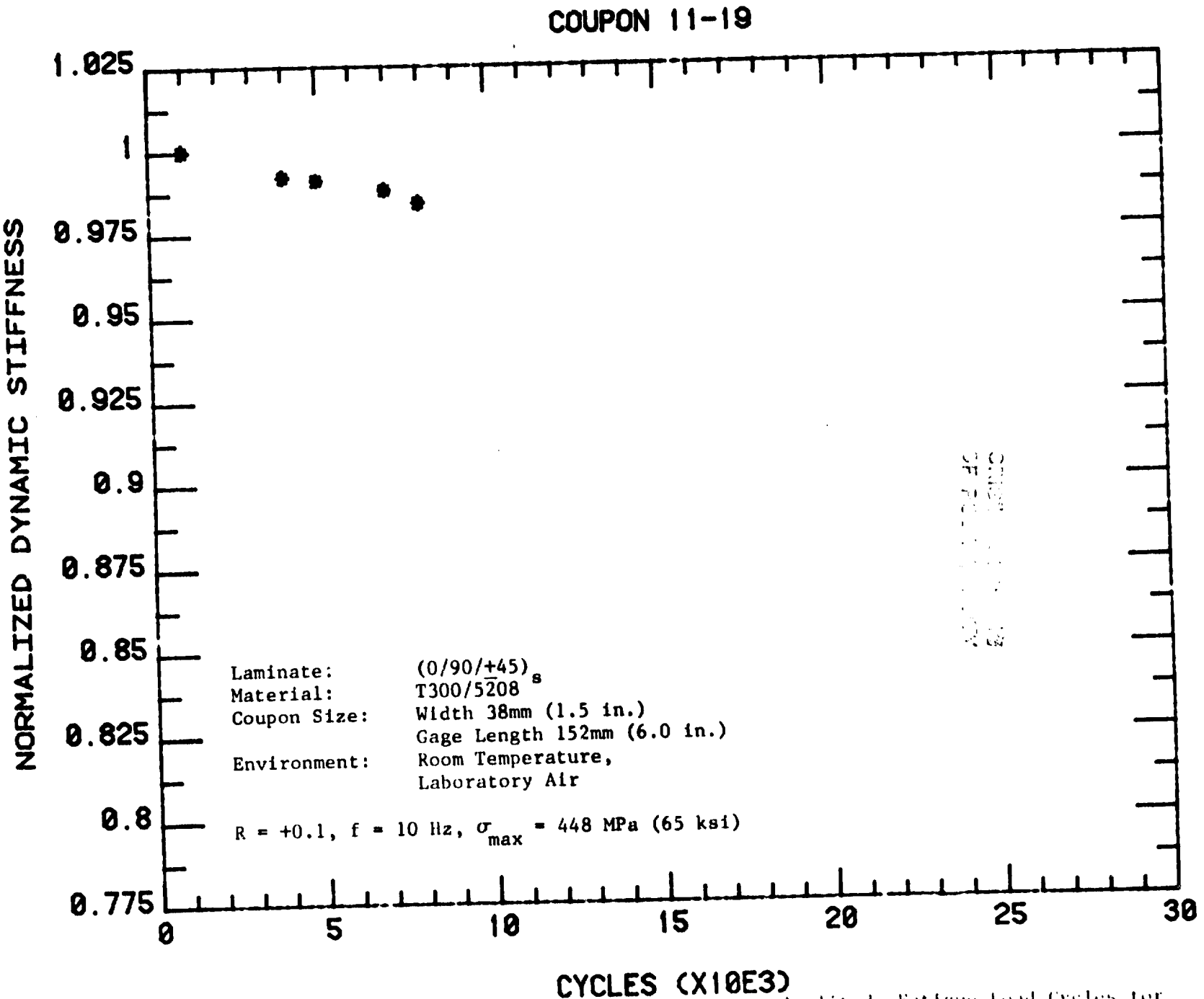

Figure C22 Normalized Dynamic Stiffness vs. Constant Amplitude Fatigue Load Cycles for (0/90/+45) Laminate Coupon 11-19, σ_{max} = 448 MPa (65 ksi)

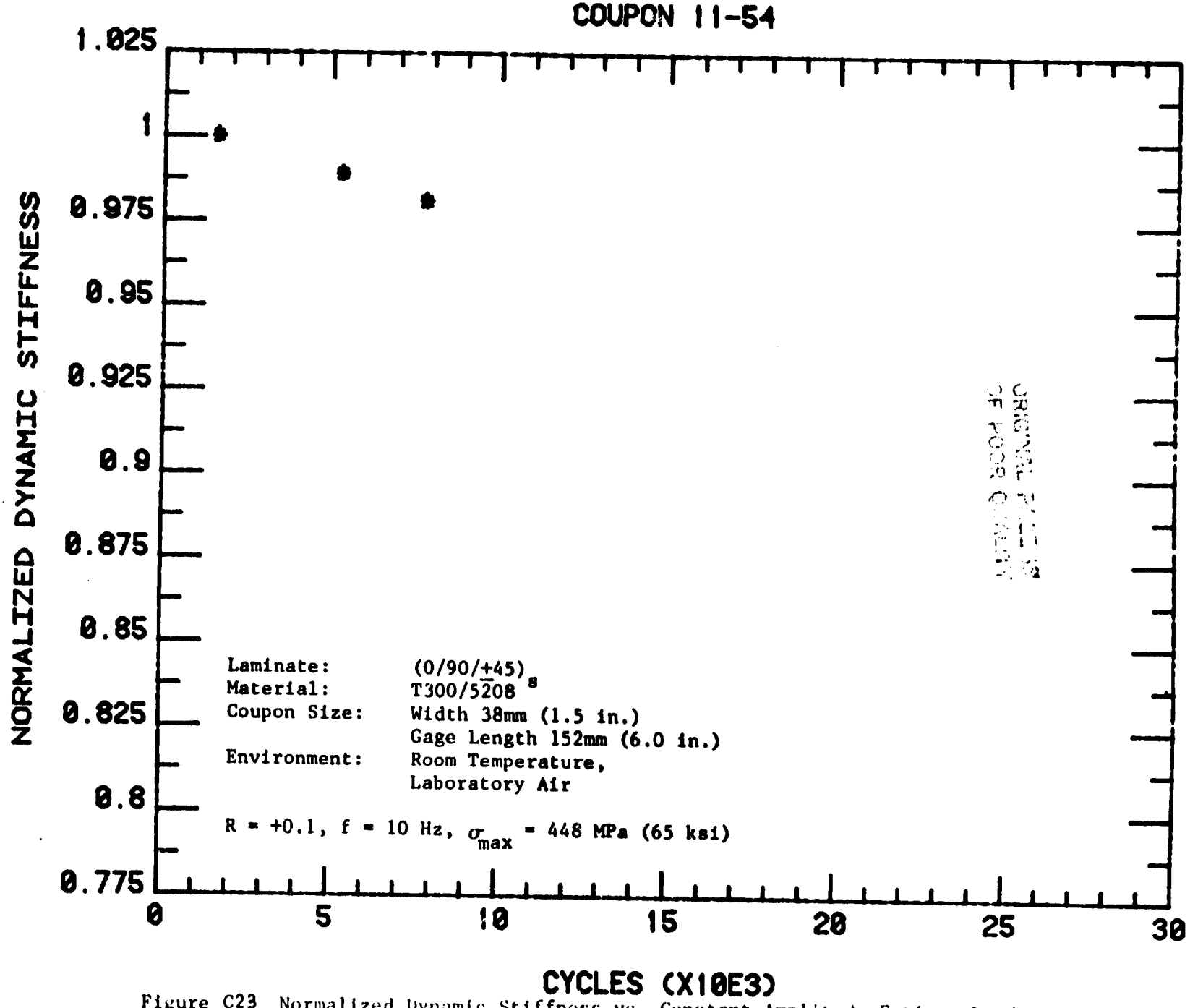

Figure C23 Normalized Dynamic Stiffness vs. Constant Amplitude Fatigue Load Cycles For $(0/90/\pm45)_s$ Laminate Coupon 11-54, σ_{max} = 448 MPa (65 ksi)

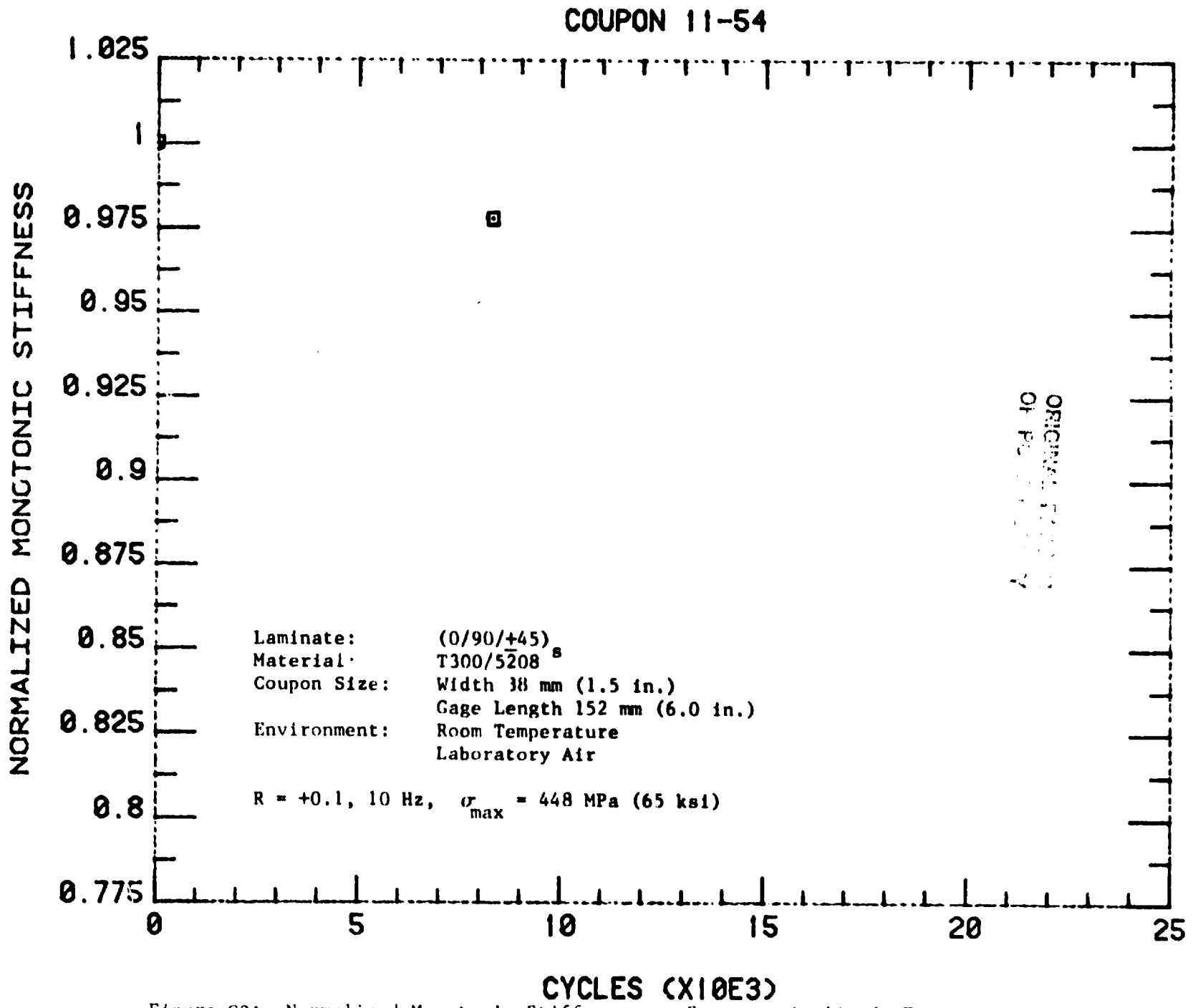

Figure C24 Normalized Monotonic Stiffness vs. Constant Amplitude Fatigue Load Cycles for $(0/90/\pm45)_s$ Laminate Coupon 11-54, σ_{max} = 448 MPa (65 ksi)

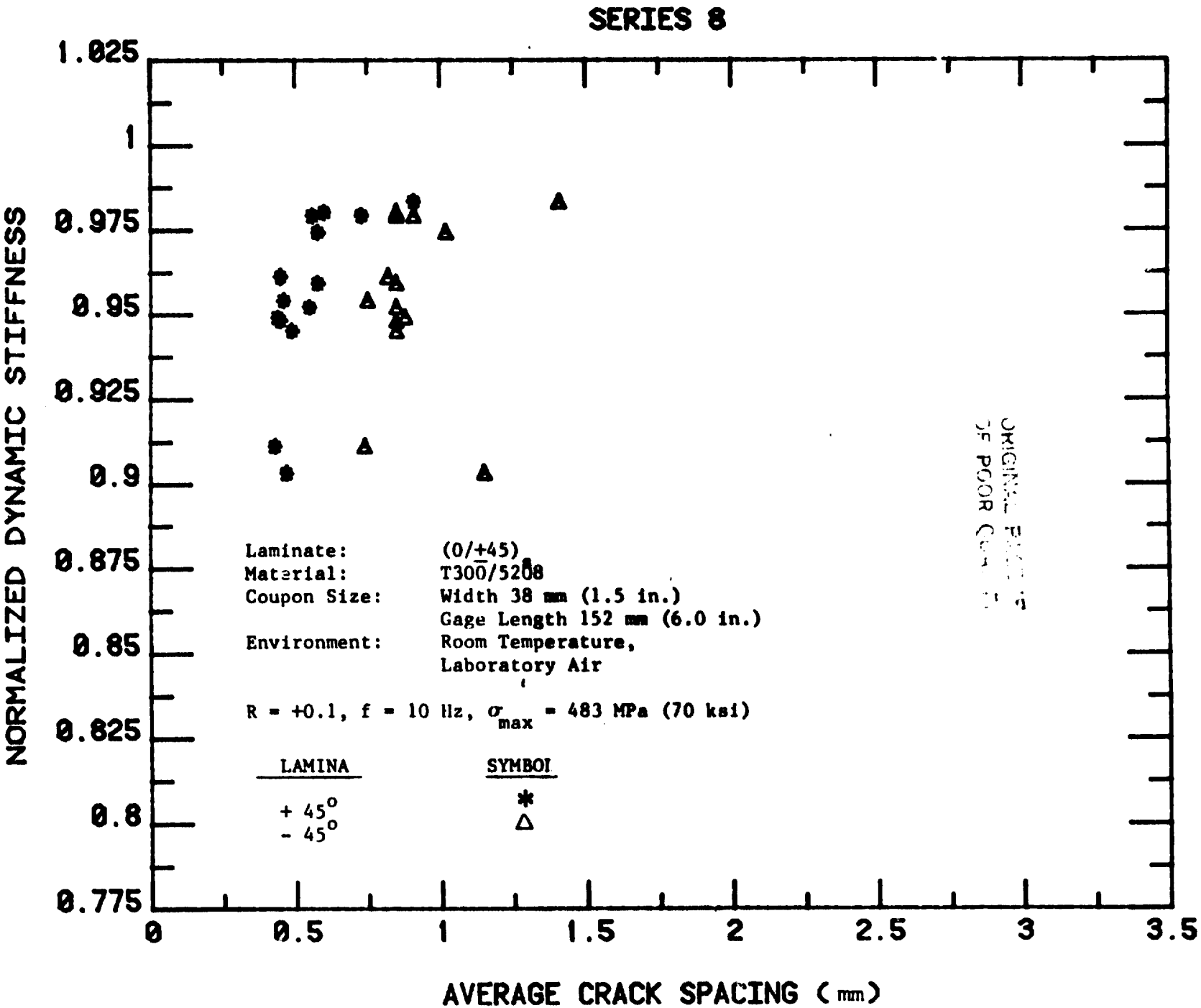

Figure C25 Normalized Dynamic Stiffness vs. Average Matrix Cracking Spacing for $(0/\pm45)_s$ Laminate Coupons Subjected to Constant Amplitude Fatigue Load, σ_{max} = 483 MPa (70 ksi)

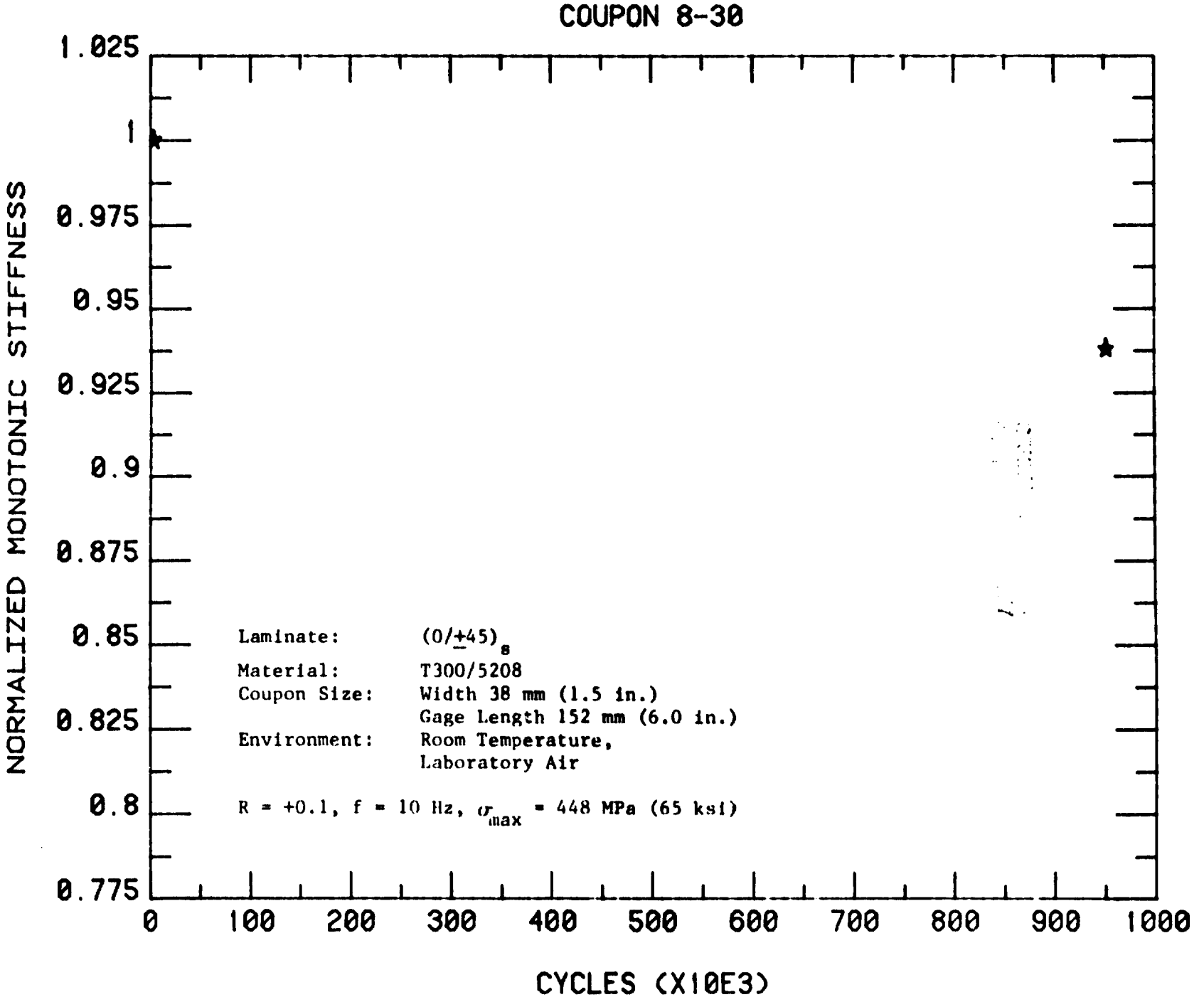

Figure C26 Normalized Monotonic Stiffness vs. Constant Amplitude Fatigue Load Cycles for (0/±45) Laminate Coupon 8-30, σ_{max} = 448 MPa (65 ksi)

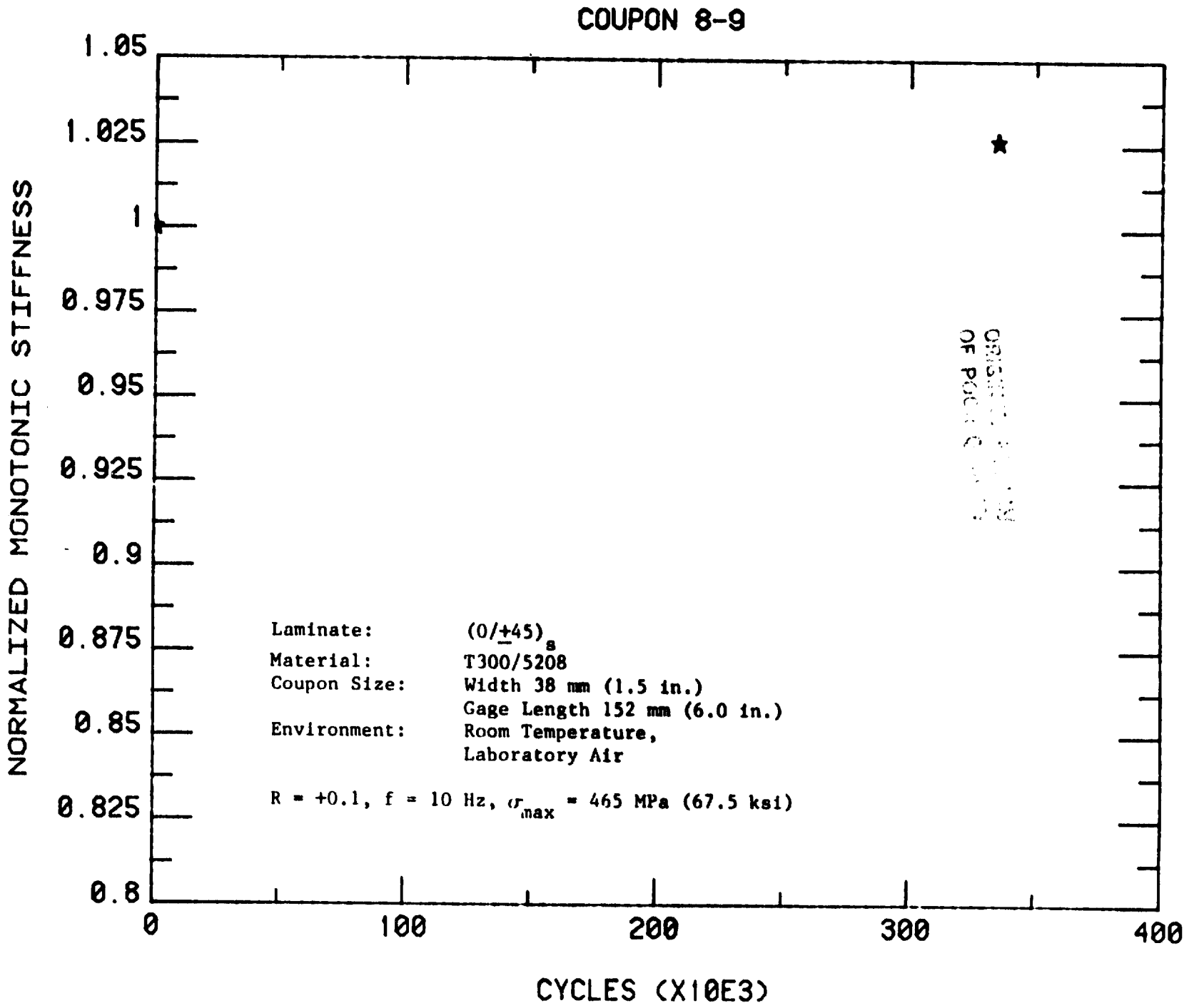

Figure C27 Normalized Monotonic Stiffness vs. Constant Amplitude Fatigue Load Cycles for $(0/\pm45)_s$ Laminate Coupon 8- 9, σ_{max} = 465 MPa (67.5 ksi)

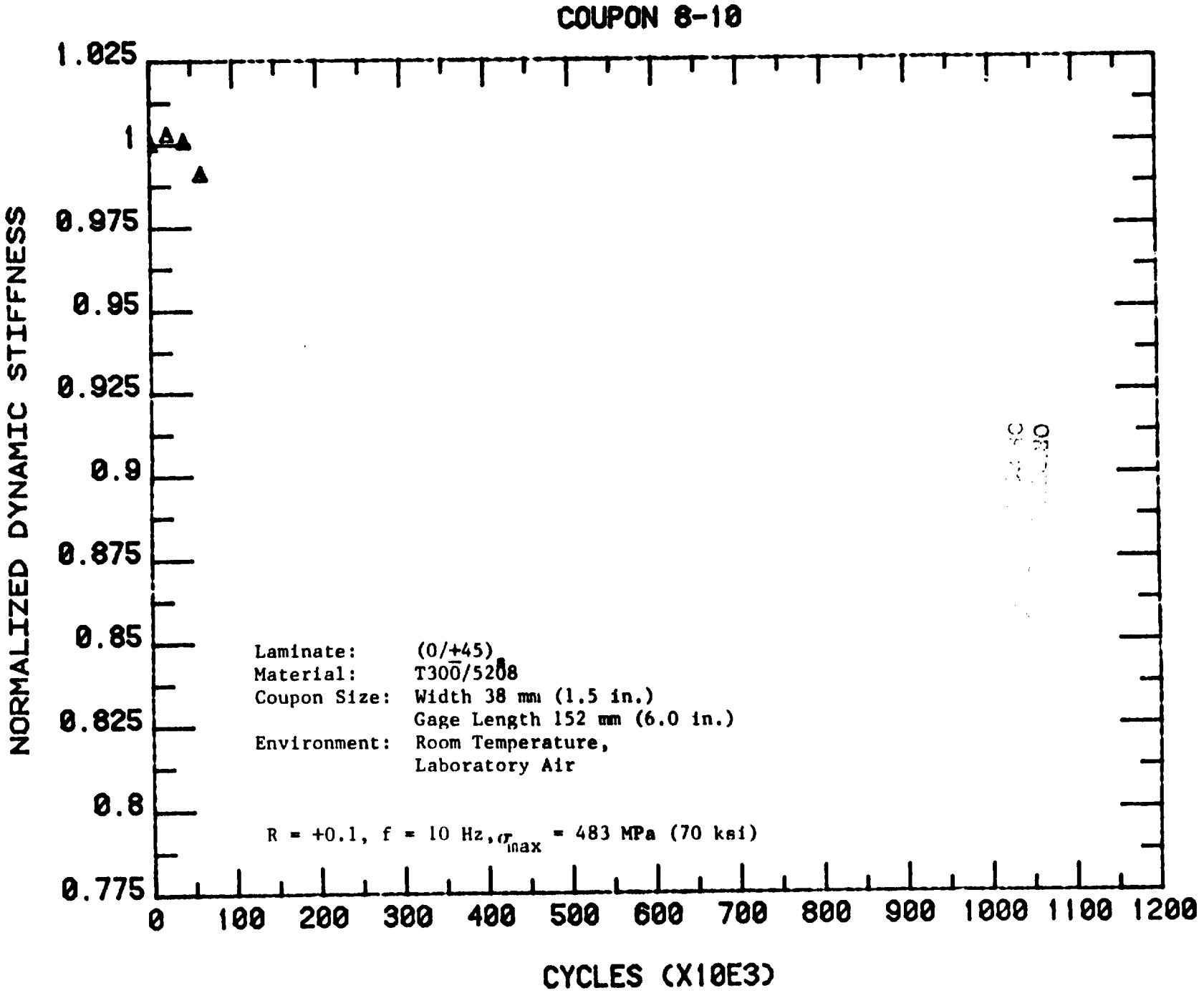

Figure C28 Normalized Dynamic Stiffness vs. Constant Amplitude Fatigue Load Cycles for $(0/\pm45)_s$ Laminate Coupon 8-10, σ_{max} = 483 MPa (70 ksi)

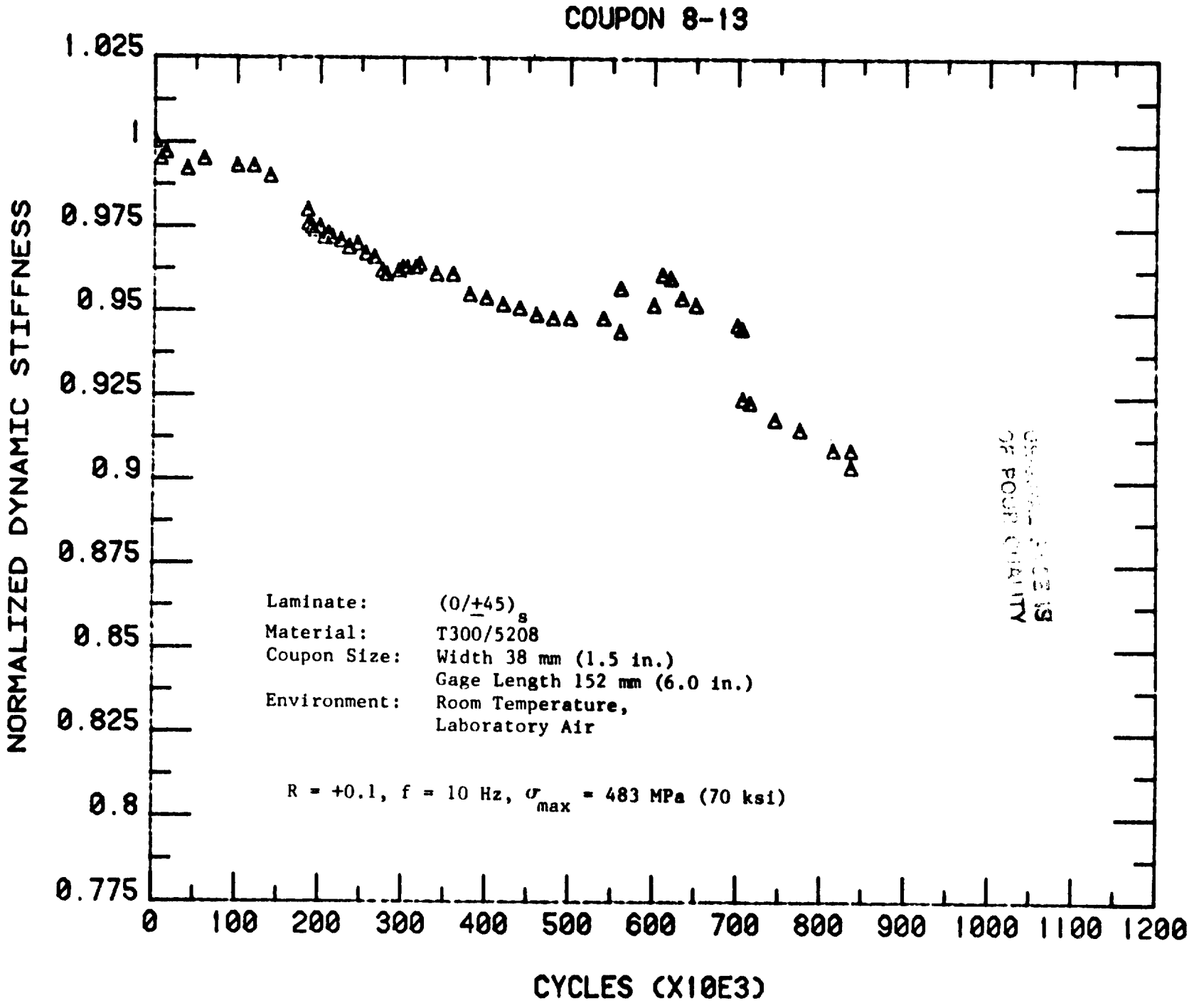

Figure C29 Normalized Dynamic Stiffness vs. Constant Amplitude Fatigue Load Cycles for $(0/\pm45)_s$ Laminate Coupon 8-13, σ_{max} = 483 MPa (70 ksi)

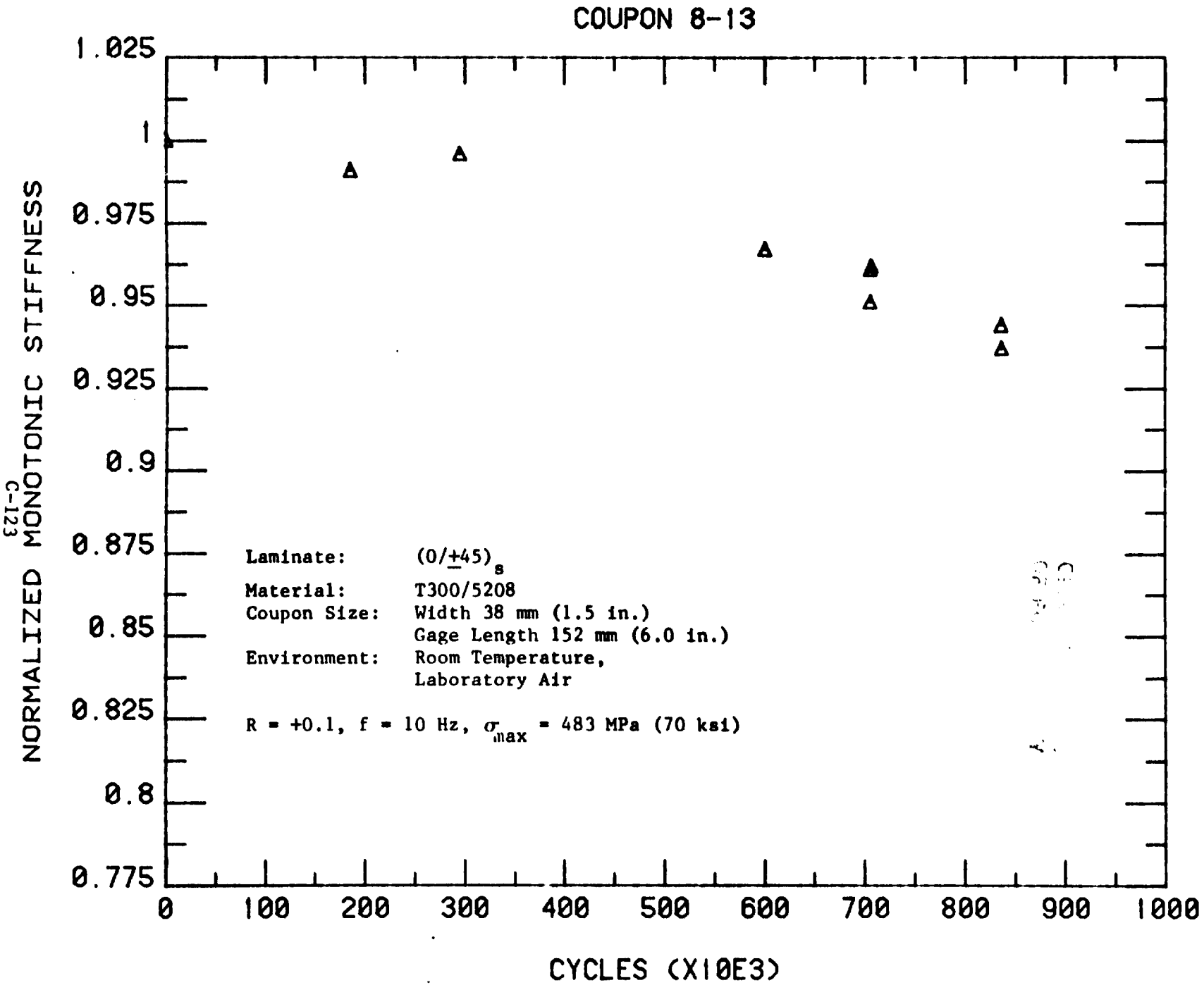

Figure C30 Normalized Monotonic Stiffness vs. Constant Amplitude Fatigue Load Cycles for $(0/\pm45)_s$ Laminate Coupon 8-13, σ_{max} = 483 MPa (70 ksi)

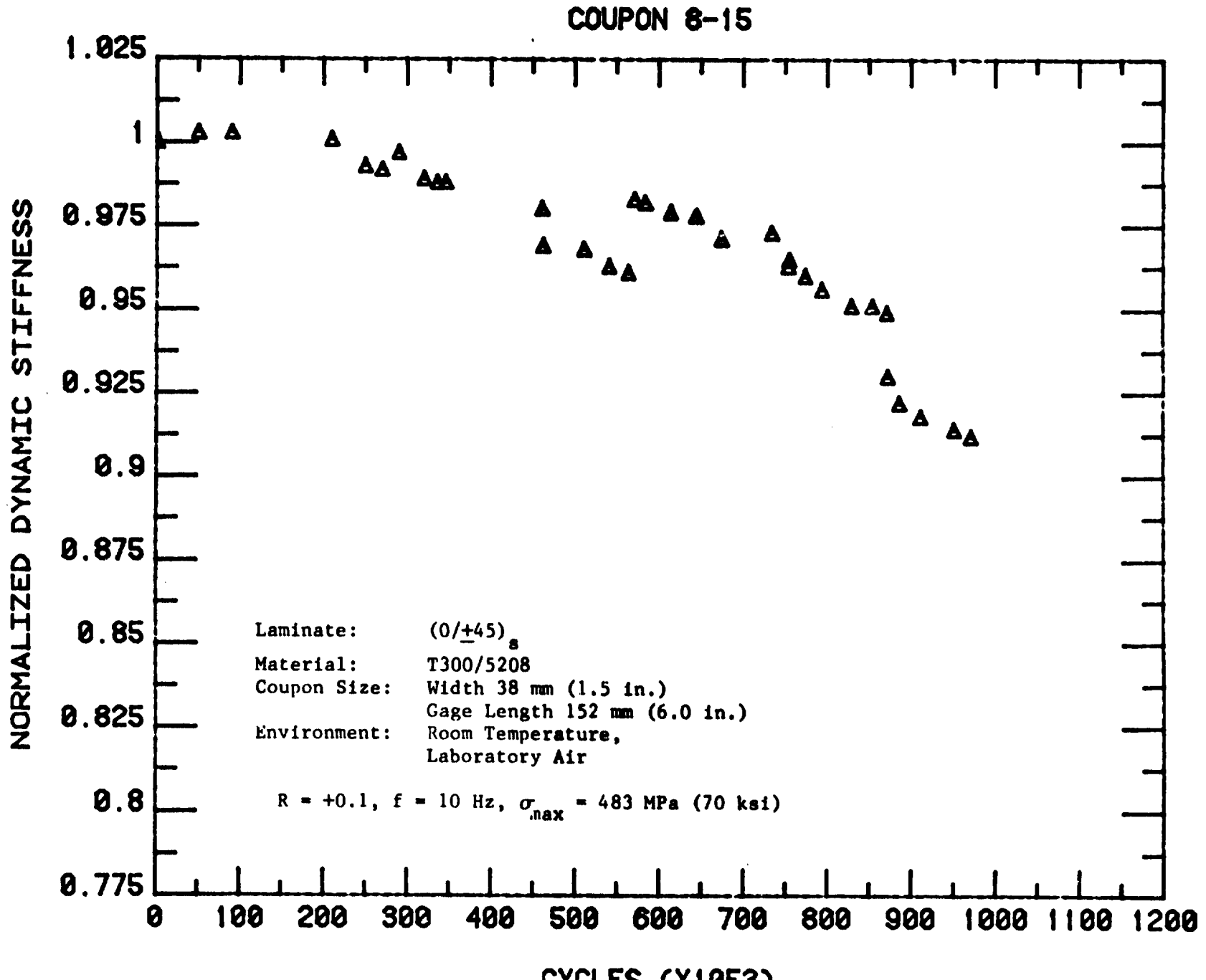

Figure C31 Normalized Dynamic Stiffness vs. Constant Amplitude Fatigue Load Cycles for $(0/\pm45)_s$ Laminate Coupon 8-15, σ_{max} = 483 MPa (70 ksi)

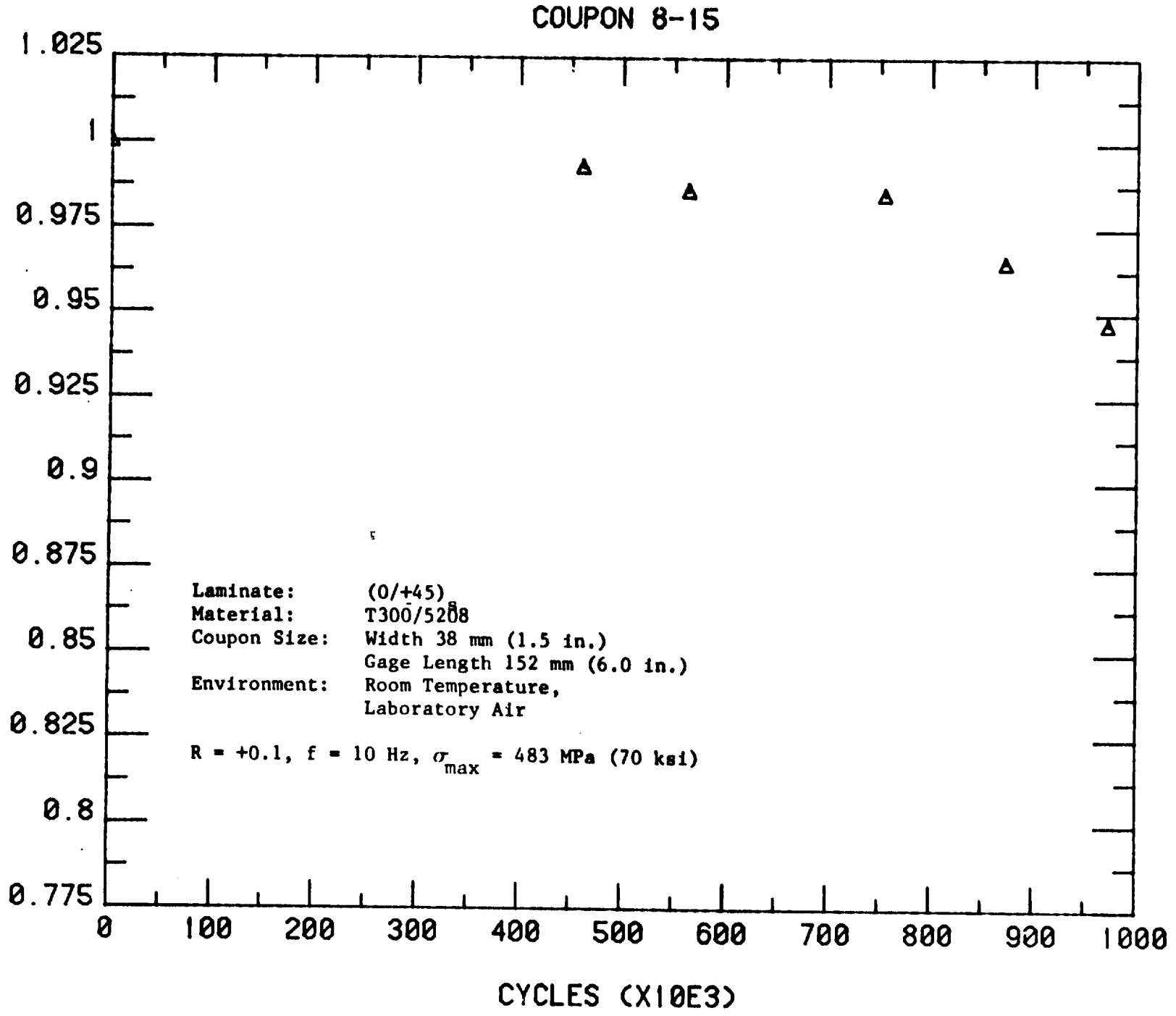

Figure C32 Normalized Monotonic Stiffness vs. Constant Amplitude Fatigue Load Cycles for $(0/\pm45)_s$ Laminate Coupon 8-15, σ_{max} = 483 MPa (70 ksi)

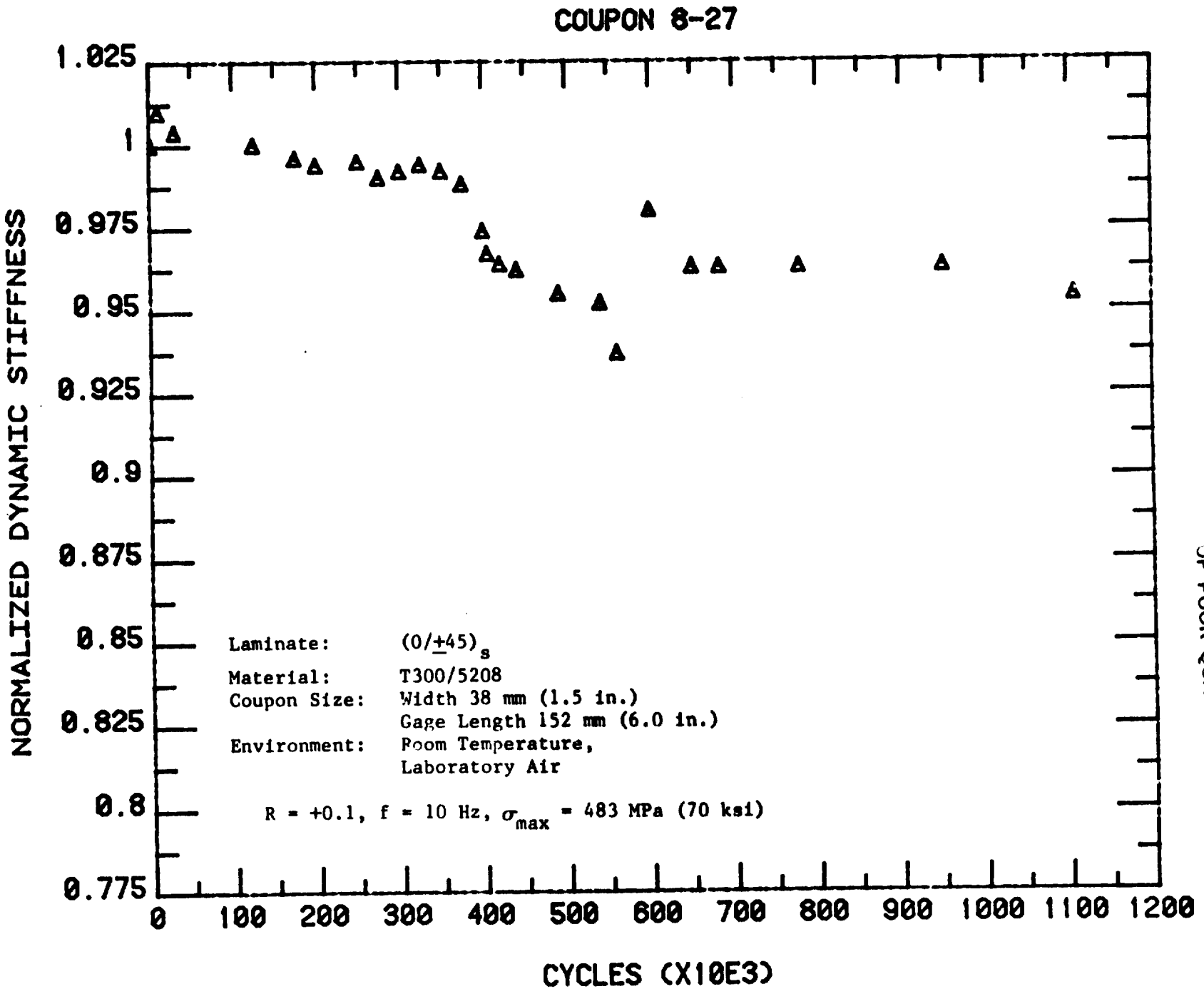

Figure C38 Normalized Dynamic Stiffness vs. Constant Amplitude Fatigue Load Cycles for $(0/\pm45)_s$ Laminate Coupon 8-27, σ_{max} = 483 MPa (70 ksi)

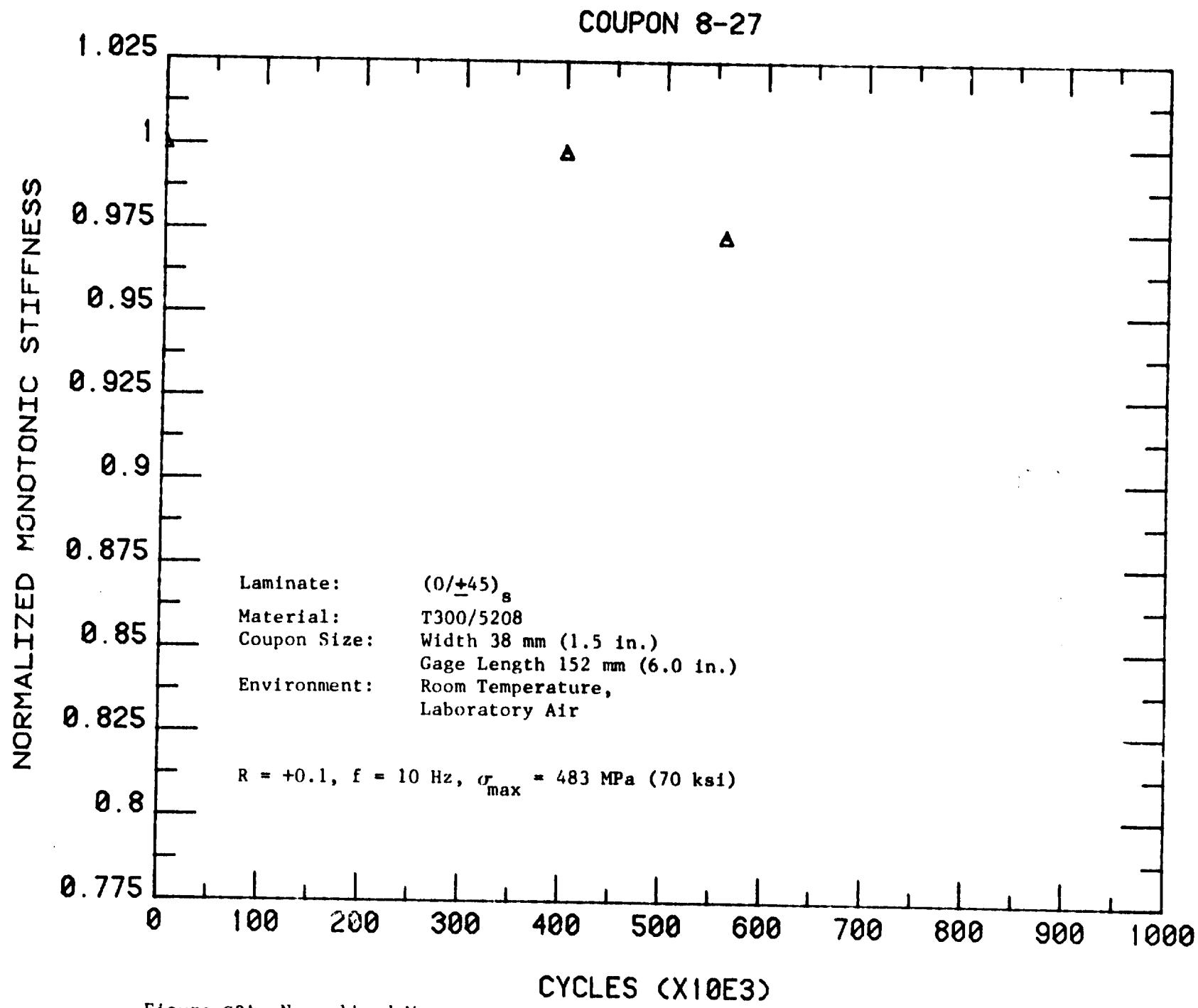

Figure C34 Normalized Monotonic Stiffness vs. Constant Amplitude Fatigue Load Cycles for $(0/\pm45)_s$ Laminate 8-27, σ_{max} = 483 MPa (70 ksi)

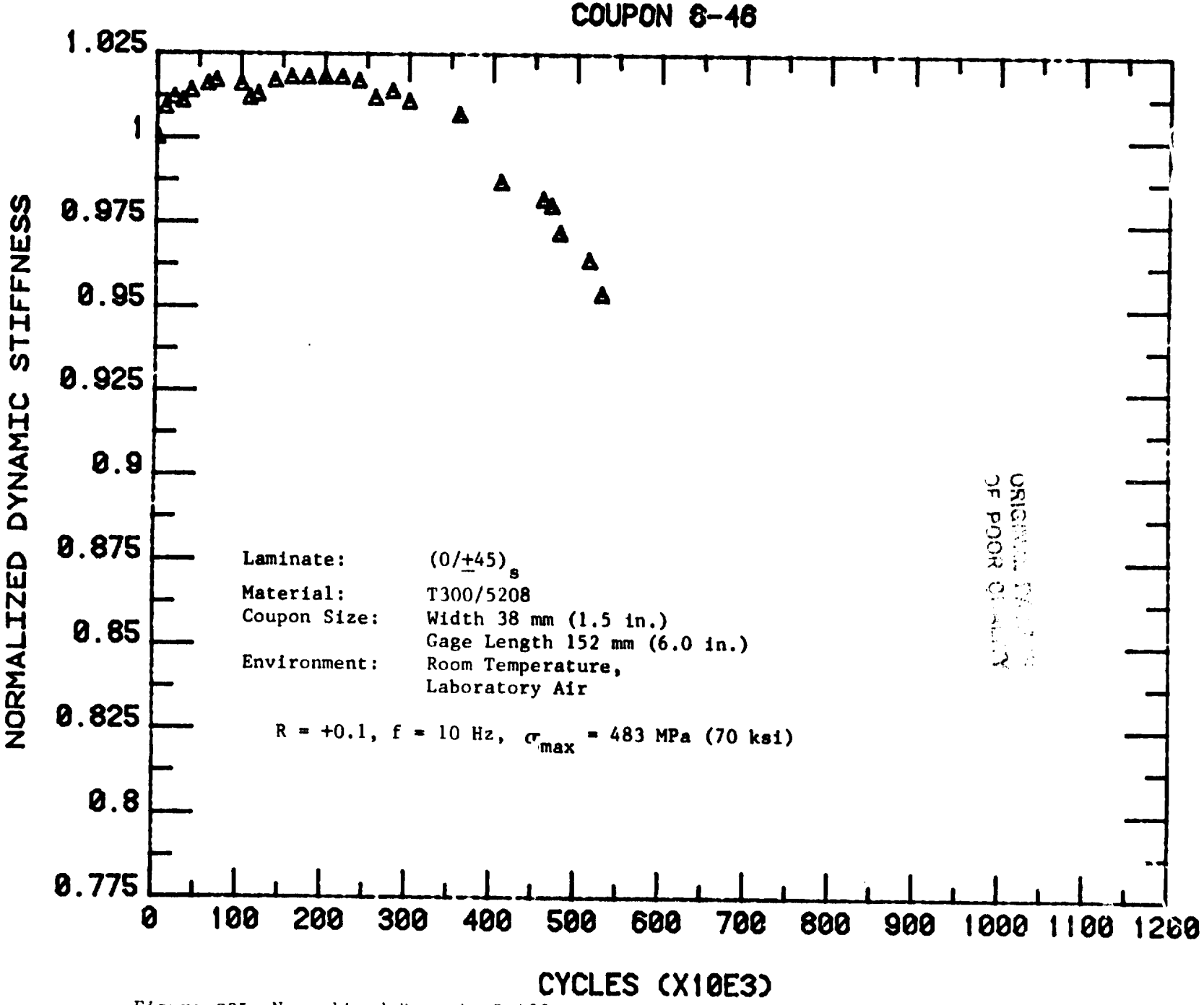

Figure C35 Normalized Dynamic Stiffness vs. Constant Amplitude Fatigue Load Cycles for $(0/\pm45)_s$ Laminate Coupon 8-46, σ_{max} = 483 MPa (70 ksi)

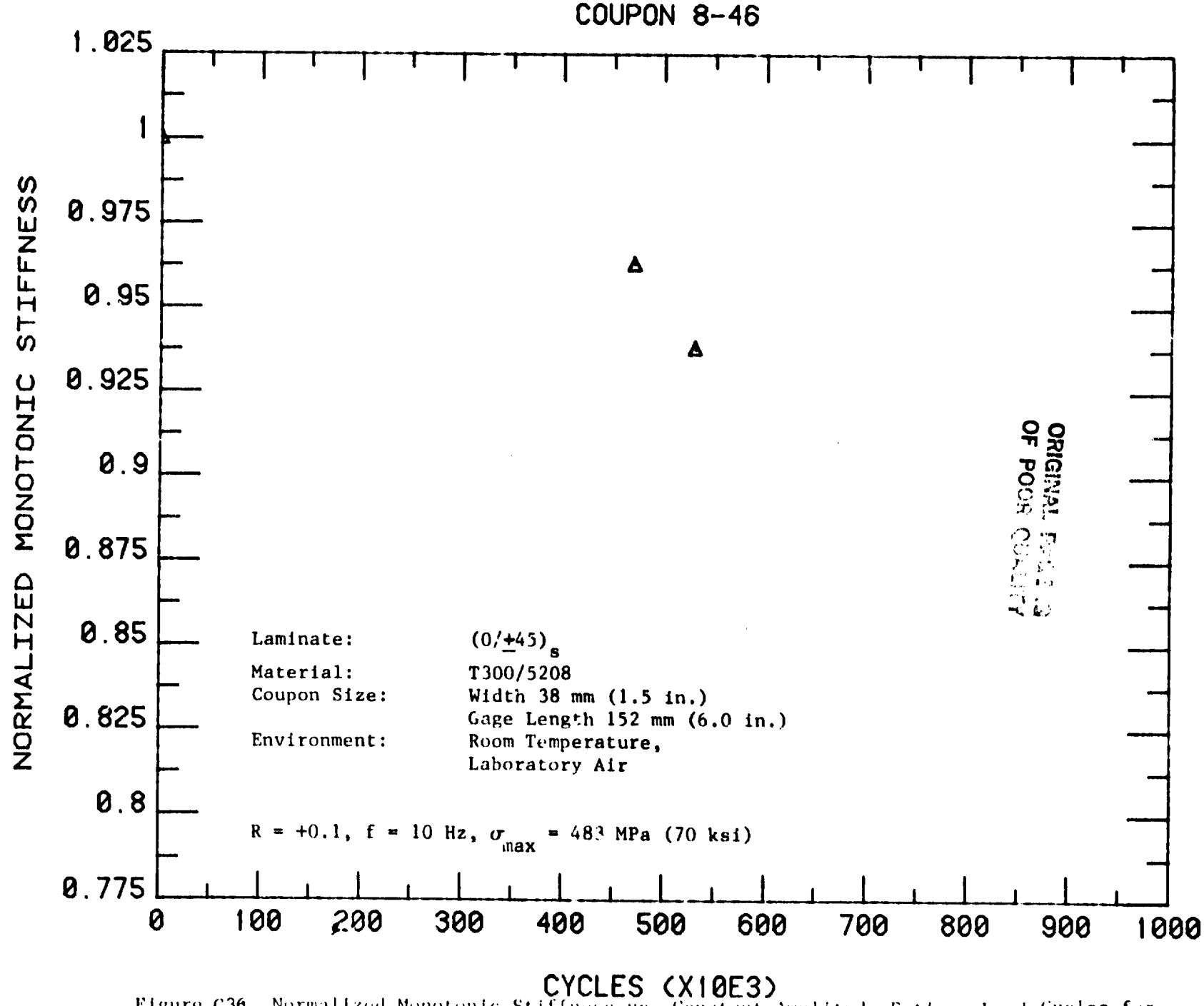

Figure C36 Normalized Monotonic Stiffness vs. Constant Amplitude Fatigue Load Cycles for $(0/\pm45)_s$ Laminate 8-46, σ_{max} = 483 MPa (70 ksi)

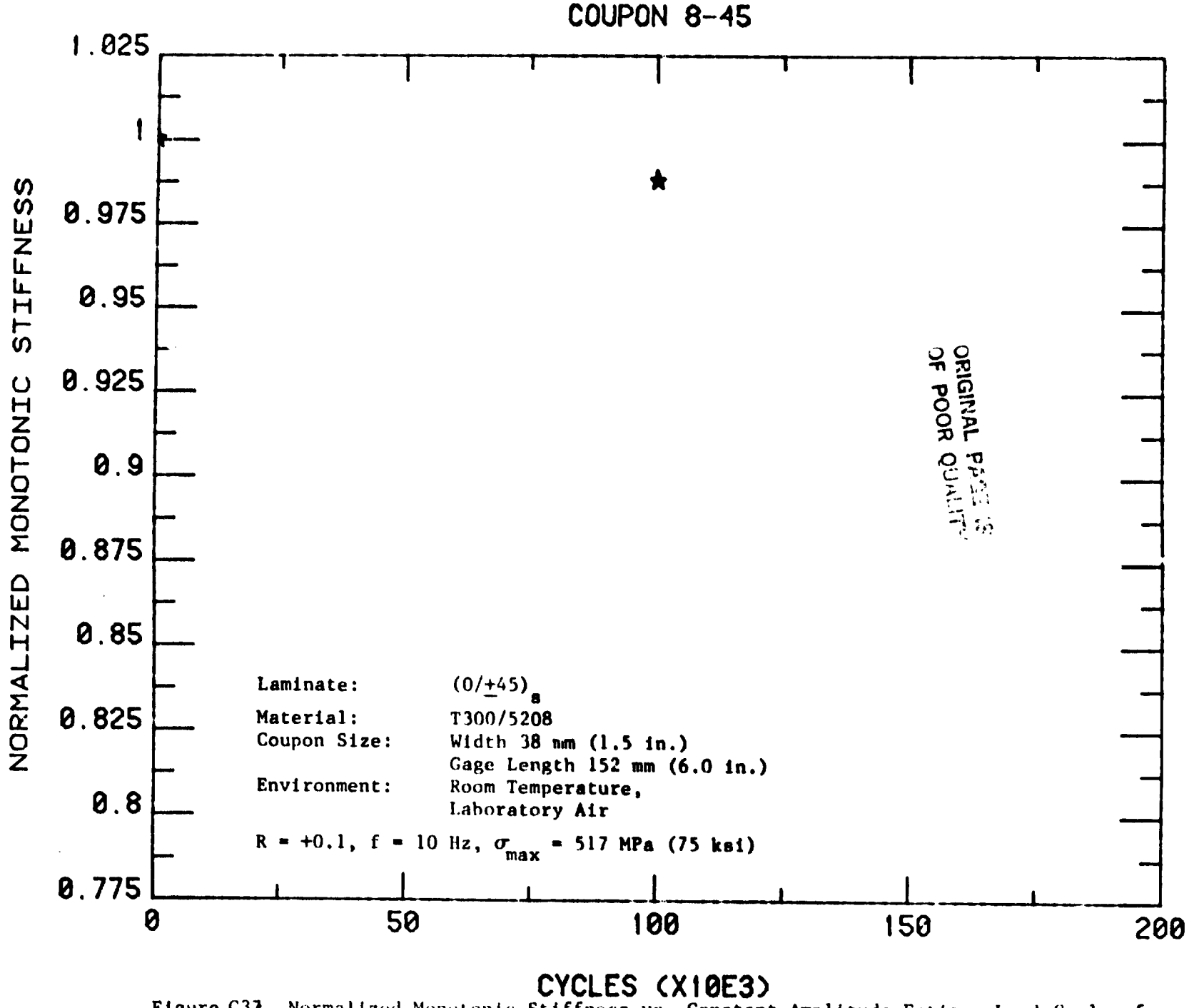

Figure C32 Normalized Monotonic Stiffness vs. Constant Amplitude Fatigue Load Cycles for $(0/\pm45)_s$ Laminate 8-45, σ_{max} = 517 MPa (75 ksi)

APPENDIX D
COMPUTER AIDED MODELING PROCEDURES

D.1 MATHEMATICAL/COMPUTER MODELING APPROACH

Two Lockheed computer codes developed as aids for the analysis of composite laminate stresses and strains were employed in this research. LPARL*ADVLAM is a laminate code for determining inplane ply stresses. The material may be linear elastic, nonlinear elastic, or linear viscoelastic. During a time-incremental analysis, through thickness gradients of temperature and moisture are calculated. Thermal and hygroscopic ply expansions and temperature and moisture altered viscoelastic properties are incrementally updated during the analysis[70,71]. The second code is LAPRL*FREEVIS, a generalized plane-strain, finite element program. This code employs constant strain and three noded triangular elements to solve the elastic or linear viscoelastic stress field of a structure which can be modeled under generalized plane strain conditions (i.e., ϵ_x = constant in all elements). Out of plane shear strains are permitted and one may prescribe nodal displacements, nodal forces, or average surface tractions as boundary conditions. This code has been used to model: 1) free edge laminate staresses due to mechanical,[56] thermal,[67] and hydroscopic[96] loads; 2) the effect of moisture absorption on the redistribution of stresses in a single lap viscoelastic adhesive bonded joint[97]; and 3) the micromechanical stresses generated in the fiber and matrix under prescribed combinations of average normal and shear tractions.[98]

The use of simple triangular elements in FREEVIS requires a linear division of the structure to be modeled rather than elements based on displacement fields fitted with higher order polynomials or hybrid stress elements. These simple elements are employed because of the ease with which the stress

field in the model can be interpreted. Triangular elements also have the advantage that they can be employed with Rybicki and Kanninen's virtual crack closure procedure[65] to analyze the strain energy rate, G, associated with transverse matrix cracks or delaminations. Furthermore, G can be subdivided into energy associated with Mode I, II or III crack opening modes.[11,12] Other higher-order finite elements cannot be used to successfully partition the crack opening energy release rate.

For the purpose of analyzing stresses and stiffnesses of dry T300/5208 laminates, static and fatigue tested at room temperature, the codes described above were previously shown to be more than powerful enough. Studies on hygrothermal damage mechanianisms in T300/5208 laminates[86] and recent work by Kriz et al;[99] have demonstrated that viscoelastic effects can be ignored in dry laminates tested at room temperature. Furthermore, at tensile strains below 1 percent even the shear modulus G_{12} can be considered linear to an error of less than 10 percent. Therefore, a linear elastic stress analysis was conducted which included elastic thermal residual stresses due to cooling from the stress free temperature. Studies of $(0_4/90_4)$ non-symmetric T300/5208 laminates havve shown that the stress free temperature is approximately 170°C.[86]

Figure D1 shows a schematic of the free-edge damage which has been observed by Reifsnider et al;[57] in an AS/3501 $(0/90/\pm45)_s$ laminate subject to a tensile stress history. The damage shown in Figure D1 is what the investigators termed the characteristic damage state (CDS) which was hypothesized to be load history independent and thus to form under either static or fatigue loading. The CDS in this laminate consists of transverse cracks in the 90 and $\pm45^\circ$ plies. The density of cracks in a laminate usually reaches a saturation level which has been reasonably well predicted by a shear lag analysis and a finite difference solution procedure[58]. Similar predictions of crack spacing based on an energy approach have been done using the FREEVIS finite element code.[59,60] Using the finite element procedure to calculate the crack density in individual layers of an arbit-

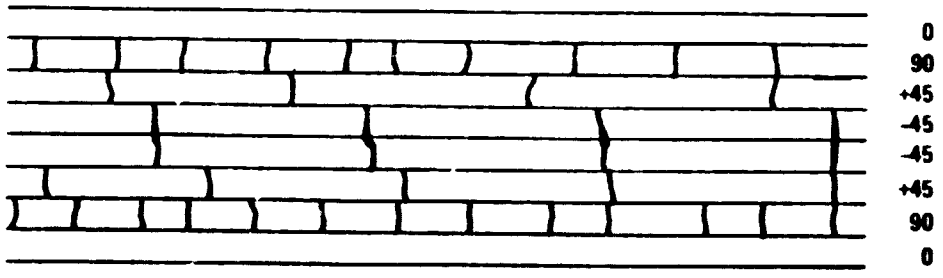

Characteristic damage state for $(0/90/45/-45)_s$

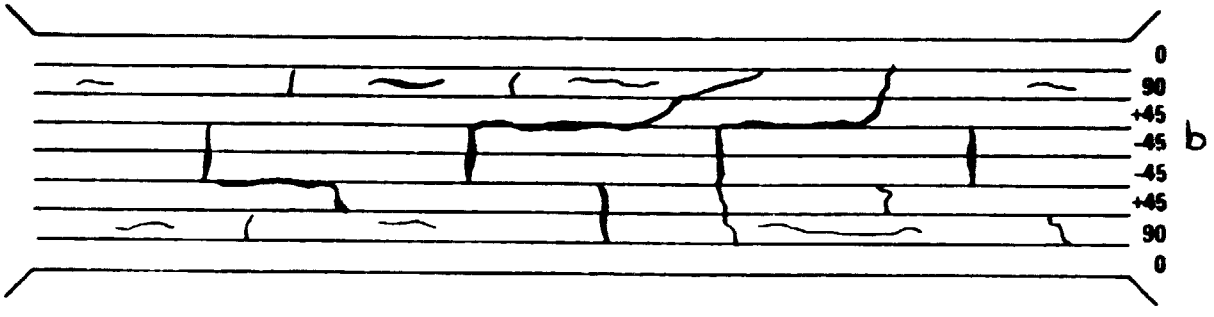

Pre-fracture crack patterns showing a breakdown of the characteristic damage state by crack coupling and longitudinal cracking.

Figure D1: Characteristic damage state progression.[57]

rary laminate stacking sequence has an advantage over the use of finite difference procedures in the ease with which boundary conditions can be changed if the stacking sequence is altered. The difficulties inherent in the finite difference approach are evident from the discussion in Reference 58.

By way of a comment, development of a characteristic damage state with a saturated crack density is not always noted in other laminate configurations. For example, the density of transverse cracks in a $(\pm 25/90_2)_s$ laminate were found at Lockheed to increase monotonically with tensile load (Figure D2) until failure. Even if such a state does occur, the significance is not clear. See Section 1 and 4 for further discussion of this point.

Figure D1b shows the free edge damage state observed just prior to fatigue failure of the $(0/90/\pm 45)_s$ laminate. In addition to transverse cracks, delamination between ± 45 layers and longitudinal splitting of the 90° ply is common. Taking X as the direction of tensile loading and Z as the through thickness direction, one can model this damage as cracks in a finite element model of a typical X-Z plane section at the specimen surface. This model will determine laminate stiffness and layer stresses associated with the surface damage. However, this information is not sufficient to model the stiffness degradation of the laminate as a whole or even to realistically predict the failure stresses in the zero degree ply during redistribution of stresses caused by the local damage accumulation.[86]

The reason for this is explained by recent work by Bader et al[61] and Wang,[49] mentioned previously, which showed that one critical stress for transverse fracture in composites is volume dependent. Experimental and analytical studies by Wang and Crossman[11,12] have shown that the onset of temperature cracking and ply delamination can be predicted by modeling crack growth with the FREEVIS code and calculating the strain energy release rate associated with each crack growth process. Figure D3 shows a comparison

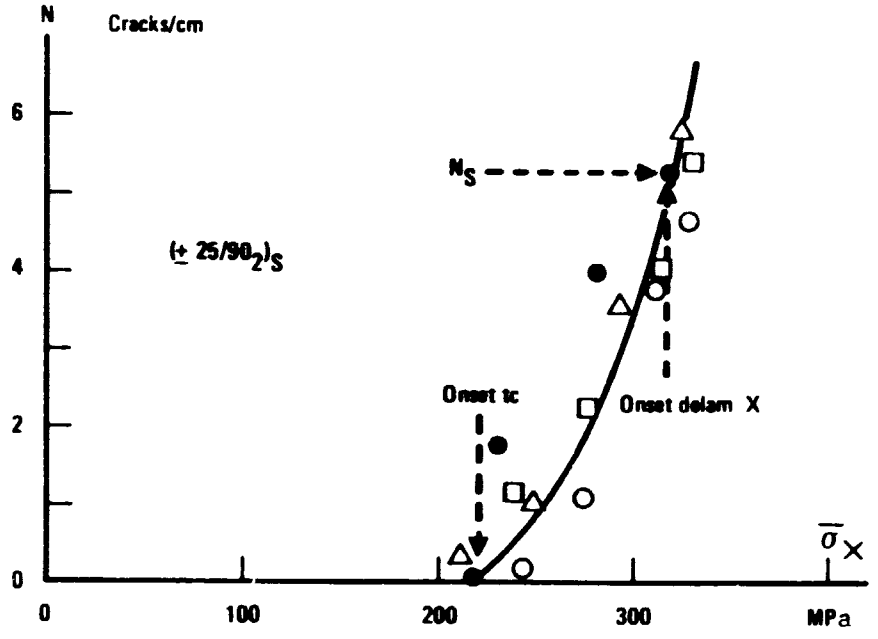

Figure D2: Transverse crack density vs. applied load. $(\pm 25/90_2)_s$. (Based on DIB X-Radiographs of Four Incrementally Tensile Loaded Specimens).

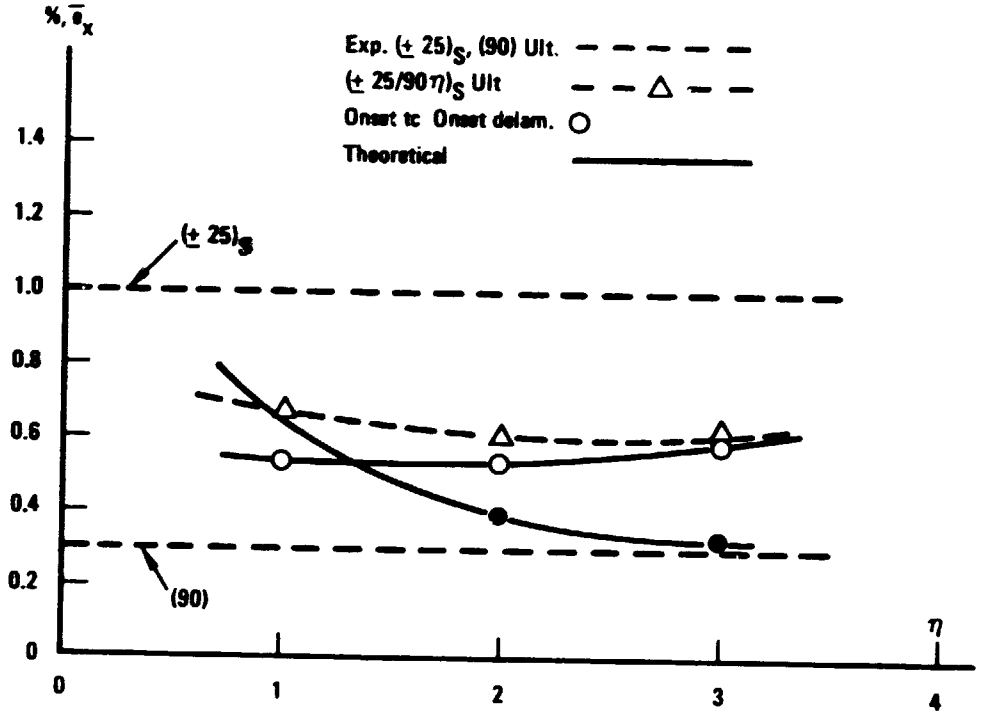

Figure D3: Failure modes and the associated strains vs 90^{o} - layer thickness in a series of tensile $(\pm 25/90_n)_s$. T300/934 laminates.

between the predicted and observed onset strains for transverse cracking of 90° plies and for delamination in a series of T300/934 $(\pm 25/90_n)_s$, n = 1, 2, 3 laminates.

In the present study the following output information was stored on disk files upon completion of the stress analysis:

- o Laminate Stiffness
- o Element Stresses, Strain Energy and Strain Energy Density
- o Nodal Forces
- o Nodal Displacements
- o Nodal coordinates and element centroids.

To provide graphical display of information generated by FREEVIS and to provide speed and flexibility in modeling, the GIFTS Interactive Graphics Software System (developed by the University of Arizona) was used as a pre and post processor to the FREEVIS analyzer. GIFTS software is available for CDC and DEC computers and requires a Tektronics CRT terminal like the 4010. Models and computation of stresses were run on the LMSC, Palo Alto, Applied Mechanics Laboratory's VAX 11/780 DEC computer which has 2 billion bytes of virtual memory storage. Analysis and computation was done in an interactive mode using GIFTS to define the finite element model, running the stress analysis, storing data files and disk, and then using GIFTS plotting capability to graphically display results. A few commands to the GIFTS processor were used to create a finite element model from scratch and to define element corrections, material properties and boundary conditions. The resulting node and element positions were quickly displayed for checking prior to analysis. Figure D4 shows GIFTS display of output in terms of contour plots or principal stress sectors. Lockheed developed graphics program were used to display a given stress or energy density as a function of position.

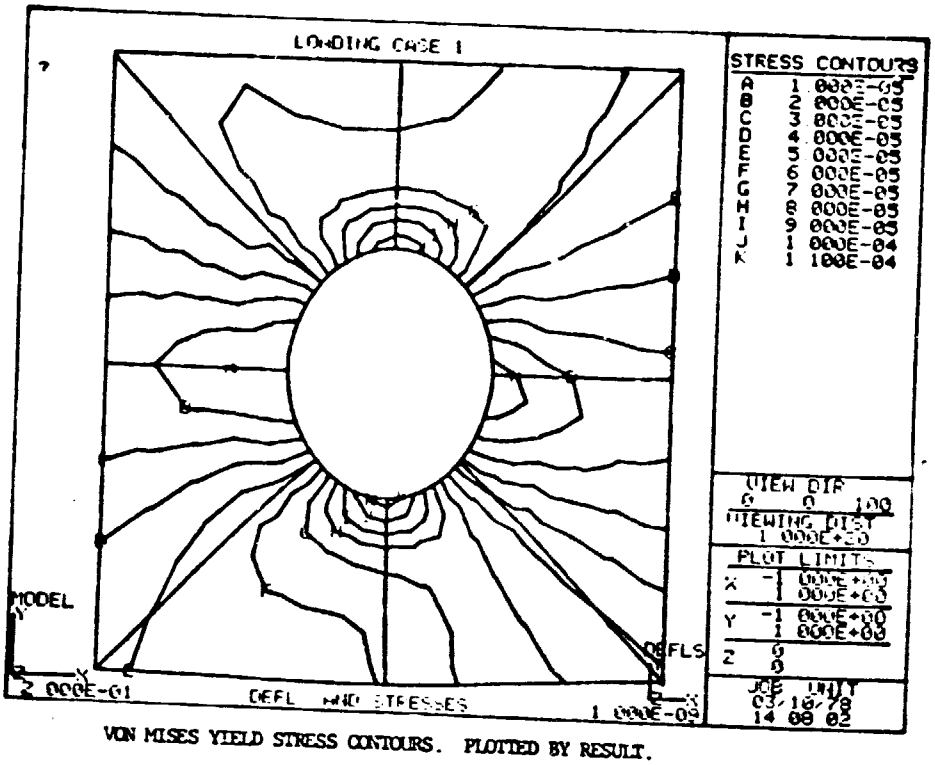

VON MISES YIELD STRESS CONTOURS. PLOTTED BY RESULT.

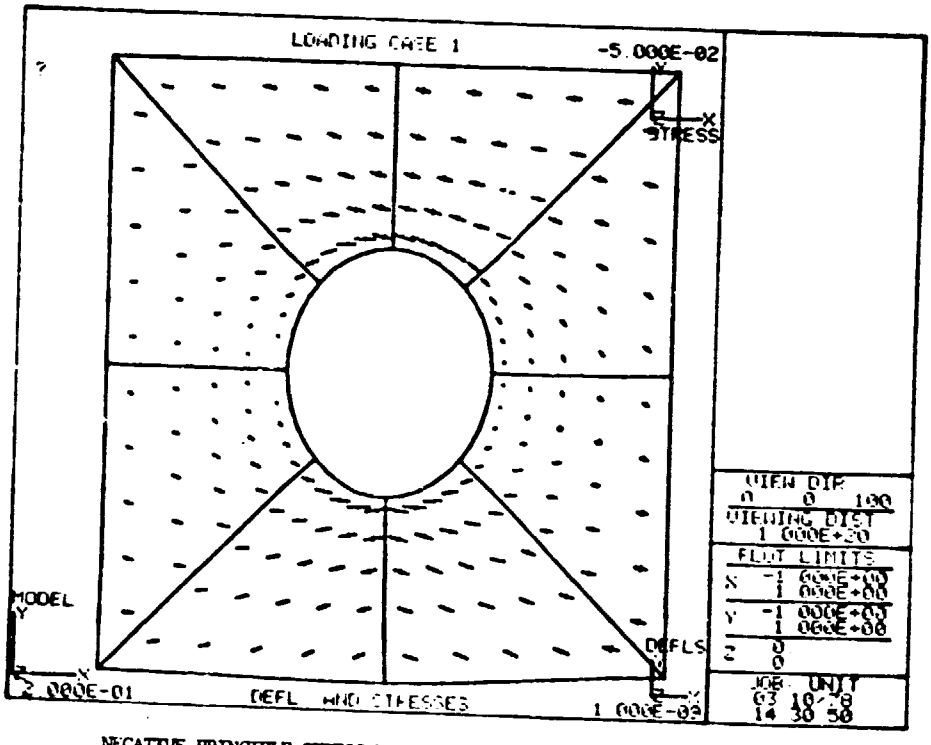

NEGATIVE PRINCIPLE STRESS VECTOR PLOT IN SELECTED COSUB. PLOTTED BY RESULT.

Figure D4: GIFTS display of stress field.

D.2 REVIEW AND EXAMPLE OF COMPUTATIONAL PROCEDURE

The following discussion provides a review of the computational steps taken to carry out modeling of stress distribution in a $(0/90/45/-45)_s$ laminate, selected as an example, loaded in uniaxial tension along the 0^o fiber axis (which is the Y axis in the model).

1. Construction of the Finite Element Model

(a) Make a sketch of the model in terms of multiple element grids.

(b) Choose the locations of points in x, y, z coordinates.

(c) Draw the model and label the key point (KPOINT) and lines connecting the points (SLINE).

(d) Generate the GIFTS model with the BULKM processor. Note the OLB (On-Line-Batch) file generation is preferred over the fully interactive model generation when modifications in the finite element grid are planned to model accumulation of damage during laminate loading. The OLB file can be easily modified in a text-editing mode.

Figure D5 shows the coarse grid network whose coordinates must be inputed point-by-point. Figures D6 - D8 show the fine grid generated by GIFTS based on the original coarse network, the nodal numbers, and the element numbers using the GIFTS display processor EDITM.

2. Transfer from GIFTS to FREEVIS (G2F) Forematting

The GIFTS processor is run to put the GIFTS files containing the model geometry into a format compatible with the FREEVIS finite element analyzer. Figures D9a - D9f show the interactive command structure of GIFTS which prompts the user for the required boundary conditions, elastic constants, layer orientations and output requirements.

In the modeling of the $(0/90/45/-45)_s$ laminate the G12 and E22 moduli of the 45^o layers were reduced to values equivalent to a crack spacing of 8t (t is the ply thickness). A crack in the 90^o layer at the left hand boundary of the model was introduced and a

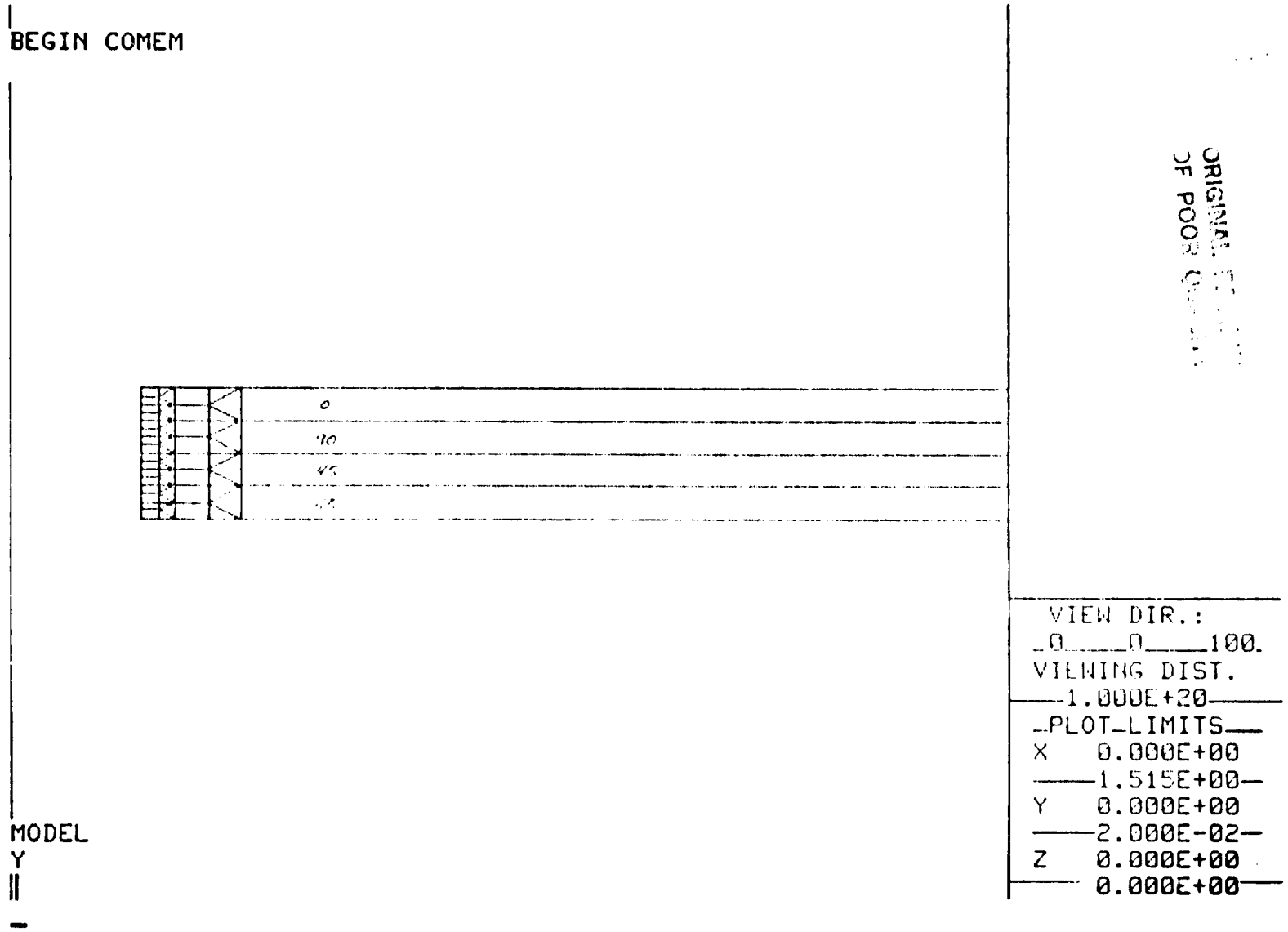

FIGURE D5: Four Layer Model

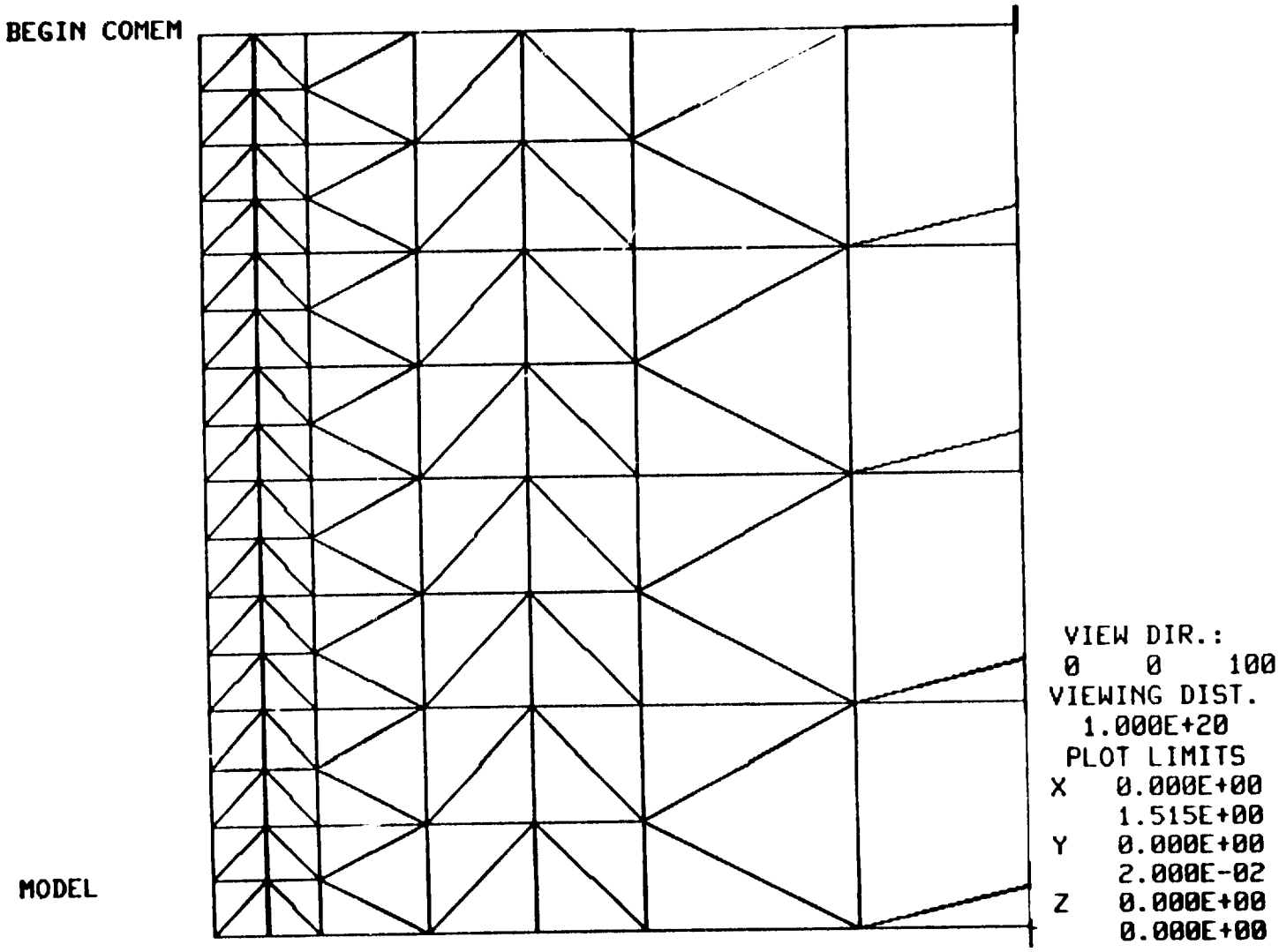

FIGURE D6: Elements

BEGIN COMEM

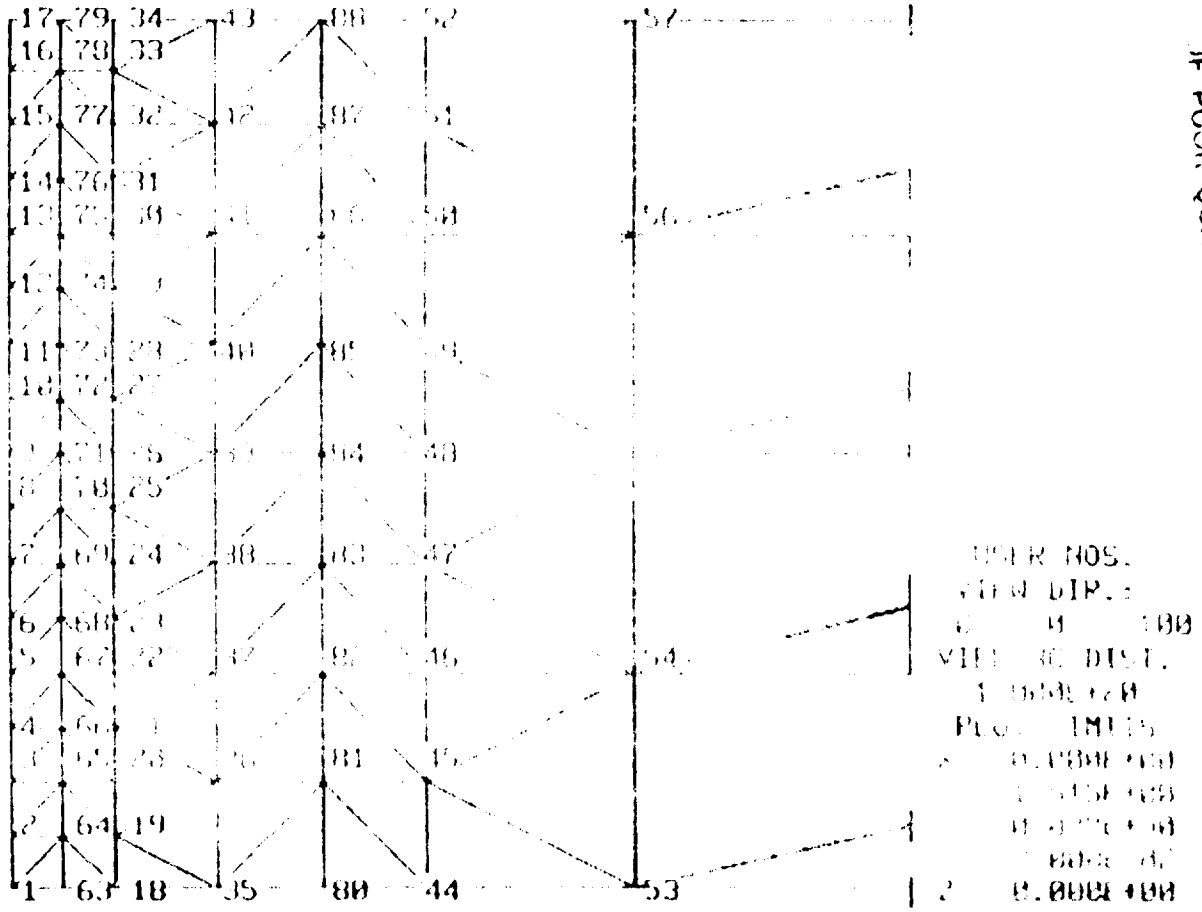

MODEL
Y

-

HOPF ... Points

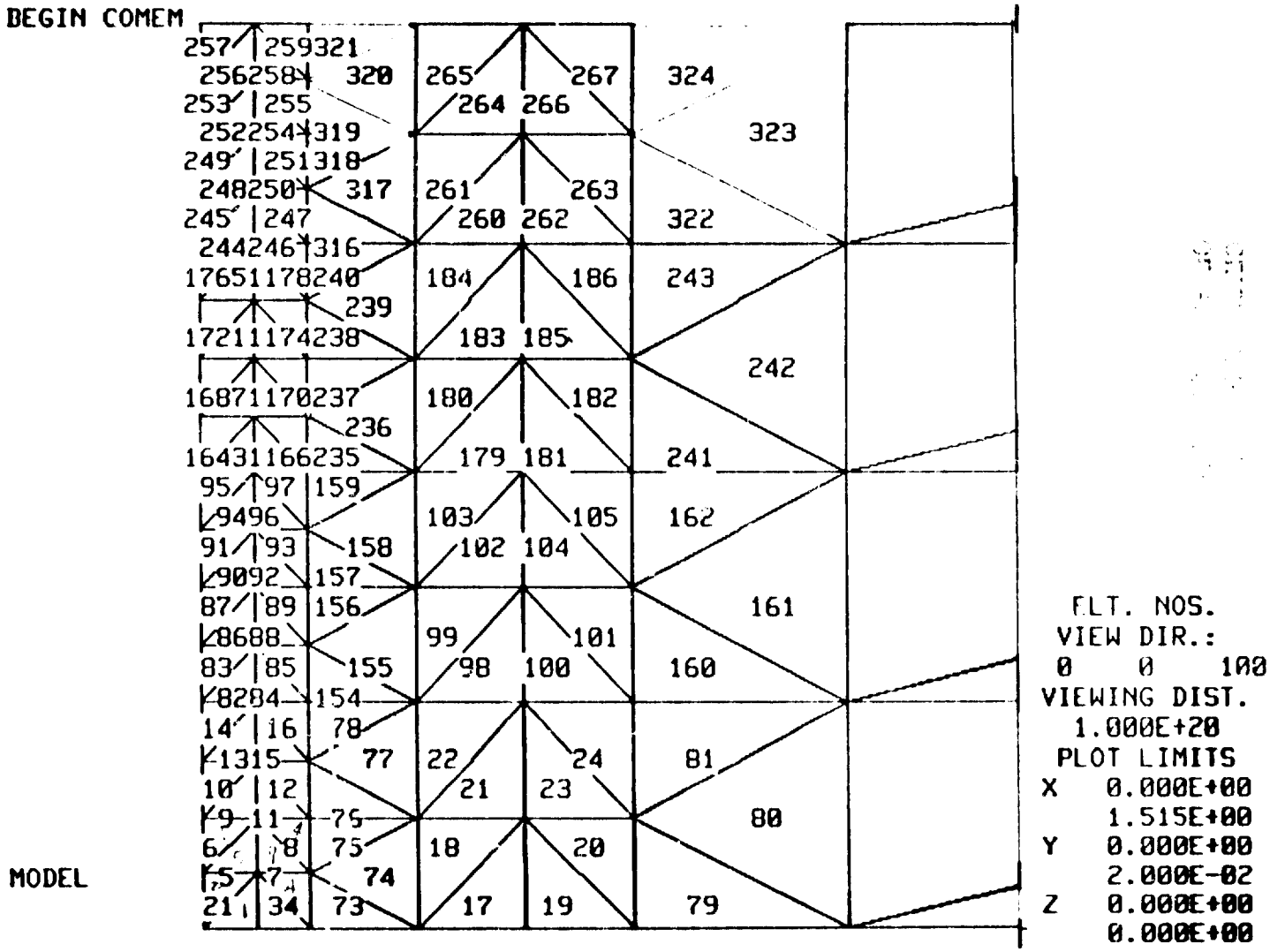

FIGURE D8: Element Numbers

```
$ GIFV

<<>>G I F V  [GIFTS-FREE*VIS INTERFACE]   V1.0/VAX

ENTER GIFTS-5 CASE NAME:  MMMM

GIFTS PARAMETERS:
        NUMBER OF SYSTEM NODE POINTS =  203
        NUMBER OF USER NODE POINTS =  203
        NUMBER OF ELEMENTS =  324
        NUMBER OF MATERIALS =    4


IF A GIFTS-FREE*VIS CONVERSION IS DESIRED, ENTER  G2F  ;
IF A FREE*VIS-GIFTS CONVERSION IS DESIRED, ENTER  F2G  .
ENTER CONVERSION TYPE: G2F
BEGIN REFORMATTING GIFTS-5 MODEL INFORMATION. PLEASE WAIT.
    GIFTS-5 NODE DATA REFORMATTED.
    GIFTS-5 ELEMENT DATA REFORMATTED.
    GIFTS-5 MATERIAL DATA REFORMATTED.
REFORMATTING COMPLETE; BEGIN PROMPTED USER INPUTS.

ENTER ESTIMATED SIZE OF THE  A  MATRIX : 50000

IS NODE AND ELEMENT DATA TO BE PRINTED BY FREE*VIS (YES/NO)? YES
ARE NODAL FORCES TO BE PRINTED BY FREE*VIS (YES/NO)? YES
ARE NODAL DISPLACEMENTS TO BE PRINTED BY FREE*VIS (YES/NO)? YES
ARE ELEMENT STRESSES TO BE PRINTED BY FREE*VIS (YES/NO)? YES

ARE THE RESULTS OF THE ANALYSIS TO BE SAVED (YES/NO)? YES

    ENTER THE NAME OF THE FILE ON WHICH THE RESULTS ARE
    TO BE SAVED (8 CHARACTERS MAX.) : MBB_
```

FIGURE D.1: Interactive Command Structure of GIFV

```
    ENTER THE NAME OF THE MATERIAL PROPERTY TO BE MODIFIED,
    OR ENTER  LIST  TO DISPLAY THE CURRENT PROPERTIES FOR THIS MATERIAL,
    OR ENTER  END  TO CONTINUE :  V13
FOR MATERIAL # 9, V13 IS CURRENTLY  0.290     ; ENTER NEW VALUE : .30
    ENTER THE NAME OF THE MATERIAL PROPERTY TO BE MODIFIED,
    OR ENTER  LIST  TO DISPLAY THE CURRENT PROPERTIES FOR THIS MATERIAL,
    OR ENTER  END  TO CONTINUE :  END

THE MATERIAL PROPERTIES SPECIFIED IN GIFTS MAY BE
MODIFIED, OR YOU MAY CONTINUE AND COMPLETE THE REST
OF THE FREE*VIS INPUTS.  ENTER  MODF  OR  CONT  : CONT

WARNING: THE NUMBER OF GIFTS-5 THICKNESS GROUPS IS
         LESS THAN THE NUMBER OF GIFTS-5 MATERIAL GROUPS; IT
         WILL BE ASSUMED THAT THE GIFTS-5 MATERIAL NUMBER
         FOR EACH ELEMENT IS ALSO THE FREE*VIS LAYER NUMBER
         FOR THAT ELEMENT.

ENTER THE GIFTS-5 MATERIAL NUMBER TO BE USED FOR EACH LAYER:
    ENTER MATERIAL NUMBER FOR LAYER # 1 : 1
    ENTER MATERIAL NUMBER FOR LAYER # 2 : 2
    ENTER MATERIAL NUMBER FOR LAYER # 3 : 3
    ENTER MATERIAL NUMBER FOR LAYER # 4 : 4

ENTER THE ANGLE (IN DEGREES) OF THE FIBERS IN EACH
LAYER WITH RESPECT TO THE X-DIRECTION.  NOTE THAT
THE THICKNESS GROUP ASSOCIATED WITH EACH GIFTS 5
ELEMENT IS TREATED AS A LAYER NUMBER BY FREE*VIS.
    ENTER ANGLE FOR LAYER # 1 : 45
    ENTER ANGLE FOR LAYER # 2 : -45
    ENTER ANGLE FOR LAYER # 3 : 90
    ENTER ANGLE FOR LAYER # 4 : 0

HOW MANY NODES HAVE APPLIED DISPLACEMENTS? _
```

FIGURE [illegible]. Interactive Command Structure of GIFV-Continued

```
    ENTER THE NAME OF THE FILE ON WHICH THE RESULTS ARE
    TO BE SAVED (8 CHARACTERS MAX.) : MBB

ARE NODAL MOISTURE CONCENTRATIONS TO BE READ FROM A
NODECONC.DAT FILE CREATED BY A SORPTION*ANALYSIS RUN (YES/NO)? NO

    ENTER THE EQUILIBRIUM MOISTURE CONTENT (IN PPM): 0.0

ENTER THE TEMPERATURE DIFFERENCE BETWEEN THE STRESS
FREE TEMPERATURE AND THE ANALYSIS TEMPERATURE (USE
THE SAME TEMPERATURE UNITS AS FOR CTE VALUES): 0.0

IS STRESS OR STRAIN TO BE SPECIFIED IN THE X-DIRECTION? STRESS

    ENTER X-DIRECTION SURFACE TRACTION (TYPICALLY IN PSI): 0.0

THE MATERIAL PROPERTIES SPECIFIED IN GIFTS MAY BE
MODIFIED, OR YOU MAY CONTINUE AND COMPLETE THE REST
OF THE FREE*VIS INPUTS.  ENTER  MODF  OR  CONT  : MODF

    THERE ARE  4 MATERIALS IN THE GIFTS MODEL;
    ENTER THE NUMBER OF THE MATERIAL TO BE LISTED : 1

THE CURRENT MATERIAL PROPERTIES FOR MATERIAL # 1 ARE :

 E11    E22    E33    G12    G23    G13  (MSI)  V12    V23    V13
29.50  29.50  29.50  11.43  11.43  11.43         0.290  0.290  0.290

 AL     AT     AZ  (MICRO-E/T)  BL     BT     BZ  (%STRAIN/%M)
0.00   0.00   0.00              0.00   0.00   0.00

    ENTER THE NAME OF THE MATERIAL PROPERTY TO BE MODIFIED,
    OR ENTER  LIST  TO DISPLAY THE CURRENT PROPERTIES FOR THIS MATERIAL,
    OR ENTER  END  TO CONTINUE : _
```

FIGURE [illegible]: Interactive Command Structure of GIFV - Continued

```
AL     AT     AZ  (MICRO-E/T)  BL     BT     BZ  (%STRAIN/%M)
0.00   0.00   0.00             0.00   0.00   0.00

    ENTER THE NAME OF THE MATERIAL PROPERTY TO BE MODIFIED,
    OR ENTER  LIST  TO DISPLAY THE CURRENT PROPERTIES FOR THIS MATERIAL,
    OR ENTER  END  TO CONTINUE :  E11
FOR MATERIAL # 1, E11 IS CURRENTLY 29.500  MSI; ENTER NEW VALUE : 23.7
    ENTER THE NAME OF THE MATERIAL PROPERTY TO BE MODIFIED,
    OR ENTER  LIST  TO DISPLAY THE CURRENT PROPERTIES FOR THIS MATERIAL,
    OR ENTER  END  TO CONTINUE :  E22
FOR MATERIAL # 2, E22 IS CURRENTLY 29.500  MSI; ENTER NEW VALUE : 1.48
    ENTER THE NAME OF THE MATERIAL PROPERTY TO BE MODIFIED,
    OR ENTER  LIST  TO DISPLAY THE CURRENT PROPERTIES FOR THIS MATERIAL,
    OR ENTER  END  TO CONTINUE :  E33
FOR MATERIAL # 3, E33 IS CURRENTLY 29.500  MSI; ENTER NEW VALUE : 1.48
    ENTER THE NAME OF THE MATERIAL PROPERTY TO BE MODIFIED,
    OR ENTER  LIST  TO DISPLAY THE CURRENT PROPERTIES FOR THIS MATERIAL,
    OR ENTER  END  TO CONTINUE :  G12
FOR MATERIAL # 4, G12 IS CURRENTLY 11.434  MSI; ENTER NEW VALUE : .94
    ENTER THE NAME OF THE MATERIAL PROPERTY TO BE MODIFIED,
    OR ENTER  LIST  TO DISPLAY THE CURRENT PROPERTIES FOR THIS MATERIAL,
    OR ENTER  END  TO CONTINUE :  G23
FOR MATERIAL # 5, G23 IS CURRENTLY 11.434  MSI; ENTER NEW VALUE : .50
    ENTER THE NAME OF THE MATERIAL PROPERTY TO BE MODIFIED,
    OR ENTER  LIST  TO DISPLAY THE CURRENT PROPERTIES FOR THIS MATERIAL,
    OR ENTER  END  TO CONTINUE :  G13
FOR MATERIAL # 6, G13 IS CURRENTLY 11.434  MSI; ENTER NEW VALUE : .94
    ENTER THE NAME OF THE MATERIAL PROPERTY TO BE MODIFIED,
    OR ENTER  LIST  TO DISPLAY THE CURRENT PROPERTIES FOR THIS MATERIAL,
    OR ENTER  END  TO CONTINUE :  V12
FOR MATERIAL # 7, V12 IS CURRENTLY  0.290      ; ENTER NEW VALUE : .30
    ENTER THE NAME OF THE MATERIAL PROPERTY TO BE MODIFIED,
    OR ENTER  LIST  TO DISPLAY THE CURRENT PROPERTIES FOR THIS MATERIAL,
    OR ENTER  END  TO CONTINUE :  _
```

FIGURE D.1: Interactive Command Structure of GIFV - Continued

```
    OR ENTER  LIST  TO DISPLAY THE CURRENT PROPERTIES FOR THIS MATERIAL,
    OR ENTER  END  TO CONTINUE :  END

THE MATERIAL PROPERTIES SPECIFIED IN GIFTS MAY BE
MODIFIED, OR YOU MAY CONTINUE AND COMPLETE THE REST
OF THE FREE*VIS INPUTS.  ENTER  MODF  OR  CONT  : CONT

WARNING: THE NUMBER OF GIFTS-5 THICKNESS GROUPS IS
         LESS THAN THE NUMBER OF GIFTS-5 MATERIAL GROUPS; IT
         WILL BE ASSUMED THAT THE GIFTS-5 MATERIAL NUMBER
         FOR EACH ELEMENT IS ALSO THE FREE*VIS LAYER NUMBER
         FOR THAT ELEMENT.

ENTER THE GIFTS-5 MATERIAL NUMBER TO BE USED FOR EACH LAYER:
    ENTER MATERIAL NUMBER FOR LAYER # 1 : 1
    ENTER MATERIAL NUMBER FOR LAYER # 2 : 2
    ENTER MATERIAL NUMBER FOR LAYER # 3 : 3
    ENTER MATERIAL NUMBER FOR LAYER # 4 : 4

ENTER THE ANGLE (IN DEGREES) OF THE FIBERS IN EACH
LAYER WITH RESPECT TO THE X-DIRECTION.  NOTE THAT
THE THICKNESS GROUP ASSOCIATED WITH EACH GIFTS-5
ELEMENT IS TREATED AS A LAYER NUMBER BY FREE*VIS.
    ENTER ANGLE FOR LAYER # 1 : 45
    ENTER ANGLE FOR LAYER # 2 : -45
    ENTER ANGLE FOR LAYER # 3 : 90
    ENTER ANGLE FOR LAYER # 4 : 0

HOW MANY NODES HAVE APPLIED DISPLACEMENTS? 3

    ENTER GIFTS NODE NUMBER, RESTRAINT CODE (SEPARATE WITH A COMMA):
    FOR RESTRAINED NODE #   1 : 1,010
    ENTER APPLIED DISPLACEMENT (IN MICROINCHES) FOR Y- DIRECTION : 0
_   FOR RESTRAINED NODE #   2 : 2,010
```

FIGURE D9c: Interactive Command Structure of GIFV - Continued

```
 HOW MANY NODES HAVE APPLIED FORCES? 0

 HOW MANY CONSTRAINED NODE SETS? 0

 FREE*VIS PARAMETERS:
        NUMBER  OF NODE POINTS =  203
        NUMBER OF ELEMENTS =  324
        NUMBER OF MATERIALS =    4

 CONVERSION COMPLETE. THE FREE*VIS CARD IMAGE INPUT
 FILE IS THE HIGHEST VERSION OF  MMMM.G2F      .
$
 END  G I F V    V1.0/VAX
$
$
$
$
$
$
$
$
$
$
$
$
$
$
$
$
$
$
$
$ _
```

FIGURE D9f: Interactive Command Structure of GIFV - Continued

uniform y displacement along a y = 8t line was applied.

3. FREEVIS Analysis

The finite element analysis can be run in interactive or batch mode and an output file containing information chosen by the user in GIFTS is saved.

4. FREEVIS to GIFTS File Forematting

Following the analysis, the output file can be examined by the VAX plot processors or a second file in GIFTS format can be created to examine the results using the GIFTS graphical displays. Figure D10 shows the commands needed to complete the FREEVIS-to-GIFTS (F2G) formatting. One must choose only one stress component to be displayed in contour format, and multiple calls to F2G can be made to develop contours for all six stress components.

5. Post-Processing Graphics

(a) a call to the GIFTS RESULT processor can display the stress contours and/or the magnified deflections of the model. Figure D11 in fact shows that the original boundary conditions used to simulate a 90^{o} crack allowed the crack to extend into the neighboring 0^{o} and 45^{o} plies by mistake. This error was seen immediately in the graphical display and corrected.

(b) The displacements can also be displayed by a call to the EPLOT processor on the VAX system, Figure D12, and plotted on the Versatek printer/plotter as shown in Figure D13. The correct crack displacements are evident in Figure D13.

(c) The stress components can be plotted as a function of y or z coordinates by a call to the SPLOT processor and by specifying a window in y or z coordinates in the interactive plotting queries shown in Figure D14. The yy stress as a function of z is plotted in Figure D15. The windows in y coordinates used for this plot are indicated at the bottom of Figure D16.

D3 FREE-EDGE STRESSES IN THE $(0/90/45/-45)_s$ LAMINATE

The free edge stresses in a $(0/90/\pm45)_s$ laminate were calculated. Figures

```
$ GIFV

 <<>>G I F V  [GIFTS-FREE*VIS INTERFACE]   V1.0/VAX

 ENTER GIFTS-5 CASE NAME:  MMMM

 GIFTS PARAMETERS:
        NUMBER OF SYSTEM NODE POINTS =  203
        NUMBER OF USER NODE POINTS =  203
        NUMBER OF ELEMENTS =  324
        NUMBER OF MATERIALS =    4


 IF A GIFTS-FREE*VIS CONVERSION IS DESIRED, ENTER  G2F  ;
 IF A FREE*VIS-GIFTS CONVERSION IS DESIRED, ENTER  F2G  .
 ENTER CONVERSION TYPE: F2G

 ENTER FREE*VIS STRESS TO BE CONTOURED ( XX, YY, ZZ, YZ, XZ, XY) : XX

 BEGIN REFORMATTING FREE*VIS ANALYSIS RESULTS. PLEASE WAIT.
+++  OPEN, 16 = MBBB                    , Acc= DIRECT   , Stat=   OLD
     FREE*VIS DEFLECTION RESULTS REFORMATTED.
     FREE*VIS STRESS RESULTS REFORMATTED.
 REFORMATTING COMPLETE.

 CONVERSION COMPLETE. THE RESULTS OF THE ANALYSIS
 FOR CASE  MMMM      MAY BE EXAMINED USING GIFTS-5.

 END  G I F V    V1.0/VAX
$
$
$
$ _
```

FIGURE D10: F2G and G2F Formatting

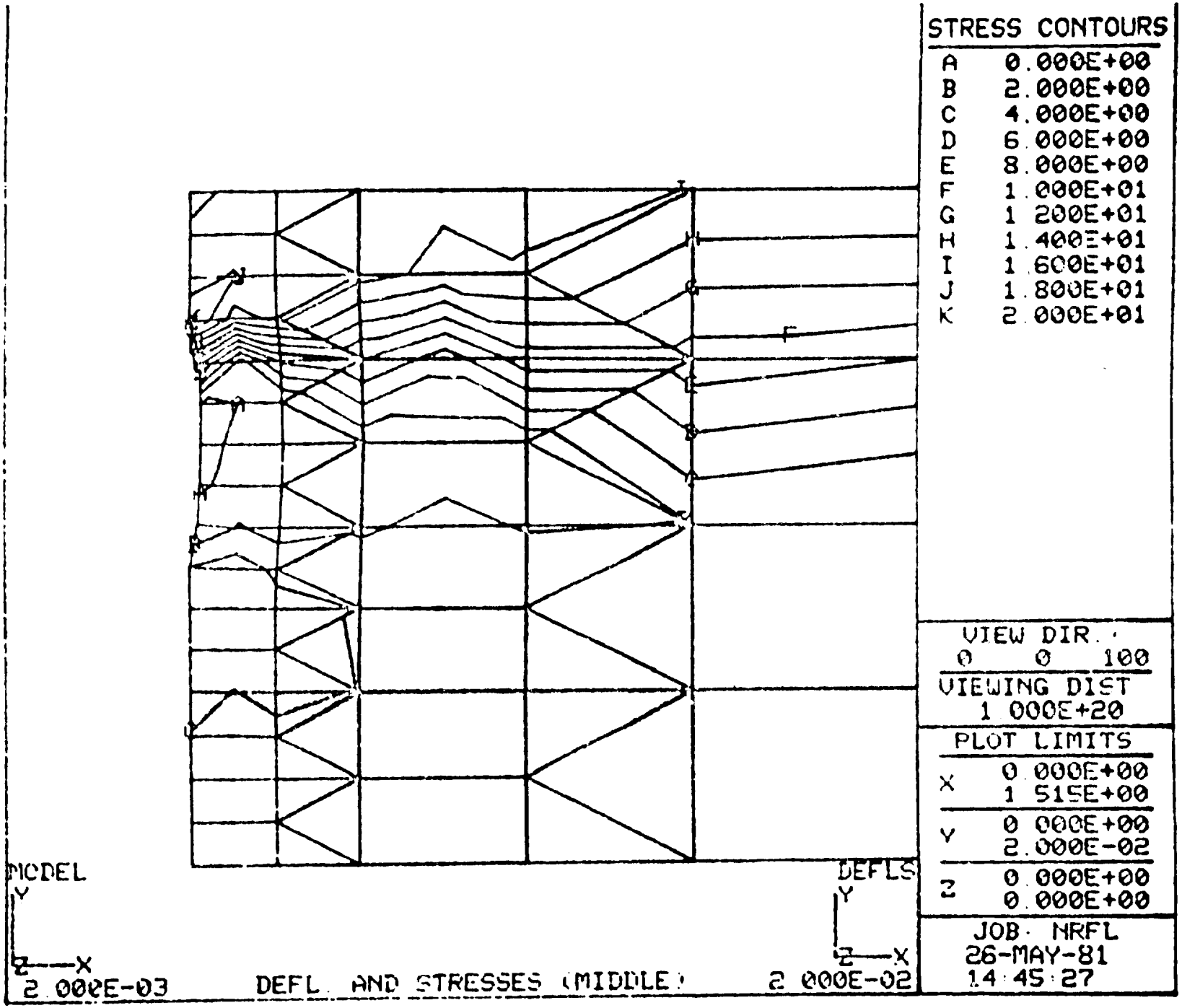

FIGURE 011: X-Stress Contour Plot Containing Error

```
$
$ EPLOT

 ENTER  PREP  IF PRE-PROCESSING IS DESIRED, OR  POST  IF
 POST-PROCESSING IS DESIRED.
POST

 ENTER NAME OF DMGASP FILE CONTAINING MESH AND RESULTS.
MBBB

+++  OPEN, 14 = MBBB                          , Acc= DIRECT    , Stat=   OLD
MBBB

THE CURRENT MODEL USES  324 ELEMENTS,  203 NODES,
AND  4 MATERIALS.

  ENTER THE NUMBER OF MATERIALS TO BE SEARCHED: 4

LIMITS OF THIS MODEL ARE:  XMIN=    0.000 , XMAX=    1.515
                           YMIN=    0.000 , YMAX=    0.020 .

  ENTER SEARCH AREA LIMITS: SXMIN,SXMAX,SYMIN,SYMAX (FREE FIELD FORMAT).
0.0,0.04,0.0,0.02

  ENTER  FULL  ,  SHRINK  ,OR  BORDER  AS THE TYPE OF MESH TO BE DRAWN
  FOR EACH MATERIAL (ALPHANUMERIC INPUT).

     ENTER MODE FOR MATERIAL # 1 :  FULL
     ENTER MODE FOR MATERIAL # 2 :  FULL
     ENTER MODE FOR MATERIAL # 3 :  FULL
     ENTER MODE FOR MATERIAL # 4 :  FULL

  ENTER  FULL  FOR FULL SCALE PLOT, OR  PAGE  FOR FULL
  PAGE PLOT, OR  MAGNIFY TO ENLARGE PLOT (ALPHA INPUT): MAGNIFY_
```

FIGURE D12a: Example of EPLOT

```
 ENTER  FULL  FOR FULL SCALE PLOT, OR  PAGE  FOR FULL
 PAGE PLOT, OR  MAGNIFY TO ENLARGE PLOT (ALPHA INPUT): MAGNIFY

 ENTER MAGNIFICATION RATIO FOR HORIZONTAL, THEN VERTICAL
 AXIS (FREE FIELD FORMAT).
200,200

 USE THE VERSAPLOT CHANGE ROUTINE TO SET XMAX=    10.00000

 ENTER  ORIGINAL  FOR UNDEFORMED MESH, OR  DEFORMED  FOR DEFLECTED MESH ,
 OR  BOTH  FOR BOTH ORIGINAL AND DEFORMED MESHES:  DEFORMED

 ENTER INCREMENT NUMBER TO BE PLOTTED: 1

THE MAXIMUM AND MINIMUM DISPLACEMENT MAGNITUDES (IN MICROINCHES) ARE:
                        DXMIN=     0.000 ,DXMAX=     0.025
                        DYMIN=     0.000 ,DYMAX=     0.005

 ENTER HORIZONTAL AND VERTICAL DISPLACEMENT
 MAGNIFICATIONS (FREE FIELD FORMAT).
10000,1000

* Mapped-vector algorithm *

 NIBSX,ISCAN,NSCAN,NWORD,NSTRIP,NBAND
       829          32          100         3200              1              9
THE SUBROUTINE  CHANGE  MAY NOW BE USED TO MODIFY
ANY OF THE FOLLOWING GLOBAL PLOTTING PARAMETERS:
XMIN,YMIN,XMAX,YMAX,MSGLVL,XSTART,YSTART,SCALE,
XFACT,YFACT,STRIP,STRIP0,LYNES.
THE COMMANDS FOR USING  CHANGE  ARE:
    PARAMETER=VALUE          WHERE PARAMETER IS THE
                             PLOTTING PARAMETER TO BE
    -                        CHANGED AND VALUE IS THE
```

FIGURE D12b: Example of EPLOT

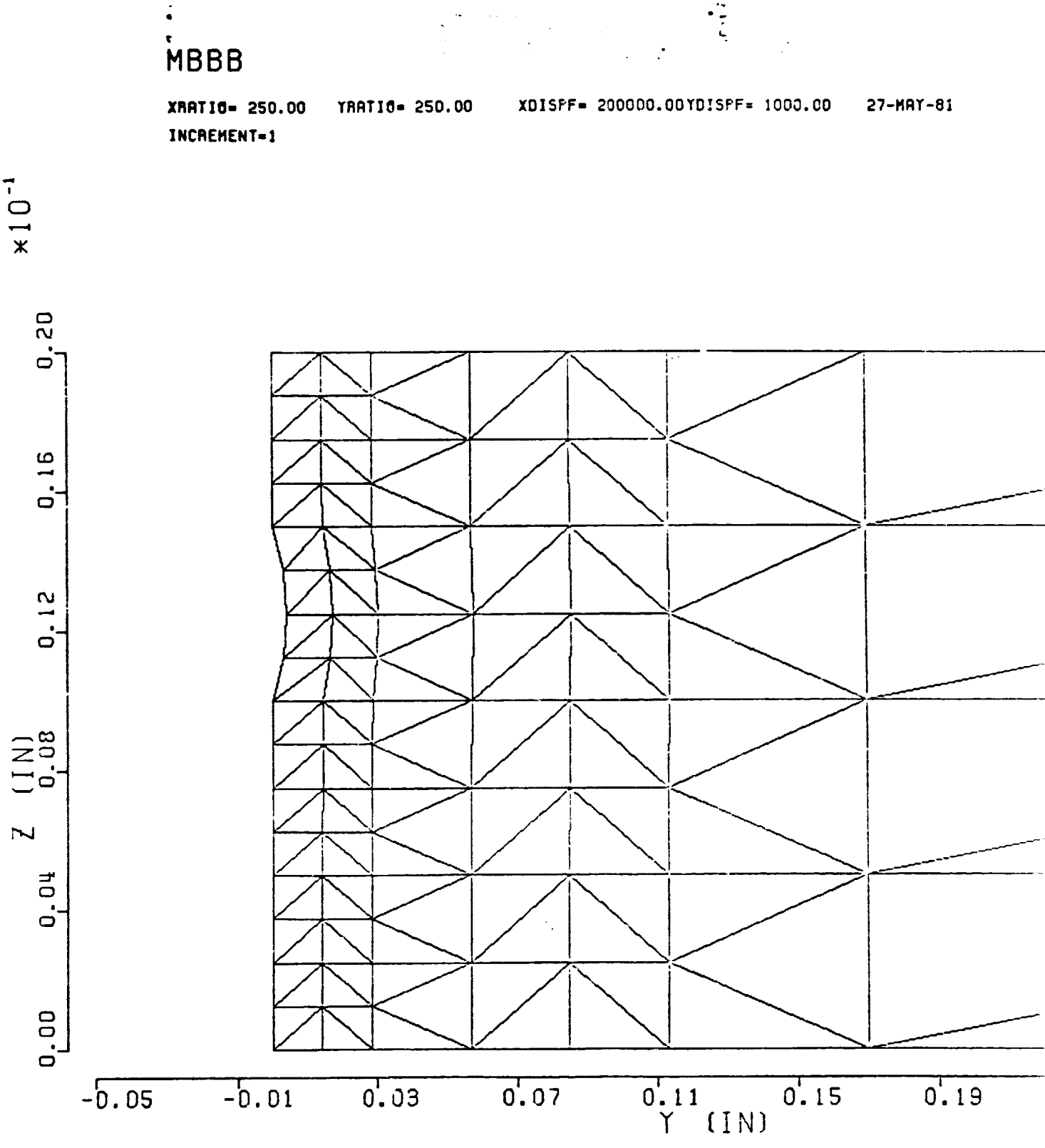

FIGURE D13: Example of Versatek Plot Showing Correct Crack Displacements

```
$
$
$ SPLOT
 ENTER THE TYPE OF OUTPUT:1(S,Y),2(S,Z),3(3D).
2
 ENTER OUTPUT DEVICE:  TEKTRONIX  OR VERSATEC  .
VERSATEC
 ENTER DMGASP FILENAME CONTAINING RESULTS OF ANALYSIS.
MBBB
+++  OPEN,  14 = MBBB                        , Acc= DIRECT , Stat= OLD


 INPUT THE NUMBER OF CURVES (<=6):
3
 INPUT INCREMENT NUMBER FOR EACH CURVE:
1,1,1
 INPUT YMIN,YMAX,ZMIN,ZMAX AND TIME FOR EACH CURVE:
 VALUES FOR CURVE 1:0.0,0.000625,0.0,0.02,1
 VALUES FOR CURVE 2:0.000625,0.00125,0.0,0.02,1
 VALUES FOR CURVE 3:0.025,0.0375,0.0,0.02,1
 INPUT STRESS TO BE PLOTTED(1=X,2=Y,3=Z,4=YZ,5=XZ,6=XY):
2
 INPUT (Y,Z) LOCATION OF LEGEND, IN INCHES:
1,1
 INPUT MIDPLANE RADIUS(0=FLAT), X-STRAIN, PLY THICKNESS:
0,1,1
 IF INTERMEDIATE RESULTS ARE TO BE PRINTED, ENTER 1 :
1
* Mapped-vector algorithm *

                *****PLOT OPTIONS IN EFFECT*****

MODEL   =       1110   ,XMIN   =        0.00   ,XMAX   =       10.23
YMIN    =       0.00   ,YMAX   =   _   10.23   ,MSGLVL =           1
```

FIGURE D14a: SPLOT Interactive Queries

```
                *****PLOT OPTIONS IN EFFECT*****

MODEL  =      1110  ,XMIN   =      0.00  ,XMAX   =     10.23
YMIN   =      0.00  ,YMAX   =     10.23  ,MSGLVL =        1
XSTART =      0.00  ,YSTART =      0.00  ,SCALE  =     1.00
XFACT  =      1.00  ,YFACT  =      1.00  ,UNITS  =     1.00
STRIP  =     10.24  ,STRIP0 =      0.00  ,SPACE  =     10.23
I2FLG  =         2  ,OUT    =     -1.00  ,LYNES  =      600
NSCAN  =       100

FINDER:NEF(NPF),MATCK,MAT(N),X,Y
         2           0          1  4.1666665E-04  8.3333330E-04
         6           0          1  4.1666665E-04  2.0833334E-03
        10           0          1  4.1666665E-04  3.3333332E-03
        14           0          1  4.1666665E-04  4.5833332E-03
        83           0          2  4.1666665E-04  5.8333334E-03
        87           0          2  4.1666665E-04  7.0833336E-03
        91           0          2  4.1666665E-04  8.3333338E-03
        95           0          2  4.1666665E-04  9.5833335E-03
       164           0          3  4.1666665E-04  1.0833334E-02
       168           0          3  4.1666665E-04  1.2083334E-02
       172           0          3  4.1666665E-04  1.3333333E-02
       176           0          3  4.1666665E-04  1.4583333E-02
       245           0          4  4.1666665E-04  1.5833333E-02
       249           0          4  4.1666665E-04  1.7083334E-02
       253           0          4  4.1666665E-04  1.8333334E-02
       257           0          4  4.1666665E-04  1.9583333E-02
FINDER:NPF,XMIN,XMAX,YMIN,YMAX          16  0.0000000E+00  6.2499999E-04
 0.0000000E+00  2.0000000E-02
FINDER:WINDOW:  0.0000000E+00  1.2500000E-03  0.0000000E+00  2.0000000E-02
SORTER:NPFI,NPFF:            1           16
         1           2  8.3333330E-04   3.775175
         2           6  2.0833334E-03   3.780551
```

FIGURE [illegible] SPLOT Interactive Queries

```
           3          187  1.1666667E-02  0.8905433
           4          268  1.1666668E-02   15.62877
 PREPRO:NPFI,NPFF:                 1              4
 SZPLOT:SUMF,SUMM:  0.0000000E+00  0.0000000E+00
 AVE=  0.03125, TIME= 0.1000E+01
 AVE=  0.03125, TIME= 0.1000E+01
 AVE=  0.00031, TIME= 0.1000E+01
 AVE=  0.00094, TIME= 0.1000E+01
 AVE=  0.03125, TIME= 0.1000E+01
  ENTER  NEXT  FOR ANOTHER STRESS COMPONENT, OR  AGAIN
  FOR ANOTHER Z-SECTION PLOT, OR  RETURN  TO RETURN TO
  THE MAIN PROGRAM:
NEXT
  INPUT STRESS TO BE PLOTTED(1=X,2=Y,3=Z,4=YZ,5=XZ,6=XY):
3
  INPUT (Y,Z) LOCATION OF LEGEND, IN INCHES:
1,1
  INPUT MIDPLANE RADIUS(0=FLAT), X-STRAIN, PLY THICKNESS:
0,1,1
  IF INTERMEDIATE RESULTS ARE TO BE PRINTED, ENTER 1 :
1
FINDER:NEF(NPF),MATCK,MAT(N),X,Y
           2          0          1  4.1666665E-04  8.3333330E-04
           6          0          1  4.1666665E-04  2.0833334E-03
          10          0          1  4.1666665E-04  3.3333332E-03
          14          0          1  4.1666665E-04  4.5833332E-03
          83          0          2  4.1666665E-04  5.8333334E-03
          87          0          2  4.1666665E-04  7.0833336E-03
          91          0          2  4.1666665E-04  8.3333338E-03
          95          0          2  4.1666665E-04  9.5833335E-03
         164          0          3  4.1666665E-04  1.0833334E-02
         168          0          3  4.1666665E-04  1.2083334E-02
         172          0          3  4.1666665E-04  1.3333333E-02
         176          0          3  4.1666665E-04  1.4583333E-02
```

Z-SECTION STRESSES FOR MBBB

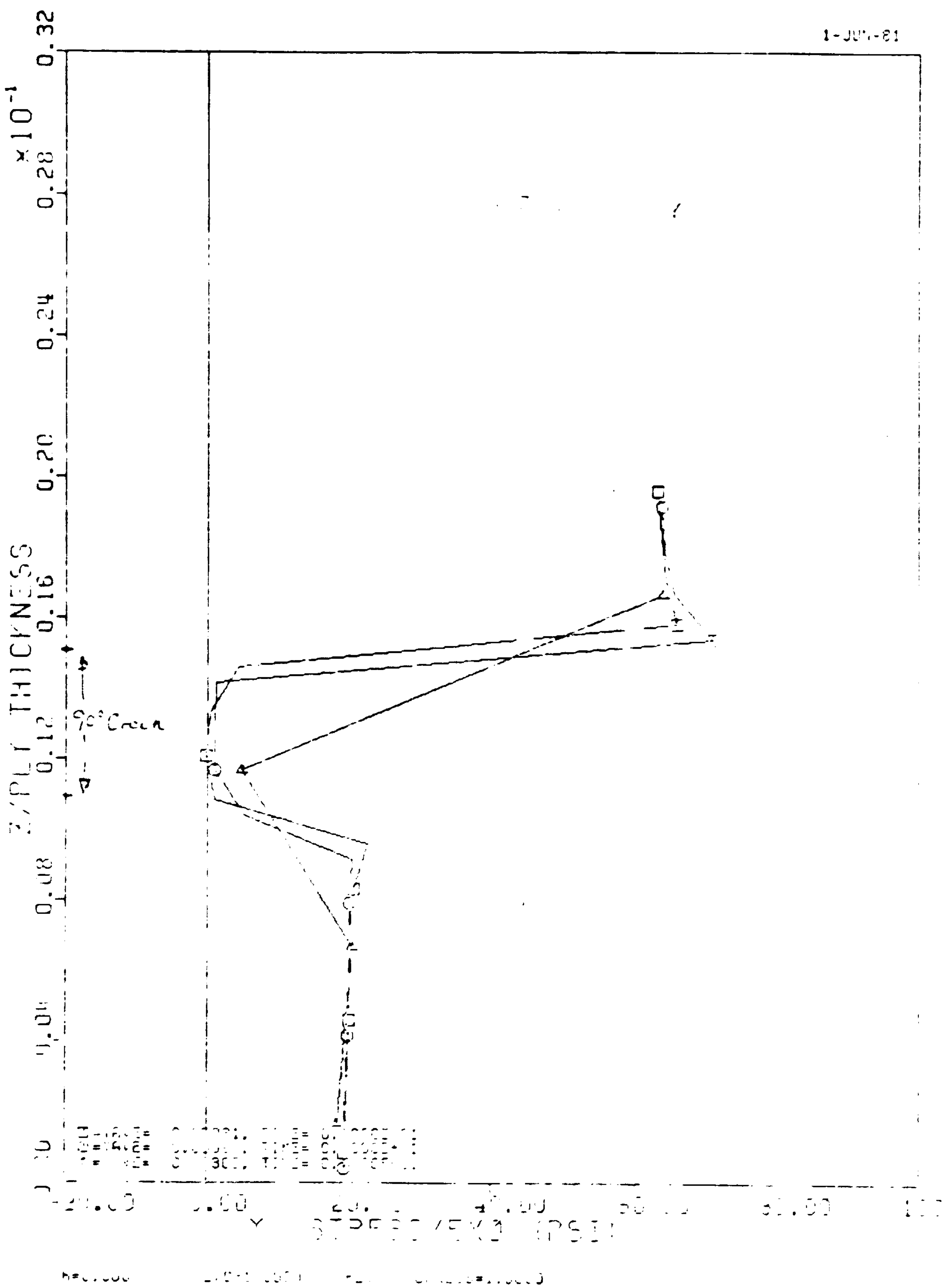

FIGURE D15: σ_{yy} Stress as a Function of z

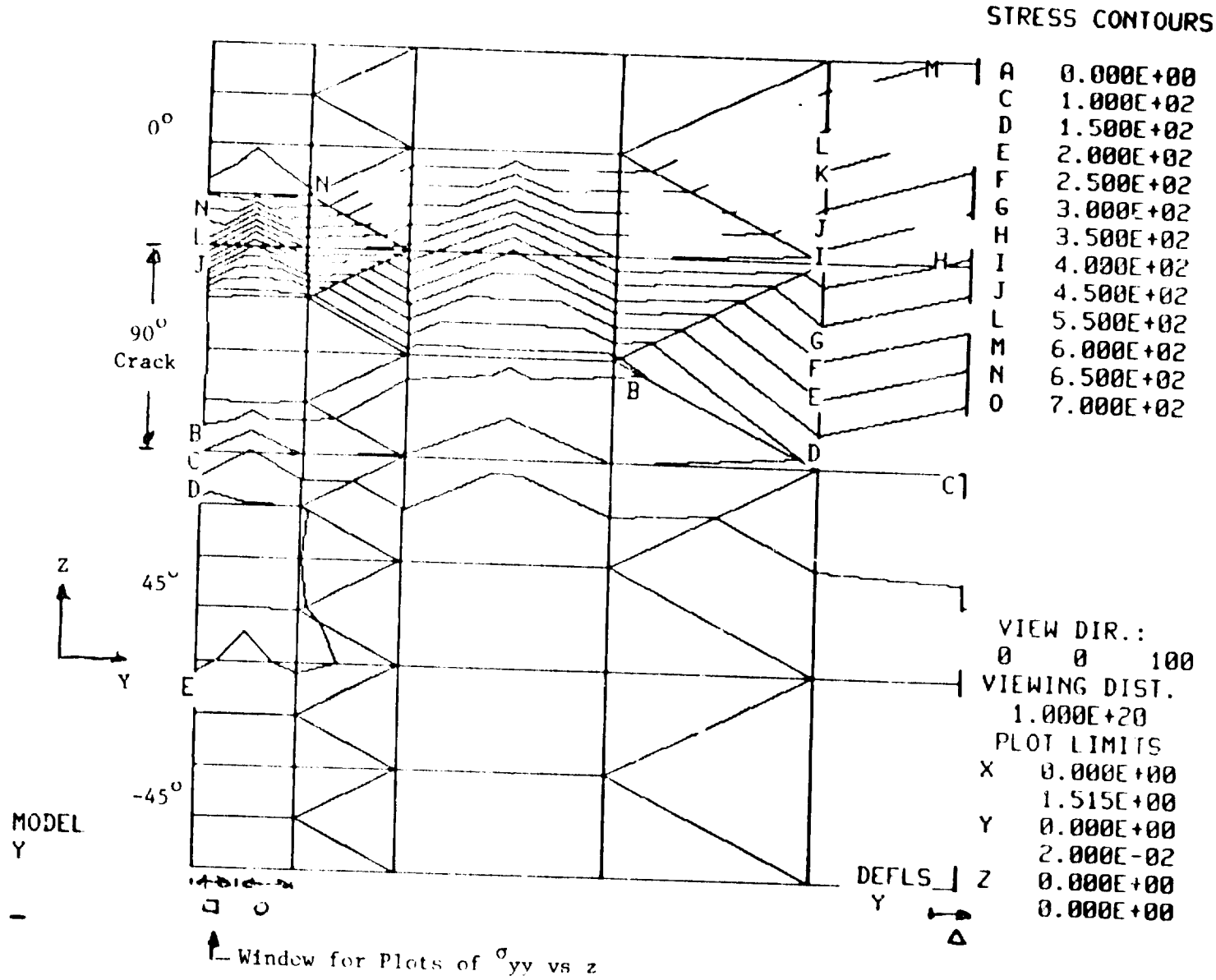

FIGURE [illegible] Loading Case 1, σ_{yy} Applied Stress (0/90/45/-45)

D17 through D18 show the GIFTS generated finite element grid used to calculate the free-edge stresses in the quasi-isotropic laminate under two different loadings: first, under a uniform tensile strain applied in the x direction; and second, under a uniform temperature change of 3.5°C (7°F) with traction free bboundary conditions. In Figures D19 to D30, the through-the-thickness stress components σ_{zz}, σ_{yz}, and σ_{xz} are plotted vs. z and y along slices through the model indicated in Figure D18. The thermal and mechanical stresses could be superposed for any arbitrary combination of thermal change, ΔR, and applied tensile strain, σ_x.

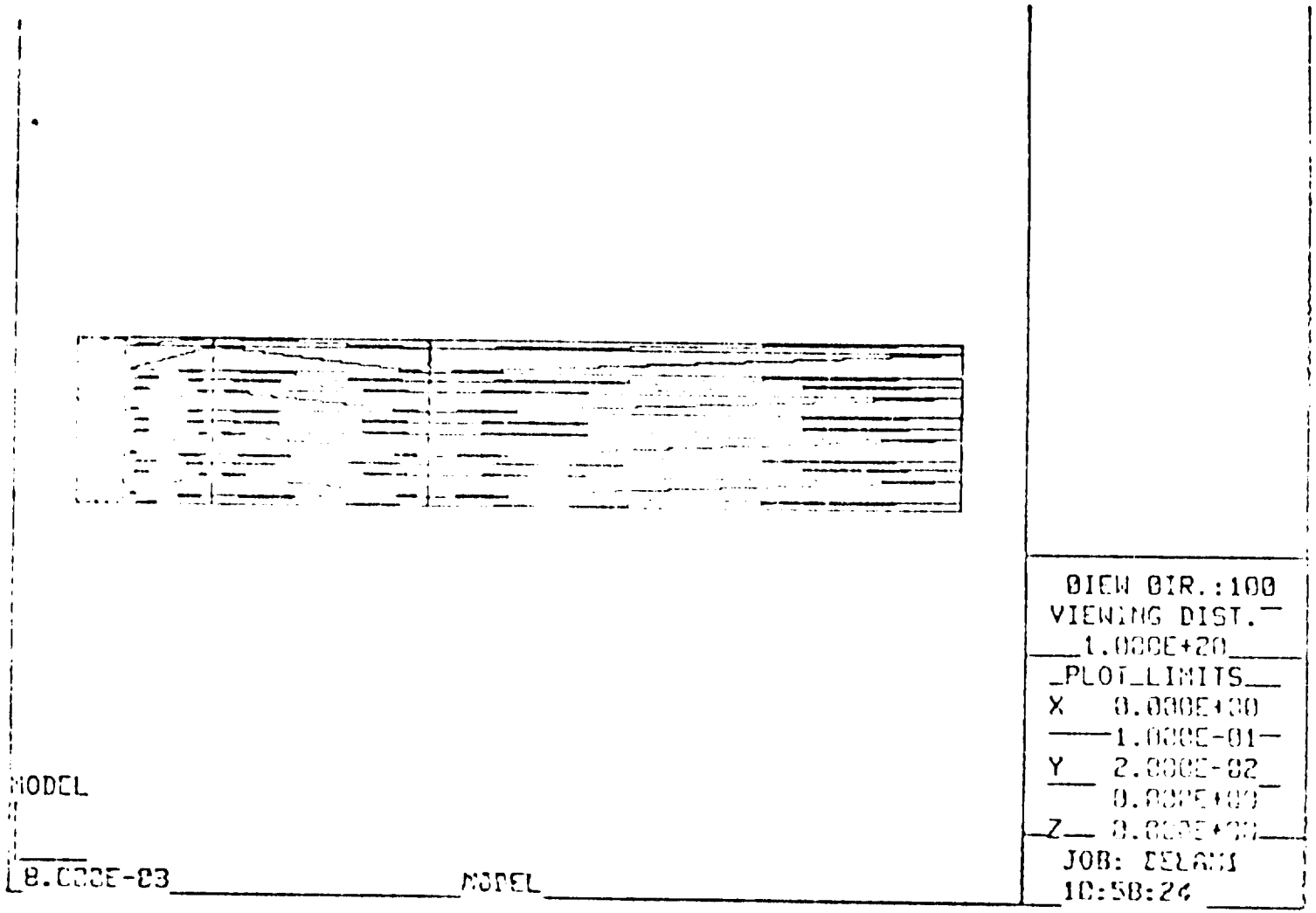

Figure D17 Finite Element Model Used to Calculate Free Edge Stresses in $(0/90/\pm 45)_s$ Laminate

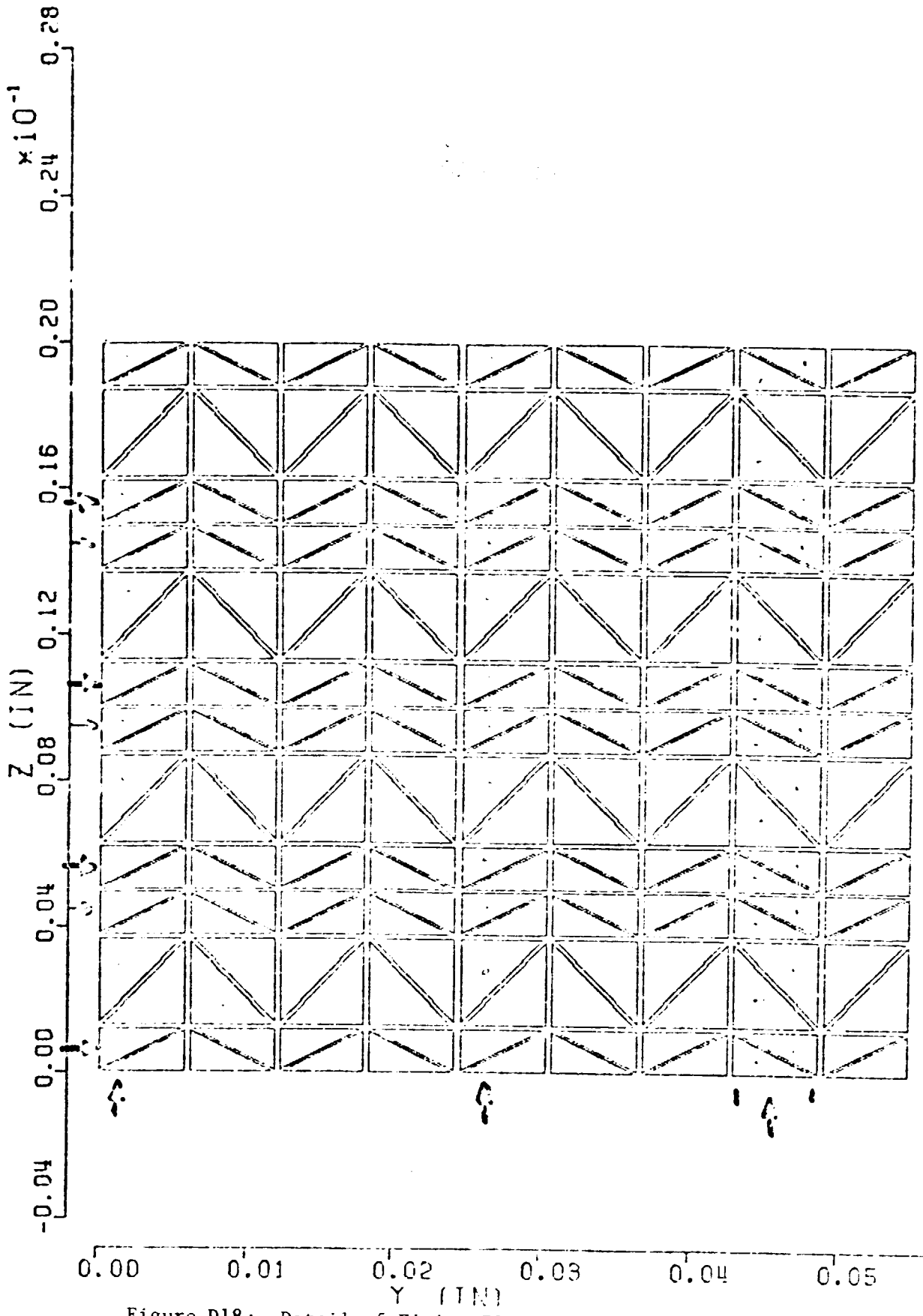

Figure D18: Detail of Finite Element Model Used to Calculate Free Edge Stresses in $(0/90/\pm45)_s$ Laminate.

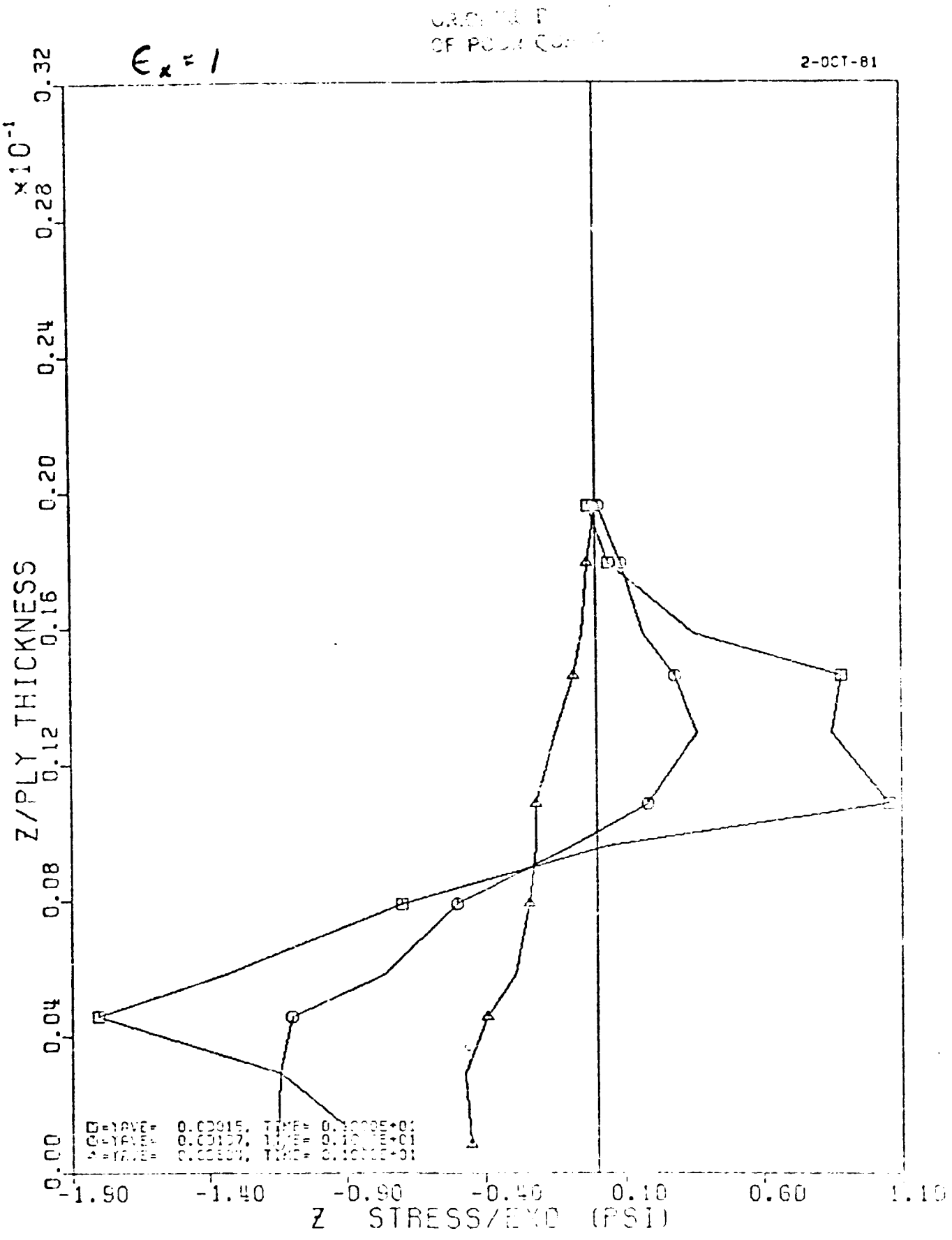

Figure D19 σ_z Free Edge Stress for $(0/90/\pm45)_s$ Laminate as a Function of Z, Uniform Tensile Strain.

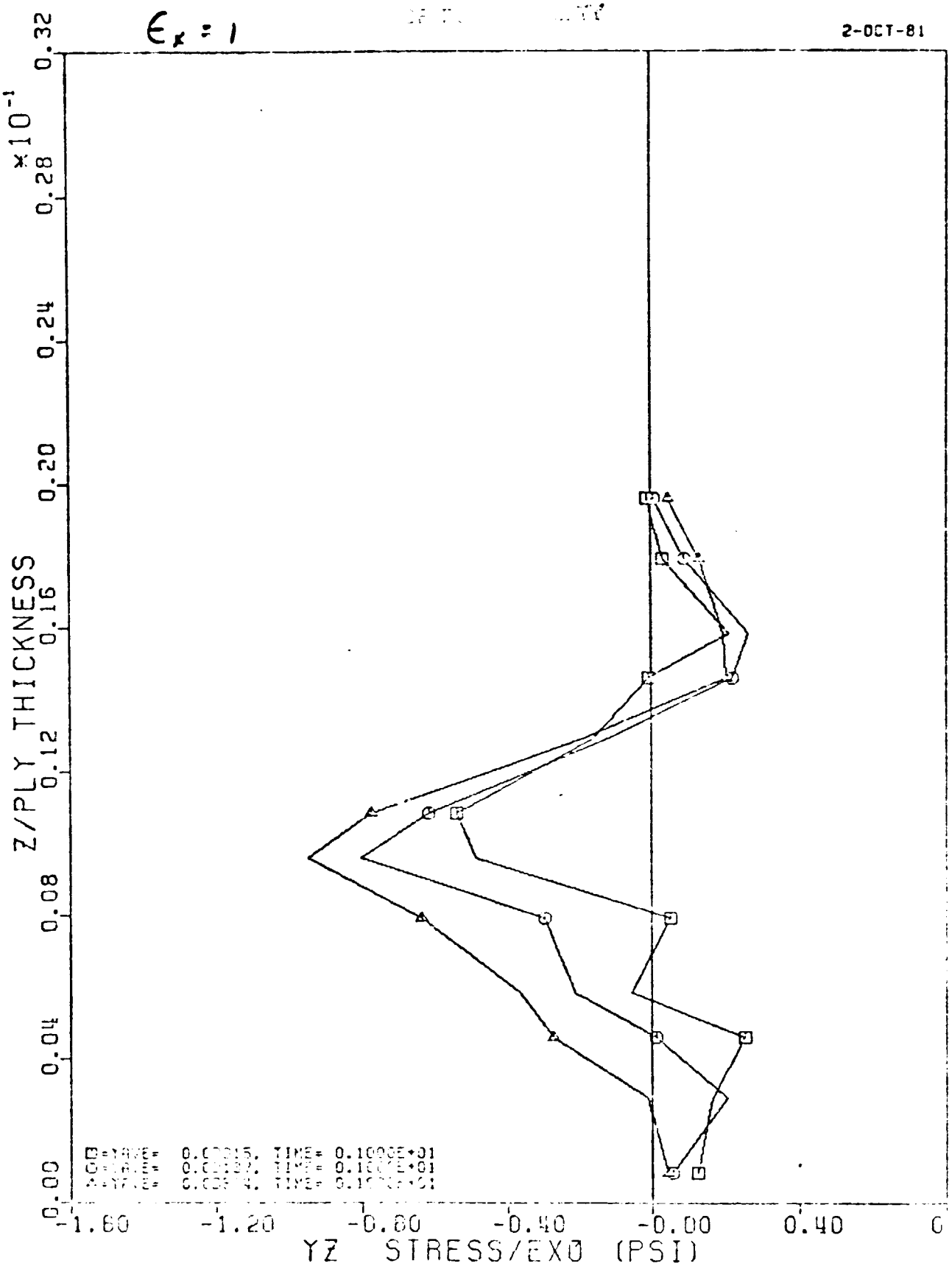
Z-SECTION STRESSES FOR DELM1
$\epsilon_x = 1$
2-OCT-81
Z/PLY THICKNESS
$\times 10^{-1}$
0.32
0.28
0.24
0.20
0.16
0.12
0.08
0.04
0.00
-1.60
-1.20
-0.80
-0.40
-0.00
0.40
YZ STRESS/EXO (PSI)

Figure D20:

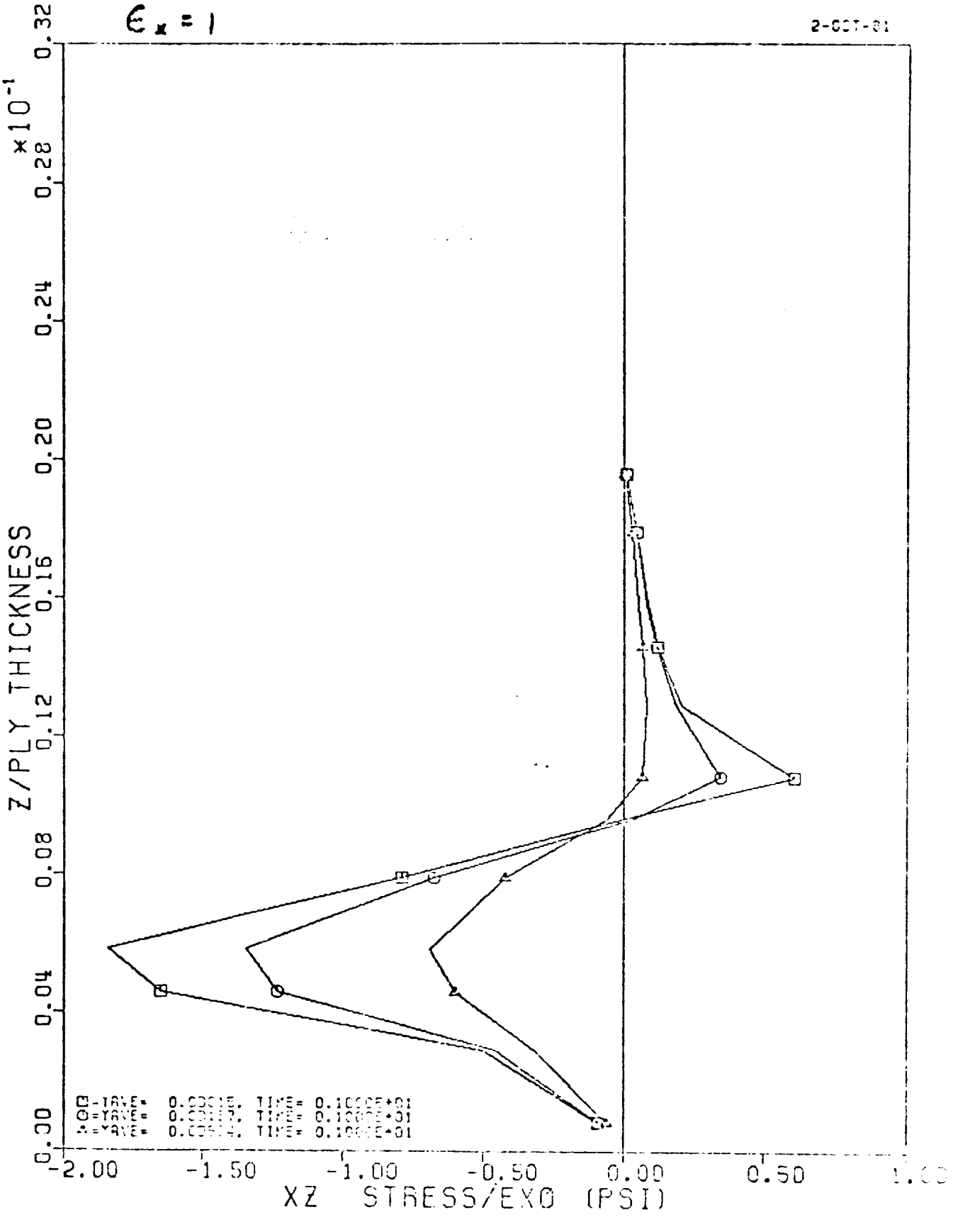
$\epsilon_x = 1$
2-OCT-81
Z/PLY THICKNESS
$\times 10^{-1}$
0.00
0.04
0.08
0.12
0.16
0.20
0.24
0.28
0.32
-2.00
-1.50
-1.00
-0.50
0.00
0.50
XZ STRESS/EXO (PSI)
R=0.000
PLY THICKNESS=1.0000

Figure D21

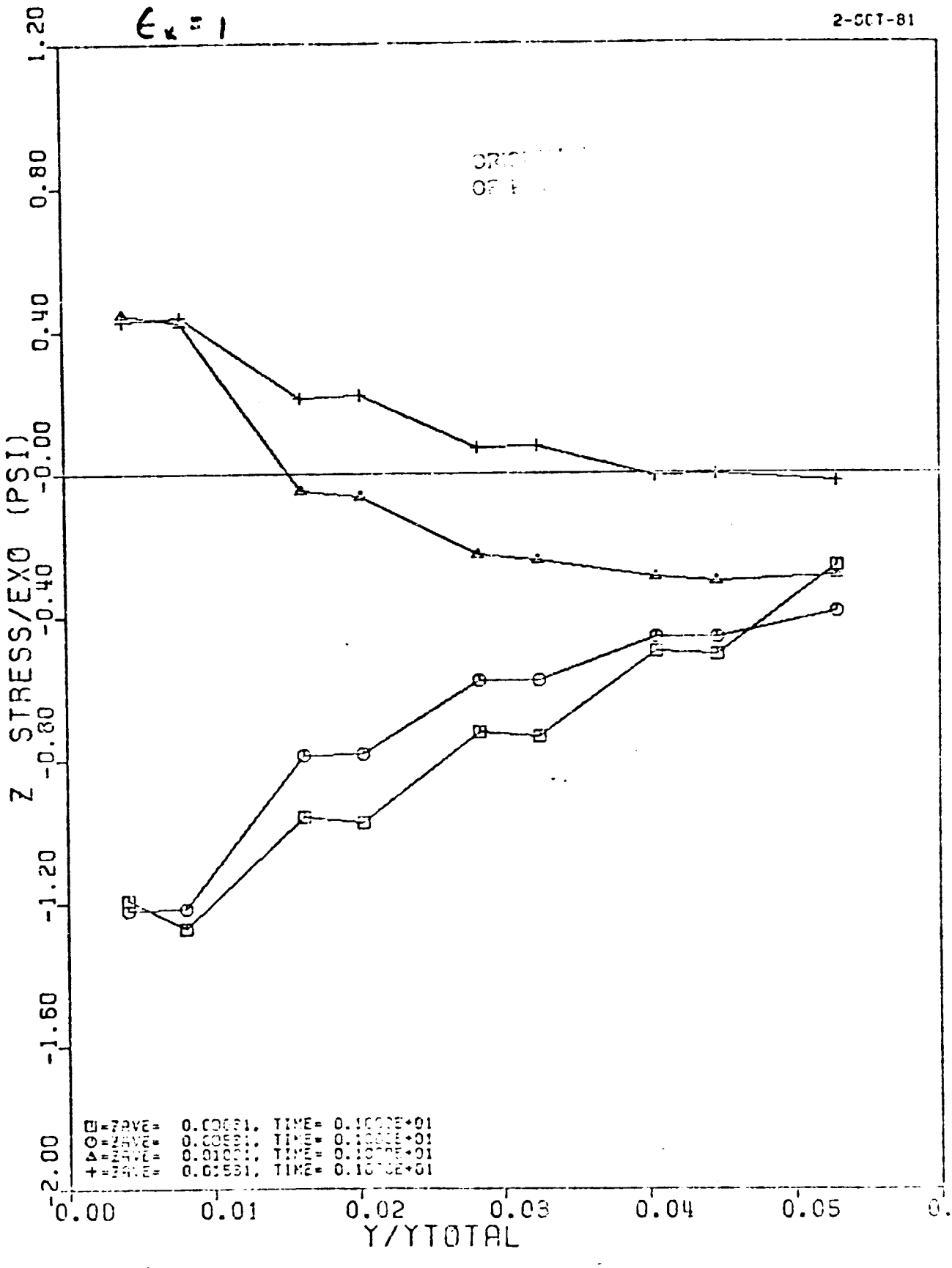

Figure D22: σ_z Free Edge Stress for $(0/90/\pm45)_s$ Laminate as a Function of Y, Uniform Tensile Strain, ϵ_x

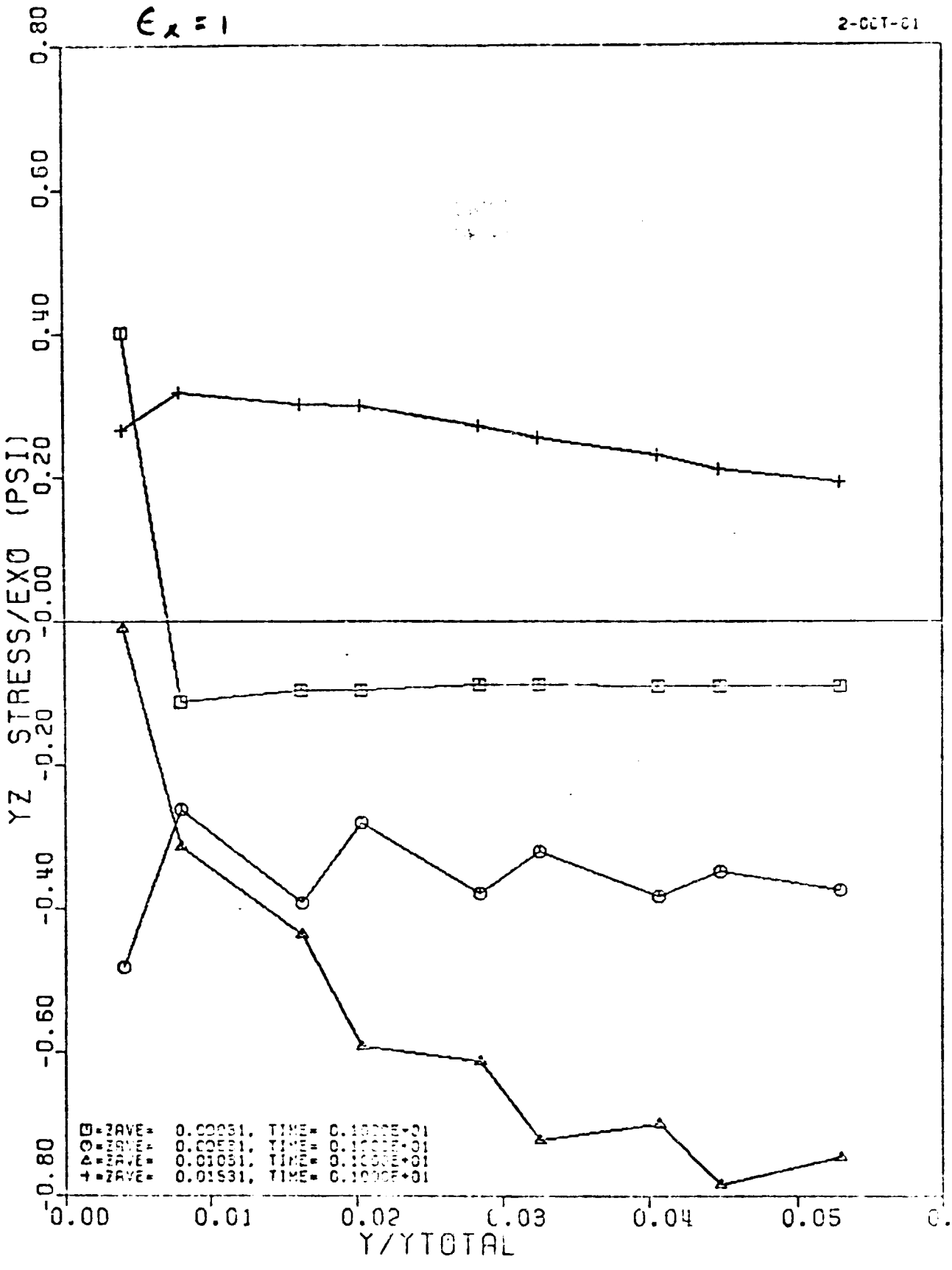

Figure D23: σ_{yz} Free Edge Stress for $(0/90/\pm45)_s$ Laminate as a Function of Y, Uniform Tensile Strain, ϵ_x

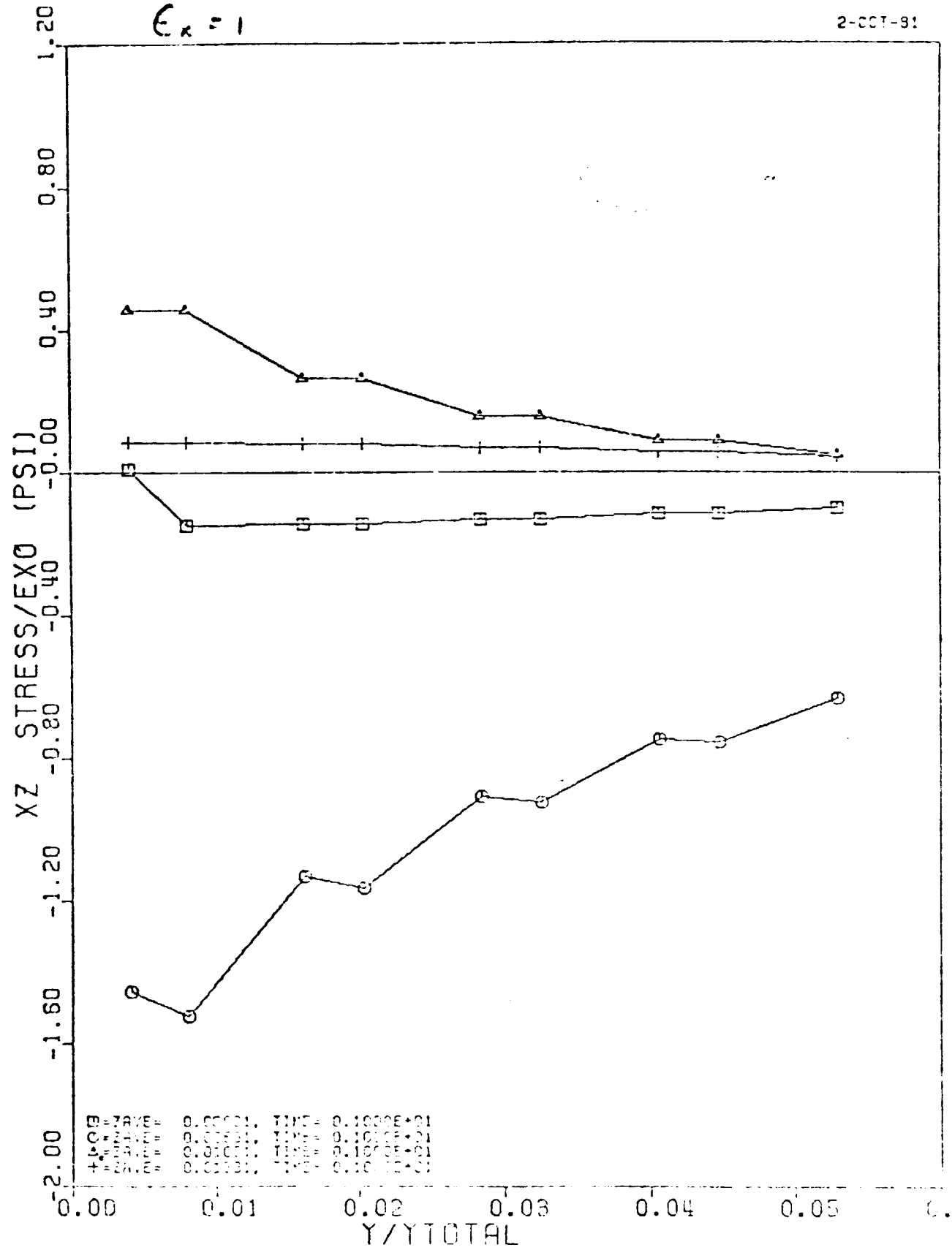

Figure D24: σ_{xz} Free Edge Stress for $(0/90/\pm45)_s$ Laminate as a Function of Y, Uniform Tensile Strain, ϵ_x

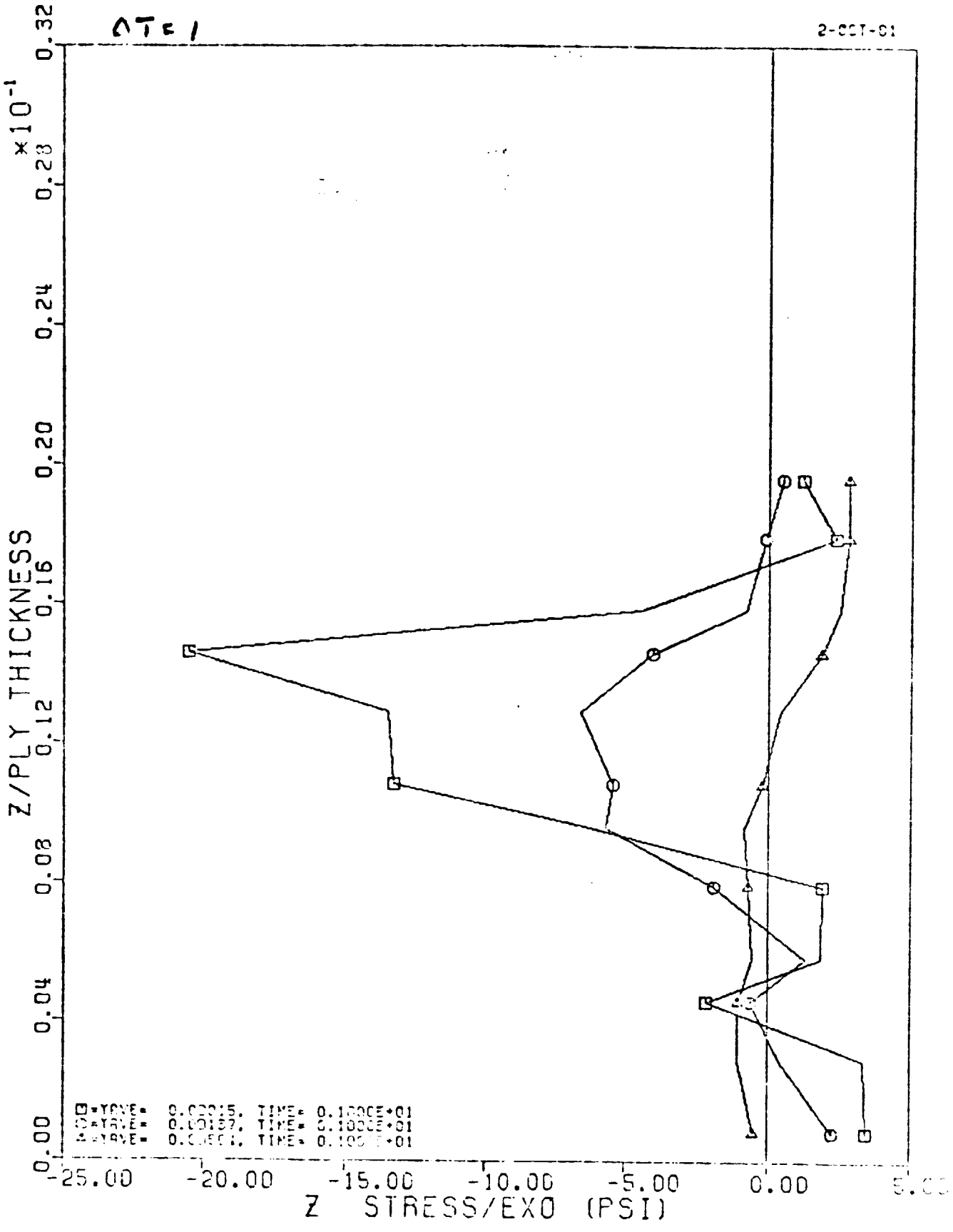

Figure D25: σ_z Free Edge Stress for (0/90/+45)$_s$ Laminate as a Function of Z, Uniform temperature Change $-55^{\circ}C$ ($100^{\circ}F$)

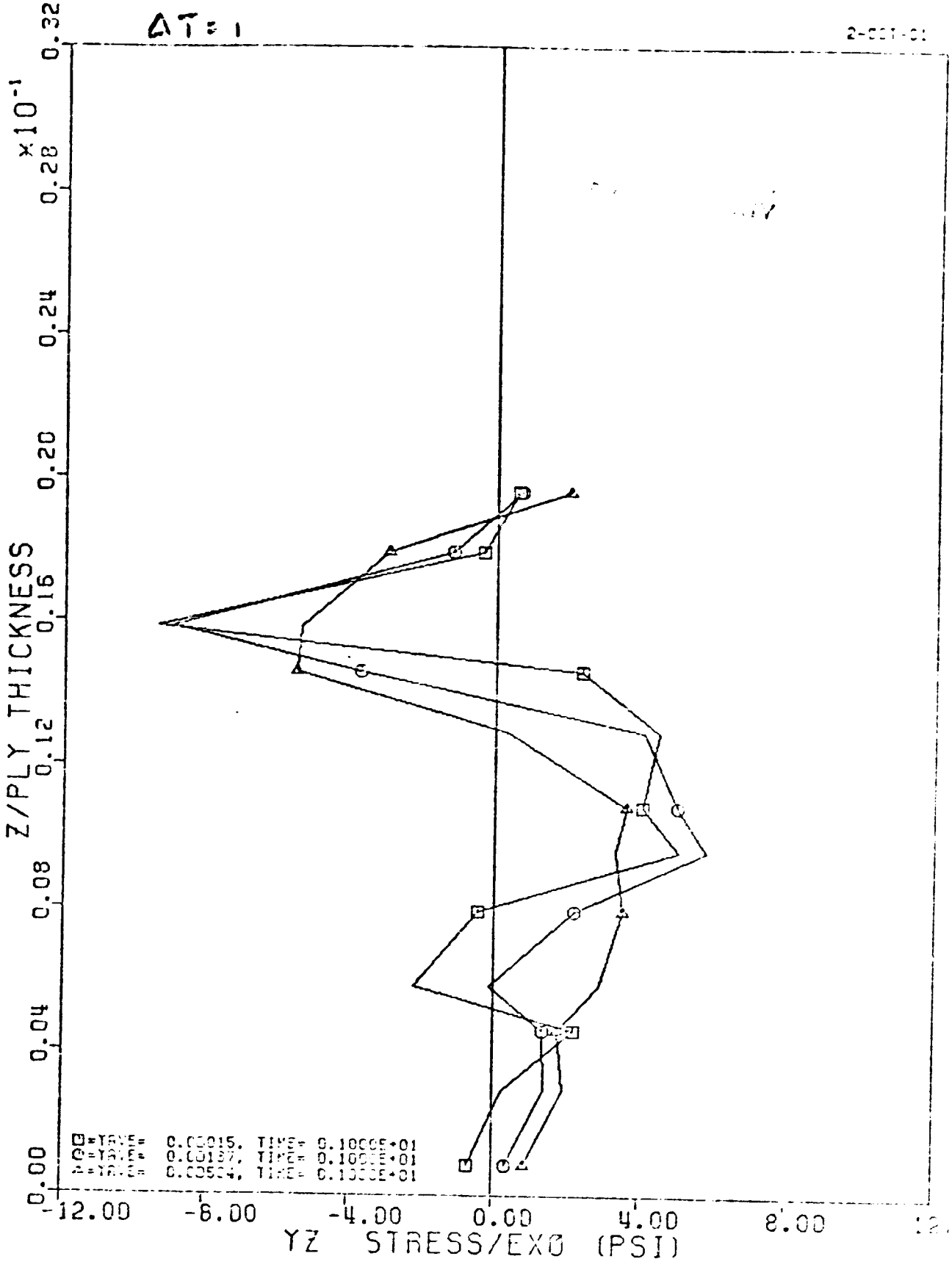

Figure D26: σ_z Free Edge Stress for $(0/90/\pm45)_s$ Laminate as a Function of Uniform Temperature Change, 0.5°C (10°F)

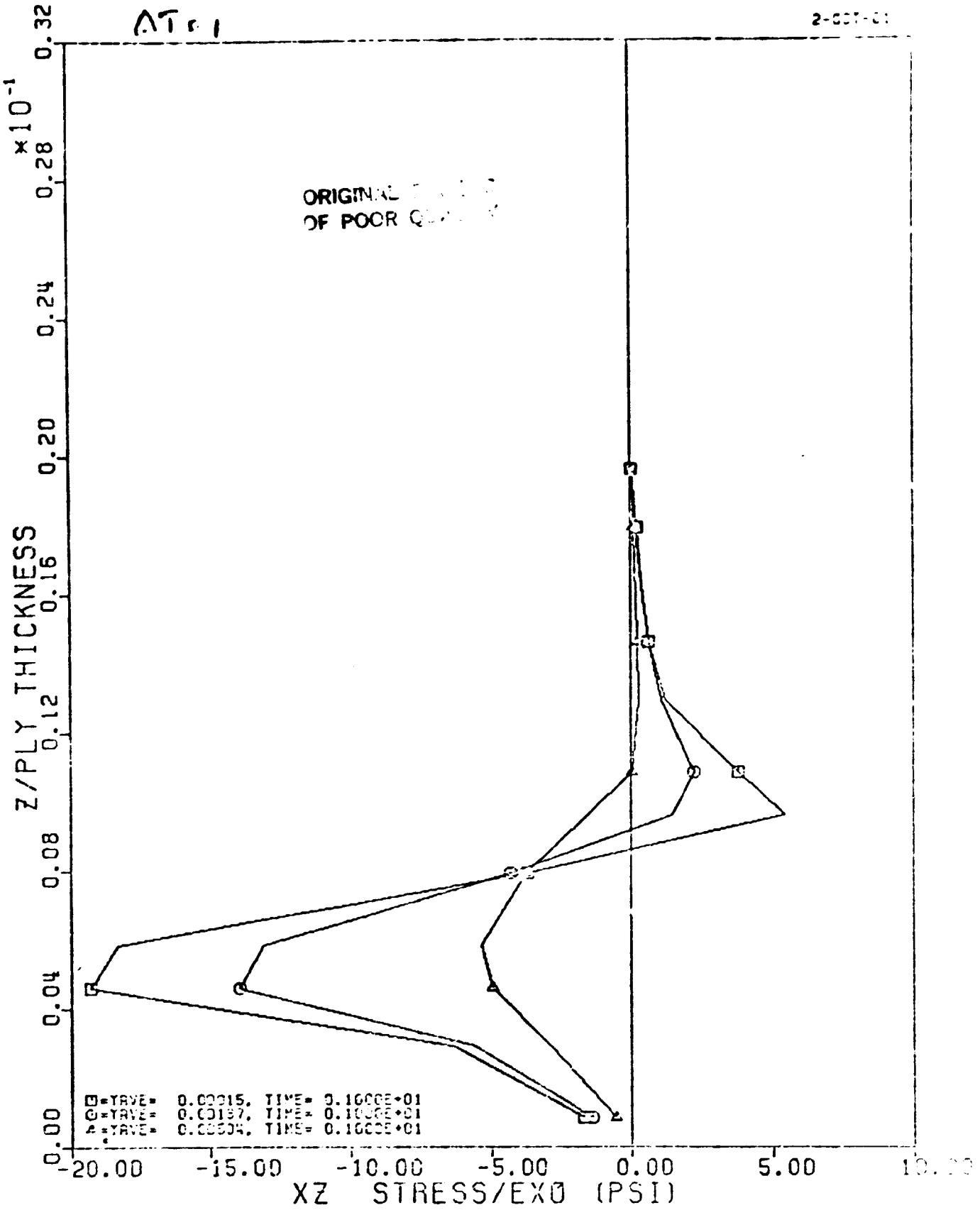

Figure D27: σ_z Free Edge Stress for $(0/90/\pm45)_s$ Laminate as a Function of Z, Uniform Temperature Change, 0.5°C (10°F).

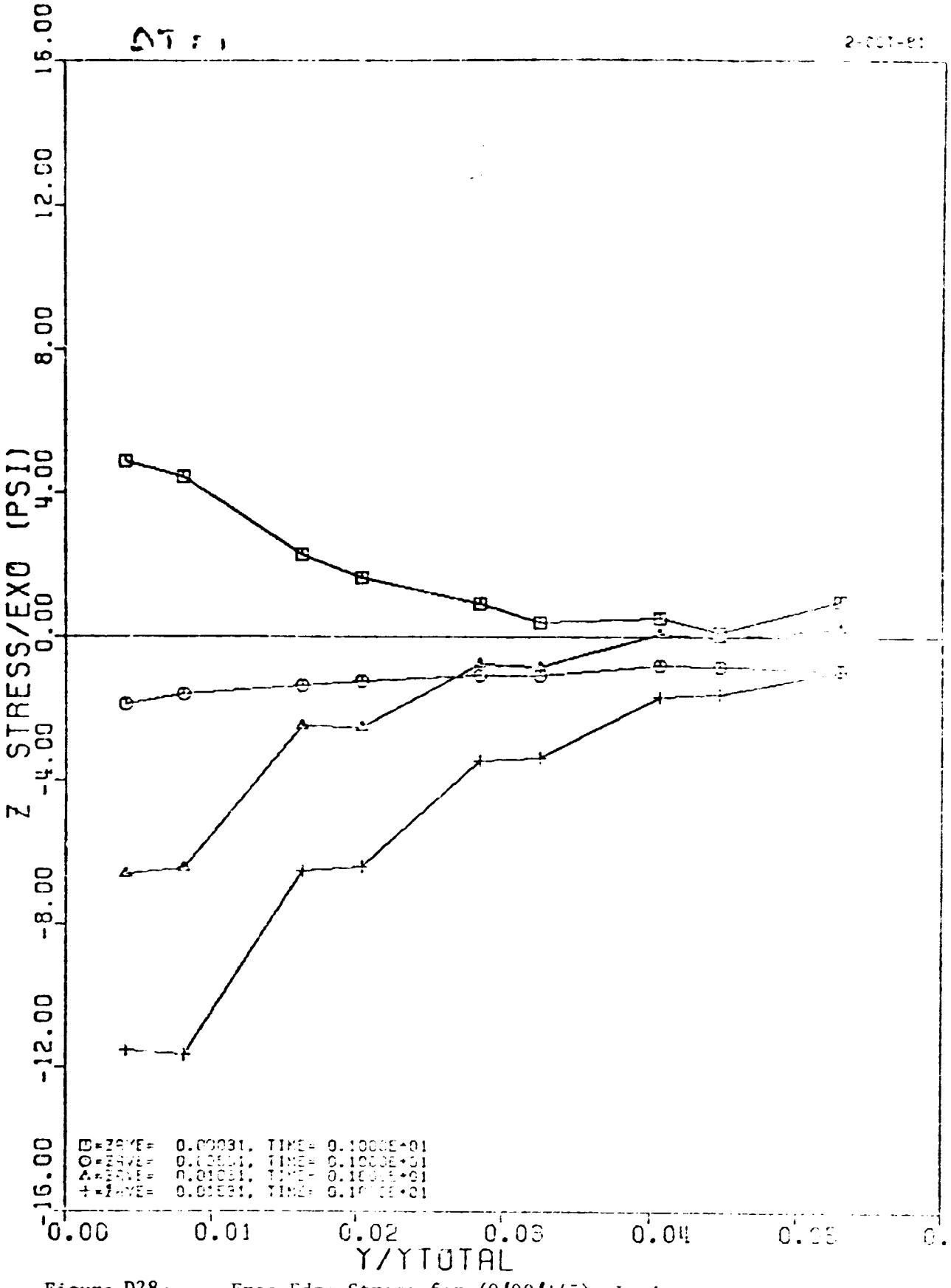

Figure D28: σ_z Free Edge Stress for $(0/90/\pm45)_s$ Laminate as a Function of Y, Uniform Temperature Change, 0.5°C (10°F).

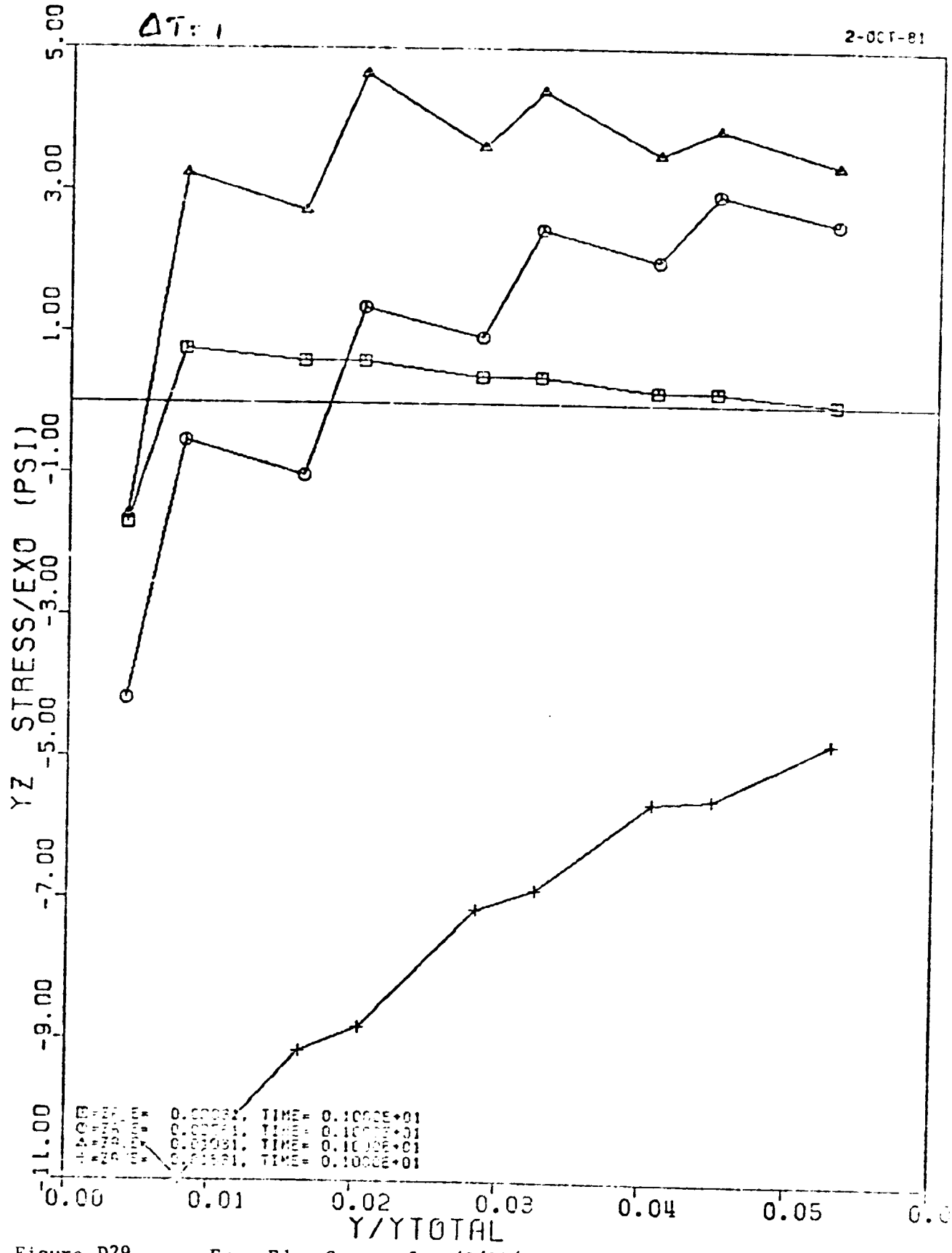

Figure D29 σ_{yz} Free Edge Stress for (0/90/±45) Laminate as a Function of Y, Uniform Temperature Change, 0.5°C (10°F).

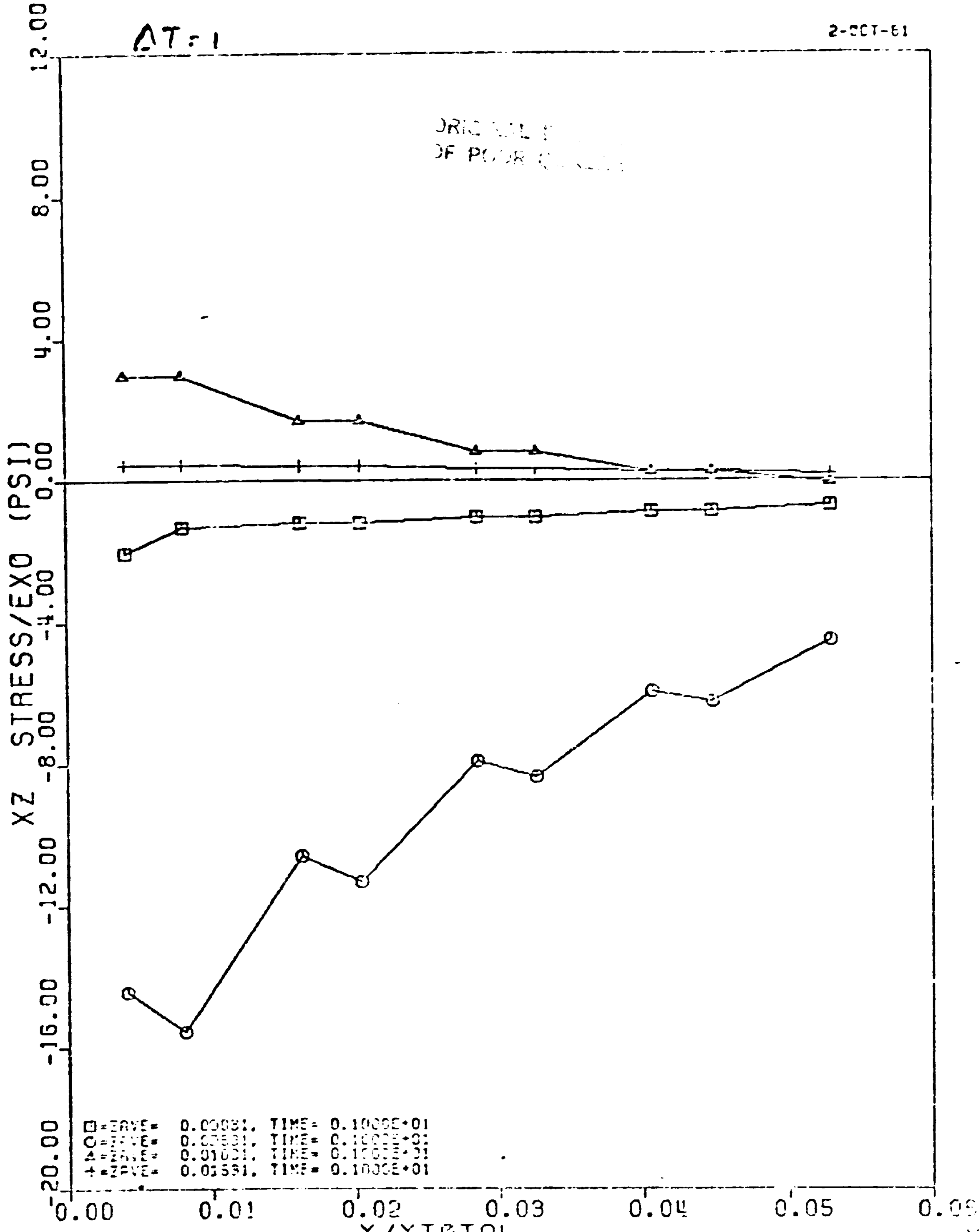

Figure D30: σ_{xz} Free Edge Stress for (0/90/±45)s Laminate as a Function of Y. Uniform Temperature Change, 0.5°C (10°F)

END

DATE

FILMED

OCT 17 1984